PROCEEDINGS OF ICSF-1

FIRST INTERNATIONAL CONFERENCE ON SCOUR OF FOUNDATIONS

NOVEMBER 17-20, 2002
TEXAS A&M UNIVERSITY
COLLEGE STATION, TEXAS, USA

SPONSORED BY
Main Sponsors:
International Society for Soil Mechanics and Geotechnical Engineering
Texas Transportation Institute

Gold Level Sponsors:
Federal Highway Administration
National Science Foundation

Silver Level Sponsors:
ADSC, The International Association of Foundation Drilling
American Society of Civil Engineers (ASCE)
Coasts, Oceans, Ports, and Rivers Institute of ASCE
Environmental & Water Resources Institute of ASCE
Geo-Institute of ASCE
Structural Engineering Institute of ASCE
Texas A&M University Department of Civil Engineering
Transportation Research Board (TRB)

ADDITIONAL COPIES OF THIS BOOK CAN BE OBTAINED FROM

Texas Transportation Institute
Publications Dept.
Tel: (979) 845-4853
Fax: (979) 862-3703
Email: sales@ttimail.tamu.edu
Internet: http://tti.tamu.edu/product/

CONFERENCE COMMITTEES

Chairman of the Conference: Jean-Louis Briaud
Vice-Chairman of the Conference: Hamn-Ching Chen
Editors of the Proceedings: Hamn-Ching Chen and Jean-Louis Briaud

National Advisory Committee:

George Annandale, Larry Arneson, Jean-Louis Briaud, Hamn-Ching Chen, Tom Dahl, Stan Davis, Jerry DiMaggio, Dave Froelich, Daryl Greer, Larry Harrison, Robert Henthorne, Carlton Ho, Rollin Hotchkiss, Beatrice Hunt, Peggy Johnson, Sterling Jones, Ed Kent, Peter Lagasse, Melinda Luna, Shawn McClemore, William Moore, Jorge E. Pagan-Ortiz, Gary Parker, Art Parola, Richard Phillips, Everett Richardson, Max Sheppard, Peter Smith, Steve Smith, David Stolpa, Phil Thompson, Mehmet Tumay

International Advisory Committee:

Laila Abed, Marco Falcon Ascanio, A. (Tony) Bracegirdle, Jean-Louis Briaud, Yee-Meng Chiew, Michael Heibaum, Sangseom Jeong, Hellgi Johannesson, Sterling Jones, Soo-Sam Kim, Boleslaw A. Klosinski, Raul A. Lopardo, Bruce Melville, Zlatko Mihalinec, Yahia E-A. Mohamedzein, Gaton Laporte Molina, A.V.S.R. Murty, Jorge E. Pagan-Ortiz, L. Rakoczi, Everett V. Richardson, A.M.M. Saffiullah, Makoto Shimamura, Testsuro Tsujimoto, Dirceu de Alencar Velloso, Narimantas Zdankus

Organizing Committee:

Michelle Benoit, Jamie Blakeney, Jean-Louis Briaud, Hamn-Ching Chen, Billy Edge, Richard Gehle, Harlow Landphair, Ya Li, Kathy Montemayor, Prahoro Nurtjahyo, Tobey Nutt, Josh Reinbolt, Susan Robertson, Jun Wang

Technical Program Committee:

Jean-Louis Briaud, Hamn-Ching Chen, Michael Heibaum, Bruce Melville, Jorge Pagan, Art Parola, Everett Richardson, Stephen Wright

Prediction Event Committee:

Jean-Louis Briaud, Kuang-An Chang, Hamn-Ching Chen, Jerry DiMaggio, Al DiMillio, Sterling Jones, Ya Li, Dave Mueller, Jorge Pagan, Jun Wang

PREFACE

Texas A&M University
September 16, 2002

Many people have contributed to making this conference a success. The teamwork that led to this event and to the proceedings will remain a very bright moment in my career. I would like to single out one person however for his tremendous contribution to this conference. Thank you Professor Chen for being such a great teammate and for your very demanding role as the main person responsible for the proceedings. You are definitely the MVP of this conference. I would also like to thank the reviewers for taking the time to review a large number of manuscripts in a relatively short period of time: Brian Barkdoll, Liang Cheng, Yee-Meng Chiew, Chen Onn Chin, Sung-Uk Choi, Keith E. Dennett, Duowen Ding, Robert Ettema, Oktay Guven, Willi H. Hager, Faruque Mia, Michael H. Heibaum, Sangseom Jeong, Yafei Jia, Peggy A. Johnson, J. Sterling Jones, Paul Kirshen, Peter Lagasse, Ya Li, Siow-Yong Lim, Richard May, Bruce Melville, David S. Mueller, Tatsuaki Nakato, Prahoro Nurtjahyo, Kunihiro Ogihara, Michael W. O'Neill, James D. Schall, D. Max Sheppard, Makoto Shimamura, Nels J. Sultan, B.Mutlu Sumer, Jun Wang. Richard Gehle and Josh Reinbolt were very helpful in assembling the proceedings electronically and in the details of the conference organization.

Our sponsors were numerous and very helpful: The International Society for Soil Mechanics and Geotechnical Engineering (Kenji Ishihara, William Van Impe), The Texas Transportation Institute (Herbert Richardson, Dennis Christiansen), The Federal Highway Administration (Sterling Jones, Al DiMillio, Jorge Pagan, Jerry DiMaggio), The National Science Foundation (Cliff Astill, Rick Fragaszy), ADSC: The International Association of Foundation Drilling (Scot Litke), American Society of Civil Engineers (ASCE), The Geo-Institute of ASCE (Carol Bowers, Gail Sor), The Environmental & Water Resources Institute of ASCE (Bryan Parsons), The Coasts, Oceans, Ports, and Rivers Institute of ASCE (Patricia Brown), The Structural Engineering Institute of ASCE (Jim Rossberg), The Transportation Research Board: TRB (Jay Jayaprakash), Texas A&M University Department of Civil Engineering (John Niedzwecki).

And then there was all the help from the various committees: International Advisory Committee, National Advisory Committee, Technical Program Committee, Prediction Event Committee, Organizing Committee. You can find the complete list of committee members within the previous page.

The Prediction Event was also a major undertaking. The Federal Highway Administration and the Texas A&M University Department of Civil Engineering were the two main sponsors with help from the USGS and several DOTs: many thanks to Sterling Jones, Dave Mueller, K. Van Wilson, Paul H. Rydlund, Richard J. Huizinga. At Texas A&M University, the flume tests were performed by Ya Li and Jun Wang with the cooperation of John Reed and Bob Randall.

I also wish to thank my wife Janet who was such a great support during all the time spent on the preparation of this conference.

Jean-Louis Briaud

Chairman of ICSF-1

First International Conference on Scour of Foundations ICSF-1
Texas A&M University, November 17 –20, 2002

Final Program

SUNDAY, NOVEMBER 17, 2002

9:00 a.m.-12:00 Noon	**ISSMGE TC-33 – Geotechnics of Soil Erosion Committee Meeting**
12:00 Noon-1:30 p.m.	**Lunch** – on your own
1:30 p.m.-3:00 p.m.	**Short Course:** Scour of Foundations **Organizers:** *J. E. Pagan*, (USA); S. Jones (USA); *J-L. Briaud*, (USA)
3:00 p.m.-3:30 p.m.	**Break**
3:30 p.m.-5:00 p.m.	**Short Course:** Scour of Foundations **Organizers:** *J. E. Pagan*, (USA); S. Jones (USA); *J-L. Briaud*, (USA)
5:30 p.m.-8:00 p.m.	**Reception in the Exhibits Hall - Registration**

MONDAY, NOVEMBER 18, 2002

7:00 a.m.-8:00 a.m.	**Breakfast and Registration in Exhibits Hall**
8:00 a.m.-8:30 a.m.	**WELCOME – Grand Ballroom** H. H. Richardson, Director, Texas Transportation Institute J. M. Niedzwecki, Head, Department of Civil Engineering J-L. Briaud, Chairman, ICSF-1, Acknowledgements
8:30 a.m.-10:00 a.m.	**SESSION (1): PLENARY SESSION I – Grand ballroom** **Session Chairs:** M. Tumay, P. Smith. **Invited Lecture 1.1:** *Scour Protection and Repair by Filtering Geosynthetic Containers.* M. H. Heibaum (Germany). **Invited Lecture 1.2:** Numerical Simulation of Scour Around Complex Piers in Cohesive Soil. *H-C. Chen* (USA). **Invited Lecture 1.3:** Unconventional Interpretation of Local Scour Downstream a Large Dam Stilling Basin. R. A. Lopardo (Argentina), J. M. Casado, M. C. Lopardo.
10:00 a.m.-10:30 a.m.	**Break in the Exhibits Hall**
10:30 a.m.-12:00 Noon	**Concurrent Sessions**
	SESSION (2): SCOUR PREDICTIONS I – Ballroom 1 **Session Chairs:** J. Audibert, C. Weber. **Invited Lecture 2.1:** *Indirect Methods of Measuring Shear Stress in the Bottom of a Scour Hole*. J. S. Jones (USA). **Presentation 2.2:** Shear Stress Approach to Pier Scour Predictions. Y. Li (USA), J-L. Briaud, H-C. Chen, P. Nurtjahyo, J. Wang. **Presentation 2.3:** A Review of Predictive Methods for General Scour. R. Bettess (UK). **Presentation 2.4:** Prediction of Local Scour Below Offshore Pipelines – A Review. L. Cheng (Australia). **Presentation 2.5:** Comparison of General Scour Prediction Equations for River Crossings. C. Lauchlan (UK), R. May.

SESSION (3): SCOUR MEASUREMENTS I – Ballroom 2
Session Chairs: C. Monk, N. Jaynes.
Invited Lecture 3.1*:* Local Scour Around Structures in Tidal Flows. R. W. P. May (UK), M. Escarameia.
Presentation 3.2*:* Movement of Bridge Pier by Water Flow Under Flood Condition. K. Ogihara (Japan), H. Muraishi, S. Masahiko, D. Nakajima.
Presentation 3.3: 3-Dimensional Measured and Simulated Flow for Scour Near Spur Dikes. R. Kuhnle (USA), Y. Jia, C. Alonso.
Presentation 3.4: Scour Experiments on Dike Angle, Porosity, and Hook for a Thin Dike. E. Martinez (USA), R. Ettema, A. Lachhab.
Presentation 3.5: Shallow Water Effect on Pier Scour in Clays. Y. Li (USA), J-L. Briaud, H-C. Chen, P. Nurtjahyo, J. Wang.

12:00 Noon-1:30 p.m. **Lunch** – **Oakwood Ballroom** (provided)

1:30 p.m.-3:00 p.m. **Concurrent Sessions**

SESSION (4): SCOUR PREDICTIONS II – Ballroom 1
Session Chairs: P. D'Odorico, D. Stolpa.
Invited Lecture 4.1: *Effect of Suspended Fine Sediment on Local Scour.* M. Sheppard (USA).
Presentation 4.2: *Numerical Simulations of 3-D Flows Around Bridge Piers.* S-U. Choi (Korea), W. Yang.
Presentation 4.3: *3-D Numerical Model for Wave-Induced Dynamic Behavior of Sand Beds at Bridge Piers*. F. Mia (Japan), H. Nago, S. Maeno.
Presentation 4.4: *Pier Scour at Woodrow Wilson Bridge and SRICOS Method.* K. Kwak (Korea), J-L. Briaud, Y. Cao, M-K. Chung, B. Hunt, S. Davis.
Presentation 4.5: *Bed Shear Stress Around Rectangular Pier: Numerical Approach*. P. Nurtjahyo (USA) H-C. Chen, J-L. Briaud, Y. Li, J. Wang.

SESSION (5): SCOUR MEASUREMENTS II – Ballroom 2
Session Chairs: W. Edge, R. Melek.
Invited Lecture 5.1: *Flume Experiments on Abutment Scour: Confronting Complexities in Process and Similitude.* R. Ettema (USA).
Presentation 5.2: *Scouring Downstream of Sluice Gate*. S-Y. Lim (Singapore), G. Yu.
Presentation 5.3: *Development of the New Inspection Method on Scour Condition Around Existing Bridge Foundations.* J. Fukui (Japan), M. Otuka.
Presentation 5.4: *Experimental Study on Toe Scour of Seawall Covered with Armor Units Due to Waves*. T. Sakakiyama (Japan), R. Kajima.
Presentation 5.5: *Scour Around Rubble-Mound Breakwater Head of Cheju Outer Port*. H. Kim, (Korea), B. C. Oh, B-S. Jung, S-Z Youn.

3:00 p.m.-3:30 p.m. **Break in the Exhibits Hall**

3:30 p.m.-5:00 p.m. **Concurrent Sessions**

SESSION (6): SCOUR PREDICTIONS III – Ballroom 1
Session Chairs: K. A. Chang, P. Nurtjahyo
Invited Lecture 6.1: *Analysis of Pier Scour Predictions and Real-Time Field Measurements*. D. S. Mueller (USA), C. R. Wagner.
Presentation 6.2: *Future Hydrographs and Scour Risk Analysis.* J-L. Briaud (USA), P. D'Odorico, E. J. Jeon
Presentation 6.3: *Database Program for Highway Bridge-Scour Data.* K. Farrag (USA), M. Morvant.
Presentation 6.4: *Nondimensional Analysis of Clear-Water Scour at Bridge*

Contractions in Cohesive Soils. O. Guven (USA), J. G. Melville, J. E. Curry.
Presentation 6.5: *FE Analysis of Coastal Cliff Erosion due to Ocean Wave Assailing*. K. Yasuhara (Japan), S. Murakami, Y. Kanno, Z. Wu.

SESSION (7): GEOTECHNICAL ASPECTS I - Ballroom 2
Session Chairs: C. Aubeny, X. Long.
Invited Lecture 7.1: *Theoretical and Practice Aspects of Rock Scour Prediction*. G. W. Annandale (USA), E. Bollaert, A. Schleiss.
Presentation 7.2: *Erosion Function Apparatus Overview and Discussion of Influence Factors on Cohesive Soil Erosion Rate in EFA Test*. Y. Cao (USA), J. Wang, J-L. Briaud, H-C. Chen, Y. Li, P. Nurtjahyo.
Presentation 7.3: *Identification of Dispersive Clays in Gaza Strip Area*; *and Filter Effects on Dam Safety*. M. A. Awad (Palestine).
Presentation 7.4: *Effects of Cohesion on Bridge Scour*. A. Molinas (USA), S. J. Jones.
Presentation 7.5: *Scour Around Submarine Pipeline in Clayey Soil.* S. Neelamani (India), A. Vijaya kumar, S. Narasimha Rao.

5:30 p.m.-6:30 p.m. **2001 TERZAGHI LECTURE – Grand Ballroom**
Session Chairs: P. Jeanjean, A. Niederoda.
Geotechnical Solutions for the Offshore: Synergy of Research and Practice S. Lacasse, (Norway)

7:00 p.m.-9:00 p.m. **Reception in the new Texas A&M University Hydraulic Laboratory**
(Buses leave every 10 minutes starting at 6:45 p.m.)

7:00 p.m.-10:00 p.m. **Committee Meetings – Mockingbird rooms**

TUESDAY, NOVEMBER 19, 2002

7:00 a.m.-8:00 a.m. **Breakfast and Registration in Exhibits Hall**

8:30 a.m.-10:00 a.m. **SESSION (8): PLENARY SESSION II – Grand Ballroom**
Session Chairs: S. Wright, B. Hunt.
Invited Lecture 8.1: Survey of Bridge Damages Due to a Heavy Rain in Northern Part of Kanto Region, Japan. J. Fukui (Japan), M. Nishitani.
Invited Lecture 8.2: The SRICOS-EFA Method**.** J-L. Briaud (USA).
Invited Lecture 8.3: *Failure Mechanisms of Riprap Layer Around Bridge Piers.* Y-M. Chiew (Singapore).

10:00 a.m.-10:30 a.m. **Break in the Exhibits Hall**

10:30 a.m.-12:00 Noon **Concurrent Sessions**

SESSION (9): COUNTERMEASURES I – Ballroom 1
Session Chairs: H. Landphair, W. Wang.
Invited Lecture 9.1: *Scour Protection Around Gravity Based Structures Using Small Size Rock*. K. J. Bos (Netherlands), H. J. Verheij, G. Kant, A. C. H. Kruisbrink.
Presentation 9.2: *Riprap as Permanent Scour Protection Around Bridge Piers*. C. D. Anglin (Canada), F. Itamunoala, G. Millen.
Presentation 9.3: *Riprap at Rectangular Bridge Piers Under Oblique Incident Flow*. J. A. Sainz (Spain), R. Salgado.
Presentation 9.4: *Countermeasure Construction Using Jet Grouting Methods to Combat Foundation Scour.* D. W. Boehm (USA).

Presentation 9.5: *Field Evaluation and Countermeasure Selection for Scour Critical Bridges in the Commonwealth of Kentucky*. K. J. Schaefer (USA), R. W. Gardner.

SESSION (10): GEOTECHNICAL ASPECTS II – Ballroom 2
Session Chairs: G. Biscontin, H. Hu.
Invited Lecture: 10.1. *GIS-Based Bridge Scour Prioritization.* C. L. Ho (USA), J. M. Di Stasi, P. Rees.
Presentation 10.2: *Erodibility Tests of Shale-Rock Samples Taken from Bridge Pier Construction Site on the Mississippi River.* T. Nakato (USA).
Presentation 10.3: *The Driving Force on Soil Grains and Its Effect on Scouring the Channel of Foundation.* L. Zhang (USA), D. Ding, W. Zhou.
Presentation 10.4: *Depth of Mobile Layer Under Severe Wave Conditions: Liquefaction Effect.* S. Sassa. (Japan).
Presentation 10.5: *Essence of Silt Factor for Scour Calculation Around Bridge Foundation.* R.K. Dhiman,(India), D. K. Mohapatra.

12:00 Noon-1:30 p.m. **Lunch** – **Oakwood Ballroom** (provided)

1:30 p.m.-3:00 p.m. **Concurrent Sessions**

SESSION (11): COUNTERMEASURES II – Ballroom 1
Session Chairs: D. Laefer, J. B. Seo.
Invited Lecture 11.1: *Impact of the Federal Highway Administration's Scour Evaluation Program in the United States of North America's Highway Bridges.* J. E. Pagan-Ortiz (USA).
Presentation 11.2: *Evaluation of Strategies to Control Erosion along U.S. Highway 50 Between Carson City and Lake Tahoe.* K. Dennett (USA), P. Fricthel, R. Siddharthan, A. Soltani.
Presentation 11.3: *Optimisation of Scour Protection Measures.* G. B. H. Spaan (Netherlands), M. H. Lindo, G. Kant.
Presentation 11.4: *Design and Construction of Bridge Scour Countermeasures Along the Salt River, Phoenix, Arizona*. D. L. Richards (USA).
Presentation: 11.5.

SESSION (12): ABUTMENTS AND EMBANKMENTS – Ballroom 2
Session Chairs: T. Dahl, S. Hilbrich.
Invited Lecture 12.1: *Abutment Scour Countermeasures: A Review* .B. Barkdoll (USA), R. Ettema, R. Kuhnle, B. Melville, T. Parchure, A. Parola, C. Alonso.
Presentation 12.2: *Countermeasures for Scour at Spill-Through Bridge Abutments.* B. Melville (New Zealand), S. Coleman, D. Hoe.
Presentation 12.3: *Hugo Reservoir Embankment Depression Study.* J. B. Nevels, Jr. (USA).
Presentation 12.4: *Pier and Abutment Scour-New Laboratory Data.* W. H. Hager (Switzerland), J. Unger, G. Oliveto.
Presentation 12.5: *Flow and Scouring in Main Channel due to Abutments.* G. Yu (Singapore), S-Y. Lim, S-K. Tan.

3:00 p.m.-3:30 p.m. **Break in the Exhibits Hall**

3:30 p.m.-5:00 p.m. **Concurrent Sessions**

SESSION (13): COUNTERMEASURES III – Ballroom 1
Session Chairs: S. Dunlap, X. Zhang.

Invited Lecture 13.1: *Treating Channel Instability at Bridges*. P. A. Johnson (USA).
Presentation 13.2: *Scour Hazard Mitigation for Tick Canyon Wash Bridge.* M. S. Islam (USA), J. Zha, A. Abghari.
Presentation 13.3: *Final Stages of Butte City Bridge Erosion Control Project.* S. K. Mishra (USA), W. B. Lindsey.
Presentation 13.4: Riprap Protection Around Bridge Piers in a Degrading Channel. *Y- M. Chiew* (Singapore).
Presentation 13.5: *Scour at a Submerged Rock Dike, Willapa Bay, Washington.* N. Sultan (USA). R. Phillips, H. Bermudez.

SESSION (14): PIER SCOUR – Ballroom 2
Session Chairs: S. Davis, J. Wang.
Invited Lecture 14.1: *3-D Numerical Modeling of Flow and Scour Around a Pile.* A. Roulund (Denmark), B. M. Sumer, J. Fredsoe, J. Michelsen.
Presentation 14.2: *New Approach to Scour Evaluation of Complex Bridge Piers.* E. V. Richardson (USA), J. S. Jones, D. M. Sheppard.
Presentation 14.3: *Time Rate of Local Scour at a Circular Pile.* W. Miller, Jr. (USA), D. M. Sheppard.
Presentation 14.4: *A Case Study of the Possible Effects of Long-Term Climate Change on Bridge Scour.* P. Kirshen (USA), L. Edgers, J. Edelmann, M. Percher, B. Bettencourt, E. Lewandowski.
Presentation 14.5: *Analysis of Pile Groups Considering Riverbed Scouring.* S. Jeong (Korea), J. Won, J. Suh.

5:30 p.m.-6:30 p.m. — **2002 BUCHANAN LECTURE – Grand Ballroom**
Session Chair: J-L. Briaud.
"The World Trade Center: Construction, Destruction, Reconstruction. A. Aronowitz, (USA)

7:00 p.m.-9:00p.m. — **Reception at the George Bush Presidential Library and Museum**
(Buses leave every 10 minutes starting at 6:45 p.m.)

WEDNESDAY, November 20, 2002

7:00 a.m.-8:00 a.m. — **Breakfast and Registration in Exhibits Hall**

8:30 a.m.-10:00 a.m. — **SESSION (15): PLENARY SESSION III – Grand Ballroom**
Session Chairs: A. Kosicki, H. Johanesson.
Invited Lecture 15.1: On the Challenges of Scour Prediction. G. Hoffmans (Netherlands), H. Verheij.
Invited Lecture 15.2: A Geotechnical Perspective: Design and Construction of Highway Bridge Foundations for Scour. C. E. Dumas (USA), J. Krolack.
Invited Lecture 15.3: Local Scour Depths at Bridge Foundations: New Zealand Methodology. B. Melville (New Zealand).

10:00 a.m.-10:30 a.m. — **Break in the Exhibits Hall**

10:30 a.m.-12:00 Noon — **Concurrent Sessions**

SESSION (16): SCOUR PROBLEMS I – Ballroom 1
Session Chairs: M. Luna, E. McDonald.
Invited Lecture 16.1: *Study on the Disasters of Bridge and Bed Protection Works During the Passage of Typhoon Herb*. C. Lin (Taiwan), T-C. Ho, P-H. Chiu, K-A. Chang.

Presentation 16.2: *Damages of the Roads-Bridges by Erosion and Remedial Measures in Albania*. L. Bozo (Albania), Y. Muceku.
Presentation 16.3: *Bridge Pier Scour in Bouldery Bed – Indian Scenario.* R. Singh (India), K. K. Razdan, R. K. Dhiman.
Presentation 16.4: *Scour Monitoring of Railway Bridge Piers via Inclination Detection.* N. Kobayashi (Japan), S. Kitsunai, M. Shimamura.
Presentation 16.5: *Non-Destructive Testing to Determine Unknown Pile Lengths Under Existing Bridges*. F. Rausche (USA), M. Huessin, M. Bixler.

SESSION (17): SCOUR MONITORING – Ballroom 2
Session Chairs: S. Smith, K. Y. Rhee.
Invited Lecture 17.1: *Instruments to Measure and Monitor Bridge Scour.* E. V. Richardson (USA).
Presentation 17.2: *Development and Implementation of a Scour Monitoring Program for Selected Bridges Crossing the Trukee River.* K. E. Dennett (USA), P. Fritchel, R. Siddharthan, A. Soltani.
Presentation 17.3: *Seismic Methods to Identify Scour Depth Around Deep Bridge Foundations.* E. J. Mercado (USA), E. B. Davies, J. A. McDonald, M. W. O'Neill.
Presentation 17.4: *Portable Scour Monitoring Research.* J. D. Schall (USA), G. R. Price.
Presentation 17.5: *Active Scour Monitor Instrumentation in the California Transportation System*. S. Ng (USA).

12:00 Noon-1:30 p.m. **Lunch** – **Oakwood Ballroom** (provided)

1:30 p.m.-3:00 p.m. **Concurrent Sessions**

SESSION (18): SCOUR PROBLEMS II – Ballroom 1
Session Chairs: R. Whitehouse, H. Shi.
Invited Lecture 18.1: *Determination of Unknown Bridge Foundation Depths with NDE Methods*. L. D. Olson (USA).
Presentation 18.2: *Scour of Railway Embankment Foundation Located on Sea-Cliff in Japan***.** H. Suzuki (Japan), M. Shimamura.
Presentation 18.3: *Design and Construction of Scour Foundations for Electric Power Transmission Line Structures.* P. M. Kandaris (USA), R. E. Kondziolka, J. P. Adams.
Presentation 18.4: *Propeller Induced Scour.* C-O. Chin (Singapore), W. Li.
Presentation 18.5: *Confederation Bridge – New Scour Design Methodology for Complex Materials.* R. B. Nairn (Canada), C. D. Anglin.

SESSION (19): CASE HISTORIES – Ballroom 2
Session Chairs: L. Arneson, Z. Lu.
Invited Lecture 19.1: *A Methodology for Predicting Channel Migration NCHRP Project No. 24-16.* P. Lagasse (USA), W. Spitz, L. Zevenbergen.
Presentation 19.2: *Predicting Meander Migration: Evaluation of Some Existing Techniques*. J-L. Briaud (USA), H-C. Chen, S. Park.
Presentation 19.3: *Collapse and Erosion of Khon Kaen Loess with Treatment Option.* P. Punrattanasin (Thailand), A. Subjarassang, O. Kusakabe, T. Nishimura.
Presentation 19.4: *Analysis of Contraction and Abutment Scour at Two Sites in Minnesota.* C. R. Wagner (USA), D. S. Mueller.
Presentation 19.5: *Factors Affecting Stream and Foundation Stability at Existing Bridges in New Jersey.* S. M. Baig (USA), J. J. Zarriello, M. A. Khan.

3:00 p.m.-3:30 p.m.	**Break in the Exhibits Hall**
3:30 p.m.-4:00 p.m.	**SESSION (20): PREDICTION EVENT – Grand Ballroom** **Session Chairs:** J. Benn, Y. Li. **Presentation: 20.1.** *Results of the FHWA Prediction Event.* J-L. Briaud (USA)
4:00 p.m. – 5:00 p.m.	**SESSION (21): *FUTURE SCOUR NEEDS. PANEL DISCUSSION* – Grand Ballroom** **Moderator:** J-L. Briaud (USA). **Panelists:** B. Melville (New Zealand). S. Jones (USA). J. Fukui (Japan). R. Whitehouse (UK). G. Hoffmans (Netherlands). C. Dumas (USA).
5:00 p.m.-9:00 p.m.	**Closing Ceremony – Reception at Janet and Jean-Louis Briaud's House** (3013 Coronado Drive, College Station, T: 979-693-3969).

TABLE OF CONTENTS

Page

VOLUME I

PLENARY

"Scour Protection and Repair by Filtering Geosynthetic Containers."
M. H. Heibaum **(Invited Lecture)** 1

"Numerical Simulation of Scour Around Complex Piers in Cohesive Soil."
H-C. Chen **(Invited Lecture)** 14

"Unconventional Interpretation of Local Scour Downstream a Large Dam Stilling Basin."
R. A. Lopardo, J. M. Casado, M. C. Lopardo **(Invited Lecture)** 34

"Survey of Bridge Damages Due to a Heavy Rain in Northern Part of Kanto Region, Japan."
J. Fukui, M. Nishitani **(Invited Lecture)** 47

"The SRICOS-EFA Method."
J-L. Briaud **(Invited Lecture)** 57

"Failure Mechanisms of Riprap Layer Around Bridge Piers."
Y- M. Chiew **(Invited Lecture)** 70

"On the Challenges of Scour Prediction."
G. Hoffmans, H. J. Verheij **(Invited Lecture)** 92

"A Geotechnical Perspective: Design and Construction of Highway Bridge Foundations for Scour." C. E. Dumas, J. Krolack **(Invited Lecture)** 112

"Local Scour Depths at Bridge Foundations: New Zealand Methodology."
B. Melville **(Invited Lecture)** 120

SCOUR PREDICTION

"Indirect Methods of Measuring Shear Stress in the Bottom of a Scour Hole."
J. S. Jones **(Invited Lecture)** 140

"Shear Stress Approach to Pier Scour Predictions."
Y. Li, J-L. Briaud, H-C. Chen, P. Nurtjahyo, J. Wang 156

"A Review of Predictive Methods for General Scour."
R. Bettess 162

"Prediction of Local Scour Below Offshore Pipelines – A Review."
L. Cheng 175

"Comparison of General Scour Prediction Equations for River Crossings."
C. Lauchlan, R. W. P. May 184

"Effect of Suspended Fine Sediment on Local Scour."
D. M. Sheppard **(Invited Lecture)** 198

"Numerical Simulations of 3-D Flows Around Bridge Piers."
S-U. Choi, W. Yang 206

"3-D Numerical Model for Wave-Induced Dynamic Behavior of Sand Beds at Bridge Piers."
F. Mia, H. Nago, S. Maeno 218

"Pier Scour at Woodrow Wilson Bridge and SRICOS Method."
K. Kwak, J-L. Briaud, Y. Cao, M-K. Chung, B. Hunt, S. Davis 227

"Bed Shear Stress Around Rectangular Pier: Numerical Approach."
P. Nurtjahyo, H-C. Chen, J-L. Briaud, Y. Li, J. Wang 242

"Analysis of Pier Scour Predictions and Real-Time Field Measurements."
D. S. Mueller, C. R. Wagner **(Invited Lecture)** 257

"Future Hydrographs and Scour Risk Analysis."
J-L. Briaud, P. D'Odorico, E. J. Jeon 272

"Database Program for Highway Bridge-Scour Data."
K. Farrag, M. Morvant 283

"Nondimensional Analysis of Clear-Water Scour at Bridge Contractions in Cohesive Soils."
O. Guven, J. G. Melville, J. E. Curry 292

"FE Analysis of Coastal Cliff Erosion due to Ocean Wave Assailing."
K. Yasuhara, S. Murakami, Y. Kanno, Z. Wu 307

SCOUR MEASUREMENTS

"Local Scour Around Structures in Tidal Flows."
R. W. P. May, M. Escarameia **(Invited Lecture)** 320

"Movement of Bridge Pier by Water Flow Under Flood Condition."
K. Ogihara, H. Muraishi, S. Masahiko, D. Nakajima 337

"3-Dimensional Measured and Simulated Flow for Scour Near Spur Dikes."
R. Kuhnle, Y. Jia, C. Alonso 349

"Scour Experiments on Dike Angle, Porosity, and Hook for a Thin Dike."
E. Martinez, R. Ettema, A. Lachhab 364

"Shallow Water Effect on Pier Scour in Clays."
Y. Li, J-L. Briaud, H-C. Chen, P. Nurtjahyo, J. Wang 373

"Flume Experiments on Abutment Scour: Confronting Complexities in Process and Similitude."
R. Ettema **(Invited Lecture)** 383

"Scouring Downstream of Sluice Gate."
S-Y. Lim, G. Yu 395

"Development of the New Inspection Method on Scour Condition Around Existing Bridge Foundations." J. Fukui, M. Otuka 410

"Experimental Study on Toe Scour of Seawall Covered with Armor Units Due to Waves."
T. Sakakiyama, R. Kajima 421

"Scour Around Rubble-Mound Breakwater Head of Cheju Outer Port."
H. Kim, B. C. Oh, B-S. Jung, S-Z Youn 437

GEOTECHNICAL ASPECTS

"Theoretical and Practice Aspects of Rock Scour Prediction."
G. W. Annandale, E. Bollaert, A. Schleiss **(Invited Lecture)** 449

"Erosion Function Apparatus Overview and Discussion of Influence Factors on Cohesive Soil Erosion Rate in EFA Test."
Y. Cao, J. Wang J-L. Briaud, H-C. Chen, Y. Li, P. Nurtjahyo 459

"Identification of Dispersive Clays in Gaza Strip Area; and Filter Effects on Dam Safety."
M. A. Awad 471

"Effects of Cohesion on Bridge Scour."
A. Molinas, S. J. Jones 485

"Scour Around Submarine Pipeline in Clayey Soil."
S. Neelamani, A. Vijaya kumar, S. Narasimha Rao 500

"GIS-Based Bridge Scour Prioritization."
C. L. Ho, J. M. Di Stasi, P. Rees **(Invited Lecture)** 516

"Erodibility Tests of Shale-Rock Samples Taken from Bridge Pier Construction Site on the Mississippi River." T. Nakato 528

"The Driving Force on Soil Grains and Its Effect on Scouring the Channel of Foundation."
L. Zhang, D. Ding, W. Zhou 540

"Depth of Mobile Layer Under Severe Wave Conditions: Liquefaction Effect."
S. Sassa. 546

"Essence of Silt Factor for Scour Calculation Around Bridge Foundation."
R. K. Dhiman, D. K. Mohapatra 560

VOLUME II

COUNTERMEASURES

"Scour Protection Around Gravity Based Structures Using Small Size Rock."
K. J. Bos, H. J. Verheij, G. Kant, A. C. H. Kruisbrink **(Invited Lecture)** 567

"Riprap as Permanent Scour Protection Around Bridge Piers."
C. D. Anglin, F. Itamunoala, G. Millen 582

"Riprap at Rectangular Bridge Piers Under Oblique Incident Flow."
J. A. Sainz, R. Salgado 597

"Countermeasure Construction Using Jet Grouting Methods to Combat Foundation Scour."
D. W. Boehm 609

"Field Evaluation and Countermeasure Selection for Scour Critical Bridges in the Commonwealth of Kentucky."
K. J. Schaefer, R. W. Gardner 623

"Impact of the Federal Highway Administration's Scour Evaluation Program in the United States of North America's Highway Bridges."
J. E. Pagan-Ortiz **(Invited Lecture)** 636

"Evaluation of Strategies to Control Erosion along U.S. Highway 50 Between Carson City and Lake Tahoe."
K. E. Dennett, P. Fricthel, R. Siddharthan, A. Soltani 642

"Optimisation of Scour Protection Measures."
G. B. H. Spaan, M. H. Lindo, G. Kant 656

"Design and Construction of Bridge Scour Countermeasures Along the Salt River, Phoenix, Arizona." D. L. Richards 670

"Treating Channel Instability at Bridges."
P. A. Johnson **(Invited Lecture)** 678

"Scour Hazard Mitigation for Tick Canyon Wash Bridge."
M. S. Islam, J. Zha, A. Abghari 684

"Final Stages of Butte City Bridge Erosion Control Project."
S. K. Mishra, W. B. Lindsey 699

"Riprap Protection Around Bridge Piers in a Degrading Channel."
Y-M. Chiew 707

"Scour at a Submerged Rock Dike, Willapa Bay, Washington."
N. Sultan, R. Phillips, H. Bermudez 719

ABUTMENTS AND EMBANKMENTS

"Abutment Scour Countermeasures: A Review."
B. Barkdoll, R. Ettema, R. Kuhnle, B. Melville, T. Parchure, A. Parola, C. Alonso
(Invited Lecture) 734

"Countermeasures for Scour at Spill-Through Bridge Abutments."
B. Melville, S. Coleman, D. Hoe 749

"Hugo Reservoir Embankment Depression Study."
J. B. Nevels, Jr. 764

"Pier and Abutment Scour-New Laboratory Data."
W. H. Hager, J. Unger, G. Oliveto 774

"Flow and Scouring in Main Channel due to Abutments."
G. Yu, S-Y. Lim, S-K. Tan 785

PIER SCOUR

"3-D Numerical Modeling of Flow and Scour Around a Pile."
A. Roulund, B. M. Sumer, J. Fredsoe, J. Michelsen **(Invited Lecture)** 795

"New Approach to Scour Evaluation of Complex Bridge Piers."
E. V. Richardson, J. S. Jones, D. M. Sheppard 810

"Time Rate of Local Scour at a Circular Pile."
W. Miller, Jr., D. M. Sheppard 827

"A Case Study of the Possible Effects of Long-Term Climate Change on Bridge Scour."
P. Kirshen, L. Edgers, J. Edelmann, M. Percher, B. Bettencourt, E. Lewandowski 842

"Analysis of Pile Groups Considering Riverbed Scouring."
S. Jeong, J. Won, J. Suh 854

SCOUR PROBLEMS

"Study on the Disasters of Bridge and Bed Protection Works During the Passage of Typhoon Herb." C. Lin, T-C. Ho, P-H. Chiu, K-A. Chang **(Invited Lecture)** 869

"Damages of the Roads-Bridges by Erosion and Remedial Measures in Albania."
L. Bozo, Y. Muceku 884

"Bridge Pier Scour in Bouldery Bed – Indian Scenario."
R. Singh, K. K. Razdan, R. K. Dhiman 896

"Scour Monitoring of Bridge Piers via Inclination Detection."
N. Kobayashi, S. Kitsunai, M. Shimamura 910

"Non-Destructive Testing to Determine Unknown Pile Lengths Under Existing Bridges."
F. Rausche, M. Huessin, M. Bixler 918

"Determination of Unknown Bridge Foundation Depths with NDE Methods."
L. D. Olson **(Invited Lecture)** 929

"Scour of Railway Embankment Foundation Located on Sea-Cliff in Japan."
H. Suzuki, M. Shimamura 945

"Design and Construction of Scour Foundations for Electric Power Transmission Line Structures." P. M. Kandaris, R. E. Kondziolka, J. P. Adams 954

"Propeller Induced Scour."
C-O. Chin, W. Li 968

"Confederation Bridge – New Scour Design Methodology for Complex Materials."
R. B. Nairn, C. D. Anglin 978

SCOUR MONTORING

"Instruments to Measure and Monitor Bridge Scour."
E. V. Richardson **(Invited Lecture)** 993

"Development and Implementation of a Scour Monitoring Program for Selected Bridges Crossing the Trukee River."
K. E. Dennett, P. Fritchel, R. Siddharthan, A. Soltani 1008

"Seismic Methods to Identify Scour Depth Around Deep Bridge Foundations."
E. J. Mercado, E. B. Davies, J. A. McDonald, M. W. O'Neill 1019

"Portable Scour Monitoring Research."
J. D. Schall, G. R. Price 1032

"Active Scour Monitor Instrumentation in the California Transportation System."
S. Ng 1042

CASE HISTORIES

"A Methodology for Predicting Channel Migration NCHRP Project No. 24-16."
P. Lagasse, W. Spitz, L. Zevenbergen **(Invited Lecture)** 1051

"Predicting Meander Migration: Evaluation of Some Existing Techniques."
J-L. Briaud, H-C. Chen, S. Park 1061

"Collapse and Erosion of Khon Kaen Loess with Treatment Option."
P. Punrattanasi, A. Subjarassang, O. Kusakabe, T. Nishimura 1081

"Analysis of Contraction and Abutment Scour at Two Sites in Minnesota."
C. R. Wagner, D. S. Mueller 1096

"Factors Affecting Stream and Foundation Stability at Existing Bridges in New Jersey."
S. M. Baig, J. J. Zarriello, M. A. Khan 1111

VOLUME III
PREDICTION EVENT

PREDICTION REQUEST

"Prediction Request for ICSF-1"
Prediction Event Committee 1127

PREDICTION PAPERS

"Pier Scour Prediction for Mississippi River Bridge / Pier 11 for the 08-03-93 flood event / Bridge Case 7." Guillermo Ferrando, Carlos Cian 1152

"Pier Scour Prediction for Mississippi River Bridge / Pier 17L for the 05-01-91 flood event / Bridge Case 8" Guillermo Ferrando, Carlos Cian 1155

"On the Prediction of the Maximum Depth of a Scour Hole Around Cylindrical Bridge Piers in Non Cohesive Soils" Oscar Link, Ulrich Zanke 1160

"Contribution Prediction Van Oord ACZ" T. Piepers 1166

"Prediction of Local Scour of Non-Cohesive Sediments Around Bridge Piers Using FVM-Based CCHE2D Model" Weiming Wu, Sam S. Y. Wang 1176

"Numerical Simulation of Local Scouring Around a Cylindrical Pier" Yafei Jia, Yichun Xu, Sam S. Y. Wang 1181

FLUME TESTS RESULTS

"Flume Tests Results" Ya Li , Jun Wang, Wei Wang, Jean-Louis Briaud , Hamn-Ching Chen 1188

COMPARISON BETWEEN PREDICTIONS AND MEASUREMENTS

"Comparison Between Predictions and Measurements" Ya Li, Jun Wang, Wei Wang, Jean-Louis Briaud, Hamn-Ching Chen 1208

Scour Protection and Repair by Filtering Geosynthetic Containers

By

Michael H. Heibaum[1]

ABSTRACT

Scour protection may be realised either by reducing the scouring impact by river or coastal training structures or by increasing the erosion resistance of the channel bed by protective systems. When designing such a system, an armour has to be chosen with high resistance against direct hydraulic loading and with the necessary weight to guarantee a sufficient state of stress in the subsoil. Additionally a filter (granular or geosynthetic) is a must. Often it is necessary to place the filter under water which creates extra problems. So for a successful scour protection measure to be built under water and loaded by currents and waves, elements are needed that combine filter capacity and sufficient weight to resist the hydraulic load. Such elements can be geosynthetic containers. They can be used in active and passive scour protection measures and can be adapted to the individual demands regarding geometry, strength, filter properties, flexibility and many more.

INTRODUCTION

Scour protection or scour repair can be done either by reducing the stress (load) or by increasing the resistance. To reduce the hydraulic load in rivers, river training measures can be built like groynes and longitudinal dikes. At the coast, breakwaters, groynes, or other coastal protection systems are installed to improve the flow pattern. Such measures are named "active", since the load condition is altered in such a way that scour will not develop.

"Passive" countermeasures leave the hydraulic load pattern as it is. To increase the resistance, the subsoil has to be strengthened or an armour system is installed on the soil surface that is hydraulically loaded.

The choice of the appropriate measure is dependent on many factors. It may be that the alteration or reduction of hydraulic loads by active systems cannot be realised, because the coastal or river training works installed to protect a certain area will create unwanted effects elsewhere. Then the advantages at one place will be followed by disadvantages at another. So one has to check very carefully which system will perform best. The comparison of the overall costs of a training measure or a measure to increase the resistance will show in the individual case which measure should be chosen.

[1] Bundesanstalt für Wasserbau (Federal Waterways Engineering and Research Institute), Kussmaulst. 17, 76187 Karlsruhe, Germany, Tel.: +49 721 9726-3820, Fax: +49 721 9726-4830, e-mail: mhb@baw.de

SCOUR: THE RESULT OF THE INTERACTION OF SOIL AND WATER

Scour will develop when the hydraulic load acting on soil and rock exceeds their resistance against these loads. Hydraulic loads may origin either from natural hydrodynamic processes or from navigation. Once a scour hole has developed it has to be checked if an equilibrium is reached and stability is not endangered. If further scouring is to be expected or if the state of scouring reached threatens a structure, a countermeasure has to be planned.

The development of scour is always an interaction of soil and water. That seems to be a simple statement, but very often it is forgotten, that water is to be found both inside the soil and on the surface of the soil. Both pore water and surface water will contribute to the scour process. As a consequence, not only the interaction of soil and water but also the interaction of the surface water and the pore water has to be considered. Impermeable covers as scour protection will prevent the direct interaction. But there is still an indirect interaction if the water pressures of the surface water on one side and the pore water on the other side of an impermeable layer are different: The resulting excess water pressure on one side of the protection has to be taken into account in the design.

The resistance of soil and rock against scouring is given by the intergranular strength which is expressed in terms of internal angle of friction and cohesion. While cohesion is more or less independent of the intergranular stresses (but stress history has an influence on the magnitude of cohesion), the shear strength caused by friction is linearly dependent on the effective stress in the soil. Effective stress is directly dependant on pore water pressure: the higher the pore water pressure in a certain point, the less the effective stress. Therefore it is very important to consider pore water pressure in design – in cohesionless soils even more than in cohesive soils.

A SPECIAL LOAD TO CONSIDER: TIME DEPENDENT PORE WATER PRESSURE

The pore water pressure in the subsoil below a channel with steady flow is quasi hydrostatic. But flowing water may generate an unsteady pore water pressure due to turbulence, vortices, large or small eddies. Unsteady pore water pressure will also be created by regular or irregular changes of the hydraulic head, originated by a sudden increase or drop of the water level or by waves.

Measurements revealed that pore water pressure may not only be unsteady but may also show a certain time delay (Nago, Maeno1981). This means that the pore water pressure at a certain point does not change simultaneously with the hydraulic head above that point. It can be observed a damping of the pressure variation with depth z and a lag in phase (fig. 1). The effect would vanish when an ideal (= incompressible) fluid is used. The reason is that natural water always contains some air, so it is not an ideal fluid (Köhler 1993, Heibaum 2002). the effect is increasing with an increasing air content of the water and a decreasing permeability of the soil.

The phase lag will result in certain time steps in an excess pore water pressure (shaded area in fig. 1). As stated above, pore water pressure reduces the effective stress in the soil and therefore the resistance of the soil against all kinds of loading. If a high excess pore water pressure is created, the effective stress may be so low that failure in the soil occurs. Soils with a low permeability but without cohesion (e.g. fine or silty sand) will be endangered most. On a bank this will cause sliding of a soil layer and on the bottom, the soil may get into the state of suspension down to a certain depth. In both cases, erosion will start at already low hydraulic loads and will develop to a larger

extent than without excess pore water pressure. To balance the excess pore water pressure, the effective stress in the soil has to be increased which can be done by an appropriate surcharge.

GEOSYNTHETIC CONTAINERS

Geosynthetics is a term for all textile structure that are used in geotechnical engineering. That term also incorporates natural fibres like jute, coir, ramie etc that are used like synthetic fibres to manufacture one of the "geo-elements". Nearly any shape can be created: separation or reinforcing layers, filters, drains, linings, bags, tubes, mattresses, meshes. The number of applications is still growing. The majority of geosynthetic fabric for geotechnical use is either woven or nonwoven. Knitted fabric, nets, cells or else are applied for special purposes only. Geosynthetics have the advantage of being easily transported due to their low weight. Manufacturing of geosynthetic products can be done very precisely resulting in special fabric for special applications.

Sandbags are known since long, for example as immediate repair of dikes, protection during floods etc. These elements have been developed further resulting in a wide field of application in geotechnical and hydraulic engineering. So the more general term of "geosynthetic containers" or "geosystems" (Pilarczyk 2000) has been established. Today this term encompasses all elements that use a geosynthetic fabric as an envelope or a casing (fig. 2). The elements may be filled with air, water, sand, mortar or waste. Often additional functions are provided: For example the fabric may be designed as a filter or it may be used as reinforcement.

The list of possible applications of containers in scour protection is very long. Small elements filled with concrete are used to replace missing elements in pitched revetments or quay walls. Concrete mattresses are used to create an impervious lining, stone mattresses provide a permeable lining. Pillow mats, i.e. mattresses of concrete filled pillows with permeable junctions, are the combination of the before named. Due to their flexibility they allow for perfect scour protection in rivers and at the coast. Mesh-like concrete mattresses are found in erosion protection. Bags are the most common type of containers and the most versatile concerning possible applications. Today bags of all sizes and of many shapes can be manufactured up to one single large container in a hopper barge or with a very large length to create tubes.

STRUCTURES FOR ACTIVE SCOUR PREVENTION USING GEOTEXTILE CONTAINERS

Training structures are build to avoid scouring by altering the flow pattern of a river or the longshore current. In this context, geosynthetic containers can be used to build artificial reefs, longitudinal dikes, groynes or else to form an active scour protection. In these cases the advantage of using geosynthetic containers is the fact that often cheap local fill material can be used that would be eroded immediately without confinement, e. g. silty or fine sands. Or the current is so high that even material of larger grain sizes like riprap cannot be used to build the structure.

A common construction method is to use containers (bags or tubes) as a core of groynes and dikes with a cover layer of armour stones to protect the core against high mechanical and hydraulic impact. If there are only low mechanical loads and no or only short exposition to UV radiation, because the container is permanently under water or because it is a temporary structure, an armour layer may not be necessary.

There may be double advantage from using geosynthetic containers when a fabric is chosen that is not only a casing but also a filter or a reinforcement. Details concerning armour and filter are given below when discussing protection systems

SCOUR PROTECTION SYSTEMS

As it has been said above, the subsoil can be strengthened or an armour system can be put on the soil surface to increase the resistance. The most common protection method will be to place an armour layer on top of the soil. By doing this, the stress in the subsoil is increased and the surface is protected against direct hydraulic impact. Basically there is also the option to increase the strength of the soil without increasing the state of stress, e. g. by grouting the soil or by using any kind of soil reinforcement (e. g. soil nails, geosynthetic reinforcement etc.). Such types of scour protection will not be discussed here.

To achieve stability, any protection system needs two essential parts: the armour and the filter. An armour layer provides the protection against the direct hydraulic and - if acting - mechanical loading. At the same time, an armour layer should be heavy enough to increases the effective stresses in the subsoil. This is of importance when an excess pore water pressure - which also could be named an indirect hydraulic loading - destabilises the subsoil as discussed above. In the armour layer no excess pore water pressure must develop. This will be guaranteed by all layers with high hydraulic conductivity.

Armour material, e.g. riprap, may resist the hydraulic load, but it will not provide the filter stability necessary to prevent erosion of the subsoil through the armour. And armour elements without a filter may sink into the subsoil when the soil is fluidised. Only a filter keeps the grains of the subsoil in place while the armour contributes the necessary strength. A filter can be either a granular or a geosynthetic filter.

ARMOUR LAYER

The armour layer may consist of single elements, mattresses or continuous linings. As to single elements, riprap is the most often used material. If such material is sufficiently available, good solutions at reasonable costs can be attained.

Concrete elements are used when natural material is not available to the necessary extent. The production costs are much higher but the transportation distance is usually rather short; sometimes they may even be produced on-site. There is a large variety of concrete elements that are used as an armour layer: Elements of many different shapes used like natural stones, blocks placed regularly ("paved") and mutually connected elements.

A paved cover layer shows an increased resistance against hydraulic loads while being limited in thickness. But the high resistance is lost if only one element is missing. So connected or confined elements may perform better. Examples are interlocking concrete blocks (articulated concrete blocks, ACB), cable connected concrete blocks, stone mattresses. In any case the armour layer has to be thick enough to provide a sufficient state of stress in the subsoil to avoid fluidisation.

FILTER LAYER

While grain filters are known since long time, geotextile filters are used since approximately 30 years. Sometimes a filter is considered not to be necessary. This may be true, when the hydraulic load at the interface of soil and armour is (permanently!) so low that the fine grains will definitely not be moved, e.g. because the armour layer is so thick, that the energy of the hydraulic load acting on the armour surface is dissipated in the armour layer. In all other cases a filter is inevitable.

GEOSYNTHETIC FILTERS

Filters in scour protection measures are loaded by unsteady, turbulent, pulsating and reversing flow. Most of the design rules for geosynthetic filters are developed for unidirectional flow. Only few are reliable in case of dynamic hydraulic loading. The development of excess pore water pressure in the subsoil due to the fast change in the hydraulic head complicates the proper filter design (Köhler 1993). So often performance tests may be necessary, e.g. turbulence tests (MAG 1993), were it has to be proven that the amount of soil washed through the geotextile is limited and is decreasing with time when loaded by a turbulent reversing flow. Filter rules basing on the opening size (e.g. Holtz, Christopher & Berg 1995) may be used as a first estimate and may be sufficient when the hydraulic load at the interface of soil and geotextile is only low, e.g. due to energy dissipation by the armour layer.

To achieve higher tensile strength when using nonwovens. a smaller opening size may be preferred. But care has to be taken that the clogging potential is not increased.

GRANULAR FILTER

Many rules for the design of grain filters are available. Schuler & Brauns (1993) have given a detailed overview on most of the filter criteria. Well known criteria for soil retention ask for certain ratios $d_{15,F}/d_{85,B}$ (grain size at 15% by weight of the filter and at 85% of the base soil, respectively). Some also incorporate the interval $d_{50,F}/d_{50,B}$ or $d_{15,F}/d_{15,B}$. Limit values however are rather different: Terzaghi asks for $d_{15,F}/d_{85,B} \leq 4$, while Bertram allows for 6 to 11 (simultaneously asking for $d_{15,F}/d_{15,B} \leq 8$ to 15). The range of permissible d_{50}-interval is given from 4 to 58, depending on different parameters. Most of the grain filter rules are restricted to well graded material. One of the most general approaches is the design chart of Cistin / Ziems (fig. 3; Busch & Luckner 1974), because it takes into account the coefficient of uniformity (C_U; in fig.3 U is used like in the original literature) of the soil and the filter, so poorly graded material is included. Limits of application are exceeded only for $C_U > 20$. According to that rule the mean diameter $d_{50,II}$ (grain size diameter of 50% finer by weight) of the coarser material (filter) must not exceed the mean diameter $d_{50,I}$ of the finer material multiplied by a factor A_{50}. The factor A_{50} is found on the vertical axis depending on the coefficient of uniformity of the finer material on the horizontal axis (U_I in fig.3) and the coefficient of uniformity of the coarser material as curve parameter (U_{II} in fig.3).

Looking at the grain size distributions of filter and base, then generally speaking a broadly graded filter is favourable, while the gradation of the base is of less influence. This can be clearly seen from the Cistin/Ziems-Diagram. But with broadly graded filters, placement problems increase which is discussed later.

It is important that limits are adhered to strictly for the interface filter to armour, since the hydraulic load is the more severe the nearer to the surface the interface of two layers is situated.

PLACEMENT PROBLEMS

It was stated above that any effective scour protection measure needs a well designed filter. To build a good filter, care has to be taken when placing it. Often it is necessary to place the filter under water which creates problems for both granular filter and geotextile filter.

Placing a geosynthetic filter cloth will be impossible in many cases because of the depth of the water, the flow or the wave action. The stability of the geotextile filter can be increased by certain measures but only up to a certain hydraulic load. While in former times iron chains or spreaders have been used, today a geocomposite is used, namely a "sandmat", i.e. a sand fill up to 9 kg/m² confined between two geosynthetic layers. The two layers are sewn or needlepunched to keep the sand in place. Stability can be achieved up to a flow velocity of ca. 1 m/s.

Placing granular filter is similarly difficult: at least the first filter layer often consists of small sized grains, so the material may be eroded nearly as easily as the subsoil. When using a broadly graded filter placement in the wet is even more difficult (even with no adverse effects due to flow), since dumping such material through water will cause segregation. Fine grains will sink more slowly than coarse grains, so an "inverse" filter is created with the fines on top, actually no filter.

To overcome placement problems, many attempts have been made. Combined elements have been developed to allow for a save placement.

The oldest forms of such a system is the fascine mattress. i.e. willow bundles with a diameter of 10 to 40 cm tied together crosswise (fig. 4). In the beginning only fascines and brushwood were combined to a mattress, the brushwood acting as a filter. Later a woven geotextile was used as the base (and filter) and the fascine bundles were tied on it. If necessary a brushwood layer was added to protect the geotextile from mechanical impact. Fascine mattresses are prefabricated according to the desired geometry on land, then they are pulled to the desired position and sunk by dumping the armour material upon. Today, a woven and a nonwoven fabric are combined to increase the filtration capacity. If they have to be placed around structures like groynes or piers, either some smaller fascines could be placed, overlapping each other, or one large fascine is manufactured with a gap. Fascine mattresses can be prepared in all sizes, but usually they are effective only when larger areas are to be covered. They can not be used if the subgrade is very uneven or significantly inclined. So in many cases they cannot be used for scour repair after a scour hole has already developed.

A combined armour and filter system is provided by certain mattresses, e.g. concrete blocks cast on a woven geotextile or concrete cushion mattresses. Block mattresses usually are assembled in the dry and placed by special cranes. Geosynthetic cushion mattresses are filled in place with concrete. One has to consider that the filtration capacity of these mattresses is limited, since the filtration area is restricted to the webs which might not be wide enough to guarantee an unhindered flow through the system to avoid the development of excess water pressure below the protection layer. There are also limits for the mass per unit area.

As a consequence of the placement problems when building scour countermeasures, it becomes clear that elements are needed that combine filter capacity and sufficient weight. The weight is necessary to guarantee a placement at the desired spot in spite of the hydraulic load. Safe placement has to be possible at greater depth and under current and wave loading. The protection sys-

tem also should be able to adapt at any subsoil geometry (including existing scour holes) and it should be flexible to follow further scouring, e. g. at the edges of the scour protection. All these requirements are met by geosynthetic containers (and a suitable placement procedure). The container fabric can be designed as a filter, but also granular filter can be installed safely using geosynthetic containers. Due to being confined in the container, even a widely graded granular filter may be used. If the container fabric is needed only as a casing, material can be used that will degrade after the placement, e. g. natural fibres.

DESIGN OF GEOSYNTHETIC CONTAINERS FOR SCOUR COUNTERMEASURES

Usually the geotextile container is intended to act as a filter itself. In few cases it is designed only as a casing for granular filter material. A double line of defence will be provided when filling granular filter material into a container which is designed as a geotextile filter. Filter rules for geosynthetics and granular material have been discussed above.

The size of geosynthetic containers has to be chosen according to the hydraulic demands and to operational restrictions. From the hydraulic point of view they should be as large as possible, since the larger the lesser they are displaced. This is impressively shown by the large containers (400 tons sand fill) that are used to build artificial reefs off the Australian coast (Hornsey 2002). But such elements can only be placed by special equipment, e.g. split barges. Standard equipment is sufficient for containers up to 1 m^3 . This size has been used several times, being placed in the wet as well as in the dry.

For a safe placement, for high serviceability and for sufficient long term resistance, the container material has to be chosen such that it will resist all mechanical loads. Usually there is a choice of wovens and nonwovens. The first have the advantage of high tensile strength, the second the advantage of large straining capacity. If a casing material is damaged, a woven cloth might be more susceptible to crack propagation (the zip effect) than a nonwoven. Nonwoven fabric usually has a high straining capacity, so the tensile strength may be less to provide a similar resistance against mechanical impact. By allowing large deformations it will be able to withstand the impact load when hitting the ground as well as when the stones are dumped upon. A minimum mass per unit area of 500 g/m^2 and a minimum tensile strength of 25 kN/m are recommended, the strain at rupture should be larger than 50%.

Since the container has to sustain abrasive forces due to rocking armour stones or due to bedload transport, any geosynthetic material used for containers either needs a high resistance against abrasion. The elements of any cover layer will rock and/or move in the immediate period after installation due to dynamic hydraulic loads and due to deformation of the subsoil caused by the new load. this effect can be reduced by partial grouting when riprap is used as armour.

Special care has to be taken concerning the seams of the container. On three sides, the seam is prefabricated at the manufacturer's. Usually a strength approximately as high as the geotextile itself is guaranteed. The container usually is closed by sewing double chain stitch seams at the top. One seam is straight and the second one is curved to allow for straining of the geotextile if the first seam is broken. A new development is closing the container by velcro. In 2001 first promising tests were made.

Often containers are used in scour protection measures in such a way that they are exposed to sunlight at least some time (fig. 5). So the fabric has to show a sufficient resistance against weathering in general and against UV radiation in particular.

FILLING THE CONTAINERS

Very large container are filled in a split barge, so the filling process is not a critical load during installation. Tubes are filled in situ, therefore the filling process usually will create less stress than the service state. Smaller containers (≈ 1 m^3) are filled before being placed. To avoid high stress or strain when filling, the container should not hang under a funnel but should touch the ground when being filled, since it should not be stretched by the filling process (fig. 6).

The fill has to be chosen according to the requirement for the individual application. Rounded grains are favourable, since the puncture and abrasion impact is much less.

The amount of fill of the container should not exceed 80% of the theoretical volume, since tightly filled geocontainers are too stiff to adjust themselves to the subsoil, to structures or to the neighbouring containers.

INSTALLATION OF GEOSYNTHETIC CONTAINERS

For large containers dumped from a split barge, the installation process may be the highest load for the element during its lifetime. Design calculations are given by Pilarczyk (2000).

Tubes are installed without fill, so when placed under water, similar difficulties have to be overcome as during the placement of geosynthetic filters.

Single geocontainers usually are placed by an excavator. Numerous geocontainers also may be dumped by side dumping vessels or split barges. Care has to be taken that the area to be protected is covered completely. Special equipment allows for very precise placement of geocontainers, for example the lattice girder device shown on fig. 7 that enables the precise installation to a depth up to 25 m.

SUMMARY

Scour protection can be done in two manners: stress (load) has to be reduced or resistance has to be increased. To reduce the load, river training measures are built or coastal systems are installed to improve the flow pattern. To increase the strength, armour systems are put on the soil surface that is hydraulically loaded. In both cases, geosynthetic containers can be used.

Geosynthetic containers developed from the traditional sand bags, but today they can be manufactured in may forms like bags, mattresses or tubes. So scour protection measures can be built according to the individual requirements of the actual situation.

Geosynthetic containers can be used to build artificial reefs, longitudinal dikes, groynes or else to form an active scour protection by changing the flow respectively the current. Or they can be part of a protection system to avoid erosion of the river or sea bed.

To achieve stability, two essential parts are necessary for a successful scour protection: a filter and an armour layer. The filter can be either a granular or a geosynthetic filter. Often it is necessary to place the filter under water which creates problems for both types. Geosynthetic containers can combine filter and sufficient weight to resist the hydraulic load. If there is no large mechanical load and no UV radiation, geosynthetic containers can be installed without armour or they can act as an armour themselves. They also can be used to place a broadly graded granular filter. the combination of a geosynthetic container designed as a filter and a fill of granular filter material will increase the filter reliability of the protection system.

REFERENCES

1. Brauns, J.; Schuler, U.: Behaviour of coarse and well-graded filters. In: Brauns, Heibaum, Schuler (Hrsg.): Filters in geotechnical and hydraulic Engineering S.3-18. Rotterdam: Balkema, 1993.
2. Busch, K.-F.; Luckner, L.: Geohydraulik. Stuttgart: Enke 1974
3. Heibaum, M.: Geotechnical Parameters of Scouring And Scour Countermeasures. In: Mitteilungsblatt der Bundesanstalt für Wasserbau Karlsruhe: BAW 2002 to be published
4. Holtz, R.D., Christopher, B.R., Berg, R.R.: Geosynthetic Engineering. Bitech Publishers, Richmond, Canada, 1997.
5. Hornsey, W..: Case studies showing the growth and development of geotextile sand containers – an Australian perspective. In: Geotextiles & Geomembranes, to be published
6. Köhler, H.-J.: The influence of hydraulic head and hydraulic gradient on the filtration process. In: Brauns, Heibaum, Schuler (Ed.): Filters in Geotechnical and Hydraulic Engineering, pp 225-240. Rotterdam: Balkema 1993.
7. Nago, H..; Maeno, S.: Liquefaction of highly saturated sand layer under oscillating water pressure. In: Memoirs of the School of Engineering, Okayama Univ., Vol.16, No.1, pp. 91-104, 1981.
8. Pilarczyk, K.: Geosynthetics and Geosystems in Hydraulic and Coastal Engineering. Rotterdam, The Netherlands: A. A. Balkema Publishers 2000

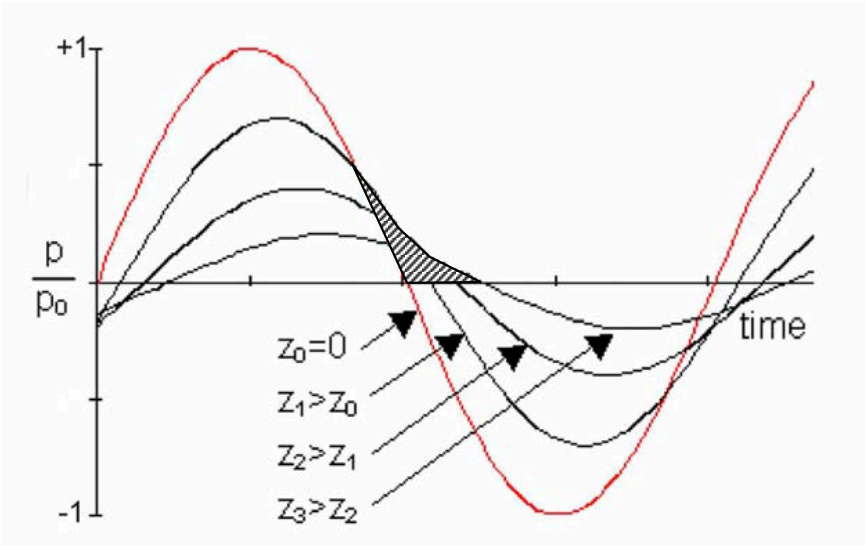

Fig. 1 – Water pressure development depending on time and depth

= excess pore water pressure

Fig. 2 – Geosynthetic containers: bag, mesh, mattress, mesh with plant openings (photo: Hydrotex)

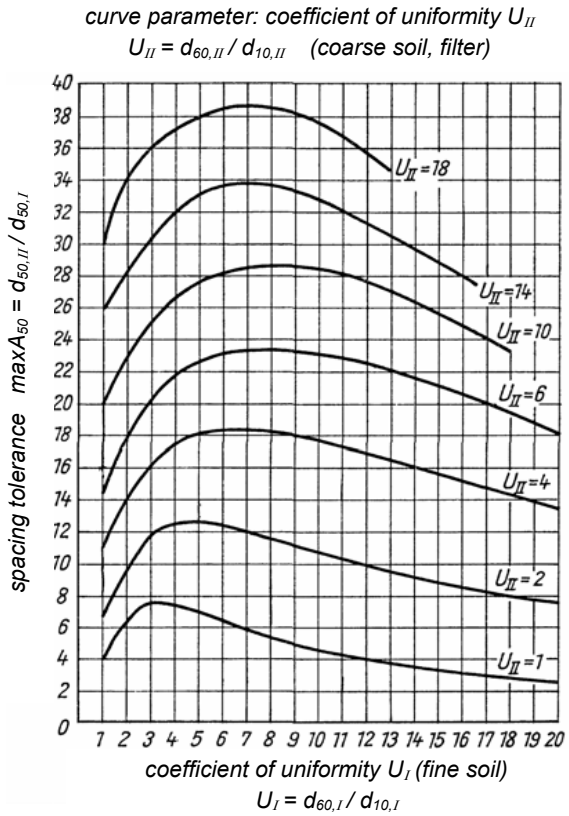

Fig. 3 – Filter design chart according to Cistin / Ziems

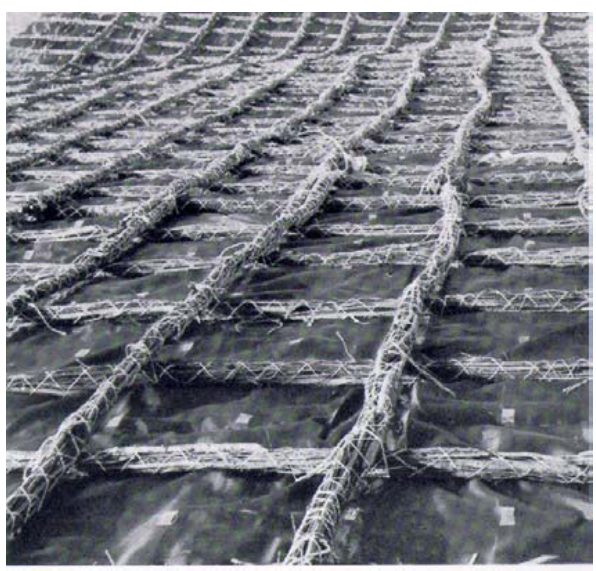

Fig. 4 – Fascine mattress

Fig. 5 – Geosynthetic containers for coastal protection (photo: WWF)

Fig. 6 – Filling geosynthetic container (1 m³)

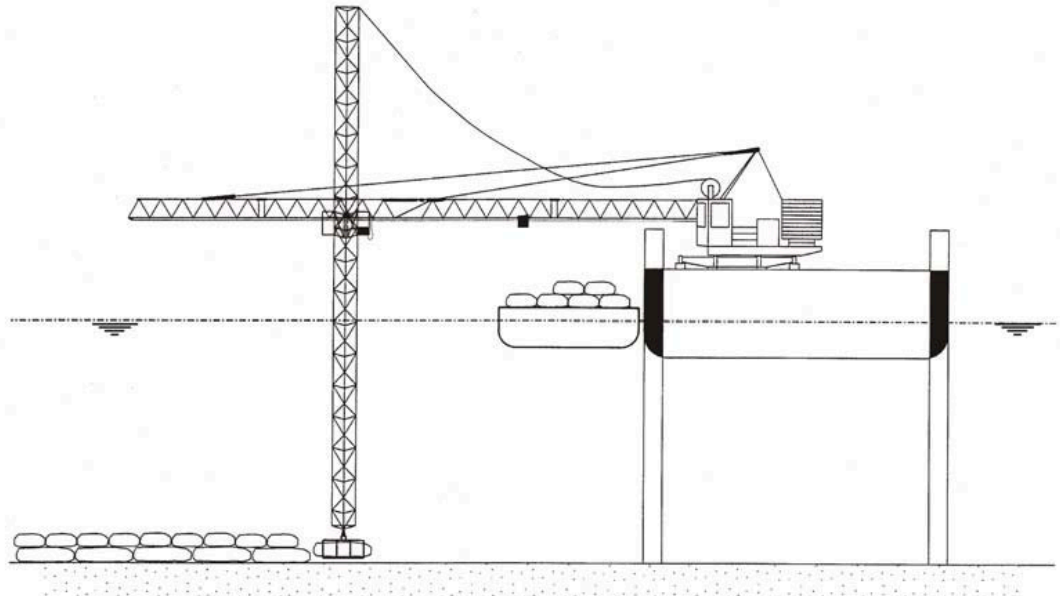

Fig. 7 – Lattice girder device for placing geosynthetic containers (courtesy Colcrete-von Essen)

Numerical Simulation of Scour Around Complex Piers in Cohesive Soil

Hamn-Ching Chen[1]

ABSTRACT

A chimera Reynolds-Averaged Navier-Stokes (RANS) method has been employed in conjunction with a scour rate equation for time-domain simulation of scour around complex piers in cohesive soils. The method solves unsteady RANS equations in a general curvilinear coordinate system using a chimera domain decomposition approach. The scour depth at each point of the streambed is determined in terms of the local shear stress using a simple scour rate equation. Calculations were performed for a model scale complex rectangular piers and a prototype circular complex pier configuration to illustrate the general capabilities of the method for prediction of combined contraction and local pier scours.

INTRODUCTION

Scour is the erosive action of water which excavates soils from streambeds and banks. The types of scour occur at a bridge site may include general scour, contraction scour, and local scour. General scour is associated with natural processes of river flow irrespective of the presence of the bridge, whereas contraction scour and local scour are directly attributed to the presence of the bridge. Contraction scour results from river channel blockage at the bridge site and is characterized by a general lowering in the local bed elevation. Local scour is caused by the three-dimensional turbulent flow around the abutment and bridge piers, and is characterized by the formation of scour holes around the bridge foundation. The present paper is concerned with the simulation of the scour processes around complex piers including the abutment and multiple piers.

In a channel with erosive bed materials, the scour hole is formed in the vicinity of the abutment and bridge piers due to the large shear forces there. As the scour hole enlarges, the velocity near the bottom of the hole decreases gradually. When the velocity near the bottom of the scour hole decreases to a certain value, the streambed shear stresses become less than the critical shear stress necessary to initiate scour and the scour rate drops to zero. For clear-water scour, an equilibrium condition of the final scour hole will be attained if the shear stresses are below the critical shear stress everywhere in the hole.

Many parameters influence the contraction and local scours in complex pier configurations. They include fluid viscosity and density, upstream velocity, streambed

[1] Professor, Department of Civil Engineering, Texas A&M University, College Station, Texas 77843-3136, USA (hcchen@civilmail.tamu.edu)

slope and flow depth, abutment length, pier shape, pier size, flow angle of attack, and properties of the streambed soil such as plasticity, density, grain size, grain form, shear strength, cohesion, and chemical properties. In scour research, streambed soils are usually classified into cohesive soils and non-cohesive soils, although most streambed soils contain both cohesive and non-cohesive particles. Scour of cohesive soils is fundamentally different from that of non-cohesive soils. It involves more complicated physical and chemical mechanism. Once eroded, cohesive materials remain in suspension such that the clear-water scour process always prevails. Moreover, the slope of the scour hole can be very steep due to soil cohesion. In some cases, slope of 90° may be approached.

In recent years, computational fluid dynamics (CFD) has been widely used to determine fluid flow behavior in industrial and environmental applications. However, due to the complexities of both the flow field and the scour mechanism, numerical modeling of the scour process around bridge piers remains a difficult research topic. The flow field has a three-dimensional separated boundary layer flow which is accompanied by complex horseshoe vortex and wake vortex systems. During the scour process, both the horseshoe vortices and wake flows change continuously due to the continuous erosion of the streambed materials. Computation of such a transient, three-dimensional flow field requires the use of more sophisticated numerical techniques and much more computer CPU time than that of a steady flow with fixed boundaries. Particularly, erosion computation must be incorporated with the flow calculations, and grid redistribution must be performed throughout the computation to conform to the instantaneous streambed. In addition, since the flow field varies greatly close to the wall and the scour depth gradient is large around the pier, the grids ought to be sufficiently fine near the streambed and the bridge piers for accurate prediction of turbulent boundary layers and streambed shear stresses. Numerical computations of bridge pier scour were performed recently by Olsen and Melaaen (1993), Olsen (1996), Du (1997), Chen et al. (1999) and Roulund (2000), but no literature can be found for the simulation of scour around complex piers.

Recently, Chen (1995a,b) developed a multiblock RANS method for detailed resolution of the horseshoe vortex system around wing-body junctions and practical submarine configurations. The method was further extended to incorporate a chimera domain decomposition technique for time-domain simulation of ship berthing operations (Chen and Chen, 1998; Chen et al., 2000), ship roll motions (Chen et al., 2002b), and multiple ship interactions in shallow navigation channel (Chen et al., 2002a). In this study, the chimera method has been employed in conjunction with a scour rate equation for time-domain simulation of scour around complex piers in cohesive soils. Calculations were performed for two complex pier configurations with rectangular and circular piers to illustrate the capability of the chimera RANS method.

CHIMERA RANS METHOD

In the present study, the chimera RANS method of Chen (1995a,b), and Chen et al. (1998, 2002a,b) has been extended to incorporate the scour rate equation for time-domain simulation of the scour process in cohesive soils around complex bridge piers. The

computational domain was divided into a number of smaller grid blocks, which allow complex configurations and flow conditions to be modeled efficiently through the judicious selection of different block topology and boundary conditions. The chimera domain decomposition technique was utilized to connect the overlapped or embedded grids by interpolating information across the block boundaries. The Reynolds stresses were evaluated using the two-layer turbulence model of Chen and Patel (1988). The mean flow and turbulence quantities were calculated using the finite-analytical method of Chen, Patel, and Ju (1990). The PISO/SIMPLER pressure-velocity coupling approach of Chen and Korpus (1993) and Chen and Chen (1998) was used to solve the pressure field. The scour hole shape was determined through a scour rate equation which expresses the erosion rate as a function of the streambed shear stress. More detailed descriptions of the chimera RANS method were given in Chen and Chen (1998) and Chen et al. (2002a,b).

The present method solves the dimensionless Reynolds-Averaged Navier-Stokes (RANS) equations for incompressible flow in general curvilinear coordinates (ξ^i, t):

$$U^i_{,i} = 0 \tag{1}$$

$$\frac{\partial U^i}{\partial t} + U^j U^i_{,j} + (\overline{u^i u^j})_{,j} = -g^{ij} p_{,j} + \frac{1}{Re} U^i_{,jk} = 0 \tag{2}$$

where U^i and u^i represent the mean and fluctuating velocity components, and g^{ij} is the conjugate metric tensor. t is time p is pressure, and Re = $U_o L/\nu$ is the Reynolds number based on a characteristic length L, a reference velocity U_o, and the kinematic viscosity ν. Equations (1) and (2) represent the continuity and mean momentum equations, respectively. The equations are written in tensor form with the subscripts, $,j$ and $,jk$, represent the covariant derivatives. In the present study, the two-layer k-ε model of Chen and Patel (1988) is employed to provide closure for the Reynolds stress tensor $\overline{u^i u^j}$.

The free surface boundary conditions for viscous flow consist of one kinematic condition and three dynamic conditions. The kinematic condition ensures that the free surface fluid particles always stay on the free surface:

$$\eta_t + U\eta_x + V\eta_y - W = 0 \qquad on \quad z = \eta \tag{3}$$

where η is the wave elevation and (U,V,W) are the mean velocity components on the free surface. The dynamic conditions represent the continuity of stresses on the free surface. When the surface tension and free surface turbulence are neglected, the dynamic boundary conditions reduce to zero velocity gradient and constant total pressure on the free surface. A more detailed description of the chimera RANS/free-surface method was given in Chen and Chen (1998) and Chen et al. (2000, 20002a,b).

In order to simulate the scour hole development, a scour rate equation was incorporated into the unsteady RANS method to compute the scour pattern around complex piers. For a given cohesive soil, it is known that the scour rate, defined as the change of scour depth per unit time, depends mainly on the shear stress at the streambed surface. The initiation

of the scour process is determined by the critical shear stress which represents the smallest streambed shear stress to start erosion. Based on this concept, the scour rate can be expressed as a function of the streambed shear stress and the critical shear stress. The scour rate equation can be written in the following dimensional form

$$\dot{Z} = \dot{Z}(\tau_b, \tau_c); \quad \tau_b = \mu \frac{\partial q}{\partial n} \tag{4}$$

where $\dot{Z}$ is the scour rate, τ_b is the streambed shear stress, τ_c is the critical shear stress, $q = \sqrt{U^2 + V^2 + W^2}$ is the magnitude of flow velocity, μ is the dynamic viscosity of water, and n is the normal distance from the streambed. After the flow field is obtained, the soil erosion rate at each grid point on the streambed is determined by the scour rate equation. The increase of scour depth is then evaluated by multiplying the scour rate by the time increment. In the present study, the scour rate is assumed to be linearly proportional to the streambed shear stress as follows:

$$\dot{Z} = \begin{cases} c(\tau_b - \tau_c), & \tau_b > \tau_c \\ 0, & \tau_b \le \tau_c \end{cases} \tag{5}$$

The above equation has been incorporated into the chimera RANS code to facilitate the simulation of scour hole developments. During each time step, the incremental scour depths at each streambed point were computed using the scour rate equation. After the new scour depth distribution was obtained, the coordinate of each bed point was updated and the streambed was moved to the new elevation. The numerical grids were then adjusted vertically to conform to the updated bathymetry of the scoured streambed.

RESULTS AND DISCUSSION

Numerical simulations have been performed first for a complex pier configuration with abutments and four rectangular piers as shown in Figure 1. The present configuration is identical to that tested by Li (2002) at Texas A&M University except that the water depth was reduced from 20 cm to 12 cm. The channel width upstream and downstream of the bridge is B_1 = 1.5 m. Each abutment is 0.48 m long and 0.06 m wide. Four rectangular piers of 0.02 m × 0.06 m were placed between the abutments with uniform pier spacing of 0.108 m. The blockage by the abutments and the bridge piers reduces the effective channel width to B_2 = 0.46 m with a large channel contraction ratio of B_1/B_2 = 3.26. A uniform upstream velocity of 0.2 m/s was used in the present simulation. To reduce the CPU time and memory requirement, the computations were performed for one-half of the solution domain and the flow was assumed to be symmetric along the channel centerline. The solution domain was divided into 8 computational blocks with a total of 508,710 grid points. An overlap region was added to all interior block boundaries to ensure the complete continuity of the solutions between adjacent grid blocks. The numerical grids were adjusted to follow both the exact free surface and instantaneous streambed elevations at every time step.

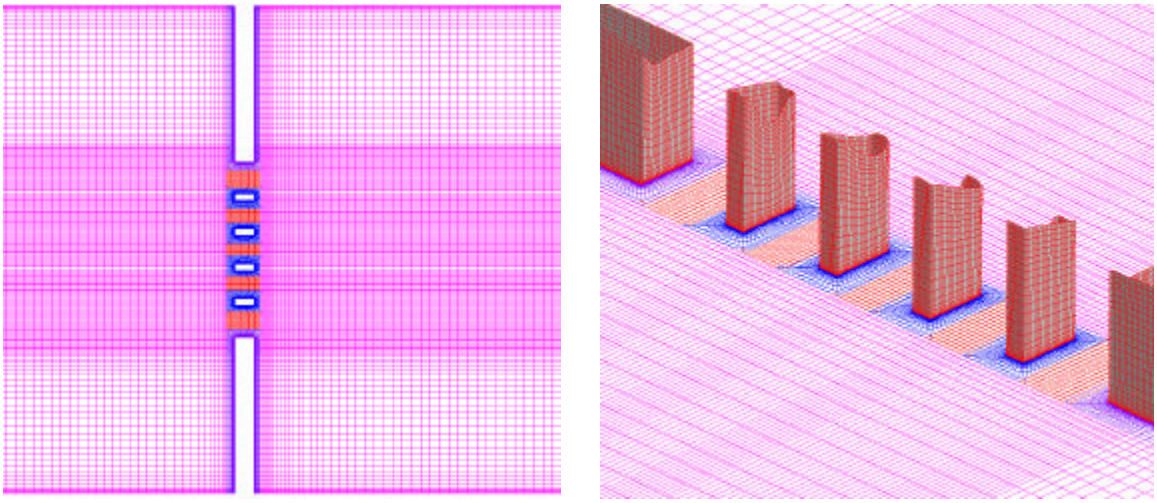

Figure 1. Bridge configuration and numerical grid for complex rectangular piers

Computations were performed first for flat bed configuration without erosion (i.e., $\boldsymbol{c} = 0$ in equation (5)) until the steady state is attained. Figure 2 shows the water elevation profiles under steady flow conditions. It is seen that there is a significant drop in free surface elevation between the piers. The highest water elevation upstream of the pier is about 1.15 cm above the mean water level, and the lowest water elevation was seen along the inner side of the two outer piers with an elevation of –3.3 cm from the mean water surface. The change in water elevation is quite significant comparing to the total water depth. However, the free surface effect was observed to diminish gradually in the flume test as the scour hole develops and the channel deepened.

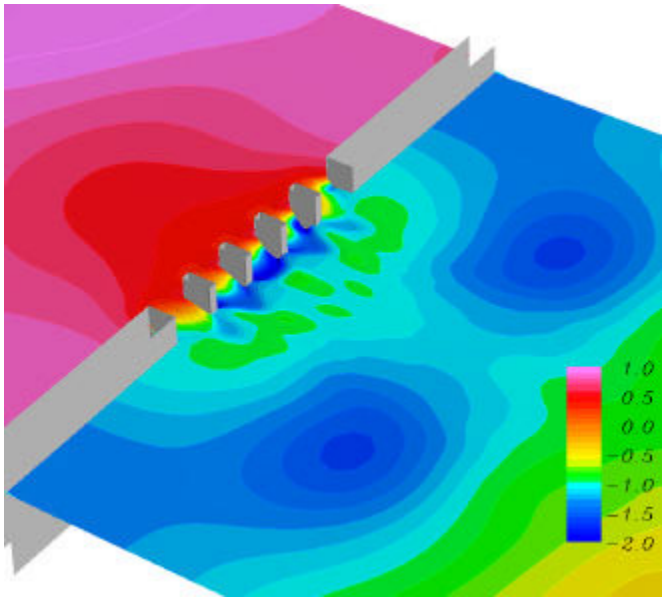

Figure 2. Free surface elevation contours around the bridge

In addition to the rather significant change in free surface elevations, the abutments and bridge piers also produce strong flow accelerations as seen in Figure 3 as a result of the narrowing of channel cross section at the bridge location. The strongest acceleration was observed between the bridge piers with a maximum velocity of nearly 0.852 m/s or 4.26 times of the upstream flow velocity. It is also noted that the stream flow separated behind the abutments and formed a pair of large recirculation regions. In addition, smaller regions of flow reversal were also observed in the wake of each pier.

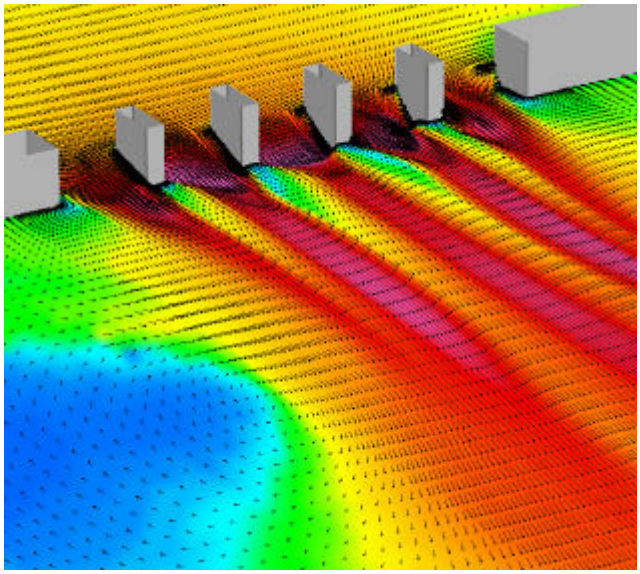

Figure 3. Free surface velocity field in the vicinity of piers

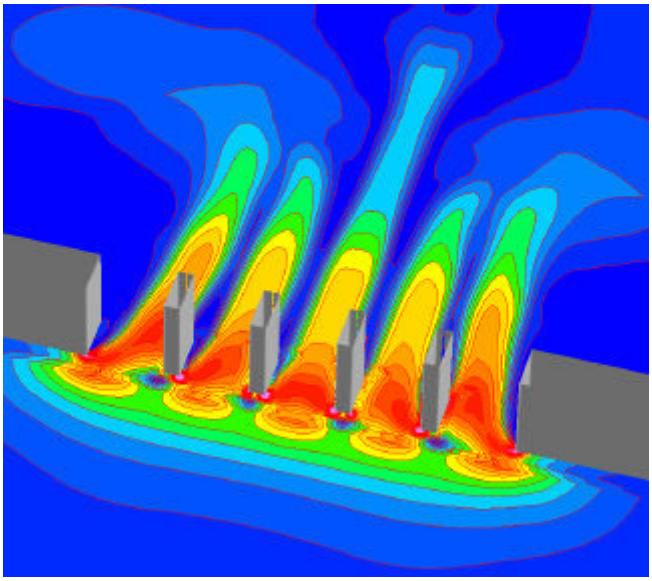

Figure 4. Shear stress distribution before scour initiation

As noted earlier, the shear stresses were computed directly from the velocity gradients on the streambed surface using eq. (4). Figure 4 shows the initial shear stress distribution

before the scour take place. It is quite clear that the shear stresses are high in the middle of each passage since the flow was forced to accelerate between the piers, and between the abutments and piers. A detailed examination of the streambed shear stresses indicated that the maximum shear stress occurs at the front corner of each abutment and around the inner front corner of each rectangular pier. It is also interesting to note that the mainstream flow approached the outer two piers with a large angle of attack. The flow angle of attack is considerably smaller for the inner two piers since the flow in the middle section of the channel is nearly parallel to the channel bank. As noted earlier, erosion occurs in the regions where the bed shear stress is greater than the critical shear stress. Therefore, the size and shape of the scour hole is expected to be dependent upon the critical shear stress as well as the streambed shear stresses.

After successful simulation of the complex pier flow for a flat streambed, the present method was coupled with the scour rate equation to predict the contraction and local scour due to complex piers. For simplicity, the free surface effects were ignored in the present simulation of complex pier scour. This is a reasonable approximation since the water depth is rather deep comparing to the pier size and the free surface does not significantly influence the scour depth. As noted earlier, the critical shear stress determines both the initiation and the end of the scour process. For accurate simulation of the scour hole development, it is necessary to determine the scour rate vs. shear stress curve from the measurement. Since neither the critical shear stress nor the scour rate was available, we will use a simple scour rate equation to illustrate the capability of the present method. In the present simulation, the dimensionless critical shear stress was chosen to be $\tau_c/\rho U_0^2 = 0.015$ which corresponds to a τ_c value of 0.6 N/m^2. The slope of the scour rate vs. shear stress curve was assumed to be c = 0.006 m^3/(N·hr). Simulations were performed for 6000 time steps using a constant time increment of Δt = 150 sec. It should be noted that the maximum initial shear stress is 4.3 N/m^2, or about 7 times of the critical shear stress, at the beginning of the scour processes.

In order to facilitate a detailed examination of the scour hole development and the associated shear stress variations, the numerical solution for the entire streambed was saved in a movie file at a 25 min interval (i.e., every 10 time steps). Figure 6 shows the predicted scour pattern and the corresponding shear stress distributions (normalized by ρU_0^2 = 40 N/m^2) at 12 selected time instants. It is clearly seen that the scour was initiated in the high shear stress regions between the piers and gradually propagates towards the downstream and upstream of the bridge. For the first several hours, the scour hole in each passage develops almost independently while very little erosions were observed behind the abutments and piers. It is noted that there are five separate valleys downstream of the bridges until t = 1,000 min. During the initial stage of scour hole development, the shear stress dropped very quickly as the valleys deepened gradually. The high shear stress region was shifted gradually to the middle passage while the streambed shear stress becomes quite low in the two outermost passages. This clearly indicated that more water was flowing through the middle section of the channel while the flow rate in the outer passages was significantly reduced.

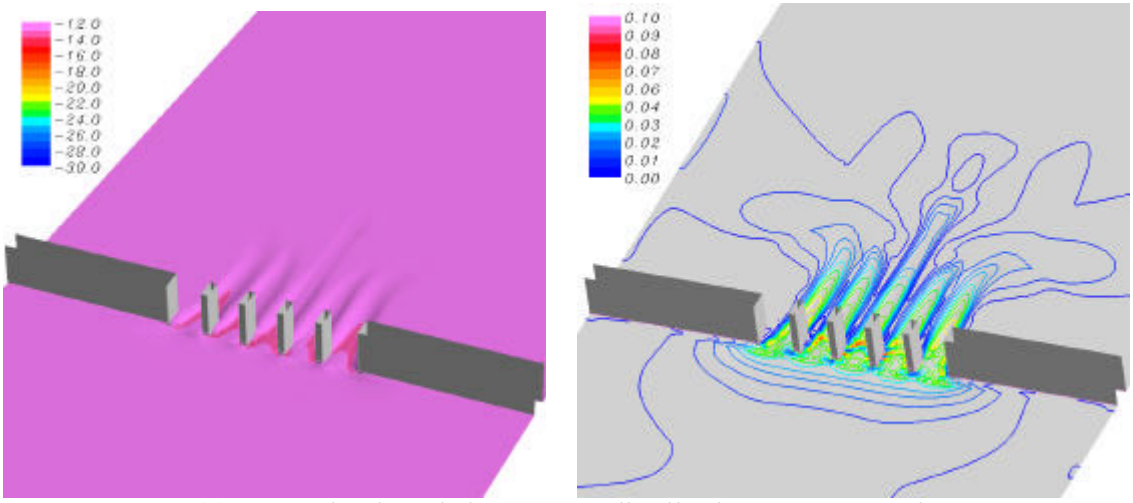

(a) Scour depth and shear stress distributions at t = 25 min

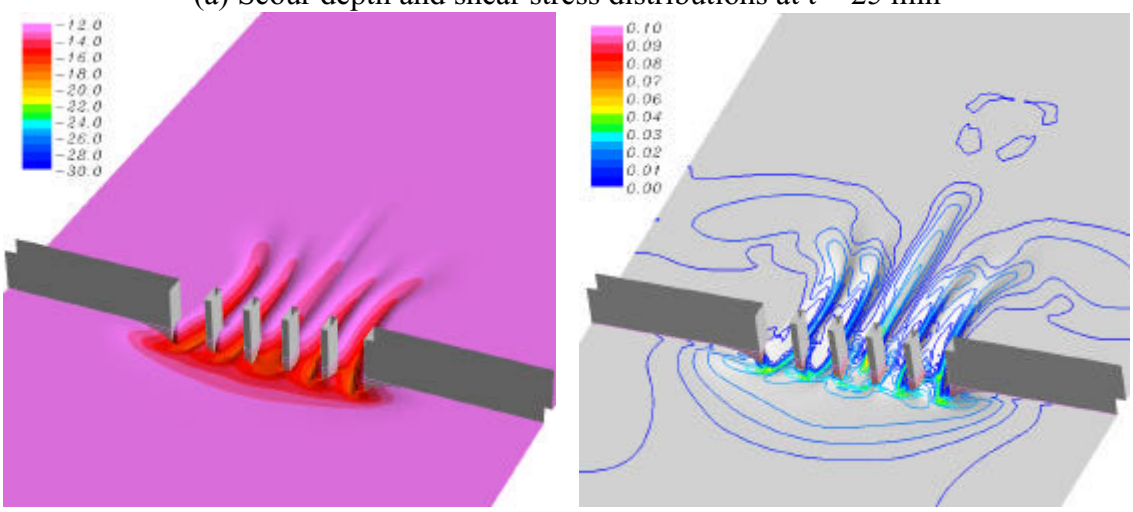

(b) Scour depth and shear stress distributions at t = 500 min

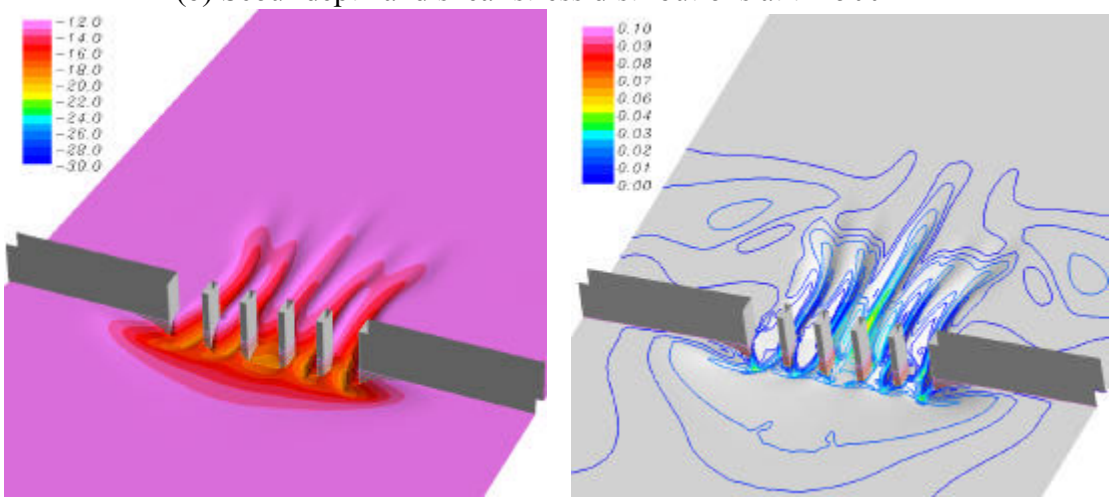

(c) Scour depth and shear stress distributions at t = 1000 min

Figure 5. Predicted scour hole shape and streambed shear stresses around complex rectangular pier configuration: (a) t = 25 min, (b) t = 500 min, (c) t = 1000 min

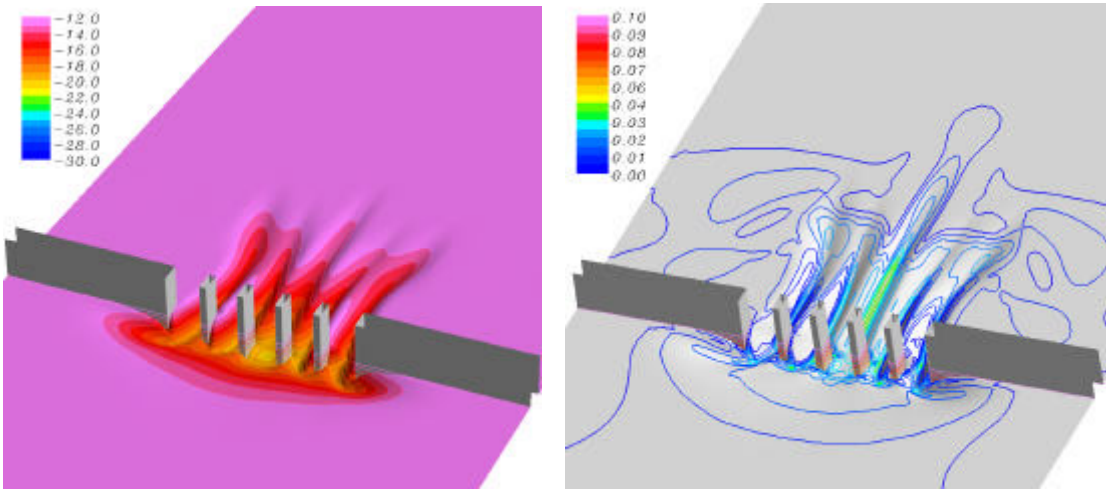

(d) Scour depth and shear stress distributions at t = 1500 min

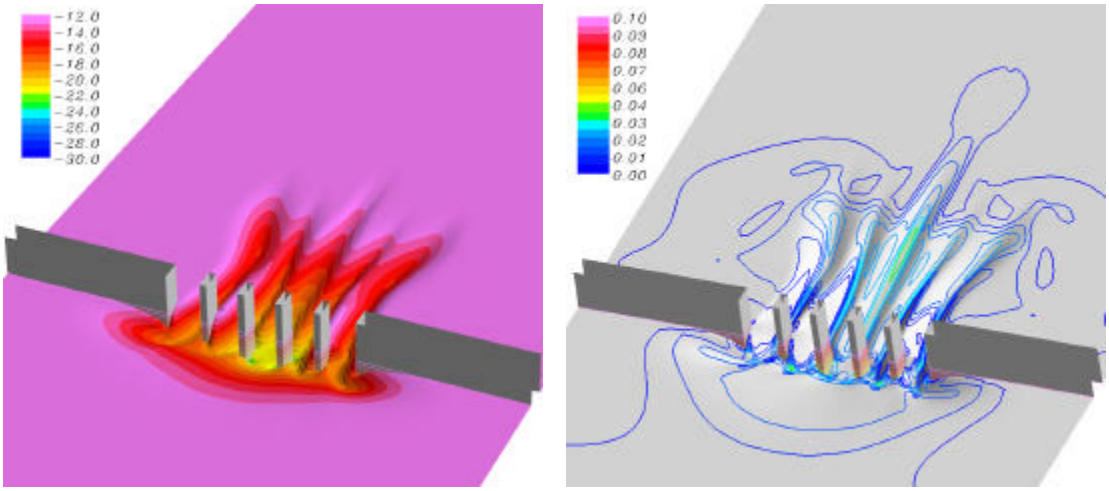

(e) Scour depth and shear stress distributions at t = 2000 min

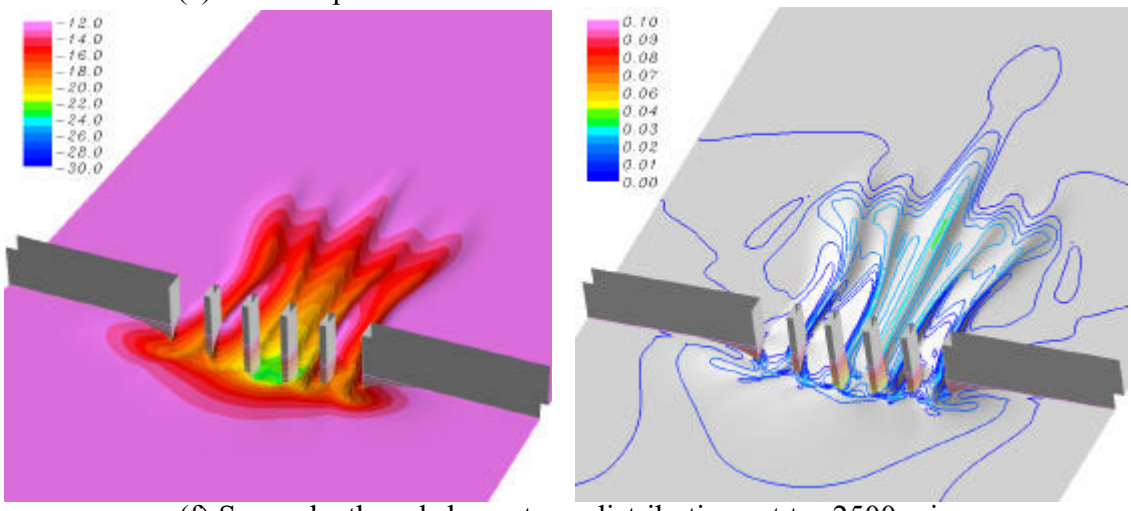

(f) Scour depth and shear stress distributions at t = 2500 min

Figure 5. Continued: (d) t = 1500 min, (e) t = 2000 min, (f) t = 2500 min

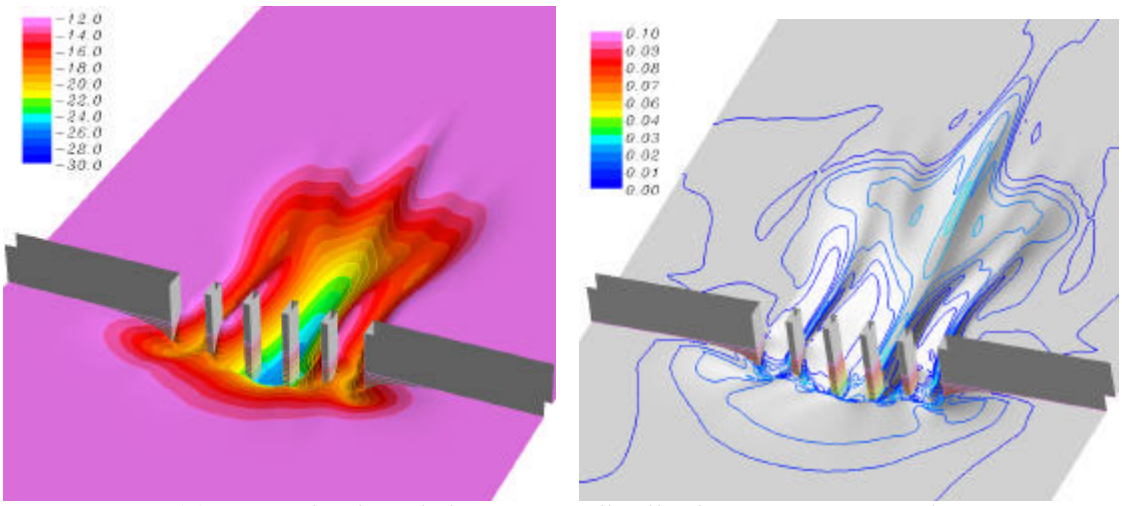

(g) Scour depth and shear stress distributions at t = 3750 min

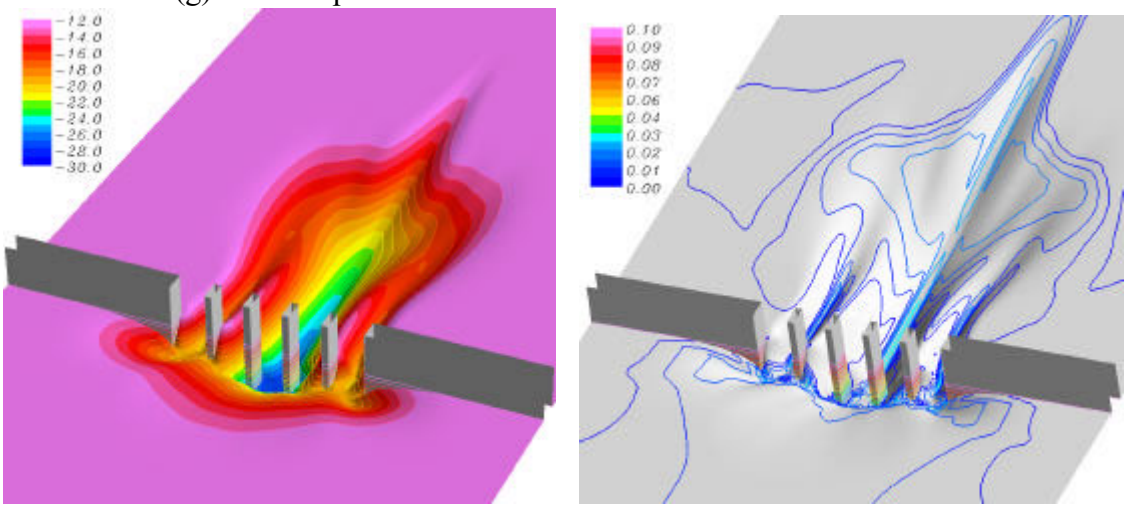

(h) Scour depth and shear stress distributions at t = 6000 min

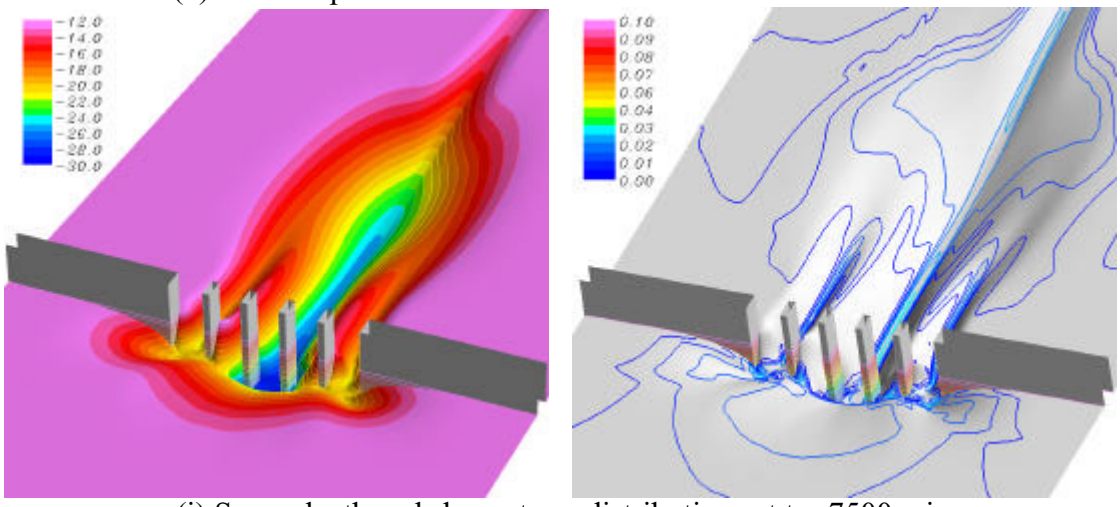

(i) Scour depth and shear stress distributions at t = 7500 min

Figure 5. Continued: (g) t = 3750 min, (h) t = 6000 min, (i) t = 7500 min

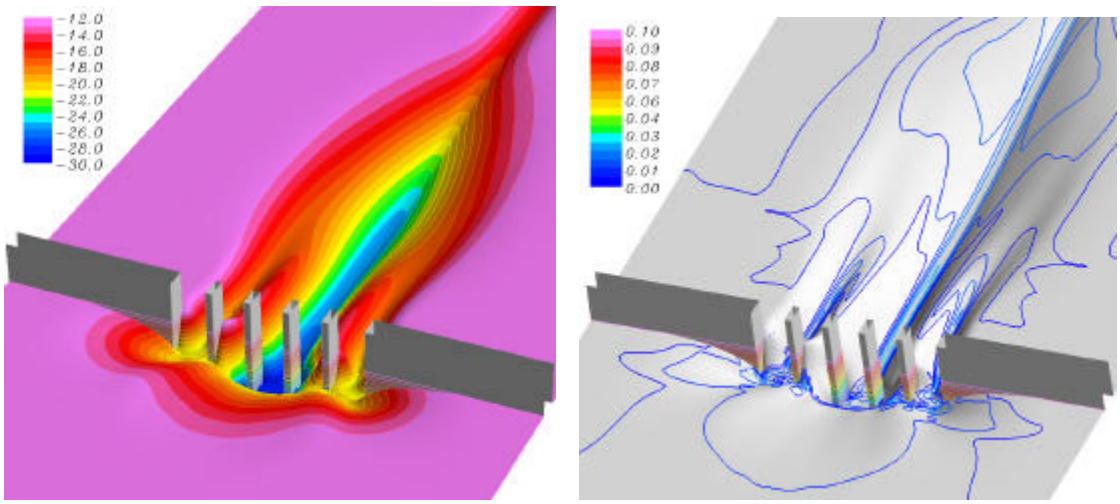

(j) Scour depth and shear stress distributions at t = 10000 min

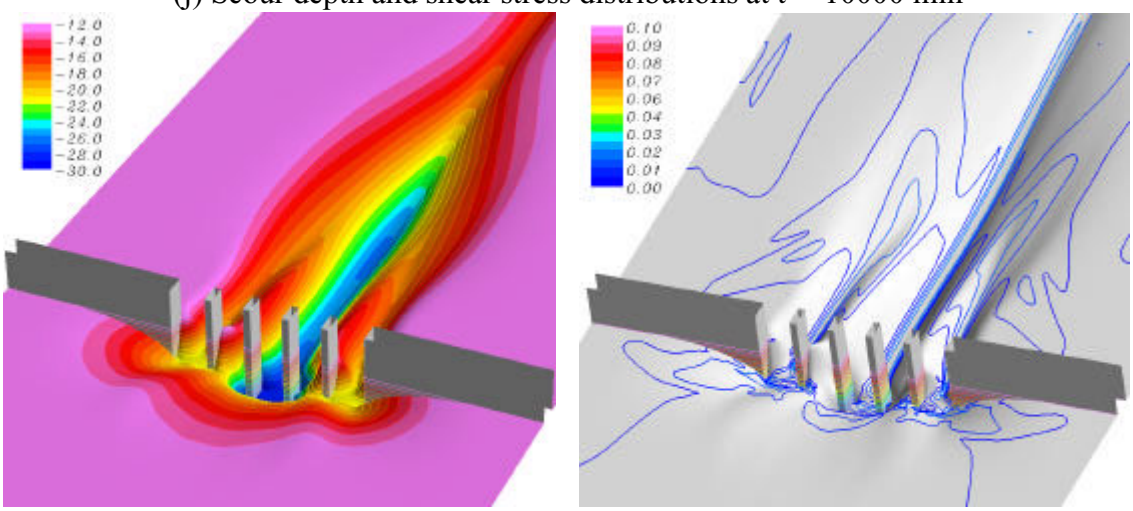

(k) Scour depth and shear stress distributions at t = 12500 min

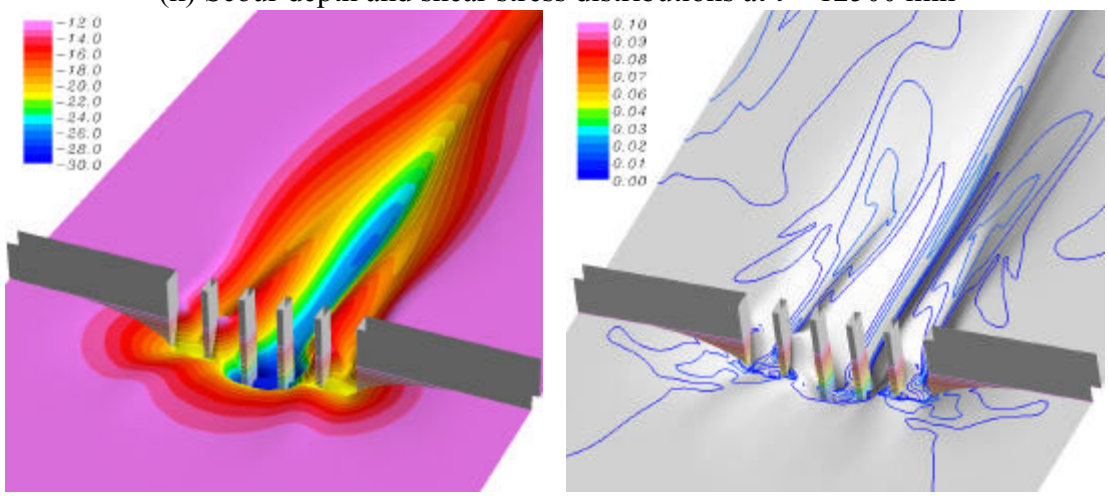

(l) Scour depth and shear stress distributions at t = 15000 min

Figure 5. Continued: (d) t = 10000 min, (e) t = 12500 min, (f) t = 15000 min

After about t = 20 hr, the ridges behind the piers also began to erode as the valleys deepened and widened continuously. As a result of this ridge erosion, the deep valleys merged into a large scour hole downstream of the pier. It is quite clear that the erosion between two central piers is significantly faster than the neighboring areas surrounding the outer piers and the abutments. Beyond t = 7,500 min, most of the new erosion took place near the middle section of the channel with only minor additional scour around the outer two piers and the abutments. The scour hole between the two inner piers continued to lengthen until about t = 12,500 min. At the end of the simulation (i.e., t = 15,000 min), the maximum shear stress reduces to about 0.91 N/m^2 and the deepest scour hole is about –22.7 cm (–34.6 cm below the free surface) or nearly twice of the water depth. The deepest scour hole was located on the outer back corner of the two inner piers and was produced by a combination of the contraction scour between the piers and the local scours around the piers.

Finally, we shall examine also the horseshoe vortex systems for complex pier configurations. Figure 6 shows the horseshoe vortices around the pier and the abutment at t = 12,500 min. It should be noted that the flow around the piers and abutments are highly three-dimensional with large lateral velocity components. In order to facilitate the visualization of horseshoe vortex systems, it is desirable to plot only the horizontal and vertical velocities while suppressing the lateral velocity components as shown in Figure 6. It is clearly seen that there is a large horseshoe vortex in front of the abutment. A smaller horseshoe vortex was also observed in front of the pier. As the scour hole size increases, the extent of the horseshoe vortex also increases. However, the strength of the horseshoe vortex decays gradually since the stream flow slows down at the bridge location as the scour hole was enlarged.

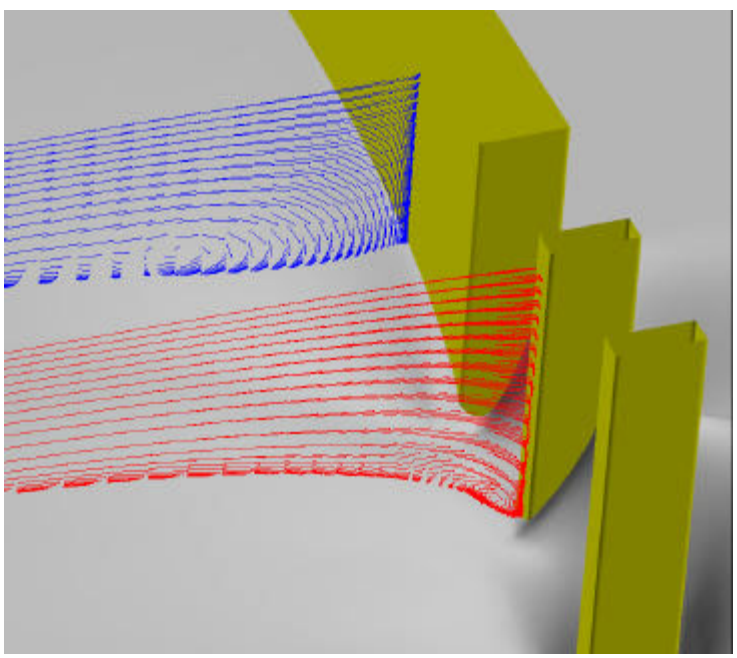

Figure 6. Horseshoe vortices around the pier and abutment

In order to further evaluate the capability of the present method, simulations were also performed for another complex pier configuration at full scale as shown in Figure 7. In this case, the channel width is 200 m and the length of each abutment is 50 m. Instead of the rectangular piers considered earlier, four circular piers of 4-m diameter each were placed between the abutments with uniform pier spacing of 20 meters. The water depth was chosen to be 12 m and the approach flow velocity was assumed to be 1 m/s. In order to reduce the CPU time and memory requirements, the computations were performed for only one-half of the solution domain with the symmetry conditions applied along the centerline of channel. The solution domain was divided into 6 computational blocks with a total of 579,847 grid points. It is noted that the cylindrical pier grid blocks were completely embedded in the rectangular channel grids using a chimera domain decomposition approach. This enables us to simplify the grid generation process and improve the resolution of turbulent boundary layers and wakes around the piers. When the streambed was eroded due to contraction and/or local scour, the numerical grids were redistributed in the vertical direction to conform to the new streambed elevation.

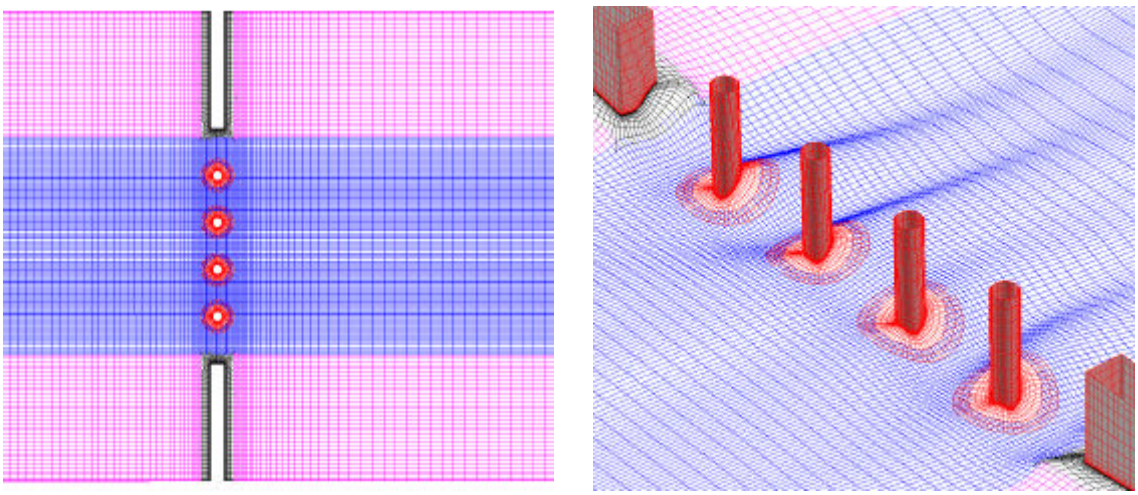

Figure 7. Bridge geometry and numerical grids for complex circular piers

Computations were performed first for the flat bed configuration without erosion until the steady flow condition is attained. For simplicity, the free surface effects were neglected. It is anticipated that the free surface may have only minor influence on the scour pattern since the water depth is quite large compared to the pier diameter. Figure 8 shows the predicted velocity distributions at the mean water surface. It is seen that the abutments and bridge piers produced strong flow accelerations at the bridge location similar to those observed in the previous case. The strongest acceleration was observed in the middle section downstream of the bridge piers. The maximum velocity was nearly 3.2 m/s or 3.2 times of the upstream flow velocity. This flow acceleration is somewhat lower than that shown in previous case since the contraction ratio due to the abutments and piers is only 2.27:1. There are again two large recirculation regions behind the abutment while the mainstream was directed towards the middle section of the channel. It is also clearly seen that the stream flow approaches the outer two piers at a fairly large skew angle.

The angle of the attack for the two central piers are considerably smaller and the wakes behind these piers are nearly parallel to the channel bank.

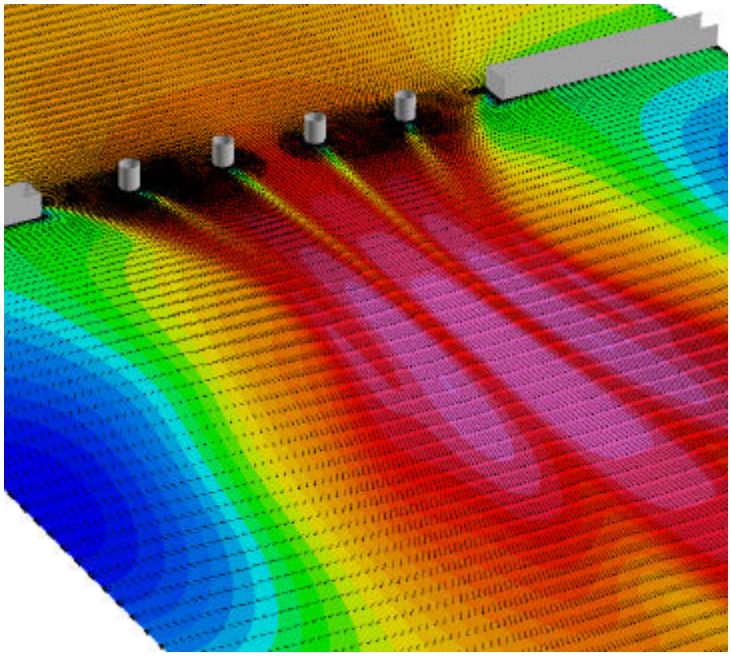

Figure 8. Free surface velocity field around complex circular pier configuration

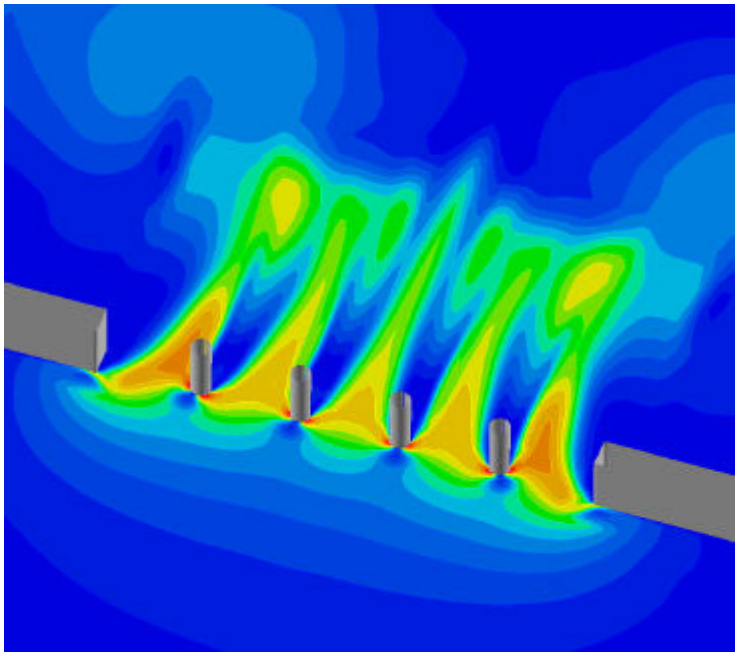

Figure 9. Shear stress distribution at the scour initiation

Figure 9 shows the initial shear stress distribution before the scour take place. It is quite clear that the shear stresses are high in the middle section of each passage since the flow

was forced to accelerate between the piers, and between the abutments and piers. The maximum shear stress was about 20.2 N/m^2. This is significantly higher than those predicted earlier for model scale piers because the upstream flow velocity is much higher for the present full-scale simulation. It is noted that the wakes behind the circular piers are significantly wide than those observed earlier for slender rectangular piers. The wider wakes was caused by the earlier separation of boundary layer flow around the circular pier. For slender rectangular piers, the flow separates nearly the leading corners, but tends to reattach in the middle section of the pier surface before separating again nearly the back face of the pier.

After the steady-state solution was obtained, the scour process was initiated using a critical shear stress of 1.0 N/m^2 (i.e., $\boldsymbol{\tau_c/\rho U_0^2 = 0.001}$). The slope of the scour rate vs. shear stress curve was assumed to be $\boldsymbol{c}$ = 0.006 m^3/(N·hr). Simulations were performed for 6000 time steps using a constant time increment of Δt = 0.1 hr. As noted earlier, the maximum shear stress is about 20.2 N/m^2 or about 20 times of the critical shear stress, at the initiation of scour processes.

In order to facilitate a detailed examination of the scour hole development and the associated shear stress variations, the numerical solution for the entire streambed was saved in a movie file at a 1.0 hr interval (i.e., every 10 time steps). Figure 10 shows the predicted scour pattern and the corresponding shear stress distributions (normalized by $\boldsymbol{\rho U_0^2}$ = 1,000 N/m^2) at 9 selected time instants. It is clearly seen that the scour was initiated in the high shear stress regions between the piers and gradually propagates towards the downstream and upstream of the bridge. During the initial stage of streambed erosion, the scour hole in each passage develops almost independently with five separate valleys downstream of the bridges. As time increases, however, the scour hole shape develops in a very different manner comparing to that seen earlier for the rectangular piers. More specifically, the scour hole not only expands in the longitudinal direction, but also extends laterally toward the channel bank with a pair of deep scour holes behind the abutments. This may be attributed, at least in part, to the relatively short abutment which enables the mainstream flow to impinge on the bank and produce a strong recirculation flow region near the channel bank. The combination of short abutment length and high streambed shear stresses produced a much wider scour hole for the prototype configuration.

A detailed comparison of the scour hole patterns for the rectangular and circular pier configurations indicated that the location of the deepest scour hole depends strongly on the complex pier configurations. For the model scale rectangular piers, the maximum scour depth was observed around the two middle piers due to combined contraction and local scours. For the prototype circular piers, however, the maximum scour occurs much farther downstream of the bridge and away from the channel centerline. The local scour around the piers and abutments were relatively small comparing to the contraction scour. It is quite clear that the scour hole development for the present circular pier configuration is dominated by the contraction scour.

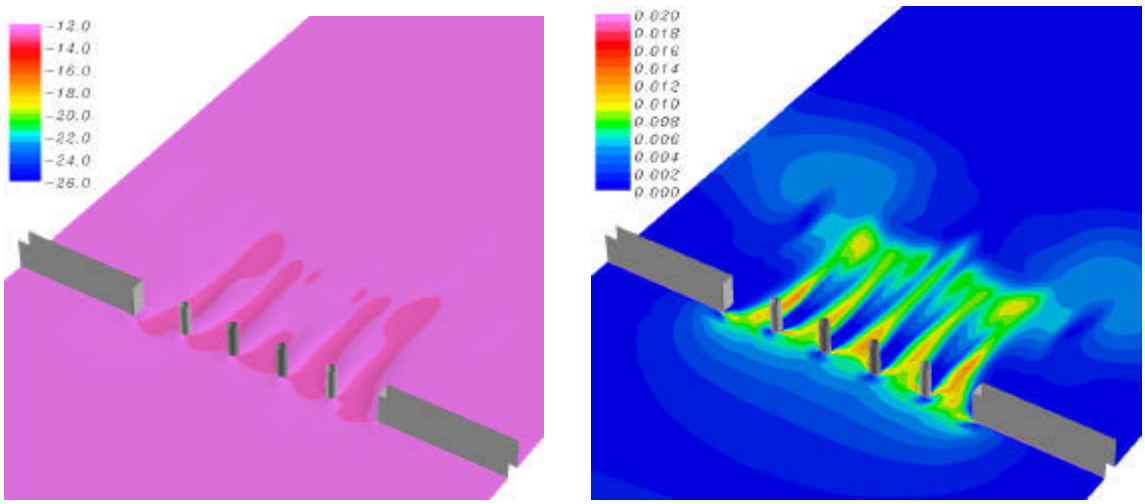

(a) Scour depth and shear stress distributions at t = 15 hr

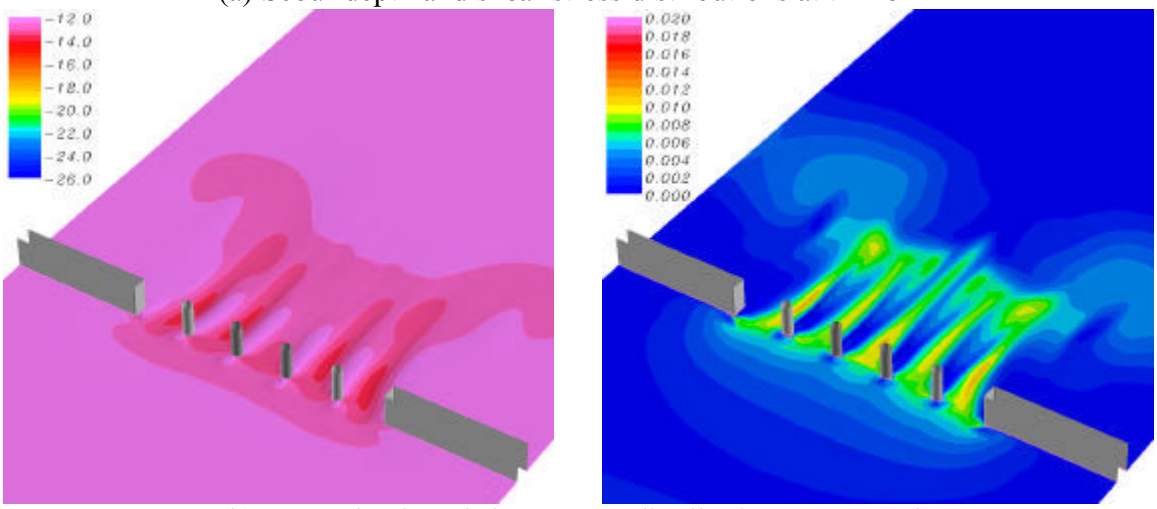

(b) Scour depth and shear stress distributions at t = 30 hr

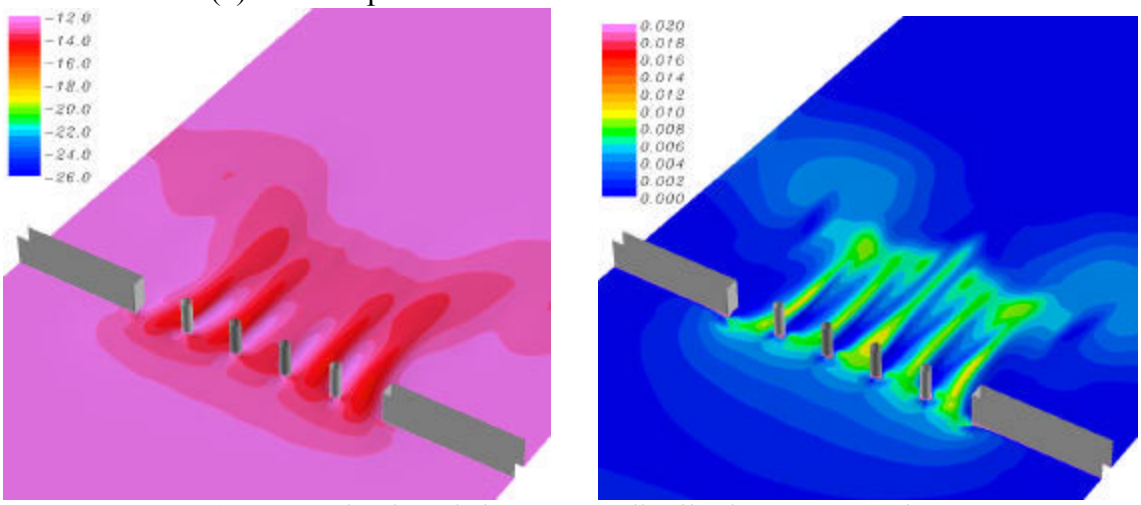

(c) Scour depth and shear stress distributions at t = 50 hr

Figure 10. Predicted scour hole shape and streambed shear stresses around complex circular pier configuration: (a) t = 15 hr, (b) t = 30 hr, (c) t = 50 hr

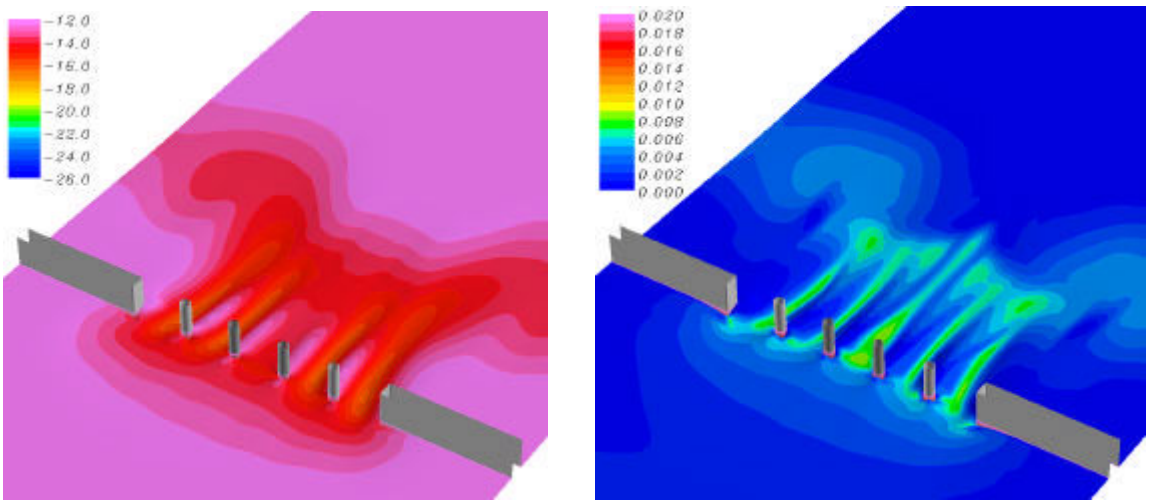

(d) Scour depth and shear stress distributions at t = 100 hr

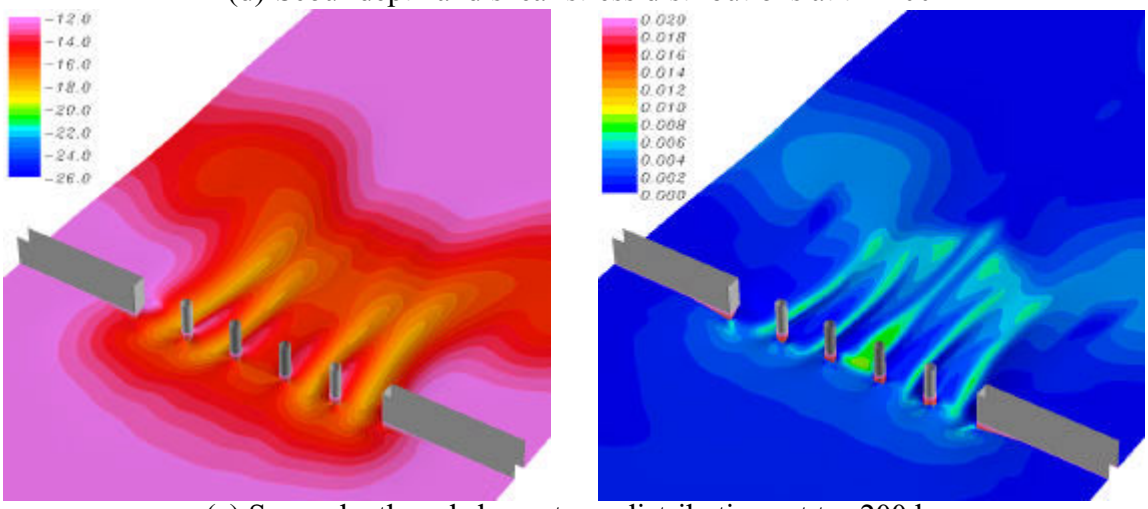

(e) Scour depth and shear stress distributions at t = 200 hr

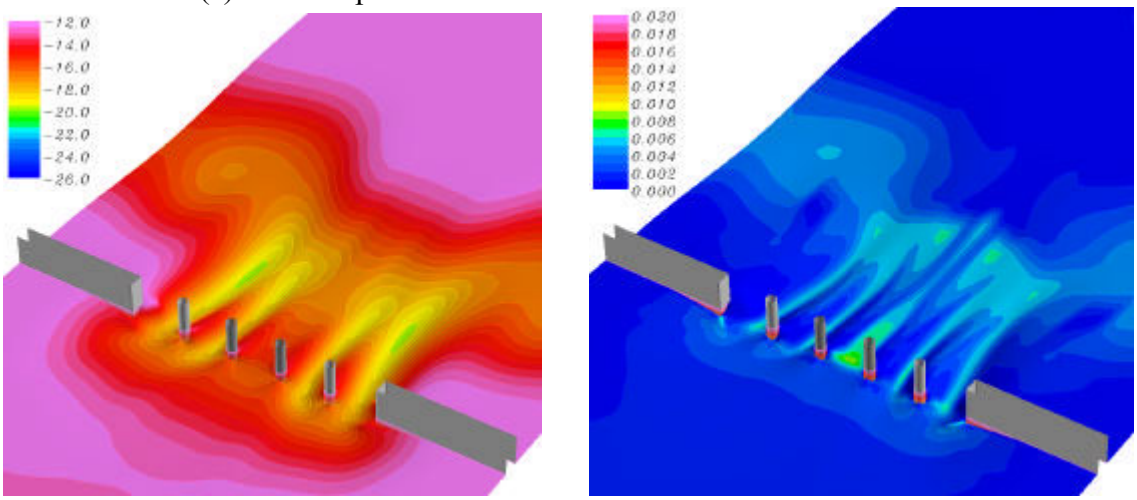

(f) Scour depth and shear stress distributions at t = 300 hr

Figure 10. Continued: (d) t = 100 hr, (e) t = 200 hr, (f) t = 300 hr

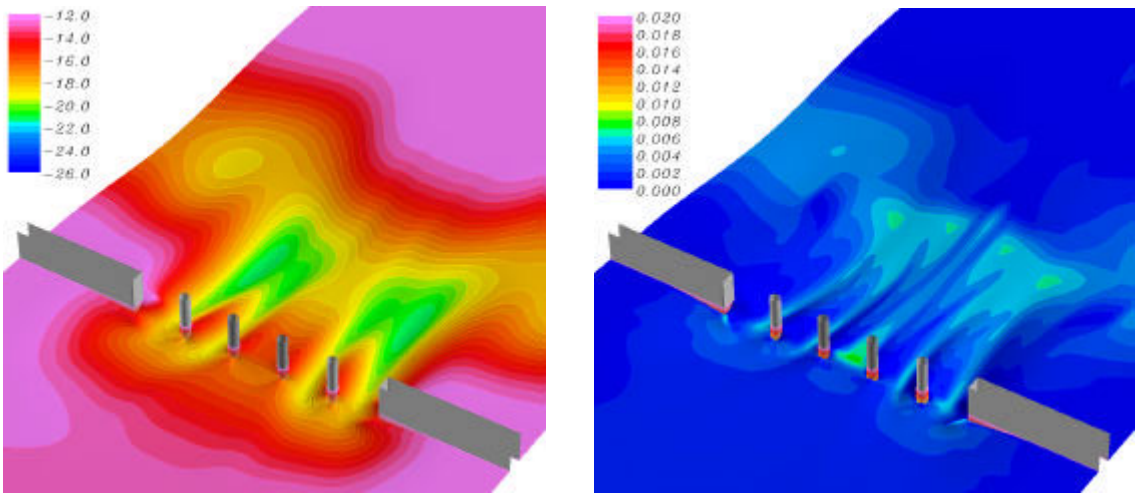

(g) Scour depth and shear stress distributions at t = 400 hr

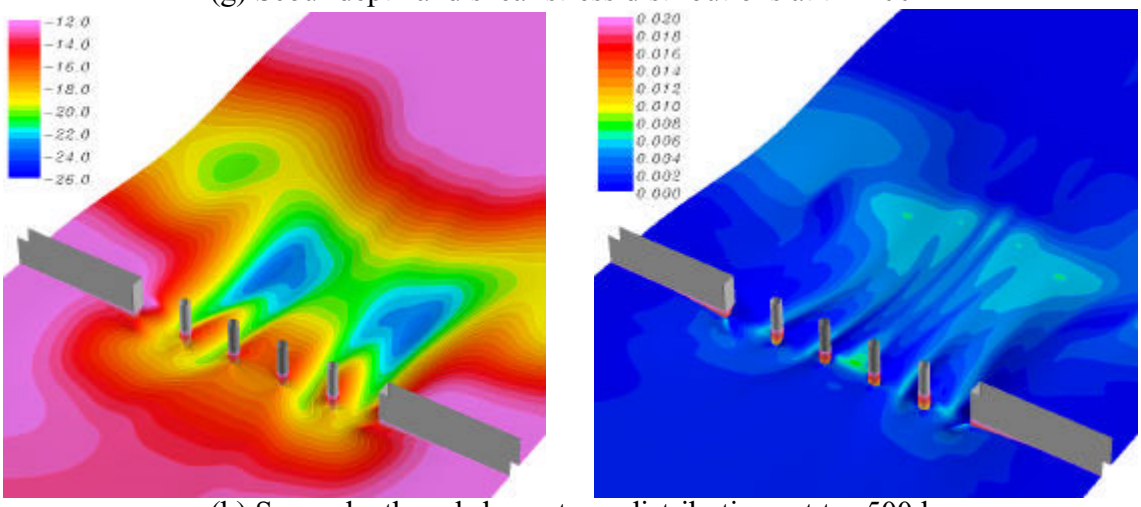

(h) Scour depth and shear stress distributions at t = 500 hr

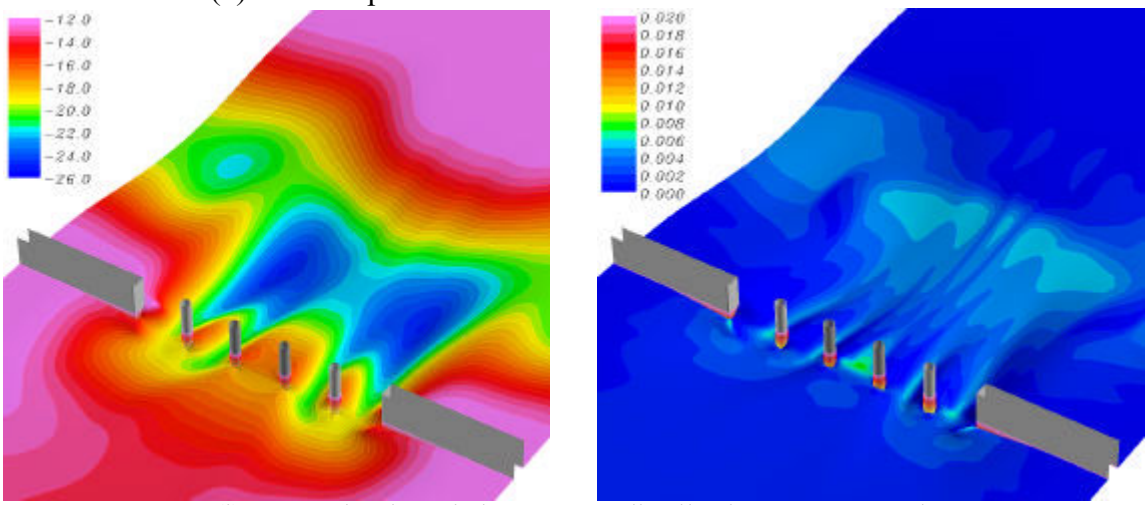

(i) Scour depth and shear stress distributions at t = 600 hr

Figure 10. Continued: (g) t = 400 hr, (h) t = 500 hr, (i) t = 600 hr

For completeness, we shall examine also the change in shear stresses as the scour hole developed. It is interesting to note that the shear stress decays rather slowly for the present configuration. It took about 45 hours for the maximum bed shear stress to drop from the initial 20.2 N/m^2 down to 10 N/m^2. A detailed examination of the time history indicated that the maximum shear stress actually increases slightly between t = 100 hr and 125 hr in the region between the two middle piers. This is most likely caused by a change in scour hole shape and an increase of local flow velocity while the flow was re-directed through the bridge. After t = 125 hr, the shear stress continued to decrease slowly while the scour hole deepened at a significantly faster rate. At the end of the simulation (t = 600 hr), the maximum shear stress remains quite high at 7.49 N/m^2 or about 7.5 times of the critical shear stress. The maximum scour depth is –13.1 m (–25.1 m below the free surface). Since the bed shear stress is still above critical shear stress in the bottom of the scour hole, it is anticipated that a much longer simulation time will be needed in order to attain the ultimate scour depth under the present flow conditions. However, if our primary interest is to determine the ultimate scour depth, then it is possible to use a larger slope for the scour rate equation so that the final scour depth can be obtained much more quickly.

Finally, it should be emphasized that the scour rate, in general, is a nonlinear function of the shear stress and must be determined experimentally. It is also important to note that the scour rate may also depend on other fluid flow characteristics such as the turbulence structure, vortex shedding, or pressure gradients. In order to further improve the predictive capability of the present method, it is necessary to develop a more general scour rate equation for more accurate representation of the erodibility function for cohesive soils.

SUMMARY AND CONCLUSIONS

A chimera RANS method has been employed in conjunction with a scour rate equation for the simulation of scour process in cohesive soils around two complex pier configurations. The method successfully resolved many important flow features for contraction and local scours around complex piers. The contraction and local scour patterns were found to depend on the abutment length, pier sharp, and pier spacing. To further improve the predictive capability of the present method, it is important to obtain an accurate critical shear stress and scour rate equation through laboratory experiments.

ACKNOWLEDGEMENTS

Many organizations and individuals have contributed to the development of the scour research program at Texas A&M University. They are all thanked sincerely. Texas DOT, NCHRP, Maryland SHA, North Carolina DOT, Minnesota DOT, Illinois DOT, Texas Transportation Institute, Humboldt, Jean-Louis Briaud, Francis Ting, Ya Li, Jun Wang, Prahoro Nurtjahyo, Kiseok Kwak, Yiwen Cao, Seung-Woon Han, Rao Gudavalli, Suresh Perugu, Gengshen Wei, Peter Smith, Tony Schneider, Melinda Luna, Kim Culp, Jay Vose, Tom Dahl, David Stolpa, Mark McClelland, John Delphia, Andy Kosicki, Stan

Davis, John Boynton, Ryhad Wahad, Bill Moore, Steven Smith, Larry Arneson, Daryl Greer, Robert Henthorne, Richard Phillips, Mehmet Tumay, Sterling Jones, Tim Hess, Mahir Al-Nadaf.

REFERENCES

1. Chen, H.C., 1995a, "Submarine Flows Studied by Second-Moment Closure," Journal of Engineering Mechanics, Vol. 121, No. 10, pp. 1136-1146, October 1995.
2. Chen, H.C., 1995b, "Assessment of a Reynolds Stress Closure Model for Appendage-Hull Junction Flows," Journal of Fluids Engineering, Vol. 117, No. 4, pp. 557-563.
3. Chen, H.C., Briaud, J.-L., Ting, F.C.K., Wei, G., Gudavalli, R. and Perugu, S., 1999, "Numerical Simulation of Scour Processes Around a Prototype Pier Under Flood Conditions," Proceedings of the 13th ASCE Engineering Mechanics Conference, Johns Hopkins University, Baltimore, MD.
4. Chen, H.C. and Chen, M., 1998, "Chimera RANS Simulation of a Berthing DDG-51 Ship in Translational and Rotational Motions," International Journal of Offshore and Polar Engineering, Vol. 8, No. 3, pp. 182-191.
5. Chen, H.C. and Korpus, R., 1993, "A Multi-block Finite-Analytic Reynolds-Averaged Navier-Stokes Method for 3D Incompressible Flows," ASME FED-Vol. 150, pp. 113-121, ASME Fluids Engineering Conference, Washington, D.C..
6. Chen, H.C., Lin, W.M., and Hwang, Y.W., 2002a, "Validation and Application of Chimera RANS Method for Ship-Ship Interactions in Shallow Water and Restricted Waterway," Proceedings, 24th Symposium on Naval Hydrodynamics, Fukuoka, Japan.
7. Chen, H.C., Liu, T., and Huang, E.T. 2002b, "Time-Domain Simulation of Large Amplitude Ship Roll Motions by a Chimera RANS Method," International Journal of Offshore and Polar Engineering, Vol. 12, No. 3, pp. 206-212.
8. Chen, H.C., Liu, T., Huang, E.T. and Davis, D.A., 2000, "Chimera RANS Simulation of Ship and Fender Coupling for Berthing Operations," International Journal of Offshore and Polar Engineering, Vol. 10, No. 2, pp. 112-122.
9. Chen, H.C. and Patel, V.C., 1988, "Near-Wall Turbulence Models for Complex Flows Including Separation," AIAA Journal, Vol. 26, No. 6, pp. 641-648.
10. Chen, H.C., Patel, V.C. and Ju, S., 1990, "Solutions of Reynolds-Averaged Navier-Stokes Equations for Three-Dimensional Incompressible Flows," Journal of Computational Physics, Vol. 88, No. 2, pp. 305-336.
11. Du, X., 1997, "Numerical Simulation of Three-Dimensional Flow Field and Local Scour at Bridge Crossings." Ph.D. Dissertation, The University of Mississippi.
12. Li, Y., 2002, private communications.
13. Olsen, N. R. B., 1996, "Three-dimensional numerical modeling of local scour," Hydroinformatics'96, Zurich, Switzerland.
14. Olsen, N. R. B. and Melaaen, M.C. (1993), "Three-dimensional calculation of scour around cylinders," Journal of Hydraulic Engineering, Vol. 119, No. 9, pp. 1048-1054.
15. Roulund, A., 2000, "Three-dimensional Numerical Modeling of Flow Around a Bottom-Mounted Pile and Its Application to Scour," Ph.D. Thesis, Technical University of Denmark.

Unconventional Interpretation of Local Scour Downstream a Large Dam Stilling Basin

Raúl A. LOPARDO, José M. CASADO and María Cecilia LOPARDO
ARGENTINA

Instituto Nacional del Agua
C.C. 46, (1802) Aeropuerto Ezeiza, ARGENTINA
E-mail: rlopardo@ina.gov.ar

ABSTRACT

The stilling basin of Rio Hondo Dam, Argentina, constructed fifty years ago, was designed to contain entirely the hydraulic jump and it was verified by means of hydraulic model tests.

The sediment discontinuity produced by the dam generates a progressive degradation of the river bed elevation downstream the structure, decreasing the bed level 3 m below the original bed. The hydrodynamic study developed shows for flow discharges between 500 m^3/s and 2248 m^3/s (maximum discharge), the Froude Number over the end sill is practically F1 = 1. This condition indicates accelerated flow at the end of the basin.

The local scour downstream this structure was analyzed: a) as a case of scour downstream ski-jump with important energy losses in the way, b) assuming the scour below an horizontal flow jet, and c) as a conventional scour downstream a conventional hydraulic jump stilling basin.

The performance of each one of the eight empirical equations used is considered for the comparison with prototype scour measurements for discharge Q = 1400 m^3/s. All the equations are applied to all discharges, reaching the maximum discharge.

A mixed protection solution (structural and non structural) was proposed. It needs the execution of diverse works and a continuous bed river behavior monitoring.

INTRODUCTION

Río Hondo Dam is located on the Dulce River, in the northern region of Argentina and it has different goals, as flood attenuation, irrigation and hydroelectric power supply.

The discharge structures of the dam are composed by a spillway, two outlet works and four valves for water derivation. The spillway has a free length L = 151 m and design head H = 3m, allowing a maximum spillway discharge of 1,525 m^3/s. The maximum discharge flowing by all the outlet devices is Q = 2,248 m^3/s. The spillway and outlet structures discharge in an horizontal stilling basin with 80 m length, topographic level +245.92, upstream wide 166.5 m and downstream wide 182.5 m. It has inside a line of baffle piers and it finish with a stepped end sill, with topographic top level +249 m.

The dam began to work in the sixties. The “wall” produced an abrupt discontinuity in sediment transport in the river, starting a typical process of “erosion downstream dams in fluvial channels”, developed along several kilometers as a progressive and permanent phenomena, searching in an asymptotic form a new riverbed profile. In the proximity of the stilling basin the bed level decreased from +250 m to less than + 247 m (Figure 1).

Due to this process, the hydrodynamic conditions are extremely modified downstream the stilling basin, and the erosion effect on the riverbed is more severe than the designers considered long time ago. The hydraulic jump cannot be located into the concrete structure and a jet jumps on the end sill to the riverbed, changing the conditions of local scour.

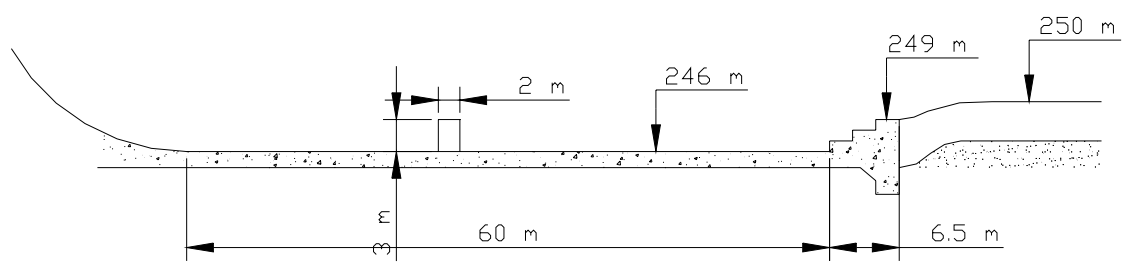

Figure 1: Río Hondo Dam stilling basin

HYDRAULIC ASPECTS

The first verification consisted on the spillway acting alone, with all other outlet devices closed. Then, it is possible to obtain the following data: Q = 1550 m^3/s, Reservoir topographic level: H_0 = +275 m, stilling basin topographic level H_p = +245.92 m, stilling basin wide at the spillway toe b = 166.5 m, and inflow specific discharge to the stilling basin: q = 9.31 m^2/s.

Applying the energy conservation and continuity principles it is possible to estimate the inflow water depth h_1 = 0.44 m, and the inflow velocity U_1 = 21.16 m/s, giving an incident Froude Number F_1 = 10.3.

The length of the stilling basin is L_c = 80 m, with baffle piers and end sill. This stilling basin was designed for hydraulic jump location and energy dissipation.

For this purpose, the flow must change from supercritical to sub critical in the structure, avoiding the macrotubulent transition on the riverbed because the possibility of severe local scour.

With the calculated values it is possible to estimate the “sequent depth” of a free hydraulic jump h_2 = 6.2 m. With the addition of this value up to the stilling basin bed level the downstream water level needed for the hydraulic jump stable condition will be +252.12. When the riverbed level was +250 m (at the beginning of the dam operation) the downstream level was clearly over that value.

According with Smetana, the length of hydraulic jump can be estimated by $L = 6 (h_2 - h_1)$ = 34.56 m, that implies L/ Lc = 0.43. However, local scour was detected downstream the structure.

The maximum measured discharge through the spillway along forty years of operation was Q = 1400 m^3/s, with a downstream level of +250.8 and it occurs recently.

The maximum local scour at the bed reaches the level + 245.5 m. the topographic level of the top of the end sill is + 249 m, the stilling basing wide at the end sill location is B = 182.5 m, the specific discharge over the end sill is q = 7.67 m^2/s and the mean velocity over the end sill was U_d = 4.26 m/s.

For different upstream reservoir levels (Hups) and the downstream water levels (Hdown) calculated by means of the HEC-RAS model it is possible to calculate the hydrodynamic conditions over the end sill for discharges between Q = 500 m^3/s and Q = 2248 m^3/s (Table 1).

In Table 1 it was also calculated the specific inflow discharge "q", the specific discharge over the end sill "q_d", the velocity "U_d", the water depth over the end sill "h_d" y and the Froude Number in this section "F_d".

TABLE 1: HYDRODYNAMIC CONDITIONS OVER THE END SILL

Hups (m)	Hdown (m)	Q (m3/s)	q (m2/s)	qd (m2/s)	Ud (m/s)	hd (m)	Fd
273.41	249.90	500	3.00	2.74	3.04	0.90	1.02
273.59	250.05	600	3.60	3.29	3.13	1.05	0.98
273.77	250.13	700	4.20	3.84	3.39	1.13	1.02
273.93	250.25	800	4.80	4.38	3.51	1.25	1.00
274.09	250.37	900	5.41	4.93	3.60	1.37	0.98
274.24	250.45	1000	6.01	5.48	3.78	1.45	1.00
274.53	250.65	1200	7.21	6.58	3.99	1.65	0.99
274.80	250.82	1400	8.41	7.67	4.21	1.82	1.00
275.00	250.93	1550	9.31	8.49	4.40	1.93	1.01
275.00	251.13	1800	10.81	9.86	4.63	2.13	1.01
275.00	251.27	2000	12.01	10.96	4.83	2.27	1.02
275.00	251.50	2248	13.50	12.32	4.93	2.50	0.99

The condition $F_d = 1$ implies that in this section a critical flow is produced and it will be considered as a control section (hydraulic upstream conditions are independent from downstream conditions). Downstream the end sill the flow must to be accelerated, with severe instability, waves formation and a new jump process over the riverbed. This phenomena contributes on the local scour process downstream the structure.

LOCAL SCOUR DOWNSTREAM SKI JUMP STRUCUTRES

The maximum depth of scour "y" , measured from the tailwater level, (Figure 2) is a function of the water density ρ, the viscosity μ, the grain representative diameter d_s of the riverbed material, the grain density ρ_s, the specific discharge "q", the fall distance between the reservoir level to the tailwater level ΔH, the tailwater depth h_r, the submerged gravity g (s - 1), where $s = \rho_s/\rho$, and the angle α of the jet.

$$y/\Delta H = F\,(q/(g\,\Delta H^3)^{0.5},\ h_r/\Delta H,\ d_s/h_r,\ \alpha)\ ,$$

and if Z* is called the "fall Number" $Z^* = q/(g\,\Delta H^3)^{0.5}$, the expression can be reduced to:

$$y/\Delta H = F\,(Z^*,\ h_r/\Delta H,\ d_s/h_r,\ \alpha)\ . \qquad [1]$$

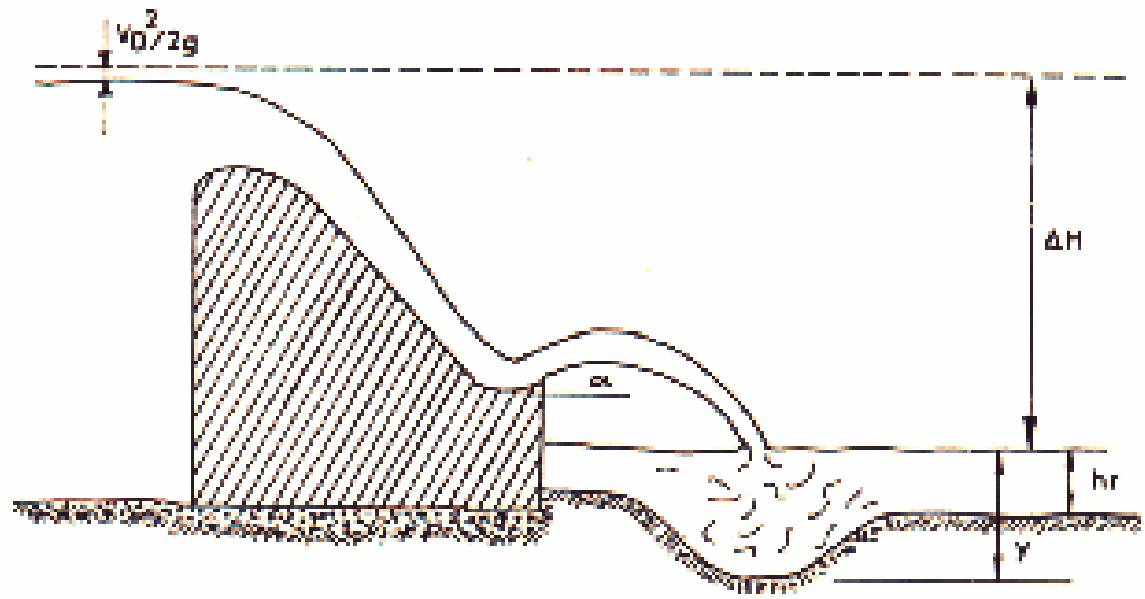

Figure 2: Ski-jump local scour notation

There are a lot of equations proposed by several authors (1) with the objective to give an experimental relationship between the variables involved in [1] with more or less complexity and simplification. An intentionally oversimplified formula for the estimation of the maximum depth of scour downstream ski-jump spillways, including only y, q, g y ΔH, or in other words the parameters $y/\Delta H$ and Z^*, is known as the INCYTH equation (2), published in 1983, in order to be of use as an initial estimation.

This equation can be expressed as:

$$y/\Delta H = K\, Z^{*0.5}\,, \qquad [2]$$

and it is it has a mean value of K = 2.5 and a maximum value for K = 3.25 (3).

The equation was developed by means of laboratory tests carried out by the authors and sixty six laboratory experimental results of other authors (with standard deviation of 18%) and seventeen prototype results (with standard deviation of 26%).

The INCYTH equation requires only the knowledge of the unit discharge and the fall height from the reservoir level to tailwater level. It should be noted that during the design stage many parameters are usually unknown, such as the size of blocks formed by fracture of the rock at different depths near the jet impact. For prototype preliminary calculations, this equation demonstrates acceptable performance, taking into account prototype results obtained from other authors, as the published data of Colbún (4), Tarbela (5), Cabora Bassa (6) and several dams in China (7).

LOCAL SCOUR DOWNSTREAM STILLING BASINS

The hydraulic jump is usually designed to be on a stilling basin with concrete floor, in order to avoid severe local scour of the riverbed downstream the spillway. Nevertheless, there are numerous references showing erosion and damages downstream hydraulic jump stilling basins. The macroturbulent flow generated by the jump has influence on this process.

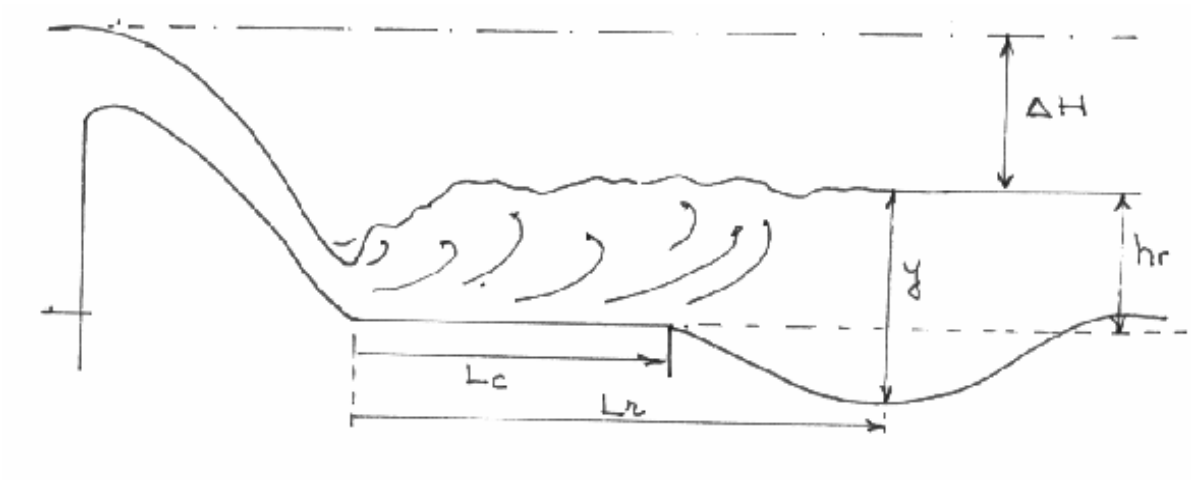

Figure 4: Local scour downstream hydraulic jump stilling basin

As the local scour downstream ski-jump spillways, it is possible to estimate the maximum depth of scour "y" (Figure Nº 4) by means of:

$$y/\Delta H = F\ (F_1,\ h_r/\Delta H,\ d_s/h_r,\ L_c/L_r), \quad [4]$$

where L_r is the length of the jump and y L_c is the length of the stilling basin.

In a first analysis, the case of a very short concrete bed is considered (L_c = 0). Empiric expression were proposed for this configuration by Schoklitsch in 1935 and Veronese in 1937, both without dimensional accord. Jaeger proposed an adaptation of Veronese's expression:

$$y/\Delta H = 10.62\ (q/(g\ \Delta H^3)^{0.5})^{0.5}\ (h_r/d_{90})^{0.33}, \quad [6]$$

On the other hand , Eggenber y Müller adapted Schoklitsch's formula:

$$y/\Delta H = 45.39\ (q/(g\ \Delta H^3)^{0.5})^{0.6}\ (\Delta H/d_{90})^{0.4}. \quad [7]$$

There are more up to date equations in the same direction, as the proposed by Kotoulas:

$$y = 1{,}9\ g^{-0{,}35}\ \Delta H^{0{,}35}\ q^{0{,}7}\ d_{95}^{-0{,}4}, \quad [8]$$

where d_{95} is the maximum diameter of the rock protection.

Altinbilek and Basmaci (8) proposed for the flow downstream a sluice gate with contracted depth h_c the equation:

$$y/h_c = (tg\Phi/(d_s/h_c))\ (F_c/(s-1)^{0.5}) , \qquad [9]$$

where Φ is the angle of the bed material and F_c the Froude Number calculated with the velocity and h_c.

Franke (9) for the same configuration proposed:

$$y/\Delta H = 1.21\ Z^{*0.3}\ (d_{90}/\Delta H)^{-0.4} . \qquad [10']$$

The experience of China in the subject (10) can be summarized in the following formula:

$$y = 1{,}25\ (q^2/g)^{1/3}\ \Delta H^{0{,}26}\ d_{95}^{-0{,}22}\ h_r^{-0.04} . \qquad [11]$$

Taking into account the case of hydraulic jump stilling basins with length not less than the jump length, there are in the literature other empirical equations. One of these expressions was proposed long time ago by Schoklitsch (11):

$$y = 4.5\ \alpha\ ß\ (\Sigma b/B)^{1/4}\ z^{1/6}\ H^{1/2}\ q^{1/3} + 2.15\ a\ , \quad [12]$$

where, Σb is the total free wide of the spillway, B is the river wide at the downstream section, z is the time period (in hours) of the flow, q is the specific discharge, α is a coefficient which depends of the stilling basin shape (for example α = 0.36 for a horizontal floor and $0.17 < \alpha < 0.25$ for a stilling basin with a Rehbock end sill), ß is other coefficient which take into account the flow dissymmetry and "a" is the difference between the level of the top of the end sill and the level of the river bottom.

Mostly of the literature on the subject includes the influence of the riverbed material size. This is the case of the equation proposed by Catakli et Al (12) for a stilling basin with length $L_c = 5\ h_2$.

$$y = K\ q^{0.6}\ (\Delta H + h_r)^{0.2}\ d_{90}^{-0.1} , \qquad [13]$$

where d_{90} is expressed in mm, K is a shape factor (K = 1.62 when the basin has not end sill and K = 1.42 when it has end sill with height of 10% to 12% of the hydraulic jump sequent depth.

As it is considered by Breusers and Raudkivi (13) there are not general expressions wit capacity for maximum local scour prediction downstream stilling basins. They mentioned two equations for estimated calculations: one proposed by Dietz and other by Blench. Dietz ,in 1969, proposed the following formula:

$$(y - h_r)/h_r = (U_{max} - U_c)/\ U_c . \qquad [15]$$

where U_{max} is the mean velocity of the flow downstream the stilling basin and U_c is the critical velocity of sediment drag, which is function of the grain diameter, for example by means of the Neill equation:

$$U_c^2 = 2\ g\ (s - 1)\ d\ (h_r/d)^{1/3}.$$

On the other hand Blench, in 1957, based in the "regime theory" proposed an equation for estimation of the maximum depth of scour downstream hydraulic jump stilling basins. This equation is

$$y_{max} = (0{,}75 \text{ a } 1{,}25)\ y_{2r} + h_r \qquad [16]$$

where y_{2r} is el the "regime depth" for two-dimensional flow: $y_{2r} = 1{,}34\ (q^2/f)$, and "f" is the "sediment factor" , which can be calculated as: $f = 1{,}76\ [d(mm)]^{1/2}$.

Briefly, among the different factors capable to generate a severe local scour downstream a hydraulic jump stilling basin (14) two of them can be specially mentioned: an uncalculated decrease of the tailwater level and an eventual deficiency of symmetry of the spillway discharge distribution.

LOCAL SCOUR FOR THE MAXIMUM MEASURED DISCHARGE

As it was mentioned above, the maximum flow discharge through the spillway of the Río Hondo Dam was Q = 1,400 m^3/s. For that flow condition the reservoir water level was + 274.8 and the tailwater level was +250.8 m (tailwater depth h_r = 3,8 m) over a riverbed with a main bottom level + 247 m. Therefore, the total head was ΔH = 24 m y and the specific discharge over the end sill was q = 7,67 m^2/s. The measured maximum depth of scour for long time of operation was y = 5,53 m, reaching a topographic level + 245.5 m.

Verification as ski-jump condition

As the stilling basin is not capable to have the hydraulic jump into its dimensions, because the tailwater level is not enough, the flow is accelerated again and the contact with the river bottom is rather similar than a ski-jump spillway. It can be considered as a first approximation the use of this hypothesis for a maximum local scour depth. This final depth of scour can be estimated by the INCYTH expression [2], where K = 2.5, giving the value y = 9.06 m, reaching the topographic level + 241.76 m.

There are several objections for the direct application of this expression, even for ski-jump usual cases. The difference between experimental data and the use of this formula for the Río Hondo Dam local scour is obviously due to these objections Firstly, the equation is valid for equilibrium scour depth, and the time required to attain this depth in the nature is extremely large. Secondly, and more essential objection in this case, between the reservoir water level and the tailwater level there are very important energy losses (baffle piers action, end sill action and friction losses) and they were not considered in the

calculation. Finally, the equation [2] don't take into account the river bottom material size.

Verification as hydraulic jump stilling basin condition

With this hypothesis of configuration the hydraulic jump length don't exceeds the stilling basin length and the flow downstream the structure must be in fluvial regime. The riverbed material is granular and composed by silt and fine sand.

The Schoklitsch empirical equation [12] is applied to the Río Hondo maximum discharge measured. With B = 182.5 m, z = 1, q_d = 7.67 m^2/s, α = 0.17, ß =1 and a = 1 m, the maximum depth of scour calculated is y = 9.24 m, and minimum topographic level + 241.56 m.

For the knowledge of the sediment characteristics on the river bottom downstream the stilling basin some representative soil data were obtained. The collection was near the surface (between 0.5 and 1 m depth) at sections located between 500 m and 750 m downstream the end sill.

By means of this sediment information, the representative diameter selected was $d = (d_{15} \cdot d_{85})^{1/2}$ = 1.51 mm, and a bed armoring diameter d_{85} = 19 mm.

With this basic condition and the hydrodynamic data obtained for the maximum reorded flood it is possible the application of Catakli's formula [13], giving in this case y = 6.93 m, reaching the topographic level + 243.87 m, more than 1.5 down the experimental data (+ 245.5 m).

Applying the methodology proposed by Dietz [15], the critical velocity is V_c = 1.89 m/s. The maximum depth of scour calculated was y = 8.49 m, and this value implies a topographic level + 242.31 m. Breusers y Raudkivi (28) considered that values predicted by Dietz can be extremely large.

By means of the Blench equation the maximum depth of scour is (as a mean value) y = 5.85 m. As the tailwater level is +250,82 m , the erosin can reach the level +244.97m. Even considering that the hydraulic jump is contained in the stilling basin the calculated scour is more than the measured in the prototype.

The calculations of the maximum depth of scour downstream the Río hondo Dam stilling basin by the different equations previously mentioned are shown in Table 2.

TABLE 2

MAXIMUM DEPTH OF LOCAL SCOUR ESTIMATIONS DOWNSTREAM THE RÍO HONDO DAM										
Basic data			Estimation as a ski-jump spillway		Maximum depth of scour estimation downstream hydraulic jump stilling basins				Maximum depth of scour without stilling basin	
Hreservoir	Hdownstream	Q (m3/s)	yAuthors	yINCYTH	yBlench	ySchoklitsch	yDietz	yCatakli	yKotoulas	yWang
(m)	(m)	(m3/s)	(m)	(m)	(m)	(m)	(m)	(m)	(m)	(m)
273.41	249.58	500	3.60	5.41	2.94	7.18	4.87	5.27	9.70	12.85
273.59	249.83	600	3.72	5.92	3.50	7.48	5.23	5.88	11.01	14.43
273.77	250.08	700	3.89	6.39	4.04	7.75	5.79	6.45	12.26	15.91
273.93	250.32	800	4.09	6.83	4.55	7.99	6.17	6.98	13.44	17.31
274.09	250.46	900	4.35	7.24	4.96	8.23	6.53	7.49	14.60	18.68
274.24	250.55	1000	4.65	7.64	5.30	8.45	6.99	7.99	15.73	20.02
274.53	250.70	1200	5.23	8.38	5.94	8.86	7.73	8.92	17.91	22.57
274.80	250.82	1400	5.80	9.06	6.51	9.24	8.49	9.79	19.99	25.00
275.00	250.89	1550	6.23	9.55	6.91	9.50	9.08	10.42	21.51	26.76
275.00	251.09	1800	6.83	10.27	7.64	9.84	9.95	11.38	23.82	29.41
275.00	251.24	2000	7.29	10.81	8.19	10.08	10.67	12.11	25.58	31.43
275.00	251.50	2248	7.75	11.43	8.94	10.35	11.38	12.97	27.66	33.77

Proposal of an unconventional methodology of calculation

Table 2 summarizes the maximum depth of scour estimated for several hydrodynamic conditions (presented in Table 1) downstream Río Hondo Dam stilling basin, for application of the equations of different authors, based on the ski-jump configuration and scour downstream stilling basins hypothesis.

Even if it is usual to have a large dispersion between the results obtained by means of equations of different authors, developed for diverse hydrodynamic and river bottom conditions, Table 2 shows that the maximum depth of scour predicted as ski-jump configuration expressions and predicted with equations for erosion downstream stilling basins is in all cases bigger than the data measured in prototype.

The authors propose an unconventional methodology, based in the following idea: even if the structure is a stilling basin with baffle piers for forced energy dissipation, the critical flow over the end sill generates a new hydrodynamic condition, and the accelerated flow acts on the river bottom as a submerged jet, such as the hydrodynamic configuration of a ski-jump spillway, but with very low hydraulic head.

The proposed methodology of maximum depth of scour estimation is based in the equation [3], considered that the “ski-jump floor” level is given by the top of the end sill level, and the total head (Hups – Hdown) must to be calculated as:

$$\Delta H = h_d + V_d^2/(2\ g).$$

This equation takes into account the friction energy losses along the flow through the spillway and the stilling basin and the local energy losses due to the baffle piers and end sill.

By means of the authors proposed methodology the maximum depth of scour estimated for the maximum recorded flood was y = 5.26 m (as it is showed in Table 2), very closed with the measured value in prototype.

This methodology is proposed for maximum depth of scour downstream stilling basins when the sediment discontinuity generates an important decreas of the tailwater level and a critical flow is produced at the end of the structure. This abnormal situation is frequent in small dams in the northwest region of Argentina.

CONCLUSIONS

Due to the progressive decrease of the river bottom downstream Río Hondo Dam produced by the reservoir sedimentation, during more than forty years, the tailwater level is now below the sequent depth and the hydraulic jump cannot be contained in the stilling basin.

From discharge of 500 m^3/s to the maximum design discharge of 2248 m^3/s, the Froude Number over the end sill is practically Fd = 1, and the end sill acts as a control section. The flow downstream the stilling basin is accelerated with the obvious effect of the increasing the local scour. The structure acts as a ski-jump but with strong energy losses along the spillway and stilling basin (due to baffle piers, friction losses and end sill).

The authors propose an unconventional methodology, based in the following idea: even if the structure is a stilling basin with baffle piers for forced energy dissipation, the critical flow over the end sill generates a new hydrodynamic condition, and the accelerated flow acts on the river bottom as a submerged jet, such as the hydrodynamic configuration of a ski-jump spillway, but with very low hydraulic head.

Taking into account this study, the authors proposed two actions that can be developed in different stages.

First of all, the bed protection by means of two layers of graduated stones over a synthetic filter.

The second action can be delayed in time. The goal is to avoid the bed degradation downstream the dam, by means of the bed control with small sills constructed with local elements, increasing gradually the tailwater level to allow the hydraulic jump location into the stilling basin.

As it is showed, a mixed protection solution (structural and non structural) was proposed. It needs the execution of diverse works and a continuous bed river behavior monitoring.

REFERENCES

(1) MASON, P.J. and ARUMUGAM, K.: "Free jet scour below dams and flip buckets", en ASCE, J. of Hydraulic Engineering, 1985, Vol. 111, Nº 2, pp. 220-235.

(2) CHIVIDINI, M., LOPARDO, R.A., VERNET, G.F. and ANGELACCIO, C.M.; "Evaluación de la socavación máxima aguas abajo de aliviaderos en saltos de esquí" *(Maximum scour estimation downstream ski-jump spillways),* Anales del XI Congreso Nacional del Agua, Córdoba, Argentina, Vol. 6, 1983, pp. 187-210.

(3) LOPARDO, R.A. and SLY, E.: "Constatación de la profundidad de erosión aguas abajo de aliviaderos en salto de esquí" *(Verification of scour depth downstream ski-jump spillways),* 1991, Revista Latinoamericana de Hidráulica, São Paulo, Brazil, Nº 4, 1992, pp. 7-23

(4) RIEDEL GRUNWALDT, R.: "Socavación aguas abajo del salto de esquí del vertedero de la presa de Colbún" *(Scour downstream the Colbún ski-jump spillway")*, IX Congreso Nacional de la Sociedad Chilena de Ingeniería Hidráulica, Santiago, Chile, 1989.

(5) SPURR, K.J.W.: "Energy approach to estimating scour downstream of large dams", en Water Power and Dam Construction, jully 1985, pp. 81-89.
(6) LEMOS, F. O. and RAMOS, C.M.: "Hydraulic modelling of free jet energy dissipation", Symposium on Scale Effects in Modelling Hydraulic Structures, edited by H. KOBUS, Esslingen am Neckar, Germany, 1984, pp. 7.6/1-7.6/5.
(7) KEMING, A. and CHUANLONG, W.: "Free jet scour to rock riverbed", en XXII Congrès IAHR, Seminaire sur Dissipation d'énergie, Lausanne, Suitzerland, 1987.
(8) ALTINBILEK, H.D. and BASMACI, Y.: "Localised scour at the downstream of outlet structures", XI Congrès des Grands Barrages, Madrid, Spain, 1973, Q. 41, R. 7, pp. 105-122.
(9) FRANKE, P.: "Über kolkbildung und kolkformen", Osterreichische Wasserwirstschaft, Jargang 12, Heft 1, 1960, pp. 11-16.
(10) WANG, Shixia: "Scouring of riverbeds below sluices and dams", Design of Hydraulic Structures, edited by A. R. KIA y M. L. ALBERTSON, Colorado State University, Fort Collins, USA, 1987, pp.295-3046.
(11) BOUVARD, M.: Barrages mobiles et prises d'eau en rivières, Eyrolles, Paris, France1960.
(12) CATAKLI et Al.: "A study of scours at the end of stilling basin and use of horizontal blams as energy dissipators", XI Congrès des Grands Barrages, Madrid, 1973, pp. 25-37.
(13) BREUSERS, H.N.C. and RAUDKIVI, A.J.: Scouring, Balkema, Rotterdam, 1991.
(14) LOPARDO, R.A.: Erosión local aguas abajo de estructuras hidráulicas, *(Local scour downstream hydraulic structures),* Curso Internacional sobre Ingeniería de Ríos, Universidad Nacional de La Plata, Argentina,2000.

Survey of Bridge Damages Due to a Heavy Rain in Northern Part of Kanto Region, Japan

Jiro Fukui[1] and Masahiro Nishitani[2]

ABSTRACT

Many kinds of damages due to the deterioration of structural member, earthquake, scour and ground deformation have occurred at the bridge foundations in Japan. Among them, the scour damages during floods are extensive. First, in this paper, the authors present the actual situation on the damage due to the bridge scour in Japan, particularly highlighting of damages occurred due to the heavy rain on August of 1998 in Fukushima and Tochigi prefectures (Northern Part of Kanto Region). Then, they try to analyze the characteristics of the foundation type incident to be damaged by scour.

1. INTRODUCTION

A concentrated intensive rainfall in the northern part of Kanto region at the end of August 1998 brought a cumulative rainfall of 1,200 mm and a maximum rainfall of 90 mm/hour, causing serious damages in the region (Fig. 1). Not only did the number of dead, the number of missing people, and the number of dwelling damaged all reach levels rarely seen in recent years, the rain inflicted severe damages on the road traffic infrastructures with inundations, sediment disasters, and damaged bridges forcing the closing of both expressways and national highways (hereafter, N.H.), etc. at 645 locations. This paper summarizes results of the survey of bridge damages caused by the rainfall.

2. SURVEY RESULTS

2.1 Outline of Damages

It was confirmed that 14 of 16 bridges examined in this survey had been damaged in some way. The damages are presented in Table 1.

[1] Team Leader, Structures Research Group, Public Works Research Institute, Independent Administrative Institute, 1-6 Minamihara, Tsukuba, Ibaraki, 305-8516, Japan
[2] Senior Researcher, ditto

A breakdown of the type of damage reveals that bridge abutments were damaged at 11 bridges and that damage to bridge piers occurred at 3 bridges.

One characteristic of this disaster is that the access road behind the abutment was washed away at 10 of 11 bridges that suffered abutment damages with the only exception being the Kumagawa Bridge. Among these bridges, the bodies of the left bank abutment of the Yosasa Bridge (N.H. No.4) and of the right bank abutment of the Kurokawa Bridge (Prefectural Road) were also washed away, allowing the spans they supported to collapse. At the Habuto Bridge, scouring caused the downstream side of the abutment to settle down and tilt. Damage to piers was, in all cases, settlement and tilting caused by scouring.

2.2 Characteristics of the Damage

2.2.1 Washing Away of the Access Road behind an Abutment (Yosasa Bridge, N.H. No.294)

The Yosasa Bridge is a simple RCT girder bridge with four spans and a total length of 37.4 m across the Yosasa River (constructed in 1927). The foundations of both abutments and piers are spread foundations.

This deluge washed away the soil behind the abutment on the right bank along with a 60 m long section of the access road (Photo 1). Moreover, on the left bank side, soil was washed away (length of 10 m) on the downstream side of access road. The examination of the superstructure revealed that part of the railing was damaged by overflow water, but no damage was found on the body of the substructure. The following process caused the damage to the soil behind the right bank side abutment.

Because the flood was much greater than the capacity of a channel section of the river, flood water overflowed at the slightly curved right bank close to 200 m upstream of the Yosasa Bridge, and as they flowed, they washed away the access road. The damage behind the left bank abutment was caused by the suction of the soil resulting from the increased flow.

2.2.2 Scouring of an Abutment at Water Colliding Front (Habuto Bridge)

The Habuto Bridge is a simple RCT girder bridge with 4 spans and a total length of 84 m across the Abukuma River (constructed in 1969). The foundations of both abutments and piers are spread foundations. The Abukuma River bends gently towards the right near this bridge.

The flood tilted the abutment on the left bank side that was the outside of this curve to the downstream side and twisted the superstructure. This resulted in cracking, apparently caused by shearing, in two girders on the upstream side.

As Photo 2 shows, on the downstream side of the abutment, the soil behind the abutment washed away with even some soil on the upstream side washed away.

It is assumed that the scouring damage was caused by the direct impact of the flood water on the revetment near the left bank side abutment, and suction of the soil resulting from the vortex which were formed during the flood.

2.2.3 Settlement and Tilt of a Pier Caused by Scouring (Kumado Bridge)

The Kumado Bridge is a simple RCT girder bridge with 3 spans and a total length of 30 m across the Kumado River (constructed in 1935). The foundations of both abutments and piers are spread foundations. Like the Habuto Bridge, it is constructed at a point on the Kumado River where the river bends greatly to the right.

Its left bank side abutment was undamaged because it was protected by a concrete revetment and a spur dike, but the pier on the outside of the bend in the river was damaged by scouring.

As shown in Photo 3, the damaged pier settled 2.3 m on the upstream side and tilted by about 20 degrees to the upstream side. This was accompanied by serious deformation of the superstructure and damage such as pulling out of anchor bolts at the bearing, damage to the railings and so on.

In order to clarify the state of streambed near the pier following the flood, the river was partly blocked to alter its flow and a survey was performed, but because of secondary sedimentation, it was not possible to visually confirm the state of scouring.

For this reason, boring explorations were performed at two locations about 4 m upstream from the pier foundation, and although the results for both boring confirmed that there were a clay and a silty layer respectively that were resistant to scouring near the bottom surface of the pier foundations, it was difficult to decisively relate this to the scouring depth.

2.2.4 Settlement and Tilt of a Pier by Scouring (Hosokura Bridge)

The Hosokura Bridge is a simple steel I girder bridge with 6 spans and a total length of 123 m across the Abukuma River. It has spread foundations. The river near this bridge is straight, but because the river is wide and there is a curve about 700 m upstream from the bridge, it is hypothesized that the axis of the flooding stream was located near the left bank. In the following explanation, the piers will be called P1 to P5 from the left bank.

As shown in Photo 4, it was confirmed that P1 settled and tilted and that this pulling out anchor bolts at the upstream side bearing supports on P1 and the

downstream side bearing supports on P2. The results of measurements performed at the road surface reveal that the settlement of P1 was 80 cm on the upstream side and 60 cm on the downstream side, and that this caused an angle of tilt of 4.3 degrees in the upstream - downstream direction.

In order to survey the state of scouring near the damaged P1, a radio-controlled boat was used to measure the shape of the streambed. Fig. 2 shows the results of this survey. An attempt was made to also measure the downstream side of the pier during this survey, but it was impossible to do so because the boat came up many times with numerous obstructions on the streambed.

As Fig. 2 clearly shows, the streambed is deep surrounding a location close to the upstream side of the P1, and it was possible to confirm that scouring occurred in this area.

It has been concluded that the damage occurred because near the left bank where the flow rate is high, the P1 has large flow resistance resulting in scouring of the streambed.

3. ANALYSIS

Based on the results of the survey described above, it is possible to prepare the following categorization of the highway bridge damage patterns caused by this concentrated intensive rainfall.

a. Washing away access roads behind abutments

b. Washing away abutments

c. Settlement and tilt of abutment foundations as a result of scouring

d. Settlement and tilt of pier foundations as a result of scouring

Table 2 presents the results of categorizing the bridges according to these four damage patterns.

As pointed out based on Table 2, the first characteristic of the bridge damage caused by this intensive rainfall is the fact that the most common form of damage to occur was, as stated above, damage to access roads behind abutments and that the length that was washed away ranged from about 10 m to more than 100 m. These cases of damage were not a result of a structural defect in the damaged abutment nor in the nearby revetments. Because in each case, the capacity of the channel section of the river was smaller than the quantity of flood water, the flood water overflowed the channel, washing away the soil behind the abutment.

When the abutment was subjected to the resistance of the flowing flood waters after the soil behind it had been washed away, it was extremely unstable and,

therefore, susceptible to slippage or overturning. It is not possible to draw a conclusion, but it assumed that the abutment itself was washed away as in damage pattern b.

The second characteristic is that many abutments and piers were damaged by scouring. Damage to seven bridges, that occupy half of all the damaged bridges, is one defined as damage patterns c and d. At 5 of these 7 bridges, the settlement and tilting of the substructure caused severe damage to the superstructure, and the damage was a result of insufficient embedding depth of the foundation or damage to revetments near the abutment in all cases.

The scouring at the bridges occurred near the center of the river where the river is nearly straight, but where the river is curved, the scouring appeared near the outer bank of the curve, indicating that damage is concentrated close to the location of the axis of the stream during flooding.

4. CONCLUSION AND FUTURE WORKS

In Japan, the safety of bridges against flood conditions is assessed in advance based on the results of inspections conducted at regular intervals. But in order to provide effective crisis management including guaranteeing evacuation and rescue routes during concentrated intensive rainfall, a careful and rational judgment method on the risk to highway bridges must be provided.

The Public Works Research Institute has developed a scouring monitoring system in order to meet these demands for such technology. It will be possible to use the system to measure scouring of bridge foundations in real time simply by attaching simple measurement devices to existing bridges. A trial system has been fabricated, was installed on an actual bridge, and confirmative testing of the system is now in progress. The survey method using a radio-controlled boat that was mentioned in this paper cannot be used during floods, but it is a technologies that can be used to assess the conditions of streambeds easily and cost-effectively. Beginning with work to bring these technologies to the practical stage, the authors will continue to endeavor to develop disaster prevention technologies for use during floods.

REFERENCES

1. K. Tokida, J. Fukui, M. Nishitani et al., Investigation Report on the damages due to the heavy rain on August of 1998 in Fukushima and Tochigi prefectures, Technical Memorandum of PWRI, Public Works Research Institute, No.3793, 2001.3.

2. J. Fukui and M. Otuka, Inspection Method on Scour Condition around Existing Bridge Piers, First International Conference on Scour of Foundations, 2002.11.

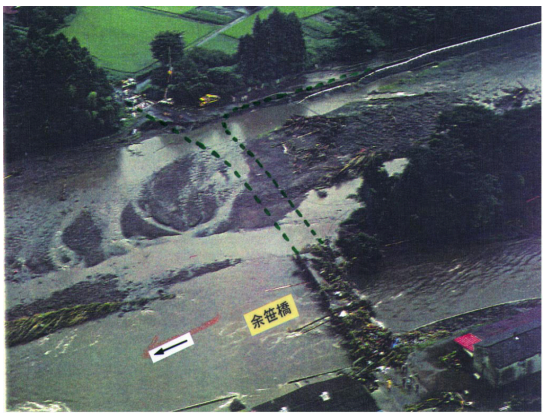

Photo 1 - Yosasa Bridge

Photo 2 - Habuto Bridge

Photo 3 - Kumado Bridge

Photo 4 - Hosokura Bridge

Table 1 - Outline of the Damage

No.	Bridge	Route Name	Number of spans	Superstructure	Substructure	Foundation	Outline of the Damage
1	Nozaki	N.H Route4	5	Simple steel box girder	RC wall type	—	・Part of the side walk and access road behind the right bank abutment were scoured.
2	Kumagawa	N.H Route4	1	Simple girder	—	—	・Revetments around the right bank abutment were scoured.
3	Yosasa	N.H Route4	6	Simple girder	Rigid frame type	Spread foundation	・The left bank abutment and access road were washed away for about 60m, and one girder supported by this abutment fell down. ・Revetments around the right bank abutment were scoured.
4	Yosasa	N.H Route294	4	Simple RCT girder	Abutment: semi-gravity type Pier: RC rigid frame type	Spread foundation	・The access road behind right bank abutment was washed away for about 60m, and the downstream side backfill of left bank abutment was scoured for about 10 m. ・Part of the railing was damaged by overflow.
5	Kyowa	Municipal Road	5	—	—	—	・The access road behind left bank abutment was washed away for about 150m. ・Three of the five girders were washed away.
6	Terako	Regional Road	3	Simple RCT girder	Abutment: gravity type Pier: wall type	—	・The access road behind right bank abutment was washed away for about 35m. ・Part of the railing was damaged by overflow.
7	Kurokawa	Regional Road	1	Simple RCT girder	Abutment: gravity type Pier: wall type	Spread foundation	・The access road behind right bank abutment was washed away for about 10m. ・Part of the railing was damaged by overflow.
8	Kurokawa	Prefectural Road	2	Simple RCT girder	Abutment: gravity type Pier: wall type	Spread foundation	・The right bank abutment and access road were washed away for about 10m, and one girder supported by this abutment was also washed away. ・Part of the railing was damaged by overflow.
9	Habuto	Principal Regional Road	4	Simple RCT girder	Abutment: gravity type Pier: wall type	Spread foundation	・The left bank abutment was tilted in the downstream direction with settlement about 1.2m on the downstream side by scouring of backfill on the downstream side. ・The tilt of this abutment caused cracking of the abutment wall and the girder, and damage to the railings.
10	Kaishin	Prefectural Road	1	Simple RCT girder	Abutment: gravity type	Spread foundation	・When the road was widened, this bridge was expanded by constructing new abutments on its downstream side. Scouring caused old abutments to settle down about 2 m at both banks resulting in the collapse of the girder. ・Backfill of abutments on the upstream side of the right bank and the downstream side of the left bank was washed away.
11	Kumado	N.H Route294	3	Simple RCT girder	Abutment: gravity type Pier: wall type	Spread foundation	・The pier on left bank side settled by 2.3 m on the upstream side, and its body tilted by 20 degrees under the effects of scouring. ・Settlement and tilt of the pier caused the girder to settle and damaged railings.
12	Itahagi	Municipal Road	4	Simple RC girder	Abutment: gravity type Pier: pile bent type	Spread foundation	・Scouring caused settlement of the piers about 10 cm at the center of the river.
13	Heisei	Municipal Road	1	Simple RCT girder or PCT girder	Abutment: reverse T type	—	・The access road behind left bank abutment was washed away for about 10 m.
14	Hosokura	Municipal Road	6	Simple Steel I Girder	Pier: wall type	Spread foundation	・Scouring caused the pier closest to the left bank to settle about 50 cm, and to tilt in the upstream direction. ・Settlement and tilt of the pier twisted the girder and pulled anchor bolts from the bearing supports.

(Note) N.H. = National Highway

Table 2 - Damage Patterns

No.	Bridge	Route	Damage Pattern				Fatal Deformation of the Superstructure or Bridge Collapse
			a	b	c	d	
1	Nozaki	N.H. Route4	○				
2	Kumagawa	N.H. Route 4			○		
3	Yosasa	N.H. Route 4	○	○	○		○ (by Pattern b)
4	Yosasa	N.H. Route 294	○				
5	Kyowa	Municipal Road				○	○
6	Terako	Principal Regional Road	○				
7	Kurokawa	Principal Regional Road	○				
8	Kurokawa	Prefectural Road	○	○			○ (by Pattern b)
9	Habuto	Principal Regional Road	○		○		○ (by Pattern c)
10	Kaishin	Prefectural Road	○		○		○ (by Pattern c)
11	Kumado	N.H. Route 294	○			○	○ (by Pattern d)
12	Itahagi	Municipal Road				○	○ (by Pattern d)
13	Heisei	Municipal Road	○				
14	Hosokura	Municipal Road				○	○ (by Pattern d)

(Note) N.H. = National Highway

Damage Patterns
a: Washing away of access roads behind abutments
b: Washing away of abutments
c: Settlement and tilt of abutment foundations as a result of scouring
d: Settlement and tilt of pier foundations as a results of scouring

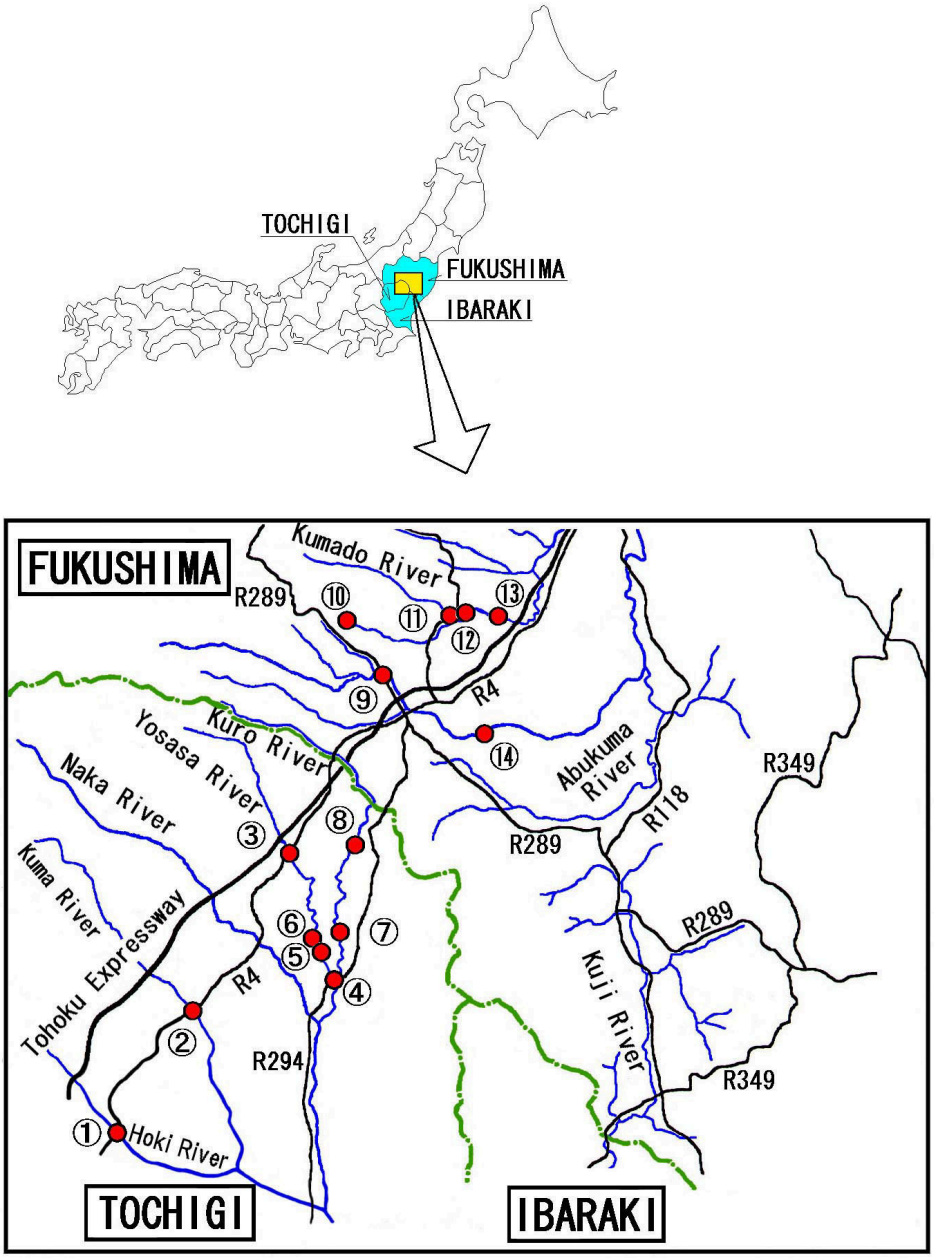

(Note) ①-⑭ : see Table 1

Fig.1 - Map of the Disaster Region
(Rivers, Principal Road and Bridge Location)

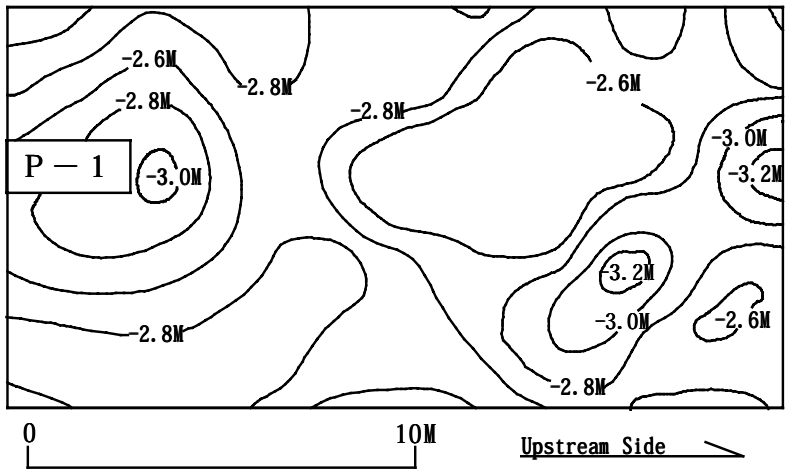

Figure 2. Contour Map of the River Bed
at the Hosokura Bridge

The SRICOS-EFA Method

Jean-Louis Briaud[1]

ABSTRACT

The SRICOS-EFA method is used to predict the scour depth versus time curve for complex pier and contraction scour in soils including sands, silts, clays, and soft rock. It consists of taking soil samples at the site, testing them in the EFA (Erosion Function Apparatus), and using the results as input to the SRICOS computer program. A hand calculation version of the method for preliminary design purposes also exists. The method is presented and comparisons between predictions and measurements at full scale are shown. A new approach to predict future hydrographs and perform risk evaluation is included.

SOIL CATEGORIES

Soils can be defined as loosely bound to unbound naturally occurring materials which cover the top few hundred meters of the Earth. By opposition, rock is a strongly bound naturally occurring material found within similar depths or deeper. At the boundary between soils and rocks are intermediate geo-materials. Classification tests and mechanical properties help to distinguish between those three types of naturally occurring materials and between different categories of soils. For soils, the classification tests consist of grain size analysis and Atterberg limits (Das, 2001). The D_{50} grain size is the grain size corresponding to 50% by weight of the soil passing a sieve of opening equal to D_{50}. The first major division in soils classification is between large-grained soils and fine-grained soils; large-grained soils have D_{50} larger than 0.075mm while fine-grained soils have D_{50} smaller than 0.075mm. Large-grained soils include gravels and sands which are identified on the basis of their grain size. Fine grained soils include silts and clays which are identified on the basis of Atterberg Limits. Large grained soils are typically referred to as cohesionless soils while silts and clays are typically referred to as cohesive soils.

ERODIBILITY: A DEFINITION

Erodibility is a term often used in scour and erosion studies. Erodibility may be thought of as one number which characterizes the rate at which a soil is eroded by the flowing water. With this concept erosion resistant soils would have a low erodibility index and erosion sensitive soils would have a high erodibility index. This concept is not appropriate; indeed the water velocity can vary drastically in rivers from 0 m/s to 5 m/s or more and therefore the erodibility is a not a single number but a relationship between the velocity applied and the corresponding erosion rate experienced by the soils. While this is an improved definition of erodibility, it still presents some problems because water

Professor and Holder of the Spencer J. Buchanan Chair, Dpt. of Civil Engineering, Texas A&M University, College Station, Texas 77843-3136, USA (briaud@tamu.edu)

velocity is a vector quantity which varies everywhere in the flow. It is much preferable to quantify the action of the water on the soil by using the shear stress applied by the water on the soil at the water-soil interface. Erodibility is therefore defined here as the relationship between the erosion rate $\dot{z}$ and the hydraulic shear stress applied τ (Figure 1). This relationship is called the erosion function $\dot{z}(\tau)$. The erodibility of a soil or a rock is represented by the erosion function of that soil or rock

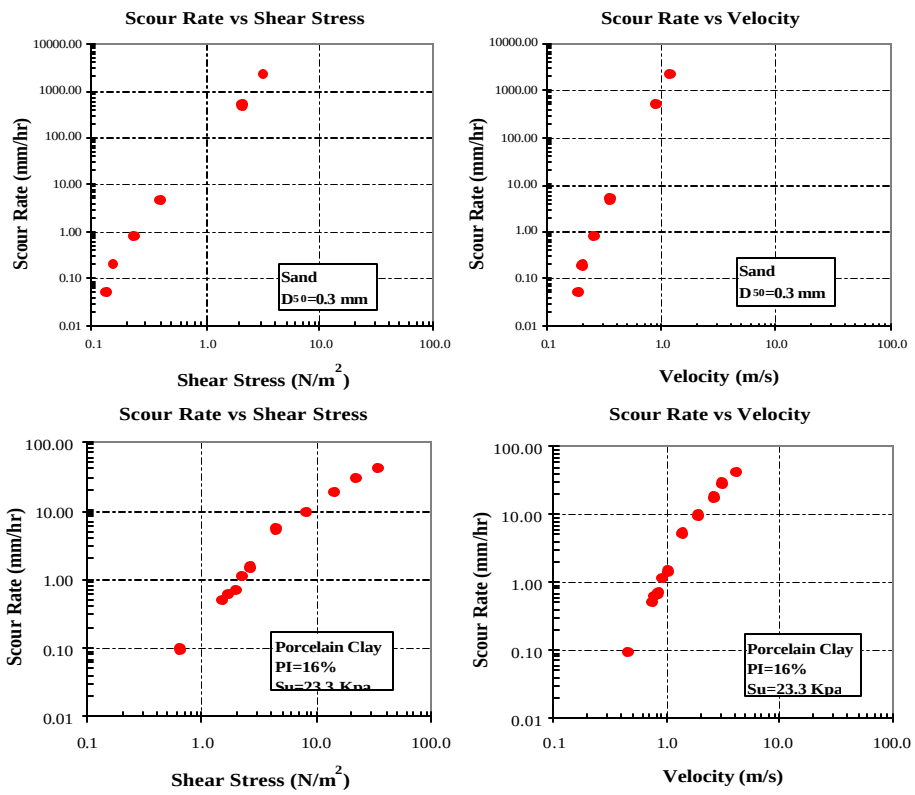

Fig. 1: Example of Erodibility Functions

THE EFA: EROSION FUNCTION APPARATUS

The EFA or Erosion Function Apparatus (Figures 2 and 3) (Briaud et al. 1999, 2001a) (http://www.humboldtmfg.com/pdf2/hm4000ds.pdf , http://tti.tamu.edu/geotech/scour) was conceived in 1991, designed in 1992, and built in 1993. The sample of soil, fine-grained or not, is taken in the field by pushing an ASTM standard Shelby tube with a 76.2 mm outside diameter (ASTM D1587) or by coring a soft rock sample (ASTM D2113). One end of the sampling tube full of soil or soft rock is placed through a circular opening in the bottom of a rectangular cross section conduit. A snug fit and an O-ring establish a leak proof connection. The cross section of the rectangular conduit is 101.6 mm by 50.8 mm. The conduit is about 1 m long and has a flow straightener at one end. The water is driven through the conduit by a pump. A valve regulates the flow and a flow meter is used to measure the flow rate. The range of mean flow velocities is 0.1 m/s to 6 m/s. The end of the sampling tube is held flush with the bottom of the rectangular conduit. A piston at the bottom end of the sampling tube pushes the soil until it protrudes 1 mm into the rectangular conduit at the other end. This 1 mm protrusion of soil is eroded

by the water flowing over it. The test measurements consist of the discharge from the flow meter and the time required for eroding the 1 mm protrusion. Several velocities are used and for each velocity, the erosion rate is measured. The data reduction consists of calculating the erosion rate $\dot{z}$ and the shear stress τ at the soil water interface. The shear stress is obtained from the velocity by using Moody's chart for pipe flow. The details are in Briaud et al.(2001a). The result of an EFA test is the erosion function (Figure 1). Over the years, a database of about 100 erosion functions on different soils and soft rocks has been accumulated at Texas A&M University. Repeated attempts at correlating some of the parameters describing the erosion function to basic soil properties failed to yield R^2 values higher than about 0.1 (Briaud et al., 2002). Therefore even if the concept of erodibility index was valid, it is very unlikely that a simple correlation with basic soil or soft rock properties exists.

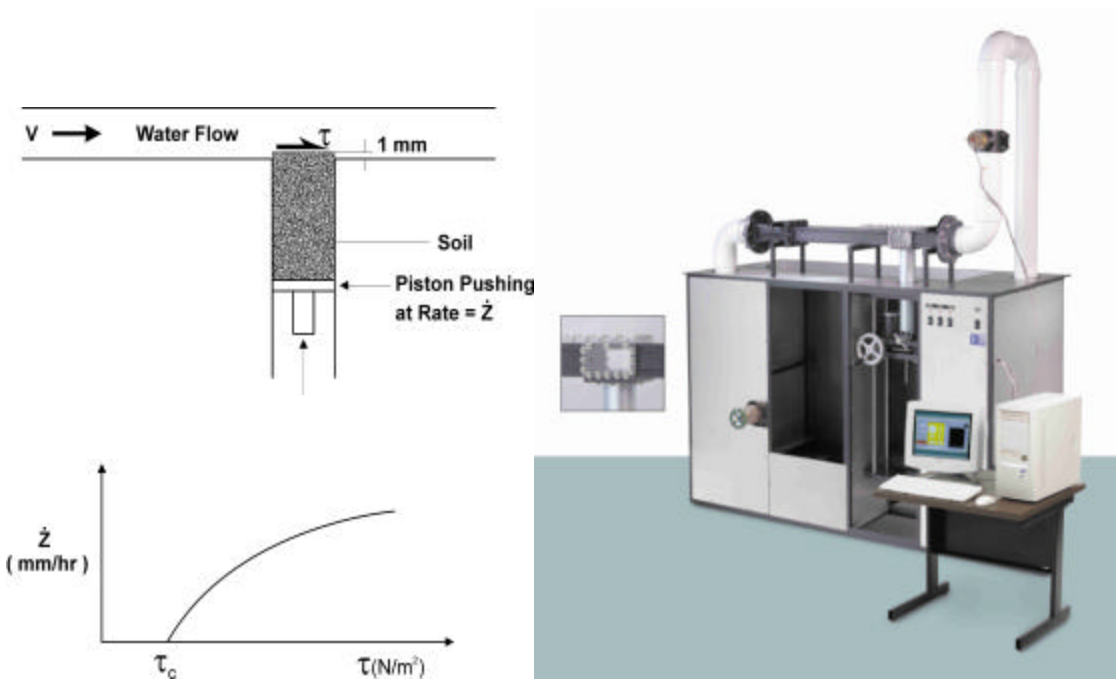

Fig. 2: Schematic Diagram, Result, and Photo of the EFA (Erosion Function Apparatus)

THE SRICOS-EFA METHOD

Now that the erodibility function or erosion function is obtained on a site specific basis with the EFA it is possible to use it to predict the scour depth versus time curve. In cohesionless soils, it is usually sufficient to calculate the maximum scour depth due to the design flood. Indeed, the scour rate in cohesionless soils is fast enough that one flood is long enough to generate the maximum scour depth for that velocity. This is rarely the case in cohesive soils and in rocks where only a fraction of the maximum scour depth may occur during the design flood. In cohesive soils and in rocks it can be very advantageous to predict the scour depth vs. time curve because ignoring it can be very conservative and costly. Ignoring the rate of erosion effect in cohesive soils may lead to unnecessarily deeper and more expensive foundations. An example of the difference

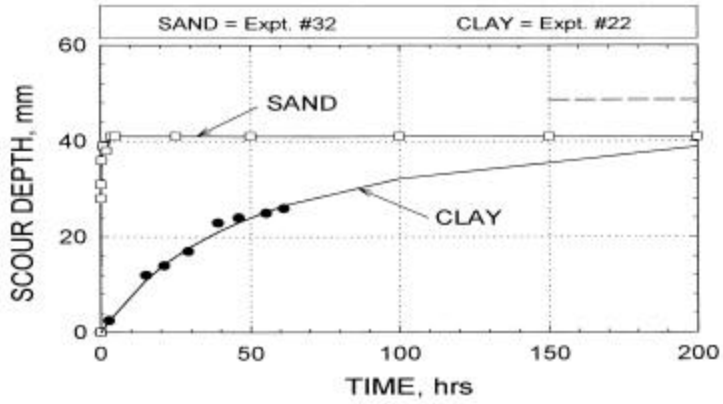

Fig. 3: Comparison between scour rate in sand and in clay for two flume experiments

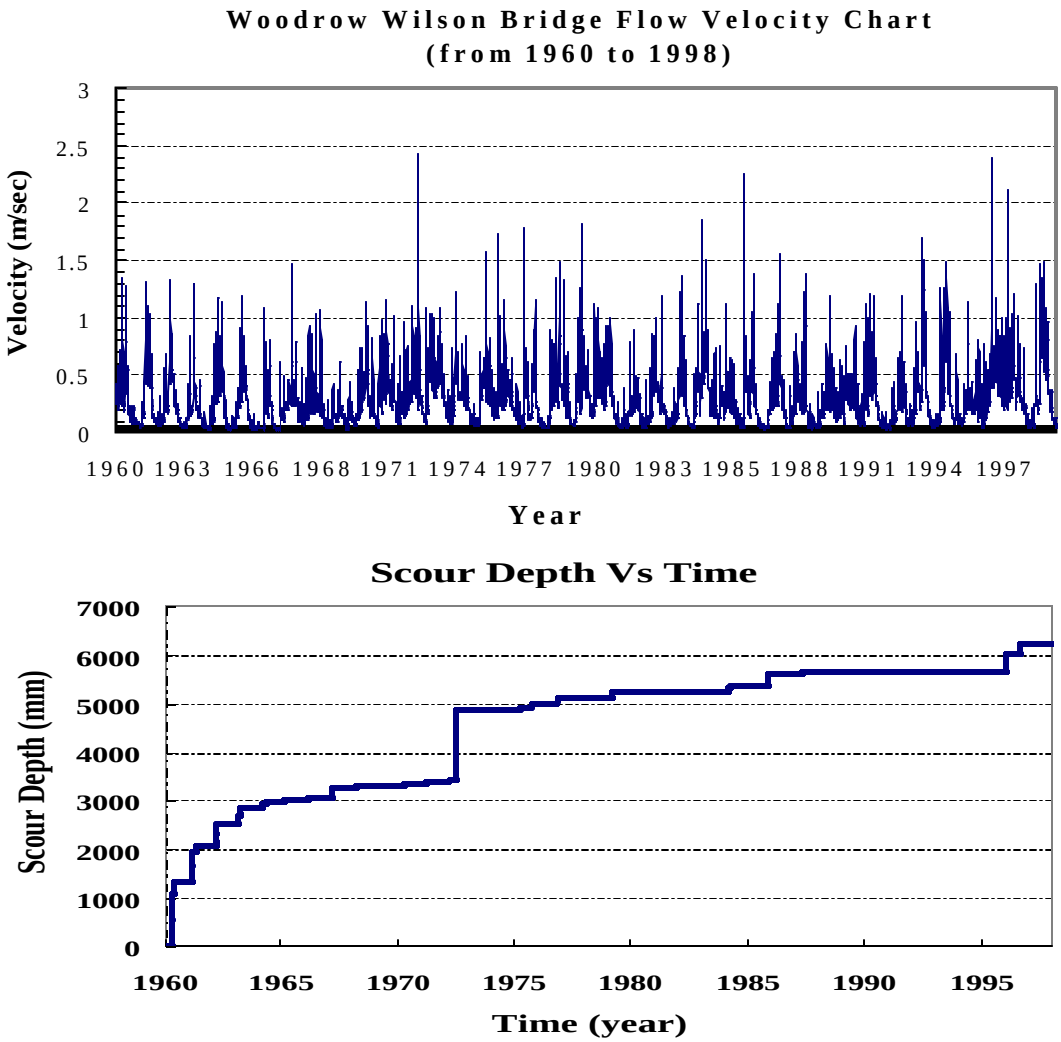

Fig. 4: Example of Output generated by the SRICOS-EFA Program.

between a scour depth versus time curve in a cohesionless soil and a cohesive soil is shown in Figure 3.

Figure 3 shows the scour depth vs. time curve for a constant velocity; however in reality the mean depth velocity in a river (Figure 4) varies significantly during the life of a bridge. The SRICOS-EFA method (Briaud et al., 2001b) was developed to predict the scour depth vs. time curve for bridges subjected to a varying velocity-time history in a layered soil or soft rock. The method can handle pier scour, contraction scour and the combination of the two occurring simultaneously. The solution for abutment scour is under development. The pier scour prediction includes circular and rectangular piers, shallow and deep water depth, different angles of attack, and the effect of pier spacing. The contraction scour prediction includes the effect of the contraction ratio, the length of the contracted channel, the water depth, and the transition angle.

The method consists of the following steps (Briaud et al., 2002):

1. Collect the input data: velocity and water depth hydrograph, geometry of the pier and of the contracted channel, erosion functions of the soil layers.
2. Calculate the maximum contraction scour depth for the ith velocity in the hydrograph.
3. Calculate the maximum complex pier scour depth using the ith velocity in the hydrograph at the pier location if there is no contraction scour in step 2, or the critical velocity for the soil if there is contraction scour in step 2.
4. Calculate the total pier scour depth as the total of step 2 and step 3.
5. Calculate the initial maximum shear stress for pier scour using the ith velocity in the hydrograph.
6. Read the initial scour rate corresponding to the initial maximum shear stress of step 5 on the erosion function of the soil layer corresponding to the current scour depth.
7. Use the results of steps 4 and 6 to construct the hyperbola describing the scour depth vs time for the pier.
8. Calculate the equivalent time for the given curve of step 7. The equivalent time is the time required for the ith velocity on the hydrograph to scour the soil to a depth equal to the depth scoured by all the velocities occurring prior to the ith velocity.
9. Read the additional scour generated by the ith velocity starting at the equivalent time and ending at the equivalent time plus the time increment.
10. Repeat steps 2 to 9 for the (i+1)th velocity and so on until the entire hydrograph is consumed.

The equations for the maximum scour depth values were developed on the basis of flume tests while the equations for the initial shear stress were developed from numerical simulations. The accumulation algorithms for velocity history and layering systems were constructed by using the concept of an equivalent time. Care was taken not to simply add the pier scour depth and the contraction scour depth. The details of the method as well as the manual for the SRICOS-EFA program can be found in Briaud et al. (2002). A simplified version of the method was also developed for preliminary design purposes. An example of that method is shown in Figure 5.

Problem: *Maximum flood velocity = 3 m/s*
Bridge design life = 75 years
Pier diameter = 2 m
Water depth = 5 m
What is the depth of scour after 75 years?

Solution: *S-SRICOS Method*

1. *Results of EFA tests gave the* $\dot{z}$ *vs* τ *curve shown.*
2. *Maximum hydraulic shear stress around the pier is:*

$$\tau_{max} = 0.094\ \rho v^2 \left(\frac{1}{logRe} - \frac{1}{10} \right) = 40\ N/m^2$$

3. *The initial rate of scour* $\dot{z}_i$ *is read on the EFA curve at* $\tau = \tau_{max}$. $\dot{z}_i = 6\ mm/hr$
4. *The maximum depth of scour* z_{max} *is*

$$z_{max} = 0.18\ Re^{0.635} = 3626\ mm$$

5. *Equivalent time*

$$t_e = 73 \left(t_{hydro} \right)^{0.126} \left(v_{max} \right)^{1.706} \left(\dot{z}_i \right)^{-0.2} = 573\ hrs.$$

6. *The equation for the* $z(t)$ *curve is*

$$z = \frac{t}{\frac{1}{\dot{z}_i} + \frac{t}{z_{max}}} = 1765\ mm\ \ after\ 75\ years$$

$z_{75\ years}$ *is 49% of* z_{max}

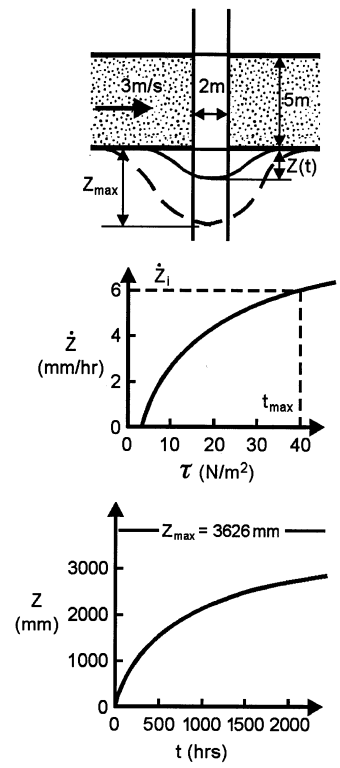

Fig. 5: Example of scour calculations by the simplified SRICOS-EFA method.

FUTURE HYDROGRAPHS AND SCOUR RISK ANALYSIS

Since the SRICOS-EFA method predicts the scour depth as a function of time, one of the input is the velocity versus time curve or hydrograph at the foundation location. This hydrograph should cover the period over which the scour depth must be predicted. A typical bridge is designed for 75 years. Therefore the design for a new bridge requires the knowledge of the hydrograph from the year of construction until that year plus 75 years. The question is: how can one obtain the future hydrograph covering that long period of time? This requires predicting the future over a 75-year period!

One solution is to use a hydrograph recorded at a nearby gauge station over the last 75 years and assume that the future hydrograph will be equal to the past hydrograph. If the gauge is not at the future bridge location, the discharge can be multiplied by the ratio of the drainage area at the bridge site over the drainage area at the gauge site. If the record at the gauge station is not 75 years long, one can simply repeat the recorded hydrograph until it covers the 75-year period. If the recorded hydrograph does not include the design flood (100 year flood or 500 year flood), one can spike the hydrograph with one or more of those floods before running the SRICOS program (Figure 6).

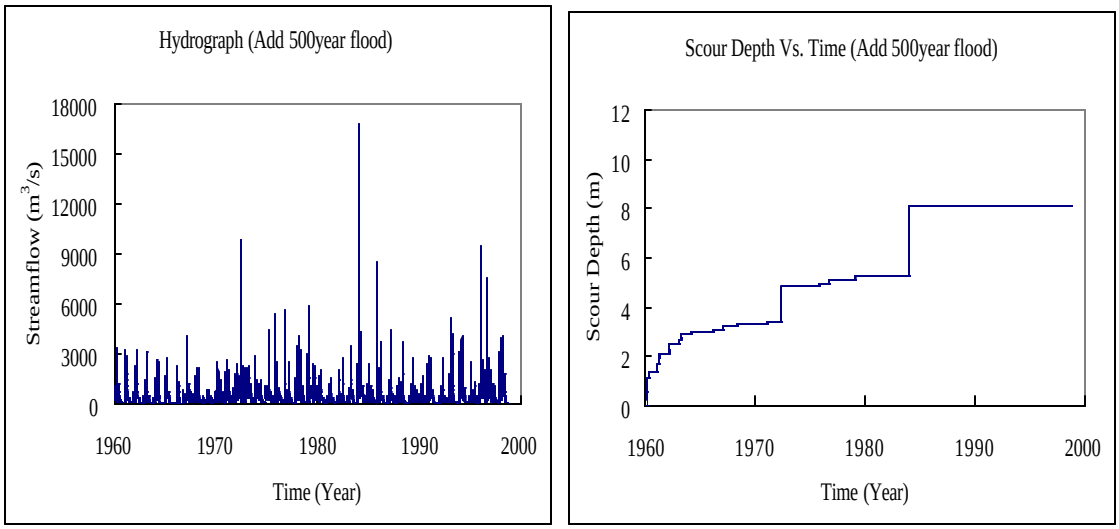

(a) Hydrograph (b) Scour Depth Vs. Time Curve

Fig. 6: Woodrow Wilson Measured Hydrograph spiked with a 500-year Flood

Another approach (Briaud, D'Odorico, 2002) consists of using a past hydrograph, preparing the frequency distribution plot for the floods within that hydrograph, sampling the distribution randomly and preparing a future hydrograph, for the required period, which has the same mean and standard deviation as the measured hydrograph (Figure 7). This process is repeated 10,000 times and, for each hydrograph, a final scour depth (the depth reached after 75 years of flow) is generated. These 10,000 final depths of scour are organized in a frequency distribution plot with a mean and a standard deviation. That plot can be used to quote a scour depth with a corresponding probability of occurrence, or better, to choose a risk level and quote the corresponding final depth of scour (Figure 8).

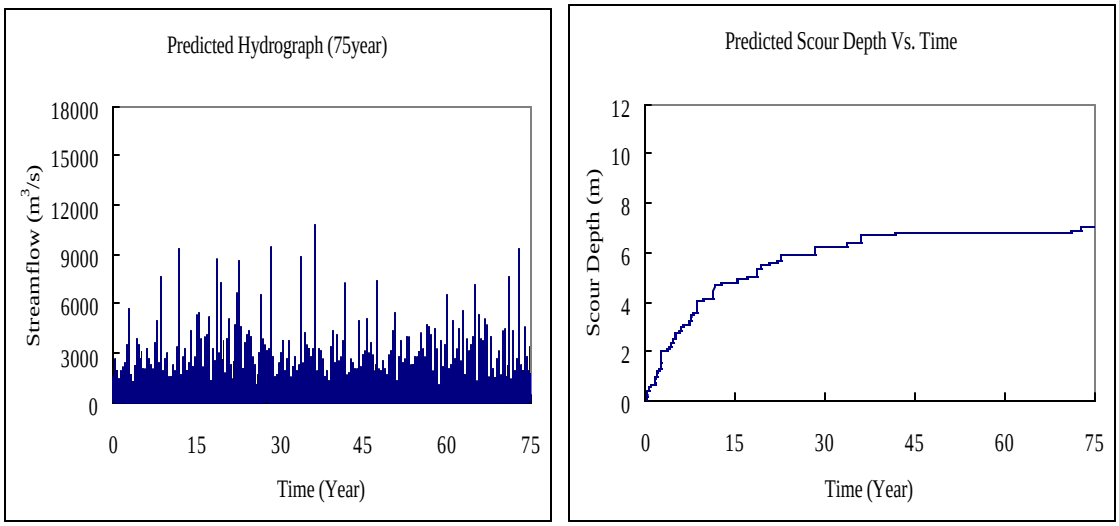

(a) Hydrograph (b) Scour Depth vs. Time

Fig. 7: Predicted Hydrograph and Scour Depth vs. Time Curve at Woodrow Wilson Bridge Site (Project time = 75year)

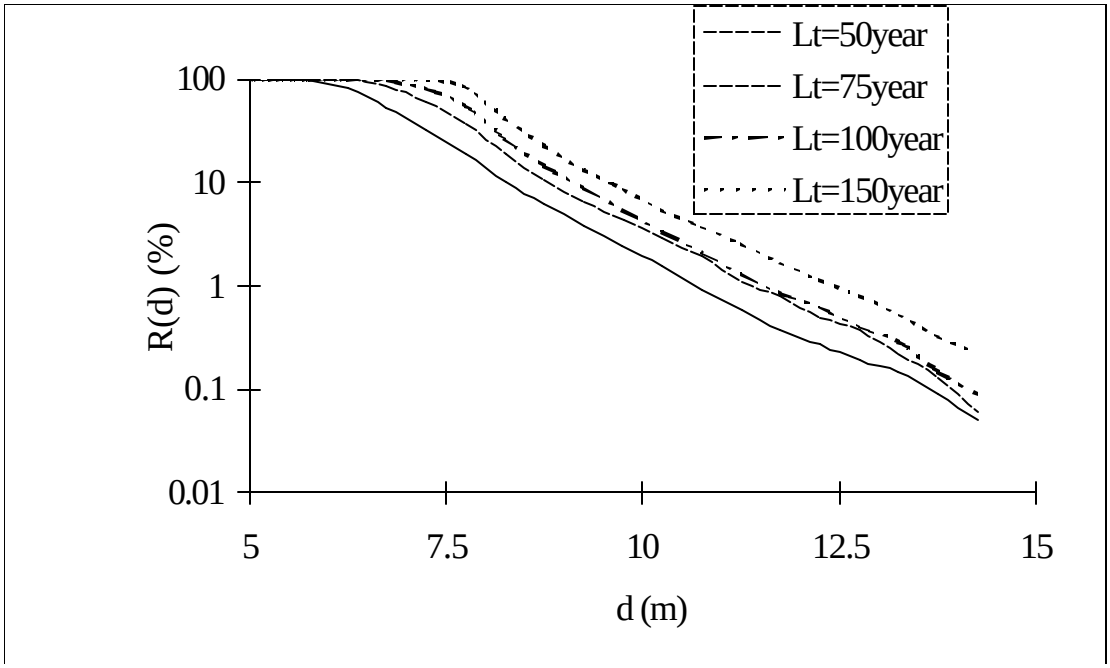

Fig. 8: Risk associated with different design values of the final scour depth, *d*, and different lengths of the project life, L_t

OBSERVATIONS ON CURRENT RISK LEVELS

In current design practice, the 100 year flood and the 500 year flood are used. If the design life of the bridge is L_t, the probability of exceedence or risk R for a flood having a return period T_r is given by:

$$R = 1 - (1 - 1/Tr)^{Lt} \quad (1)$$

If the design life of the bridge is 75 years, the probability that the flood with a return period of 100 year will be exceeded during the 75 year design life is 53% according to equation 1. Therefore the risk that the 100 year flood will be exceeded during the 75 years is 53% or about one chance out of two. For the 500 year flood, and for the same 75 year design life, the risk is 14% or one chance in about seven.

Even if a bridge designed for a 100 or 500 year flood experiences a 1000 year flood, this bridge may not collapse. Indeed collapse of the bridge is based on a different criterion than just exceedence of the design flood. There are numerous inherent redundancies in the design of a bridge and many design parameters have to be exceeded before collapse occurs. Nevertheless, the risk level associated with the floods used in everyday design appears very high compared to risk levels in other disciplines within Civil Engineering. For example the structural engineers have based their codes on a risk level of about 0.1%. The geotechnical engineers probably operate at about 1%. The scour engineers seem to operate at a much higher risk level. This is particularly worrisome since there is no factor of safety on the depth of scour passed on from the scour engineer to the geotechnical engineer for him to calculate the pile length.

VERIFICATION OF THE SRICOS-EFA METHOD

In order to evaluate the SRICOS-EFA method, 8 bridges were selected in Texas. These bridges all satisfied the following requirements: the predominant soil type was fine grained soils according to existing borings, the river bottom profiles were measured at two dates separated by at least several years, these river bottom profiles indicated anywhere from 0.05m to 4.57m of scour, a USGS gaging station existed near the bridge, and drilling access was relatively easy. The data for all bridges is listed in Tables 1 and 2.

For each bridge, Shelby tube samples were retrieved, tested in the EFA and the SRICOS-EFA method was used to predict the local scour at the chosen bridge pier location. One pier was selected for each bridge except for the Navasota River bridge at SH7 and the Trinity River bridge at FM787 for which two piers were selected. Therefore a total of 10 predictions were made for these 8 bridges. These predictions are not Class A predictions since the measured values were known before the prediction process started. However the predictions were not modified once they were obtained. The results are shown in Figure 9 and indicate a good comparison.

In addition to this verification process, the SRICOS-EFA method was compared to the to the HEC-18 method (Richardson, Davis, 2001) for complex pier scour using the data base developed by Mueller (1996). The results are shown on Figure 10 and 11. The good and safe comparison obtained for this predominently cohesionless soils database and the similarity of results with the HEC-18 method indicates that the range of applications of the SRICOS-EFA method is not limited to cohesive soils. One might ask: If the SRICOS-EFA method gives the same results as the HEC-18 method why do we need the SRICOS-EFA method? The answer is that the HEC-18 method cannot predict the rate of scour while the SRICOS-EFA method can. It is however reassuring to see that the SRICOS-EFA method is consistent with the HEC-18 method when it comes to the maximum depth of scour.

CONCLUSIONS

The SRICOS-EFA method was developed starting in 1991 and has matured over the last 11 years. The method makes use of the SRICOS computer program. A hand calculation version of the method also exists. The SRICOS-EFA method can handle the prediction of the scour depth versus time curve for complex piers and for contraction scour where the soil is sand, silt, clay, or soft rock. It has been verified against full-scale case histories and against large databases. The SRICOS-EFA method for abutment scour is being developed.

Table 1: Full Scale Bridges as Case Histories

Bridge	Pier Bent No.	Pier Width (m)	Pier Length (m)	Pier Shape	Skew Angle (°)	River Slope	Manning's Coefficient n	Max. Velocity (m/s)	True Duration of Hydrograph (yrs)
Navasota River at SH 7	3	0.36	0.36	Square	5	0.0010	0.035	2.54	41
Navasota River at SH 7	5	0.36	8.53	Square Nose	5	0.0010	0.035	3.82	41
Brazos River at US 90A	3	0.91	8.53	Round Nose	0	0.0011	0.035	4.20	33
San Jacinto River at US 90	43	0.85	0.85	Square	15	0.0012	0.035	3.07	10
Trinity River at FM 787	3	0.91	7.30	Round Nose	25	0.0011	0.035	2.00	17
Trinity River at FM 787	4	0.91	7.30	Round Nose	25	0.0011	0.035	4.06	17
San Marcos River at SH 80	9	0.91	14.2	Round Nose	0	0.0010	0.035	1.89	60
Sims Bayou at SH 35	3	0.76	0.76	Circular	5	0.0001	0.035	0.95	3
Bedias Creek at US 75	26	0.86	0.86	Square	0	0.0005	0.035	2.19	50
Bedias Creek at SH 90	6	0.38	0.38	Square	5	0.0010	0.035	1.54	18

Bridge	Distance between Pier and Boring (m)	Max. Shear Stress (N/m2)	Initial Erosion Rate (mm/hr)	Equivalent Time (hrs)	Predicted Local Scour (m)		Measured Local Scour (m)	Measured Total Scour (m)	Predicted Max. Local Scour (m)
					E-SRICOS	S-SRICOS			
Navasota River at SH 7	6.5	41.46	8.91	368.8	0.76	0.82	0.76	-	1.10
Navasota River at SH 7	16.1	86.53	22.39	616.0	1.24	1.29	1.41	1.80	1.42
Brazos River at US 90A	55.4	85.86	65.26	568.4	2.59	2.54	2.87	4.43	2.72
San Jacinto River at US 90	146.3	49.62	17.44	373.1	1.30	1.66	1.47	3.17	2.14
Trinity River at FM 787	37.8	22.46	50.60	155.1	1.53	1.40	2.17	4.57	1.70
Trinity River at FM 787	78.4	80.93	39.82	544.6	2.26	2.37	2.17	4.57	2.66
San Marcos River at SH 80	57.3	20.30	61.75	158.4	1.07	1.40	1.27	2.66	1.64
Sims Bayou at SH 35	20.0	26.71	2.69	63.0	0.29	0.14	0.05	-	0.95
Bedias Creek at US 75	33.0	16.31	127.44	172.5	1.66	1.61	1.35	2.13	1.74
Bedias Creek at SH 90	2.9	5.92	44.25	102.8	0.70	0.70	0.61	-	0.83

Table 2: Soil Properties at the Bridge Sites

Soil Properties	Bridge	Navasota		Brazos	San Jacinto			Sims
	Layer No.	1	2	1, 2	1, 2	3	4	1
	Depth (m)	1.8–2.4	4.9–5.5	13.0–13.7	5.3-6.1	6.9-7.6	7.6-8.4	3.0-3.7
Liquid Limit (%)		27.72	26.42	24.49	22.04	-	37.50	84.16
Plastic Limit (%)		14.29	6.25	9.41	9.09	-	12.71	16.05
Plasticity Index (%)		13.43	20.17	15.08	12.95	-	24.79	68.11
Water Content (%)		19.80	26.60	17.32	151.57	26.88	27.75	25.25
Mean Diameter, D_{50} (mm)		0.125	-	0.265	-	-	-	0.0012
Shear Strength (kPa)		43.10	32.10	45.49	23.94	4.78	21.53	23.00
Unit Weight (kN/m^3)		19.20	18.80	20.20	19.60	16.70	20.80	19.60
% Passing #200 Sieve		26.20	57.70	30.09	50.36	60.71	94.50	99.07

Soil Properties	Bridge	Trinity		San Marcos		Bedias 75		Bedias 90
	Layer No.	1	2	1	2	1	2	1
	Depth (m)	10.7-11.4	13.0-13.7	6.1-6.6	7.0-7.5	6.1-6.9	6.9-7.6	1.5-2.3
Liquid Limit (%)		-	42.24	41.34	40.31	47.86	-	55.08
Plastic Limit (%)		-	8.70	16.67	19.18	13.56	-	15.79
Plasticity Index (%)		-	33.54	24.67	21.13	34.30	-	39.29
Water Content (%)		7.67	22.22	22.00	24.40	18.07	17.50	23.63
Mean Diameter, D_{50} (mm)		6.00	-	-	-	0.048	0.130	0.040
Shear Strength (kPa)		9.57	11.48	27.30	29.67	10.00	32.00	62.00
Unit Weight (kN/m^3)		22.00	22.10	19.60	20.20	20.04	21.30	19.60
% Passing #200 Sieve		11.52	68.40	78.30	73.40	86.81	35.14	91.31

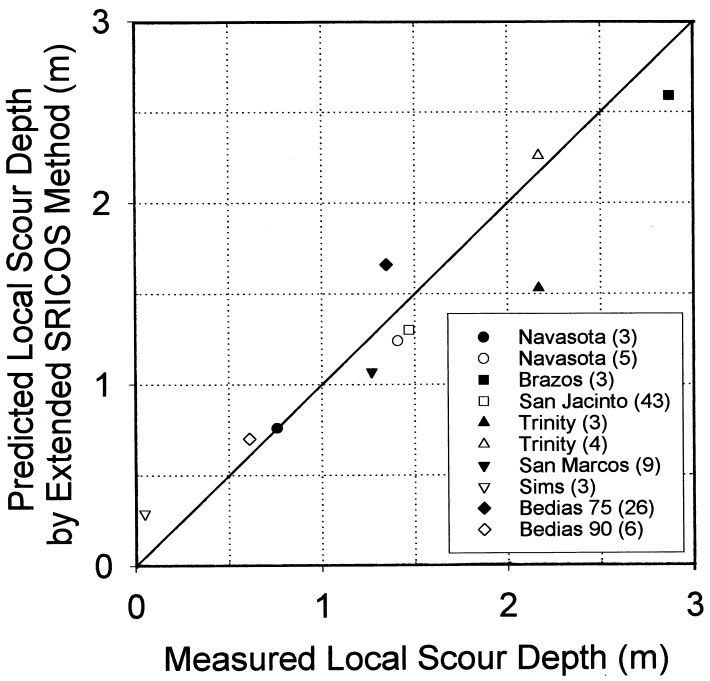

Fig. 9: Predicted vs Measured Local Scour for the E-SRICOS method.

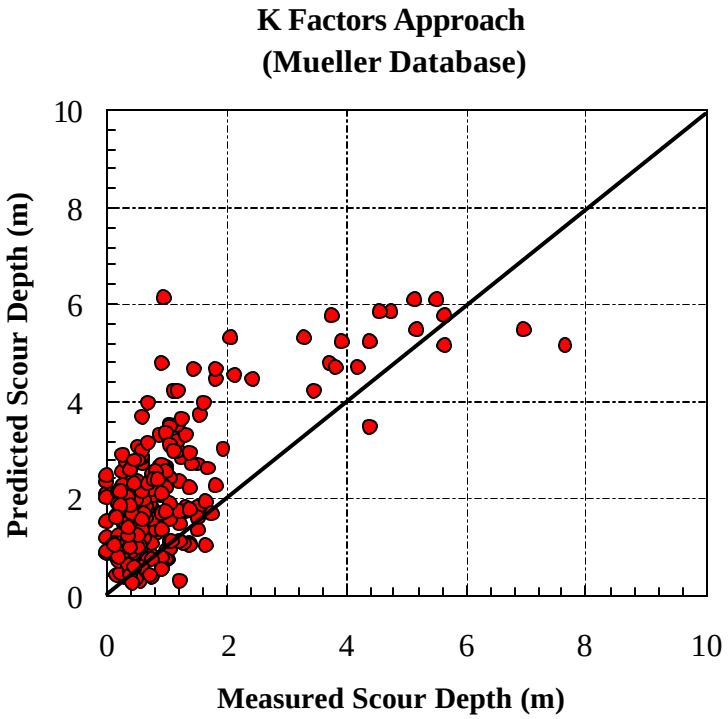

Fig. 10: SRICOS-EFA Predictions against Mueller (1996) Database

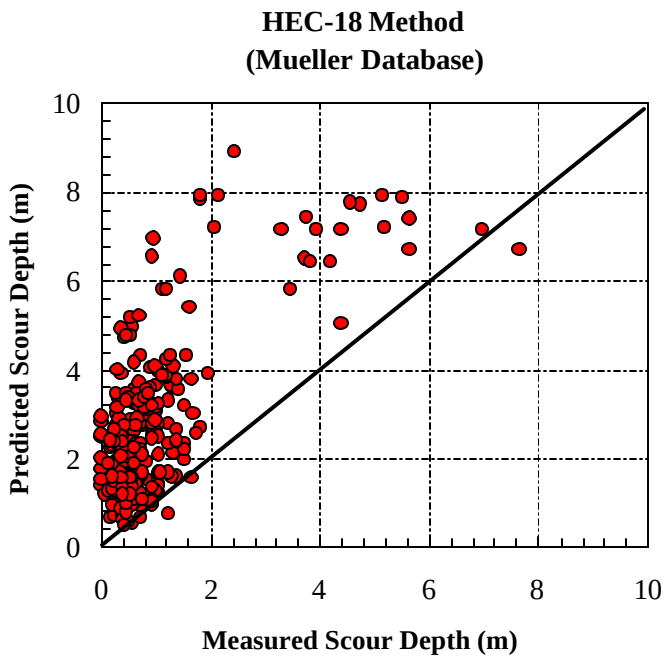

Fig. 11: HEC-18 Predictions against Mueller (1996) Database

ACKNOWLEDGEMENTS

Many organizations and individuals have contributed to the development of the SRICOS-EFA method. They are all thanked sincerely. Texas DOT, NCHRP, Maryland SHA, North Carolina DOT, Minnesota DOT, Illinois DOT, Texas Transportation Institute, Humboldt, H.-C. Chen, Francis Ting, Ya Li, Jun Wang, Prahoro Nurtjahyo, Kiseok Kwak, Yiwen Cao, Seung-Woon Han, Rao Gudavalli, Suresh Perugu, Gengshen Wei, Peter Smith, Tony Schneider, Melinda luna, Kim Culp, Jay Vose, Mark McClelland, John Delphia, Andy Kosicki, Stan Davis, John Boynton, Ryhad Wahad, Bill Moore, Steven Smith, Larry Arneson, Daryl Greer, Robert Henthorne, Rochard Phillips, Mehmet Tumay, Sterling Jones, Tim Hess, Mahir Al-Nadaf.

REFERENCES

1. Briaud, J.-L., Ting, F., Chen, H.C., Gudavalli, S.R., Perugu, S., and Wei, G., 1999, "SRICOS: Prediction of Scour Rate in Cohesive Soils at Bridge Piers", Journal of Geotechnical and Geoenvironmental Engineering, Vol.125, pp. 237-246, ASCE, Reston, Virginia, USA.
2. Briaud J.-L., Ting F., Chen H.C., Cao Y., Han S.-W., Kwak K., 2001a, "Erosion Function Apparatus for Scour Rate Predictions". Journal of Geotechnical and Geoenvironmental Engineering, Vol.127, No. 2, pp.105-113, ASCE, Reston, Virginia, USA.
3. Briaud, J. L., Chen, H. C. Kwak K., Han S-W., Ting F., 2001b, "Multiflood and Multilayer Method for Scour Rate Prediction at Bridge Piers", Journal of

Geotechnical and Geoenvironmental Engineering, Vol.127, No. 2, 2001b, pp.105-113, ASCE, Reston, Virginia, USA.

4. Briaud J.-L., Chen H.-C., Li Y., Nurtjahyo P., Wang J., 2002, "Complex Pier Scour and Contraction Scour in Cohesive Soils", Final Report for NCHRP Project 24-15, National Cooperative Highway Research Program, Transportation Research Board, Washington DC.
5. Briaud J.-L., D'Odorico P., 2002, "Future Hydrographs and Scour Risk Analysis", Proceedings of the First International Conference on Scour of Foundations, Texas Transportation Institute, College Station, Texas, USA.
6. Das B.J., 2001, "Principles of Geotechnical Engineering", Fifth Edition, Brooks and Cole, Pacific Grove, California, USA.
7. Mueller D.S. and Landers M., 1996, "Channel Scour at Bridges in the United States", Report FHWA-RD-95-184, Federal Highway Administration, Washington DC, USA.
8. Richardson, E. V., Davis, S. M., 2001, "Evaluating Scour at Bridges", Fourth Edition, Publication No. FWHA-NHI-01-001, HEC No.18, Federal Highway Administration, US Department of Transportation, Washington, D. C.

Failure Mechanisms of Riprap Layer Around Bridge Piers

By

Yee-Meng Chiew[1]

ABSTRACT

By summarizing research efforts on using riprap as a pier countermeasure over the previous decade, the paper highlights the deficiencies of riprap in arresting pier scour. To this end, five failure mechanisms are identified. They are shear failure, winnowing failure, edge failure, bedform-induced failure and bed-degradation induced failure. Each failure mechanism can singly or, more likely, combine to cause the eventual breakdown of the riprap layer. The study shows that a riprap layer is most vulnerable when subjected to bedform-induced failure, which is dominant under a condition where large dunes are present. This failure mechanism leads to embedment of the riprap layer, rendering it ineffective in arresting scour. It is postulated that a pragmatic solution is to adopt innovative idea, such as seepage induction, to reduce the size of the migrating dunes during high flows past the riprap layer.

INTRODUCTION

Much damage to bridges at river crossings can be attributed to scouring at bridge foundations. Citing examples of 143 bridge failures dating as far back as 1847, Smith (1976) reported that 66 failures were scour related. Using data collected in the USA, Shirole and Holt (1991) stated that 60% of the 1,000 plus bridges that failed could be attributed to scour. In the widely cited bridge failure that occurred in New York and New England in 1987, 17 bridges were either damaged or destroyed by scour (Richardson and Davis 1995). Melville and Coleman (2000) reported that at least one serious bridge failure each year on the average could be attributed to scour in New Zealand. All these data point towards an important relationship between bridge failure and scour at bridge foundation.

The threat of pier scour on the integrity of a bridge has been known for many years. The classical works on bridge pier scour was that by Chabert and Engeldinger (1956) and Laursen and Toch (1956). These early works and many others published in that era are summarized in the state-of-the art paper initiated by the IAHR Section on Fluvial Hydraulics. The result of the labor of the task

[1] Associate Professor, School of Civil & Environmental Engineering, Nanyang Technological University, Nanyang Avenue, Singapore 639798 (cymchiew@ntu.edu.sg)

force was published in Breusers et al. (1977). It is interesting to note that in the 42-pages paper, which comprises nine sections; only one section (Section 7) with approximately two full pages was devoted to pier scour protection. Three different types of scour countermeasures were discussed therein: (1) foundation caisson; (2) additional structures placed upstream: piles; and (3) riprap mats. The concerted effort of scour research undertaken in New Zealand over the past three decades (Melville and Coleman 2000) also revealed the lack of emphasis placed on the study of scour countermeasures. Citing the thirty-seven published reports between 1975-1994 from the New Zealand efforts, it is significant to note that only one was on riprap protection on pier scour.

Despite the apparent lack of research effort on methods to reduce pier scour, engineers throughout the ages have used many ingenious methods in an attempt to arrest pier scour, thereby safe-guarding the bridge from failure during floods. Engineering methods that were devised to deal with pier scour problems are not sophisticated. They can be categorized generally into two distinctive groups: flow-altering and armoring countermeasures. The function of the first group of pier scour protection method is the provision of a means to reduce the power of the eroding agents; i.e., the downflow and horseshoe vortex, which are primarily responsible for causing scour at the pier. The flow-altering group involves one of the following three methods:

(a) Installation of some form of structures upstream of the pier (e.g., sacrificial piles or sills);
(b) Modification of pier shape; and
(c) Provision of scour reduction devices on the pier (e.g., collars, plates or slots).

The function of the second group of scour countermeasure is to provide a physical barrier against scouring. The barrier is designed to withstand the eroding power of the local flow field around the bridge pier. In practice, it is in the form of large, heavy units that are not easily eroded. Parker et al. (1998) and Melville and Coleman (2000) provide excellent descriptions of examples of these two methods used as pier scour countermeasure.

When comparing the use of these two groups of countermeasures in the field, it is clear that the latter (i.e., armoring countermeasure) is used much more extensively in both hydraulic and coastal engineering. Use of a flow-altering countermeasure is limited; even testing of such devices in the laboratory is not extensive and is exclusively conducted under clear-water conditions. On the other hand, use of an armoring countermeasure is comparatively much more prevalent, especially the use of riprap. Engels (1929) dated the possible use of riprap at bridge sites as far back as 1893. Besides using riprap as a means to reduce pier scour, there are other alternative armoring devices such as cabled-tied blocks, reno mattresses, gabion mattresses, concrete-filled mats and bags,

concrete apron, dolos, tetrapods, etc. Some of these methods, such as dolos and tetrapods, are "borrowed" from coastal engineering practices. Their success as a pier scour countermeasure is as yet uncertain.

Although armoring countermeasures, especially riprap, have been used as a means to protect bridge piers against scour for more than a century, research efforts to-date inadequately examine how riprap behaves around bridge piers. Many earlier design recommendations (Neill 1973) were "loaned" from riprap practices used on riverbanks in alluvial rivers. No specific research has been conducted to explore riprap in the 3-dimensional flow field around piers. In recent years, this deficiency has begun to be addressed by growing research efforts. The main objective of this paper is to summarize knowledge gained from these recent research efforts. Highlighted herein are the deficiencies in riprap as a method for protecting bridge piers from scour. The paper also recommends further research into new and innovative ideas so as to render riprap a more reliable countermeasure in arresting scour.

FAILURE BEHAVIOR OF RIPRAP AROUND BRIDGE PIERS

The earlier studies on using riprap as a scour countermeasure at bridge piers were mainly conducted under clear-water conditions, which pertain to a stage of flow where no bedload sediment transport occurs in a channel. In other words, the undisturbed mean flow velocity is less than the critical velocity for bed sediment entrainment. Examples of some of these studies are Bonasoundas (1973), Neill (1973), Posey (1974), Hjorth (1975), Breusers et al. (1977), Richardson and Davies (1995) and Chiew (1995).

Based on a study conducted under clear-water conditions, Chiew (1995) identified three failure mechanisms that may destabilize riprap stones and lead to the breakdown of a riprap layer:

(a) Shear failure – where the riprap stones are entrained by the local flow field around the pier;
(b) Winnowing failure – where the finer underlying bed material is eroded through the voids or interstices of the coarser riprap stones under the action of turbulence and seepage; and
(c) Edge failure – where bed scouring at the periphery of the riprap layer undermines the armor stones.

Whilst the above mechanisms were originally identified as the main cause of failure for riprap layer around a bridge pier under clear-water conditions, it was subsequently confirmed (Chiew and Lim, 2000; Lauchlan and Melville, 2001) that they are also present under live-bed conditions. However, there is an additional failure mechanism associated with riprap protection that is unique in live-bed conditions where bedforms, such as dunes are present. Lim (1998) and

Chiew and Lim (2000) called it *bed feature destabilization,* and it was later referred to as *bedform undermining* by Melville and Coleman (2000). This mode of failure mechanism, which is called *bedform-induced failure* in this paper, was found to be the dominant mode of failure under conditions where large bed features are present in the flow.

All the four failure mechanisms have been observed in live-bed conditions when the undisturbed mean bed level of the river remains unchanged; i.e., in the absence of general scour of the alluvial bed. When the channel bed degrades, which can be caused by changes to the land use of the river catchment or more specifically due to direct human intervention such as excessive streambed mining and dam starvation, an additional mode of failure mechanism may destabilize the riprap. This type of failure may be called *bed-degradation induced failure*. As far as the author is aware, there have been only two studies on this failure mechanism to-date (Lauchlan and Melville 2002, and Chiew 2002). There are, however, distinct differences between the two studies and they are discussed in a latter section of the paper.

Shear Failure

Shear failure of a riprap layer around a bridge pier refers to the entrainment of the riprap stones by the local flow field. This occurrence simply means that the stones are not large or heavy enough to withstand the downflow and horseshoe vortex associated with the pier-scour mechanism for the given flow condition. Among all the five failure mechanisms outlined above, this is the easiest to conceptualize as one can clearly see the entrainment of individual stones in a laboratory experiment. For this reason, it is the most studied of all the failure mechanisms. To-date, there are a host of formulas available for use by bridge engineers seeking to find the appropriate riprap stone size. Lauchlan (1999), in her doctoral dissertation, compiled a list of these published equations and compared their performance. Some of these equations and their comparisons, which are also shown in Melville and Coleman (2000), are reproduced in Table 1 and Figure 1, respectively.

It must be pointed out that some of the 12 equations listed in Table 1 were derived semi-empirically, such as the equations proposed by Breusers and Raudkivi (1991) and Chiew (1995), whereas the others are purely empirically fitted equations, such as those by Bonasoundas (1973), Quazi and Peterson (1973) and Parola (1993). With the latter type, it is important to recognize the definition of failure - the criterion pre-determined by the researchers to assess whether a riprap layer has failed or not. In his work, Parola (1993) spelt out his definition of the critical condition, which is defined as "exposure of a portion of the painted gravel (stones in the middle of a 3-layer thick riprap layer), without removal of the painted layer over a period of about 30 minutes". It can be inferred from this definition that Parola considered the riprap layer has begun to

fail when one of the stones on the first layer of his riprap is entrained within a 30-minute duration. Conversely, the definition of failure in Croad (1997) refers to the condition where the riprap layer is completely disintegrated. Which of these two definitions accurately depicts actual failure is a matter yet to be determined. There is still no consensus amongst researchers as to the precise definition of failure of the riprap layer in laboratory studies. As a result, care is needed when comparing the results obtained from these equations.

Some of the equations listed in Table 1 were not originally designed for use in a bridge pier. Farraday and Charlton's (1983) equation is in fact the equation proposed by Maynord (1978) for bank or streambed erosion. This type of equation is no different from the design curve cited in Neill (1973); both of which were not originally intended for use in pier scour condition. Additionally, the commonly cited HEC 18 equation by Richardson and Davies (1995) was in fact a modified form of the Isbash equation, which again was not formulated specifically for bridge pier application. This predicament likewise applies to the equation proposed by Breusers et al. (1977), who also used the Isbash equation. Whether one could really use these equations designed for streambed and bank erosion and apply them in a pier-scour condition is debatable. The difference between the flow field responsible for erosion in both these conditions is unmistakable, and there is really no reason whatsoever that they should be transferable.

Notwithstanding the difficulties outlined above, these equations have formed a basis from which engineers and researchers in the field of pier scour protection would continue to explore new ways to arrive at a more reliable method for sizing riprap. The designers, on the other hand, would have to be satisfied with them until such time that a better set of equation becomes available.

A comparison of these 12 equations was done by Lauchlan (1999), and is reproduced in Figure 1. Although researchers in the area of the pure sciences may be appall with the lack of consistency of the data, researchers in sediment transport area is not unfamiliar with such variations. In fact, when compared with other sediment transport predictive equations, the bulk of the equations do give reasonably consistent results.

Notwithstanding the drawbacks of the equations discussed above, engineers are not overly concerned with this form of erosion – shear failure of the riprap stone. Generally, this mechanism seems not to be the controlling failure mechanism as larger stones than are necessary can always be used to avert this failure mechanism.

Winnowing Failure

In an alluvial channel, the process of winnowing occurs when a sediment bed comprising a layer of coarse particles overlay a bed of finer sediments. It refers to the erosion of finer sediment particles through the voids between the coarser ones. The extent of winnowing is dependent on the magnitude and type of flow, and the relative size of the overlying coarse and underlying fine sediment particles. Chiew (1995) described some experiments conducted in a 2-dimensional flow where winnowing is the dominant mode of erosion. In a 3-dimensional flow field, as is the case of flow around a bridge pier, winnowing is even more conducive because of the high level of turbulence. This is especially apparent if there are less than three layers of coarse stones making up the riprap layer. Experimental observations (Chiew 1995, Chiew and Lim 2000, Lauchlan and Melville 2001) have clearly revealed the importance of winnowing on the degradation of a riprap layer. Under such a condition, the riprap stone is large enough to resist shear failure, but the underlying finer sediments were entrained through the process of winnowing. Published experimental results (Chiew 1995 in clear-water conditions; Chiew and Lim; 2000 and Lauchlan and Melville; 2001 in live-bed conditions) show the importance of winnowing failure when assessing the performance of a riprap layer. Degradation of the riprap layer can be significant even though the riprap stones themselves may remain intact. Chiew and Lim (2000) called this type of failure *embedment failure* and it can have dire consequences on the performance of the riprap layer. To this end, they have published a figure, which is reproduced in this paper as Figure 2 to demarcate embedment failure (caused primarily by winnowing failure) from total disintegration failure (caused primarily by shear failure).

Edge Failure

The third type of failure associated with riprap protection around bridge pier is edge failure. This occurs at the periphery of the coarse riprap stones and fine bed sediment interface. Chiew (1995) first documented this type of failure, and attributed it to the increase in shear stress on the finer sediment bed as water flows from the coarse to the fine bed boundary. It is not uncommon in flume experiments involving a rigid-loose bed interface. At such a location, a scour hole inevitably forms on the downstream erodible bed.

With riprap protection around a bridge pier, edge failure can occur when the coarse riprap stones remain intact; i.e., they can resist shear failure. With the intact riprap layer in place, the downstream finer sediment particles are entrained by the flow because of their lower critical shear stress. When this happens, a local depression forms, exposing the larger riprap stones. The stones at the edge thus roll or slide into the depression, as illustrated in Figure 3. Chiew (1995) observed the occurrence of edge erosion at the downstream end of the riprap layer. Such erosion takes place at low velocity ratio where shear

and winnowing erosion are normally absent, and constitutes the first sign of failure of the riprap layer. With the erosion of some of the larger riprap stones due to edge erosion, shear erosion and subsequently winnowing erosion may set in. He described total disintegration or embedment of the riprap layer with the aid of a series of six photographs, beginning with edge failure at the downstream of the riprap layer. He claimed that how the riprap layer would progress beyond edge failure was very much dependent on its aerial coverage and thickness. This aspect of scour research is still not thoroughly investigated.

Edge failure was also observed at the upstream end of the bridge pier. Describing this type of occurrence, Lauchlan and Melville (2002) stated that "as the scour (at the upstream location) progresses deeper, edge stones in the riprap layer begin to experience undercutting, causing them to subside into the scour region. With the edge stones removed the inner riprap is exposed. These stones gradually subside as sand is winnowed from beneath them".

Edge failure, whether it occurs at the upstream or downstream end of the bridge pier, serves as an important function in weakening the riprap layer. By itself, edge failure will not render the demise of the riprap layer. Its role is indirect in that it -

(a) Exposes the larger stones in the coarse-fine sediment interface, rendering it more susceptible to erosion; and
(b) Reduces the thickness of the riprap layer, thereby promoting winnowing failure.

In summary, edge failure hastens the eventual demise of the riprap layer as it enhances either winnowing or shear failure. The former leads to embedment while the latter enhances disintegration of the riprap layer.

Bedform-Induced Failure

Shear failure, winnowing failure and edge failure occur under both clear-water and live-bed conditions. Bedform-induced failure, however, only occurs in live-bed conditions. It is especially prevalent where large dunes are present on the approaching bed. It is the dominant failure mode and can easily overshadow the other three types of failure.

Lim and Chiew (1997) first described how the propagating bedforms interact with the riprap stones. The mechanism of bedform-induced failure was described in more detail by Chiew and Lim (2000) in which they stated that "bed-feature destabilization (or bedform-induced failure) is prompted by the fluctuation of the bed level due to the propagation of bed features (ripples and dunes) past the pier. The fluctuating bed level causes the riprap stones to lose support, and therefore stability. When the troughs of these dunes arrive at the

riprap layer, high level of turbulence is generated at the reattached zone of the flow over the dune crest. This combines with the flow field that formed at the pier to pluck and erode additional riprap stones from the degraded riprap layer. Once these stones are eroded, the degraded layer becomes thinner and is further loosened, which gives an impetus for winnowing, resulting in the embedment of the riprap layer".

Chiew and Lim (2000) have also devised an experiment to distinguish bedform-induced failure from the other three types of failure. It includes two tests which were both conducted under transition flat bed conditions at a velocity ratio, $U/U_c = 4.5$. All the other conditions for both the tests were identical except that in the first test, the flow velocity was increased as quickly as practicable so that transition flat bed was formed immediately after the onset of the test. The objective of such a procedure was to avoid the formation of ripples or dunes on the approaching bed so as to negate any bedform-induced failure at the riprap layer before the test was conducted. With the second test, velocity was increased incrementally to allow ripples and dunes to form prior to the final test with $U/U_c = 4.5$.

Figure 4 shows the results of the two tests, and it depicts the temporal scour depth fluctuation at $U/U_c = 4.5$ where transition flat bed was present on the approaching bed. The horizontal lines in Figures 4(a) and 4(b) represent the depth of the riprap layer – the level at which the riprap layer has degraded. The results show that the levels of riprap degradation, d_{rp} for Test 1 and 2 are 133 mm and 176 mm, respectively. In Test 1, the scour depth expectedly fluctuates with time and it is due to avalanches of the sediment particles on the upstream slope of the scour hole. It shows that the riprap layer has clearly degraded to the same level as the maximum scour depth. On the other hand, d_{rp} associated with Test 2 is deeper than the observed maximum scour depth at $U/U_c = 4.5$. The reason for the deeper d_{rp} is because of the antecedent condition where ripples and dunes were allowed to form before the later test was conducted. The differential of 43 mm (difference between 176 and 133 mm) is caused by bedform-induced failure.

The importance of bedform-induced failure at riprap layers is also highlighted in Parker et al. (1998) and Lauchlan and Melville (2001). In the latter study, the authors concluded that destabilization of a riprap layer by the progression of bedforms past the pier is the dominant failure mode under live-bed conditions, whereas shear, winnowing and edge failures play a secondary role.

Research studies published to-date are unanimous that bedform-induced failure is of prime importance in affecting riprap layer around bridge piers. This failure mechanism highlights the reality that, when considering riprap stability around bridge pier, it is just not sufficient to consider the ability of the stone itself to resist erosion; i.e., shear failure alone, as was done by early researchers when

considering riprap stability under clear-water conditions. In a nutshell, the stability of a riprap stone depends not only on its ability to resist shear, but also on the firmness of its foundation.

Bed-Degradation Induced Failure

The fifth and final type of failure affecting riprap failure at bridge piers is bed-degradation induced failure. Unlike the other four, this type of failure will only occur under a condition when general scour is present. Under this condition, there is a net loss of sediment over the reach of the alluvial channel at which the bridge is founded.

Lauchlan and Melville (2002) used a specially designed flume to investigate this failure mechanism. It consists of a sediment recess in which a vertically adjustable table was installed. This set-up was originally used by Chin (1985) to study streambed armoring. A unique feature of the set-up is that the shear stress of the sediment bed could be kept constant throughout the experiment. This is because the adjustable table allows the sediment bed to be raised such that it is subjected to a constant shear stress. While such a set-up reduces the effort in conducting the tests immensely, because no sediment needs to be placed upstream of the test section, it does not replicate the actual field condition on two counts. First, the shear stress in a degrading channel under a steady flow condition is not a constant but decreases with time. At the limiting condition, the shear stress approaches the critical shear stress of the bed sediment, at which time bed degradation ceases. At this juncture, the riprap layer is exposed to a much lower shear stress than that simulated in the test conducted by Lauchlan and Melville (2002). Second, bedform-induced failure is altogether absent in their study because the upstream bed in their test is rigid and no approaching bedform is present.

Chiew (2002) did not have the benefit of an adjustable table in his flume, and had to resort to a much more labor-intensive study. Even with the help of (and thanks to) research students, only three sets of experiments were conducted in an 8-months period. The study is reported in a separate paper in this conference and only the essence is presented here. At the commencement of his study, the bed sediment was eroded causing general scour. At the same time, edge and to a limited extent, shear and winnowing failure were observed at the riprap layer. With time, dunes were formed on the approaching bed. When they approached the bridge pier, a certain degree of bed degradation was observed as bedform-induced failure set in. This, however, took place at the same time that the entire bed was degrading, resulting in a reduction of the approach shear stress. With time, two important features resulted:

(1) The approach flow shear stress reduces so much that the riprap stones become effectively more stable as compared with those before general scour has taken place; and
(2) The decreasing mobility of the bed sediment reduces the size of the migrating bedforms. At the limiting condition were no inflow of sediment particles was provided, an immobile plane bed was formed.

The cumulative effect of these two features is the formation of a stable mound consisting of riprap stones around the bridge pier, as is shown in Figure 5. Chiew (2002) further showed that the riprap mound might be susceptible to failure when it is subjected to another flood accompanied by large dunes.

The observations of Chiew (2002) are very different from that reported in Lauchlan and Melville (2002). In the latter's study, the riprap mound was not observed, primarily because shear stress was kept constant throughout their experiment. As the bed (artificially) degraded with the raising bed, the riprap stones increasingly protruded above the general bed level, causing them to have a reduced critical shear stress (Chin and Chiew 1993). The result is that they eventually are entrained, or subjected to shear failure. Based on such an observation, Lauchlan and Melville (2002) concluded that "riprap installed as local scour protection around bridge piers is inadequate for protecting the pier in rivers where significant degradation of the channel bed is likely to occur. The overall degradation of the sediment bed causes the riprap stones to subside into the degrading bed. After substantial degradation the riprap layer disintegrates and can no longer prevent local scouring around the pier". This conclusion may not be so in the field if the shear stress is reduced as a consequence of bed degradation.

Notwithstanding this concern, general scour does cause riprap stones (in the form of a mound) to protrude above the bed level, resulting in a reduced critical shear stress needed to entrain the stones. If the stones are subjected to subsequent floods, especially with large approaching dunes, they are very likely to be entrained, causing the riprap mound to disintegrate.

In summary, bed-degradation induced failure constitutes another facet of riprap failure at bridge piers. Under a steady flow condition with an unchanged downstream control point, general bed degradation results in a reduction in bed shear stress, causing an apparent stable riprap mound to form. This gives a subtle impression that the riprap layer, albeit having a modified form, can function as planned in arresting scour. Research shows that subsequently floods, especially if large dunes accompany them, can cause total disintegration of the riprap mound.

FUTURE STUDY

Arising from the knowledge gained from research studies conducted over the last 10 years, we are now in a better position to assess how a riprap layer around bridge piers fails. The early emphasis on searching for an equation to size riprap stones for a particular application had only addressed the issue on shear failure. While an appropriately sized stone is very important in riprap design, the question on coverage and thickness of the riprap layer is still not well understood. A carefully planned research study in this area is still lacking. Moreover, the other four failure mechanisms outlined in this paper are not overcome merely through the use of large stones. Lim and Chiew (2001) present a series of experimental results, showing that riprap layers with different geometrical properties would fail if subjected to high flows accompanied by large dunes.

Published results so far appear to suggest that the critical factor in augmenting riprap failure is large dunes that accompany high flows. Dunes have a twofold influences:

(a) Reattachment of the main flow over the dune crest as it attacks the riprap layer; and
(b) Undermining of the riprap layer as the dune troughs propagate past the pier.

To a large extent, both these influences can be negated if one were able to reduce their height as dunes migrate past the bridge pier. One way is to explore innovative methods to reduce the size of propagating bedforms past the pier. With this, it is surmise that the threat of bedform-induced failure of the riprap layer can be significantly reduced, and thereby increasing the reliability of the riprap as a pier-scour countermeasure.

To this end, the present writer has conducted some very preliminary studies on seepage effect on dune geometry. These data are encouraging in that the dune geometry does appear to change as bedforms translate past a region subjected to upward seepage or suction. Previous studies on both seepage and suction (Cheng and Chiew, 1998; 1999 and Chen and Chiew, 2001) have shown a close correlation between such flows on the turbulence characteristics of the main flow field. This, in turn, affects the sediment transport behavior of the river. It, therefore, would not be inappropriate to surmise that either seepage or suction could have a positive influence in reducing the size of the dunes. Figure 6 shows the preliminary results of the effect of relative seepage velocity, v_s/U on the dune steepness, h/λ, where v_s = seepage velocity in which a positive v_s denotes upward seepage and vice-versa; U = undisturbed mean flow velocity; h = dune height; and λ = wavelength of dune. These data appear to show that the dune steepness increases and decreases with suction and upward seepage,

respectively. If we are able to exploit this, the problem engineers faced in designing for an effective riprap as a pier-scour countermeasure may be overcome. At this juncture, it is by no means clear whether the seepage idea would lead to a realistic and practical solution to overcoming bedform-induced failure. Additional research is necessary to explore its applicability.

CONCLUSIONS

A riprap layer around bridge piers is subjected to five failure mechanisms. They are shear failure, winnowing failure, edge failure, bedform-induced failure and bed-degradation induced failure. Each of these failure mechanisms plays a role in causing the eventual breakdown of the riprap layer. The first three failures occur in both clear-water and live-bed conditions, whereas the latter two only occur in live-bed conditions. Moreover, bed-degradation induced failure will only take place in a river where general scour occurs. The other four failure mechanisms may occur in either a non-degrading or degrading channel.

It is important to note that a riprap layer may fail either in the form of embedment or total disintegration. The former mode is closely related to winnowing and bedform-induced failure whereas the latter is cause by shear failure. Whether a riprap layer will embed or totally disintegrate depends not only on the size of the riprap layer, but also on its aerial coverage and thickness. The latter two parameters are as yet not adequately researched on. Under a live-bed condition where large dunes are present, embedment failure is the principal mode of failure because the dune trough has the tendency to undermine the riprap layer. Edge failure serves to initiate failure especially under conditions of comparatively low flow velocity. An interesting failure mechanism is bed-degradation induced failure, which can cause the formation of a riprap mound around the bridge pier. When subjected to subsequent floods with large dunes, it may also fail.

Recent studies show the vulnerability of a riprap layer when subject to high flows accompanied by large dunes. Bedform-induced failure can be so dominant that it readily causes riprap layer embedment, rendering it completely ineffective in arresting pier scour. It is postulated that a solution to increase riprap reliability is to reduce the size of the propagating bedforms. Innovative ideas, such as using seepage to reduce dune geometry, are necessary to effect a pragmatic method that can curtail bedform-induced failure so that a more reliably riprap layer can be built.

REFERENCES

1. Bonasoundas, M., 1973, “Flow Structures and problems at Circular Bridge Piers”, Report No. 28, Oskar V. Miller Inst., Tech. Univ. Munich, Germany.
2. Breusers, H. N. C., Nicollet, G., and Shen, H. W., 1977, “Local Scour around Cylindrical Piers”, Journal of Hydraulic Research, IAHR, Vol. 15, No. 3, pp. 211-252.
3. Breusers, H. N. C., and Raudkivi, A. J., 1991, “Scouring”, IAHR Hydraulic Structures Design Manual 2, A. A. Balkema, Rotterdam, The Netherlands.
4. Chabert, J. and Engeldinger, P., 1956, “Etude des Affouillements autour des Piles des Ponts”, *Laboratoire National d’Hydraulique*, Chatou, France.
5. Chen, X., and Chiew, Y. M., 2001, "Bed Shear Stress in Open Channel Flow with Bed Suction" Proceedings of the XXIX IAHR Congress, Theme D, Vol. 1, Beijing, pp. 276-281.
6. Cheng, N. S., and Chiew, Y. M., 1998, “Turbulent Open-Channel Flow with Upward Seepage” Journal of Hydraulic Research, IAHR, Vol. 36, No. 3, pp. 415-431.
7. Cheng, N. S., and Chiew, Y. M., 1999, “Incipient Sediment Motion with Upward Seepage" Journal of Hydraulic Research, IAHR, Vol. 37, No. 5, pp. 665-681.
8. Chiew, Y. M., 1995, "Mechanics of Riprap Failure at Bridge Piers", Journal of Hydraulic Engineering, ASCE, Vol. 121, No. 9, pp. 635-643.
9. Chiew, Y. M., 2002, “Riprap Protection around Bridge Piers in a Degrading Channel”, to be published in Proc. First International Conference on Scour of Foundations ICSF-1, College Station, Texas, November 17-20, 2002.
10. Chiew, Y. M., and Lim, F. H., 2000, "Failure Behavior of Riprap Layer at Bridge Piers under Live-Bed Conditions", Journal of Hydraulic Engineering, ASCE, Vol. 126, No. 1, pp. 43-55.
11. Chin, C. O., 1985, “Stream Bed Armouring”, Report No. 403, School of Engineering, University of Auckland, Auckland, New Zealand.
12. Chin, C. O., and Chiew, Y. M., 1993, "Effect of Bed Surface Structures on Particle Stability" Journal of Waterway, Port, Coastal, and Ocean Engineering, ASCE, vol. 119, no. 3, pp. 231-242.
13. Croad, R. N., 1997, “Protection from Scour of Bridge Piers using Riprap”, Transit New Zealand Research Report No. PR3-0071, Transit NZ, Wellington, New Zealand, 77pp.
14. Engels, H., 1929, “Experiments Pertaining to the Protection of Bridge Piers against Undermining”, Hydraulics Laboratory Practice, Chapter V, ASME, N.Y., USA.
15. Farraday, R. V., and Charlton, F. G., 1983, “Hydraulic Factors in Bridge Design”, Hydraulic Research Station, Wallingford, England, 102pp.

16. Hjorth, P., 1975, “Studies on the Nature of Local Scour”, Bulletin, Series A, No. 46, Department of water Resources Engineering, Lund Institute of Technology, University of Lund, 191pp.
17. Lauchlan, C. S., 1999, “Countermeasure for Pier Scour”, pH.D Thesis, The University of Auckland, Auckland, New Zealand.
18. Lauchlan, C. S., and Melville, B. W., 2001, “Riprap Protection at Bridge Piers”, Journal of Hydraulic Engineering, ASCE, Vol. 127, No. 5, pp. 412-418.
19. Lauchlan, C. S., and Melville, B. W., 2002, “Effect of Bed Degradation on Riprap Protection at Bridge Piers”, Proceedings of the Institution of Civil Engineers, Water and Maritime Engineering, Vol. 154, Issue 1, pp. 19-27.
20. Laursen, E. M., and Toch, A., 1956, “Scour around Bridge Piers and Abutments”, Bulletin No. 4, Iowa Highway Research Board.
21. Lim, F. H., 1998, “Riprap Protection and Its Failure Mechanisms”, A thesis submitted to the School of Civil and Structural Engineering, Nanyang Technological University, Singapore in fulfillment of the requirement for the degree of Doctor of Philosophy.
22. Lim, F. H. and Chiew, Y. M., 1997, “Failure Behavior of Riprap Layer around Bridge Pier”, Proceedings of the XXVII IAHR Congress, Theme A - Managing Water: Coping with Scarcity and Abundance, San Francisco, pp. 184-189.
23. Lim, F. H. and Chiew, Y. M., 2001, “Parametric Study of Riprap Failure around Bridge Piers”, Journal of Hydraulic Research, IAHR, Vol. 39, No. 1, pp. 61-72.
24. Maynord, S. T., 1978, “Practical Riprap Design”, Misc. Paper H-78-7, U.S. Army Engineer Waterway Experiment Station, Vicksburg, Mississippi.
25. Melville, B. W., and Coleman, S. E., 2000, “Bridge Scour”, Water Resources Publication, LLC, CO., USA.
26. Neill, C. R., 1973, “Guide to Bridge Hydraulics”, Roads and Transportation Association of Canada, University of Toronto Press, Toronto, Canada, 191pp.
27. Parker, G., Toro-Escobar, C., and Voigt, R. L., 1998, "Countermeasures to Protect Bridge Piers from Scour." Final Report prepared for National Highway Research Program, Transportation Research Board, National Research Council, University of Minnesota, Minneapolis, December, 360pp.
28. Parola, A. C., 1993, “Stability of Riprap at Bridge Piers”, Journal of Hydraulic Engineering, ASCE, Vol. 119, No. 10, pp. 1080-1093.
29. Posey, C. J., 1974, “Tests of Scour Protection for Bridge Piers”, Journal of Hydraulic Division, ASCE, Vol. 100, No. 12, pp. 1773-1783.
30. Quasi, M. E., and Peterson, A. W., 1973, “A Method of Bridge Pier Riprap Design”, Proceedings, First Canadian Hydraulic Conferences, Edmonton, Canada, pp. 96-106.

31. Richardson, E. V., and Davies, S. R., 1995, "Evaluating Scour at Bridges", 3rd Edition, HEC 18, U. S. Department of Transportation, Federal Highway Administration.
32. Shirole, A. M., and Holt, R. C., 1991, “Planning for a Comprehensive Bridge Safety Assurance Program”, Transp. Res. Rec. No. 1290, Transportation Research Board, Washington D.C., 39-50.
33. Smith, D. F., 1976, “Bridge Failures”, Proceedings of the Institution of Civil Engineers, Vol. 60, No. 1, pp. 367-383.

Table 1. Equation for sizing riprap at bridge piers (Melville and Coleman 2000)

Reference	Original Equation	Equation used for Comparison	Symbols
Bonasoundas (1973)	$d_r(cm) = 6 - 3.3V + 4V^2$		Apply to stones with $S_s = 2.65$; V = mean approach velocity (m/s)
Quazi and Peterson (1973)	$N_{sc} = 1.14\left(\frac{d_r}{y}\right)^{-0.2}$	$\frac{d_r}{y} = \frac{0.85}{(S_s - 1)^{1.25}} Fr^{2.5}$	N_{sc} = critical Stability Number = $V^2/[g(S_s-1)d_r]$; Fr = Froude number = $V/(gy)^{0.5}$
Breusers et al. (1977)	$V = 0.42\sqrt{2g(S_s - 1)d_r}$	$\frac{d_r}{y} = \frac{2.83}{(S_s - 1)} Fr^2$	y = undisturbed approach flow depth
Farraday and Charlton[2] (1983)	$\frac{d_r}{y} = CFr^3$	$\frac{d_r}{y} = 0.547Fr^3$	C = coefficient and is dependent on the bank slope and the factor of safety, SF, selected. For a flat slope, C = 0.22, 0.25 and 0.28 for SF = 1, 1.5 and 2, respectively. Moreover, there is a velocity multiplier depending on whether the pier is sited in a straight channel (1.25); bends (1.5) or nose of groins or guide banks (2.0).
Parola and Jones (1989)	$\frac{d_r}{y} = \frac{C^*}{(S_s - 1)} Fr^2$	$\frac{d_r}{y} = \frac{C^*}{(S_s - 1)} Fr^2$	C* = coefficient for pier shape = 1.0 (rectangular), 0.61 (round-nose)
Breusers and Raudkivi (1991)	$V = 4.8\sqrt{S_s - 1}\, d_r^{1/2} y^{1/6}$	$\frac{d_r}{y} = \frac{0.278}{(S_s - 1)^{1.5}} Fr^3$	
Austroads (1994)	$\frac{d_r}{y} = \frac{0.58K_pK_v}{(S_s - 1)} Fr^2$	$\frac{d_r}{y} = \frac{0.58K_pK_v}{(S_s - 1)} Fr^2$	K_p = pier shape factor = 2.25 (round nose), 2.89 (rectangular) K_v = velocity factor, varying from 0.81 for a pier near the bank of a straight channel to 2.89 for a pier at the outside bend in the main channel

[2] For the formula proposed in Faraday and Charlton (1983), Melville and Coleman (2000) used a coefficient of 0.547. This is obtained by assuming a flat bed and a factor of safety of 2.0, yielding C = 0.28. They assume the pier is sited on a straight river reach, thus giving a velocity multiplier of 1.25. As a result of this the coefficient becomes $0.28*1.25^3 = 0.547$.

Reference	Original Equation	Equation used for Comparison	Symbols
Richardson and Davies (1995)	$d_r = \frac{0.692(f_1 f_2 V)^2}{(S_s - 1)2g}$	$\frac{d_r}{y} = \frac{0.346 f_1^2 f_2^2}{(S_s - 1)} Fr^2$	f_1 = pier shape factor = 1.5 (round nose), 1.7 (rectangular) f_2 = factor ranging from 0.9 for a pier near the bank of a straight reach to 1.7 for a pier in the main current at a bend
Chiew (1995)	$d_r = \frac{0.168}{\sqrt{y}} \left(\frac{V}{U_* \sqrt{(S_s - 1)g}} \right)^3$	$\frac{d_r}{y} = \frac{0.168}{(S_s - 1)^{1.5} U_*^3} Fr^3 \; U_* = \frac{0.3}{K_d K_y}$ K_d = sediment size factor; K_y = flow depth factor	$K_y = 0.783 \left(\frac{y}{b} \right)^{0.322} - 0.106 \qquad 0 \le \frac{y}{b} < 3$ $K_y = 1 \qquad \frac{y}{b} \ge 3$ $K_d = 0.398 \ln\left(\frac{b}{d_r} \right) - 0.034 \left[\ln\left(\frac{b}{d_r} \right) \right]^2 \qquad 1 \le \frac{b}{d_r} < 50$ $K_d = 1 \qquad \frac{b}{d_r} \ge 50$
Parola (1993)	<u>Rectangular</u>: $N_{sc} = 0.8 \qquad 20 < \frac{b}{d_r} < 33$ $N_{sc} = 1.0 \qquad 7 < \frac{b}{d_r} < 14$ $N_{sc} = 1.2 \qquad 4 < \frac{b}{d_r} < 7$ *<u>Aligned Round-nose:</u>* $N_{sc} = 1.4$	$\frac{d_r}{y} = \frac{f_1 f_3}{(S_s - 1)} Fr^2$	f_1 = pier shape factor = 1.0 (rectangular), 0.71 (round-nose if aligned) f_3 = pier size factor $f_3 = 0.83 \qquad 4 < \frac{b}{d_r} < 7$ $f_3 = 1.0 \qquad 7 < \frac{b}{d_r} < 14$ $f_3 = 1.25 \qquad 20 < \frac{b}{d_r} < 33$

Reference	Original Equation	Equation used for Comparison	Symbols
Croad (1997)	$\frac{V}{A\sqrt{(S_s-1)gd_r}} = 1.16\left(\frac{y}{d_r}-2\right)^{1/6}$ $d_r = 17\ d_{50}$	$\frac{d_r}{y}\sqrt{\left(1-\frac{2d_r}{y}\right)} = \frac{0.641}{A^3(S_s-1)^{1.5}}Fr^3$ *use larger of computed d_r or 17 d_{50}*	A = acceleration factor = 0.45 (circular and slab piers), = 0.35 (square and sharp edge piers). Equation given for factor of safety = 1.25.
Lauchlan (1999)	$\frac{d_r}{y} = 0.3SF\left(1-\frac{Y_r}{y}\right)^{2.75} Fr^{1.2}$	$\frac{d_r}{y} = 0.3SF\left(1-\frac{Y_r}{y}\right)^{2.75} Fr^{1.2}$	SF = factor of safety, with a minimum recommended value = 1.1 Y_r = placement depth below bed level

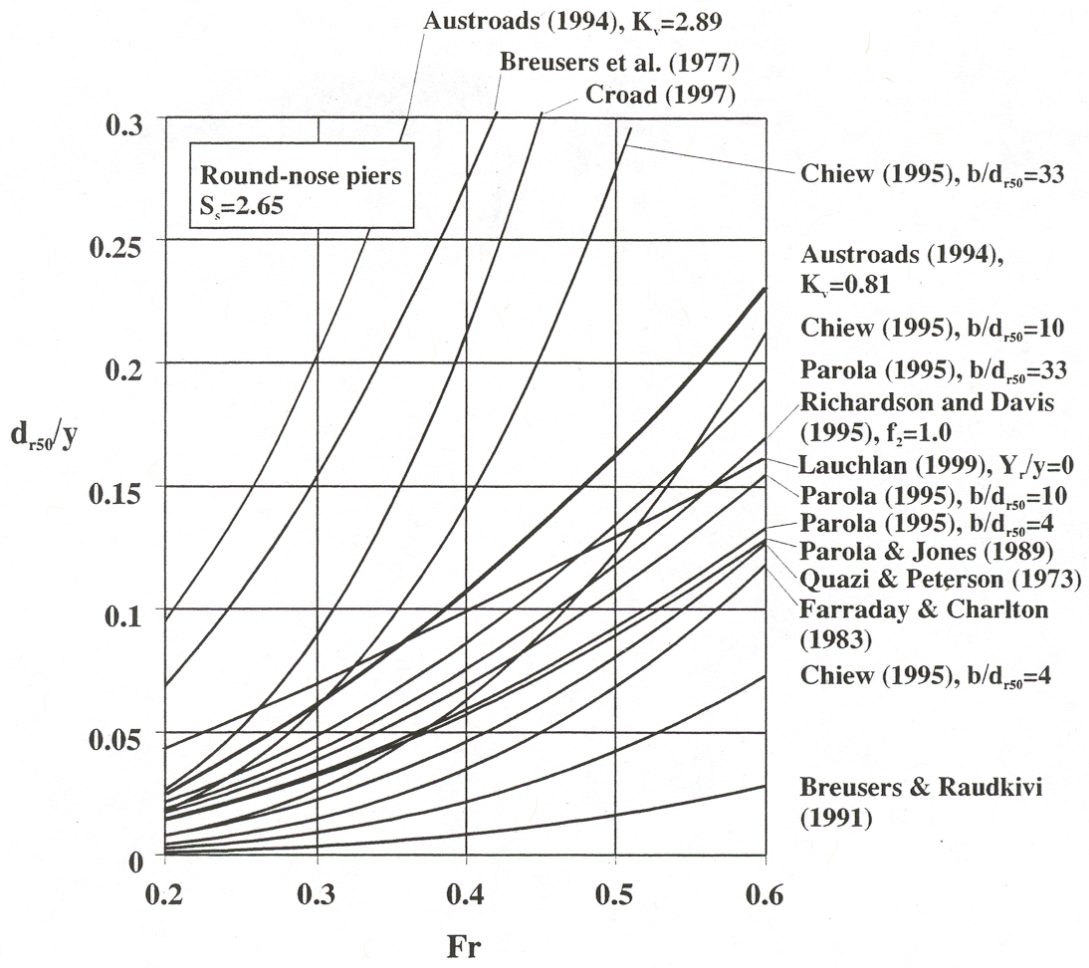

Figure 1. Comparison of Equations for Sizing Riprap at Bridge Piers (Melville and Coleman 2000)

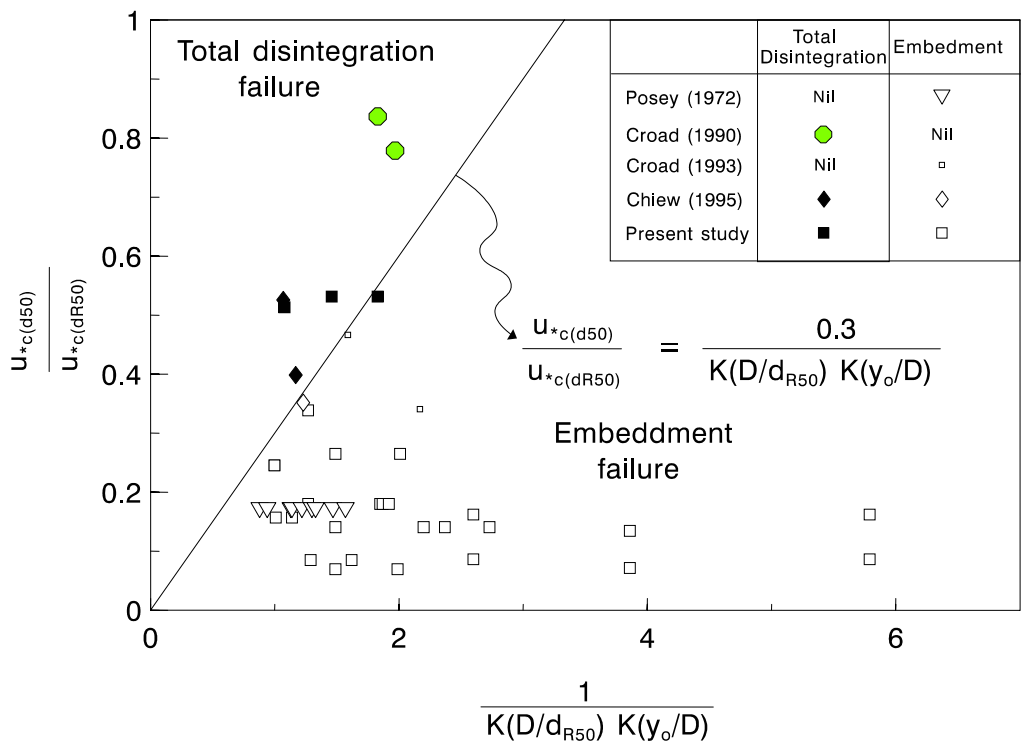

Figure 2. Classification of Failure Mode of riprap Layer (Chiew and Lim 2000)

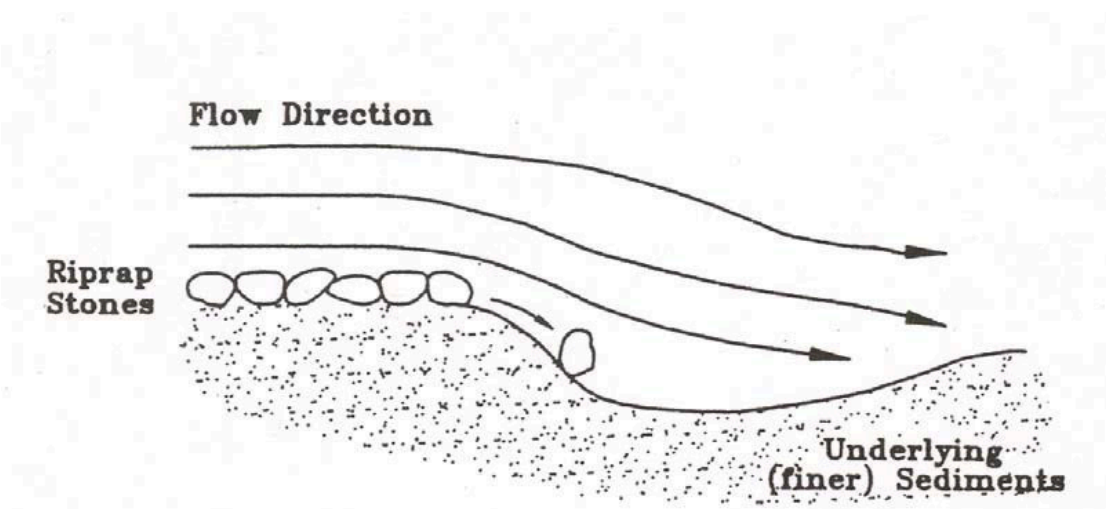

Figure 3. Schematic Illustration of Edge Failure (Chiew 1995)

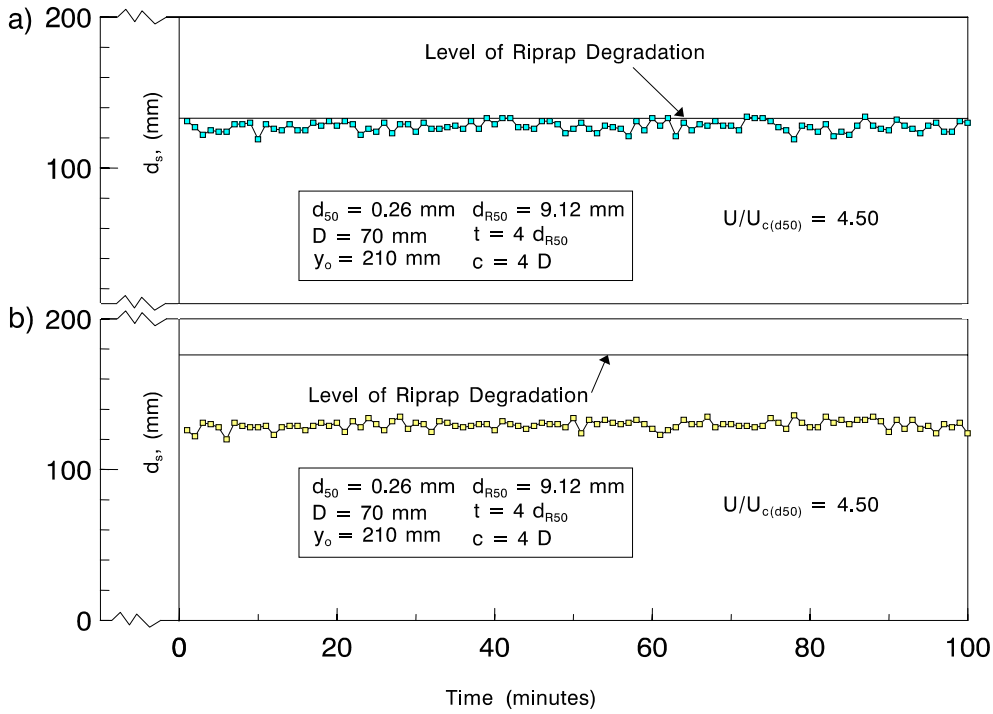

Figure 4. Temporal Variation of Scour Depth in Transition Flat Bed Regime with Different Antecedent Bedforms: (a) Immobile Plane Bed; (b) Immobile Plane Bed, Ripples and Dunes (Chiew and Lim 2000)

Figure 5. Formation of riprap mound around bridge pier in a degrading bed (Flow from right to left)

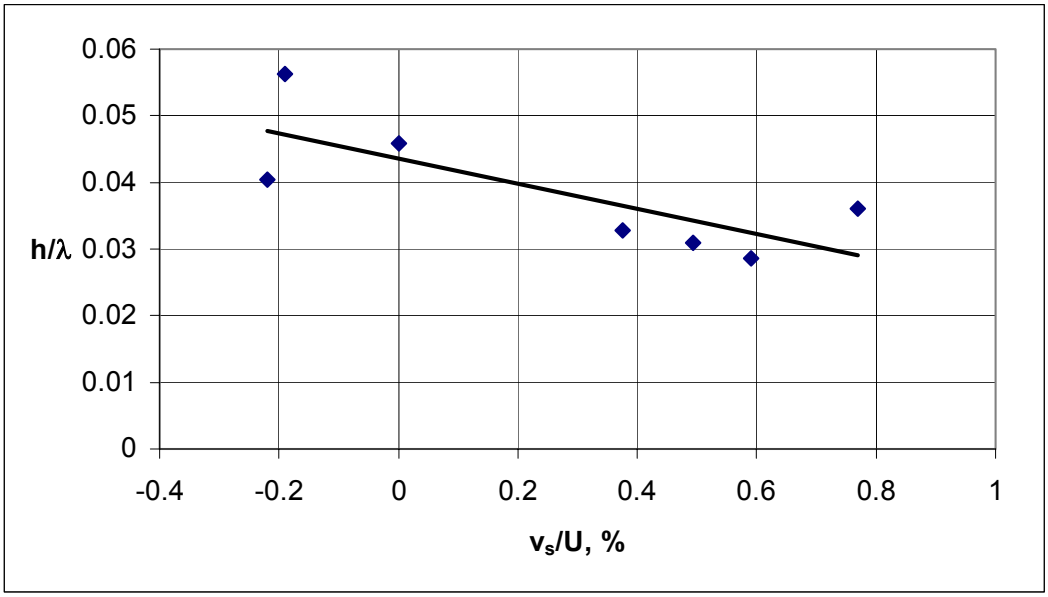

Figure 6. Effect of relative seepage velocity on dune steepness

On the Challenges of Scour Prediction

by

Gijs Hoffmans[1] and Henk Verheij[2]

ABSTRACT

In principle, empirical structure-specific formulas are still used to predict scour. Turbulence and probability distributions for relevant parameters, such as critical shear stress, are taken into account only incidentally. This lecture describes the Dutch approach to scour by presenting a concept for a generally applicable, structure-independent scour prediction formula, as well as the results of turbulence research and a stochastic approach to the transport mechanism. Examples of projects and research carried out are presented to illustrate the possibilities afforded by and also the need for an integrated approach. Finally, some aspects of scour that require further research are defined.

INTRODUCTION

Prior to the design of hydraulic structures it is necessary to establish boundary conditions. Information is required about water levels, flow velocities and soil mechanical aspects, and, in addition, the expected local bed levels under extreme conditions should also be known. The bed level in a river varies in time, due to discharge variations as well as continuing aggregation by sedimentation or degradation by erosion. Moreover, the hydraulic structure may influence the bed level, because the flow field changes and this may initiate the formation of a lower bed-level. Three types of phenomena contribute to the bed level, viz.: 'general scour', 'natural scour' and 'local scour'. General scour is the continuous degradation of the bed level due to human changes in the river basin and the river. In some cases aggradation may occur. Causes of this include the building of reservoirs and changes in land use. Natural scour is the result of natural river processes due to local flow field changes; examples are bend scour, confluence scour, constriction scour and protrusion scour (e.g. scour upstream of a sudden constriction). Local scour is the result of flow field changes due to the presence of a structure.

Today natural and local scour are still predicted by using empirical formulas. In the scour manuals each structure has its own chapter and formula (see for instance the Scour Manual by Hoffmans & Verheij, 1997). Coefficients take into account particular conditions, such as the shape of the bridge piers, or the heads of the spurs. Sometimes the affects of turbulence and stochastics are also taken into account. The same holds for general scour, where empirical sediment transport formulas are most often used, although stochastic predictors are available (van Rijn, 1993). Very recently, transport prediction near the threshold for motion was successful using a stochastic approach taking into account hiding-exposure and hindrance effects (Kleinhans & van Rijn, 2002).

In this lecture results of Dutch research on scour and scour-related items will be considered.

---

[1] Hydraulic specialist, Ministry of Public Works and Water Management, Dept. of Hydraulic Engineering, Delft, The Netherlands (email: g.j.c.m.hoffmans@dww.rws.minvenw.nl)

[2] Senior Hydraulic Engineer, WL | Delft Hydraulics, Delft, The Netherlands (email: henk.verheij@wldelft.nl)

Firstly, the Dutch approach to scour prediction will be discussed, viz. the development of a generally-applicable (e.g. structure-independent) formula for natural and local scour, including turbulence and probability distributions for all parameters and an integration of all aspects involved. In the next section turbulence will be discussed, followed by a treatment of the transport mechanism. Subsequently, examples of the Dutch approach are presented. Finally, the needs for further research are presented.

DUTCH SCOUR APPROACH

Scour is the result of erosion of bed material, i.e. in conditions in which the bed shear stress is greater than the critical one (see section transport mechanism). In principle, the presence of a hydraulic structure influences the flow field and thus the bed shear stress, which may eventually result in scouring. It is believed that the blockage of a river, resulting in accelerating flow upstream and adjacent to the hydraulic structure and decelerating flow with a higher turbulence level downstream of the structure, determines the shear stress acting on the bed material. In other words: the relative geometrical parameters (relative to the water depth or river width) determine the bed shear stress and its turbulence and not the absolute values of geometrical parameters. This makes it possible to assume that a structure-independent scour relation could be determined which could replace the many formula currently used.

Scour research in the Netherlands is therefore focussed on the following issues ('Dutch scour approach'):

- Development of a generally applicable, structure-independent, scour formula.
- Implementation of turbulence.
- Implementation of stochastics to account for uncertainties in transport mechanism, values of parameters and coefficients.
- Numerical scour prediction by using morphological models, taking into account the mutual influence of flow field, scouring and morphology.

Firstly, the concept of a generally applicable scour formula will be presented. The second and third issues will be treated in subsequent sections. The last item will be illustrated by examples of projects carried out by WL|Delft Hydraulics.

A first attempt to derive a generally applicable scour formula was presented by Hoffmans & Verheij in the Scour Manual (1997). An improved version reads (Fig. 1):

$$y_m = y_{m,e}\ f(t) \quad \text{with} \quad y_{m,e} / L_s = \prod_{i=1}^{n} f_i \quad \text{and} \quad f(t) = 1 - \exp\left(-\lambda\left(t / t_1\right)^{\gamma}\right) \qquad (1)$$

where y_m = time-dependent scour, $y_{m,e}$ = final equilibrium scour, $f(t)$ = function describing the time-dependent scour development, L_s = characteristic length, f_i = coefficients for various influences (for instance: f_1 = flow velocity relative to initiation of motion, f_2 = influence of current and wave loads and their mutual relevance), t = time, t_1 = characteristic time scale in which $y_m = L_s$ and $\lambda = -\ln(1 - L_s/y_{m,e})$ and γ is a constant. The formula accounts for the subsequent scour phases: initial phase, phase of development, stabilisation phase and equilibrium phase.

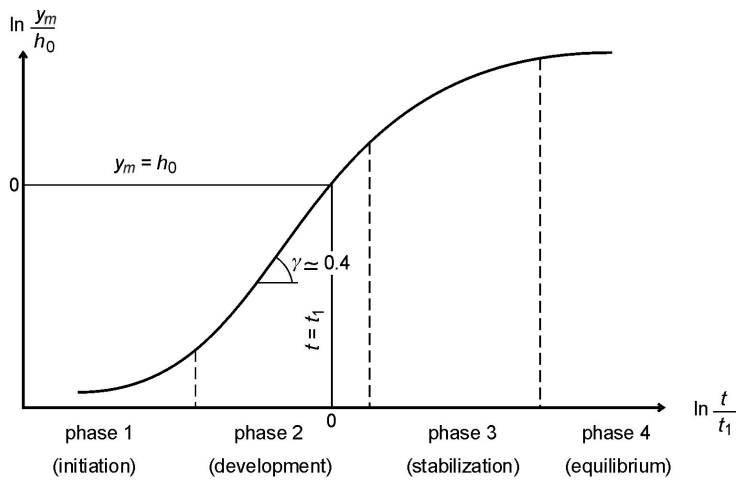

This concept was presented by Breusers *et al.* (1977) and adapted by various researchers (e.g. HEC-18, 1995; Escarameia & May, 1999; Melville & Coleman, 2000; Sumer *et al*., 1993; Whitehouse, 1998; Cardoso & Bettess, 1999).

However, most of these relations focus on one dominant process in a particular situation and often the time factor is not included.

Fig. 1 - Scour development process($L_s = h_0$, e.g. downstream of sill)

Bos *et al.* (2002) present an application of the above-mentioned relation for a submerged gravity based structure attacked by the combined action of currents and waves.

The characteristic length L_s is usually related to the flow depth (h_0) or to geometrical properties such as the diameter of a bridge pier or the length (b) of a spur. Breusers *et al.* (1977) had already included an empirical formula to describe the scour process around slender and large structures. We propose:

$$L_s = h_0\left((1-m)^{-2/3} - 1\right) + b\tanh\left(h_0 / b\right) \qquad (2)$$

in which $m = b/B$ in which B is the width of the river. The first term represents the constriction of the channel by the presence of an abutment or a bridge pier. For relatively large depths (say $b/h_0 < 0.5$) or slender piers the length scale is equal to b, whereas the length scale equals the flow depth for shallow water conditions ($b/h_0 > 1.5$) or large structures. For intermediate structures $0.5 < b/h_0 < 1.5$ the relation between either L_s and b or L_s and h_0 is not unambiguous. We believe that the influence of the width (l_s) to (L_s) is important in predicting the scour process. Table 1 shows different types of structures that are related to values of the ratios l_s/h_0 and b/h_0. By applying this concept the length scale (L_s) has to be smaller than $y_{m.e}$.

The governing parameters in (1) depend on the flow characteristics, the characteristics of the bed material, or geometrical values. For example f_1 is a function of:

$$f_1 = \alpha_{\ell,1} U_\ell / U_c - 1 \quad \text{with} \quad \alpha_{\ell,1} = 1 + 3r_{0,\ell} \qquad (3)$$

This allows the incorporation of turbulence, for instance via the local turbulence parameter $r_{0,\ell}$ (see next section) and a stochastic approach with respect to U_ℓ (local depth-averaged flow velocity) and U_c (local and depth-averaged critical velocity).

Based on earlier research activities of Breusers *et al.* (1977), the time scale (t_1) can be expressed for both two and three-dimensional flow (Fig. 4):

$$t_1 = \textbf{constant} \cdot L_s^2 \;/\left(\alpha_\ell U_\ell - U_c\right)^{4.3} \quad \text{with} \quad \alpha_\ell = 1.5 + 5r_{0,\ell} \qquad (4)$$

Other definitions are also possible, for instance, the one proposed by Escarameia & May (1999), who define t_1 as the time in which 50% of the final equilibrium scour depth is reached.

The parameter γ determines the erosion velocity during the stage in which the scour develops. Obviously, relevant aspects are the critical bed shear stress (sand results in a faster scour process than clay), the flow complexity (2D or 3D) and the geometry. For two-dimensional flow behind sills $\gamma = 0.4$. In the literature values in the range from 0.2 to 0.8 are presented (Hoffmans & Verheij, 1997), however, these values are not related to a proper length scale L_s.

Recently, research has been started in the Netherlands into breaching in cohesive soils within the framework of establishing dike safety and inundation risk. In this respect critical flow velocities of cohesive soils have also been studied (Verheij, 2002).

Although the basic principles, related to turbulence and a stochastic approach to the initiation of motion are already known, at present research aimed at further develop the generally applicable scour formula is in progress.

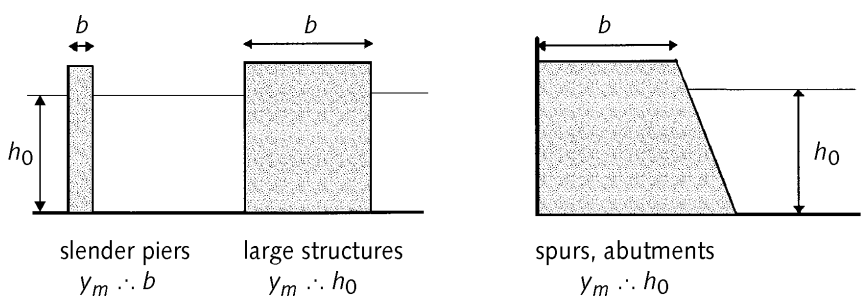

Figure 2 – Value of L_s for different structures

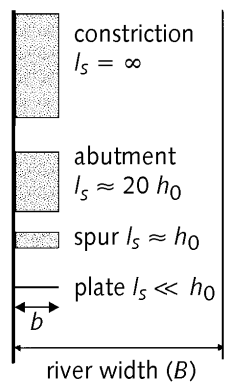

Fig 3 Definition of l_s

TURBULENCE

In a turbulent flow the particles of fluid move erratically producing eddies. It is difficult to follow the paths of individual particles. However, the behaviour of the fluid can be examined by considering average conditions. The (mean) bed shear stress (τ_0) and the standard deviation (σ_0) of the instantaneous bed shear stress are often used to express the loading on bed particles (see also section Transport Mechanism). In this section a definition of a depth-averaged turbulence-intensity (r_0), which has been successfully applied in predicting the scour process downstream of the storm surge barrier in the Eastern Scheldt will be discussed.

The bed shear stress is defined as:

$$\tau_0 = \rho u_*^2 \tag{5}$$

where u_* is the bed shear velocity and ρ is the fluid density. For uniform flow the depth-averaged flow velocity (U_0) is (Chézy equation):

$$U_0 = u_* \frac{C}{\sqrt{g}} \tag{6}$$

where C is the Chézy coefficient and g is the acceleration of gravity. The depth-averaged turbulence intensity (r_0) is defined as:

$$r_0 = \frac{1}{U_0 h_0} \int_0^{h_0} \sigma_u(z) \mathbf{d}z \tag{7}$$

where h_0 is the flow depth, z is the vertical distance and σ_u is standard deviation of the longitudinal flow velocity. Applying the definition of the turbulence energy k (or the turbulent kinetic energy) as function of the vertical:

$$k(z) = \tfrac{1}{2}\left(\sigma_u^2(z) + \sigma_v^2(z) + \sigma_w^2(z)\right) \tag{8}$$

the depth-averaged turbulence intensity can also be written as:

$$r_0 = \frac{\sqrt{\frac{1}{h_0} \int_0^{h_0} k(z)\, \mathbf{d}z}}{U_0} \tag{9}$$

	l_s		
b	$<< h_0$	$\approx h_0$	$>> h_0$
$<< h_0$	slender piers		
$\approx h_0$		wide piers	
$>> h_0$	spur modelled as plate	spur	abutment constriction

Table 1 - Classification of structures

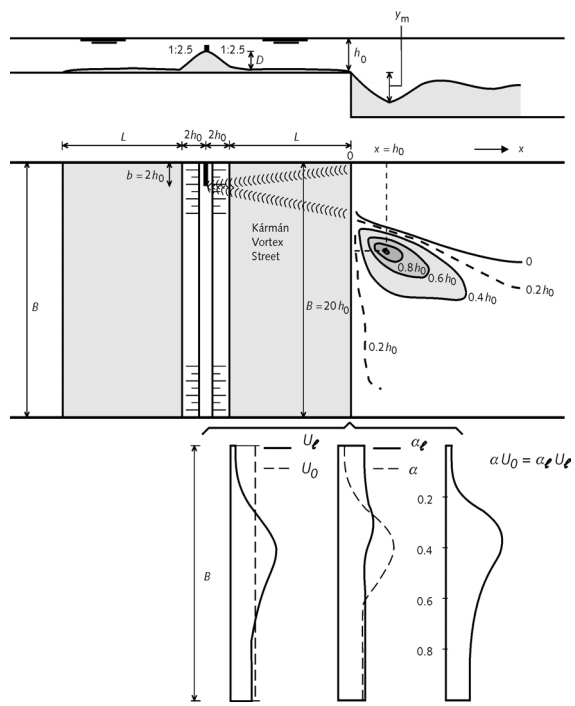

Fig. 4 – Two-dimensional flow field for a horizontal constriction

For uniform flow this can easily be verified when using model relations proposed by Nezu (1977). Following Nezu, the turbulence parameters σ_u, σ_v (= standard deviation in transverse direction) and σ_w (= standard deviation in vertical direction) could be approximated by:

$$\sigma_v(z) = 0.7\,\sigma_u(z) \qquad \sigma\ \ (z) = 0.55\,\sigma_u(z) \qquad \sigma_u(z) = 1.92\,u_* \exp\left(-z/h_0\right) \tag{10}$$

Combining (6), (7) and (10) r_0 is for *uniform flow* (Hoffmans, 1993):

$$r_0 = 1.21\frac{u_*}{U_0} = 1.21\frac{\sqrt{g}}{C} \tag{11}$$

For hydraulically smooth conditions (C = 75 m$^{1/2}$/s) r_0 = 0.05 and for hydraulically rough conditions (C = 35 m$^{1/2}$/s) r_0 = 0.10.

Non-uniform flow measurements of Van Mierlo & De Ruiter (1988) showed that the turbulence energy (k_m) in the centre of the mixing layer (with horizontal axis) grows rapidly to a maximum and vanishes where the new wall boundary layer is well developed. The turbulence energy (k_0) (close to the bed) then approaches an equilibrium value, which consists largely of turbulence generated at the bed (Fig. 5 and 6).

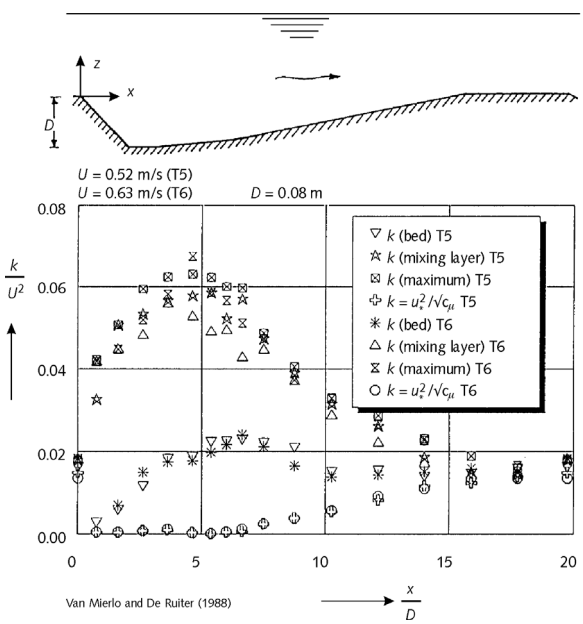

Fig. 5 – Measurements of k as function of x above an artificial dune

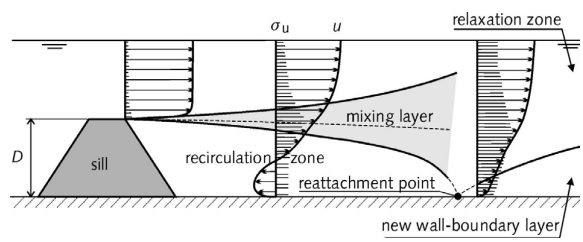

Fig. 6 - Flow downstream of sill

Downstream of the point of reattachment, the turbulence energy (k_η) in the relaxation zone decreases gradually and becomes small compared to the turbulence energy (k_0). Earlier studies of Hoffmans (1992) have shown that in a scour hole the turbulence energy (k_b) near the bed can be represented by a combination of the turbulence energy (k_η) and the turbulence energy (k_0).

$$k_b(x) = \omega k_\eta(x) + k_0(x) \qquad \text{with} \qquad k_0(x) = \frac{u_*^2(x)}{\sqrt{c_\mu}} \tag{12}$$

with c_μ (= 0.09) a coefficient used in k-ε-models and x is the longitudinal coordinate. It should be noted that in the deceleration zone $k_0 << \omega k_\eta$ ($\omega \cong 0.3$); this can be ascribed to the small flow gradients close to the bed.

To analyse the decay of the turbulence in the relaxation zone, an analogy with the decay of the turbulence energy and the dissipation in grid turbulence can be used (Launder & Spalding,

1972). When the zone downstream of the point of reattachment is considered and the production and diffusion terms in the transport equations of the turbulence energy and the dissipation are neglected, k_η can be given by (Booij, 1989):

$$k_\eta(x) = k_m \left(\frac{x - x_R}{\lambda_r} + 1 \right)^{\alpha_k} \tag{13}$$

where x_R ($\cong 6D$) is the x-coordinate where the flow reattaches the bed, D is the height of the sill, λ_r ($\cong$ ½ c_λ h_0/β_m) is a relaxation length, c_λ ($\cong$ 1.2) is a relaxation coefficient, β_m ($\cong$ 0.09) is the angle of the mixing layer and α_k ($\cong$ -1.08) is a coefficient that is directly related to the turbulence coefficients used in k-ε-models. The hypothesis of self-preservation (Townsend, 1976) requires constant turbulence energy in the mixing layer up to the point where the boundaries have reached the surface and the bed. An appropriate value is:

$$k_m = C_k U^2 \tag{14}$$

in which C_k ($\cong$ 0.045) is a coefficient and U is the depth-averaged flow velocity above the sill. In analogy to (13) the turbulence energy averaged over the depth, from which r_0 can be determined downstream of a sill, can be given by:

$$\frac{1}{h_0} \int_0^{h_0} k(x,z)\mathbf{d}z = \beta_k k_\eta(x) + c_0 u_*^2(x) \tag{15}$$

where β_k ($\cong$ 0.5) and c_0 ($\cong$ 1.45) are constants. If the geometry of the tests consists of a horizontal bed where the flow is sub-critical above a sill, the following relation for r_0 can be deduced by combining (9), (12), (13), (14) and (15), (Hoffmans, 1993):

$$r_0 = \sqrt{0.0225\left(1 - \frac{D}{h_0}\right)^{-2} \left(\frac{L - 6D}{6.67 h_0} + 1 \right)^{-1.08} + 1.45 \frac{\sqrt{g}}{C}} \quad \text{for} \quad L > 6D \tag{16}$$

For reasons of safety, the length L of the bed protection will always extend beyond the point of reattachment. More than 250 experiments were used to calibrate and verify (16). In these laboratory experiments both the hydraulic conditions and the geometrical parameters were varied.

TRANSPORT MECHANISM

Particle transport or scouring occurs when there is no balance between loading (instantaneous bed shear stress) and strength (instantaneous critical bed shear stress). When the load is less than some critical value, the bed material remains motionless. The bed can then be considered as fully stable; but when the load over the bed attains or exceeds its critical value, particle motion begins. The beginning of motion is difficult to define and this can be ascribed to phenomena that are random in time and space. Usually particle transport is modelled by formulas that include the difference either in velocity (or shear stress) or in turbulence or both. Based on the concepts of Shields, Grass (1970) and Raudkivi (1998) a stability formula is discussed for describing the initiation of motion.

Shields published his experimental results for the initiation of movement of uniform granular material on a flat bed, later known as the Shields-criterion although Rouse proposed the well-known curve (Fig. 7).

Several researchers investigated the influence of turbulence on bed load. As given by Kalinske and Einstein, the instantaneous velocity varies according to a Gaussian distribution. Grass

(1970) extended these ideas. The weakness of these classical stochastic models is that they do not incorporate modern turbulence knowledge. For example, measurements show that for uniform flow the influence of sweeps, which are directed towards the bed, and ejections, which are moving away from the bed, is not included in the Gaussian distribution (Fig. 8). Sweeps and ejections contribute most to the turbulent shear stress.

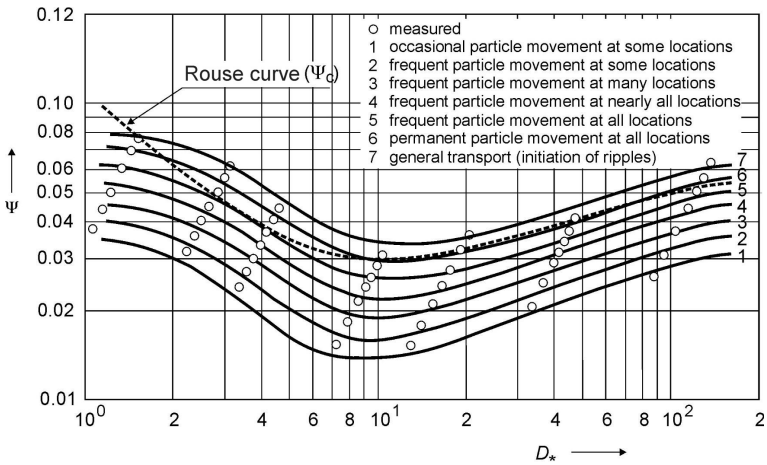

Figure 7 – Shields Diagram ($D_* = d_{50}(\Delta g/\nu^2)^{1/3}$

In the Shields diagram, the influence of fluctuating shear stresses on bed particles is not directly specified. In the sixties WL|Delft Hydraulics studied the initiation of movement of bed material in detail and distinguished 7 qualitative criteria. These introduced criteria all lie in the broad belt as originally given by Shields thus confirming the earlier research activities of Shields

However, there is more to the difference than the enhanced skew in the instantaneous bed shear stress. Under non-uniform flow conditions, there is no clear relation between the instantaneous sediment transport and the instantaneous bed shear stress. Near-bed measurements of turbulent correlations (Reynolds stresses) are estimates of momentum flux, but are only related to the force acting on the bed when it is averaged over a long period of time. This being so, some assumptions are made in order to model important design parameters for both turbulence and scouring.

When dealing with the concept of Grass, the exact shape of the distribution of loading and strength is irrelevant because a characteristic bed shear stress can be defined, this being a time-averaged value and a fluctuating term that originates from the turbulence near the bed. The characteristic value is a value that is higher or lower than the time-averaged value. Usually characteristic values are expressed as a mean value and a fraction or a multiple of the standard deviation. In fact, the problem of bed stability will now be expressed in terms of the magnitude of this fluctuation. In addition to the random nature of the load, another random variable in the process of initial instability is determined by the strength of the particles close to the bed.

To make an adaptation to non-uniform flow it is useful to analyse the influence of the turbulence in the vicinity of the bed on uniform flow. For this exercise the concept of Grass (1970) can be applied, this being based on statistical assumptions for both the loading and strength parameters (Fig. 9). The characteristic bed shear stress ($\tau_{0,k}$) and the characteristic strength, which is the critical bed shear stress ($\tau_{c,k}$) can be respectively written as:

$$\tau_{0,k} = \tau_0 + \gamma\sigma_0 \qquad \tau_{c,k} = \tau_G - \gamma\sigma_c \tag{17}$$

where γ is determined by an allowable transport of the bed material, σ_c is the standard deviation of the instantaneous critical bed shear stress and τ_G is the time-averaged critical bed shear stress according to Grass. A specific transport will occur if $\tau_{0,k} = \tau_{c,k}$; this will be elucidated later.

If the characteristic loading near the bed is equal to the characteristic strength (thus $\tau_{0,k} = \tau_{c,k}$)

and if $\sigma_c = \alpha_c \tau_G$ with $\tau_G = \Psi_{c,G} \Delta \rho g d_{50}$ (analogous to the Shields concept) and assuming $\gamma_{strength} = \gamma_{load} = \gamma$, a general relation for the upper layer of bed protection follows:

$$\Delta d_{50} = \frac{\tau_0 + \gamma \sigma_0}{\Psi_{c,G} \rho g (1 - \alpha_c \gamma)} \tag{18}$$

where d_{50} is the medium grain size, g is the acceleration of gravity, α_c is a coefficient representing the variation of the material characteristics, ν is kinematic viscosity, ρ is the fluid density, Δ is the relative density and $\Psi_{c,G}$ mobility parameter according to Grass. For uniform flow ($\sigma_0 \cong 0.4\tau_0$) Grass found that a bed of nearly uniform sand ($\alpha_c \cong 0.3$) was completely stable for $\gamma = 1$ and for $\gamma = 0$ a significant transport of sediment particles was observed. Based on his experiments, he reported that for $\gamma = 0.625$ the criterion of Shields was met for the initial movement of sands up to a size of 250 µm. In his opinion the $\gamma = 0.625$ criterion was also in agreement with observations of Vanoni and Tison when using the Rouse curve as a basis for the critical shear stress prediction. The critical bed shear stress τ_G is approximately 1.54 times higher than the time-averaged bed shear stress and thus 1.54 times higher than the mean critical value according to Rouse.

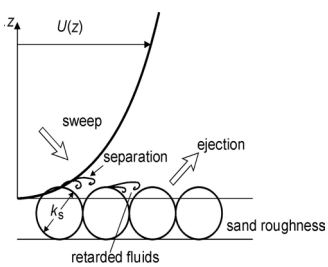

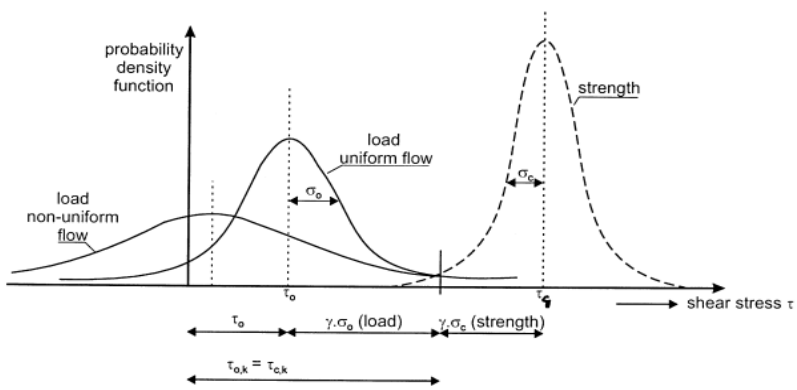

Fig. 8 Sweeps and ejections Fig. 9 Probability functions of loading and strength parameters

With equation (18) the influence of particle gradation on the stability of the bed material can be explained in a qualitative way. A broadly graded material has more fines than a more uniform material. Consequently a broadly graded material is given an average grain size that is larger than for uniform material. These predictions correspond with observations in flume experiments.

Raudkivi (1998) pointed out that the beginning of movement is a function of the mean bed shear stress, its turbulence intensity, particle size and its distribution. For uniform flow the production of energy is at maximum near the bed and determined by the roughness (size and distribution). However, downstream of a sill, the turbulence intensity can be ten times that of the downstream uniform flow of the same depth.

In laminar flow when there is no turbulence (Reynolds number $R_* << 0$), σ_0 equals zero. In these flows the forces acting on the particles are marginal if compared to their weight. Hence all particles will be at rest ($\gamma >> 1$). Following De Ruiter (1980) the standard deviation of the instantaneous bed shear stress depends on the Reynolds numbers for uniform turbulent flow (Fig. 10).

For non-uniform (turbulent) flow there is no unique relation between σ_0 and R_*. The turbulence generated is strongly dependent on the geometry of the hydraulic structure and to a lesser extent to the roughness of the bed.
Following Raudkivi, equal conditions for the initiation of motion can be distinguished for both uniform and non-uniform flow (Fig. 11).

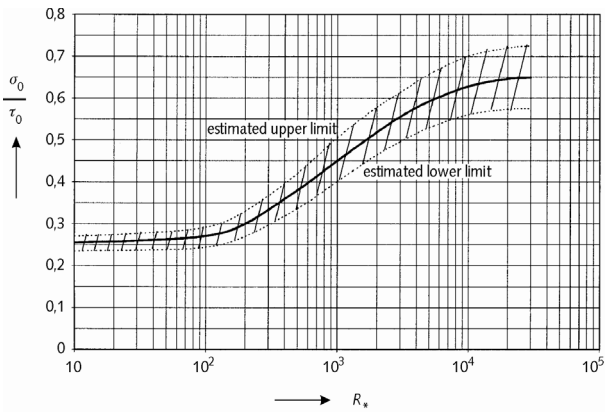

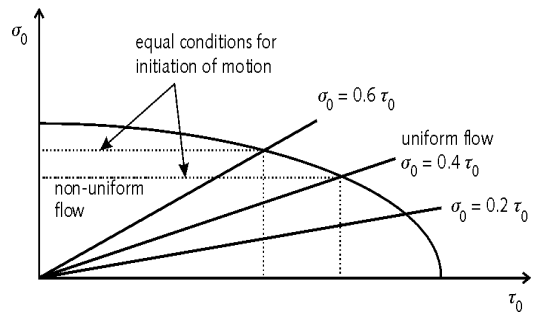

Fig- 10 - σ_0 as function of R_* (uniform flow) Fig-11 Equal conditions for initiation of motion

The area between $\sigma_0 = 0.2\tau_0$ and $\sigma_0 = 0.6\tau_0$ represents all combinations of uniform flow in which the particles are entrained by the bed shear stress. Particles can also be moved by turbulence alone at zero bed shear stress. For example, on a bed covered with ripples or dunes the bed shear stress is zero at the point of reattachment, yet the particles are in an agitated movement. Based on the experimental observations of Raudkivi, the subsequent hypothesis is introduced.

$$\tau_0 + \gamma\sigma_0 = f(\gamma)\frac{\rho}{h_0}\int_0^{h_0} k(z)\mathbf{d}z \tag{19}$$

whence follows:

$$\Delta d_{50} = 0.7\frac{(r_0 U_0)^2}{\Psi_{c,S}\, g} \tag{20}$$

where $\Psi_{c,S}$ is the critical mobility parameter according to Shields. About 90 experiments with small Froude numbers were analysed to validate (20) for flow directly downstream of a sill (Figures 5 and 6). In the tests at model scale both the hydraulic conditions and the geometrical parameters were varied. Moreover two types of transport were simulated, $\Psi_{c,S}$ = 0.032; occasional particle movement at some locations and $\Psi_{c,S}$ = 0.055, frequent particle movement at all locations. In the predictions the turbulence intensity was calculated by (16) in which the source term was neglected (Hoffmans, 2001). To evaluate the accuracy of the computed and measured values of the strength (Δd_{50}), a discrepancy ratio has been used, defined as:

$$r = \frac{(\Delta d_{50})_{\mathbf{computed}}}{(\Delta d_{50})_{\mathbf{measured}}} \tag{21}$$

About 80% of the experiments lie in the range of $0.75 < r < 1.33$.

Escarameia & May (1992) carried out tests with six different stone sizes on a flat bed at various turbulence levels. An adjustable sluice gate was designed and installed in the flume to

produce a hydraulic jump with associated turbulence upstream of the test section. The tail water depths were controlled by means of a flap gate and a valve at the downstream end of the flume (Fig. 12).

The turbulence intensities were measured with a 3D ultrasonic current meter. Fig.13 shows the relation between the loading and the strength of about 30 experiments. The loading is represented by combination of a local turbulence intensity TI(10) at 10% of the flow depth and a depth-averaged flow velocity. The strength is given by $\sqrt{(\Delta g d_{50})}$. The upper and lower boundaries in Fig.13 reflect the transport for respectively $\Psi_{c,S} = 0.06$ and $\Psi_{c,S} = 0.03$. Though the transport was not explicitly measured, all experimental results lie within a range that could be expected. Since the local turbulence intensity at 10 % almost equals the depth-averaged turbulence intensity, (20) could be used to calculate the stability of the bed protection in a preliminary phase. For underflow situations it is recommended that a model relation for r_0 in analogy of (16) should be deduced. In addition, it is advisable to validate equation (20) for horizontal constriction, flow around bridge piers and abutments.

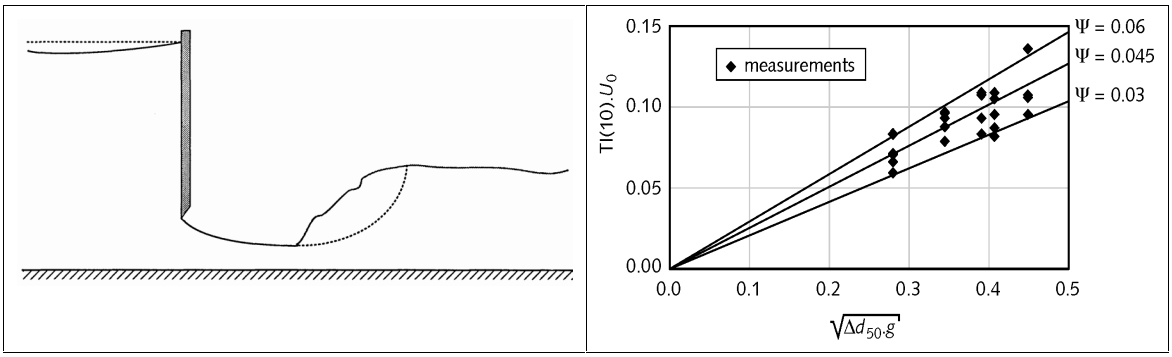

Fig. 12 - Hydraulic jump behind sluice-gate Fig.13-Relation between load and strength

EXAMPLES OF DUTCH SCOUR MODELLING

Where possible the approach described above will be applied. In this section examples of consultancy and research projects carried out by WL|Delft Hydraulics are presented.

Numerical prediction of protrusion scour

Near a factory the river width will be reduced due to the construction of a quay wall over a length of about 350 m from 220 m to 140 m at the upstream end and to 100 m at the downstream end (Fig.14 and 15). WL|Delft Hydraulics has been asked to predict the expected scour depth resulting from the construction of the structure on the right side in a river which will block about one third of the original channel width (Delft Hydraulics, 2002).

The river discharge is 2500 m^3/s, resulting in an upstream flow velocity of 2 m/s with a flow depth of 5 to 6 m. It should be noted that even if no construction is carried out the width of the river reduces from 220 m to about 130 just downstream of the proposed structure. This results in an increased flow velocity of 3 m/s.

At the left bank a “hard point” consisting of a locally more resistant bank is present and therefore protrusion scour may be expected. Protrusion scour occurs when the flow impinges on a bank or (river engineering) structure that is protruding into the flow (“hard points”), see Figure 16. The flow is forced inward and thus concentrated within a smaller width, increasing its velocity and hence its sediment transport capacity increases. The strong and sudden

concentration of flow lines may result in scour of the riverbed upstream of the protrusion. The upstream location of the scour hole distinguishes protrusion scour from local scour in which the scour hole is usually found downstream of the structure and the scour process is related to eddies and vortices inclusive a high turbulence level. We observed major scour holes upstream of hard points for the first time as a different type of scour during the Meghna River project (Haskoning, 1992).

The scour prediction for the construction of the quay wall is based on a mathematical simulation of the situation using Delft3D (http://www.wldelft.nl/). The size of the grid cells is 5 x 4 metres near the corners of the structure and in the narrow part downstream. A period of 2 days was simulated morphologically. The results are shown in Fig. 14 and 15.

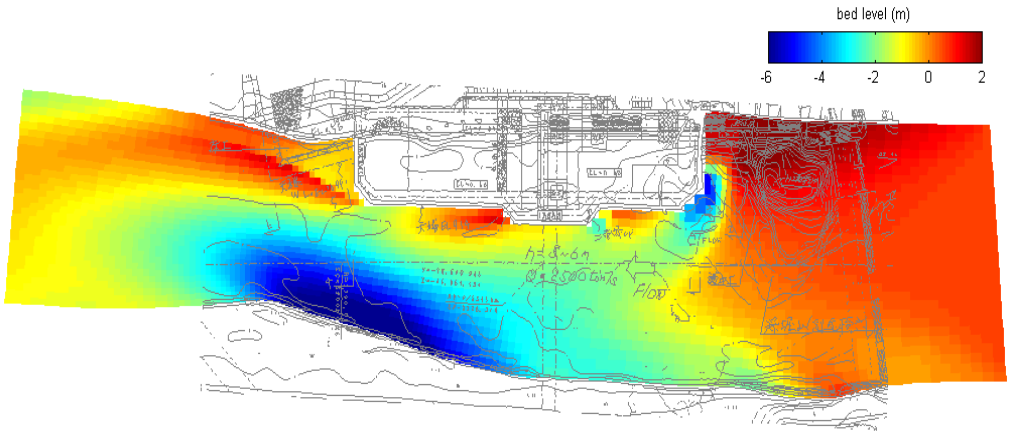

Figure 14 - Bed levels after 2 days of continuous discharge of 2500 m3/s.

(flow direction from right to left)

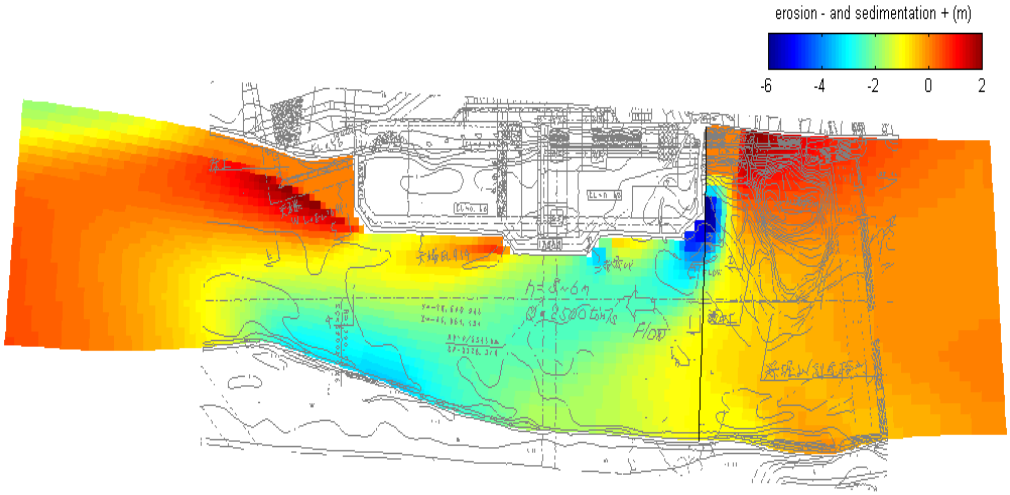

Figure 15 - Erosion and sedimentation pattern

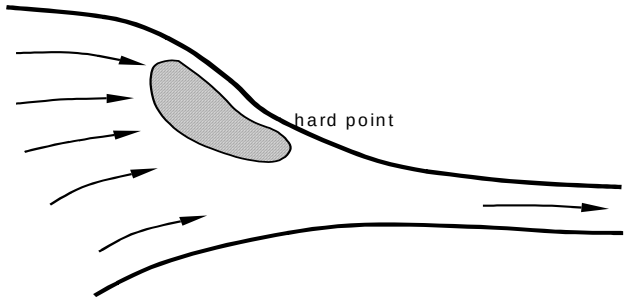

Figure 16 - Principle of protrusion

The constriction caused by the structure results in a general increase in the flow velocities alongside of it, up to 4 m/s. Vortices develop downstream of the structure. Near the upstream edge of the construction no flow separation was observed.

A scour hole with a depth of 6 m relative to the initial bed level quickly develops at the upstream edge of the structure. From the scour hole a channel forms that connects it with the existing scour hole close to the left bank. This scour hole deepens from 4 m to 7 m below the initial bed level. Furthermore, the simulation indicated that downstream of the structure close to the right bank sedimentation will occur despite the vortices and the high turbulence. In general, a local scour hole should be expected at this location.

Local scour holes and macroscale river morphology

Scour studies often use a two-step approach with a far-field and a near-field model. The far-field model is usually a mathematical model, whereas the near-field model is usually a physical model or an empirical scour formula. This approach ignores the feedback from the local scour hole in the near-field model to the morphology in the far-field model. Manuals on river engineering and scour do not deal with this feedback. However, the feedback may change the approach flow conditions in such a way that the local scour hole becomes deeper. This implies that the strong interaction between local scour and river morphology on a large scale is not taken into account.

Mosselman & Sloff (2002) discussed this phenomenon. For this purpose they carried out morphological simulations with the Delft3D model for a 15 km long reach of the River Waal in the Netherlands. As the mathematical model does not yet possess the functionality to create local scour, an initial scour hole is included in the initial bed topography close to the right bank at 7 km downstream of the upper model boundary and this is maintained by continual sediment extraction. Figure 17 shows the channel attraction as a continuous pool develops along the right bank from the scour hole to the next bend. The fairway constriction and bend tightening is also reproduced. Figure 18 shows an additional phenomenon downstream of the scour hole, viz. a pattern of forced bars. In conditions with a regular pattern of bars and channels this pattern constitutes the approach conditions for a local scour hole, and hence determines the scour depth. However, the very presence of a local scour hole itself affects the pattern of bars and channels in return. As a result, the approach flow conditions may change in such a way that the local scour hole becomes deeper. Thus, a feedback arises which may lead to deeper scour.

The foregoing shows the need for a two-dimensional approach. This is more emphasized if we consider the following aspects. In a one-dimensional approach, the bed erodes during the rising limb of the flood hydrograph (Fig.19). Conversely, the bed aggrades during the falling

limb. The result is a lower riverbed during floods. Two-dimensional effects, however, may produce the opposite effect (Fig.20). Main low-water channels may experience sedimentation when the flood is conveyed over a much larger flow width. These channels are incised during the fall of the flood, partly by retarded scour across shallow channels. Thus, the riverbed can be higher during floods. Measurements of this phenomenon have been documented for the Jamuna River in Bangladesh (Delft Hydraulics, DHI & EGIS, 1996).

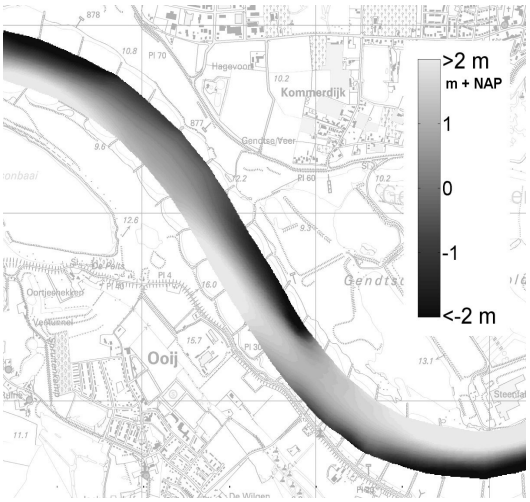

Figure 17 - Computed bed topography after 2 years. For case with continual sediment extraction to maintain scour hole (flow from right to left).

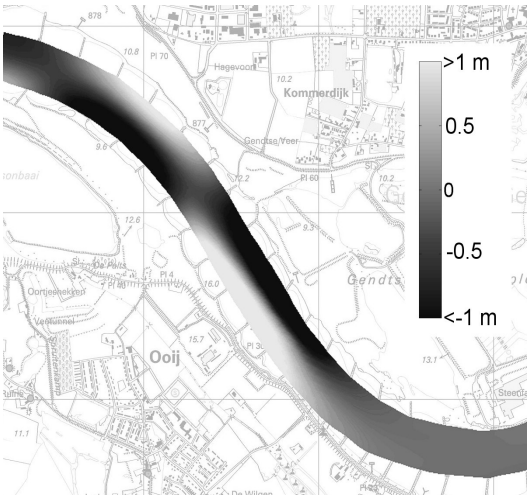

Figure 18 – Computed total erosion and sedimentation.

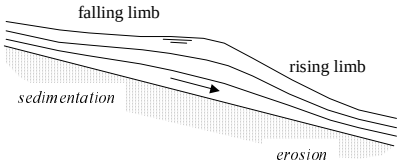

Fig. 19 - Longitudinal profile of flood Wave

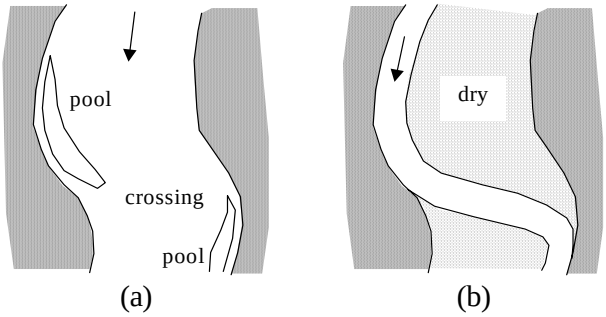

Fig. 20 - Bed topography during flood (a) and low flow (b)

Summarizing: scour studies for the design of structures on alluvial rivers require a two-dimensional approach, including a feedback from near-field models to far-field models, because channel attraction, bend tightening, channel narrowing (constriction) and downstream superimposition of forced bars due to local scour holes affect macro-scale river morphology. Manuals on river engineering and scour usually ignore this effect, which may lead to underestimates of scour depths.

Stability of scour hole slopes

Scouring is of no importance as long as no structures are threatened by the instability of the scour hole slopes. Scour holes of up to 50 m deep were considered to be acceptable near the

Eastern Scheldt barrier. However, a special schedule of regular dumping of gravel and stones were designed to keep the scour hole slopes gentle enough to remain stable (Davis & De Groot, 1983).

In most cases with limited scour hole depth (up to 5 to 10 m) and sandy bed, the natural slope of ca 1V : 1.5H is stable. Outflowing pore water, e.g. due to relatively quick descent of the water level may reduce the critical slope angle to 1V: 2H or 1V: 2.5H. Sometimes a weak clay or peat layer causes a similar reduction of the critical slope angle. The deeper scour holes, however, are often faced with two phenomena which cause a reduction of the critical slope angle to 1V : 4H or even more gentle: liquefaction of sand and breaching.

The sand in rivers and estuaries is often loosely packed, and thus liquefiable. Liquefaction flow slides may occur in scour hole slopes. The looser the sand and the deeper the scour hole, the more gentle is the slope critical for flow slides (Silvis & De Groot, 1995). A sophisticated analysis requires knowledge about the sensitivity to liquefaction of the sand and about its relative density (Stoutjesdijk *et al.*, 1998).

Breaching is a process well analysed on behalf of suction dredging in sand (Van Rhee & Bezuijen, 1998): sand is dredged away from the toe of a slope, causing a steep and unstable part of the slope. The instability propagates upstream more or less slowly and a sand water mixture flows downstream. The process stops, if no further dredging is done, either when the instability has reached the top of the slope or earlier in case of a too gentle slope. Whether the existing slope is too gentle and which slope results at the end, depends on the height of the slope, on the grain sizes and on the size of the initial instability. The steeper the slope, the smaller the sand grain sizes and the larger the initial instability, the more gentle the critical slope and the more gentle the resulting slope.

The same process of breaching or retrogression erosion, i.e. gradual retrogression of a steep slope, may occur in sand filled canyons or other deep natural under water slopes, but cohesive soils are also vulnerable for this process (Van den Berg *et al.* 2002). It may also occur in deep scour holes if a natural initial instability occurs, such as a (small) flow slide in some loosely packed sand layers or a local instability of a clay layer which has been undermined by the gradual scouring process.

Figure 21 shows an example of a bank collapse due to scouring and breaching, but designers should know that the same can happen at bed protection around bridge piers, downstream of sills and other structures.

Besides material parameters the stability of scour slopes also depends on hydraulic parameters. With higher flow velocities and more turbulent conditions, much steeper slopes are found (Hoffmans & Verheij, 1997).

Interaction of scour and bank protections

Bank protections attract the main flow in river channels, because of the formation of scour holes, which are local areas of reduced flow resistance due to the larger flow depth. This results in convergence of the flow towards the local scour holes that may become deeper than without the presence of a protected bank. To explain this, consider non-protected meander bends in homogeneous soils that have smooth curves (Fig.22-A). The bend migrates in a transverse (extension) and a downstream direction (translation). In front of the bank a scour

hole due to bend scour exists.

A bank protection hinders the extension (Fig.22-B) and a deeper scour hole develops compared to a non-protected bank. This scour hole attracts the flow and slows down or stops the downstream translation. Thus, the smooth curvature of the meander bend changes, resulting in deeper scour, because the approach channel impinges more perpendicularly on the bank and the curvature of the bend becomes even more pronounced.

In addition, another mechanism also plays a role when the outer bank of a rapidly migrating channel is stabilised: the input of bank erosion products stops and consequently the supply of sediment to the outer-bend pool stops. As a result the scour hole will deepen.

Figure 21 – Bank collapse due to scouring

Clearly, this phenomenon should influence the design level of the toe of the bank protection in order to prevent undermining.

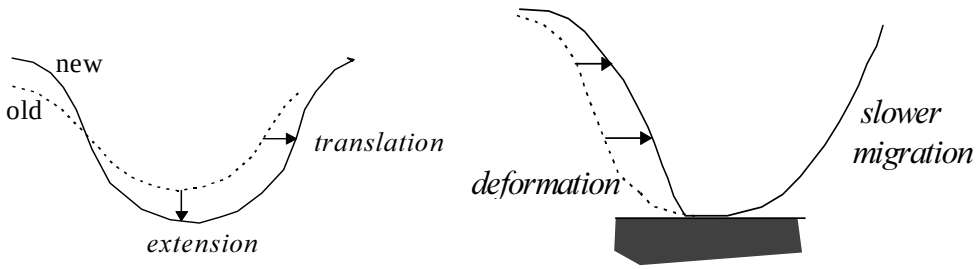

Figure 22- Meander bend deformation due to local resistance against erosion (A: smooth bends in homogeneous soil; B: hindered meandering by a bank protection).

Probabilistic approach

Usually, scouring is a combination of different types of scour. For instance, a combination of bend scour and local scour may occur near a spur. For many combinations the mode of combination is unclear, while, in addition, a lot of uncertainty exists about exact design values of parameters and coefficients. Nevertheless, the expected scour depth is a design parameter

with a high economic impact. For this reason it is recommended that a joint probability analysis, taking into account the coherence of the types of scour involved and paying sufficient attention to expected values of parameters and coefficient, should be performed.

The combination of different types of scour is the first aspect that is briefly discussed. For instance for local scour and bend scour, there are two possible ways to determine the expected scour:

1. Adding both types of scour: $h_{total} = \alpha_{bend}\, h_0 + \alpha_{local}\, h_0 = (\alpha_{bend} + \alpha_{local})\, h_0$ (22)
2. Multiplying both coefficients: $h_{total} = \alpha_{bend}\, \alpha_{local}\, h_0$ (23)

Probably, the first approach is correct. Mesbahi (1992) proved this with small-scale experiments. Based on approximately 1000 experiments both at model and prototype scale Hoffmans (1995) showed that the total scour around bridge piers and abutments in channel flow is the sum of constriction scour and local scour (see relation 2). Some empirical formulas also include different types of scour. However, for most of the combinations of types of scour, we do not have a formal methodology to determine the scour. Thus, for the time being sound engineering judgement is required and a need for more research into this issue.

To overcome some of the problems it is possible to carry out a probabilistic approach. Then, the joint scour depth for a range of exceedance probabilities may be determined, for instance with a level II probabilistic method. To illustrate the possibilities: suppose that we will know the equilibrium scour depth for a slender structure, then:

$$y_{m,e} = L_s f_1 \cong b\left(\left(1+3r_0\right) U_\ell / U_c - 1\right) \tag{24}$$

Each parameter is characterized by a probability distribution, for instance expressed by the average value μ and standard deviation σ. However, it is not sufficient to use just r_0; it has to be expressed as:

$$r_0 = \sqrt{c_s + 1.45\sqrt{g}/C} \tag{25}$$

where c_s is a structure-dependent turbulence factor (see e.g. relation (17). Furthermore, the flow velocity U_ℓ should be related to the local unit discharge q and its fluctuations, and not the total discharge Q. Finally, also coefficients such as 1.45 in the formula for r_0 should be defined with both an average and a standard value.

After a probabilistic calculation has been carried out for a range of selected scour depths the probabilities of exceedance can be determined. This enables designers to choose the most appropriate design scour depth, which is in accordance with other failure probabilities of the structure. In addition, a probabilistic approach also gives insight into the parameters that have the greatest influence on the scour depth.

CONCLUSIONS: SOME NEEDS FOR RESEARCH

The possible consequences of scour, viz. the instability of one or more bridge piers and hence the superstructure, or a dike breach in combination with an inundation, require a well-funded design, which takes into account accepted risk levels and a state-of-the-art calculation of the expected scour depth. For a first estimate rules of thumb may be used and these may be optimised by applying two-dimensional morphological calculations.

In this lecture both aspects are discussed. Firstly, the concept of a generally applicable scour formula, that is independent of the type of structure is presented. In addition to geometrical parameters and coefficients, the formula also takes into account turbulence and the stochastic aspects of bed material characteristics. Obviously, validation of the formula under different

hydraulic conditions and local situations requires data and time and consequently, the new scour formula is not ready for immediate use. For instance, it is only for sills that a formula for the relative turbulence r_0 has been derived, while the formula for Δd_{50} has not been validated for all types of non-uniform conditions. Aspects such as combined scour and the scour of cohesive material are not included because the existing knowledge is either insufficient or even not available.

Secondly, examples of consultancy and research projects in which the need for the application of 2D-mathematical, morphological models is shown are presented. The examples show the strong interaction between local scour and the macroscale river morphology, and the necessity for feedback between the mutual results. The mathematical models still require improvements, although some progress has been made, in particular for general and natural scour (see the presented examples). For example, the formation of a local scour has not yet been implemented in our own model Delft3D.

Summarizing, the following needs for research can be mentioned:

- Validation of the structure-independent formula for scour caused by different structures.
- Extension of equation (16) or (25) for the relative turbulence r_0 to provide a formula that is also valid for other structures.
- Validation of the stability formula (20) for horizontal constriction, flow around bridge piers and abutments, and flow in the ship's propeller jets.
- Determination of how local scour and natural scour should be combined: by just adding the separate values or by multiplying the coefficients.
- Breach processes (in sand and cohesive material) and their influence on scour, as well as determination of parameters influencing scour in cohesive materials.
- Implementation in mathematical models (and further validation) of the stochastic and fractionwise approach in order to calculate transport at the threshold of motion.

Finally, the Dutch approach is to treat scour as an integrated problem in which large-scale morphology, all types of scour, the process of breaching and soil mechanics each have a role. We strongly recommend this approach in order to prevent the underestimation of expected scour depth, which may result in undesired consequences of scour.

ACKNOWLEDGEMENTS

The authors wish to thank the Ministry of Public Works and Water Management and WL|Delft Hydraulics for their permission to present the research results described in this lecture. They also thank Mr. Maarten de Groot of Geodelft for his contribution to the lecture.

REFERENCES

1. Berg, J.H. van den, Gelder, A.van, Mastbergen, D.R., 2002, "The importance of breaching as a mechanism of subaqueous slope failure in fine sand", Sedimentology 45, pp.81-95.
2. Booij, R. 1989, "Depth-averaged k-epsilon model in ODYSSEE", Delft University of Technology, Report No.1-89, Delft. The Netherlands.

3. Bos, K.J., Verheij, H.J., Kant, G., Kruisbrink, A.C.H., 2002, “Scour protection around gravity based structures using small size rock”, First Intern.Conf. on Scour of Foundations, Texas A&M Univ., College Station, Texas, USA.

4. Breusers, H.N.C., Nicollet, G., Shen, H.W., 1977, “Local scour around cylindrical piers”, Journal of Hydraulic Research 15 (1977) No.3.

5. Cardoso, A.H., Bettess, R. 1999, “Effects of time and channel geometry on scour at bridge abutments”, ASCE, Journal of Hydraulic Engineering, Vol.125, No.4, April, 1999.

6. Davis, P.G.J., Groot M.B. de, 1983, “Economic scour protection with adequate guarantee for structural safety”, Proc. XXth IAHR Congress, Vol.III-B.d.4

7. DELFT HYDRAULICS, DHI and EGIS, 1996, “River Survey Project; Spatial representation and analysis of hydraulic and morphological data”, Special Report No. 17, Water Resources Planning Organization, Government of Bangladesh.

8. Escarameia, M., May, R.W.P.,1992, “Channel protection; Turbulence downstream of structures”, HRWallingford, Report SR 313, England.

9. Escarameia, M., May, R.W.P., 1999, “Scour around structures in tidal flows”, HR Wallingford, report SR521, April 1999.

10. Grass, A.J., 1970, “Initial instability of fine bed sand”, Proceedings of the American Society of Civil Engineers, Hydraulic Division, Vol.96, No.HY3, pp.619-632.

11. Haskoning/Delft Hydraulics/BETS, 1992, “Meghna river short-term bank protection project, Annex B: Geomorphology, and river morphology”, Prepared for BWDB.

12. HEC-18, 1995, “Evaluating Scour at Bridges” Federal Highway Administration, Hydraulics Engineering Circular No.18, Publication FHWA HI-96-031, Washington, DC, USA.

13. Hoffmans, G.J.C.M., 1992, “Two-dimensional mathematical modelling of local-scour holes”, Delft University of Technology, Doctoral thesis, Delft, The Netherlands.

14. Hoffmans, G.J.C.M. 1993, “A study concerning the influence of the relative turbulence intensity on local-scour holes”, Ministry of Public Works and Water Management, Road and Hydraulic Division, Delft, The Netherlands.

15. Hoffmans, G.J.C.M. 1995, “Scour around bridge piers and abutments”, Report W-DWW-94-312, Ministry of Public Works and Water Management, Road and Hydraulic Division, unpublished notes, Delft, The Netherlands (in Dutch).

16. Hoffmans, G.J.C.M., Verheij, H.J., 1997, “Scour Manual” A.A.Balkema Publishers, Rotterdam/Brookfield, ISBN 90.5410.673.5.

17. Hoffmans, G.J.C.M. 2001, “Predictability of depth-averaged stability concepts”, Ministry of Public Works and Water Management, Road and Hydraulic Division, unpublished notes, Delft, The Netherlands.

18. Kleinhans, M.G., Rijn, L.C. van, 2002, “Stochastic prediction of sediment transport in sand-gravel bed rivers”, Journal of Hydraulic Engineering 128(4), ASCE, pp.412-425,

special issue: Stochastic hydraulics and sediment transport.

19. Launder, B.E., Spalding, D.B., 1972, “Mathematical models of turbulence”, Academic Press, London, England.

20. Melville, B.W., Coleman, S.E., 2000, “Bridge Scour”, Water Resources Publications, LLC, Colorado, USA.

21. Mesbahi, J., 1992, “On combined scour near groynes in river bends”, Delft Hydraulics/IHE Delft, M.Sc. thesis HH132, Delft, The Netherlands.

22. Mierlo, van M.C.L.M, Ruiter, J.C. de, 1988, “Turbulent measurements above dunes”, WL|Delft Hydraulics, Report Q789, Vol.I and II, Delft, Netherlands.

23. Mosselman, E., Sloff, K., 2002, “Effect of local scour holes on macroscale river morphology”, Proc.Congress “River Flow 2002”, Louvain-la-Neuve, Belgium, September 2002

24. Nezu, I., 1977, “Turbulent structure in open-channel flows”, Department of Civil Engineering, Kyoto University, Japan ”, (translation of doctoral dissertation).

25. Raudkivi, A.J., 1998, “Loose boundary hydraulics”, Balkema, Rotterdam, The Netherlands.

26. Rhee, van C., Bezuijen, A. 1998, “The breaching of sand investigated in large-scale model tests”, Proc. Int. Conf. Coastal Engineering (ASCE), Vol. 3, pp.2509-2519.

27. Rijn, L.C. van, 1993, “Principles of sediment transport in rivers, estuaries and coastal seas”, Aqua Publications, ISBN 90.800356.2.9.

28. Ruiter, de J.C.C., 1980, “Incipient motion and pick-up of sediment as function of local variables”, WL|Delft Hydraulics, Report R 657-XI, Delft, The Netherlands.

29. Sumer, B.M., Christiansen, N., Fredsoe, J., 1993, “Influence of cross-section on wave scour around piles”, Journal of Waterway, Port, Coastal and Ocean Engineering ASCE, 119(5), pp.477-495.

30. Silvis, F., Groot, de M.B., 1995, “Flow slides in the Netherlands: experience and engineering practice”, Can. Geotechn. J. 32 pp. 1086-1092.

31. Stoutjesdijk, T.P., Groot, de M.B., Lindenberg, J., 1998, “Flow slide prediction method: influence of slope geometry”, Can. Geotechn. J. pp. 34-54.

32. Townsend, A.A., 1976, “The structure of turbulent shear flow”, Cambridge University Press, Cambridge.

33. Verheij, H.J., 2002, “Breaching in cohesive soils”, WL|Delft Hydraulics, research report Q2959, Delft (in Dutch, in preparation).

34. Whitehouse, R.J.S., 1998, “Scour at marine structures”, Thomas Telford Publications, ISBN 0.7277.2655.2.

35. WL|Delft Hydraulics, 2002, “ Scour and morphological consequences of a quay wall”, WL|Delft Hydraulics, report Q3160, Delft, The Netherlands.

A Geotechnical Perspective: Design and Construction of Highway Bridge Foundations for Scour

By
Christopher E. Dumas[1], Joseph Krolack[2]

ABSTRACT

Scour of foundation soil and rock is the most common cause of bridge failures. To address this problem, AASHTO and FHWA developed and implemented comprehensive and stringent design guidelines and codes during the late 1980's and early 1990's. Although, scour related losses have been significantly reduced as a result of their implementation, significant concurrent increases in foundation costs and construction difficulty have occurred as well.

This paper examines the causes of scour related escalation in foundation costs and constructability difficulties from a geotechnical perspective. The focus will be on: (a) key considerations within the current scour design and construction processes; (b) application of scour codes and guidelines; (c) gaps in processes and guidelines; and (d) scour research priorities.

INTRODUCTION

By far, the most common cause of bridge failure is the scouring of soil and rock from around the foundations. The seriousness of this problem with respect to the cost of direct damage, economic disruption, and loss of life led FHWA and AASHTO to develop and implement comprehensive and stringent design guidelines and codes. As a result, scour related losses have been significantly reduced since in the late 1980's and early 1990's, when these guidelines and codes were implemented. However, concurrently, there has also been a significant increase in foundation costs and construction difficulty associated with scour foundations. It is not uncommon for foundation costs increasing by a factor of between two and four. For a single $100 million bridge project, this can represent an increase foundation cost of between $10 million to $40 million. On an extremely large project, scour requirements increased the cost of a single pier foundation by $10 million. In most instances, these cost increases are attributable to:

(i) A non-interactive, compartmentalized process where little interaction/coordination exists between hydraulic, geotechnical and construction engineers.
(ii) Conservative and/or incomplete application of AASHTO and FHWA requirements
(iii) Gaps within the current guidelines
(iv) Various combinations of items i through iii.

1 Geotechnical Engineer, FHWA Eastern Resource Center, 10 South Howard Street, Suite 4000, Baltimore MD 21201
2 Hydraulic Engineer, FHWA Eastern Resource Center, 10 South Howard Street, Suite 4000, Baltimore MD 21201

This paper presents a geotechnical perspective of: (a) key considerations within the current scour design and construction process; (b) how and why Highway Agencies, consultants, should develop and fully implement detailed written protocols for the determination of foundations scour; and (c) improvements needed in processes, guidelines, and research.

SCOUR PREDICTION PROCESS

Scour is a fundamental component of bridge foundation design. Scouring of foundation soils directly impacts foundation performance and, therefore, the type, size and constructability of the foundation. At the same time, scour is fundamentally dependent upon the foundation type, size, and geometry. Therefore, foundation design, and the estimation of scour depths, should inherently be an iterative and interactive activity between Bridge Engineers, Geotechnical Engineers, and Hydraulic Engineers. The need for this interdisciplinary process is explicitly stated and implicitly embedded throughout the FHWA scour evaluation guidelines (1).

Unfortunately, the current practice by which scour prediction and foundation design are executed is not interactive, iterative or interdisciplinary. Often, the hydraulic engineer becomes involved in design at a relatively late stage of the process. They are presented with a bridge design where major structural, geometric (layout), and geotechnical elements have already been established a-priori. Unfortunately, these designs (often inefficient from a hydraulic perspective) can introduce the very factors that result in large scour magnitudes. An example is a recent interchange project where thirty percent bridge plans were developed without consideration and incorporation of issues that where known by hydraulic engineers as of importance. Piers were designed skewed to the stream and flood plain flow, and the selected foundations cause significant flow constrictions. The results of the subsequent hydraulics analysis showed excessive scour as well as backwater flood levels, which did not meet FEMA permitting requirements. Expensive and time consuming redesign activities ensued.

Another non interdisciplinary process is one in which each of these discipline develops their own scour prediction estimates. The hydraulic engineer makes his/her estimate based very limited, or generalized, input provided with respect to the foundation size and special geotechnical considerations. This scour prediction value is then passed onto the geotechnical engineer who in turn develops a geotechnically modified value, and sends it to the bridge engineer who then develops his modified value.

The one typical outcome of these processes is that all parties are surprised at the complexity and rapidly increasing cost of the project. In essence, all three parties have engaged in a non-interactive, non-iterative compartmentalized process does not permit any optimization. As described later in this paper, this process can be particularly costly at sites requiring scour countermeasures and those with multiple soil layers and rock.

PERMANENT SCOUR COUNTERMEASURES

Similar to scour prediction, there is a lack of focus on fundamental design and construction issues, and a lack of appropriate interaction between hydraulic, geotechnical, and construction engineers. This is demonstrated by the fact that the number one cause of failures for countermeasures is not the

hydraulic design and/or countermeasure selection, but inadequate geotechnical, geosynthetics, and installation design. Specifically, these countermeasure are based and constructed upon underwater soil slopes that typically require benching and geosynthetics.

In particular, benching is required for short term and long term stability of the slope. The countermeasure needs to be properly keyed into the soil so that it will remain stable and avoid undermining (2). To be effective, benching requires specialized knowledge of soil engineering characteristics, slope stability, and construction placement, specifications, and quality control.

Geosynthetics are essential for filtration, and bridging of the countermeasure weight. Filtration allows the water pass, but leaves the soil in place. Bridging keeps the countermeasure intact by spread the load out over a large soil area and, thereby, keeping the countermeasures from sinking non-uniformly. This requires specialized knowledge of geosynthetics and their construction (3). Selection of an appropriate geosynthetics requires knowledge of (a) material characteristics such as creep, long term filtration capability for the site specific soils, degradability, susceptibility to construction damage; (b) material specific quality control methods and testing; and (c) writing geosynthetics specifications. Successful installation requires detailed knowledge and experience in placing geosynthetics underwater, and writing effective construction specifications and quality control protocols.

GEOTECHNICAL SITE INVESTIGATION

Another area where interdisciplinary coordination is in needs of improvement is geotechnical site investigations. Specifically, field and laboratory information needed for a detailed site specific scour analysis is frequently not evaluated and incorporated into the geotechnical investigation. Investigation and laboratory testing guidance is provided in FHWA HEC 18 and the 1991 FHWA Memorandum on rock scourability. Insufficient coordination and/or incomplete application of FHWA guidance too often result in cost increases and time delays from:

a. Conservative and difficult to construct foundations. Insufficient information is collected to execute, or rely upon, a site specific scour evaluation as recommended and outlined in HEC 18 scour estimation procedure (page 2.1), and the 1991 FHWA Memorandum on rock scourability.

b. Additional drilling mobilizations and lab work. If the initial site investigation and scour prediction indicates an extremely costly scour depth, a site specific evaluation may be undertaken. Consequently, a second phase drilling will probably be required, as well as a lab program to obtain pertinent information not collected in the first phase. The costs and time associated with second phase are considerable once initiated. For example,

    - Two-months to scheduled and begin drilling, one to six month to execute drilling, and one to two months to perform lab work, and revise scour prediction and foundation calculations–four to ten months total.
    - $10,000 Mobilization Cost
    - $5,000 per day of drilling, or $100,000 per month of drilling.
    - $10,000 to $50,000 in lab testing costs.

MULTI-LAYER GROUND STRATIGAPHY

Currently, there is no direct guidance for estimating scour for sites with multi-layer ground stratigraphy. As a consequence, the scour prediction is frequently based on the very fine upper soil layer which in turn results in unrealistic scour design values–calculated scour values can significantly exceed the depth of the soil layer itself. This extremely conservative approach is one of the more frequent causes of high foundation costs. From a geotechnical perspective, scour calculations for a multi-layer site need to be performed in as series of scour calculations that emulate the sequence of scour occurring at the site. In addition, this situation strongly demonstrates the need for a site specific scour study as outlined in HEC 18.

SCOUR IN ROCK

In 1991, the FHWA Bridge Division issued a Memorandum (4) that provided "interim" guidance on empirical methods and testing to assess rock scourability, until result of ongoing research permit more accurate evaluation procedures.

Prior to this Memorandum, the lack of guidance on rock scour had frequently resulted in unrealistic conservative rock scour estimates that profoundly increased foundation costs and construction difficulty, while no quantifiable improvement to bridge reliability. Two common methods that result in these extremely conservative scour estimates where:

- Scour estimates where based on the particle size of the soil above the rock.
- Over-reliance on calculated scour values versus site specific historical behavior.

The 1991 Memorandum set out guidance to address this problem as follows:

a. Introduce some level of understanding of common geotechnical information and methods for indexing the engineering characteristics that could rationally be employed by hydraulics engineers for the prediction of rock scourability.

b. Establish and clarify that the geotechnical information is an Index Testing based approach which should be supplemented by local experience and historical data (bridge inspection reports, etc.)

c. Begin and interdisciplinary approach to scour prediction.

d. Bring an awareness of the cost and construction implications of scour

The Memorandum did succeed at many of the objectives, but a key issue not explicitly stated in this 11-year old memorandum is that the scourability of rock is typically very different than that for soil. Specifically, rock formations are not large gravel deposits for which an extrapolation of particle size and water velocity method for sands is reasonable. Rock formations are commonly large masses that have cracked in-situ over time. The rock segments are extremely large and are held in place

not only by gravity, but also by very high interlocking friction. In these cases, it is rock erode-ability that will impact the removal of support from the foundation. The Memorandum did provide recommendations on appropriate testing procedures for indexing of rock erodeability (Slake Durability, Soundness, Abrasion), but did not provide explicit guidance about how testing procedures should be used in conjunction with RQD, unconfined compressive strength, local experience, and interdisciplinary interaction.

The New River Bridge Replacement project is an excellent example of common interpretation and application of the 1991 Memorandum. The foundation design called for a spread footing keyed into the dense limestone. The limestone was horizontally bedded, and had an RQD average of about 40%. As per the Memorandums recommendation for RQD values lower than 50%, the designer called for the limestone around the footing to be removed for a considerable distance around the footing, and replaced by a rip rap countermeasure. A "strict" reading of the Memorandum and FHWA scour countermeasure guidelines (4) would have resulted in this design becoming the constructed configuration. However, in this case, review of the proposed design by the DOT and FHWA triggered the DOT to perform a more detailed site-specific geotechnical and hydraulic evaluation of the existing bridge's foundations.

The investigation found no evidence of scour, or rock erosion, at the existing foundations, and concluded that the scour performance would be better without removal and replacement. Removal techniques would further fracture the existing rock, and replacement with rip rap would change a rock erosion scour condition, to a large particle scour condition. The understanding of the nature of the site allowed design of a more suitable scour countermeasure. The site investigation saved construction time, difficulty, and cost (i.e., several million dollars) while providing a significant reduction in rock scour potential. The site investigation saved construction time, difficulty, and cost while providing a significant reduction in rock scour potential.

SCOUR ESTIMATE METHODS, AND RESEARCH NEEDS

Due to extreme complexity, foreseen and unforeseen interactions, and the highly site specific nature of soil conditions, geotechnical engineering relies heavily on semi-empirical design methods developed via correlation and calibration of field observations. Intrinsic to the effectiveness of this method is the ability to obtain direct measurements of actual performance (load testing, etc.) and site geotechnical conditions. New methods and theories are always evaluated, and calibrated with these direct field measurements.

Scour estimation is, at the least, an equally complex task that is also highly site specific and influenced by many foreseen and unforeseen interactions. From a geotechnical perspective, scour estimation and research activities should be driven by this reality. Unfortunately, this does not seem to be the case for scour. The current equations and methods for calculating bridge scour are based primarily on laboratory research. For a multitude of reasons, very little field data has been collected to verify the applicability and accuracy of the various design procedures for the range soil conditions, flow conditions, and bridge configurations.

RECOMMENDATIONS

This paper has presented a geotechnical perspective as to the causes of scour related escalation in foundation costs and construction difficulties. From this perspective, key scour design and construction processes; guidance documents, and research priorities were identified and examined. Recommendations for improvements in these areas are presented below.

1. Scour Prediction Process (Soil and Rock). Highway Agencies, Consultants, and other Organizations involved in the design and construction of bridges should develop and fully implement detailed written protocols for the determination of foundations scour. These protocols should be based on the design philosophy, concept and procedures as presented in FHWA publication HEC 18 , and reflect the iterative, interactive, and interdisciplinary nature of scour prediction for bridge foundations.

2. Permanent Scour Countermeasures. Successful design and installation of scour countermeasure requires advanced hydraulic, geotechnical, and construction engineering expertise. The depth of expertise in each of these disciplines far exceeds what a single hydraulic, geotechnical, or construction engineer will posses. Therefore, as with the scour prediction process, interactive and interdisciplinary protocols for the selections and design of countermeasures should be developed and implemented.

3. Geotechnical Site Investigation. The planning and execution of geotechnical site investigations should encompass information needed for the overall site specific scour evaluation and prediction analysis. This would include drilling locations, soils data, and lab testing as outlined in HEC 18, and the 1991 FHWA Rock Scour Memorandum.

4. Multi-Layer Ground Stratigraphy. Scour calculations for a multi-layer site should be performed in as series of scour calculations which emulate the sequence of scour occurring at the site. A possible procedure is a follows:

    i. Calculate the scour depth using hydraulic and geotechnical data for the top soil layer. If this number is greater then the depth of the top layer, the top layer is scoured away. Go to step ii.

    ii. Adjust the input parameter to account for the removal of the top soil layer. Calculate a scour depth using the adjusted input, and geotechnical data from the second layer. If this number is greater then the depth of the top layer, the top layer is scoured away. Go to step iii.

    iii. Repeat step two until a calculated scour value doesn't exceed the specific soil layers thickness.

6. Scour in Rock.

   a. Rock Scour estimates should always include consideration of specific historical behavior, and performance of rock. Estimates should not be based solely on RQD nor should they ever be based on the particle size of soil above the rock.

   b. Interdisciplinary Task Force should be assembled with the mission of developing clear guidance for differentiating between erode-able and scour-able rock. This may be best achieved by expanding the 1991 FHWA Memorandum to include more direct guidance as to how the geotechnical index tests for erode-ability should be used in conjunction with RQD, unconfined compressive strength, local experience, and interdisciplinary interaction.

   c. Develop a national Standard RQD, and Coring equipment and methods. RQD and coring methods are not homogeneous across the USA.

7. Scour Estimate Methods, and Research Needs. The number one priority of scour research and allocation of funds should be focused on:

   I. Developing equipment for accurately measuring insitu scour depth as they occur. This not a hydraulics, geotechnical, or civil engineering problem. It requires individual experts in sensor, wireless technologies, and electrical engineering. Great advances in technology for non civil engineering application have occurred over the last ten years--technologies that could be adapted to this specific use.

      An example of this is ultra high bandwidth wireless technology that can transmit signals through concrete. In addition, it is essential that the decision process for developing and implementation of such equipment and systems evaluates the cost of the system relative to the hundreds of millions of dollars that can be save in a few short years via improved scour prediction reliability, and not relative to the initial installation costs.

   II. Designing and implementing a comprehensive national monitoring program that will generate the data needed to improve the accuracy of scour predictions over a wide variety of geotechnical, hydraulic, and structural conditions. This a very similar approach to earthquake research in which instruments are installed to “listen” and record seismic events which may decades after their installation.

References

1. FHWA Hydraulic Engineering Circular Number 18, Evaluating Scour at Bridges, Fourth Edition, NHI-01-001, May 2001, **http://www.fhwa.dot.gov/bridge/hydpub.htm**

2. FHWA Hydraulic Engineering Circular Number 23, Bridge Scour Stream Instability Countermeasures, FHWA HI-97-030, July 1997, **http://www.fhwa.dot.gov/bridge/hydpub.htm**

3. FHWA Geosynthetic Design and Construction Guidelines Participant Notebook HI-95-038 PB95-270500, http://www.fhwa.dot.gov/bridge/hydpub.htm

4. FHWA Memorandum, Scourability of Rock Formations, Bridge Division, Office of Engineering, July 1991.

5. Training Course in Geotechnical and Foundation Engineering: Subsurface Investigations -Participants Manual, HI-97-021, **http://www.fhwa.dot.gov/bridge/hydpub.htm**

Local Scour Depths at Bridge Foundations: New Zealand Methodology

By

Bruce Melville[1]

ABSTRACT

A comprehensive method for estimating local scour depths at bridge foundations is presented. The method, which is presented in detail in Melville and Coleman (2000), was developed in New Zealand on the basis of an extensive series of laboratory investigations. Application of the method ensures that the various influences on local scour depths are systematically addressed. These are the characteristics of the flow approaching the bridge crossing, the shape of the river channel in the vicinity of the bridge, the characteristics of the bed sediments in the vicinity of the bridge, the geometry of the bridge foundations (piers and abutments), and the peak value and duration of the design flood. Application of the method is highlighted in two examples.

INTRODUCTION

The major damage to bridges at river crossings occurs during floods. Damage is caused for various reasons, the main reason being riverbed scour at bridge foundations, namely piers and abutments. In New Zealand, at least one serious bridge failure each year (on average) can be attributed to scour of the bridge foundations. The damage can range from minor erosion at an adjacent river bank or bridge approach, to complete failure of the bridge structure or its road approach. Complete failure results in severe disruption to local traffic flows. The frequency of bridge failures due to scour has spurred many research projects of this vexing problem.

In spite of the significant investment in bridge scour research, bridges still fail due to scour. This has been a consequence of both inadequacies in design criteria adopted for older bridges and the lack of convenient and appropriate availability of the results of the past scour research to practitioners. A comprehensive treatment of the present state of knowledge on bridge scour is now available in Melville and Coleman (2000). The monograph, which makes use of New Zealand's extensive experience with scour problems, addresses all aspects of bridge scour, including general scour, contraction scour, local scour, scour countermeasures and 31 case histories of scour failures. The methodology for local scour is summarised in this paper. Examples of application of the local scour method are included.

ESTIMATION OF LOCAL SCOUR DEPTHS

The method for estimation of local scour depths at bridge piers and abutments by Melville and Coleman (2000) is presented. The basic data required to apply the method are:

[1] Professor of Civil Engineering, The University of Auckland, Auckland, New Zealand

- ***Approach flow***, characterised by the mean velocity (V), depth (y) and Manning's coefficient (n) of the main channel. For bridge piers, the appropriate values of V and y are those, which best represent the flow approaching the particular pier.
- ***Bed sediment***, characterised by the median size (d_{50}), maximum size (d_{max}) and geometric standard deviation (σ_g) of the particle size distribution. In practice, d_{90} (or a similar size) can be used in place of d_{max}, which is unlikely to be known.
- ***Foundation geometry***, characterised by the pier width (b) and pier length (l) for piers, abutment length (L) for abutments, shape (*Sh*) and alignment (θ). Circular piers are characterised by pier diameter (D). For nonuniform piers, additional parameters are required, as described below.
- ***Channel geometry (for abutments only)***, characterised by V, y, n and the depth (y*), Manning's coefficient (n*) and width (L*) of the flood channel.

The design method is based on the following relation for the depth of local scour:

$$d_s = K_{yB} K_I K_d K_s K_\theta K_G K_t \tag{1}$$

where the K factors are empirical expressions accounting for the various influences on scour depth: K_{yB} = depth-size ≡ K_{yb} for piers and K_{yL} for abutments; K_I = flow intensity; K_d = sediment size; K_s = pier or abutment shape; K_θ = pier or abutment alignment; K_G = channel geometry ($K_G \equiv 1$ for piers); and K_t = time. K_I is formulated to include sediment gradation effects as well as flow velocity effects. $K_{yB} = f(y, B)$ and d_s have the dimension of length, while the other K factors are dimensionless.

The K factors are derived from envelope curves fitted to laboratory data. Expressions for the various K factors are summarised in Tables 1 and 2 and illustrated in Figures 1 and 2 for piers and abutments, respectively. For nonuniform piers, the pier width (b) is replaced by the equivalent pier width (b_e), as illustrated in Figure 3.

K_I is a function of the threshold velocity (V_c), the armour velocity (V_a) and the velocity parameter $[V-(V_a-V_c)]/V_c$. The procedure for estimating these velocities is explained below and summarised in Tables 1 and 2.

Maximum Possible Local Scour Depths at Piers and Abutments

The local scour depth is given by (1), in which K_I, K_d, K_G and K_t are always less than or equal to unity. Thus the maximum possible equilibrium local scour depth is

$$d_{se)\max} = K_{yB} K_s K_\theta \tag{2}$$

A simple equation for the maximum local scour depth at piers is obtained by substitution of the expression for K_{yB} for narrow piers in (2), giving

$$d_{se)\max} = 2.4 K_s K_\theta b \tag{3}$$

For design purposes, (3) is adequate for estimation of local scour depth at piers in many situations.

PHYSICAL BASIS OF SCOUR DEPTH METHODOLOGY

The K-factors in (1) represent the various physical influences on local scour depth, as determined from systematic laboratory-based tests. In the following sections, each parameter is discussed briefly.

Flow Depth - Foundation Size (Depth - Size) Factor, K_{yB}

Data, which demonstrate the influence of $K_{yB} = f(y, B)$ on local scour depth, are given in Figure 4. The plot includes the reliable pier and abutment local scour depth data that are unaffected by flow intensity, sediment size, sediment gradation, foundation shape and alignment, channel geometry and time. The data plotted are from Chabert and Engeldinger (1956), Laursen and Toch (1956), Hancu (1971), Bonasoundas (1973), Basak (1975), Jain and Fischer (1979), Chee (1982), Chiew (1984), and Ettema (1980), for piers; and Gill (1972), Wong (1982), Tey (1984), Kwan (1984, 1988), Kandasamy (1989), and Dongol (1994), for abutments.

The solid lines in Figure 4 are envelopes to the data and apply, from left to right respectively, to wide (long), intermediate width (length) and narrow (short) piers (abutments) at threshold conditions. For clear-water scour at reduced flow velocities, lesser scour depths are developed. The equations of the upper-limit lines define the depth-size factors for piers, and are given in Tables 1 and 2.

Flow Intensity Factor, K_I

K_I represents the effects of flow intensity on local scour depth. It is defined, for each set of data, as the scour depth at a particular flow intensity divided by the maximum scour depth for the data set, where V is systematically varied for each data set and all other dependent parameters are held constant. The scour maxima used occur at the threshold peak for uniform sediments and the live-bed peak for nonuniform sediments.

Figure 5 (uniform sediments) and Figure 6 (nonuniform sediments) are plots of laboratory data from many sources for local scour at piers and abutments in terms of K_I. The nonuniform sediment data are plotted in terms of a transformed velocity parameter, as shown. The transformed velocity parameter aligns the armour peaks (that is $V=V_a$) for nonuniform sediments with varying σ_g with the threshold peak (that is $V=V_a$) for uniform sediments. For uniform sediments, $V_a \equiv V_c$ and $[V-(V_a-V_c)]/V_c \equiv V/V_c$. The transformed velocity parameter incorporating V_a largely accounts for the effects of sediment nonuniformity as well as those of flow velocity, although the smaller values of scour depth at $[V-(V_a-V_c)]/V_c \approx 1$, as σ_g increases, remain. Thus, the effects of sediment nonuniformity are mostly accounted for in the flow intensity factor. It is apparent that all of the data are enveloped by a value of K_I increasing linearly from zero to unity at the threshold condition and thereafter remaining unchanged.

The velocities V_c and V_a can be determined using the logarithmic velocity distribution equation:

$$\frac{V_c}{u_{*c}} = 5.75 \log\left(5.53 \frac{y}{d_{50}}\right) \tag{4}$$

where u_{*c} is critical shear velocity determined from the Shields' diagram, and d_{50} and u_{*c} are replaced by d_{50a} (median size of the armour layer = $d_{max}/1.8$) and u_{*ca} (critical shear velocity of the armour layer), respectively, for determination of the armour peak velocity, V_a.

Figure 7 is a comparison of U.S. field data with the laboratory-based envelope curves for K_I. Because many of these data were collected at sites where the bed material is nonuniform, the transformed velocity parameter is used in Figure 7. The field scour depths are normalised using the projected pier width, b_p, to compensate for pier skewness effects inherent in the data. The armour peak velocity was determined assuming d_{84} to be representative of the maximum grain size in the bed material. The laboratory-derived K_I function also envelops the field data.

Sediment Size Factor, K_d

The pier data by Ettema (1980), Chiew (1984) and Baker (1986) and the abutment data by Dongol (1994) are plotted in Figure 8 in terms of the sediment size multiplying factor, K_d, which is defined generally as the ratio of the scour depth for a particular B/d_{50} to that for $B/d_{50} \geq 50$. The data for uniform and nonuniform sediments are plotted separately. The plots show that the influence of relative sediment size on scour depth is the same for both piers and abutments, although few data are shown for abutments. Because the condition $L/d_{50}<50$ is unlikely in practice, it is considered that the few abutment data shown in Figure 8 are adequate for definition of K_d for abutments.

Nonuniform sediments are characterised by channel bed armouring as discussed earlier. The nonuniform sediment data in Figure 8 are plotted for different values of the velocity parameter $[V-(V_a-V_c)]/V_c$ = 1.0, 2.0, 3.0 and 4.0. The data are plotted in terms of b/d_{50a} or L/d_{50a} because the median size of the armour layer is considered to be the characteristic sediment size. The envelope curves in Figure 8 define the sediment size factor for design purposes.

Foundation Shape Factor, K_s

The shape factor K_s is defined as the ratio of the scour depth for a particular foundation shape to that for the standard shapes, namely circular piers and vertical-wall abutments.

Recommended shape factors for uniform piers, i.e. piers having constant cross-sectional shape, are given in Table 1. These factors, taken from Melville (1997), show that shape is relatively insignificant for uniform piers. The shape factors should only be used where the pier is aligned with the flow, that is, K_s=1 for a skewed pier.

The four cases of local scour at nonuniform piers, where the pier is founded on a wider element (caissons, slab footings and pile caps), are shown in Figure 3. For ***Case I***, the local scour is estimated using the pier width b. For ***Case II***, a procedure given by Melville and Raudkivi (1996) to estimate the size of an equivalent uniform pier can be applied. The equivalent uniform pier induces (at least) the same scour as the nonuniform pier. The procedure is therefore conservative. Melville and Raudkivi (1996), who measured scour depths at a circular pier founded on a larger concentric, circular caisson, give the following relation:

$$b_e = b\left(\frac{y+Y}{y+b^*}\right) + b^*\left(\frac{b^*-Y}{b^*+y}\right) \tag{5}$$

where b_e = width of an equivalent uniform pier; b* = caisson width; and the equation is restricted to the range defined by $Y \leq b^*$ and $-Y \leq y$, where Y represents the elevation of the top surface of the caisson (Figure 3). The relation for b_e can be used for Case II nonuniform piers that are geometrically similar to the caisson foundation shown in Figure 3, including piers founded on slab footings and piled foundations, unless the footing or the pile cap is

undermined by the scour. Equation 5 also applies to ***Case III*** caisson foundations and may be used to give conservative scour estimates for Case III piled foundations. For ***Case IV*** caisson foundations, the local scour is estimated using the caisson width b*. This approach would also give a conservative estimate of Case IV local scour at a piled foundation.

Also given in Figure 3 and Table 1 is a method to determine the effective size of a bridge pier having a raft of floating debris material attached.

Shape factors, based on data by Hannah (1978), for piled pier foundations where the pile cap is clear of the water surface (Case V) are given in Table 1 and illustrated in Figure 3 (Case V). The pile-group shape factor values are shown in Table 1 for a single row and a double row of piles in terms of approach flow angle, θ, pile diameter, D_p and pile spacing (measured centre-to-centre), S_p. The single-row values apply also to a pier comprising a row of cylinders. The values shown include pier alignment effects and shape effects, that is, they represent K_sK_θ.

Recommended shape factors for shorter abutments are given in Table 2. For longer abutments, shape effects are less significant, and an adjusted shape factor K_s^* is applied. K_s* is given in Table 2.

Foundation Alignment Factor, K_θ

The alignment factor K_θ is defined as the ratio of the local scour depth at a skewed bridge foundation to that at an aligned foundation. Bridge piers are aligned if $\theta = 0°$, while abutments are considered to be aligned where $\theta = 90°$. An equation for K_θ for non-cylindrical piers is given in Table 1.

Recommended alignment factors for longer abutments are given in Table 2. For shorter abutments, alignment effects are less significant. The adjusted alignment factor K_θ^* for shorter abutments is given in Table 2.

Approach Channel Geometry Factor, K_G

The approach channel geometry factor K_G is the ratio of the local scour depth at a bridge foundation to that at the same foundation sited in the equivalent rectangular channel. The local scour at bridge piers is considered to be unaffected by approach channel geometry as long as appropriate values of y and V are used to estimate the scour depth. If values of y and V are selected to be representative of the flow approaching the particular pier, K_G=1.0.

For bridge abutments in rectangular channels (Case A of Figure 2), K_G=1.0 by definition. For abutments in compound channels, K_G depends on the position of the abutment in the compound channel (Figure 2). At Case B abutments, the equation given in Table 2 is recommended, where L and L* = total projected length of the abutment (including the bridge approach) and projected length of the abutment (including the bridge approach) spanning the flood channel, respectively; y and y* = flow depths in the main and flood channels, respectively; and n and n* = Manning roughness coefficients for the main and flood channels, respectively. The equation is derived from a simple theoretical analysis based on the ratio of flows deflected by the abutment, including the bridge approach, in a compound channel to such flows in the corresponding rectangular channel. The equation is plotted in Figure 9 for ranges of values of the ratios (L*/L), (y/y*) and (n/n*). Case C can be considered to be a special condition of Case A if the flow in the main channel is ignored; thus K_G=1.0. For Case D abutments where the abutment is sited at about the edge of the main channel, K_G can be estimated from the equation for Case B, with L*/L=1.0. No specific information is available to aid estimation of K_G for other Case D abutments; such situations could be treated by

interpolating conservatively between scour depth estimates for longer (Case B) and shorter (Case C) abutments sited in the same channel.

Time Factor, K_t

The time factor is defined as the ratio of local scour depth d_s at a particular time t to the equilibrium scour depth d_{se}, which occurs at time t_e. The value of K_t at a site depends on whether conditions are clear-water or live-bed. Under live-bed conditions, the equilibrium depth of local scour is attained rapidly and $K_t = 1.0$ can be assumed.

Functions for the time factor at piers and abutments are given in Tables 1 and 2, respectively. The latter is derived from recent research and represents an updating of the recommendations in Melville and Coleman (2000). K_t depends on t_e, the time to equilibrium scour depth. Equations for estimation of t_e are also given in Tables 1 and 2.

EXAMPLES OF APPLICATION OF METHODOLOGY

Local scour at piers

A bridge pier, comprising a piled foundation, is situated in the 310 m wide flood channel of a river crossing, as illustrated in Figure 10. The peak flow rate in the flood channel is 500 m^3/s and this persists for 1 day. The calculations are presented in Table 3, showing a local scour depth of 1.71 m.

Local scour at abutments (including contraction scour)

A bridge is situated at a channel bend, as illustrated in Figure 11. The sediment is a medium sand with d_{50} = 0.5 mm. The peak flow rate is 440 m^3/s and this lasts for 2 days. The calculations are presented in Table 4, showing local scour depth of 3.83 m.

Contraction scour would occur due to the bridge narrowing the channel. Mobile-bed conditions would exist (Table 4). Laursen's (1960) equation for contraction scour is used to estimate the contraction scour depth. The equation is

$$\frac{y_2}{y_1} = \left(\frac{Q_2}{Q_{1m}}\right)^{6/7} \left(\frac{W_1}{W_2}\right)^{k_1} \tag{5}$$

where y_1 = average depth in the approach main channel; y_2 = average depth in the main channel of the contracted section; W_1 = bottom width of the approach main channel; W_2 = bottom width of the main channel in the contracted section; Q_{1m} = discharge in the approach main channel transporting sediment; Q_2 = total discharge through the bridge; and k_1 = a coefficient depending on the mode of sediment transport. For the given example $Q_{1m} = Q_2$.

REFERENCES

Basak, V. (1975) "Scour at square piles," Report No. 583, Devlet Su isteri genel mudurlugu, Ankara, Turkey.

Bonasoundas, M. (1973) "Strömungsvorgang und kolkproblem," Report No. 28, Oskar v. Miller Institu, Tech. Univ. Munich, Germany.

Baker, R.E. (1986) "Local scour at bridge piers in non-uniform sediment," Report No. 402, School of Engineering, The University of Auckland, Auckland, New Zealand, 91pp.

Chabert, J. and Engeldinger, P. (1956) "Etude des affouillements autour des piles des ponts," Laboratoire d'Hydraulique, Chatou, France (in French).

Chee, R.K.W. (1982) "Live-bed scour at bridge piers," Report No. 290, School of Engineering, The University of Auckland, Auckland, New Zealand, 79pp.

Chiew, Y.M. (1984) "Local scour at bridge piers," Report No. 355, School of Engineering, The University of Auckland, Auckland, New Zealand, 200pp.

Dongol, D. M. S. (1994). "Local scour at bridge abutments." Report No. 544, School of Engineering, The University of Auckland, Auckland, New Zealand, 409pp.

Ettema, R. (1980) "Scour at bridge piers," Report No. 216, School of Engineering, The University of Auckland, Auckland, New Zealand, 527pp.

Gill, M.A. (1972) "Erosion of sand beds around spur dikes," Journal of the Hydraulics Division, A.S.C.E., 98(9), 1587-1602.

Hancu, S. (1971) "Sur le calcul des affouillements locaux dams la zone des piles des ponts," Proc., 14th. I.A.H.R. Congress, Paris, France, Vol. 3, 299-313.

Hannah, C.R. (1978) "Scour at pile groups," Report No. 78-3, Department of Civil Engineering, University of Canterbury, Christchurch, New Zealand, 92pp.

Jain, S.C. and Fischer, E.E. (1979) "Scour around bridge piers at high Froude numbers," Report No. FH-WA-RD-79-104, Federal Highway Administration, U.S. Department of Transportation, Washington, D.C., U.S.A.

Kandasamy, J.K. (1989) "Abutment scour," Report No. 458, School of Engineering, The University of Auckland, Auckland, New Zealand, 278pp.

Kwan, T. F. (1984). "Study of abutment scour." Report No. 328, School of Engineering, The University of Auckland, Auckland, New Zealand, 225pp.

Kwan, T.F. (1988) "A study of abutment scour," Report No. 451, School of Engineering, The University of Auckland, Auckland, New Zealand, 461pp.

Laursen, E.M. (1960) "Scour at bridge crossings," Journal of the Hydraulics Division, A.S.C.E., 86(2), 39-54.

Laursen, E.M. and Toch, A. (1956) "Scour around bridge piers and abutments," Bulletin No.4, Iowa Highways Research Board, Ames, Iowa, U.S.A.

Melville, B. W. (1997). “Pier and abutment scour - an integrated approach.” J. Hyd. Engrg., ASCE, 123(2), 125-136.

Melville, B. W., and Chiew, Y. M. (1999). “Time scale for local scour at bridge piers.” J. Hyd. Engrg., ASCE, 125(1), 59-65.

Melville, B. W., and Coleman, S. E. (2000). Bridge scour. Water Resources Publications, LLC, Colorado, U.S.A. 550pp.

Melville, B.W. and Raudkivi, A.J. (1996) “Effects of foundation geometry on bridge pier scour, “Journal of Hydraulic Engineering, A.S.C.E., 122(4), 203-209.

Neill, C.R. (1987) “Bridge hydraulics - An update report,” Roads and Transportation Assoc. of Canada, Ottawa, Canada, 75pp.

Tey, C. B. (1984). “Local scour at bridge abutments.” Report No. 329, School of Engineering, The University of Auckland, Auckland, New Zealand, 111pp.

Wong, W.H. (1982) “Scour at bridge abutments,” Report No. 275, School of Engineering, The University of Auckland, Auckland, New Zealand, 109pp.

Table 1 Factors influencing local scour depth at bridge piers

Factor	K	Method of Estimation				
Depth-size factor	K_{yb}	$K_{yb} = 2.4b$	$\frac{b}{y} < 0.7$			
		$K_{yb} = 2\sqrt{yb}$	$0.7 < \frac{b}{y} < 5$			
		$K_{yb} = 4.5y$	$\frac{b}{y} > 5$			
Flow intensity factor	K_I	For uniform sediments: $d_{50a} \equiv d_{50}$ and $V_a \equiv V_c$ For nonuniform sediments: $d_{50a} = d_{max}/1.8 \approx d_{84}/1.8 = \sigma_g d_{50}/1.8$; and $V_a = 0.8V_{ca}$, where V_{ca} is V_c calculated for d_{50a}				
		$K_I = \frac{V-(V_a-V_c)}{V_c}$	$\frac{V-(V_a-V_c)}{V_c} < 1$			
		$K_I = 1$	$\frac{V-(V_a-V_c)}{V_c} \geq 1$			
Sediment size factor	K_d	$K_d = 0.57 \log\left(2.24 \frac{b}{d_{50}}\right)$	$\frac{b}{d_{50}} \leq 25$			
		$K_d = 1.0$	$\frac{b}{d_{50}} > 25$			
Shape factor	K_s	Shape				K_s
		Circular				1.0
		Round Nosed				1.0
		Square Nosed				1.1
		Sharp Nosed				0.9
		Skewed piers				1.0
Equivalent size for nonuniform piers	b_e	$b_e = b$				Case I
		$b_e = b\left(\frac{y+Y}{y+b^*}\right) + b^*\left(\frac{b^*-Y}{b^*+y}\right) \quad Y \leq b^*, -Y \leq y$				Case II Case III
		$b_e = b^*$				Case IV
Multiplying factors for pile groups	K_sK_θ	Type	S_p/D_p	K_sK_θ		
				$\theta<5°$	$\theta=5°\rightarrow45°$	$\theta=90°$
		Single Row	2	1.12	1.40	1.20
			4	1.12	1.20	1.10
			6	1.07	1.16	1.08
			8	1.04	1.12	1.02
			10	1.00	1.00	1.00
		Double Row	2	1.50	1.80	-
			4	1.35	1.50	-
Alignment factor	K_θ	$K_\theta = \left(\frac{l}{b}\sin\theta + \cos\theta\right)^{0.65}$	non - circular piers			
		$K_\theta = 1.0$	circular piers			

Time factor	K_t	$K_t = \exp\left\{-0.03\left\lvert\frac{V_c}{V}\ln\left(\frac{t}{t_e}\right)\right\rvert^{1.6}\right\}$	$\frac{V}{V_c} \le 1$
		$K_t = 1.0$	$\frac{V}{V_c} > 1$
Equilibrium time	t_e	$t_e(days) = 48.26\frac{b}{V}\left(\frac{V}{V_c} - 0.4\right)$	$\frac{y}{b} > 6, \frac{V}{V_c} > 0.4$
		$t_e(days) = 30.89\frac{b}{V}\left(\frac{V}{V_c} - 0.4\right)\left(\frac{y}{b}\right)^{0.25}$	$\frac{y}{b} \le 6, \frac{V}{V_c} > 0.4$
Equivalent size - pier with debris	b_e	$b_e = \frac{0.52T_d b_d + (y - 0.52T_d)b}{y}$	

Table 2 Factors influencing local scour depth at bridge abutments

Factor	K	Method of Estimation	
Flow depth-abutment size	K_{yL}	$K_{yL} = 10y$	$\frac{y}{L} \le 0.04$
		$K_{yL} = 2\sqrt{yL}$	$0.04 < \frac{y}{L} \le 1$
		$K_{yL} = 2L$	$\frac{y}{L} > 1$
Flow intensity	K_I	For uniform sediments: $d_{50a} \equiv d_{50}$ and $V_a \equiv V_c$ For nonuniform sediments: $d_{50a} = d_{max}/1.8 \approx d_{84}/1.8 = \sigma_g d_{50}/1.8$; and $V_a = 0.8V_{ca}$, where V_{ca} is V_c calculated for d_{50a}	
		$K_I = \frac{V - (V_a - V_c)}{V_c}$	for $[V-(V_a-V_c)]/V_c < 1$
		$K_I = 1.0$	for $[V-(V_a-V_c)]/V_c \ge 1$
Sediment size	K_d	$K_d = 1.0$	$\frac{L}{d_{50a}} > 60$
Foundation shape		Shape	K_s
	K_s	Vertical-wall	1.0
		Wing-wall	0.75
		Spill-through 0.5:1 (H:V)	0.6
		Spill-through 1:1	0.5
		Spill-through 1.5:1	0.45
	K_s^*	$K_s^* = K_s$	$\frac{L}{y} \le 10$
		$K_s^* = K_s + 0.667(1 - K_s)\left(0.1\frac{L}{y} - 1\right)$	$10 < \frac{L}{y} < 25$
		$K_s^* = 1.0$	$\frac{L}{y} \ge 25$

Foundation alignment	K_θ	θ (°)	30	45	60	90	120	135	150
		K_θ	0.90	0.95	0.98	1.0	1.05	1.07	1.08
	K_θ^*	$K_\theta^* = 1.0$						$\frac{L}{y} \le 1$	
		$K_\theta^* = K_\theta + (1 - K_\theta)\left(1.5 - 0.5\frac{L}{y}\right)$						$1 < \frac{L}{y} < 3$	
		$K_\theta^* = 1.0$						$\frac{L}{y} \le 1$	
Approach-channel geometry		Case A (Fig. 2): [Simple rectangular river channel] $K_G \equiv 1.0$							
		Case C (Fig. 2): [Abutment well back from the flood-channel edge] Consider only the flood channel flows of y* and set $K_G = 1.0$							
	K_G	Case B (Fig. 2): [Abutment in the main channel] $K_G = \sqrt{1 - \left(\frac{L^*}{L}\right)\left[1 - \left(\frac{y^*}{y}\right)^{5/3}\left(\frac{n}{n^*}\right)\right]}$							
		Case D (Fig. 2): [Abutment near the flood channel edge] Abutment at about the flood-channel edge: Case B with L*/L=1.0.							
Time		$t_e(days) = 20.83\frac{L}{V}\left(\frac{V}{V_c}\right)^3\left(\frac{y}{L}\right)^{0.8}$ for y/L < 1							
		$t_e(days) = 20.83\frac{L}{V}\left(\frac{V}{V_c}\right)^3$ for y/L ≥ 1							
	K_t	$K_t = \exp\left[-0.07\left(\frac{V}{V_c}\right)^{-1}\left\lvert\ln\left(\frac{t}{t_e}\right)\right\rvert^{1.5}\right]$ for $V/V_c < 1$							
		$K_t = 1.0$ for $V/V_c \ge 1$							

Table 3 Pier Scour Example

$b_e = b\left(\frac{y_f + Y}{y_f + b^*}\right) + b^*\left(\frac{b^* - Y}{b^* + y_f}\right) = 0.6\left(\frac{2.0 - 0.6}{2.0 + 1.5}\right) + 1.5\left(\frac{1.5 + 0.6}{1.5 + 2.0}\right) = 1.14\,\text{m}$
$\frac{b_e}{y} = 0.57, K_{yb} = 2.4b_e = 2.74\,\text{m}$
$K_s = 1.0,$ for skewed pier
$K_\theta = \left(\frac{l}{b_e}\sin\theta + \cos\theta\right)^{0.65} = 1.93$
$V = \frac{Q_f}{W_{1f}y_f} = \frac{500}{310 \times 2} = 0.81\,\text{m/s}$

From grading curve, $d_{max} = 27$ mm $d_{50a} = \frac{d_{max}}{1.8} = 15$ mm, $u_{*c} = 0.067$ m/s, $u_{*ca} = 0.118$ m/s $V_c = 1.29$ m/s, $V_{ca} = 1.95$ m/s, $V_a = 1.56$ m/s, $\frac{V-(V_a - V_c)}{V_c} = 0.42, K_I = 0.42$
$\frac{y}{b_e} = 1.75, t_e(days) = 30.89\frac{b_e}{V}\left(\frac{V}{V_c} - 0.4\right)\left(\frac{y}{b_e}\right)^{0.25} = 11.4$ days
$K_t = \exp\left\{-0.03\left\lvert\frac{V_c}{V}\ln\left(\frac{t}{t_e}\right)\right\rvert^{1.6}\right\} = 0.77$
$\frac{b_e}{d_{50}} = 228, \frac{b_e}{d_{50a}} = 76, K_d = 1.0$
$d_s = K_{yb}K_I K_d K_s K_\theta K_t = 1.71$ m

Table 4 Abutment Scour Example

The threshold velocity is, $V_c = 1.3$ m/s, for y = 6 m and $d_{50} = 0.5$ mm (using Neill's 1987 competent velocity chart. $V_2 = \frac{Q}{W_2 y} = \frac{440}{19 \times 6} = 3.86 \text{ m/s} >> V_c$ and conditions are live-bed
Using (5) with $k_1 = 0.69$ to estimate contraction scour: $\frac{d_s}{y_1} = \left(\frac{W_1}{W_2}\right)^{k_1} - 1, d_{s)contraction} = 1.25$ m $d_{s)contraction} = 1.5$ m, RHS, $d_{s)contraction} = 1.0$ m, LHS It is assumed that the contraction scour is distributed as shown in Figure 11
Flow depth after contraction scour is: $y = 6 + d_{s)_{contraction}} = 7.25$ m
$\frac{L}{y} = 0.42, K_{yL} = 6$ m
$V = \frac{Q}{W_1 y} = \frac{440}{25 \times 7.25} = 2.43$ m / s
$u_{*c} = 0.016$ m/s, $V_c = 0.45$ m/s, $\frac{V}{V_c} = 5.4, K_I = 1.0$ and $K_t = 1.0$ for live - bed conditions
$\frac{L}{d_{50}} > 25, K_d = 1.0$
$K_s = 0.75$, for wing - wall abutment, $K_s^* = K_s$
$\frac{L}{y} < 1, K_{\theta)LHS} = K_{\theta)RHS} = 1.0$
$K_G = 1.0$
$d_s = K_{yL}K_I K_d K_s K_\theta K_G K_t, d_s = 4.5$ m

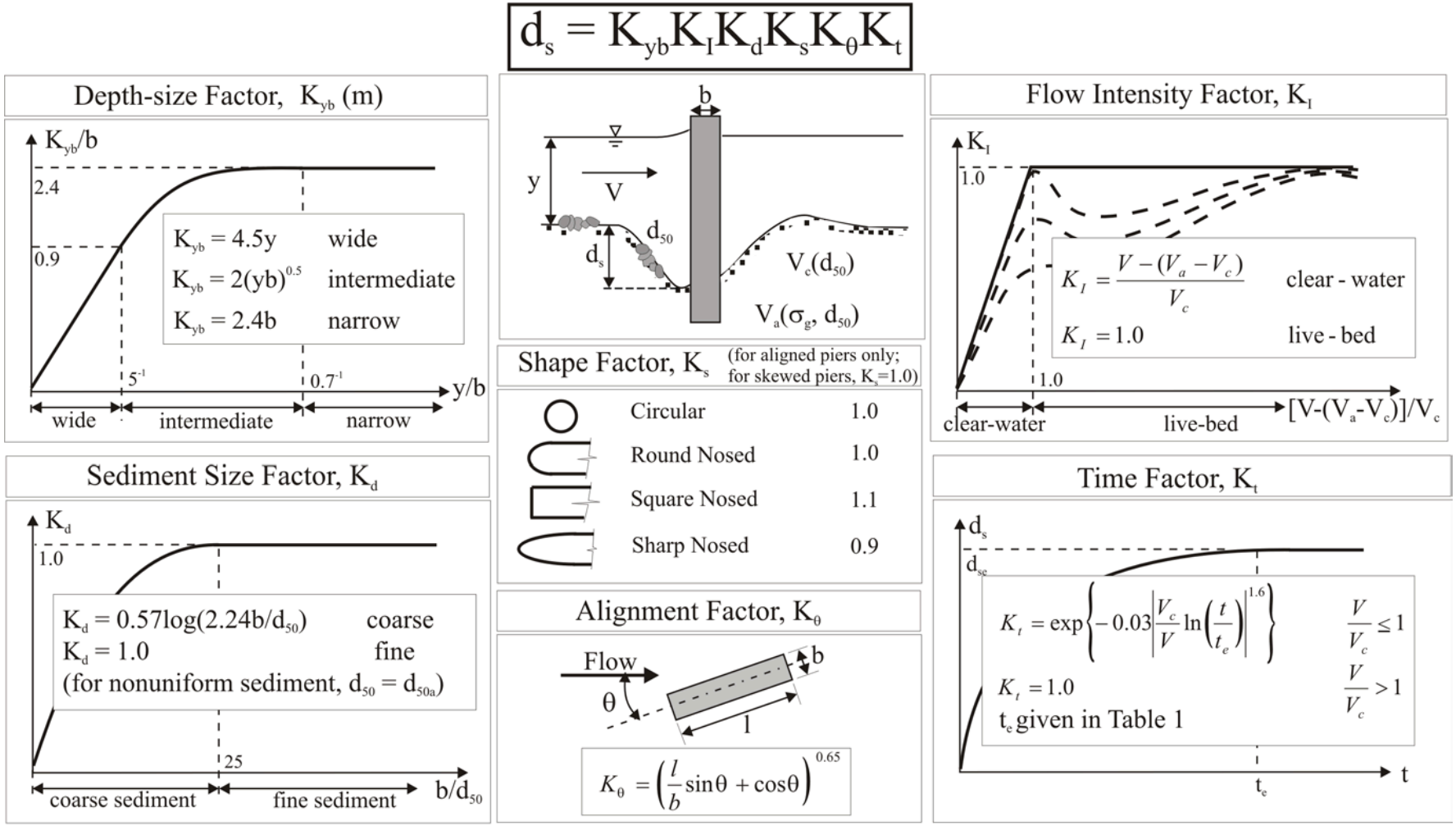

Figure 1 Method for estimation of local scour depth at piers.

$$d_s = K_{yL} K_I K_d K_s K_\theta K_G K_t$$

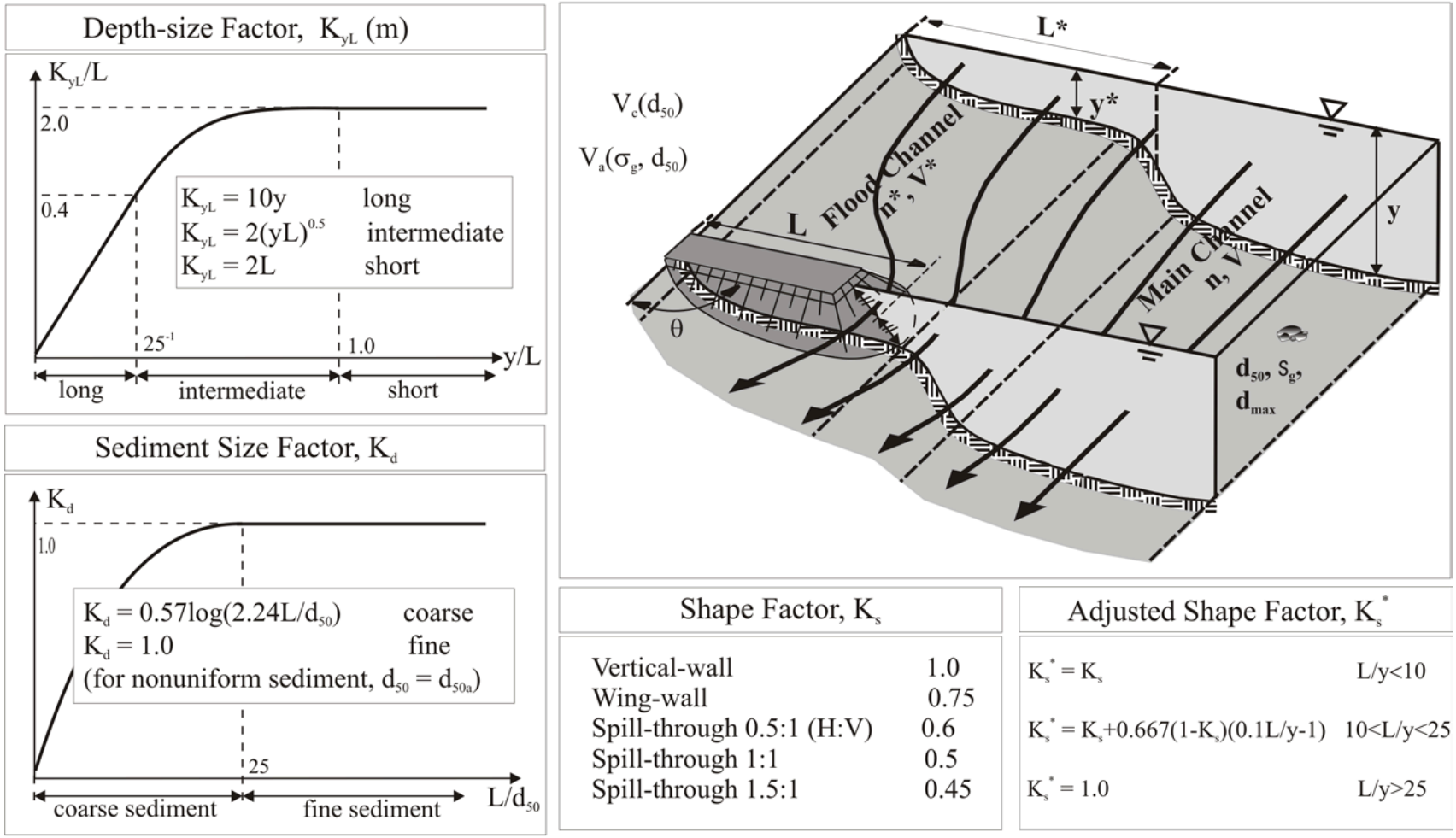

Figure 2 Method for estimation of local scour depth at abutments.

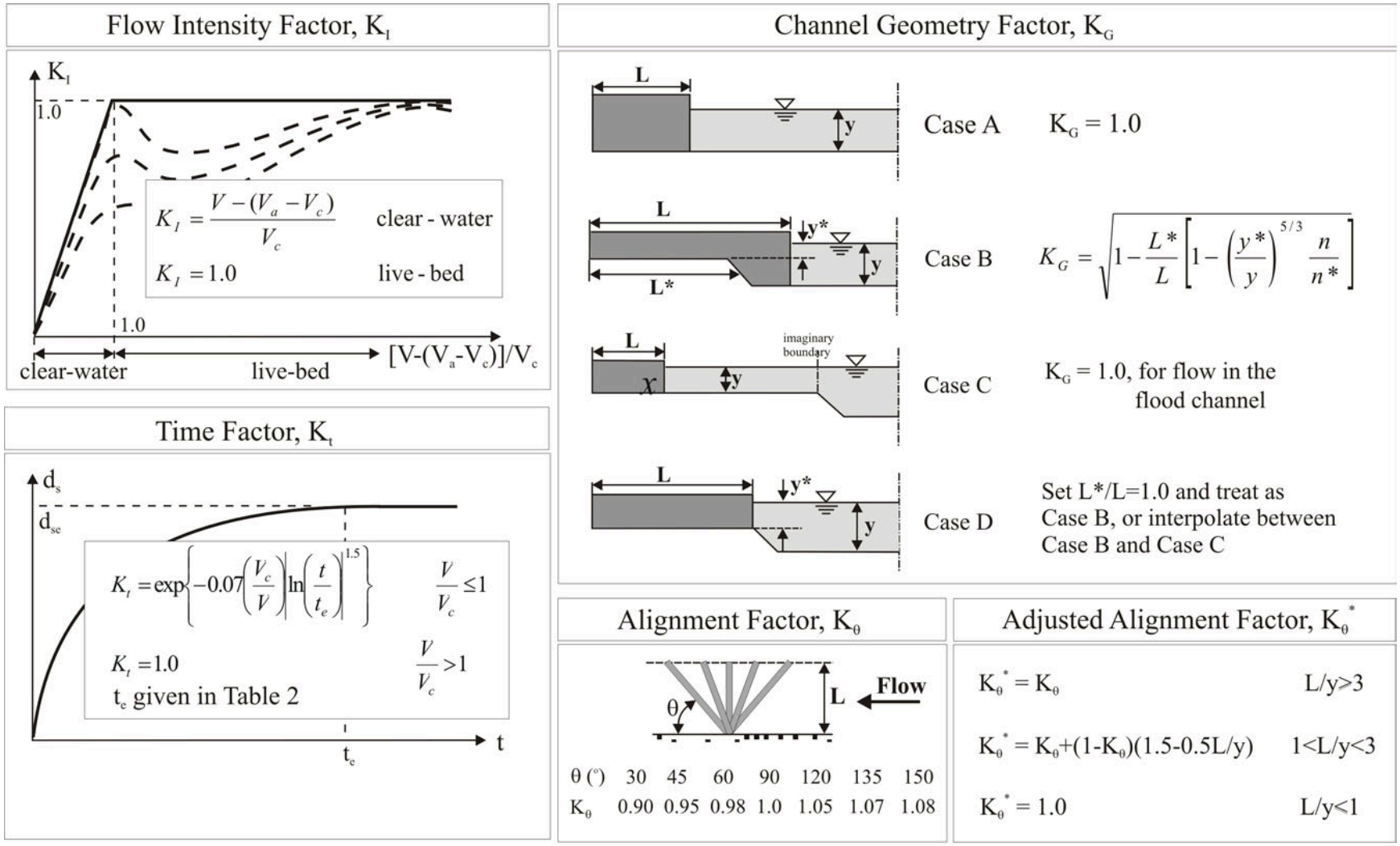

Figure 2 (cont.) Method for estimation of local scour depth at abutments.

CASE I

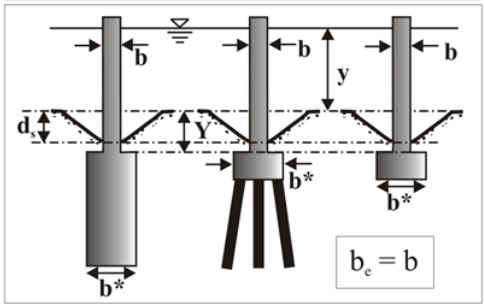

CASE II

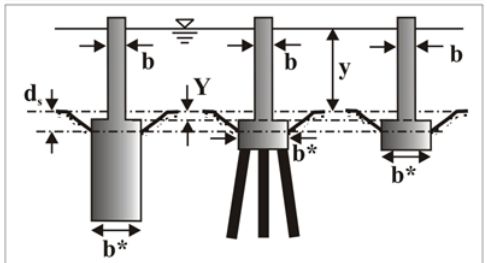

$$b_e = b\left(\frac{y+Y}{y+b^*}\right) + b^*\left(\frac{b^*-Y}{b^*+y}\right)$$

CASE III

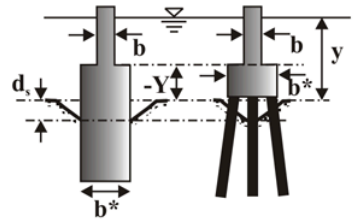

$$b_e = b\left(\frac{y+Y}{y+b^*}\right) + b^*\left(\frac{b^*-Y}{b^*+y}\right)$$

(conservative for piled foundations)

Note: Y is negative for Case III

CASE IV

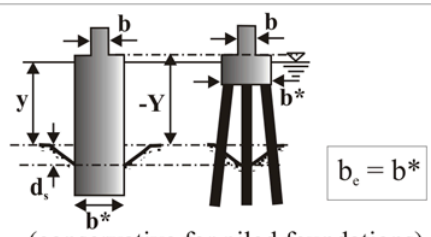

(conservative for piled foundations)

CASE V (Pile cap above W.L.)

Type	S_p/D_p	K_sK_θ		
		θ<5°	θ=5° to 45°	θ=90°
Single Row	2	1.12	1.40	1.20
	4	1.12	1.20	1.10
	6	1.07	1.16	1.08
	8	1.04	1.12	1.02
	10	1.00	1.00	1.00
Double Row	2	1.50	1.80	-
	4	1.35	1.50	-

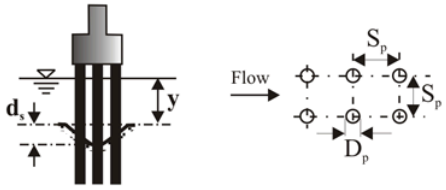

Floating Debris

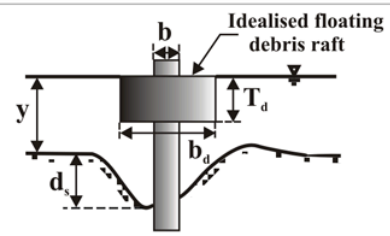

$$b_e = \frac{0.52T_d b_d + (y - 0.52T_d)b}{y}$$

Figure 3 Method for estimation of local scour depth at nonuniform piers

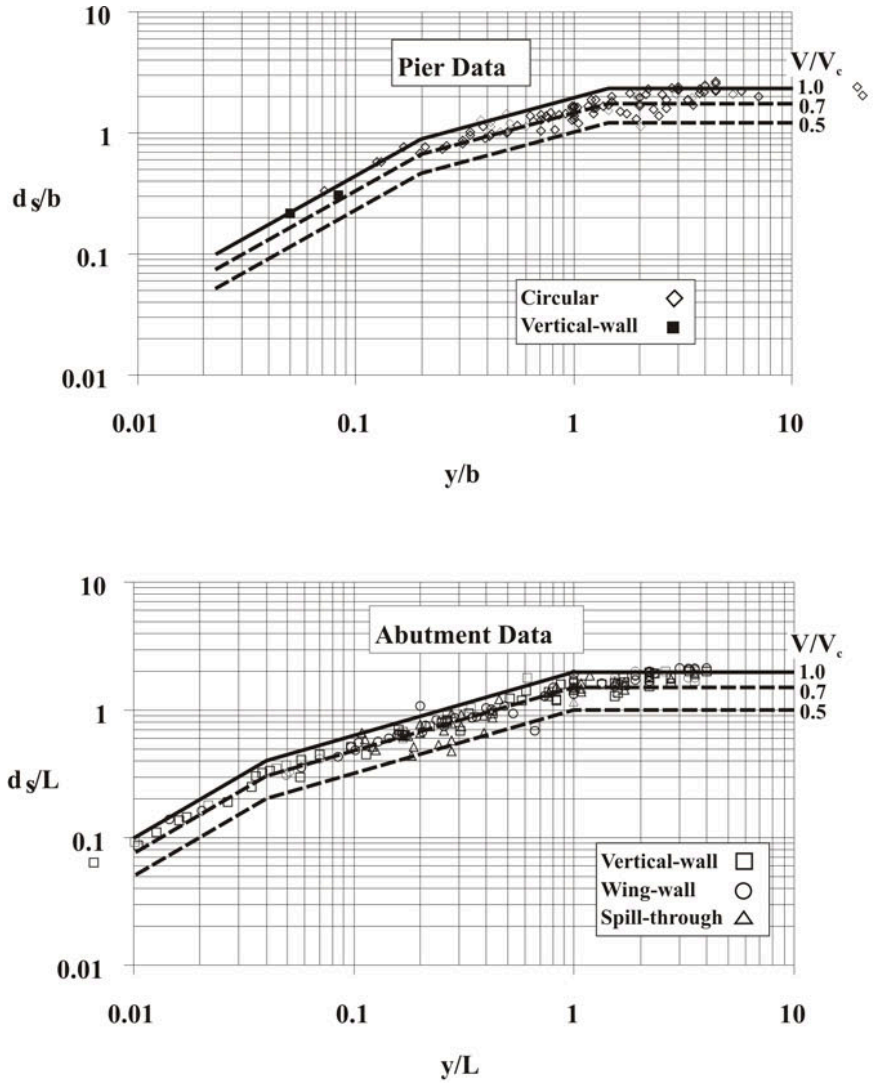

Figure 4 The influence of flow shallowness on local scour depth

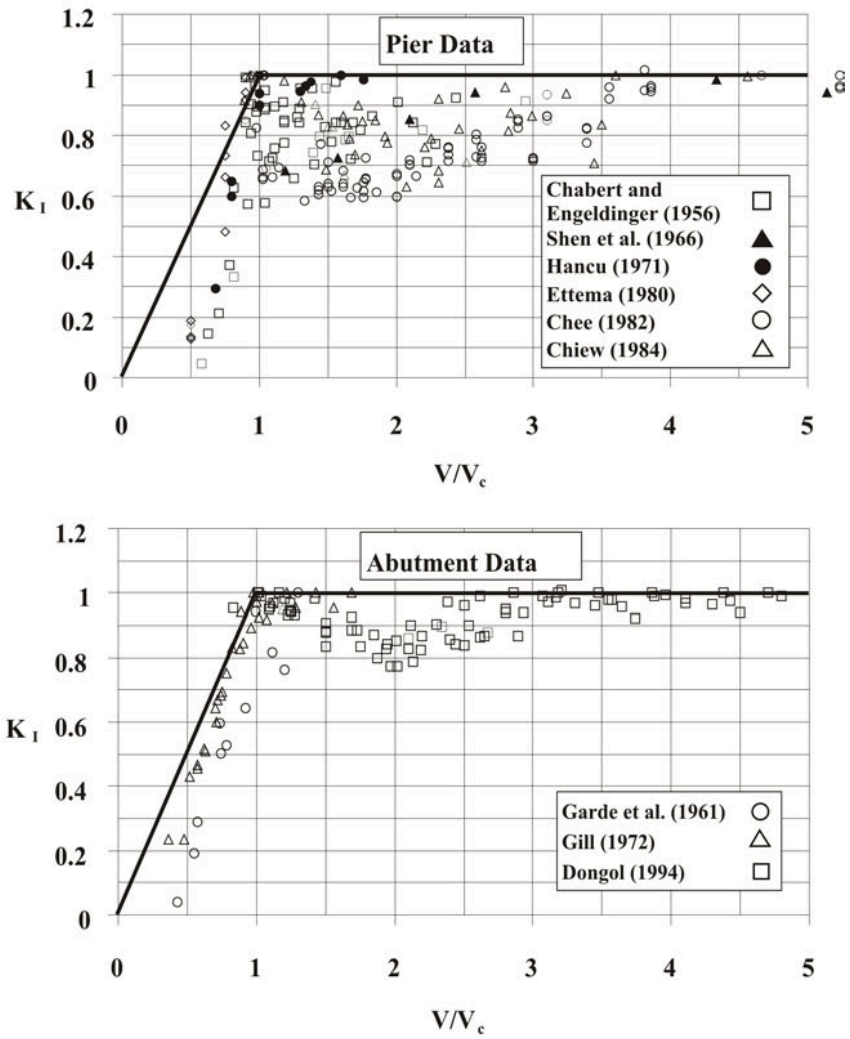

Figure 5 The influence of flow intensity on local scour depth in uniform sediment

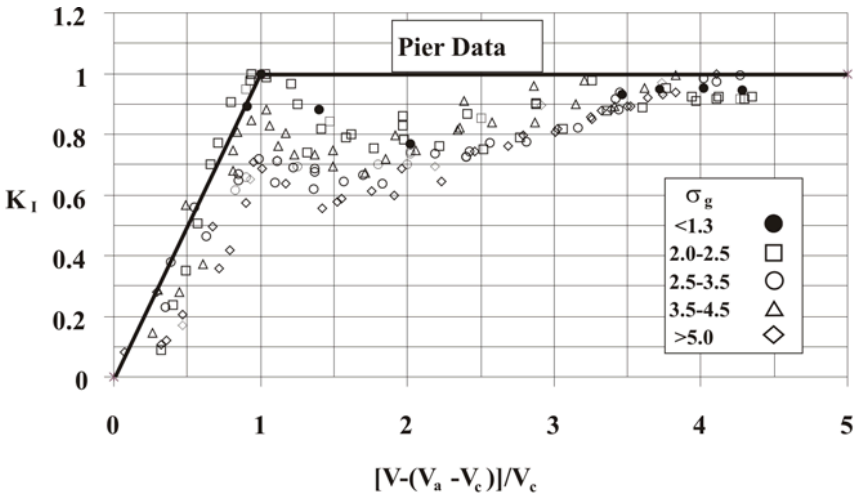

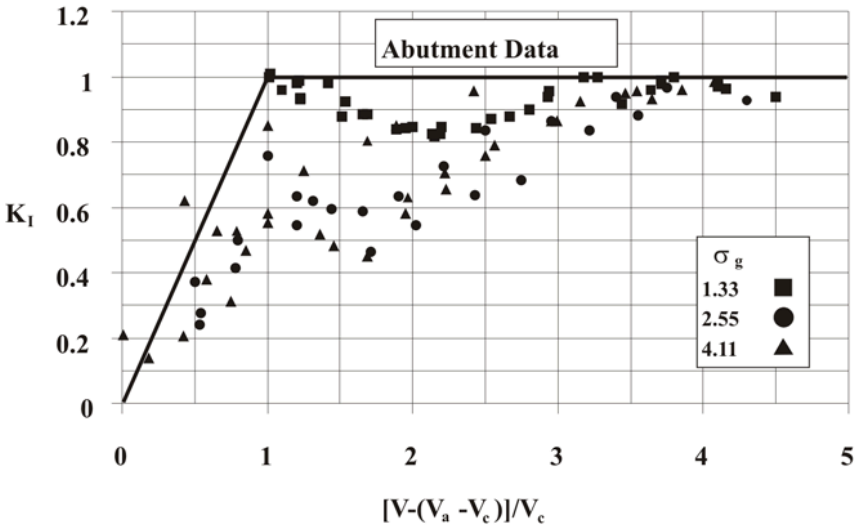

Figure 6 Influence of flow intensity on local scour depth in nonuniform sediment

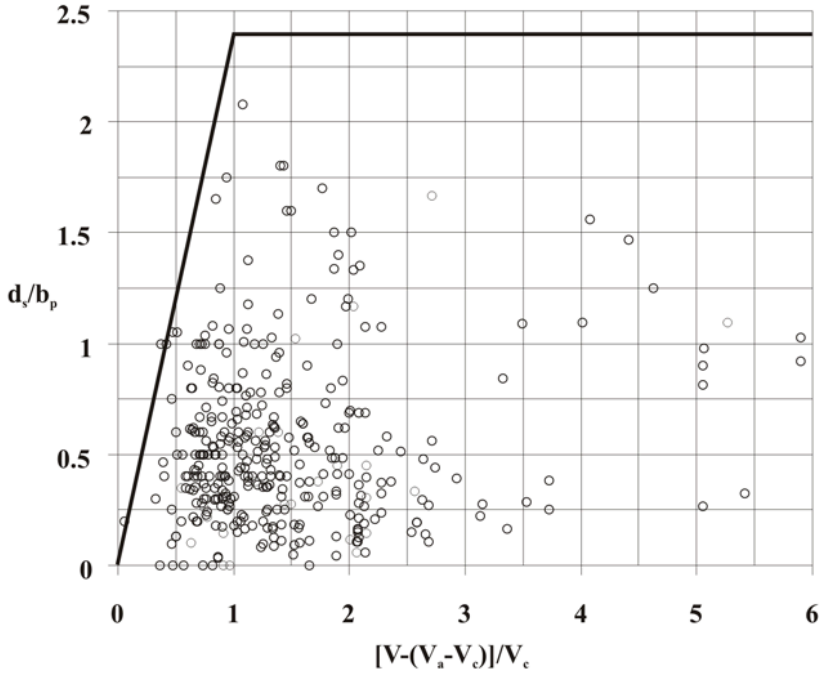

Figure 7 Comparison of field data with flow intensity curves

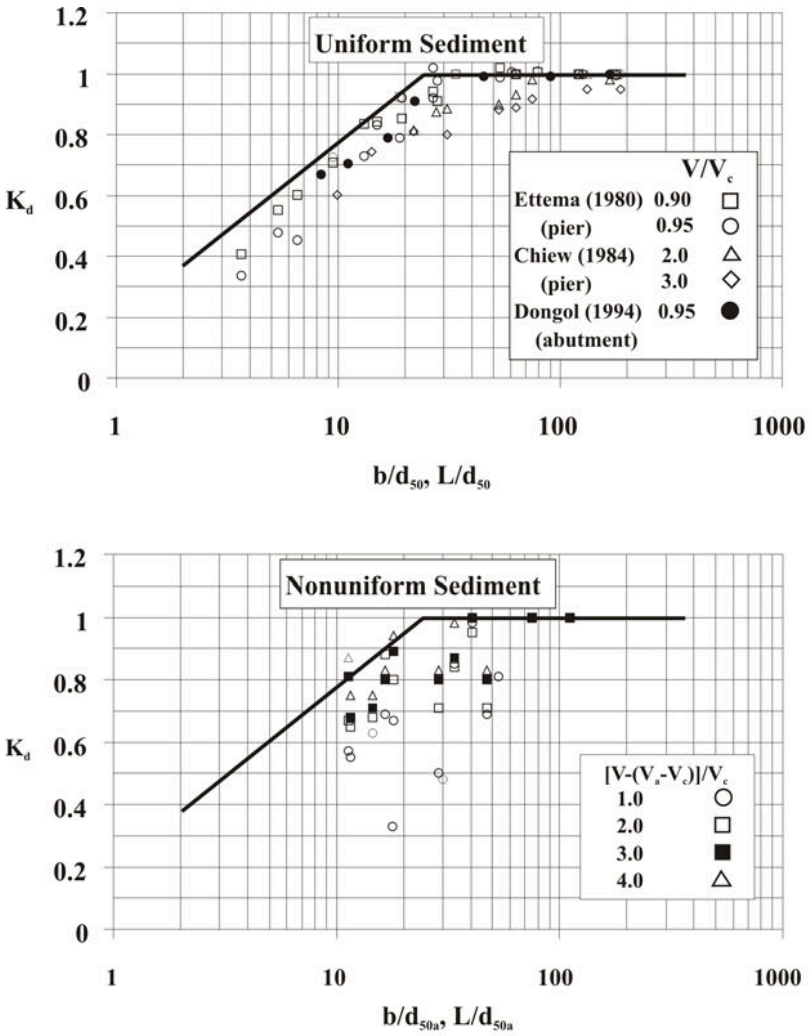

Figure 8 Influence of sediment coarseness on local scour depth

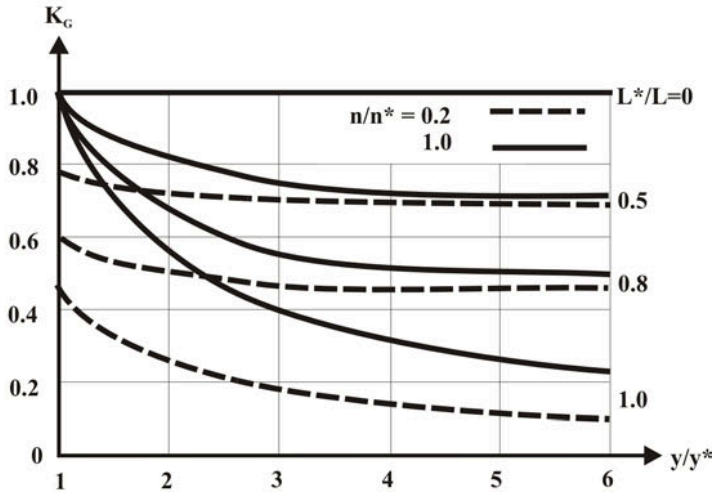

Figure 9 Influence of channel geometry on local scour depth at bridge abutments

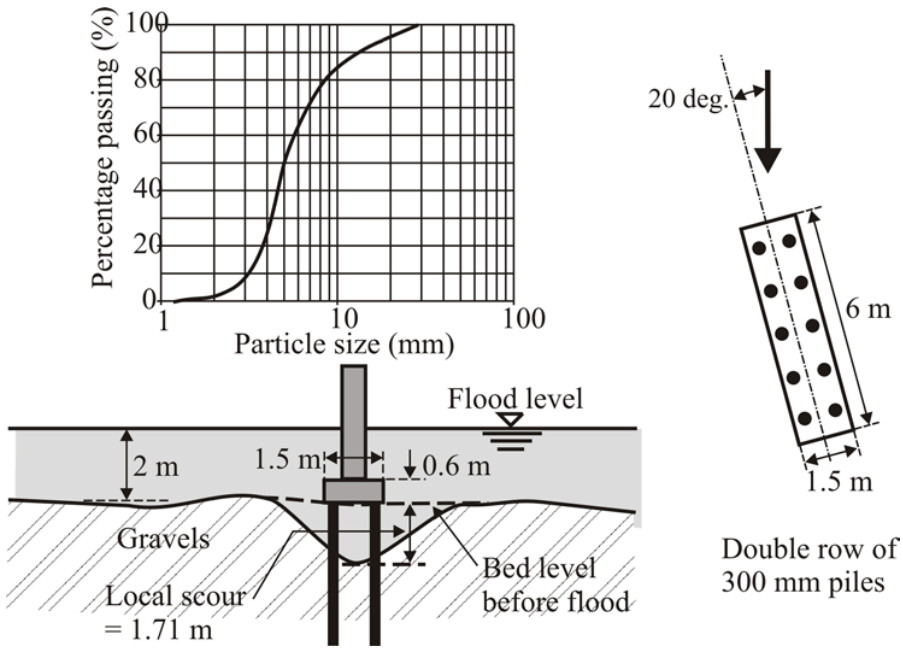

Figure 10 Diagram for pier scour example

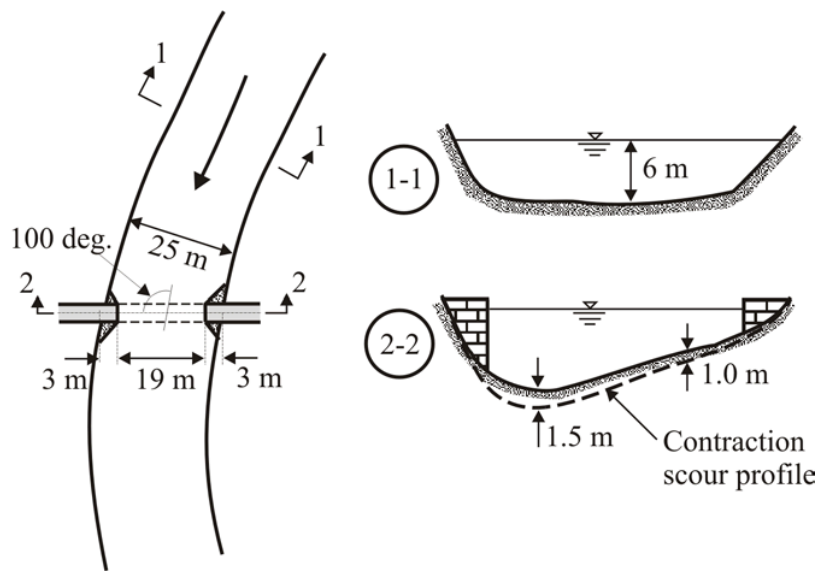

Figure 11 Diagram for abutment scour example

Indirect Methods of Measuring Shear Stress in the Bottom of a Scour Hole

By
J. Sterling Jones

INTRODUCTION

Most rational methods for estimating scour in cohesive or consolidated bed materials are time dependent and are in terms of excess shear stress or excess stream power. To apply the logic of these methodologies to the bridge pier scour problem one would need to somehow determine the shear stress or stream power in the scour hole as a function of the depth of the scour hole. The challenge, for scour evaluations to link with the technology that has evolved from erosion research, is to find a way to track the maximum shear stress in the scour hole.

The magnitude of the approach flow shear stress is amplified several fold at the beginning of scour but it decays as the scour hole gets deeper. Shear stress is a very logical concept, but it is very difficult to measure even in a laboratory. Engineers typically compute shear stresses based on fully developed normal flow or on an assumed ideal velocity distribution. The highly complex flow patterns around a bridge pier are anything but either of these conditions as illustrated by the flow visualization photo in figure 1. Direct measuring devices such as dynamometers designed to measure a drag force on a small element of the channel bed and shear stress pads which measure the velocity gradient near the bed probably do not capture the effects of the diving currents and vortices that are primarily responsible for dislodging the particles that are scoured out of the scour hole. Even sophisticated 3-D models, which can generate a shear stress for any element in the flow field, probably do not reflect the erodibility effects of the diving currents and vortices that dominate of the scour process unless they have been calibrated for those kind of secondary currents.

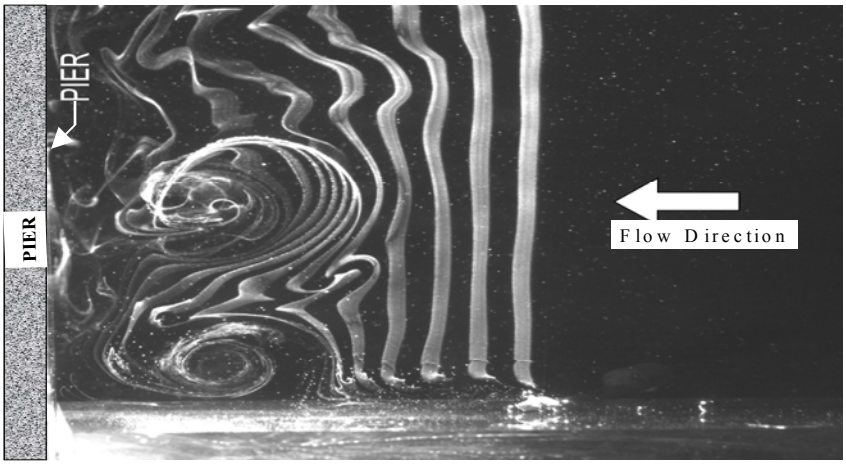

Figure 1. Photo of Visualized Flow in Front of a Bridge Pier

When researchers at the FHWA TFHRC Hydraulics laboratory were confronted with the problem of finding a practical way of determining shear stresses around bridge piers, a

number of alternatives were considered. One was a calibrated shear stress hemisphere which was an assortment of small hemispheres that could be placed anywhere along the bed. The idea was to keep exchanging hemispheres to find the one that just barely moved and that one would be an indirect measure of the shear stress at that point. Dr. Peggy Johnson, who was working at the lab at that time, reasoned that we could accomplish almost the same thing by using different size sand particles by running experiments long enough to reach the point that the sand particles were barely moving. Based on that logic, researchers at the lab embarked on an experimental program of long duration scour tests to indirectly measure effective shear stresses and stream power in scour holes at different. depths. The key word in that endeavor was ”effective” because we were really trying to characterize all the forces that act on a particle to dislodge it as a single parameter that could be related to the shear stress in the approach flow where the typical assumptions for computing shear stress are valid.

We published a technical paper based on this study in the proceedings of the ASCE Water Resources Conference’98 held in Memphis TN.[1] That paper documented the technique used to extrapolate shorter duration runs to predict equilibrium scour for a much longer duration run, but it did not document the process used to develop shear stress ratios that are the key to coupling erosion concepts with scour computations.

Previous Studies

Johnson conducted a study using marbles to indirectly measure shear stress at the base of piers at various preformed scour depths.[2] Marbles make a convenient particle for sediment studies because they have approximately the same specific gravity as granite sand and they are very uniform in size. The problem with marbles is they roll by themselves unless they are packed against one another. Johnson concluded that the effective shear stress at the base of a pier varied from 2.8 to 1.4 times the shear stress in the approach flow depending on the depth of scour.

Parola conducted a study of riprap sizes necessary to protect bridge piers against scour. [3] He used gravel particles to indirectly determine the effective velocity at the base of a pier. He compared the approach velocity required to move a particle at the base of a pier to the velocity that would be required to move the same size particle in unobstructed flow and concluded that the effective velocity at the base of a pier must be approximately 1.5 to 1.7 times the approach velocity. Since shear stress is related to velocity squared, it follows that Parola’s effective shear stress was 2.2 to 2.9 times the shear stress in the approach.

Pagan conducted a similar study of riprap protection for bridge abutments and found that the effective velocity at the base of abutments must be approximately two times the average contracted velocity through the bridge opening; hence his maximum effective shear stresses at the base of abutments represented an amplification of approximately four times the average shear stress in the contracted section.[4]

Both Parola and Pagan were looking at the amplification factor for zero scour depth, but Johnson did attempt to determine the decay rate as the scour hole got deeper.

to reach an equilibrium depth for clear water experiments, the *effective* shear stress in the bottom of the scour hole must have reached critical for that sediment size.

The experiments were designed to determine how much the approach flow shear stress is effectively amplified at the base of a pier as a function of the local scour depth. Each experiment provided one point on a shear stress amplification curve where the approach flow shear stress (always equal or less than critical for the sediment size) could be computed from the velocity and flow depth, the shear stress at the base of the pier could be computed as the critical shear stress for the sediment size, from Shields or other similar criteria, and the equilibrium scour depth was a measured quantity. The sediment particles themselves were indirectly measuring all the forces acting to cause motion in the complicated flow field around the pier. The combined effects of these forces could be represented as an effective shear stress that is comparable to the shear stress that is associated with one-dimensional flow such as the flow past a sediment sample in the Texas A&M erosion function apparatus (EFA).

The primary procedural issue in running these experiments was how long to run each test so that the equilibrium scour depth could be estimated with reasonable confidence. Theoretically clear water scour never reaches equilibrium but is asymptotic with time, but most of the scour occurs in a relatively short time. Scour depths measured from a few very long duration experiments, as long as 10 days, were compared with scour depths from shorter duration experiments to establish criteria for extrapolating equilibrium scour depths from short duration data. Techniques for extrapolating short-duration scour measurements was the topic of the 1998 ASCE paper by Bertoldi, et al.[1]

For the conditions used in these experiments, the following percentages of equilibrium scour depths were used to extrapolate short duration scour measurements.

Approximately 75% of equilibrium scour occurred in the first 24 hours.
Approximately 81% of equilibrium scour occurred in the first 48 hours
Approximately 90% of equilibrium scour occurred in the first 72 hours
Approximately 100% of equilibrium scour occurred after 8 days.

Extrapolations from 24-hour measurements are much less reliable than extrapolations from 48-hour or longer measurements. Unfortunately most of the experiments in this study were 24-hour experiments.

Computation of Approach Flow Shear Stress

An underlying consideration in this study was that one could compute and/or measure the shear stress in the unobstructed approach flow whereas it is nearly impossible to calculate or measure shear stress in the chaotic flow region immediately in front of a pier. The notion was that we could use laboratory experiments to determine an amplification factor to be applied to the computed approach flow shear stress as an indirect measure of the shear stress in the vicinity of a pier.

Even in the relatively orderly approach flow, there are a number of ways to compute the shear stress.

The average bed shear stress in a segment of flow can be derived from Newton's first law of physics. The simplest derivation is for a segment of closed conduit flow as illustrated in figure 2.

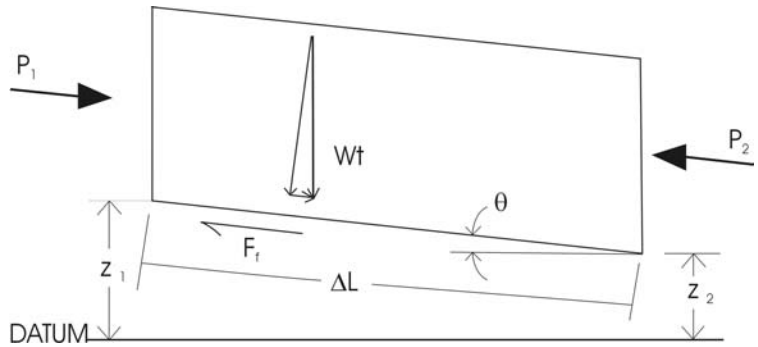

Figure 2. Free Body Diagram of Forces on a Segment of Closed Conduit Flow

$\Sigma F_x = m\, a_x$

$P_1 - P_2 - F_f + Wt \sin\theta = m\, a_x = \rho Q\,(V_2 - V_1)$

$p_1A_1 - p_2A_2 - \tau\, WP\, \Delta L + \gamma\, 1/2(A_1 + A_2)\, \Delta L \sin\theta = \rho Q\,(V_2 - V_1)$

but $A_1 = A_2 = A$ and $V_1 = V_2$

$p_1 - p_2 - \tau\, WP/A\, \Delta L + \gamma\, \Delta L \sin\theta = 0$

$\tau = \gamma\, A/WP\, (\Delta p/\gamma + \Delta L \sin\theta)/\Delta L = 0$

but $A/WP = R_H$; $\Delta L \sin\theta = \Delta Z$; $(\Delta p/\gamma + \Delta Z) = H_{Lf}$; $H_{Lf}/\Delta L = S_F$

Substitution and simplifying yields the familiar expression for average boundary shear stress

$$\boxed{\tau = \gamma R_H S_F}$$

where: τ = average boundary shear stress
R_H = Hydraulic Radius = A/WP = Area / Wetted Perimeter
S_F = friction slope

Chow used a little more algebraic manipulation to derive the same expression for the average boundary shear stress in a segment of gradually varied open channel flow in a unit channel width as illustrated in figure 3.

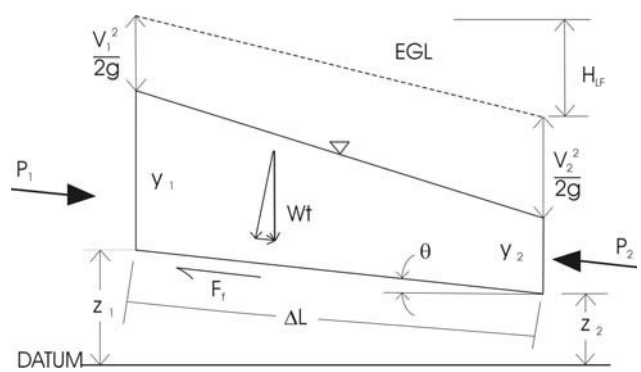

Figure 3. Free Body Diagram of Forces on a Segment of Gradually Varied Open Channel Flow

$\Sigma F_x = m\, a_x$

$P_1 - P_2 - F_f + Wt \sin\theta = m\, a_x = \rho Q\, (V_2 - V_1)$

But,

$P_1 = ½\, \gamma\, (1)\, y_1^2$; $P_2 = ½\, \gamma\, (1)\, y_2^2$;

$$Q = A_{AVG}\, V_{AVG} = \frac{(1)\times(y_1 + y_2)}{2} \times \frac{V_1 + V_2}{2}$$

$$Wt = \gamma \times (1)\left(\frac{y_1 + y_2}{2}\right)\Delta L$$

Substitution yields

$½\, \gamma\, (y_1^2 - y_2^2) - \tau\, WP\, \Delta L + ½\, \gamma\, (y_1 + y_2)\, \Delta L \sin\theta = \rho\, [½\, (y_1 + y_2)\, ½\, (V_1 + V_2)]\, (V_2 - V_1)$

Recall: $(y_1^2 - y_2^2) = (y_1 + y_2)\, (y_1 - y_2)$

Then,

$$y_1 - y_2 - \frac{\tau \times WP \times \Delta L}{\gamma\ (y_1 + y_2)/2} + \Delta L \sin\theta = 1/2\, \frac{\rho}{\gamma}\left(V_2^2 - V_1^2\right) = \frac{V_2^2}{2g} - \frac{V_1^2}{2g}$$

But, $\Delta L \sin\theta = \Delta Z = Z_1 - Z_2$

Rearranging and simplifying yields

$$\tau = \gamma\, R_H \left\{\left[\frac{V_1^2}{2g} + y_1 + Z_1\right] - \left[\frac{V_1^2}{2g} + y_2 + Z_2\right]\right\} / \Delta L = \gamma\, R_H\, H_{Lf} / \Delta L$$

$$\boxed{\tau = \gamma R_H\, S_F}$$

The obvious way to measure the approach shear stress would be very precisely measure the total energy head at two sections of flow on each side of the point of interest. Then one could compute the friction slope and shear stress from the laws of physics. However we did not take such precise measurements for these experiments. We recorded depth averaged approach velocities and approach flow depths in gradually varied flow. To compute shear stresses from the recorded average approach velocity we assumed a log velocity distribution.

Annandale proposed an erodibilty index method for estimating scour limits in rock formations.[5] He expressed average stream power in one dimensional flow as

$$SP = \gamma q S_F = \gamma V y S_F = \tau V$$

Shear stress is related to velocity squared, stream power is related to velocity cubed and it follows that shear stress is proportional to stream power raised to the exponent 2/3. Annandale later derived stream power decay equations from data provided by the TFHRC Hydraulic lab that is represented in this paper. Annandale's equations were:

$$\frac{SP_{pier}}{SP_{appr}} = 3.30\left(\frac{y_s}{y_{s\,max}}\right)^2 - 9.66\left(\frac{y_s}{y_{s\,max}}\right) + 7.66 \qquad \text{for circular piers}$$

$$\frac{SP_{pier}}{SP_{appr}} = 11.64\left(\frac{y_s}{y_{s\,max}}\right)^2 - 22.71\left(\frac{y_s}{y_{s\,max}}\right) + 12.61 \quad \text{for rectangular piers}$$

Where: SP_{pier} = max stream power around the pier at scour depth y_s

SP_{appr} = stream power in the approach flow

y_s = scour depth

$y_{s\,max}$ = maximum scour that would occur in a sand bed channel . Annandale suggested using the FHWA HEC-18 pier scour to estimate this term

At zero scour Annandale's equations indicate that the approach flow stream power is amplified around the pier by 7.66 for circular piers and by 12.61 for rectangular piers. Assuming that the shear stress is proportional to the stream power raised to the 2/3 exponent, it follows that the corresponding shear stress amplifications would be 3.9 and 5.4.

Purpose of this Paper

Data for this paper is the same as the data provided to Annandale for his analysis. This paper will evaluate shear stresses whereas Annandale was interested in stream power for the erodibility index method. Moreover the data behind the analyses have never been published. The data includes some long duration experiments that are not likely to be repeated. Part of the purpose of this paper is to make that data and the logic we used in presenting the results available for other researchers to use and build upon.

Experimental Procedure

Moveable bed experiments were conducted in the six-foot wide by seventy-foot long Tilting flume in the FHWA hydraulics lab located in McLean, Virginia. Four different sediment sizes and four pier models were used in the experiments. Sediment sizes were 0.3mm, 1.2mm, 2.4mm and 5mm. Pier models were a 152 mm (6 inch) diameter cylindrical pier, a 152 mm by 152 mm (6 inch by 6 inch) square pier, a 75mm by 300 mm (3 inch by12 inch) round nose oblong pier and a 75 mm by 300 mm (3 inch by12 inch) rectangular pier. The round nose oblong and rectangular piers were tested at 0°, 15°, and 30° skew angles. The approach velocity was varied for each experiment, but it was always at or below the critical incipient motion velocity for the sediment

$$\frac{V}{U_*} = 5.75 \ \text{Log} \left(\frac{12.27 \ x \ y_0}{K_s}\right)$$

where: V = depth averaged velocity

U_* = shear velocity = $(\tau/\rho)^{1/2}$

y_0 = flow depth

K_s = grain roughness, use $K_s = D_{50}$ for uniform grain sizes

x = viscosity correction factor found in figure 2.97 of ASCE Manual No. 54

We fit several functions to the correction factor graph in figure 2.97 to facilitate T&E solution to determine τ from the above equation on a spreadsheet.

There are other methods such as Manning-Strickler and Moody to estimate the shear stress in the approach flow but we selected the assumed log velocity distribution to estimate shear stress from the data we recorded.

Computation of Shear Stress at the Pier

The second assumption was that the shear stress at the pier in the bottom of the scour hole must be the "effective" incipient motion (critical) shear stress when the scour hole reached equilibrium. We could assume critical shear stress at the pier when the scour depth reached equilibrium. All of the experiments were clear water experiments, which meant the approach flow shear stress was always less than critical; therefore there was always some amplification of the shear stress at the pier**.** The key word here is "effective" because one can argue that there are a lot more forces than boundary shear stresses that determine when particles could no longer get washed out of the scour hole. Our rational was that we were simply letting the sand particles tell us when all these forces were in balance and using a computed shear stress as an indicator of the balance.

The logistical problem was duration of experiments to reach equilibrium scour for clear water experiments. Theoretically clear water scour never reaches equilibrium but we found that practical equilibrium was reached in several days and we could use the trends from a few long duration tests to extrapolate scour depths from shorter duration experiments.

Shields diagram was used to compute the critical shear stress, which we assumed was the equilibrium condition in the bottom of the scour hole. Shields dimensionless shear stress is usually taken as a constant for boundary Reynolds numbers greater than 1000. Most of our laboratory experiments however had boundary Reynolds numbers in the range from 30 to 330. To facilitate computations we fit a regression equation to the portion of Shields diagram that we used. The equation

$$\tau_* = 0.0215\, R_*^{0.1585} \quad \text{if } 10 < R_* < 700$$

where: τ_* = Shields dimensionless shear stress

R_* = Shields boundary Reynolds number

fits the Shield's diagram quite well for our range of data.

But,

$$\tau_* = \frac{\tau_C}{(\gamma_S - \gamma) D_{50}}$$

$$R_* = \frac{\sqrt{\tau_c / \rho}\, D_{50}}{\nu}$$

where: γ = unit weight of water = 9.79 N/m^3 at 20° C ; γ_S= 2.65 γ

ρ = mass density of water = 998 Kg/m^3 at 20° C

υ = dynamic viscosity of water = 1.00 x 10^{-6} at 20° C

Combining the above three expressions yields the following equation which could be solved directly for the critical shear stress:

$$\tau_c = \left[\frac{[0.0215 \quad (\gamma_S - \gamma)\, D_{50}]}{\left(\sqrt{\rho}\ \nu\right)^{0.1585}} \right]^{1.086}$$

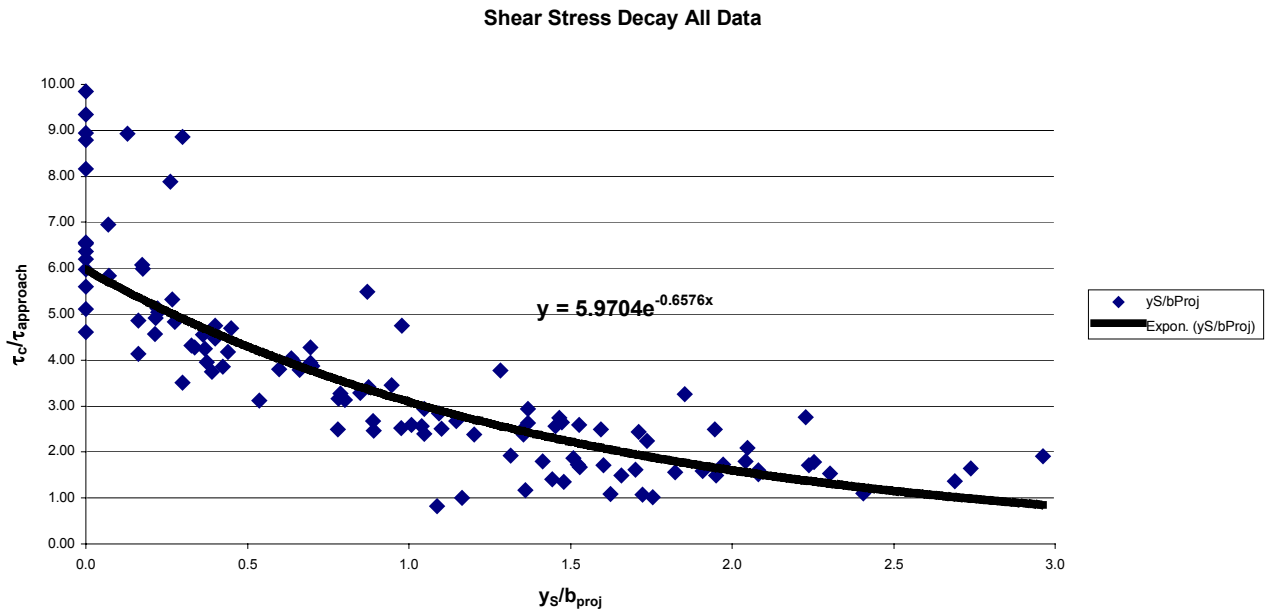

The Reynolds number, R_*, was checked for each line in the spreadsheet to ascertain that it was between 10 and 700.

Results

The ratio of critical shear stress to the approach shear stress, which was always less than critical due to the nature of the experiments, was the amplification ratio caused by the pier. The next step was to determine the equilibrium scour depth where the critical shear stress assumption was valid. A few long duration tests were run for as long as 8 days; for those tests the measured scour depth was the equilibrium scour depth. The equilibrium scour depths for shorter duration tests by extrapolating the measured scour depths as described in the 1998 ASCE paper by Bertoldi, et al.[1] We recognized that the extrapolations were not so reliable for the 24 hour tests and should have run all experiments for at least 48 hours.
Several parameters were tried for normalizing the scour depths so that the dimensionless shear stress ratio could be plotted against a dimensionless scour depth parameter. The normalizing parameter selected for this paper is the pier width so that a plot of $\tau_c/\tau_{Approach}$ vs. y_s/b could represent the shear stress amplification-decay as the scour depth got deeper. For skewed piers the projected width of the pier was used instead of the width b.

Figure 4 is a plot of all the data including round nose and rectangular piers skewed to the flow with no consideration for shape effects. It shows that the average amplification at zero scour depth is approximately 6.0. The particles tell us that the approach shear stress is amplified by a factor of six at zero scour. The amplification reduces to 1.0 at scour depths approximately 2.4 times the projected pier width. The scatter in the data can be explained in part by the large number of 24-hour tests that were in the data set.

Figure 4. Shear Stress amplification-Decay Curve for all Data

Figure 5 is a plot of circular and square piers only. It shows that the amplification is distinctly higher for the square piers than it is for circular. Figure 5 includes a single point

from exploratory PIV measurements, which are described below. The PIV point is very consistent with the indirect measurements but that came only after much discussion about how to interpret the PIV results.

were "clear water".

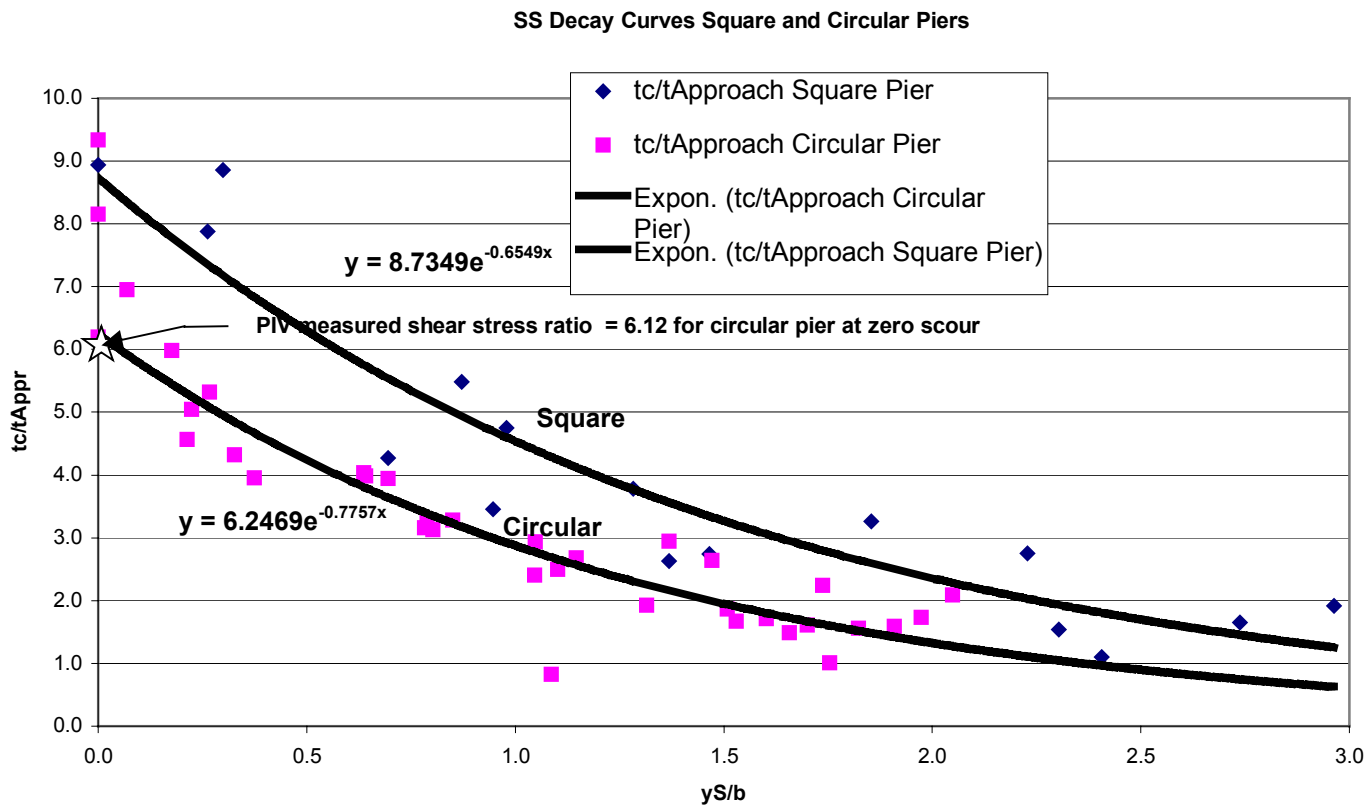

Figure 5. Shear Stress amplification-Decay Curve for Circular and Square Piers

PIV Shear Stress Measurements

Particle Image Velocimetry (PIV) is a powerful laboratory technique that utilizes laser light sheets to illuminate tracer particles in the water and high-speed digital cameras to quantify velocity fields in an experimental set-up. Researchers at the TFHRC hydraulics lab have been developing this technology as a tool for explaining some of the scour

processes we observe. We made small-scale exploratory tests to measure velocity fields very close to the boundary and compute the theoretical shear stresses as a check for the indirect measurements we made with the moveable bed scour tests. If this method works, we can accelerate the tests considerably and establish a sound theoretical basis for the results. The advantage of this method is we could perform fixed bed scour holes and test a wide range of approach flow condition to validate an inherent assumption that the **ratio** of shear stresses holds for a wide range of approach flow velocities.

The theoretical shear stress at any point in a two dimensional flow field is made up of two components- the laminar component and the turbulent component as follows:

$$\tau = \mu\left[\frac{\partial \bar{u}}{\partial y} + \frac{\partial \bar{v}}{\partial x}\right] - \rho\overline{u'v'}$$

where: The first term on the right side is the laminar component and the second term is the turbulent component

u and v are point velocities in the x and y directions respectively

u' and v' are the turbulent fluctuations

Since PIV can measure all of these quantities at discrete pixels in the flow field, it seemed reasonable that the shear stresses could be calculated from a PIV flow field. The partial derivatives are evaluated by computing the incremental changes at adjacent pixels

Figure 6 is the PIV velocity field measured in front of a very small model of a bridge pier. Figure 7 is the zoomed view of the velocity field and resulting shear stress distribution immediately upstream of the pier where vorticity seemed strongest.

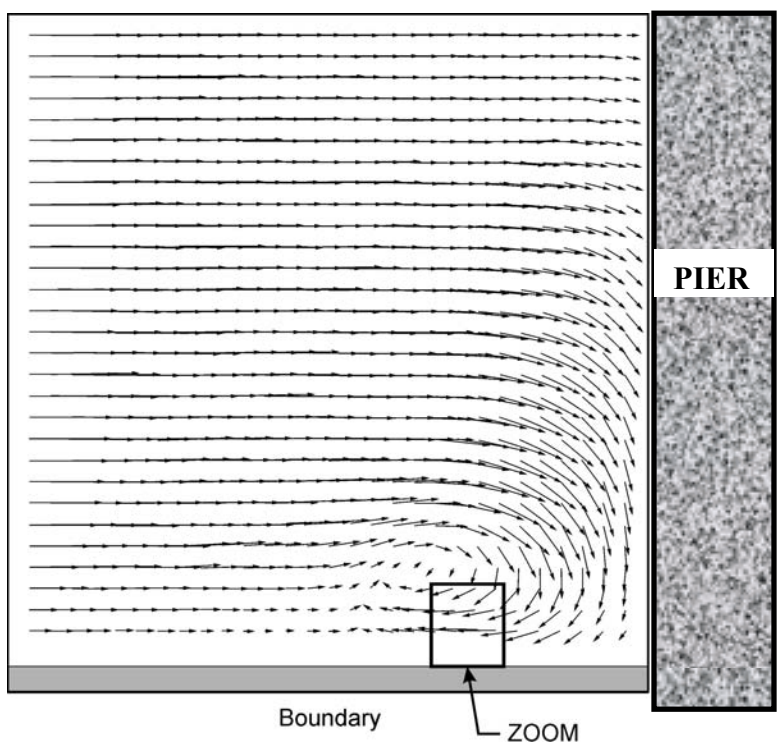

Figure 6. PIV velocity field upstream of a bridge pier model

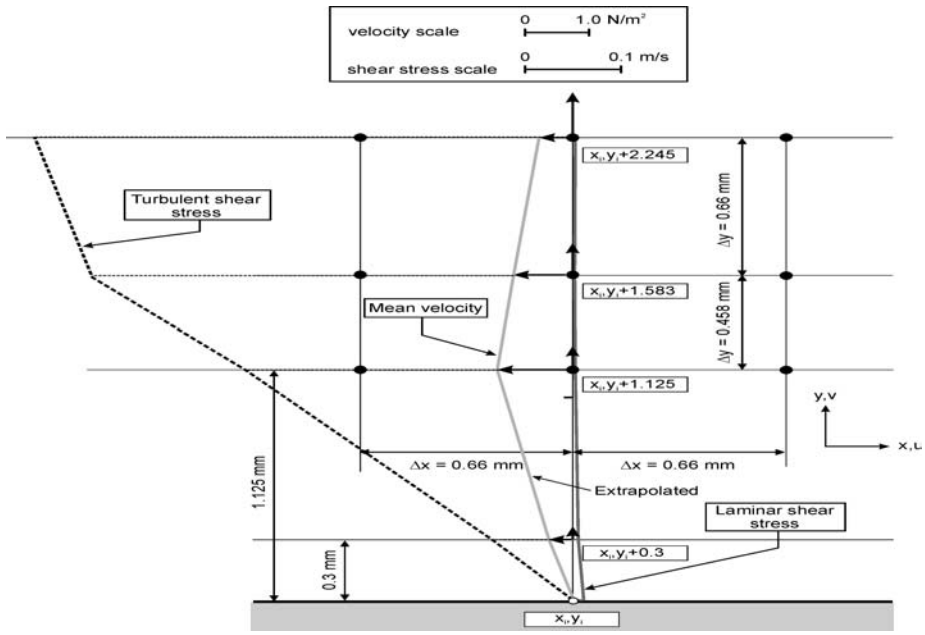

Figure 7. Zoomed Velocity Field and Shear Stress Distribution Near the Bed

The laminar shear stresses at the bed dominate in the approach flow and the turbulent shear stresses dominate in front of the pier as indicated in table 1. The problem we had was where to form the ratio because the turbulent shear stress must go to zero at a no slip boundary. If we compared shear stresses right at the bed , it would appear that the ratio was less than1.0 even at zero scour. If we compared shear stresses at the first measured pixel,which was 1.125 mm above the bed it would appear that the amplification was approximately 95. But if we extrapolated the shear stresses to a close proximity to the bed, 0.33 mm, equal to the diameter of the smallest particles used in the scour tests, then the ratio was a reasonable value of 6.15. That value was plotted on figure 5.
PIV shows promise but we need more experience to apply it to this problem. Perhaps better lens and larger scale tests will eliminate skepticism, but without the indirect measurements from the scour tests as a gage, we may never have reached a reasonable conclusion from these PIV results.

Table1. PIV Shear Stress Results

Approach Flow						
x_i	y_i	$\bar{u}$ [m/s]	$\bar{v}$ [m/s]	$\rho\overline{u'v'}$ [N/m²]	$\mu\left(\frac{\partial\bar{u}}{\partial y}+\frac{\partial\bar{v}}{\partial x}\right)$ [N/m²]	τ_{TOT} [N/m²]
x_i	$y_i + 0$	0	0	0	.254	0.254
x_i	$y_i + 0.3$	.562	0	-.0115	.21411	0.22561
x_i	$y_i + 1.125$	.213	0	-.0277	.0322	0.0599
x_i	$y_i + 1.583$	.234	0	-.019	.0389	0.0579
x_i	$y_i + 2.245$	.265	0	-.0076	.0424	0.05
In Front of Pier						

x_i	y_i	$\bar{u}$ [m/s]	$\bar{v}$ [m/s]	$\rho\overline{u'v'}$ [N/m^2]	$\mu\left(\frac{\partial\bar{u}}{\partial y}+\frac{\partial\bar{v}}{\partial x}\right)$ [N/m^2]	τ_{TOT} [N/m^2]
x_i	$y_i + 0$	0	0	0	.1366	0.1366
x_i	$y_i + 0.3$	-.024	.0114	-1.297	.0907	1.3877
x_i	$y_i + 1.125$	-.078	.0376	-5.098	.0168	5.1148
x_i	$y_i + 1.583$	-.0624	.0516	-6.606	.0296	6.6356
x_i	$y_i + 2.245$	-.0338	.0727	-8.446	.0480	8.494

Conclusions

Shear stress is a key to estimating scour at bridge piers especially in cohesive bed materials, but shear stresses are very difficult to quantify in the chaotic flow field in front of bridge piers.

This paper presents a simple but tedious technique for quantifying shear stresses by using sand particles as an indirect measure.

PIV shows promise as a more theoretical technique for quantifying shear stresses but we need further development and experience.

The indirect measure described in this paper will serve as a gage for more the interpretation of numerical and physical model results that may have a more theoretical basis.

References

1. Bertoldi, David A. and J. Sterling Jones, "Time to Scour Experiments as an Indirect Measure of Stream Power Around Bridge Piers." Proceedings of the ASCE International Water Resources Engineering Conference held in Memphis, TN, pp 264-269, 1998.
2. Johnson, Peggy A. and J. Sterling Jones, "Shear Stress at Base of Bridge Pier," Transportation Research Record No. 1350, Transportation Research Board, pp 14-18, 1992.
3. Parola, A.C., "The Stability of Riprap Used to Protect Bridge Piers," Publication No. FHWA-RD-91-063, Federal Highway Administration, Office of Research and Development, 1991
4. Pagan, Jorge, "Stability of Riprap for Protection at the Toe of Abutments," Publication No. FHWA-RD-91-057, Federal Highway Administration, Office of Research and Development, 1991
5. Annandale, George W., "Calculation of Pier Scour Using the Erodibility Index Method," Draft notes for a short course presented to the Maryland State Highway Administration, April 1999.
6. Annandale, George W. and Steve P. Smith, "Proposed Pier Scour Procedure for Rock Formations" Proceedings of the ASCE International Water Resources Engineering Conference held in Memphis, TN, pp 258-263, 1998.

Appendix Summary of Data

Run #	Run Time (hrs)	Description	Skew Angle (degrees)	b_{proj} (mm)	D_{50} (mm)	Flow Depth y_a (m)	Approach Velocity Va (m/s)	Measured Scour Depth y_s (m)	Estimated Equilibrium Scour Depth y_{equil} (m)	Einstein Barborosa Approach Shear Stress τ_a (N/m^2)	τ_c (N/m^2)	τ_c/τ_a	y_S/b_{Proj}
45	24	Square Pier	0	152	1.2	0.267	0.520	0.274	0.366	0.657	0.723	1.10	2.41
30	72	152mm x 152mm	0	152	1.2	0.267	0.443	0.315	0.350	0.470	0.723	1.54	2.30
56R	41		0	152	1.2	0.267	0.344	0.166	0.208	0.275	0.723	2.63	1.37
31	72		0	152	1.2	0.267	0.337	0.201	0.223	0.264	0.723	2.74	1.47
46	24		0	152	1.2	0.267	0.301	0.108	0.144	0.209	0.723	3.46	0.95
6	23.3		0	152	1.2	0.267	0.272	0.079	0.106	0.169	0.723	4.27	0.70
136	24		0	152	1.2	0.305	0.204	0.030	0.040	0.092	0.723	7.88	0.26
5	1	Incipient scour at pier	0	152	1.2	0.267	0.189	0.000	0.000	0.081	0.723	8.94	0.00
15	24	Circular Pier	0	152	1.2	0.267	0.541	0.200	0.267	0.713	0.723	1.01	1.75
47	24	152mm x 152mm	0	152	1.2	0.267	0.442	0.208	0.277	0.465	0.723	1.56	1.82
52R	24		0	152	1.2	0.267	0.434	0.194	0.258	0.449	0.723	1.61	1.70
134	72		0	152	1.2	0.267	0.422	0.219	0.244	0.422	0.723	1.71	1.60
49	24		0	152	1.2	0.267	0.352	0.126	0.167	0.289	0.723	2.50	1.10
57R	144		0	152	1.2	0.267	0.340	0.174	0.174	0.270	0.723	2.68	1.15
50	70		0	152	1.2	0.267	0.310	0.108	0.120	0.221	0.723	3.27	0.79
10	23.3		0	152	1.2	0.267	0.270	0.037	0.050	0.167	0.723	4.32	0.33
135	6		0	152	1.2	0.267	0.230	0.020	0.027	0.121	0.723	5.98	0.18
48	1	Incipientscour at pier	0	152	1.2	0.267	0.185			0.077	0.723	9.34	0.00
41	24	Round Nose Pier	0	75	1.2	0.267	0.526	0.097	0.129	0.671	0.723	1.08	1.72
42	24	75mm x 300mm	0	75	1.2	0.267	0.446	0.117	0.156	0.475	0.723	1.52	2.08
54R	24		0	75	1.2	0.267	0.435	0.117	0.156	0.451	0.723	1.60	2.08
40	67		0	75	1.2	0.267	0.352	0.090	0.101	0.290	0.723	2.49	1.35
44	70		0	75	1.2	0.267	0.303	0.059	0.066	0.212	0.723	3.42	0.88
20	23.3		0	75	1.2	0.267	0.258	0.023	0.030	0.152	0.723	4.75	0.40
16	1	Incipient	0	75	1.2	0.267	0.238			0.129	0.723	5.60	0.00
43	24	Round Nose Pier	15	150.09	1.2	0.267	0.524	0.183	0.244	0.667	0.723	1.08	1.62
29	48	75mm x 300mm	15	150.09	1.2	0.267	0.419	0.192	0.229	0.417	0.723	1.73	1.52
28	24		15	150.09	1.2	0.267	0.273	0.041	0.055	0.170	0.723	4.25	0.37
137	6		15	150.09	1.2	0.267	0.263	0.041	0.054	0.159	0.723	4.55	0.36
23	1	Incipient scour at pier	15	150.09	1.2	0.267	0.249			0.141	0.723	5.12	0.00
53R	24	Round Nose Pier	30	214.95	1.2	0.267	0.544	0.188	0.250	0.720	0.723	1.00	1.16
38	24	75mm x 300mm	30	214.95	1.2	0.267	0.505	0.219	0.293	0.616	0.723	1.17	1.36
39	24		30	214.95	1.2	0.267	0.413	0.228	0.304	0.403	0.723	1.79	1.41

Run #	Run Time (hrs)	Description	Skew Angle (degrees)	b_{proj} (mm)	D_{50} (mm)	Flow Depth y_a (m)	Approach Velocity Va (m/s)	Measured Scour Depth y_s (m)	Estimated Equilibrium Scour Depth y_{equil} (m)	Einstein Barborosa Approach Shear Stress τ_a (N/m^2)	τ_c (N/m^2)	τ_c/τ_a	y_S/b_{Proj}
35	24		30	214.95	1.2	0.267	0.348	0.168	0.224	0.283	0.723	2.56	1.04
36	24		30	214.95	1.2	0.267	0.287	0.096	0.128	0.190	0.723	3.81	0.60
37	24		30	214.95	1.2	0.267	0.266	0.065	0.086	0.161	0.723	4.48	0.40
138	24		30	214.95	1.2	0.267	0.256	0.045	0.059	0.150	0.723	4.83	0.28
34	1	Incipient scour at pier	30	214.95	1.2	0.267	0.220			0.110	0.723	6.57	0.00
58	192	Circular Pier	0	152.00	0.3	0.267	0.289	0.165	0.165	0.154	0.126	0.82	1.09
62	24	Square Pier	0	152.00	2.4	0.267	0.645	0.307	0.409	1.271	1.729	1.36	2.69
133	24	152mm x 152mm	0	152.00	2.4	0.267	0.480	0.266	0.296	0.694	1.729	2.49	1.95
85	24		0	152.00	2.4	0.267	0.485	0.195	0.260	0.711	1.729	2.43	1.71
59	24		0	152.00	2.4	0.267	0.479	0.182	0.242	0.693	1.729	2.49	1.59
60	24		0	152.00	2.4	0.267	0.387	0.080	0.106	0.447	1.729	3.87	0.70
61	72		0	152.00	2.4	0.267	0.352	0.062	0.068	0.369	1.729	4.69	0.45
130	6		0	152.00	2.4	0.267	0.257	0.018	0.020	0.194	1.729	8.93	0.13
84	1	Incipient scour at pier	0	152.00	2.4	0.267	0.259			0.197	1.729	8.79	0.00
67	24	Circular Pier	0	152.00	2.4	0.267	0.618	0.189	0.252	1.163	1.729	1.49	1.66
127	24		0	152.00	2.4	0.267	0.583	0.174	0.232	1.035	1.729	1.67	1.53
128	144		0	152.00	2.4	0.267	0.544	0.200	0.200	0.897	1.729	1.93	1.32
65	72	152mm x 152mm	0	152.00	2.4	0.267	0.488	0.143	0.159	0.720	1.729	2.40	1.05
87*	24		0	152.00	2.4	0.267	0.442	0.156	0.208	0.587	1.729	2.94	1.37
129	24		0	152.00	2.4	0.267	0.443	0.119	0.159	0.589	1.729	2.94	1.05
86	72		0	152.00	2.4	0.267	0.429	0.110	0.122	0.553	1.729	3.13	0.80
74	144		0	152.00	2.4	0.267	0.427	0.119	0.119	0.546	1.729	3.16	0.78
64	24		0	152.00	2.4	0.267	0.383	0.043	0.057	0.437	1.729	3.96	0.37
63	24		0	152.00	2.4	0.267	0.357	0.024	0.033	0.379	1.729	4.57	0.21
66	1	Incipient scour at pier	0	152.00	2.4	0.267	0.308			0.279	1.729	6.20	0.00
70	24	Round Nose	0	75.00	2.4	0.267	0.618	0.110	0.146	1.163	1.729	1.49	1.95
132	24		0	75.00	2.4	0.267	0.490	0.076	0.102	0.724	1.729	2.39	1.35
71R	72	75mm x 300mm	0	75.00	2.4	0.267	0.490	0.081	0.090	0.724	1.729	2.39	1.20
69	24		0	75.00	2.4	0.267	0.477	0.055	0.073	0.686	1.729	2.52	0.98
72	24		0	75.00	2.4	0.267	0.368	0.019	0.025	0.404	1.729	4.28	0.34
131	6		0	75.00	2.4	0.267	0.346	0.009	0.012	0.356	1.729	4.86	0.16
68	1	Incipient scour at pier	0	75.00	2.4	0.267	0.355			0.375	1.729	4.61	0.00
73	24	Round Nose	15	150.09	2.4	0.267	0.647	0.166	0.222	1.278	1.729	1.35	1.48
75	24		15	150.09	2.4	0.267	0.479	0.088	0.117	0.694	1.729	2.49	0.78
76	24		15	150.09	2.4	0.267	0.393	0.044	0.059	0.462	1.729	3.75	0.39

Run #	Run Time (hrs)	Description	Skew Angle (degrees)	b_{proj} (mm)	D_{50} (mm)	Flow Depth y_a (m)	Approach Velocity Va (m/s)	Measured Scour Depth y_s (m)	Estimated Equilibrium Scour Depth y_{equil} (m)	Einstein Barborosa Approach Shear Stress τ_a (N/m^2)	τ_c (N/m^2)	τ_c/τ_a	y_S/b_{Proj}
78	24		15	150.09	2.4	0.267	0.337	0.025	0.033	0.337	1.729	5.13	0.22
77	1	Incipient scour at pier	15	150.09	2.4	0.267	0.304			0.271	1.729	6.37	0.00
80	24	Round Nose	30	214.95	2.4	0.267	0.634	0.233	0.310	1.224	1.729	1.41	1.44
81	72	75mm x 300mm	30	214.95	2.4	0.267	0.481	0.173	0.192	0.700	1.729	2.47	0.89
82	24		30	214.95	2.4	0.267	0.387	0.068	0.091	0.448	1.729	3.86	0.42
83	24		30	214.95	2.4	0.267	0.344	0.035	0.046	0.352	1.729	4.91	0.22
79	1	Incipient scour at pier	30	214.95	2.4	0.267	0.313			0.289	1.729	5.98	0.00
123	24	Square Pier	0	152.00	5	0.267	0.833	0.312	0.416	2.644	4.354	1.65	2.74
99	24	152mm x 152mm	0	152.00	5	0.267	0.773	0.338	0.450	2.275	4.354	1.91	2.96
98	72		0	152.00	5	0.267	0.644	0.305	0.339	1.581	4.354	2.75	2.23
124	72		0	152.00	5	0.267	0.592	0.254	0.282	1.336	4.354	3.26	1.85
100	24		0	152.00	5	0.267	0.550	0.146	0.195	1.152	4.354	3.78	1.28
90	24		0	152.00	5	0.267	0.491	0.112	0.149	0.917	4.354	4.75	0.98
89	24		0	152.00	5	0.267	0.457	0.099	0.132	0.794	4.354	5.48	0.87
122	6		0	152.00	5	0.267	0.359	0.034	0.046	0.491	4.354	8.86	0.30
88	1	Incipient scour at pier	0	152.00	5	0.267	0.316			0.378	4.354	11.51	0.00
96	24	Circular Pier	0	152.00	5	0.267	0.847	0.218	0.290	2.733	4.354	1.59	1.91
121	24	152mm x 152mm	0	152.00	5	0.267	0.813	0.225	0.300	2.516	4.354	1.73	1.97
125	144		0	152.00	5	0.267	0.784	0.229	0.229	2.337	4.354	1.86	1.51
97	24		0	152.00	5	0.267	0.740	0.233	0.311	2.084	4.354	2.09	2.05
126	144		0	152.00	5	0.267	0.713	0.264	0.264	1.937	4.354	2.25	1.74
95	28		0	152.00	5	0.267	0.658	0.170	0.224	1.648	4.354	2.64	1.47
109	144		0	152.00	5	0.267	0.590	0.129	0.129	1.325	4.354	3.29	0.85
120	72		0	152.00	5	0.267	0.535	0.088	0.098	1.091	4.354	3.99	0.64
94	72		0	152.00	5	0.267	0.539	0.095	0.106	1.105	4.354	3.94	0.70
93	24		0	152.00	5	0.267	0.532	0.073	0.097	1.079	4.354	4.04	0.64
110	6		0	152.00	5	0.267	0.476	0.026	0.034	0.863	4.354	5.04	0.22
92	24		0	152.00	5	0.267	0.464	0.030	0.041	0.818	4.354	5.32	0.27
111	6		0	152.00	5	0.267	0.406	0.008	0.011	0.626	4.354	6.95	0.07
91	1	Incipient scour at pier	0	152.00	5	0.267	0.375			0.534	4.354	8.15	0.00
104	24	Round Nose	0	75.00	5	0.267	0.800	0.127	0.169	2.436	4.354	1.79	2.25
103	72	75mm x 300mm	0	75.00	5	0.267	0.635	0.074	0.082	1.534	4.354	2.84	1.09
119	24		0	75.00	5	0.267	0.571	0.020	0.022	1.240	4.354	3.51	0.30
102	24		0	75.00	5	0.267	0.526	0.009	0.012	1.054	4.354	4.13	0.16
101	1	Incipient	0	75.00	5	0.267	0.419			0.667	4.354	6.53	0.00

Run #	Run Time (hrs)	Description	Skew Angle (degrees)	b_{proj} (mm)	D_{50} (mm)	Flow Depth y_a (m)	Approach Velocity Va (m/s)	Measured Scour Depth y_s (m)	Estimated Equilibrium Scour Depth y_{equil} (m)	Einstein Barborosa Approach Shear Stress τ_a (N/m^2)	τ_c (N/m^2)	τ_c/τ_a	y_S/b_{Proj}
107	24	Round Nose	15	150.09	5	0.267	0.797	0.230	0.306	2.418	4.354	1.80	2.04
108	72	75mm x 300mm	15	150.09	5	0.267	0.654	0.120	0.133	1.628	4.354	2.67	0.89
106	24		15	150.09	5	0.267	0.524	0.049	0.066	1.044	4.354	4.17	0.44
118	6		15	150.09	5	0.267	0.434	0.020	0.026	0.717	4.354	6.07	0.17
105	1	Incipient scour at pier	15	150.09	5	0.267	0.341			0.442	4.354	9.85	0.00
114	24	Round Nose	30	214.95	5	0.267	0.817	0.361	0.481	2.539	4.354	1.71	2.24
115	72	75mm x 300mm	30	214.95	5	0.267	0.668	0.281	0.312	1.699	4.354	2.56	1.45
117	24		30	214.95	5	0.267	0.665	0.246	0.328	1.684	4.354	2.59	1.53
112	24		30	214.95	5	0.267	0.550	0.107	0.142	1.151	4.354	3.78	0.66
116	6		30	214.95	5	0.267	0.443	0.012	0.015	0.746	4.354	5.84	0.07
113	1	Incipient scour at pier	30	214.95	5	0.267	0.326			0.403	4.354	10.81	0.00

Shear Stress Approach to Pier Scour Predictions

Ya Li[1], Jean-Louis Briaud[2], Hamn-Ching Chen[2], Prahoro Nurtjahyo[1], Jun Wang[1]

ABSTRACT

A shear stress approach for pier scour is developed based on the results of flume tests and numerical simulations: The final depth of pier scour, which might develop in a complex pier condition, is first correlated with the difference between the maximum shear stress and the critical shear stress of the eroding soil. Second, to simulate the time history of the scour development, a decay model of the boundary shear stress at the bottom of the scour hole is proposed. This model makes use of the erodibility function.

INTRODUCTION

One of the key yet unanswered questions in scour predictions is: "Is the maximum scour depth for a given pier subjected to a given constant velocity the same for all soils? Research at Texas A&M University (Briaud et al., 1999) indicated that the answer appeared to be Yes. The rate was drastically different for different soils but the maximum depth obtained in sand and in clay was the same in the flume experiments which were conducted. The present paper examines this question from the shear stress perspective. To begin, a shear stress approach is developed for the final pier scour prediction by integrating the maximum scour depth results from flume tests with the maximum boundary shear stress results from numerical simulations. Then, to simulate the time history of scour development, a decay model of the boundary shear stress on the bottom of the scour hole is proposed including the use of soil erodibility function.

SHEAR STRESS APPROACH FOR FINAL SCOUR DEPTH

The erosion process is assumed to be controlled by the shear stress acting on the water soil boundary of the scour hole. The shear stress on the river bottom is maximum at the beginning of the scour process and decays as the scour depth increases until an equilibrium scour depth or maximum scour depth, Z_{max}, is reached. At a certain time t during the scour process, the scour hole has a depth z and a pattern of shear stresses is distributed around the pier; the maximum value of these shear stresses for a given depth of the scour hole z is defined as the instantaneous maximum shear stress $\tau(z)$. The initial maximum shear stress (t = 0) just before scouring starts is called τ_{max} because it is the maximum shear stress among the $\tau(z)$ values.

[1] *Graduate student, Dept. of Civil Engineering, Texas A&M Univ., College Station, TX 77843, USA*

[2] *Professor., Dept. of Civil Engineering, Texas A&M Univ., College Station, TX 77843, USA*

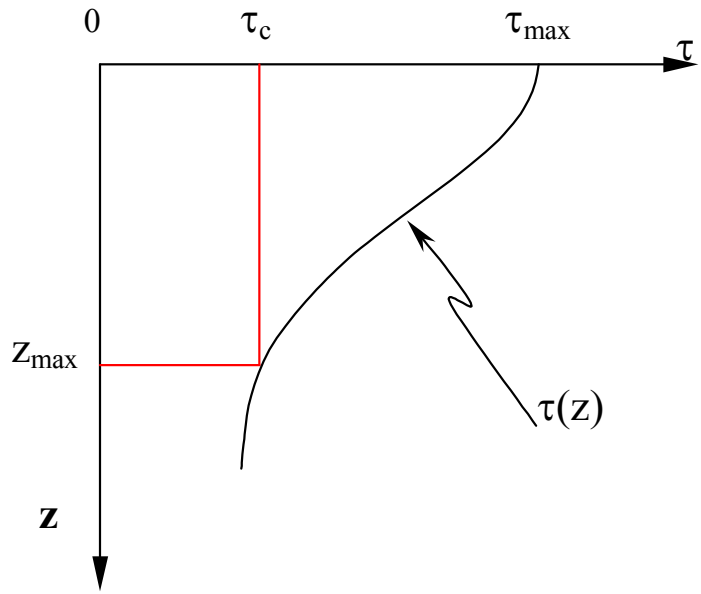

FIG 1 Diagram for Pier Scour Development

The threshold value for soil erosion is the critical shear stress τ_c, which means that scour happens only when the shear stress is larger than the critical shear stress. Unlike the decaying of the shear stress $\tau(z)$, τ_c will not change with the scour development, it is a property of the soil.

Based on the above analysis, a diagram is shown in FIG 1 to represent the scour development. The boundary and initial conditions for pier scour in clay or clear water scour in sand are:

(1) Scour starts from: ($t = 0$, $z = 0$, $\tau = \tau_{max}$)

(2) Scour terminates at: ($t = t_{final}$, $z = Z_{max}$, $\tau = \tau_c$)

To satisfy these two boundary conditions, the maximum (final) scour depth must be a function of ($\tau_{max} - \tau_c$), which means:

$$Z_{max} = \text{function of } (\tau_{max} - \tau_c) \quad \textbf{(1)}$$

In Equation (1), the maximum shear stress can be calculated numerically (Wei, 1997, Nurtjahyo, 2002) and a summarized equation is given below:

$$\tau_{\max} = K_w K_{sh} K_{sp} K_a \times 0.094 \rho V^2 \left(\frac{1}{\log \mathrm{Re}} - 0.1 \right) \quad \textbf{(2)}$$

Where, K_w, K_{sh}, K_{sp}, K_a are the correction factors for water depth effect, pier shape effect, pier spacing effect, and attack angle effect on τ_{max}. The exact equations for these factors can be found in Nurtjahyo (2002). The critical shear stress of the soil can be measured in the Erosion Function Apparatus (Briaud et al, 2001). The maximum scour depth Z_{max} was measured in a number of flume tests conducted by Gudavalli (1997) and Li (2002). These tests included pier scour tests in different clays and sands, and different complex pier scour configurations. By

using the flume test data with equation (1), the best fitting function of (τ_{max} - τ_c) was found to be:

$$\frac{Z_{\max}}{B'} = 20\left(\frac{\tau_{\max} - \tau_c}{\rho g B'}\right)^{0.4} f\left(\frac{H}{B'}\right) \quad \textbf{(3)}$$

with an upper boundary envelope of:

$$\frac{Z_{\max}}{B'} = 40\left(\frac{\tau_{\max} - \tau_c}{\rho g B'}\right)^{0.4} f\left(\frac{H}{B'}\right) \quad \textbf{(4)}$$

and a lower boundary envelope of:

$$\frac{Z_{\max}}{B'} = 10\left(\frac{\tau_{\max} - \tau_c}{\rho g B'}\right)^{0.4} f\left(\frac{H}{B'}\right) \quad \textbf{(5)}$$

where, B' is the pier projection width perpendicular to the flow and H is the water depth. The function $f\left(H/B'\right)$ is the correction function for the shallow water effect in the shear stress approach and it can be represented as (Li, 2002):

$$f\left(\frac{H}{B'}\right) = \begin{cases} 0.075e^{\left(1.88\frac{H}{B'}\right)} & H/B' < 1.383 \\ 1 & H/B' > 1.383 \end{cases} \quad \textbf{(6)}$$

SHEAR STRESS DECAY MODEL

Scour, especially in cohesive soil, is a time dependant process. Therefore a shear stress decay model is necessary to develop the time history for the progression of the scour hole. Of course the erodibility function will also be necessary to transform the shear stress information into an erosion rate parameter. The Erosion Function Apparatus (Briaud et al 2001) can provide that erodibility function. If $\tau(z)$ is the instantaneous maximum shear stress value when the scour hole is z deep, and if the erosion function for the soil is $f(\tau - \tau_c)$, then the finite difference scheme for scour development is:

$$\begin{cases} z_1 = 0 \\ z_{i+1} = z_i + \Delta t \cdot f\left(\tau\left(z_i\right) - \tau_c\right) \quad i = 1, 2, 3, \cdots\cdots \end{cases} \quad \textbf{(7)}$$

As discussed before, the shear stress decay model must pass through the initial point $(\tau_{\max}, 0)$ and the terminal point $(\tau_c, z_{\max})$ as shown in FIG 2. Accordingly, there are several possible shear stress decay models. By fitting the scour depth versus time curves obtained in the flume tests (Gudavalli 1997, Li 2002), it was found that the shear stress on the bottom of the scour hole decays in a curve which is first concave and then convex as the scour depth increases. This reverse curvature model was chosen to describe the decay curve (FIG.3):

$$\frac{\tau-\tau_c}{\tau_{\max}-\tau_c}=e^{-4\left(\frac{z}{z_{\max}}\right)^2} \quad \textbf{(8)}$$

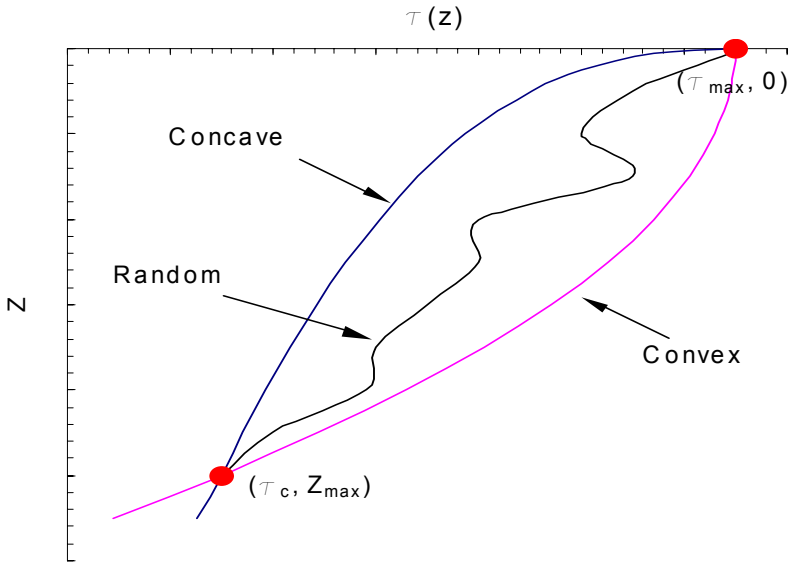

FIG 2 Different Shear Decay Curves

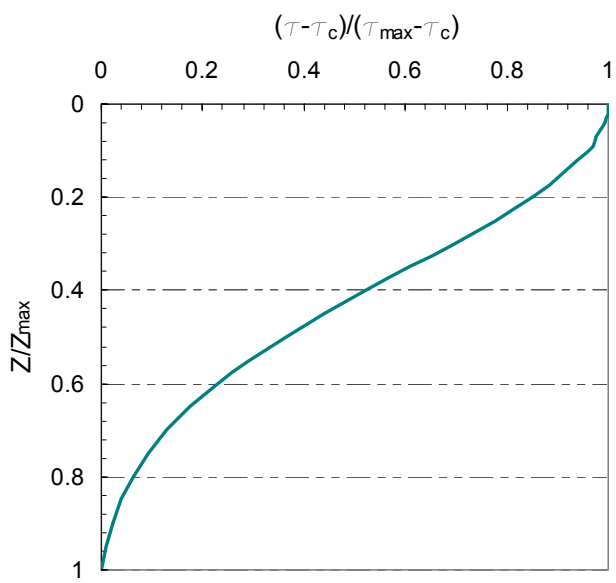

FIG 3 Normalization of Shear Decay Curve

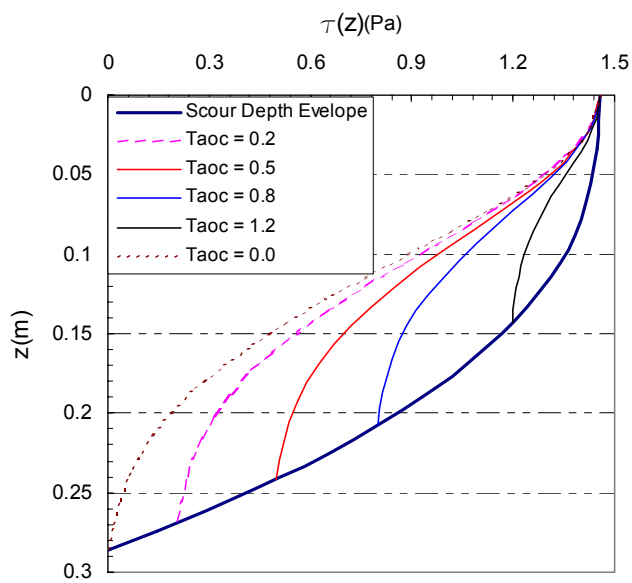

FIG 4 Relationship between Shear Stress Decay Curves and Maximum Scour Depths

An interesting relationship exists between the shear stress decay curve in Equation (8) and the shear stress approach for the maximum pier scour depth in Equation (3). As shown in FIG 4, for the same scour condition but on soils with different critical shear stresses, scour starts from the same origin but follows different tracks as defined by the decay model leading to different maximum scour depths. The envelope of the maximum scour depths is exactly described by Equation (3).

The shear stress approach introduced in this paper for a constant water velocity can also be used for a multi-flood hydrograph and a layered soil system. The reasoning used is similar to the one proposed by Briaud et al (2001) and can be found in Li (2002).

CONCLUSIONS

A shear stress approach is proposed to predict complex pier scour depth, where the scour depth is a function of the difference between the maximum shear stress and the critical shear stress of the eroding soil. The method is limited at this time to pier scour developed in cohesive soils or clear water pier scour in sands. To simulate the time histrory of scour development, a shear stress decay model which gives the evolution of the shear stress at the bottom of the scour hole as the hole deepens is proposed. The shape of that decay model has a reverse curvature with depth.

Previous work at Texas A&M University showed that sands and clays scoured to the same depth but got there at very different rates. This article argues that not only is the rate different for different soils but so is the maximum scour depth. The reason is that different soils have different critical shear stresses. The fact that previous work did not show differences between sand and clay is explained by the fact that the critical shear stresses of the sands and clays used in the flume tests were similar.

REFERENCES

1. Briaud, J.-L., Ting, F., Chen, H.C., Gudavalli, S.R., Perugu, S., and Wei, G., 1999, "SRICOS: Prediction of Scour Rate in Cohesive Soils at Bridge Piers", Journal of Geotechnical and Geoenvironmental Engineering, Vol.125, pp. 237-246, ASCE, Reston, Virginia, USA.
2. Briaud J.-L., Ting F., Chen H.C., Cao Y., Han S.-W., Kwak K., 2001a, "Erosion Function Apparatus for Scour Rate Predictions". Journal of Geotechnical and Geoenvironmental Engineering, Vol.127, No. 2, pp.105-113, ASCE, Reston, Virginia, USA.
3. Briaud, J. L., Chen, H. C. Kwak K., Han S-W., Ting F., 2001b, "Multiflood and Multilayer Method for Scour Rate Prediction at Bridge Piers", Journal of Geotechnical and Geoenvironmental Engineering, Vol.127, No. 2, 2001b, pp.105-113, ASCE, Reston, Virginia, USA.
4. Gudavalli, S. R., (1997), " *Prediction model for scour rate around bridge piers in cohesive soil on the basis of flume tests*," Ph. D. Dissertation, Department of Civil Engineering, Texas A&M University, College Station, Texas, USA.
5. Li, Y. (2002), " Bridge pier scour and contraction scour in cohesive soils on the basis of flume tests," Ph. D. Dissertation, Department of Civil Engineering, Texas A&M University, College Station, Texas, USA.

6. Nurtjahyo, P. (2002), "Bridge pier scour and contraction scour in cohesive soils on the basis of numerical simulations," Ph. D. Dissertation, Department of Civil Engineering, Texas A&M University, College Station, Texas, USA.
7. Wei G., (1997), " *Numerical simulation to study scour rate in cohesive soils,*" Master's Thesis, Department of Civil Engineering, Texas A&M University, College Station, Texas, USA.

A Review of Predictive Methods for General Scour

Professor R Bettess, Principal Scientist, HR Wallingford, Howbery Park,
Wallingford, Oxfordshire, UK
e-mail: roger@hrwallingford.co.uk

Abstract

General scour is the bed level change that can take place in a river section below the natural or normal bed level. Predicting the amount of general scour has received less attention than predicting local scour but as the two effects are additive it is equally as important. The methods used to predict general scour are frequently based on either a regime approach or on conditions for the initiation of motion of the sediment on the bed of the channel. In the paper existing methods of estimating general scour are critically reviewed. Numerical model results are presented indicating that the amount of general scour that takes place during a single flood event depends upon the duration of the flood event and that in many cases equilibrium scour depths are never achieved. This implies that in many cases the assumptions underlying methods for predicting general scour are not satisfied in the field.

1 Introduction

In designing bridge or pipeline crossings of rivers an important design parameter is the bed levels which may occur in the river during the lifetime of the structure. For bridges a lot of attention has been paid to the issue of predicting local scour around structures, perhaps because this is a well-defined and obvious problem which may be studied using laboratory experiments and more recently using numerical models. The issue of predicting general changes in river bed level has received less attention.

There are a number of potential sources of general bed level change:

- Long-term progressive degradation , either natural or man-induced may take place.
- Changes in channel shape arising from:
  - a) a change in the river type, for example, a change from a braided to a meandering river,
  - b) a change in the plan form of a river, for example, a change in the radius of curvature of the river channel,
- Changes caused by individual flood events.

It is the last topic, the changes in bed level arising during a flood event that will be discussed in this paper.

2 Definition of general scour

As alluded to above, the changes in bed level that may occur during the lifetime of a structure potentially arise from a number of different sources and so can be difficult to define. Thus different authors use different definitions and classifications. Melville and Coleman (2000) define general scour as ‘that scour occurring irrespective of the presence of any human-imposed structure’ while they define contraction scour as that

scour that ‘can occur where the foundations and/or the road approach embankments of a bridge restrict the waterway. Alternatively, contraction scour can occur if the bridge is sited at a natural contraction in the width of the river.’ Thus there is an overlap between the Melville and Coleman definitions of general scour and contraction scour.

In the following we will discuss that scour that can arise as a result of longitudinal changes in channel properties resulting from either man-made structures or natural changes. Thus this corresponds to the Melville and Coleman definition of contraction scour

3 Properties of general scour

The factors which affect contraction scour include:

a) Change in cross-sectional area of flow

It is normally assumed that the contraction is brought about by a reduction in the width of the flow. The corresponding adjustment to the bed leads to the scour. This factor is normally quantified using the parameter B1/B2, where B is the width of the channel and 1 refers to the upstream section and 2 refers to the downstream section.

b) Change in discharge

Continuity imposes that unless water is being lost out of the system that the discharge at the constricted reach must be the same as the total discharge at the upstream section. As has been pointed out, however, particularly at bridges with approach embankments, the flow upstream may be distributed between the main channel(s) and the floodplains while at the constricted section all the flow may be confined to the main channel. Thus the discharge in the main channel between the upstream and constricted sections may be different.

c) Sediment grading

Where the bed sediment contains a range of sediment sizes, differential transport of different sizes may lead to the bed in the constricted section armouring and so leading to a reduction in the scour depth in comparison with a uniform sediment

d) Sediment supply from upstream

The amount of sediment that is being transported by the channel can also affect the depth of scour. Thus in the past a distinction has been made between ‘clear water’ and ‘live-bed’ scour. It is generally considered that clear water scour in which there is no sediment input from upstream will be larger than live bed scour when there is some sediment supply from upstream

e) Duration of flow

Many theories to predict scour are based on the assumption of equilibrium conditions. Thus it is assumed that an individual flood event is sufficiently long that the scour achieves its ultimate depth. It is now clear that following a flood event the bed of the river rapidly

recovers to the pre-flood bed levels. For short duration flood events the scour may not achieve equilibrium conditions.

4 Review of predictive methods

4.1 Long contraction methods

Many approaches to the problem of predicting contraction scour are based on considering a long rectangular contraction. This assume that the upstream section is uniform and rectangular and that the length of the contraction is long enough tom establish uniform conditions in the contraction. The objective is then to predict the conditions in the contracted section and relate them to the upstream conditions. The approach seems to have been first used by Straub (1934) and subsequently extended by Laursen (1958, 1960, 1962 and 1963), Komura (1966), Ashida (1964), Gill (1981) and Keller (1983). To make this approach analytically tractable a number of assumptions have to be made:

a) the length of the contraction is long enough to establish uniform conditions
b) the energy slope in the contracted section is the same that in the upstream section
c) the flow conditions in the contracted section are such that the sediment is just at the point of initiation of motion.

Determine the critical velocity an estimate is required of the Manning's n value for the channel. This is based on the sediment diameter using Strickler's equation:

$$n = 0.034\ D_{50}^{1/6}. \qquad (1)$$

This assumes that the hydraulic roughness is predominantly skin roughness due to the sediment grains. This is often a reasonable assumption for gravel bed rivers but can underestimate the hydraulic roughness for sand bed rivers where form losses may be significant. Even for gravel bed rivers, the use of D_{50} in assessing the hydraulic roughness of a sediment bed is also rather unusual. In the context of gravel bed rivers it is normally found that the hydraulic roughness depends upon the size of the larger fractions such as the D_{90} or D_{85}. These problems may explain a subsequent recommendation that in equation (1) D_{50} should be replaced by D_m, where:

$$D_m = 1.25\ D_{50}.$$

Though one can understand the logic of using a sediment diameter larger than the D_{50} size it seems unlikely that a simple factor of 1.25 is an adequate representation of the different processes at work.

The impact of underestimating the Manning's n value is that the scour depth is also then underestimated.

Laboratory simulations of long contractions have shown that the theories give reasonable predictions of the depth within the constricted section but tend to under-estimate the observed depths. Keller presented a generalisation of the analysis of Laursen (1963) and found that it under predicted the observations by up to 13%.

Keller recommends that for design purposes the predictions of the equations should be multiplied by 1.2.

While the long contraction model is attractive to enable an analytic expression for scour depth it may not be a very realistic model of contraction scour at crossings. Where the contraction is due to a bridge and abutments its streamwise extent is rarely long enough to establish uniform conditions in the contracted reach. Nor is it is clear that in the real world the second assumption above about energy slope is valid.

Keller (1983) observed that in some of the laboratory experiments the scour at the entry to the contraction exceeded that in section where the flow had become uniform once again. This increased scour at the entry to the contraction can arise from a number of causes. In general the contractions at crossings are so short that uniform conditions are rarely established in the contracted section. The result is that in the contracted section the energy slope exceeds that in the section upstream and downstream. In abrupt contractions the flow may separate from the sides of the channel. This results in the formation of a horizontal, transverse recirculation zone. A vena contracta is present that is narrower than the width of the contracted section. This means that the effective width of the cross-section is reduced from the bank to bank width. This effective narrowing of the section will depend upon the details of the transition from upstream to downstream and will be larger in sudden transitions and less in more gradual transitions. It is likely that some estimate of the additional scour caused by this effect could be provided by estimating the width of the vena contract. Certainly an upper limit on this effect could be provided by assuming a sharp transition.

The evidence is thus that methods of estimating scour based on a long contraction approach are likely to underestimate the depth of scour.

4.2 Regime methods

Another approach to estimating contraction scour has been based on regime theory. Neill (1973) suggested that the depth of a flow in a channel during a flood could be determined using the regime theory due to Lacey (1973). This provided a method for predicting the depth in an uncontracted channel.

Previously Blench (1969) had put forward a regime approach to calculating the scour depth in a constricted channel. In this approach instead of using the discharge as the independent variable, the unit discharge is used to determine the depth of flow. Blench used the regime equation of the form:

$$V^2/d = F_b, \qquad (2)$$

where Fb is a function of the sediment. By using the equation:

$$q = Vd, \qquad (3)$$

where q is the unit discharge, the regime equation (2) becomes:

$$d = (q^2 F_b)^{1/3}. \qquad (4)$$

It would appear that Blench then proposed using this equation within the contraction to determine the depth of flow. This approach neglects the fact that equation (2) is a description of regime channels in which the flow width is free to adjust and is thus related to the other flow parameters, V and d. It does not necessarily apply, however, to channels with constrained widths. Thus equation (4) is only applicable to regime channels and does not apply to channels whose width is constrained. It thus cannot be used to predict contraction scour. This can be easily demonstrated by using the data from the laboratory experiments of Keller. All the experiments used the same sediment and so the value of F_b should be constant. Thus the value of V^2/d should be the same for all the runs. In reality the value of V^2/d varies from 0.856 to 2.649. When equation (4) is used to predict the results of the experiments the errors range from 28 to 49%. Thus the regime approach of Blench cannot be recommended for use to predict constriction scour.

The regime approach has recently been refined by May et al (2002). Although not explicit this approach makes a number of assumptions. It assumes:

a) the length of the contraction is long enough to establish uniform conditions
b) the energy slope in the contracted section is the same that in the upstream section.

The method is based on assuming that the upstream section of the channel is in regime and that in the constricted reach the area of flow is the same as that in the upstream reach. As was discussed above these assumptions are not always valid for contractions associated with crossings.

4.3 Competent velocity methods

Competent velocity methods are based on the assumption that scour will continue until the flow conditions approach those for the threshold of motion of the bed sediment. As the name implies the flow conditions for threshold of motion are expressed in terms of a critical flow velocity. We know from the work of Yalin (1977) that using flow velocity to determine critical conditions is not very reliable in comparison with using critical shear stress. Thus any estimate of scour depth using competent velocity methods must be regarded with suspicion. As described under the section on long contractions it is possible to use an estimate of the Manning's n value to overcome this problem but errors in estimating Manning's n may add to the errors in estimating scour depths rather than reduce them.

4.4 Armouring condition

One disadvantage of the methods described above is that they assume that the composition of the bed material remains constant during the flood event. It seems likely that where the bed of the river consists of a range of sediment sizes that the finer sediment is preferentially removed and so the composition of the surface or armour layer changes during the flood. Particularly when there is partial transport so that not all the sediment sizes are moving, this may inhibit the development of scour and hence lead to smaller scour depths than would be obtained in uniform sediments with the same D_{50} size.

It should be noted that in scour equations such as those of Laursen, the depth of scour is a function of the sediment diameter and reduces as the sediment diameter increases. During a flood, differential sediment transport of different sediment sizes will lead to a change in composition of the bed sediments within a constriction. This will, in general, lead to an increase in size of sediment on the bed which will act to inhibit scour. Note that this effect will take place even if all the sediment sizes are moving.

A number of approaches have been based on assessing the degree of armouring that will take place. In essence they are based on a critical flow approach but take account of the fact that with time the composition of the bed will change so modifying the critical velocity. The methods of Pemberton and Lara (1984) and Borah (1989) are only applicable where a proportion of the bed material is sufficiently large that it is not moved by the flow.

Pemberton and Lara (1984) assume that the degraded channel has the same hydraulic conditions as the existing channel. This neglect the fact that as the scour takes place the velocities in the constricted channel will reduce. It is thus likely to over-estimate the depth of scour.

In cases where the bed of the river rapidly armours with immobile sediment this is likely to lead to increased shear stresses on the river banks and hence may lead to erosion of the river banks.

4.5 Empirical methods

There are a number of empirical methods such as the New Zealand Railways method (Holmes, 1974). The method is based on field data collected in New Zealand from scour failures at a number of railway bridges. The ability of empirical equations to make realistic assumptions depends upon the basis of the form of equation used to develop the relationship. In the case of the New Zealand Railway method Neill (1987) has criticised the physical basis of the method.

4.6 Equilibrium/non-equilibrium theories

All the approaches described above assume that the duration of a flood is long enough for equilibrium conditions to be achieved. There is evidence to suggest that in many rivers the duration of the flood is not long enough for the bed to scour down to the equilibrium values. Whether equilibrium values are achieved depends upon the product of the unit discharge and the difference in sediment concentration between the upstream reach and the contracted reach and the duration of the flood. Particularly for flashy rivers with low sediment concentrations, the equilibrium value may not be achieved.

Gole and Chitale (1967) carried out studies at two bridges in India and found that the full contraction scour depth, as given by equations for scour in long rectangular contractions, was not developed at abridge where the flood hydrograph was of short duration. This is consistent with some numerical modelling carried out by Meadowcroft (1991).

Meadowcroft modelled a hypothetical bridge and subjected it to a number of different discharge hydrographs with the same peak discharge but different time bases. In all cases the channel width was 5 m and the initial bed slope was 0.0002. A total of 77 cross-sections at 25m spacing were used to represent a 1,900m length of channel. A constriction was modelled by reducing the width of two adjacent sections, 875m and 900m from the upstream boundary. A sediment size of 0.5 mm was assumed. For the results presented here a channel constriction of 0.8 was assumed.

Figure 1 shows the time development of scour for long duration flood events in which the discharge is kept constant in time at a value of 20 m^3/s. The model indicates the development of equilibrium conditions and the time that is required to achieve such an equilibrium. Figure 2 shows the discharge hydrograph and the corresponding calculated minimum bed level. The duration of the flood event is 300 hours. The model clearly shows that bed levels recover after the peak of the flood has passed. This implies that inspections after floods may not indicate the depth of scour that may have taken place during the peak of the event. A duration of 300 hours for a flood event on a small river would be unusual in the UK. Figure 2 shows the minimum bed level generated by a flood of the same magnitude as that in Figure 1 but with a duration of 30 hours, which might be more typical of rivers in the UK. It can be seen that the scour depth developed is significantly smaller than the equilibrium scour depth. This suggests that equilibrium scour theories may over-estimate the scour that occurs in practise.

It is thus likely that the predictions of equilibrium theories are conservative in some, but not all, cases.

4.7 Assessment of flood levels

A number of the scour equations discussed above, for example, in Sections 4.1, 4.2 and 4.3, predict a depth of flow within the constricted section. To determine the level of the scoured depth it is necessary to determine the water level during the flood. This aspect seems to be little discussed. In many cases it seems to be implicitly assumed that the water level to be used should be the water level one would calculate in the unscoured condition. This will over-estimate the water level and hence lead to a predicted bed level that is higher then the true scoured bed level. Little work seems to have been done on the impact of this so it is difficult to assess its impact.

4.7 Numerical modelling

Given the problems with the desk methods described above it seems natural to consider the application of numerical methods to the problems of estimating constriction scour. Meadowcroft (1991) showed that conventional one-dimensional, mobile bed river models could be used to assess constriction scour during a flood. Such a modelling approach overcomes a number of the problems associated with the methods discussed above. The water level should be assessed accurately during the flood and it is not necessary to make the assumption of a long contraction. The time development of the scour should also be taken into account. If the model can take into account the change in bed sediment composition then the impact of armouring could be included.

The use of a one-dimensional model does not, however, remove all the problems. Such models use a sediment transport equation to determine the sediment transport rate at each cross-section. The accuracy of the predictions depends upon the accuracy of this transport equation. In cases where the scour is significant this may lead to bed slopes which are significantly different from the water surface slope. In these cases it may be necessary to take this into account in predicting the sediment transport rate (Kovacs and Parker, 1994). The extent of the model upstream of the constriction should be long enough so that the predictions at the constriction are not influenced by the upstream boundary conditions, particularly the upstream sediment load.

In Section 4.1, it was pointed out the results of Keller suggested that scour depths at rapid constrictions could be influenced by the contraction of the flow and the development of a vena contracta. This effect cannot be simulated by a one-dimensional model and so for rapid contractions it may be necessary to use either two or three dimensional numerical models.

5 Conclusions

Methods for predicting constriction scour by modelling the problem as scour at a long contraction may underestimate the scour that takes place at a rapid, short constriction. By assuming that a vena contracta is developed at the constricted section it may be able to improve the scour predictions.

The regime approach proposed by Blench is fundamentally flawed and may not give accurate predictions of scour.

The methods proposed to take account of the impact of armouring assume that a proportion of the bed material is stable. This ignores cases where all or most of the sediment is moving but the bed is armoured.

Numerical model tests suggest that in many cases the time scale to develop equilibrium scour is significantly longer than the duration of a flood event. This implies that equilibrium scour equations may overestimate the depth of scour.

A number of methods of estimating constriction scour are based on estimating a depth of flow. To apply such methods a water level is needed to determine the scoured bed level. This problem has not been adequately discussed in the past.

Many of the problems of the desk methods for estimating constriction scour can be overcome by the application of numerical models. The problem with flow separation in short, rapid contractions suggests that one-dimensional models will not adequately reproduce scour under these circumstances and that two or three dimensional models may be required.

References

Ashida K, 1964, On river bed variation and stable channels in alluvial streams, Bulletin of Disaster Prevention Research Institute, Japan, Vol 14 Part 1

Blench T, 1969, Mobile-bed fluviology, University of Alberta Press, Canada

Borah D K, 1989, Scour-depth prediction under armouring conditions, J of Hyd Engng, ASCE, Vol 115, HY10, pp1421-1425

Gill M A, 1981, Bed erosion in rectangular long contraction, J of Hyd Div, ASCE, Vol 107, HY3, pp273-294

Gole C V and Chitale S V, 1967, River bed scour at bridge constrictions, Proc 12th IAHR Congress, Fort Collins, Colorado, USA, C.38.1-C38.8

Keller R J, 1983, General scour in a long contraction, Proc 20th IAHR Congress, Moscow, Vol II, pp280-289

Komura S, 1966, Equilibrium depth of scour in long constrictions, J of Hyd Div, ASCE, Vol 92, HY5

Kovacs, A. and G. Parker, 1994, A new vectorial bedload formulation and its application to the time evolution of straight rivers. *J. Fluid Mechanics,* 267:153-183.

Lacey, 1930, Stable channels in alluvium, Paper 4736, Minutes of Proc, Inst of Civ Engnrs, Vol 229, pp259-292

Laursen E M, 1958, Scour at bridge crossings, Bulletin No 8, Iowa Highway Research Board, Ames, Iowa, USA

Laursen E M, 1960, Scour at bridge crossings, J of Hyd Div, ASCE, Vol 86, HY2, pp39-54

Laursen E M, 1962, Scour at bridge crossings, Trans ASCE, Vol 127, Part 1, pp116-179

Laursen E M, 1963, Analysis of relief bridge scour, J of Hyd Div, ASCE, Vol 89, HY3, pp93-118

May R W M P, Ackers J C, Kirby A M, 2002, Manual on scour at bridges and other hydraulic structures, CIRIA Report C551,

Meadowcroft I C, 1991, A numerical model of general scour at channel constrictions, HR Wallingford Report SR 248

Melville B W and Coleman S E, 2000, Bridge scour, Water Resources Publications

Neill C R, 1973, Guide to bridge hydraulics, Road and Transportation Association of Canada, University of Toronto Press, Canada

Pemberton E L and Lara J M, 1984, Computing degradation and local scour, Technical Guideline for Bureau of Reclamation, Engineering and Research Centre, Bureau of Reclamation, Denver, Colorado

Straub L G, 1934, Effect of channel contraction works upon regimen of movable bed streams, Trans American Geophysical Union, Part II

Yalin M S, 1977, Mechanics of sediment transport, Pergamon Press, 2nd edition

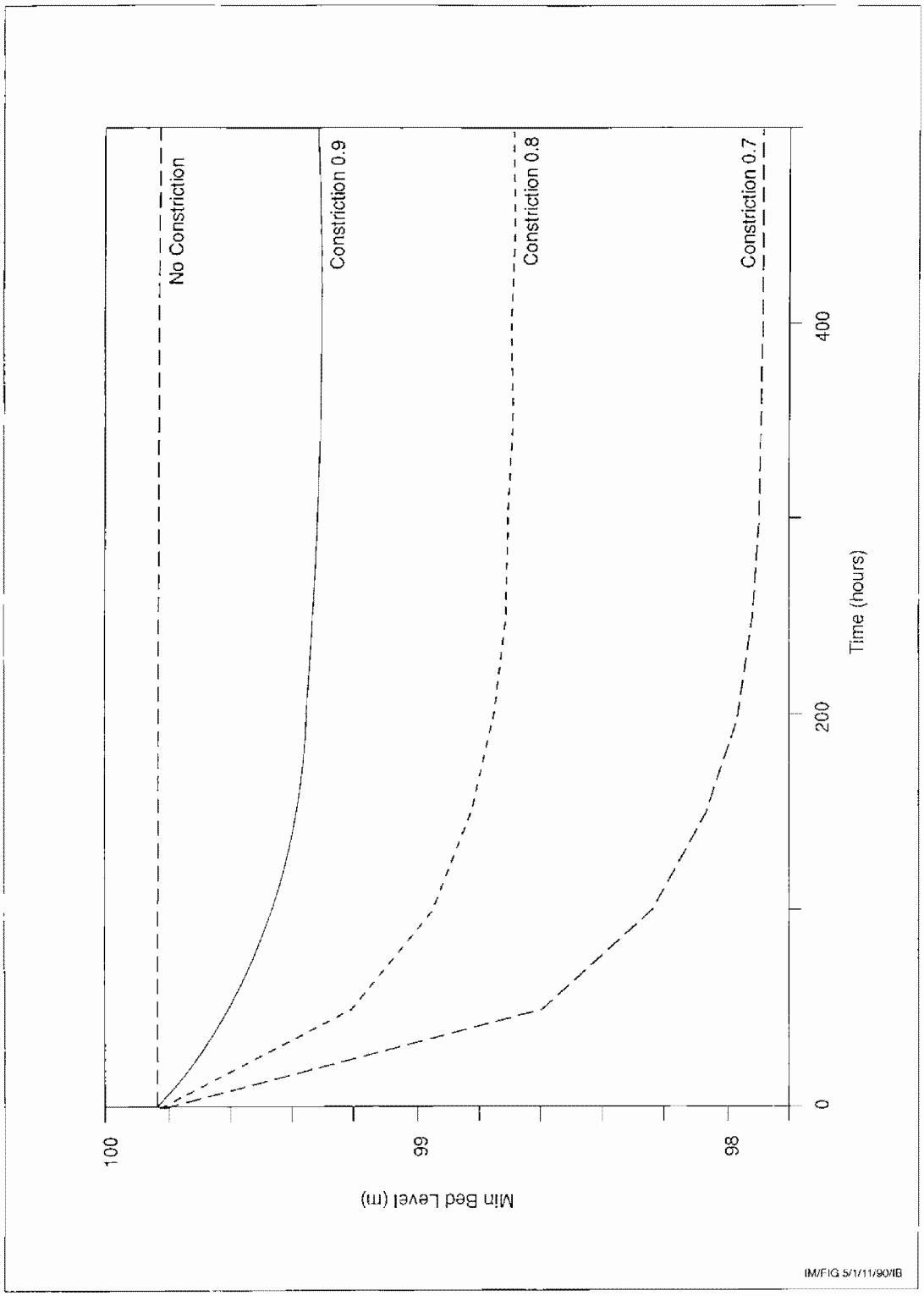

Fig 1 Minimum bed level in constricted reach: effect of different channel constrictions: Series 1

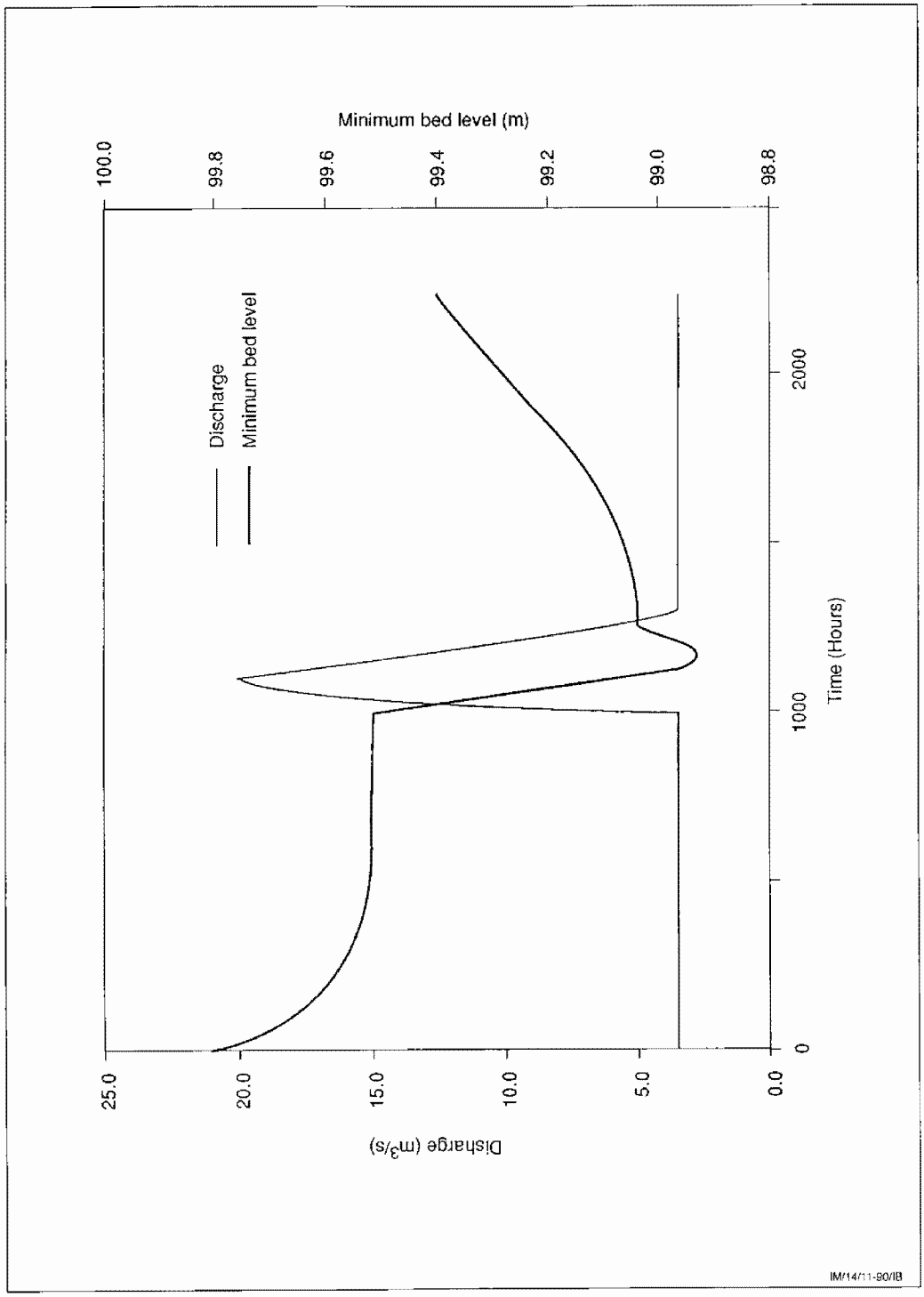

Fig 2 **300 hour flood hydrograph: Variation of minimum general scoured bed level with time, numerical model results**

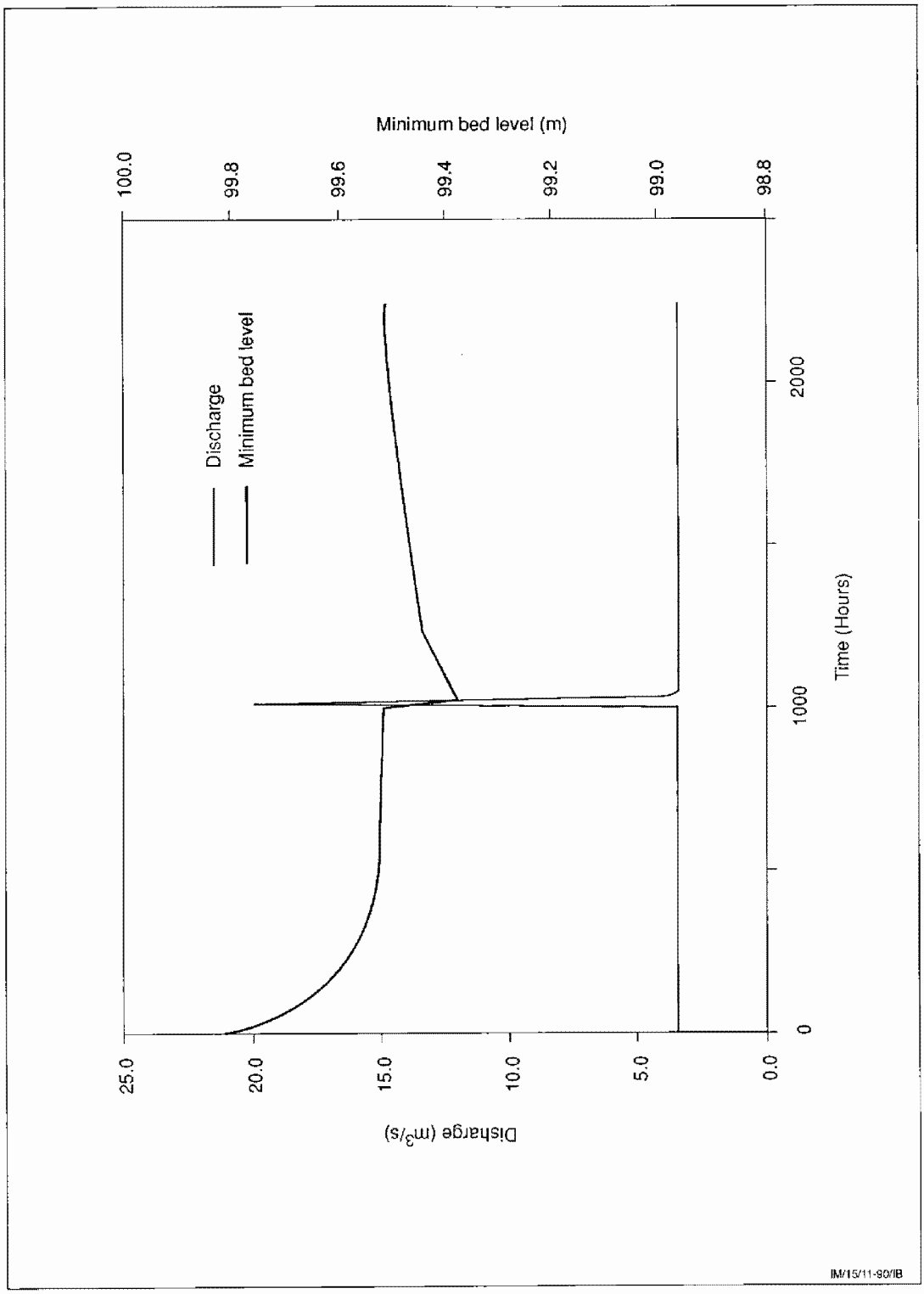

Fig 3 30 hour flood hydrograph: Variation of minimum general scoured bed level with time

Prediction of Local Scour Below Offshore Pipelines - A Review

Liang Cheng

Department of Civil and Resource Engineering
The University of Western Australia
35 Stirling Hwy, Crawley
Western Australia 6009, Australia
Tel: +61.8.9380.3076
Fax: +61.8.9380.1018
Email:cheng@civil.uwa.edu.au

ABSTRACT
This paper presents a brief review on the development of numerical model for local scour below offshore pipelines. Emphasis is given to the models developed by the author over the last three years at the University of Western Australia. The models reviewed include a potential flow scour model, a lee wake model for equilibrium scour and a turbulent model for time dependent scour processes. The limitations of these models and future research efforts are also discussed.

1 INTRODUCTION

Pipelines installed on the seabed disturb the local flow field producing an imbalance in the local sediment transport that leads to scouring of the seabed. The scouring can leave the pipeline unsupported over sections that may extend significant distances. Suspended sections of the pipeline are susceptible to damages arising from environmental forces (wave and currents forces) or human activities (fishing trawl and anchor loading). The consequences of pipeline failure would be severe both economically and environmentally.

Scour at pipelines can sometimes be beneficial where pipelines laid on the seabed may bury themselves under storm conditions due to local scouring. This phenomenon is referred to as the self-burial of pipelines. The self-burial of the pipeline can minimise or remove completely the need to trench and backfill a pipeline. If the process of self-burial could be exploited, the costs associated with installing and stabilising a pipeline can be reduced significantly. The typical costs for pipeline stabilization are in the order of 1-2 millions of US dollars per kilometre both in the North Sea and the Australian North West Shelf.

Evaluation of local scour is a very important element of pipeline design. Typical questions to be answered in the design process include: (1) under what conditions local scour will take place; (2) what is the maximum scour depth; (3) how fast the scour hole will propagate along the pipeline once the local scour initiates; (4) what are the equilibrium span length and (5) what is the time scale required for the free span to develop.

Due to the obvious significance, local scour below a pipeline has been the subject of a number of investigations over the last three decades (e.g. Kjeldsen et al. 1973; Mao 1986; Sumer and Fredsoe 1990, Li and Cheng 1999, Li and Cheng 2001a, among others). Early studies of local scour below pipelines were mainly achieved through two-dimensional flume tests where local scour profile in the plane perpendicular to the axis of the pipe was measured. Issues regarding two-dimensional scour, such as

onset of scour (Sumer and Fredsoe 1991), mechanisms of scour (Chiew 1990), scour depth (e.g. Kjeldsen et al. 1973, Sumer and Fredsoe 1990) and time scale of local scour (Fredsoe et al. 1992), have been studied experimentally. Detailed reviews on the state-of-art development of local scour research can be found in Whitehouse (1998) and Sumer and Fredsoe (1999) and will not be given here.

There is little doubt that model test is the most effective way to understand local scour process so far. However it does subject to some drawbacks. Apart from being expensive and time consuming, small-scale laboratory tests do suffer from scale effects because most of the scale-down models can not satisfy the similarity laws. There are several scale effects such as the pipe Reynolds number, pipe roughness, incoming flow turbulence, etc. (Sumer and Fredsøe, 1999). The scale effects need to be considered when the experimental results are extrapolated to prototype situations. Unfortunately little is known about these scale effects and none of these effects have been studied in a systematic manner (Sumer and Fredsøe, 1999).

In contrast to the scale-down laboratory tests, numerical models of local scour around pipelines do not suffer from scale effects. Once the numerical model is developed, it can be applied to different environmental conditions including those that could not be modelled under normal laboratory conditions. It has been widely accepted that a good numerical model can certainly be complementary to model tests and can assist design engineers to identify the most crucial cases for which model tests may be conducted. The ultimate goal of numerical models will be to replace (at least partially) the costly physical model tests and to be used directly in the design of pipelines.

Development of numerical models for local scour below pipelines has been slow, despite of their relative significance. The numerical models developed so far are mainly for the two-dimensional scour in the perpendicular direction of a fixed pipeline, and can be roughly classified into two groups. One group uses potential flow model (referred to as potential flow model) and the other employs turbulent flow model (referred to as turbulent flow model). The details of these models will be reviewed in the following sections.

2 POTENTIAL FLOW MODELS

The pioneering research in scour prediction under pipelines was conducted by Chao and Hennessy (1972). Chao and Hennessy proposed an analytical method for estimating the maximum scour depth under offshore pipelines caused by sub-surface currents. The discharge through the gap between the pipe and the eroded seabed was estimated using a potential-flow model with the assumption of a flat seabed at any depth of scouring. It was assumed that when the velocity in the scour hole is greater than the free stream velocity, which is always specified as the critical velocity, erosion would occur. The maximum scour depth is reached when the velocity difference decreases with the enlargement of the scour section. The seabed shear stress is estimated by assuming that the seabed is flat and the flow in the eroded section resembles open-channel flow characteristics. The friction factor is determined using a Reynolds number type relationship. Since too many assumptions have been made in the derivation of the model, this method can only provide an order of magnitude estimate of the possible scour hole depth

Hansen et al. (1986) proposed a numerical method to simulate the shape of the scour hole under pipelines, based on the potential-flow theory. In their method the flow

field was calculated using the modified von Müller method and the scour hole profile was obtained by a direct integration of the continuity equation for sediment transport. It was assumed that the bedload is the only form of sediment transport and the transport rate can be calculated using the Meyer-Peter and Müller formula. Although only the upstream part of the scour hole was calculated in the model, it was shown that the method predicts the scour depth under the pipeline and the shape of the upstream scour hole well.

Li and Cheng (1999) developed a curvilinear finite-difference model for calculating the maximum scour depth under pipelines. In this model, it was assumed that the flow field around the pipe is two-dimensional and can be analysed by the potential-flow theory. The equilibrium scour profile was obtained by an iteration methodology based on the Shields diagram. The main feature of the model was that it does not need to use any sediment transport formulae to calculate the shape of the scour hole. The comparison of the numerical results with the experimental data by Mao (1986) indicated that the model predicted the maximum scour depth and the upstream shape of the scour hole very well. However the model failed to predict the downstream part of the scour hole accurately. This was mainly because the potential flow model they used could not predict vortex shedding behind the pipeline, which is the main cause of the downstream scour below pipelines. Li and Cheng (1999) speculated that this could be improved if a turbulent model is used.

3 TURBULENT FLOW MODELS

Early numerical models based on k-ε turbulence models seemed to have difficulties to handle the seabed deformation due to scouring. Leeuwestein et al. (1985) developed a numerical model based upon the standard k-ε turbulence model and a sediment transport equation. A numerical package named ODYSSEE was used to calculate the turbulent flow field. As for the computation of the sediment transport and the variation in seabed topography they reported a failure in obtaining a real scour hole shape by using an empirical bed-load formula. This was ascribed to the ignorance of the suspended-load contribution in the model. In the numerical part of the investigation by Sumer et al. (1988), the so-called Cloud in Cell (CIC) method was employed to simulate the flow. It was reported that the CIC method generally gives good prediction on the gross characteristics of the organized wake behind the pipeline. However, there was no evidence in the paper showing that a numerical model was employed to calculate the seabed deformation. Instead, by comparing the effective Shields parameter with its time average value, an important conclusion was drawn that the organized wake behind the pipeline has strong effects on the profile of scour hole downstream of the pipeline. The time-averaged bed shear stress is not a suitable parameter to use in predicting the lee-wake scouring behind a pipeline.

Some improvements on k-ε based models have been achieved in 1990s. van Beek and Wind (1990) developed a numerical model based on the standard k-ε turbulence model and a transport equation for suspended sediment. The application of the model to scour prediction below a pipeline with and without an attached spoiler showed good agreement with the measured scour holes, although the predicted rate of erosion was three times as fast as in the physical model (Whitehouse, 1999). Brørs (1999) presented a model that includes the description of fluid flow by the standard k-ε turbulence and the suspended and bed-load sediment transports. Density effects were considered in the vertical momentum equation and in the turbulence equations. Flow around a surface mounted cylinder was predicted in good agreement with the experiments. However, in the scour calculation the model did not predict periodic vortex shedding, even during the later stages of scour development. The author suggested that a fine mesh (5000 nodes or more) is needed to predict the phenomena of vortex shedding. For the scour calculations, the prediction of a clear water scour hole agreed well with Mao's (1986) experimental measurements.

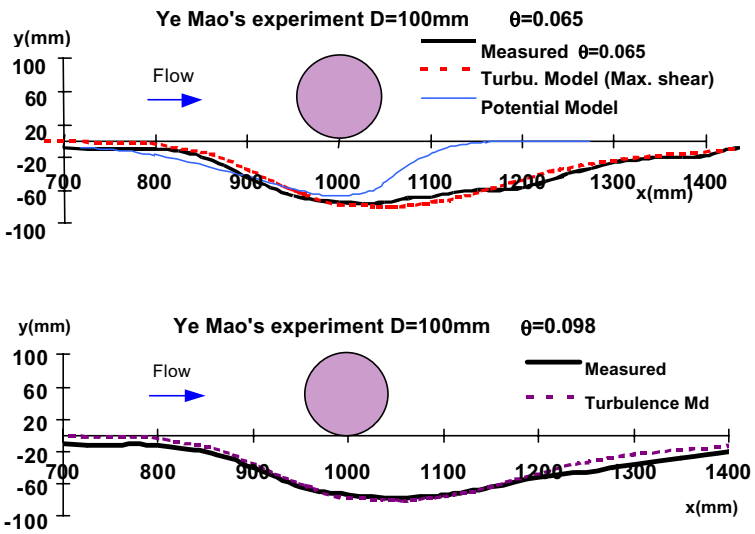

Fig 1 Predicted and measured equilibrium scour holes (Li and Cheng 2001a)

Li and Cheng (2001a) extended their potential flow model (Li and Cheng 1999) to include a turbulent flow model. The flow around the pipeline is simulated using a Large Eddy Simulation (LES) model that is capable of modeling the vortex shedding from the pipeline. The equilibrium scour hole is again determined by iterations, based on the assumption that the shear stress on the seabed is equal to the far field shear stress for live bed scour (or equal to the critical shear stress for clear-water scour) every where when the equilibrium scour hole is established (Li and Cheng 2001a). The iterative process of calculating the scour profile can be roughly described as:

1. assumption of an initial seabed profile;
2. computation of the flow field and flow induced seabed shear stress;
3. examination of the seabed shear stress assumption mentioned earlier;
4. if the seabed shear stress condition is not satisfied, adjust the seabed profile based the equations specifying the seabed shear stress assumption and go back to step 2;

5. if the seabed shear stress condition is satisfied, the seabed profile is the equilibrium scour profile.

It was found that the predicted equilibrium scour holes compared very well with the experimental results by Mao (1986). Fig. 1 shows the comparisons of the numerical results with the measured profiles by Mao (1986) for a pipeline being initially placed on the original seabed at two different Shields parameters. Fig 2 shows the comparisons of the numerical results with the measured profiles by Mao (1986) for pipelines initially placed above the seabed. The numerical results obtained using the potential flow model (Li and Cheng 1999) are also included in the figures for the purpose of comparison. It can be seen from these comparisons that the numerical model with a LES model predicted the equilibrium scour reasonably well for the both cases where the pipe was placed on the initial seabed and above the seabed. However the potential flow model failed to predict the downstream scour hole shapes accurately. This demonstrated that a correct flow model is very crucial in modeling the lee wake scour.

The advantages of the iteration model with a LES flow model are that the vortex shedding is modelled accurately and it does not use the empirical sediment transport formulae that normally contain empirical coefficients. The disadvantage of the model however is that it can not describe the time development of the scour hole due to the equilibrium assumption employed in the model.

In addition to the equilibrium model (Li and Cheng 2001a), Li and Cheng (2000) also developed a numerical model that is capable of modelling time dependent scour process. The model solves flow field using the same LES model as in the earlier work of Li and Cheng (2001a). The morphological change of the seabed was calculated using the non-equilibrium version of the general continuity equation in the same fashion as that used by Brørs (1999). The sediment deposition and entrainment rates were linked with the concentration of the suspended loads of sediment. The concentration of the suspended-load was calculated by solving the scalar transport equation of suspended-load concentration. The boundary condition for the near-bed concentration of suspended-load was specified using an empirical formula derived from experimental measurements (Zyserman and Fredsøe, 1990). The bedload

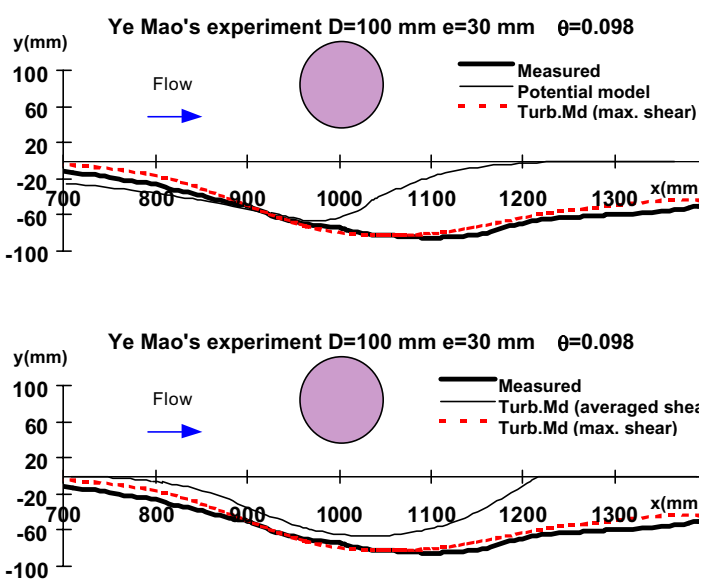

Fig 2 Predicted and measured equilibrium scour holes for a pipe initially placed above the seabed (Li and Cheng 2001a)

sediment transport was not included in the morphological model. Li and Cheng (2000) reported that this was because the inclusion of bed-load transport caused numerical instability at a rather early stage of the calculations. The reason for the numerical instability may be due to the fact that the bed-load transport under complex flow and bed slope conditions was not well understood. They argued, however, that the effect of neglecting bed-load transport on local scour is marginal for live-bed conditions. The argument was based on the experimental observation that suspended-load normally dominates bed-load under live-bed conditions. In addition, the use of the near-bed concentration formula by Zyserman & Fredsøe (1990) could partly take the bed-load transport into account in the calculation because the formula was derived from total transport rates (Zyserman & Fredsøe 1990). However, for large grain sediments and low flow rate situations bedload contribution to the scour process may be significant and further investigations are necessary. Fortunately most situations of engineering interests involve live bed sediment transport.

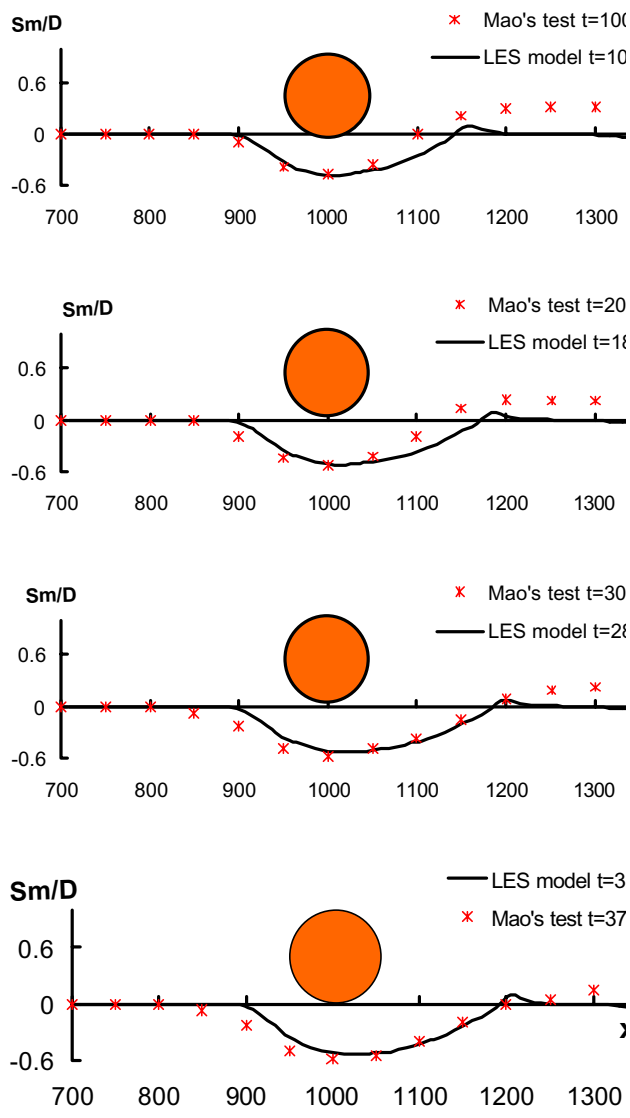

Fig. 3 Comparison of scour hole shapes, D=100 mm , e=0, θ=0.048 (Li and Cheng 2000).

The comparison of the numerical results with the experimental results by Mao (1986) indicated that the model worked quite well for both clear-water scour and live bed scour cases. Fig. 3 shows a clear water scour case and Fig. 4 gives a live bed case. It can be seen from Fig. 3 and Fig. 4 that there exist some discrepancies between the numerical and experimental results at very early stage of the scour. This was considered due to the ignorance of bedload sediment transport in the model. However the difference is noticeable only at early stage of the scour development. The numerical model does seem to predict the time scale of the scour corectly (Li and Cheng 2000).

Li and Cheng (2001) also developed a numerical model to simulate the scour deepening due to pipeline sagging. The model is very similar to the one they developed for time-dependent scour problems (2000), except that the bed load was included this model. In addition, a sliding mechanism was also introduced in this study. It was assumed that a small block of sediments can lose its stability and slide down along a slope if the slope of the scour hole at the point exceeds its angle of repose. This was implemented by moving the volume of soil at the area (where the bed surface angle is excessive to the angle of repose) to the nearest lowest location of the seabed. The conservation of soil volume was maintained in the soil relocation process.

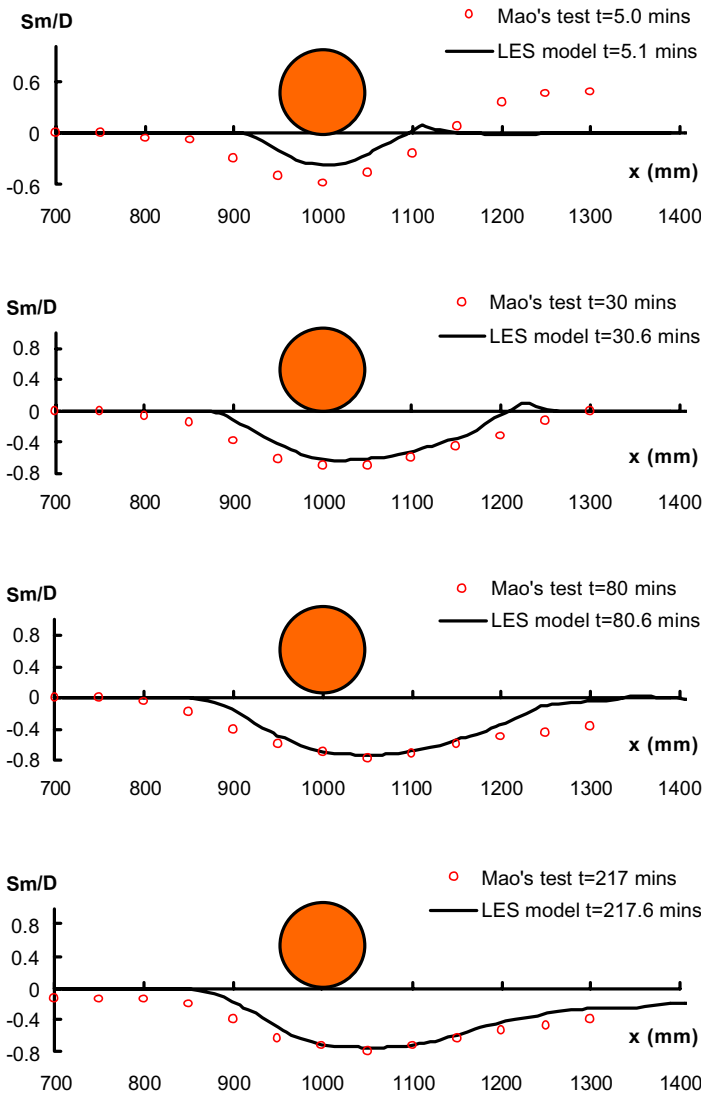

Fig. 4 Comparison of scour hole shapes, D=100 mm , e=0, θ=0.098 (Li and Cheng 2000).

The model was applied to investigating the scour deepening for different speeds of pipeline sagging. The comparison of the numerical results with the experimental results by Fredsøe et al. (1988) indicated that the model simulated the scour deepening due to pipeline sagging quite well (see Fig. 5).

4 DISCUSSIONS AND CONCLUSIONS

Evaluation of local scour is a very important element of pipeline design. Typical questions to be answered in the design process include: (1) under what conditions local scour take places; (2) how fast the scour hole propagates along the pipeline once the local scour initiates; (3) what are the equilibrium scour depth and span length and (4) how fast the scour hole develops.

Based on the above review, it is obvious that none of the current numerical models can answer all of these

questions. The mathematical modeling of local scour below pipelines is still in its early stage. The numerical models developed so far are mainly concentrated on the two-dimensional scour in the perpendicular plane to the pipeline. The current two-dimensional models seem to be able to predict

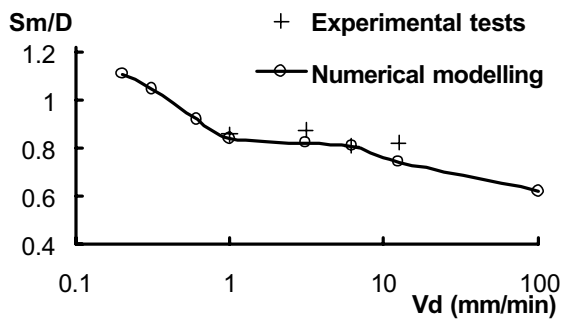

Fig. 5 Dimensionless final scour depth versus sagging speed (experimental data was taken from Fredsøe et al. 1988).

(i) the maximum scour depth due to steady currents (e.g. Hansen et al. 1986; Li and Cheng 1999);

(ii) equilibrium scour profiles due to steady currents (e.g. Li and Cheng 2001a);

(iii) time-dependent local scour processes of uniform sands subject to steady currents (e.g. Brørs 1999; Li and Cheng 2000)

(iv) time-dependent scour due to a moving pipeline in steady currents (Li and Cheng 2001);

The issues such as scour due to waves or combined waves and currents, onset of local scour, scour of non-uniform sands or cohesive sediments and three-dimensional scour, have never been addressed numerically. There is considerable amount of work to be done before numerical models can answer all of these design questions.

There seems to be no reason that the models developed for two-dimensional scour due to steady currents could not be extended to simulating local scour due to waves, the combined waves and currents and the three-dimensional scour. The research is being undertaken at the University of Western Australia to model the local scour due to waves. The rapid growth of computing power makes the development much easier than it has ever been.

ACKNOWLEDGMENTS

The work forms part of the activities of the Special Research Centre for Offshore Foundation Systems, established and supported under the Australian Research Council's Research Centres Program. The author would also like to acknowledge the supports from Australian Research Council through a Discovery Project DP0208223.

REFERENCES

Brrøs, B. (1999). "Numerical modeling of flow and scour at pipelines" J. Hydr. Engrg., ASCE,125(5), 511-523

Chao, J. L. and Hennessy,P.V. (1972). "Local scour under ocean outfall pipe-lines." J. Water Pollution Control Federation, 44(7), 1443-1447.

Chiew, Y. M. (1990). "Mechanics of local scour around submarine pipelines," J. Hydraulic Engrg., ASCE, Vol. 116, No. 4, 515-529.

Fredsφe, J. Hansen, E. A. Mao, Y. Sumer, B. M. (1988) "Three-Dimensional Scour Below Pipelines", Journal of Offshore Mechanics and Arctic Engineering, 1988, Vol. 110, 373-379.

Fredsoe, J, Sumer, B.M., and Arnskov, M.M. (1992). " Time Scale for Wave/Current Scour Below Pipelines." Int. J. of Offshore and Polar Engineering, Vol. 2. No. 1, 13-17.

Hansen, E. A., Fredsoe, J. and Mao, Y. (1986). "Two-dimensional scour below pipelines," Proc. Fifth Int. Symp. on Offshore Mech. and Arctic Engrg., American Society of Mechanical Engineers, 3, 670--678.

Kjeldsen, S. P., Gjørsvik, O., Bringaker, K. G., and Jacobsen, J. (1973). "Local scour near offshore pipelines." Proc. 2nd Int. Conf. On Port and Oc. Engrg. Under Arctic Conditions, University of Iceland, 308-331.

Leeuwestein, W., Bijker, E. A., Peerbolte, E. B. and Wind, H. G. (1985). "The natural selfburial of submarine pipelines," Proc 4th Int. Conf. on Behaviour of Offshore Structure (BOSS), Eleevier Science Publishers, 717-728.

Li, F and Cheng, L. (1999). "A numerical model for local scour under offshore pipelines" J. Hydr. Engrg., ASCE, 125(4), 400-406.

Li, F. and Cheng, L. (2000). "Non-equilibrium sediment transport process of local scour around pipelines," The 10th International Conference on Offshore and Polar Engineering, Vol. 2, 212-217.

Li, F. and Cheng, L. (2001). 'Effect of pipeline sagging on local scour below pipelines' 20th International Conference on Offshore Mechanics and Arctic Engineering, OMAE, June 3-8, 2001, Rio de Janeiro, Brazil, Paper Pipe-4027.

Li, F. and Cheng, L. (2001a). "Prediction of lee-wake scouring of pipelines in currents." J. Of Waterway, Port, Coastal, and Ocean Engineering , ASCE, 127(2), 106-112.

Mao, Y. (1986). "The interaction between a pipeline and an erodible bed," Series Paper 39, Tech. University of Denmark.

Sumer, B. M., Jensen, H. R. and Fredsøe, J. (1988). "Effect of lee-wake on scour below pipelines in current," J. of Waterway, Port, Coastal, and Ocean Engineering, Vol. 114, No. 5, 599--614.

Sumer, B. M. and Fredsøe, J. (1990). "Scour below pipelines in waves," J. of Waterway, Port, Coastal, and Ocean Engineering, Vol. 116, No. 3, 307--323.

Sumer, B. M. and Fredsøe, J. (1991). "Onset of scour below a pipeline exposed to waves," Int. J. Offshore and Polar Engineering, 1(3): 189-194.

Sumer, B. M. and Fredsøe, J. (1999). "Wave scour around structures," Advances in Coastal and Ocean Engineering, Edited by Philip L.-F. Liu, Vol. 4, 191--249.

van Beek., F. A and Wind., H. G. (1990). "Numerical modelling of erosion and sedimentation around pipelines. Coastal Engineering, 14 107-128.

Whitehouse, R. (1998). "Scour at marine structures," Thomas Telford Publications.

Zyserman, J. A. and Fredsøe, J. (1990). "Data analysis of bed concentration of suspended sediment," J. Hydraulic Engineering, Vol. 120, No. 9, 1021-1042.

Comparison of General Scour Prediction Equations for River Crossings

Christine Lauchlan[1] and Richard May[2]

ABSTRACT

Often when building structures in the river environment it is necessary to know whether the bed of a natural river is subject to degradation. For instance, the depth of burial for pipelines and the foundation requirements for bridge piers and abutments require some knowledge of what the river bed level is likely to be under certain conditions or over certain time scales. The natural scour that a site may experience can be due to long term morphological development of the system or shorter-term degradation due to higher-than-average flow velocities during floods. Both types of scour of bed material are often termed "general scour". The present study compares a variety of general scour prediction methods for estimating scour depths during a single flood event. For comparison of the methods three case studies are used. Initially, each river section was checked against 'regime' channel characteristics. Then each of the scour prediction methods was assessed for applicability to the channel type before being applied to generate an estimate of the general scour depth for a 200-year return period flood event. It was found that a wide range of predicted scour depths was possible for a single flood event in each case. The reasons for the different predictions are discussed in detail and recommendations for choosing the most appropriate prediction equation are provided.

INTRODUCTION

Natural river systems exist in a dynamic state. The flow and sediment movement in the channel(s) varies over time and space and can alter the channel dimensions. Under certain flow conditions sediment can be transported with the flow while for other flows it remains stationary. There is also often a wide range of sediment sizes present on the riverbed so the sediment transport rate can vary. In order to undertake engineering works in this type of environment it is therefore necessary to be able to quantify the likely changes to the system for given conditions or over certain time spans. Particular attention is often given to estimating how the bed level of the channel may change under flood flow conditions.

This problem involves a wide range of sediment and flow parameters including the sediment size and grading, flow velocity, channel width, depth and shape. Further complications arise as often under flood conditions the flow cannot be contained within the main channel and is distributed over floodplain regions.

Many authors have proposed empirical relations to quantify general scour depth. The basis behind these relations and general scour relationships in general is discussed in more detail in the companion paper. In the present paper we will compare a number of existing general scour prediction formulae for three different rivers. Various difficulties arose when attempting to apply each method and these are discussed in detail.

METHODOLOGY

[1] Engineer, Water and Industry Section, HR Wallingford, Howbery Park, Wallingford, OX10 8BA, United Kingdom, (csl@hrwallingford.co.uk)
[2] Technical Director, Water and Industry Section, HR Wallingford, Howbery Park, Wallingford, OX10 8BA, United Kingdom, (rwpm@hrwallingford.co.uk)

In total 11 general scour prediction equations were compared in this study. Each equation was assessed for its key parameters and applicability to particular river types or conditions. A detailed summary of each of the formulas is provided in Table 1. The general scour analysis is used to determine what the predicted bed level change would be for a short-term flood event. The long-term change of the sediment bed level is not addressed here.

In order to compare these different prediction methods it was first necessary to assess the existing river channel configuration. This relates to the 'regime' concept whereby alluvial channels that are in regime appear to operate in a quasi steady state without significant long-term variations in channel size and depth. The characteristic features are considered to be the shape and size of the main channel when flowing at just bank-full conditions and also the longitudinal gradient of the channel. The bank-full condition refers to the main incised river channel. For natural rivers this is typically found to be the peak flow rate occurring in a flood with a return period of about 1.6 years (which corresponds statistically to the most probable maximum annual flood). For this study the methodology of May, Ackers and Kirby (2002), hereafter referred to as the CIRIA Manual, was used to assess the river conditions, in conjunction with the HR Wallingford Regime Tables.

If the river channel under the dominant discharge is found to be in a regime state then the next step is to assess how the channel may adjust to a flood flow event. Using the existing channel dimensions and predicted water depths for both a 100-year and 200-year return period event estimates can then be made of the likely general scour depths. Water depths and flow areas were calculated using a one-dimensional hydraulic model. Each of the 11 formulae was applied in turn, using the same initial conditions.

CASE STUDY 1

This river has a length of 64km, with a catchment are of 1940km^2. It has an average bed slope of 0.013. The river regime is characterised by spring floods due to snowmelt and low water levels during the winter. Information supplied from gauging stations at a number of locations along the river was used to assess the dominant and flood flow conditions. The river is substantially braided over large reaches.

The river channel pattern has been shown to vary over time. In 1945 the river was extensively braided, whereas in subsequent maps there appears to be a single main channel with a number of smaller peripheral channels. There is a small channel located close to the left-bank of the floodplain in both 1955 and 1976 maps. It appears to branch off the river upstream of the crossing and follow the edge of the valley before rejoining the main river channel.

The bed sediment in the river is gravel, with a d_{50} = 39mm, and a geometric standard deviation, $\sigma_g \approx 2.2$. The bank-full, 100-year and 200-year return period discharges were 75m^3/s, 243m^3/s and 278m^3/s respectively.

The cross-sectional shape of the channel at the engineering point of interest is shown in Figure 1, while the predicted scour depths are compared in Figure 2.

CASE STUDY 2

This case study is for the same river as in Case Study 1 but located further downstream, after the confluence with a major tributary. Comparison of the river plan-form at the crossing shows a range of channel and floodplain shapes. In 1945 the river formed a single main channel with a number of smaller channels crossing the floodplain. In 1956 the river flowed in two main channels, adjacent to either side of the active channel region. Then in 1976 the river plan-form shows further changes in the period 1956 to 1976, with flow in one main channel near the northern bank and two smaller channels across the floodplain. One of the smaller channels appears to be a cutoff section of a former, larger channel.

The braided channel network appears to be very active across the entire active channel region. There are two main channels and a number of smaller interconnected channels. It can be expected that the river will continue to actively migrate across the active channel region. The same characteristic bed material sizes as for Case 1 were used. The channel slope along this section of the river is 0.007. The bank-full, 100-year and 200-year return period discharges were 150m^3/s, 500m^3/s and 595m^3/s respectively.

The cross-sectional shape of the channel at the engineering point of interest is shown in Figure 3, while the predicted scour depths are compared in Figure 4.

CASE STUDY 3

This is a large gravel bed river, whose morphology changes along its length. It has a length of 1364km, with a total catchment area of 188,000 km^2. As with the river mentioned previously, this river is characterised by spring floods due to snowmelt and low water levels during the winter.

In areas to the west it is either meandering or braided in form. Along part of its length, however, the river is confined in narrow gorge. Along its whole length there is substantial sediment transport, giving the potential for large and rapid morphological change. In particular, many areas along the river are characterised by significant lateral movement.

At the site used for the present analysis the river is characterised by a wide floodplain with a number of braided channels. There appears to be one main channel, with approximately four smaller channels criss-crossing the floodplain. Historical records show that substantial changes to the channel arrangement have occurred and the river is very active in this region.

The bed sediment in the river is gravel, with a d_{50} = 25mm, and a geometric standard deviation, $\sigma_g \approx 3.4$. There is a wide range of sediment sizes in the river and it is likely that armouring of the sediment bed occurs due to preferential movement of the finer material. The channel slope in the area under consideration is approximately 0.003. The bank-full, 100-year and 200-year return period discharges were 338m^3/s, 1241m^3/s and 1381m^3/s respectively.

The cross-sectional shape of the channel at the engineering point of interest is shown in Figure 5, while the predicted scour depths are compared in Figure 6.

DISCUSSION

A number of difference and difficulties arose when attempting to apply each of the formulae. One of the key problems was defining the main incised channel dimensions. For each of the rivers studied there were multiple braided channels with historical evidence of active channel

movement. Under flood conditions it was not known how the low-flow cross-sectional properties would change. Therefore, for the analysis the deepest low-flow channel was chosen as the main incised channel. It was also assumed that the channel would not widen under the flood flow. This was based on the idea that it is unlikely that a full adjustment of the channel to the higher flow regime would be achieved during an individual flood. This assumption has considerable impact on many of the formulae tested. A discussion of each method is provided.

Lacey (1930, 1933)

The method of Lacey (1930, 1933) is one of the earliest methods for estimation of general scour depths. It links the scoured flow depth to the flow rate and a sediment parameter. The difficulty in applying this method arose from the inclusion of the 'silt' factor. In the present case studies the bed material is gravel, with a median size of around 20-30mm. This produced very large values of f and correspondingly low scour depths. In most instances the method indicated no scour would occur for the given flood flows. This contradicted the results from the other methods tested. Due to this result the scour depths predicted by Lacey are not included in the comparison.

Blench (1969)

This method was developed for in-regime canals and has been applied satisfactorily to well-maintained sand bed irrigation canal systems. The gravel bed formula was derived based on large gravel rivers.

The method is dependent upon the flow rate, the channel width and the sand size and provides reasonable estimates of scour depths for each of the three cases. As d_{50} increases the scour depth y_s decreases, while increasing B or Q increases y_s.

Neill (1973)

This is a very general method based on the competent velocity concept for movement of the bed material. It differs from the other predictions mainly for Case 3. In this instance, there are multiple channels in the system and once the flow moves out of bank for the 200-year flood event the proportion of the total flow in this main channel is substantially reduced and the velocity in the channel reduces accordingly. This implies that the scour potential and calculated scour depths do not increase as quickly with increasing flood stage for compound and multiple channel systems.

Also, the redistribution of the channel area to account for scour is subjective. Neill suggests a graphical redistribution of area based on known characteristics of the site. For the present comparison a channel shape factor, as given in the CIRIA Manual was used so that the method can be directly compared to the other prediction formulas.

Charlton (1982)

This formula was developed specifically for application to gravel bed rivers. It requires detailed information on sediment sizes, which can be difficult to obtain, particularly the d_{50Z} term, which is the median sediment size measure along the minor axis. This would not normally be obtained from a particle size distribution curve. The channel width term was

found to be the most sensitive parameter. The method provides a way to estimate an effective channel width for scour, which is very similar to that given by Kellerhals (1967).

Simons and Albertson (1963)

This method provided scour depths similar to the overall average general scour depth for each case. The scour depth is mainly a function of the flow rate, with an empirical factor to account for the channel type. As the flow rate increases so too does the scour depth.

Kellarhals (1967)

The method of Kellarhals was developed for gravel bed rivers and is principally dependent on the channel width. The channel width used in the calculations is an effective width, based upon the flow rate. The original method does not deal with multiple channels or channels with floodplains so the flow rate chosen for the calculations was the flow rate in the main incised channel only.

Holmes (1974)

A key parameter in this method is the waterway width, which is defined as the width of channel carrying 80% of the flow. To use a width value based on this definition for the present cases would have produced very small scour depths due to the wide braided nature of the channels. It was found that a better general scour estimate was obtained by using the flow width associated with the main channel(s).

Melville and Coleman (2000) note that various authors have commented that this method does not appear to have a very logical basis and does not account for the effect of sediment size at all.

Mirtskhoulava, Ts.E (1967, 1991)

This method is applicable to non-cohesive sediments. There are also versions of this method developed especially for cohesive material and additional factors can be included to account for the effects of sediment armouring of the bed and/or scour hole.

One of the key parameters is the near-bottom velocity at the roughness height prior to scouring. The author gives guidance on how to estimate the roughness height and near-bottom velocity but these methods are not in general application. Also, it is not clear what the datum for the depth of flow after scour is, whether it is below the flood level or bank-full level.

Maza Alvarez and Echavarria Alfaro (1973)

As detailed in Melville and Coleman (2000) this method was developed using the competent velocity approach and was based on data for fine silts to coarse sands. For all cases this approach gives the highest estimate of general scour. However this is highly dependent upon the choice of shape factor. If the shape factor as defined by Maza and Alfaro is used then the total scoured depth is less than the maximum flow depth, as seen in Figure 6 where the scour depth with this shape factor was plotted instead of the CIRIA shape factor. However, if the shape factor as defined by the CIRIA Manual is used then the scour depth can be almost three

and a half times (e.g. Case 3) the deepest depth predicted by any of the other methods. The method of scaling the average and maximum scoured depths is therefore critical when applying this procedure.

CIRIA Manual (2002)

The CIRIA Manual provides a methodology for the analysis of channel response to flood conditions. Initially the HR Wallingford Regime Tables were used to assess the existing channel dimensions. However, any regime type formula/method could have been applied.

The use of a regime method as the basis of the analysis is a limitation of the methodology. Since if the channel system based on existing cross-sectional data and flow information cannot be matched to a regime dimensions then there is no way of estimating the effect of a higher flow regime. This could be seen to some degree in Case 3, where the match between the bank-full conditions and an equivalent regime channel was less clear than for the other two rivers. This may therefore have impacted upon the general scour depths predicted by the other formulas, especially those that strongly depend upon the channel width dimension.

One aspect of this approach that it not addressed by any of the other procedures is suspended sediment transport. When using the HR Wallingford Regime Tables the regime channel dimensions must be matched for sediment concentration as well as flow rate.

Comparison of Predicted Scour Depths for 100-year and 200-year Return Period Events

The resulting predicted scour depths for the 200-year return period events are provided in Figures 2, 4 and 6. General scour depths were also estimated for the 100-year return period event for each river.

For Case 1, all the prediction equations predicted smaller depths of general scour. Overall, the average predicted reduction in scour depth was around 12%. The formula of Mirtskhoulava (1967, 1991) gave the smallest reduction (8%) while that of Holmes (1974) gave the greatest (26%). These results are expected, as the flow rate for the 100-year event is 12.5% less than the 200-year event.

For Case 2 there was a wider range of changes in the predicted general scour depths. The method of Simons and Albertson (1963) predicted greater depths of general scour while all the other formulae predicted reductions in general scour ranging from 6% (Kellerhals, 1967) to 50% (Neill, 1973). The reduction in flow for the 100-year event compared to the 200-year event is 16%.

Case 3 produced the most interesting results. In many cases the general scour depths predicted for the 100-year event were in fact greater than for the 200-year event. This can be explained by examining the river cross-section. For the 100-year return period flow the highest proportion of the flow is concentrated in the main channel. However, as the flow rate increases the proportion of the total flow in the main channel actually decreases. This results in decreased velocities and decreased scour potential in the main channel.

What is shown by these results is that when considering the most critical case for general scour depths at a particular location consideration must be given to the flow and channel

configurations over a range of flows. It is not necessarily the highest return period event that produces the greatest scour depths.

CONCLUSIONS

1. There is no clear pattern shown by any of the general scour prediction equations.
2. The type of river channel system has a significant effect on the performance of the various prediction equations. The most sensitive parameter appears to be the channel width. In the analysis presented here, the channel width was assumed to remain constant with no width adjustment occurring due to the short duration of the flood event. This assumption should be investigated further. It may be more realistic to relax the constant width constraint based on an estimate likely lateral movement of the channel. Any estimate of lateral channel movement should consider sediment and slope characteristics for the bed and banks as well as flow properties.
3. Many of the methods do not explicitly account for cases where there is more than one channel, or where floodplain flows occur.
4. The definition of scour depth varies between methods, some using an average depth, others applying a shape factor. This makes direct comparison of the predicted depths more difficult. The definition of shape factor and the effect of overbank flows on the shape factor should be investigated further.
5. Given the uncertainty in the general scour estimates the use of a safety factor is recommended.

REFERENCES

1. Ackers, P. and White, W.R. 1973. Sediment Transport: a new approach and analysis, Proc. ASCE, Journal of the Hydraulics Division, 99 (HY11), pp 2041-2060
2. Blench, T. 1969. Mobile-bed fluviology, University of Alberta Press, Edmonton, Canada
3. Charlton, 1982 River stabilization and training in gravel-bed rivers, Chapter 23, Gravel-bed rivers, Editors: Hey, R.D. Bathurst, J.C., and Thorne, C.R
4. Holmes, P.S. 1974. Analysis and prediction of scour at railway bridges in New Zealand, New Zealand Engineering, Nov, 313-320
5. Kellarhals, R. Stable channels with gravel paved beds. Proc. Am. Soc. Civ. Engrs, 1967, 93, No. WW1, Feb., 63
6. Kennedy, R.G., 1895. On the prevention of silting in irrigation channels. Minutes of the Proc. ICE, 119
7. Laursen, E.M. Scour at bridge crossings. Journal of the Hydraulics Division, ASCE, 1960, 86(2), 39-54
8. May, R.W.P., Ackers, J.C., and Kirby, A.M. 2002. Manual on scour at bridges and other hydraulic structures. CIRIA, Report No. C551, London, United Kingdom
9. Maza Alvarez, J.A., and Echavarria Alfaro, F.J. 1973. Contribution to the study of general scour. Proc. International Symposium on River Mechanics, IAHR, Bangkok, Thailand, 795-803
10. Melville, B.W., and Coleman, S.E. 2000. Bridge Scour., Water Resources Publications, LLC, Colorado, USA, p550
11. Mirtskhoulava, Ts. E., 1991. Scouring by flowing water of cohesive and non-cohesive beds. Journal of Hydraulic Research., 29(3), p341-354
12. Mirtskhoulava, Ts., E. 1967. Bed Scour and Methods of Assessing their Stability, M., *Kolos*, 179p

13. Neill, C.R. (Ed) 1973. Guide to Bridge Hydraulics., Roads and Transportation Association of Canada, University of Toronto Press, Toronto, Canada, 191pp
14. Simons, D.B. and Albertson, M.L. 1960. Uniform water conveyance channels in alluvial material, Proc ASCE, 86, HY5 (May)
15. Smith, K.V.H., 1974. Comparison of prediction techniques with records and observations on the Lower Chenab canal system. University of Southampton, CE/5/74
16. U.S. Army Corps of Engineers, Hydraulic Engineering Circulars 6, 18 and 20, Hydraulic Engineering Centre, Davis, California, U.S.A.
17. White, W.R. Milli, H. and Crabbe, A.D. 1975. Sediment Transport theories: a review. Proc. ICE, Part 2, 59, pp 265-292
18. White, W.R., Paris, E., and Bettess, R. 1980b. The frictional characteristics of alluvial streams: a new approach, Proc ICE, Part 2, 69, pp 737-750
19. White, W.R., Paris, E., and Bettess, R., 1980a. River regime based on sediment transport concepts, Hydraulic Research Station, Report IT 201

SYMBOLS

B	Channel width
d_{50}	Sediment size for which 50% by weight is finer than.
d_{90}	Sediment size for which 90% by weight is finer than.
f	Lacey's silt factor.
Q	Flow rate
q	Flow rate per unit width
S	Energy slope
y_s	Scoured flow depth; refer to individual formulae for further definition
σ_g	Geometric standard deviation of the sediment size.

Table 1: Summary of General Scour Depth Prediction Methods.

Method	Description
Lacey (1930) & (1933)	$y_{ms} = 0.47\left(\frac{Q}{f}\right)^{1/3}$ where mean scoured flow depth y_{ms} (m) is defined as the wetted area divided by the surface width; Q (m^3/s) is the design discharge; and *f* is the Lacey silt. This equation is applicable to uncontracted sandy alluvial channels.
Blench (1969)	For sand of $0.06 < d_{50}$ (mm) < 2 For gravels of S = 2.65 and $d_{50} > 2$mm $y_{ms} = 1.20\left[\frac{q^{2/3}}{d_{50}^{1/6}}\right]$ $y_{ms} = 1.23\left[\frac{q^{2/3}}{d_{50}^{1/12}}\right]$ q ($m^3/s/m$) is the discharge per unit width, for the main channel if the channel has floodplains; and d_{50} (mm) is the sediment size for which 50% is finer than, and y_{ms} is the mean scoured flow depth below the free surface. The sand size sediment equation is derived for regime channels of steady discharge, steady sediment-transport rate, a dune sand bed of natural particle size distribution, suspended load too small to influence equations, and steep cohesive channel sides (hydraulically smooth). The gravel equation is derived from large gravel rivers.
Maza Alvarez and Echavarria Alfaro (1973)	$y_{ms} = 0.365\left(\frac{Q^{0.784}}{W^{0.784} d_{50}^{0.157}}\right)$ where y_{ms} (m) = flow depth from the design water level to the mean scoured bed level; Q (m^3/s) is flow rate; W (m) is water surface width; and d_{50} (m) is the median sediment size. For sands and gravels of $d_{75} < 6$mm
Kellarhals (1967)	$B = 3.26Q^{0.5}$ $y = 0.47q^{0.8} d_{90}^{-0.12}$ where B is the mean channel width, y is the mean depth of flow, and d_{90} is the size of bed material (m) such that 90% of the stones by number are smaller. This formula is based on work on gravel bed rivers.
Neill (1973)	Neill outlines four approaches to estimating the general scour depth in a river reach. Methods 1 to 3 rely on utilisation of field measurements, whereas method 4 (detailed here) is the approach to be adopted where no measurements of channel change are available. This method depends on the hypothesis that scouring will continue until the mean velocity is reduced to just above critical for bed material exposed at the scoured depth. It is considered conservative for high bed-load conditions.
	Procedure: Compute the mean velocity through the opening at the design discharge – assume no scour. Determine the corresponding depth of flow and median sediment diameter; Compare the computed velocity with the competent velocity (figure 4.12, Neill 1973). If the computed mean velocity > competent mean velocity, general scour occurs; Determine by trial the average general scour level, assuming an appropriate cross-sectional shape, so that the mean velocity is equal to the competent velocity for the material exposed at that level. The appropriate average depth of flow after scour should be used in selecting the competent velocity. For graded material armouring should be considered – perhaps by using a larger D_{50} value (but less than D_{80}); Redistribute the trapezoidal cross sectional area to give the worst expected cross-sectional shape and lowest elevation of general scour.

Method	Description
Charlton (1982)	<u>Deep channels</u> – for $3 \le y_s/d_{90} \le 80$ $B = 3.74\, K_G\, Q^{0.45}$ $y_s = \left(0.114\, K_G^{-1.82} Q^{0.42} d_{65}^{-0.38} d_{90}^{-0.24}\right) - d_{50Z}$ $S = 0.15\, K_G^{-1} Q^{-0.76} B^{0.76} d_{65}^{1.38} d_{90}^{-0.24}$ B is the channel width; y_s is the scoured flow depth; S is the energy slope. The value of the non-dimensional factor K_G depends on the type of vegetation on the banks of the channel: for grass and light vegetation, $0.9 < K_G < 1.3$; for trees and heavy vegetation, $0.7 < K_G < 1.1$. <u>Shallow channels</u> – for $y_s/d_{90} < 3$ $B = 3.74 K_G\, Q^{0.45}$ $y_s = \left(0.477\, K_G^{-1.82} Q^{0.25} d_{65}^{-0.22} d_{90}^{0.55}\right) - d_{50Z}$ $S = 0.068\, K_G^{-1} Q^{-0.45} B^{0.45} d_{65}^{1.22} d_{90}^{-0.55}$ These formulae apply to gravel-bed rivers only. Refer to CIRIA (2002) for a full discussion of this method and the various sediment and channel factors.
Simons and Albertson (1963)	$P = J_1\, Q^{1/2}$ $\quad B = 0.98\, P + 0.7$ $A = J_2\, Q^{0.87}$ $\quad R = J_3\, Q^{0.36}$ $y_s = 1.21\, R$ for $R < 2.1$ m $y_s = 0.93\, R + 0.6$ for $R > 2.1$ m where P is the length of the wetted perimeter, A is the corresponding flow cross-sectional area, R is the hydraulic radius, B is the channel width, ν is the kinematic viscosity of water (= 1.14×10^{-6} m^2/s at temperature of 15° C). All quantities in the equations should be in SI units, as defined above. The values of the coefficients vary according to the type of channel. The J coefficients are then determined based on the channel type chosen. Refer to the CIRIA Manual for a complete listing of channel types and coefficients.
Holmes (1974)	Developed to estimate the total scour at a site. General scour is not estimated as an individual quantity. $y_s = \dfrac{y_r V_1 K}{\sqrt{A/W}}$ where y_s (m) is the scoured flow depth, and $V_1 = C\left(\dfrac{Q}{A}\right)\left(\dfrac{y}{A/W}\right)^{2/3}$ and $K = \sqrt{\dfrac{W}{4.83 Q^{0.5}}} \le 1$ y (m) is the unscoured flow depth; y_r (m) is the water level rise from low water to flood stage; A (m^2) is the flow area of the unscoured profile; W (m) is the waterway width allowing for berm flow; V_1 is the approach flow velocity; C is a coefficient related to channel type. This method was developed based on field data collected in New Zealand for a range of rivers covering a wide range of sediment sizes. It incorporates a safety factor. See Melville and Coleman (2000) for a detailed description.

Method	Description
Mirtskhoulava, Ts.E (1967, 1991) and further papers	$$y_s = \left(\frac{1.25 q \Delta^b}{e m_1 m_h v_n} \right)^{\frac{1}{b+1}}$$ where y_s is the depth of flow after scour; e is a coefficient taking into account contraction of the flow and increasing specific discharge; v_n is the non-scour near bed velocity at the height of the roughness protrusion; q is the specific discharge; m_1 is the coefficient of conditions of performance; m_h is a coefficient taking into account a water layer in the flood plain in channels formed of cohesive as well as fine grained soils (n = 4 recommended); Δ is the protrusion height (taken as $0.75d_{95}$); and b is a calculated parameter. $$v_n = 1.25 \sqrt{\frac{2}{0.44 \rho_o n}} \left[g(\rho_s - \rho_o) d_{50} \right]$$ where ρ_s and ρ_o are the sediment and water densities respectively. $$b = \frac{\log \log \left(\frac{8.8 y}{d_{95}} \right)}{\log \left(\frac{y}{0.7 d_{95}} \right)}$$ where y is the average flow depth before scouring. These formulas are applicable to specific flow conditions, such as for the rivers in the present study. The river conditions should be checked against the methodology presented by Mirtskhoulava to ensure the most appropriate version of the scour prediction equation is used.
CIRIA Manual (2002)	This manual provides the following procedure for estimating the likely general scour depth due to a flood. *Procedure:* The existing cross-sectional shape of the main incised channel is checked against dimensions predicted by the HR Wallingford regime tables (or any other regime method) for the bank-full flow rate. Next the conveyance in the main channel due to the flood flow is calculated. Using a regime method assess the predicted dimensions of the incised channel if it were to reach equilibrium conditions for the flow. If the required area from (2) is greater then the available area then the channel is assumed to adjust its shape to provide the additional flow area. A shape factor is provided for use in redistributing this required area.

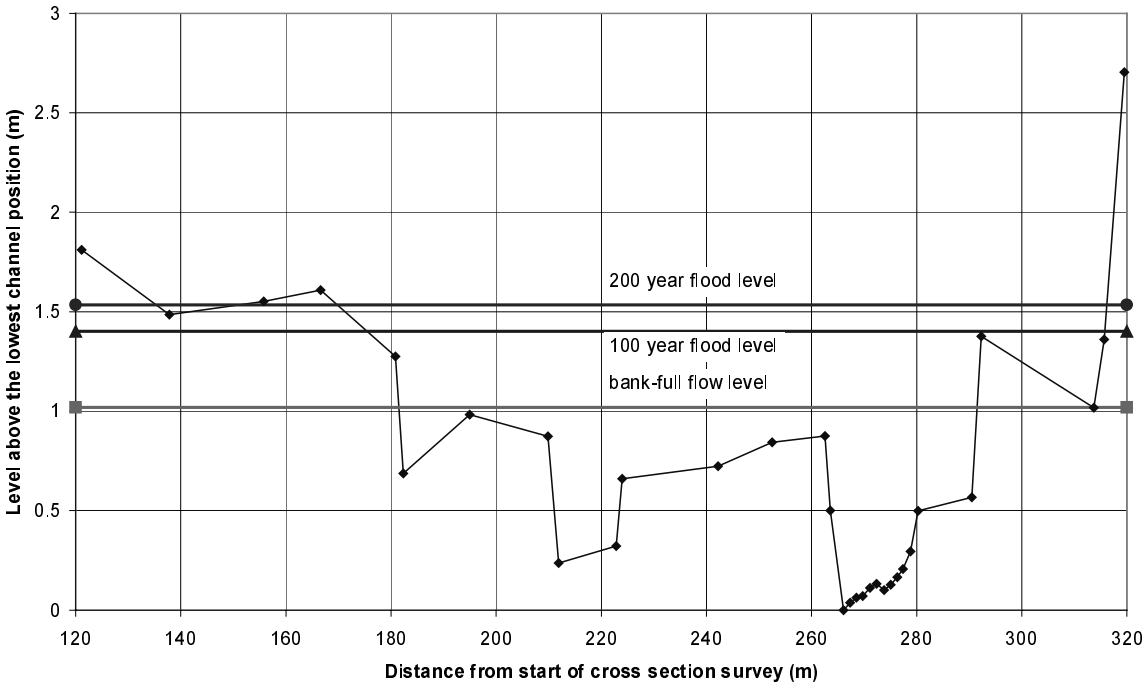

Figure 1. Cross-sectional view of Case Study 1 site.

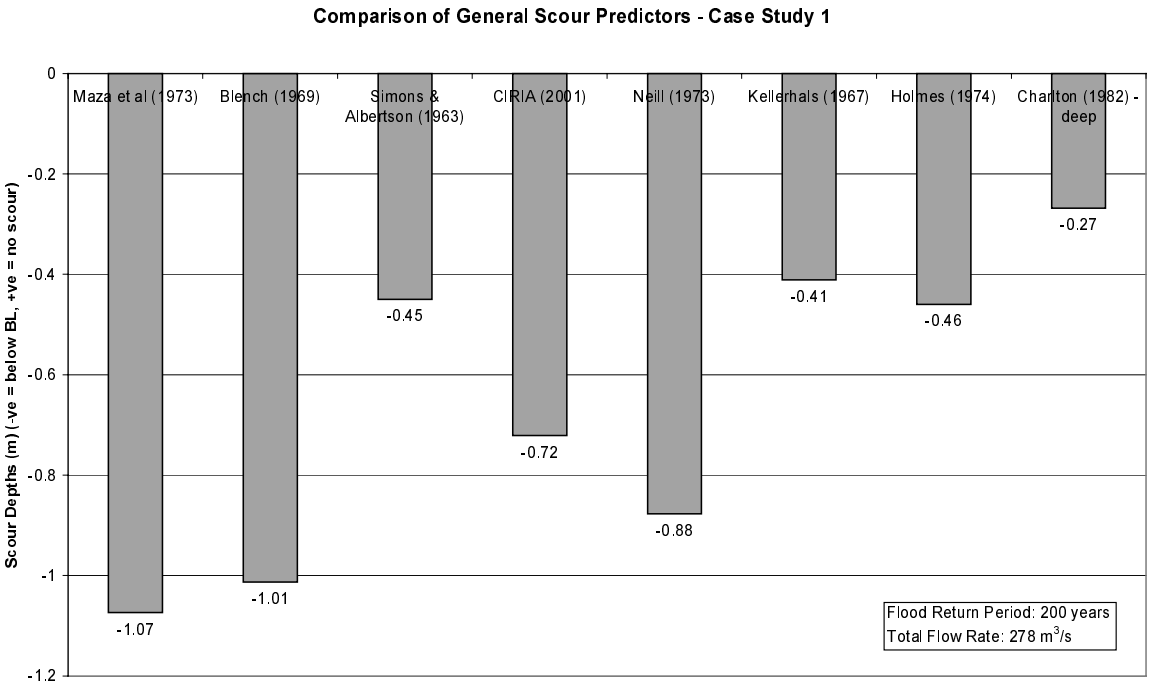

Figure 2. Comparison of General Scour Prediction Equations for Case Study 1 Site.

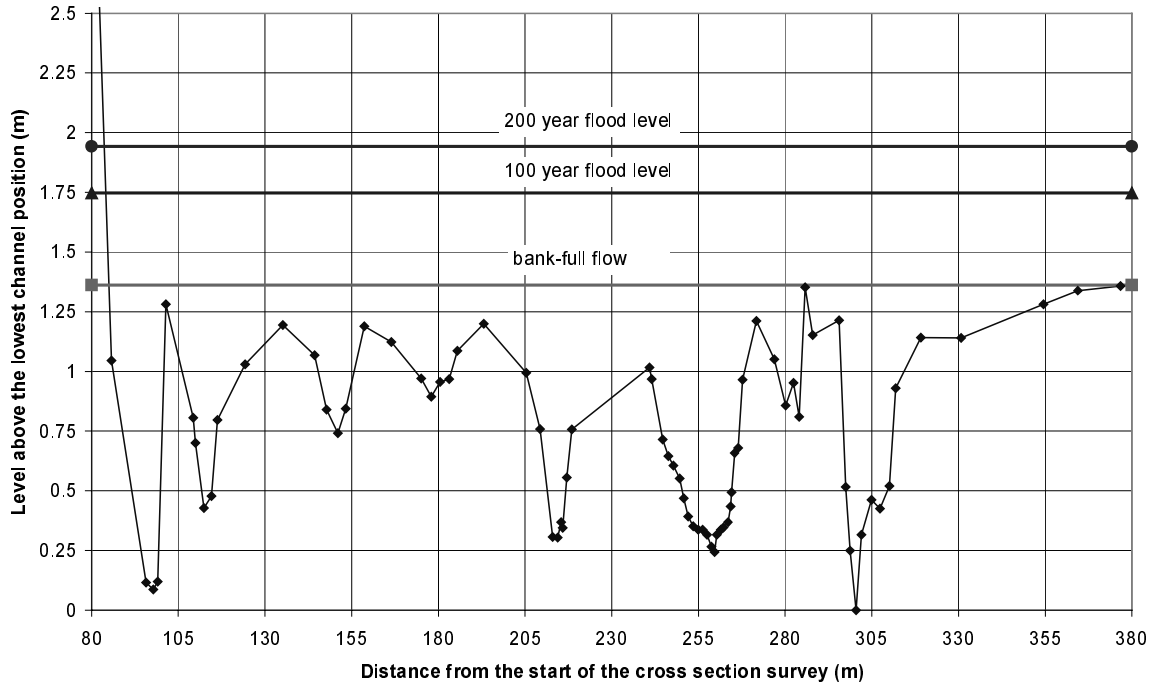

Figure 3. Cross-sectional view of Case Study 2 site.

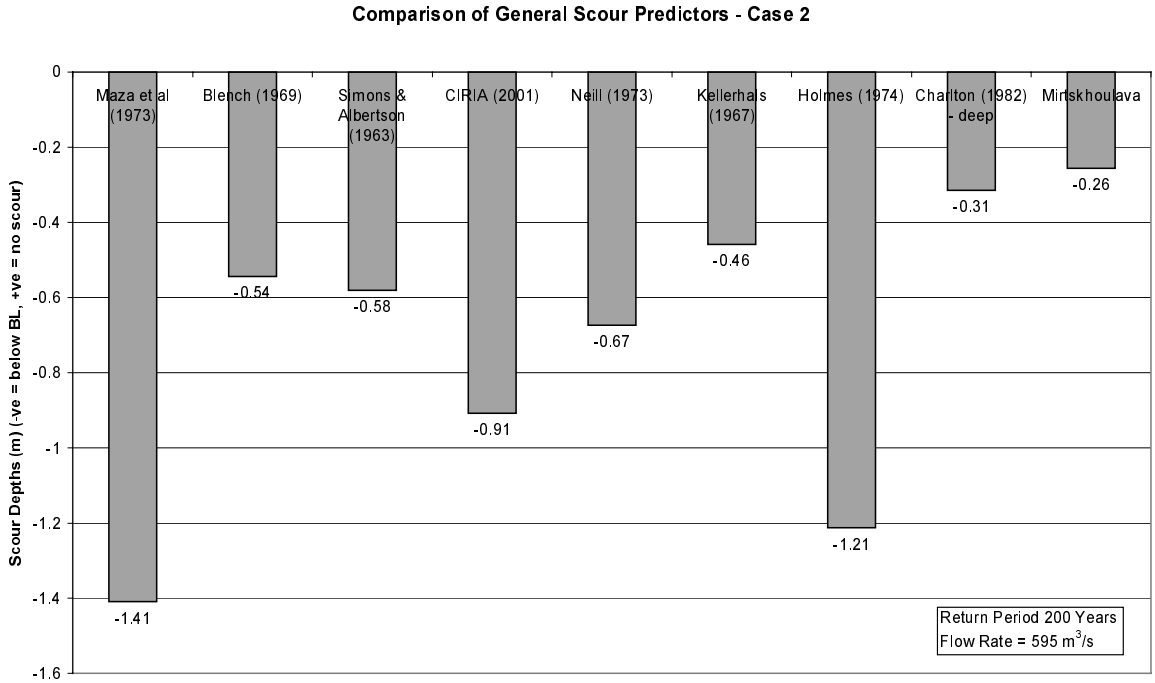

Figure 4. Comparison of General Scour Prediction Equations for Case Study 2 Site.

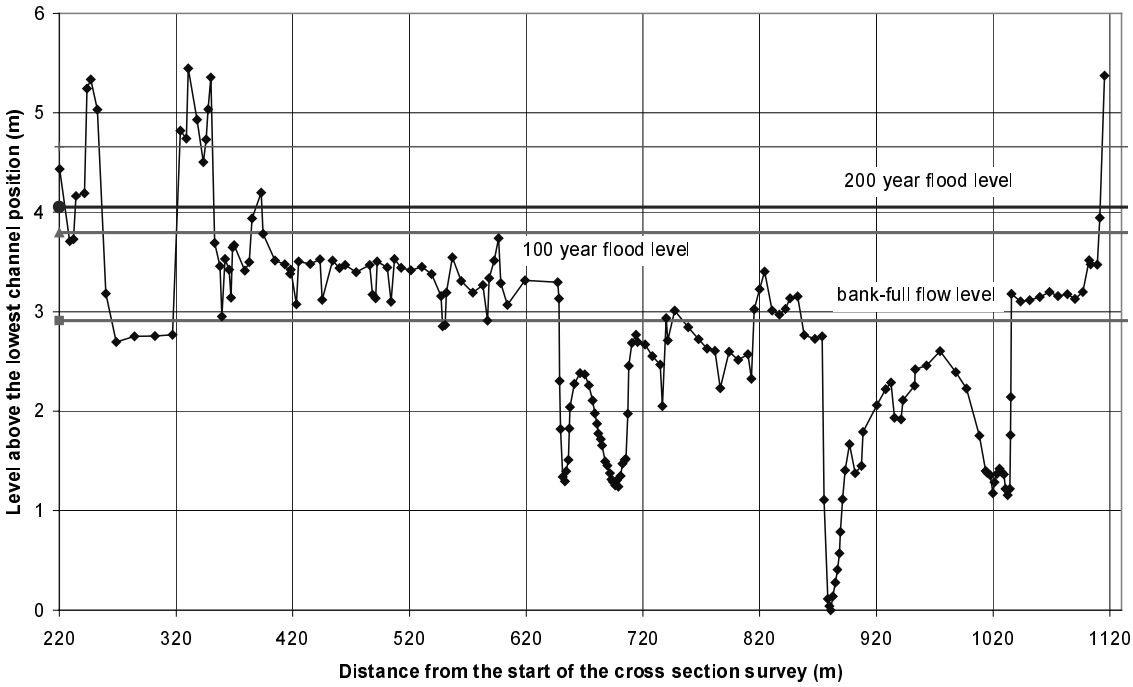

Figure 5. Cross-sectional view of Case Study 3 site.

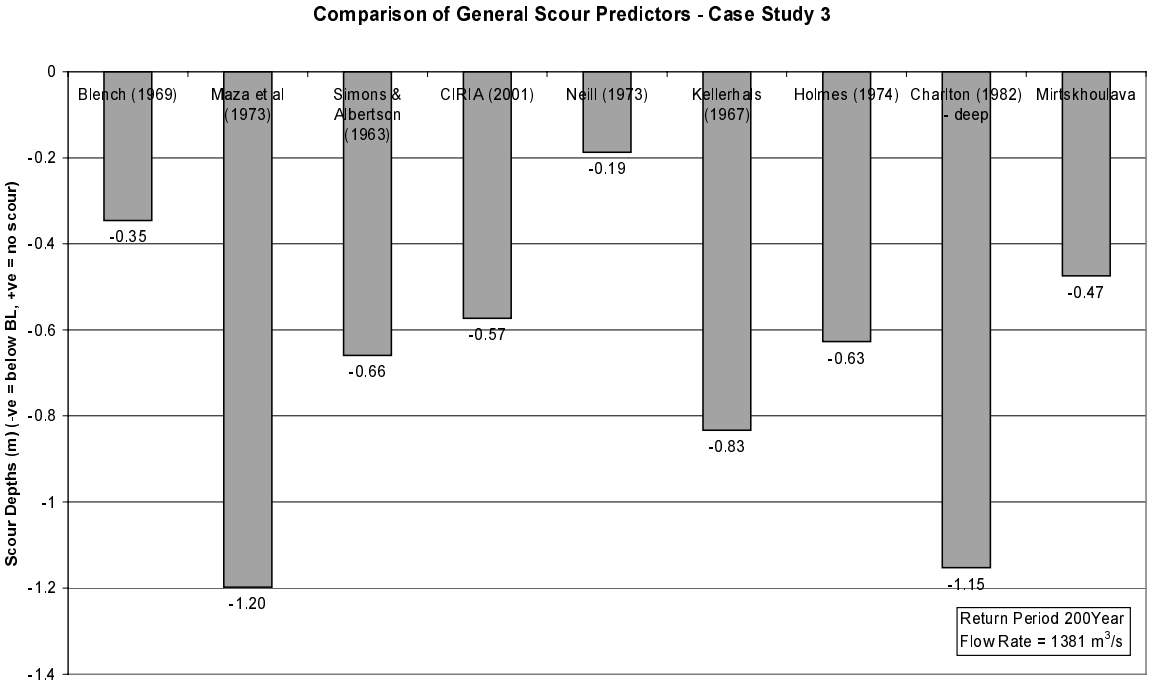

Figure 6. Comparison of General Scour Prediction Equations for Case Study 3 Site.

Effect of Suspended Fine Sediment on Local Scour

by
D. Max Sheppard[1]

ABSTRACT

The presence of suspended fine sediment in the water column has been found to impact both the rate and the value of local sediment scour depth in the clearwater scour range of velocities. This was discovered during clearwater scour tests conducted by the author in a flow-through type flume at the Conte USGS-BRD Laboratory in Turners Falls, Massachusetts. The water for these tests was supplied by a power plant reservoir adjacent to the Connecticut River. The concentration of suspended fine sediment in the reservoir would increase during times of heavy runoff and affect the scour experiments conducted in the laboratory.

Subsequent to this finding an effort to understand and quantify this phenomenon was undertaken. This is a progress report on these efforts and a presentation of the results to date.

Introduction

There have been numerous laboratory investigations of local sediment scour over the last few decades [see e.g. Charbert and Engledenger (1956), Shen, et al. (1966), Melville and Raudkivi (1977), Ettema (1980)]. Due to the complexities of the flow and sediment transport processes associated with structure-induced sediment scour and the number of quantities thought to affect both the rate of scour and the equilibrium depths, the results from the laboratory studies have been presented in a variety of ways. This has often made it difficult to compare results from the various investigations and in the cases where comparisons can be made there can be significant differences. This difficulty is nothing new for investigators working in sediment transport where orders of magnitude differences are not uncommon. There are many reasons for these differences including failure to control important parameters during the experiment, failure to measure and/or report important parameters, insufficient test duration, and perhaps the concentration of suspended fine sediment present during the experiment.

Background

Clearwater local scour experiments conducted by the author in an open, flow-through flume at the USGS-BRD Laboratory in Turners Falls, Massachusetts uncovered a dependence of equilibrium scour depth on the presence of suspended fine sediment in the water column. The supply water for this flume is a power plant reservoir located adjacent to the Connecticut River. There is no control of the constituents in the water or the temperature of the water in the reservoir and thus the water in the flume. During some of the long duration tests the concentration of suspended sediment in the reservoir increased abruptly due to stormwater and/or snow melt runoff. When this happened there was an immediate response in the rate of local scour, as can be seen in Figure 1, even though there was essentially no change in

[1] Professor of Civil and Coastal Engineering, University of Florida, Gainesville, FL 32611, sheppard@ufl.edu

discharge and depth averaged flow velocity. Even though the scour appeared to have reached an equilibrium value the test was allowed to continue for approximately 90 hours before stopping the flow. Draining the flume through the bed resulted in the deposition of a thin layer of fine sediment. The top layer of sediment was removed and replaced by clean sediment. After the suspended sediment in the reservoir settled the next test was performed. This experiment (Experiment B in Figure 1) was conducted at the same flow velocity but at a deeper water depth. The scour depths for this test were then adjusted to the conditions of the first test (i.e. adjustments for the larger water depths were made) and the results plotted on the same figure (Experiment B Modified). Note that there is a difference in both the rate of scour and the equilibrium depths. Suspended fine sediment was encountered in other tests, which were stopped immediately and the test repeated once the suspended sediment levels returned to normal. This observation was the motivation for the work reported in the paper.

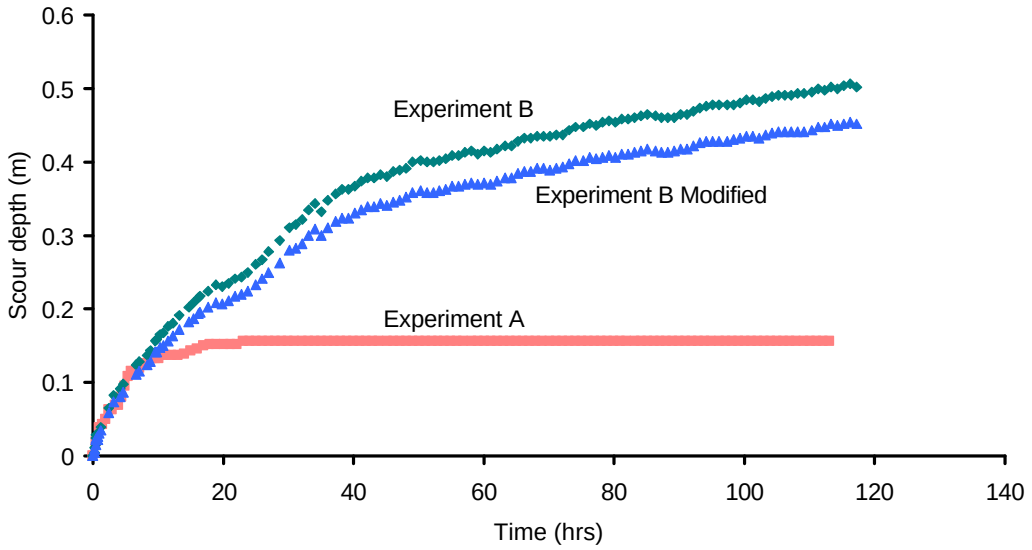

Figure 1. Local scour depths at a 0.915 m diameter circular pile in 0.22 mm diameter sand as functions of time. The flow velocities, V, for both tests were 0.3 m/s. The water depth for Experiment A was 1.2 m. The Experiment B water depth was 1.8 m. The third curve (denoted as Experiment B Modified) is Experiment B data corrected to Experiment A water depths. The sediment critical velocity for both experiments was 0.32 m/s.

The results presented here are an attempt to quantify and explain the reasons for the phenomena discovered in the clearwater local scour tests at the USGS-BRD Laboratory. Research in the field of drag reduction has shown that the presence of suspended fine sediment in the water can significantly reduce drag forces [see e.g. Gust (1976), Gust and Southard (1983), Li and Gust (2000), Wang and Larsen (1994) Wang and Larsen (1998)]. It is reasonable to assume that a reduction in bed shear stress due to suspended fine sediment, if not the only reason for reduced scour, is at least the major player in these observed phenomena. A series of clearwater and live bed tests were conducted in order to quantify the effects of suspended sediment concentration and flow velocity on local scour reduction. The first of these tests were conducted by the author

and the remainder by a civil engineering student (Dougal Clunie) at the University of Auckland in Auckland, New Zealand.

Flume Tests:

The flume used for the quantification tests is 456 mm wide, 440 deep, and 19 m long, is tilting and has the capability of recirculating the sediment as well as the water. This flume is located in the Hydraulics Laboratory in the Civil and Environmental Engineering Department at the University of Auckland in Auckland New Zealand. The test structure was a 50 mm diameter Plexiglas circular pile. A photograph of the flume and test structure is shown in Figure 2. The water depths were held constant at 150 mm for all of the tests. The sediment was sand with a median grain diameter of 0.27 mm. Bentonite was used for the fine sediment. An estimate of the water volume in the flume and return system was made in order to know the approximate amount of bentonite to mix and add to the water. Water samples were collected during the experiments and tested in order to obtain a more accurate measure of the suspended sediment concentration. The scour depths were measured with an acoustic transponder mounted just below the water surface in front of the cylinder.

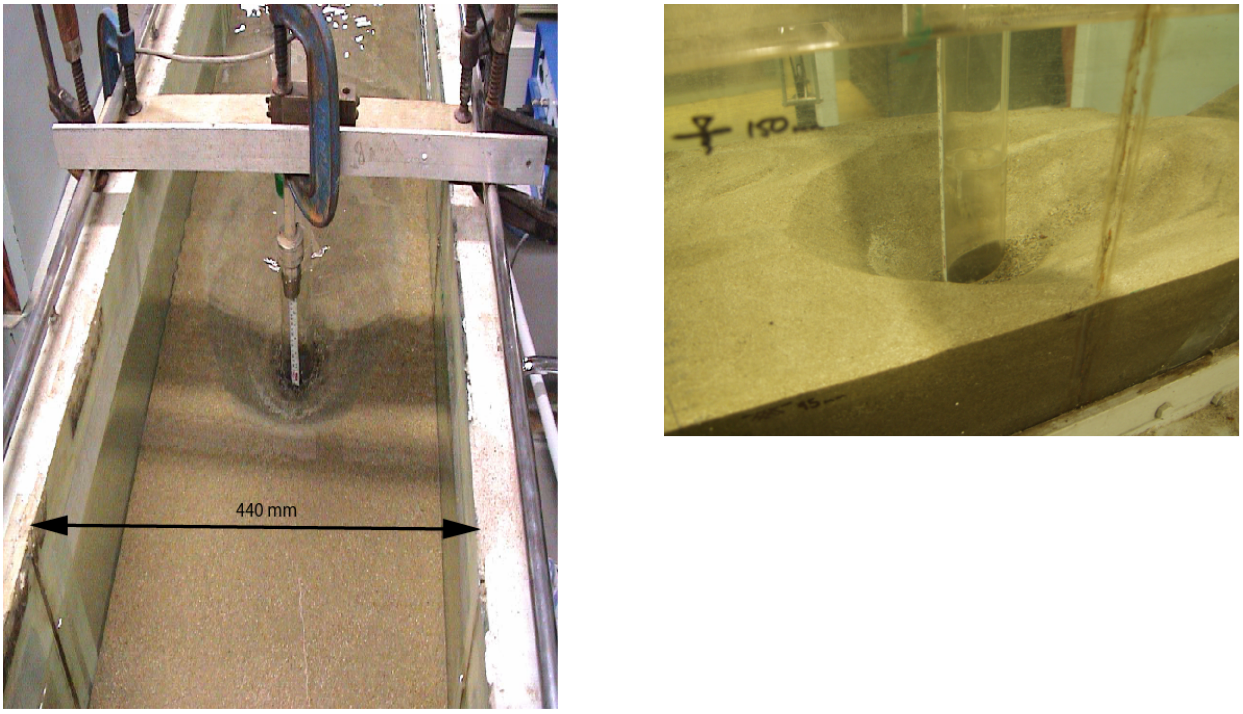

Figure 2. Photograph of the flume and test structure used in these tests. The flume is located in the Hydraulics Laboratory at the University of Auckland in Auckland, New Zealand.

A baseline study was conducted first with zero concentration (i.e. the minimum concentration obtainable) suspended sediment. This was followed by a series of tests at different concentrations and flow velocities. It became evident after a few tests that scour reduction did not occur in a measurable amount at the higher, live bed scour, velocities. It was therefore

decided to restrict the remaining tests in the lower velocity live bed and clearwater scour velocity ranges. The test conditions and results are shown in Table 1.

Table 1. Local scour test parameters and results.

D (mm)	y_0 (mm)	D_{50} (mm)	V/V_c	Concentration (gm/l)	d_{se} (mm)
50	150	0.27	0.95	0.0	78
50	150	0.27	0.95	0.1	63
50	150	0.27	0.95	0.2	67
50	150	0.27	0.95	0.3	67

Plots of scour depth versus time for suspended sediment (bentonite) concentrations of 0.0, 0.1, 0.2, 0.3 gm/l are shown in Figures 3-6. Figure 7 is a plot of projected equilibrium scour depth versus suspended sediment concentration. Additional tests are in the process of being conduced to determine the effect of flow velocity on the scour reduction. A plot of percent reduction in equilibrium scour depth as a function of suspended sediment concentration is shown in Figure 8.

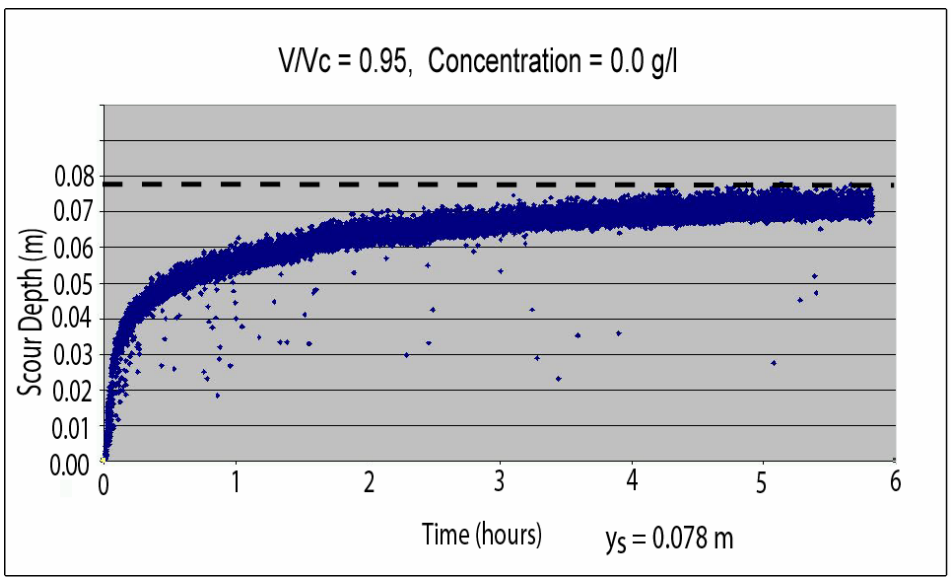

Figure 3. Scour depth versus time with zero percent bentonite concentration.

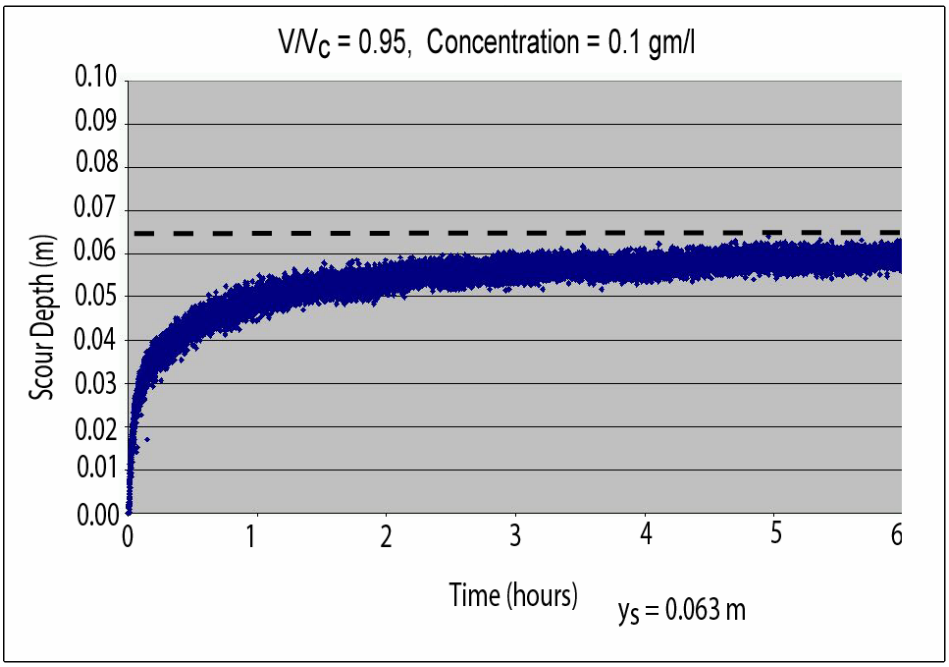

Figure 4. Scour depth versus time with 0.1 gm/l bentonite concentration suspended sediment.

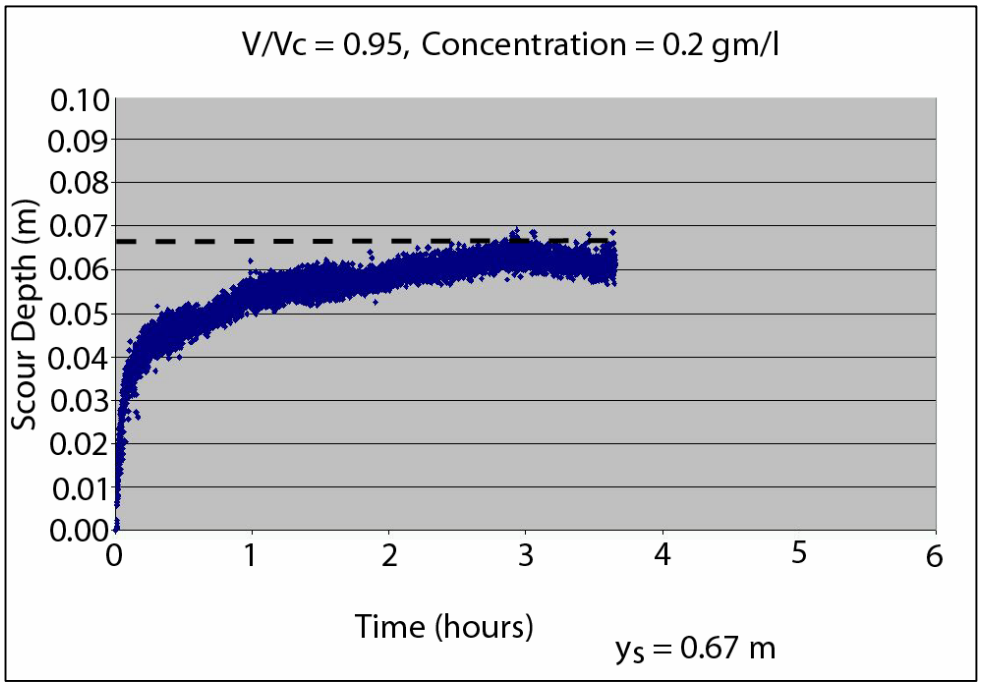

Figure 5. Scour depth versus time with 0.2 gm/l bentonite concentration suspended sediment.

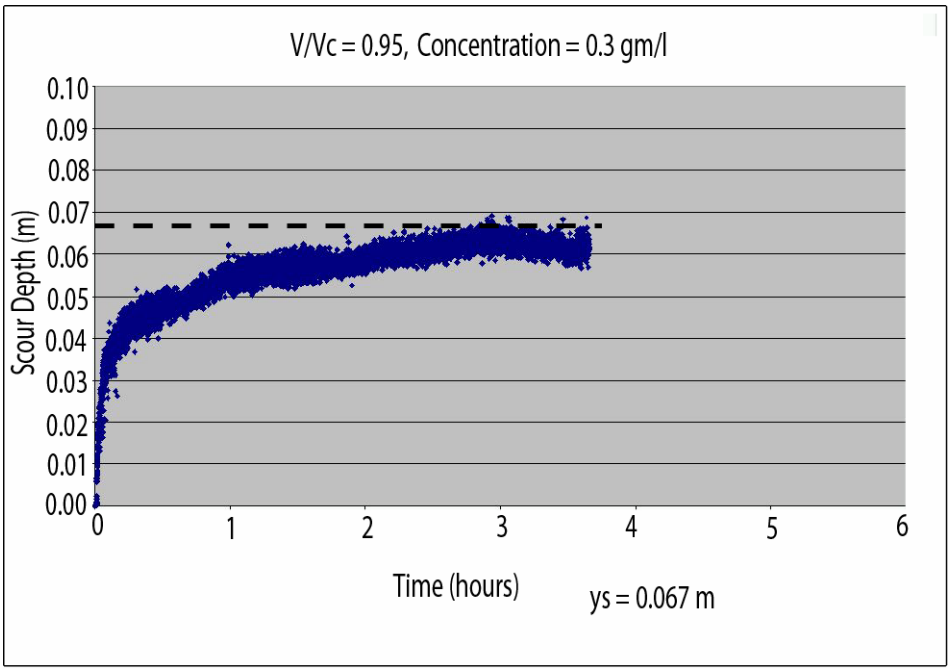

Figure 6. Scour depth versus time with 0.3 gm/l bentonite concentration suspended sediment.

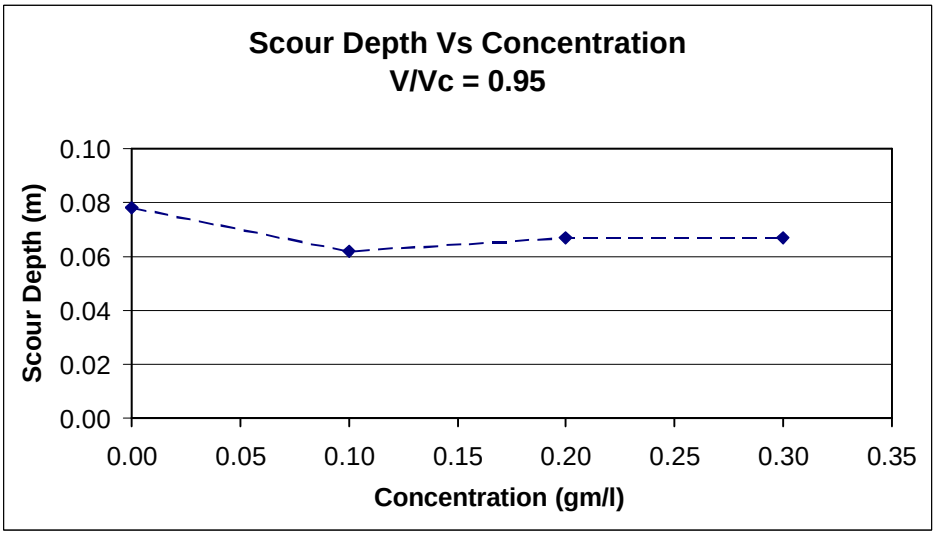

Figure 7. Scour depth versus suspended sediment concentration.

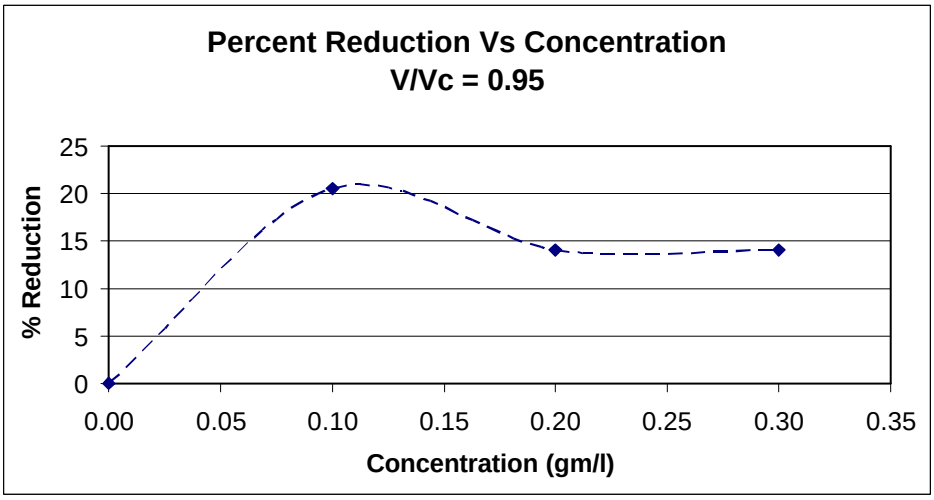

Figure 8. Percent reduction in equilibrium scour depth as a function of suspended sediment concentration.

Possible Explanations

As stated above researchers have found reductions in drag forces in water flows as a result of suspended fine sediment. The explanations given were that the presence of the suspended fine sediment caused a thickening of the viscous layer near the boundary and a reduction in the turbulence intensity (and therefore a reduction in Reynolds stresses) in the water column. It is therefore quite possible that the reduced scour depths are due to a reduction in bed shear stress caused by the suspended fine sediment. This would somewhat equivalent to reducing the flow velocity. Shear stress reduction is not the only possibility but it appears to be the most likely explanation at this time. Other possibilities include the deposition of a thin layer of the fine sediment on the bed and creating cohesive forces between the cohesionless sand grains on the surface of the bed. This would increase the sediment critical velocity and reduce the value of V/V_c ,thus reducing the equilibrium scour depth. Video cameras were located inside the 0.915 m diameter pile and recorded images of the bed throughout the tests which clearly show the increase in water turbidity. There does not, however, appear to be fine sediment deposition on the bed in the scour hole.

Summary and Conclusions

In summary, it is clear that equilibrium scour depths are reduced by the presence of suspended fine sediment at flow velocities up to the transition from clearwater to live bed scour. This could be one explanation for the scatter in laboratory local scour data. It might also be a reason why local scour depths at piers under ambient, low flow velocity conditions are often over-predicted using equations based on laboratory data where, in general, the suspended sediment concentrations are less. These findings could impact design scour predictions for situations where design velocities are low and there are sources of fine sediment that will be put into suspension during a design storm event.

It appears that the primary reason for the reduced equilibrium scour depths is the reduction in bed shear stress brought about by the presence of the suspended fine sediment. Additional work directed specifically at the measurement of wall shear stress is needed before definite conclusions can be made. Bed shear stresses are small in this velocity range and are therefore difficult to measure so this will not be an easy task.

References

Chabert, J.P. and Endeldinger, P. (1956) "Etude des Affouillements Autour des Piles des Ponts."Laboratoire National d'Hydraulique, Chatou, France.

Gust, Giselher, (1976). "Observations on turbulent-drag reduction in a dilute suspension of clay - in sea-water." Journal of Fluid Mechanics 75(1): 29-47.

Gust, Giselher, J. B. Southard, (1983). "Effects of Weak Bed Load on the Universal Law of the Wall." Journal of Geophysical Research 88(C10): 5939-5952.

Li, Michael Z., G. Gust, (2000). "Boundary layer dynamics and drag reduction in flows of high cohesive sediments." Sedimentology 47: 71-86.

Wang, Z.Y., P. Larsen, (1994). "Turbulent structure of flows of water and clay suspensions with bed load." Journal of Hydraulic Engineering 120(5): 577-600.

Wang, Zhao Yin, P. Larsen, (1998). "Resistance and Drag Reduction of Flows of Clay Suspensions." Journal of Hydraulic Engineering 124(1): 41-49.

Numerical Simulations of 3-D Flows Around Bridge Piers

By

Choi, Sung-Uk[1] and Yang, Wonjun[2]

ABSTRACT

In the present paper, the numerical simulations of the 3D flows around the bridge pier are presented. The LES and the RNG k-ε model are used for the numerical analysis of Navier-Stokes equations. Flows without and with the scour hole are simulated and compared with measured data from the experiments by Melville and Raudkivi (1977). The computed flow patterns appear to agree well with the observed patterns. However, the LES is shown to reproduce the vortex at the upstream part of the pier much better than the RNG k-ε model. Using the computed results, the downflow occurring at the frontal part of the pier is also investigated. At the location far from the pier, the downflow computed by the LES seem to be similar to that by the RNG k-ε model. However, near the pier, the downflow by the LES is observed to be much stronger than that by the RNG k-ε model.

INTRODUCTION

The flow phenomenon related with the local scour around the bridge pier is extremely complicated, and it is characterized by highly 3D turbulent motions. The downflow, the horseshoe vortex, and the wake vortex are known to be responsible for the local scour. The complex nature of flow has prevented the hydraulic engineers from applying the hydrodynamic model to this problem.

[1] Associate Prof., Department of Civil Engineering, Yonsei University, Seoul, Korea, (schoi@yonsei.ac.kr)
[2] Graduate Student, Department of Civil Engineering, Yonsei University, Seoul, Korea

Therefore, previous methods to predict the scour depth are empirical relationships such as CSU and Laursen formulas.

Recent development in computational fluid dynamics enables the hydraulic engineers to study the local scour around the bridge pier based on hydrodynamics. Olsen and Melaaen (1993) solved the Reynolds equations with the k-ε model for turbulence closure. Considering both suspended load and bedload, they solved the bed sediment conservation equation by iterating the procedure until the scour hole at an equilibrium state is obtained. Richardson and Panchang (1998) simulated the flow structures around a bridge pier with and without the scour hole. They used FLOW3D with the RNG k-ε model. Comparing the simulated with the experimental results, they found that the 3D hydrodynamic model simulates well the complex flow patterns around the bridge pier. Wang and Jia (2000) simulated an evolution of the scour hole developing around the bridge pier by using CCHE3D. In the computations, they used empirical functions for sediment transport, which were calibrated by using the experimental data. Li and Lin (2000) performed the LES to study the flow structures around a rectangular pier. They carried out the spectral analysis of turbulent and coherent structures. Tseng et al. (2000) conducted the numerical simulation with the square and the circular piers by the LES. They found that the downflow is made at the front face of the pier and this affects the creation of the horseshoe vortex. They also compared turbulent structures, lift coefficient, and drag coefficient with the experimental results, and obtained good agreements.

This paper presents an application of the 3D hydrodynamic model to the flow around the bridge pier. Herein FLOW3D is used (Sicilian et al., 1987), which solves time-dependent 3D Navier-Stokes equations by the volume-of-fluid method (Hirt and Nichols, 1981). Many techniques of turbulence modeling are available in FLOW3D. We employed the LES (Large Eddy Simulation) technique to both cases without and with the scour hole. We also use the RNG (Renormalization Group) k-ε model to see the impact from the non-isotropic turbulence assumption. First, the flowfields are simulated and compared with the measured data. Then, the downflow characteristics are investigated.

LARGE EDDY SIMULATION

The spatially-filtered Navier-Stokes equations for fluid motion are given by

$$\frac{\partial \overline{u_i}}{\partial x_i} = 0$$

$$\frac{\partial \overline{u_i}}{\partial t} + \frac{\partial}{\partial x_j}\overline{U_i U_j} = -\frac{1}{\rho}\frac{\partial \overline{p}}{\partial x_i} + \nu \frac{\partial^2 \overline{u}_i}{\partial x_j \partial x_j}$$

where U_i is the *i*-component of instantaneous velocity, $\overline{u}_i$ and $\overline{p}$ are the spatially-filtered value of U_i and pressure, respectively, ρ is the density of water, and ν is the kinematic viscosity. In the above equations, the overbar denotes the spatially-filtered value. Expanding the non-linear advective term in the momentum equation leads to

$$\overline{U_i U_j} = \overline{\overline{u}_i \overline{u}_j} + \overline{u_i' \overline{u}_j} + \overline{\overline{u}_i u_j'} + \overline{u_i' u_j'}$$

If we define the residual stress term by $\tau_{ij}^R = u_i' \overline{u}_j + \overline{u}_i u_j' + u_i' u_j'$, then we have the non-linear advective term such as

$$\frac{\partial}{\partial x_j}(\overline{U_i U_j}) = \frac{\partial}{\partial x_j}(\overline{u}_i \overline{u}_j) + \frac{\partial}{\partial x_j}(\overline{\tau}_{ij}^R)$$

Substituting the advection term into the momentum equation, we have the following form of the momentum equation:

$$\frac{\partial \overline{u}_i}{\partial t} + \frac{\partial}{\partial x_j}\left(\overline{u}_i \overline{u}_j\right) = -\frac{1}{\rho}\frac{\partial \overline{p}}{\partial x_i} + \nu \frac{\partial^2 \overline{u}_i}{\partial x_j \partial x_j} - \frac{\partial}{\partial x_j}\overline{\tau}_{ij}^r$$

where τ_{ij}^r is the deviatoric residual stress tensor defined by

$$\tau_{ij}^r = \tau_{ij}^R - \frac{2}{3}k_r \delta_{ij}$$

where k_r is the residual kinetic energy (= $1/2\tau_{ii}^R$) and δ_{ij} is the Kronecker delta. The Smagorinsky's (1963) model expresses the deviatoric residual stress tensor such as

$$\tau_{ij}^r = -2\nu_r \overline{S}_{ij}$$

where $\overline{S}_{ij}$ and ν_r are the strain rate and the turbulent viscosity of the filtered velocity. The mixing length model can be used to obtain the turbulent viscosity

of the filtered velocity, i.e.,

$$\nu_r = l_S^2 \bar{S}$$

where l_S is the characteristic length and $\bar{S}$ is the filtered characteristic strain rate ($=\left(2\bar{S}_{ij}\bar{S}_{ij}\right)^{1/2}$). In the above equation, the characteristic length is given by

$$l_S = C_S \Delta$$

where Δ is the filter size and C_S is the Smagorinsky coefficient (= 0.1).

RNG k-ε MODEL

The RNG *k*-*ε* model is known to require less reliance on empirical coefficients and provide a better solution in areas affected by high shear (Versteeg and Malalasekera, 1995). The RNG *k*-*ε* model developed by Yakhot et al. (1992) represents the effects of the small-scale turbulence by means of a random forcing function in the Reynolds equations. The RNG procedure systematically removes the small-scale motion from the governing equations by expressing their effects in terms of larger-scale motions and a modified viscosity. The equations of the time-averaged turbulent kinetic energy (*k*) and the dissipation rate (*ε*) of *k* are respectively given by (the tilde denotes the time-averaged value)

$$\frac{\partial k}{\partial t} + \frac{\partial}{\partial x_j}(k\tilde{u}_i) = \alpha_k \nu_{eff} \frac{\partial^2 k}{\partial x_j \partial x_j} + 2\nu_t E_{ij} \cdot E_{ij} - \varepsilon$$

$$\frac{\partial \varepsilon}{\partial t} + \frac{\partial}{\partial x_j}(\varepsilon\tilde{u}_i) = \alpha_k \nu_{eff} \frac{\partial^2 \varepsilon}{\partial x_j \partial x_j} + C_{1\varepsilon}^* \frac{\varepsilon}{k} 2\nu_t E_{ij} \cdot E_{ij} - C_{2\varepsilon} \frac{\varepsilon^2}{k}$$

where $\nu_{eff} = \nu + \nu_t$, $\nu_t = C_\mu k^2/\varepsilon$, C_μ = 0.0845, $\alpha_k = \alpha_\varepsilon$ = 1.39, $C_{1\varepsilon}$ = 1.42, $C_{2\varepsilon}$ = 1.68, $C_{1\varepsilon}^* = C_{1\varepsilon} - \eta(1-\eta/\eta_0)/1+\beta\eta^3$, $\eta = \left(2E_{ij} \cdot E_{ij}\right)^{1/2} k/\varepsilon$, $\eta_0 = 4.377$, and $\beta = 0.012$.

APPLICATIONS

Among the literatures published, Melville and Raudkivi (1977) provided perhaps the most detailed quantitative descriptions of the flow structures of the local scour. So, in this study, we perform the numerical simulations using the

experimental conditions in Melville and Raudkivi (1977). Fig. 1 shows the schematic figure of the flow condition used in the computation. Two cases are simulated separately, i.e., without and with the scour hole. Figs. 2(a) and (b) show the constructed grids for the cases without and with the scour hole, respectively. The number and size of the grids for each case are given in Table 1. Unfortunately, a detailed geometric description of the scour hole at the equilibrium state is not given in Melville and Raudkivi (1977). Thus, herein, the shape of the scour hole is approximated by a frustum of a cone, which is thought to be a good assumption at the upstream side of the pier (Richardson and Panchang, 1998).

Figs. 3(a)-(c) show the velocity vector fields at the vertical symmetry plane upstream of the pier. The computed results in Figs. 3(a) and (b) are from the LES and the RNG k-ε model, respectively, and Fig. 3(c) is the experimental data measured by Melville and Raudkivi (1977). In the figures, the velocity is made dimensionless by the mean approach velocity (u_o) of 0.25 m/s. It is seen that the computed and measured velocity fields show a similar flow pattern, i.e., the downflow is made along the upstream face of the pier. Compared with the measured profile, the magnitude of the downflow velocity from the numerical simulation is slightly small. Notice in Fig 3(a) that a return flow is observed nearly at the bottom. This cannot be decided to be realistic or not because the measurement is made on a too coarse grid.

The numerical simulations same as the previous ones are performed but the scour hole at the equilibrium state is included. The velocity vector fields made within the scour hole are presented in Figs. 4(a)-(c), where the first two figures are computed results by the LES and the RNG k-ε model, respectively, and the last is the measured data by Melville and Raudkivi (1977). Fig. 4(c) shows the flow descending into the scour hole along the vertical plane of symmetry and the formation of an eddy that constitutes the horseshow vortex. Among the two computed results, the LES is seen to simulate the formation of the eddy much better than the RNG k-ε model although the center of the vortex is located slightly downstream compared with Fig. 4(c).

Figs. 5(a)-(c) depict the distributions of the downflow velocity at the x-z plane parallel to the main flow direction. The distributions are given at three locations, i.e., x = 0.5D, 1D, and 2D. In the figures, both simulations without

and with the scour hole are presented, and the magnitude of the downflow velocity is made dimensionless by the mean approach velocity (u_o), and the distance from the bed by the uniform flow depth (h). In the figures, the minus downflow denotes vertically upward direction.

In the case without the scour hole, it is seen that the downflows by the LES and the RNG *k-ε* model are similar and negligible at $x = 2D$. However, as it is close to the pier, the profiles look differently and the maximum value of the downflow by the LES is seen to be larger than that by the RNG *k-ε* model. That is, as it gets close to the pier (at $x = 0.5D$), the downflow grows considerably and reaches a magnitude of $0.5u_o$ and $0.4u_o$ by the LES and by the RNG *k-ε* model, respectively.

In the case with the scour hole, the downflow profiles computed by the LES and the RNG *k-ε* model look very similar at $x = 1D$ and $2D$. However, at $x = 0.5D$, the downflow by the LES is seen to be much stronger than that by the RNG *k-ε* model. That is, the maximum values of w/u_o appear to be 0.6 and 0.2 by the LES and by the RNG *k-ε* model, respectively. This may indicate that the anisotropy of turbulence increases the strength of the downflow. Very recently, Graf and Istriarto (2001) performed laboratory experiments and showed that the maximum downflow reaches $0.6u_o$ at $x = 0.67D$, which coincides well with the results presented herein.

Fig. 6 shows the distribution of the downflow velocity at the *y-z* plane normal to the main flow direction. The profiles are provided at $0.5D$, $1D$, and $2D$. Like the previous cases, it is seen that the two simulated results look similar at $y = 2D$ but they look differently in the region close to the pier. In both cases (without and with the scour hole), the downflow velocity computed by the LES is larger than that by the RNG *k-ε* model.

CONCLUSIONS

This paper presented a 3D numerical simulation of the flow around the bridge pier. The Navier-Stokes equations were solved by using the LES and the RNG k-ε model. Flow patterns without and with the scour hole were simulated. We applied the numerical model to the experimental condition in Melville and Raudkivi (1977), and compared the computed results with their measured data.

Comparisons with the measured velocity fields revealed that the LES and the

RNG k-ε model are capable of computing the flow around the pier nicely. Specifically, the LES performed better than the RNG k-ε model in that it reproduces the vortex flow quite similarly with the observed data.

The downflow characteristics were also studied by using the simulated results. The computed downflows look similar at a distance far from the pier but, as it gets close to the pier, the maximum downflow by the LES appears larger than that by the RNG k-ε model. This may indicate that the non-isotropic nature of turbulence will increase the strength of the downflow.

ACKNOWLDEGMENT
This work was supported by grant No. 1991-1-311-002-3 from the Basic Research Program of the Korea Science & Engineering Foundation. Thanks are also due to Mr. Kiwon Hong in Soft-Tech International, Inc. in Korea for his technical support.

REFERENCES

1. Graf, W.H. and Istiarto, I. (2002). "Flow pattern in the scour hole around a cylinder." *Journal of Hydraulic Research*, IAHR, Vol. 40, No. 1, 13-20.
2. Hirt, C.W. and Nichols, B.D. (1981). "Volume of fluid (VOF) method for the dynamics of free boundaries." *Journal of Computational Physics*, Vol. 39, 201-225.
3. Li, C.W. and Lin, P. (2000). "Simulation of three-dimensional coherent and turbulent motions around a rectangular pile in an open channel flow." *Stochastic Hydraulics 2000*, Wang and Hu (eds), Beijing, China.
4. Melville, B.W. and Raudkivi, A.J. (1977). "Flow characteristics in local scour at bridge piers." *Journal of Hydraulic Research*, IAHR, Vol. 15, No. 4, 373-380.
5. Olsen, N.R.B. and Melaaen, M.C. (1993). "Three-dimensional calculation of scour around cylinders." *Journal of Hydraulic Engineering*, ASCE, Vol. 119, No. 9, 1048-1054.
6. Richardson, J.E. and Panchang, V.G. (1998). "Three-dimensional simulation of scour-inducing flow at bridge piers." *Journal of Hydraulic Engineering*, ASCE, Vol. 124, Vol. 5, 530-540.
7. Sicilian, J.M., Hirt, C.W., and Harper, R.P. (1987). FLOW3D: *Computational modeling power for scientists and engineers. FSI-87-00-1*, Flow Science, Los Alamos, NM.
8. Smagorinsky, J. (1963). "General circulation experiments with the primitive equations: I. the basic equations." *Monthly Weather Review*, 91, 2217-2226.

9. Tseng, M., Yen, C.L., and Song, C.C.S. (2000). "Computation of three-dimensional flow around square and circular piers." *International Journal for Numerical Methods in Fluids*, Vol. 34, 207-227.
10. Versteeg, H.K. and Malalasekera, W. (1995). *An Introduction to Computational Fluid Dynamics*, Longman Group Ltd, Edinburgh, England.
11. Wang, S.Y. and Jia, Y. (2000). "Computational simulations of local scour at bridge crossings-capabilities and limitations." *International Conference on Hydro-Science Engineering 2000*, CD-ROM.
12. Yakhot, V., Orszag, S.A., Thangam, S., Gatski, T.B., and Speziale, G.G. (1992). "Development of turbulence model for shear flows by a double expansion technique." *Physics of Fluids*, 4(7), 1510-1520.

Table 1. Grids used in Computation

	Simulation Type	Number of Grids	Grid Dimensions $x \times y \times z$ (m)
LES	w/o scour hole	140,000	0.004×0.002×0.001
	with scour hole	250,000	0.0003×0.002×0.0006
RNG $k-\varepsilon$	w/o scour hole	105,000	0.004×0.005×0.0012
	with scour hole	183,750	0.00098×0.0033×0.0006

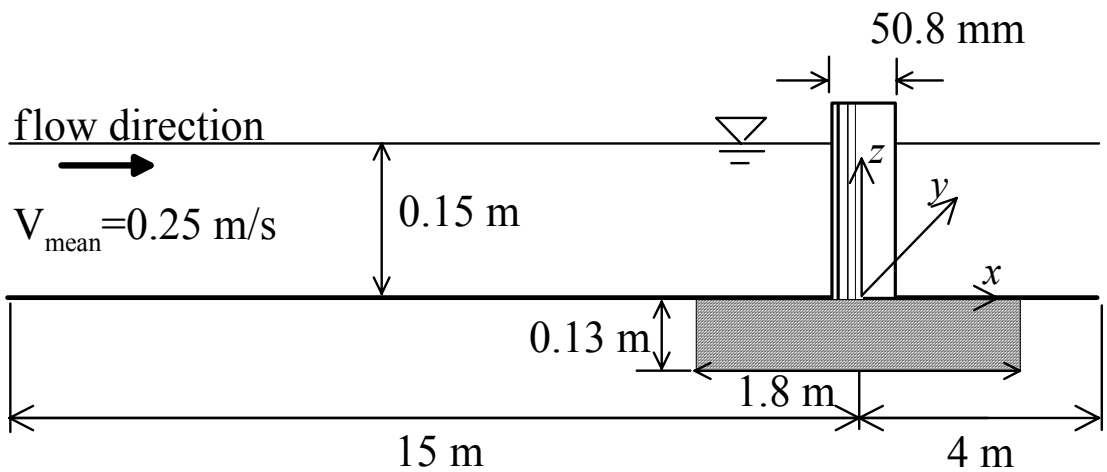

Fig 1. Schematic Figure of Experiments (Melville and Raudkivi, 1977)
(The origin is located at the center of the pier)

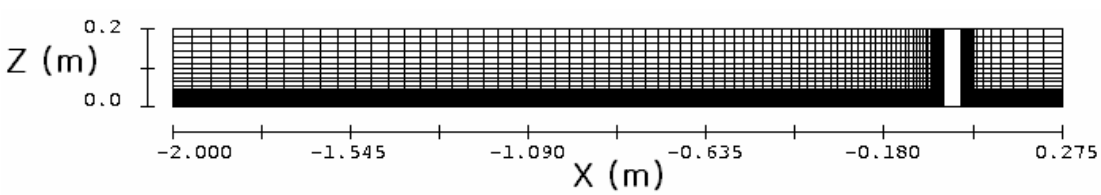

(a) Grid for Simulation without Scour Hole

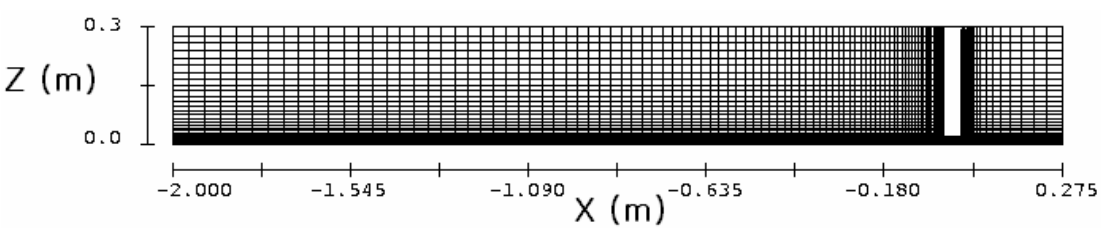

(b) Grid for Simulation with Scour Hole

Fig 2. Grid used in Computation

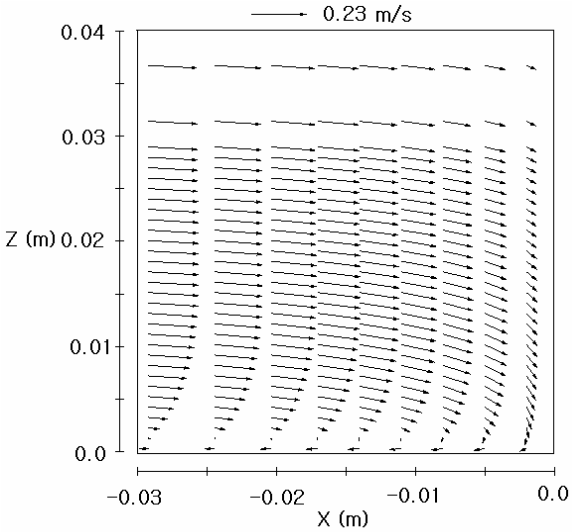

(a) LES

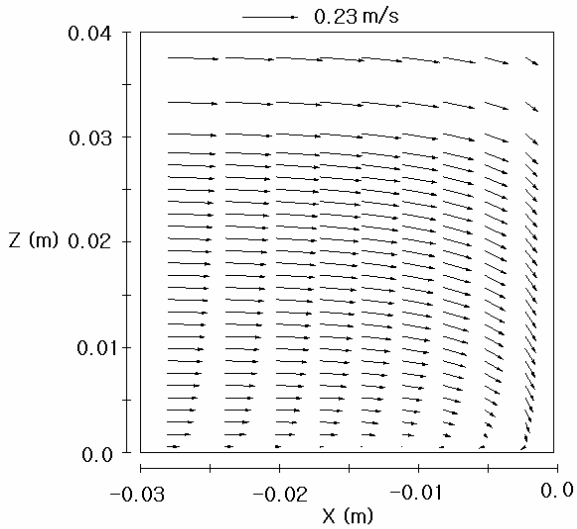

(b) RNG k−ε

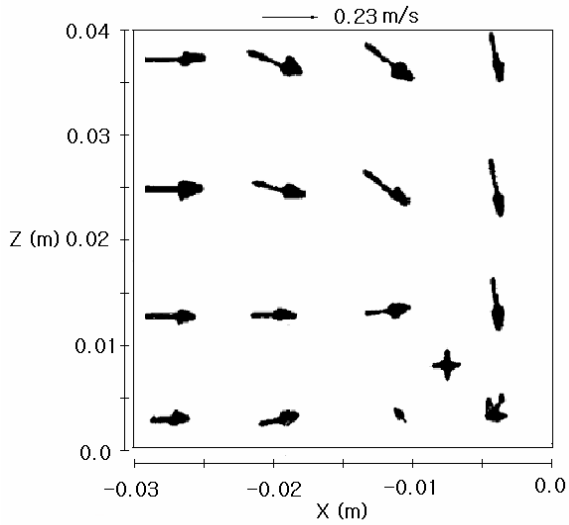

(c) Melville and Raudkivi (1977)

Fig. 3 Velocity Vectors at *x*-*z* Plane (without Scour Hole)

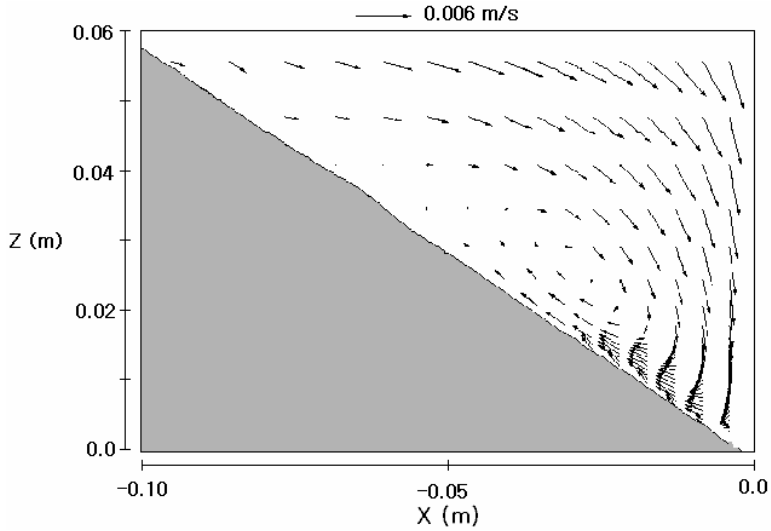

(a) LES

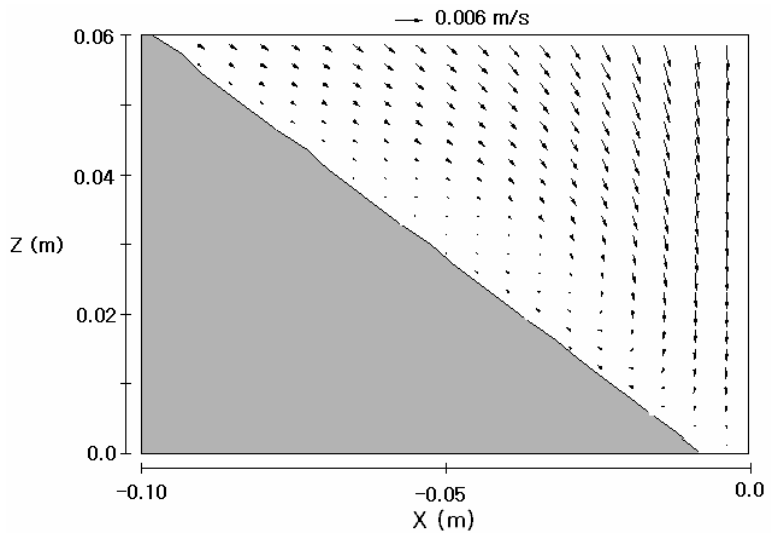

(b) RNG k-ε

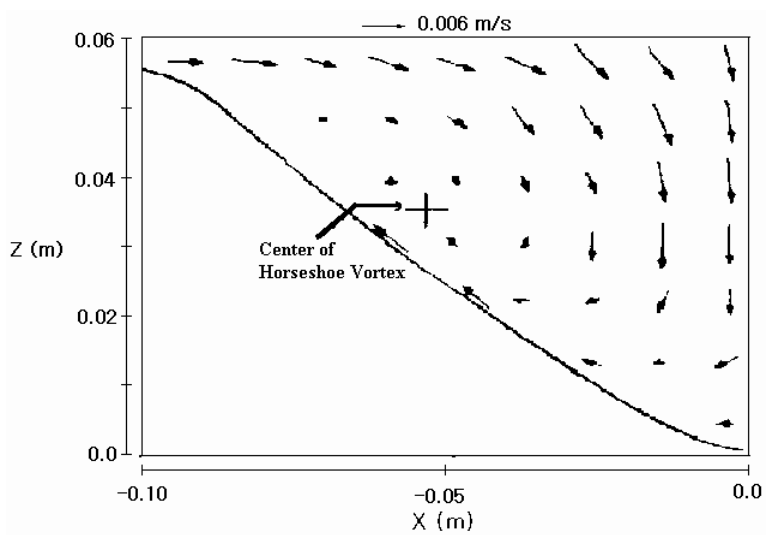

(c) Melville and Raudkivi (1977)

Fig. 4 Velocity Vectors at *y*-*z* Plane (with Scour Hole)

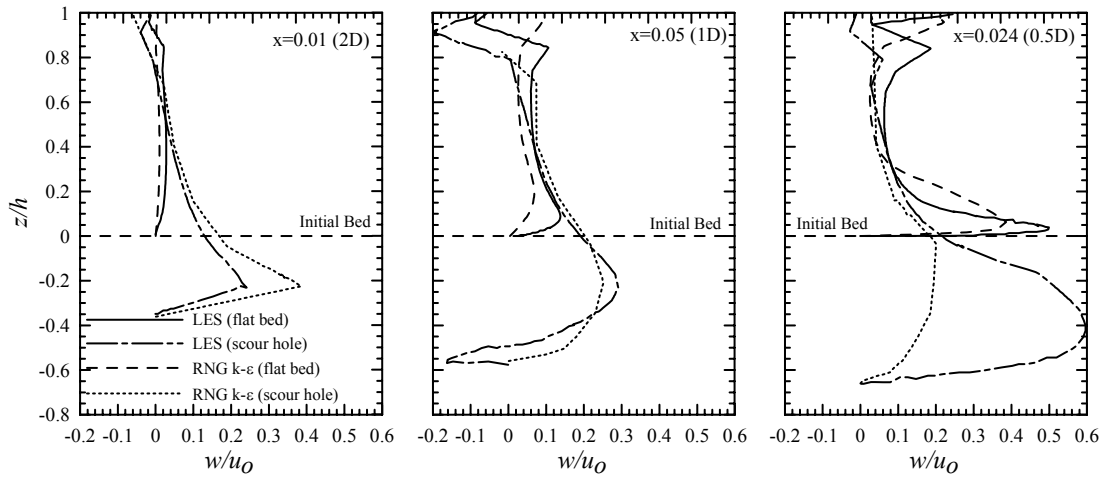

(a) at $x = 2D$ (b) at $x = 1D$ (c) at $x = 0.5D$

Fig 5. Downflow Velocity Profiles at the x-z Plane ($y = 0$)

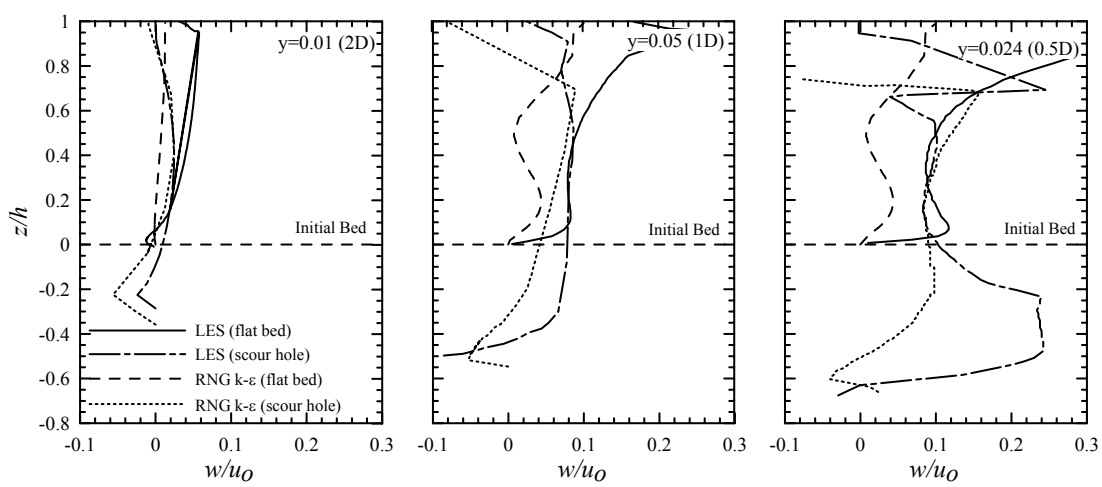

(a) at $y = 2D$ (b) at $y = 1D$ (c) at $y = 0.5D$

Fig 6. Downflow Velocity Profiles at the y-z Plane ($x = 0$)

3-D Numerical Model for Wave-Induced Dynamic Behavior of Sand Beds at Bridge Piers

By

Md. Faruque Mia[1], Hiroshi Nago[2], Shiro Maeno[3]

ABSTRACT

Bridges over water are mainly collapsed due to foundation scour and instability. The major damage to bridges specially occurs during floods or storm waves. When variation of wave pressure is subjected to fine-grained bed materials, the excess pore water pressure develops and changes with time. Depending on circumstances, the increase of the excess pore water pressure may reduce the effective stress to zero at a certain depth of foundation at bridge piers. Hence, the failure of bridges may not only occur due to scour but also due to instability of foundations under the persistent action of flood waves. A three-dimensional numerical model is therefore presented in this paper to calculate the characteristics of the pore water pressure and the effective stress variation at bridge piers under water pressure variation. The results obtained by numerical analysis are compared with laboratory data observed at a circular bridge pier. Comparisons of the computed results with experimental data reveal that the model predicts well the distribution of the pore water pressure and the distribution of the effective stress at bridge pier.

INTRODUCTION

The subject of wave-induced effective stress in sand beds is important to designing the foundations for various structures like bridges, gravity type breakwaters, offshore oil storage tanks and buried pipelines. Many bridges and offshore structures are damaged due to onslaught (i.e., violent attack) of flood waves or storm waves. Zen et al. (1991) reported that a breakwater in the West port of Niigata, Japan, was critically damaged due to a cyclone passed through the Japan Sea in October, 1976. They mentioned that the breakwater was designed against circular slip failures where the oscillating effects of wave pressure were not taken into account in the design code. Therefore, it is necessary to take into account the wave-induced dynamic behavior of the sand beds for designing purpose

[1] Consulting Engineer, PhD, Dainichi Consultant Inc., 3-1-21 Yabuta Minami, Gifu 500-8384, Japan.
[2] Professor, Dept. of Environmental & Civil Engineering, Okayama University, Tsushima-naka, Okayama 700-8530, Japan.
[3] Associate Professor, Dept. of Environmental & Civil Engineering, Okayama University, Tsushima-naka, Okayama 700-8530, Japan.

of the river and coastal structures. Hattori et al. (1984) suggested that the failure of a breakwater may be caused either by the local scour in the front edge of the rubble mound, or by the wave pressure acting directly to the caisson under attacks of storm waves. During strong waves, the strong variation of wave pressure acts on the surface of the sand bed. As a result, the pore water pressure increases and the effective stress decreases with time in the sand bed. This paper considers three-dimensional numerical analysis for wave-induced pore water pressure and effective stress of sand bed foundations based on the Biot's three-dimensional consolidation theory. The model is used to simulate the basic dynamic behavior of the sand bed around a bridge pier.

EXPERIMENTS

The experiments to investigate the dynamic behavior of sand bed were conducted in a large wave flume 1600cm long, 60cm wide and 160cm deep, located in the Hydraulics Laboratory of Okayama University, Japan. Fig. 1 shows a schematic figure of the longitudinal cross-sectional view of the experimental wave flume. A mobile bed zone 450cm long, 60cm wide and 40cm deep was prepared at a distance of 800cm from the upstream end of the flume. This zone was filled with sediment of mean particle size $d_{50} = 0.25$ mm and geometric standard deviation $\sigma_g = 1.2$. A circular pier of diameter $D = 10$ cm was used in the experiment. The experiments were conducted for the measurements of pore water pressure at the pier in the different layers of the sand bed. Fig. 2 shows the position of the pressure transducers at the pier wall. Pt.1 was placed 5cm above the bed level to measure the water pressure, which was considered as the pressure acted over the bed surface, and Pt.2, Pt.3 and Pt.4 are placed at distances of 5cm, 15cm and 25cm, respectively, below the sand surface. The data for pore water pressure were collected at the beginning and some other several time steps of the experiment for 180 sec with a frequency of $f_z = 50\ \mathrm{s}^{-1}$. Table 1 shows the detail of several experiments. The numerical model was verified with the experimental data which were observed for the condition of mean water level h_0 = 80cm, wave height H = 30cm, wave period T = 2sec and wave length L = 450cm.

GOVERNING EQUATIONS AND NUMERICAL APPROXIMATIONS

The motions of water and sand in the bed are analyzed by the method similar to that of ground water problems in an elastic aquifer (Rouse 1950). Based on the Biot's (1941) three-dimensional consolidation theory, the governing equations for equilibrium and continuity to express the pore water pressure and the effective stress under hydrodynamic forces in the three-dimensional (x, y, z) coordinate system with the z axis directed vertically downward are

$$\frac{\partial \sigma_x}{\partial x} + \frac{\partial \tau_{yx}}{\partial y} + \frac{\partial \tau_{zx}}{\partial z} = \rho g \frac{\partial h}{\partial x} \tag{1}$$

$$\frac{\partial \tau_{xy}}{\partial x} + \frac{\partial \sigma_y}{\partial y} + \frac{\partial \tau_{zy}}{\partial z} = \rho g \frac{\partial h}{\partial y} \tag{2}$$

$$\frac{\partial \tau_{xz}}{\partial x} + \frac{\partial \tau_{yz}}{\partial y} + \frac{\partial \sigma_z}{\partial z} = \rho g \frac{\partial h}{\partial z} \tag{3}$$

$$\rho g \left(\beta \lambda_w + \frac{\lambda_a}{P_0 + \rho g h} \right) \frac{\partial h}{\partial t} + \frac{\partial e}{\partial t} = k \left(\frac{\partial^2 h}{\partial x^2} + \frac{\partial^2 h}{\partial y^2} + \frac{\partial^2 h}{\partial z^2} \right) \tag{4}$$

where σ_x, σ_y, σ_z are the incremental normal stresses which are the deviations from the initial stress state, τ_{xy}, τ_{yz}, τ_{zx} are the incremental shear stresses, h is the pore water pressure, ρ is the mass density of water, g is the acceleration due to gravity, P_0 is the atmospheric pressure, β is the compressibility of water, t is the time, k is the coefficient of permeability, λ_w is the porosity occupied by the water, λ_a is the porosity occupied by the air and e is the incremental volumetric strain.

The vertical distribution of porosity occupied by air, λ_a, is not uniform along the depth of the sand bed. This varies with the absolute pressure, P ($= P_0 + \rho g h$). If λ_a for the standard pressure ($\bar{P} = P_0 + \rho g \bar{h}$) is denoted by $\bar{\lambda}_a$, then λ_a for the pressure P can be expressed as

$$\lambda_a = \left(\frac{\bar{P}}{P} \right) \bar{\lambda}_a \tag{5}$$

The computational domain is discretized with a series of 8-noded hexahedron isoparametric elements. The continuous functions for displacements components u_x, u_y, u_z, and h are approximated using the interpolation formulations over each element as

$$u_x = \sum_{j=1}^{n} a_j(t) \phi_j(x, y, z) \tag{6}$$

$$u_y = \sum_{j=1}^{n} b_j(t) \phi_j(x, y, z) \tag{7}$$

$$u_z = \sum_{j=1}^{n} c_j(t) \phi_j(x, y, z) \tag{8}$$

$$h = \sum_{j=1}^{n} d_j(t) \phi_j(x, y, z) \tag{9}$$

where n is the number of nodes in each element, a_j, b_j, c_j and d_j are the nodal values of u_x, u_y, u_z and h, respectively, and ϕ_j is the shape functions dependent only on coordinates. Applying the Galerkin method to Eq. (1) to Eq. (4), then applying Green's Theorem to the terms involving second order derivatives and using a weighted finite-difference scheme to discretize the time derivative, a system of element stiffness matrix is obtained.

The finite difference scheme to discretize the time derivative is formulated as

$$\frac{\partial f_j}{\partial t} = \frac{\left(f_j^{t+\Delta t} - f_j^{t}\right)}{\Delta t}, \qquad f_j = \theta f_j^{t+\Delta t} + \left(1-\theta\right) f_j^{t} \tag{10}$$

where Δt is the computation time interval and θ is a time discretization weighting factor. The parameter θ defines different two-level time integration methods. For example, $\theta = 0$ corresponds to the explicit Euler scheme, $\theta = 1/2$ is the centered difference Crank-Nicholson method and $\theta = 1$ will produce a completely implicit scheme. The global matrix for the whole domain is stored by superposing the element stiffness matrices and solved for each time interval using the Gauss elimination method.

NUMERICAL MODEL APPLICATION

Computations were performed with a symmetric mesh containing 1296 elements. The meshes are discretized by 8-noded hexahedral isoparametric elements. The domain for mesh discretization was considered as 60cm×60cm×40cm with 10 vertical layers. The schematic diagram for computational mesh around a bridge pier is given in Fig. 3.

Numerical calculations are performed for the parametric values of porosity occupied by water, $\lambda_w = 0.40$; porosity occupied by air, $\lambda_a = 0.005$; coefficient of permeability, $k = 0.012$ cm/s; compressibility of the sand bed, $\alpha = 1000\times10^{-11}$ m^2/N; compressibility of water, $\beta = 42.3\times10^{-11}$ m^2/N; Young's modulus, $E = 4.8\times10^{7}$ N/ m^2; Poisson's ratio, $\mu = 0.48$; incremental time step, $\Delta t = 0.02$; total depth of sand bed, $Z = 40$ cm; mean water depth, $h_0 = 80$ cm and time period, $T = 2$ sec.

NUMERICAL ANALYSIS AND DISCUSSIONS

The dynamic behavior of sand bed around bridge pier is simulated using the proposed numerical model. The experimental results for test no.2 are compared with simulated results in Fig. 4 and Fig. 5. The pore water pressure was recorded for the wave propagation of 20 sec from the beginning of the experiment. The porosity of the uniform sand bed was

0.4. Fig. 4 shows the comparison between the simulated and experimental pore water pressure at different depths. The oscillating water pressure acting on the highly saturated sand surface propagates into the sand layer with the damping in amplitude and the lag in phase. The damping ratio and phase lags largely depend on the volume of the air content in the sand layer (Nago 1981). Nago and Maeno (1987) also suggested that there is no damping of pore water pressure without the presence of air in the sand layer even under consideration of the compressibility of water and the sand bed. Therefore, the vertical distribution of porosity occupied by air (λ_a) is modeled by the Eq. (5). The oscillating water pressure is considered as recorded in the experiments and the pressure is distributed at all surface grid points assuming progressive wave flow. Fig. 4(a) to (c) represents the comparison between calculated and measured pore water pressure at the cylindrical pier at depths z = 5cm, z = 15cm and z = 25cm, respectively. Good agreement between the simulated results and the experimental data for pore water pressure is obtained for both pressure damping and phase lag.

The effective stress level is calculated from the simulated pore water pressure at different depths of sand layer at bridge pier. Fig. 5 shows the calculated and measured non-dimensional effective stress for test no. 2. There was no development of local scour at the pier. Therefore, the calculations for $\sigma_z'(t)$ were performed using the initial depth corresponding to each of the measuring points. Fig. 5(a) shows the effective stress variation with time at z = 5cm. The effective stress reduces along with the propagation of the wave generation when the wave trough comes in front of the pier. The comparison between the calculated and the measured effective stress at depths z = 15cm and z = 25cm is also shown in Fig. 5(b) and (c), respectively. If $\sigma_z'(t) \geq 1$, then the sand bed is considered to be stable. Fig. 5 shows that the value of $\sigma_z'(t)=1$ until about 4 secs, at which state the waves were not acted in the sand bed. After that the waves were generated and the effective stress reduced considerably due to the development of the pore water pressure under wave action.

CONCLUSIONS

This paper presents a three-dimensional finite element numerical model for simulating the dynamic behavior of the sand bed. The simulated results are verified with experimental data observed at cylindrical bridge pier in uniform sand bed. The numerically obtained results give good agreement with experimental results. A smaller value of effective stress is found around the bridge pier than required for stable condition. The effective stress is expected to be zero, i.e., liquefaction state, under circumstances of the wave propagation at the bridge site. Under such a state, the structure is likely to be unstable and liable of collapse. In this study, the pier diameter and wave properties were selected in such a way that no local scour was allowed. Therefore, the sand bed behavior is resulted only from the effect of the wave action. Obviously, the situation will be more severe when the foundation of the structure will be experienced by both the local scour and the liquefaction. The results also suggest that this numerical modeling technique can be used regarding to the other soil-water-structure problems such as the floatation of buried pipelines, the burial of bubble mounds and the foundation failures of the breakwaters. Since the sand of liquefied zone is supposed to remove away by the tangential incipient flow velocity, the liquefaction depth assessed by this simulation will also be useful for modeling sediment transport.

REFERENCES

1. Biot, M. A. (1941). "General theory of three-dimensional consolidation." J. of Applied Phy., (12), 155-164.
2. Hattori, C., Shibata, K., and Ohori, K. (1984). "Disasters of breakwater by wave action (part 3)." Tech. note of the Port and Harbor Res. Inst., Ministry of Trans., Japan, No. 485.
3. Nago, H. (1981). "Liquefaction of highly saturated sand layer under oscillating water pressure." Memoirs of the Sch. of Engrg., Okayama Univ., Japan, 16(1), 91-104.
4. Nago, H., and Maeno, S. (1987). "Pore pressure and effective stress in a highly saturated sand bed under water pressure variation on its surface." Natural Disaster Sc., 9(1), 23-35.
5. Rouse, H. (1950). "Engineering Hydraulics." John Wiley & Sons, New York, USA.
6. Zen, K., Yamazaki, H., and Lee, I. H. (1991). "Wave-induced liquefaction and instability of breakwaters." Proc., Geo-Coast, Port and Harbour Res. Inst., Yokohama, Japan, (1), 673-678.

TABLE 1. Details of Experiments

Test No. (1)	h_0 (cm) (2)	D (cm) (3)	d_{50} (mm) (4)	λ_w (5)	H (cm) (6)	T (sec) (7)	L (cm) (8)
1	80	10	0.25	0.46	30	2	450
2	80	10	0.25	0.40	30	2	450
3	80	10	0.25	0.45	30	3	750
4	50	10	0.25	0.40	27	2	430

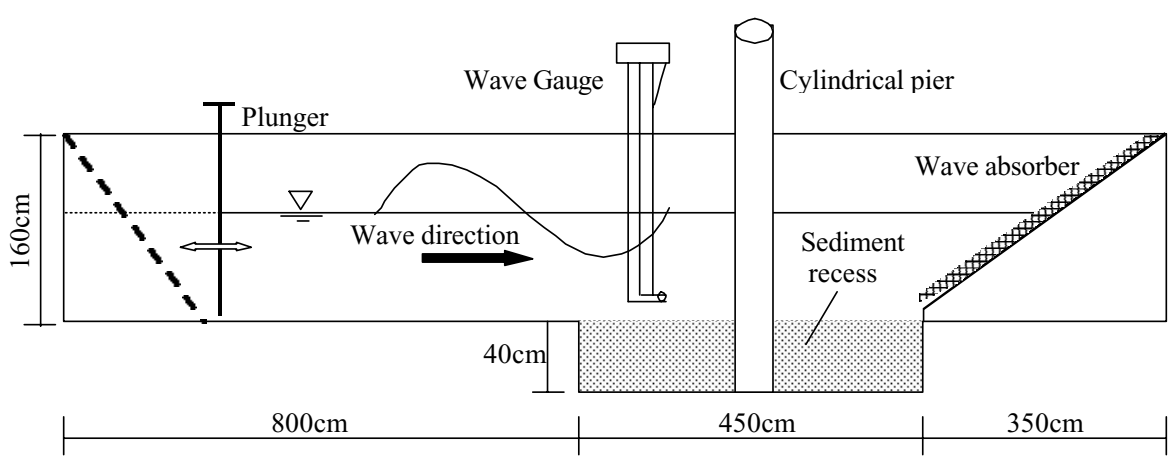

Fig. 1. Schematic diagram of the experimental wave flume

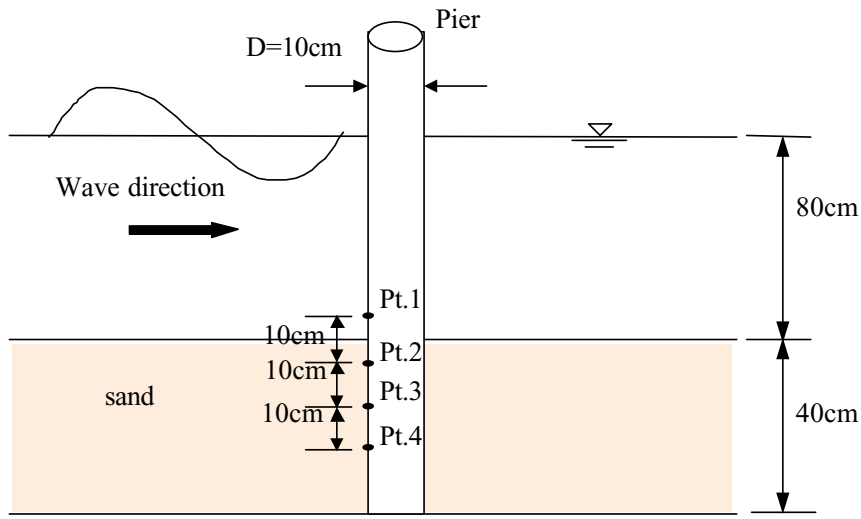

Fig.2. Position of the pressure transducers at the pier wall

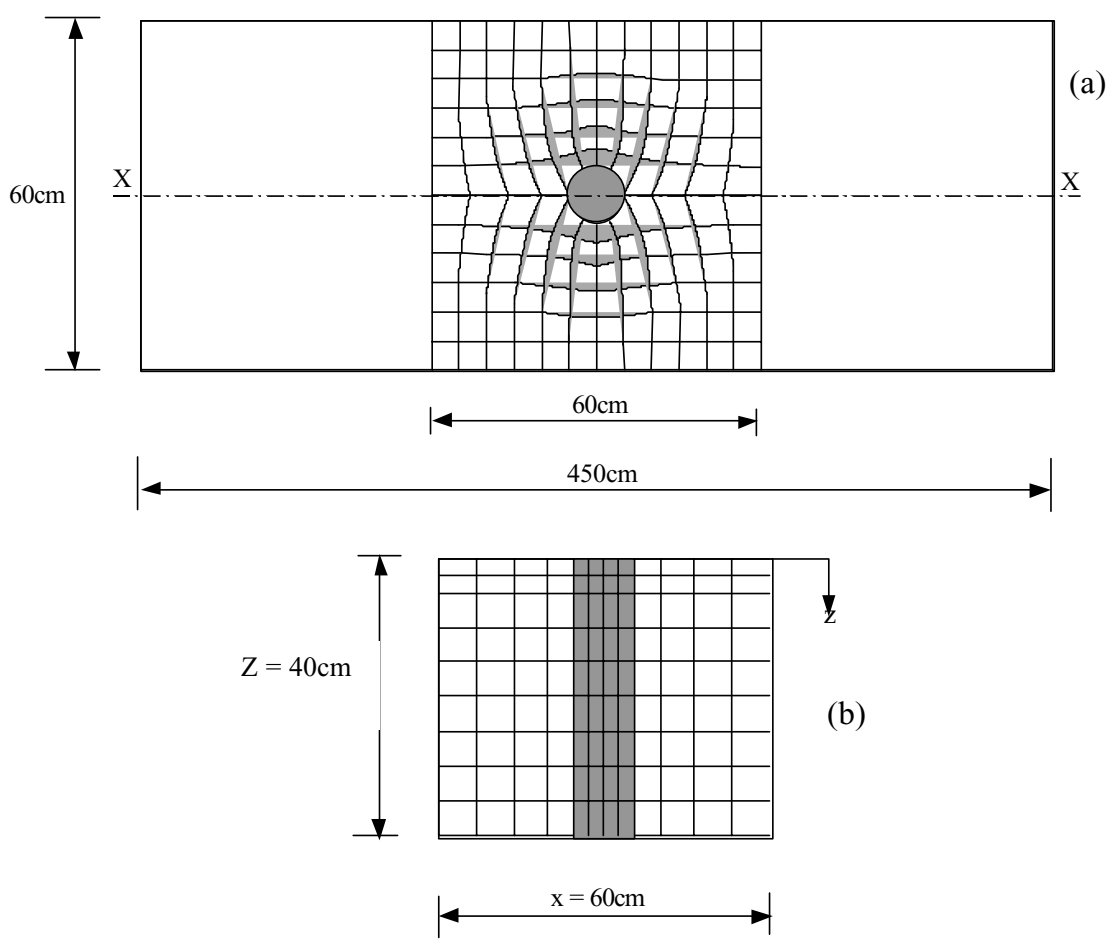

Fig. 3. Schematic diagram of sand bed and computational mesh (a) grids seen from above and (b) grids seen from vertical cross-section X-X

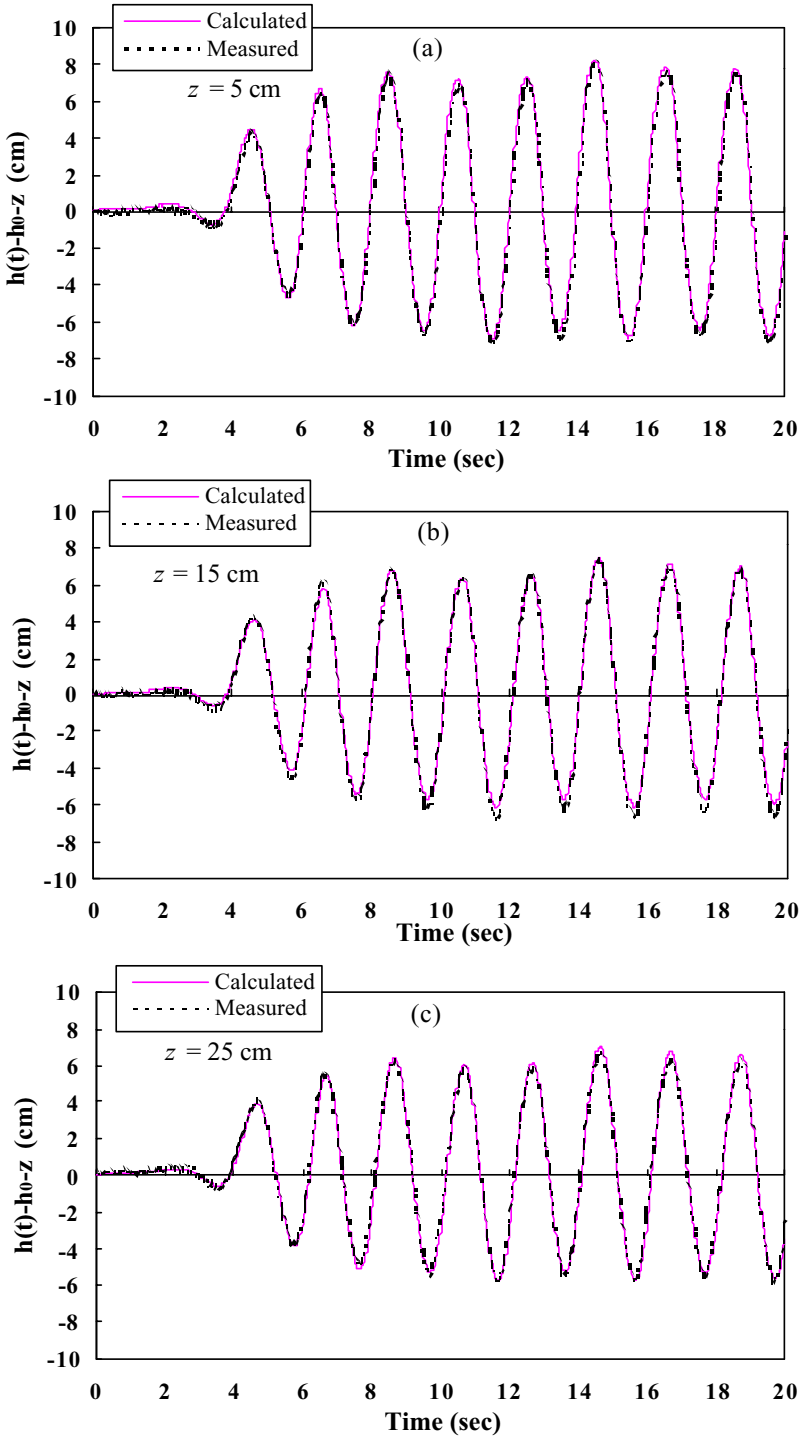

Fig. 4. Comparison between calculated and measured pore water pressure at pier for test 2, (a) at z = 5 cm, (b) at z = 15 cm and (c) at z = 25 cm

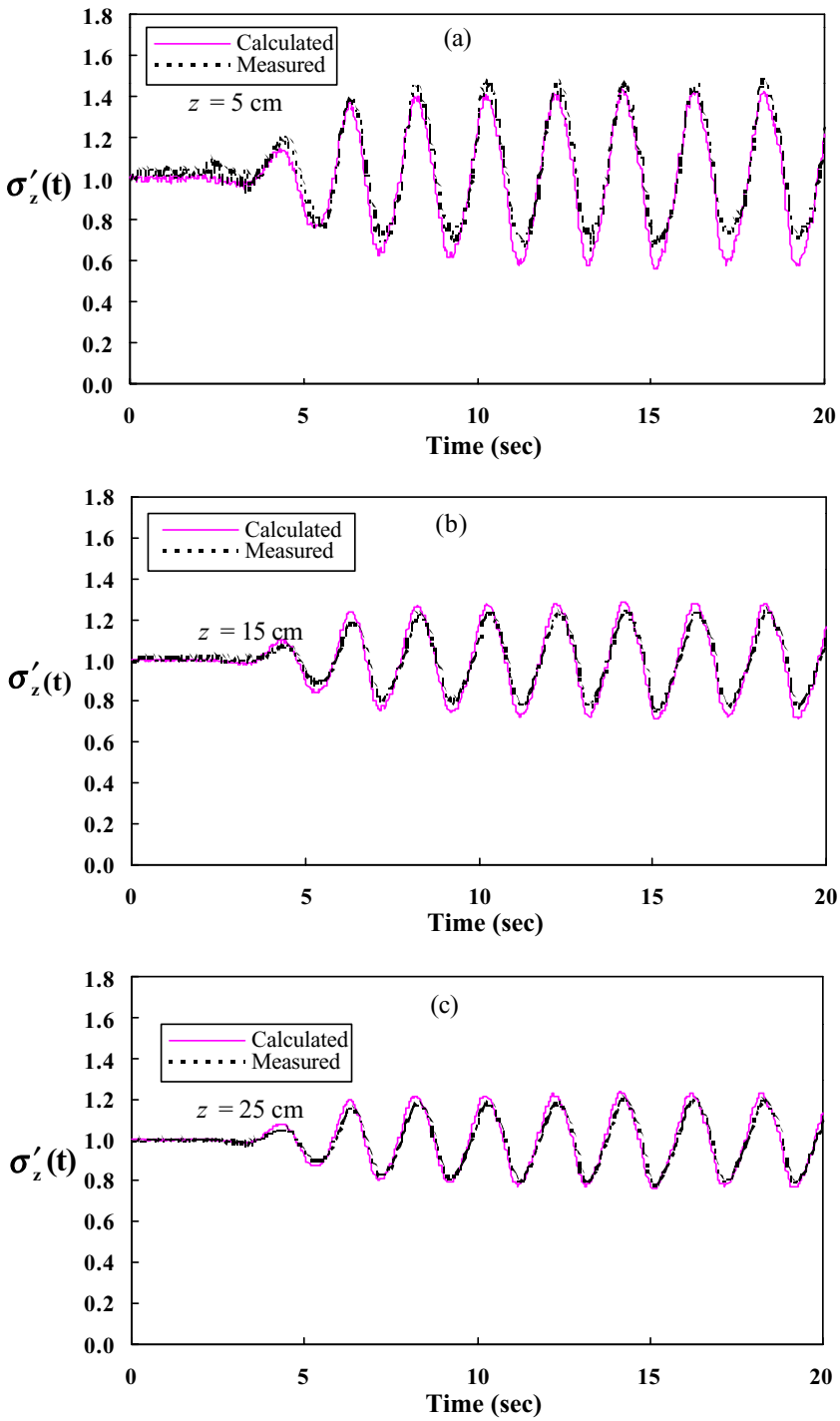

Fig. 5. Comparison between calculated and measured non-dimensional effective stress variation at pier for test.2 (a) at z = 5 cm, (b) at z = 15 cm and (c) at z = 25 cm

Pier Scour at Woodrow Wilson Bridge and SRICOS Method

By

Kiseok KWAK[1], Jean-Louis BRIAUD[2], Yiwen CAO[3], Moon-Kyung CHUNG[4], Bea HUNT[5] and Stan DAVIS[6]

ABSTRACT

The Woodrow Wilson bridge across the Potomac River in Washington D.C. is a six lane bridge which is being replaced by a twelve lane bridge due to the rapid growth of traffic. In the design process the scour depth around the bridge piers must be predicted as it affects the depth of the foundations. In this study, the scour depth at selected piers are calculated for the existing bridge and for the new bridge by using the SRICOS method. First, the bridges are described including their foundation, the soil condition, and the river at the site. Second, the calculations and the results using the SRICOS method are presented. Third, the calculated scour depths are compared to the scour depths measured at the existing bridge. A discussion follows.

THE EXISTING WOODROW WILSON BRIDGE

The existing Woodrow Wilson bridge is located in Prince George County (Maryland), Alexandria (Virginia), and Washington (D.C.) and carries Interstate Routes 95 and 495 over the Potomac River. This bridge is an essential element of the I-495/95 beltway around Washington D.C. Due to the rapid growth of traffic, a replacement bridge is being designed to handle future demand safely and efficiently.

The existing Woodrow Wilson bridge is a draw bridge which has 58 spans and is approximately 1,800 m long. It was opened to traffic in 1961 with a design capacity of 75,000 vehicles per day. The design capacity was reached just 8 years after completion of the bridge (1969). In 1998, approximately 190,000 vehicles were using the bridge everyday. The projected 2020 average daily traffic volume is 300,000 vehicles per day. The main river piers of the existing bridge are massive and embedded in the river bed. The width of the piers which cross over the river

[1] Senior Researcher, Civil Engineering Division, Korea Institute of Construction Technology, 2311 Daehwa-dong, Ilsan-gu, Koyang City, Kyonggi-do, 411-712, Korea, (kskwak@kict.re.kr).
[2] Spencer J. Buchanan Professor, Department of Civil Engineering, Texas A&M University, College Station, TX 77843-3136.
[3] Graduate Student, Department of Civil Engineering, Texas A&M University, College Station, TX 77843-3136, USA.
[4] Research Fellow, Civil Engineering Division, Korea Institute of Construction Technology, 2311 Daehwa-dong, Ilsan-gu, Koyang City, Kyonggi-do, 411-712, Korea.
[5] Hydraulic Engineer, Hardesty & Hanover, LLP, New York, NY 10036, USA.
[6] Hydraulic Engineer, Maryland State Highway Administration, Office of Bridge Development, 2nd Floor, 707 North Calvert, Baltimore, MD 21202. USA.

channels and the shape of the front of the piers are listed in Table 1. The location of the piers can be found in Fig. 1. All piers are founded on piles.

At the bridge site, the Potomac River can be divided in three areas: the main channel, the secondary channel, and the median area between the two channels. The main channel is near the west shore and is approximately 305 m wide; the secondary channel is along the east shore and is approximately 275 m wide. Fig. 1 shows a best estimate of the soil profile along the existing Woodrow Wilson bridge and the replacement Woodrow Wilson bridge. Some soil properties are listed in Table 2.

THE REPLACEMENT WOODROW WILSON BRIDGE

The replacement bridge will be built immediately south of the existing Woodrow Wilson bridge. The proposed design has two parallel six-lane bridges to replace the existing single six-lane bridge and incorporates a drawbridge for ship traffic. The overall cost of the project including the approach embankments and associated interchanges is estimated at 2.2 billion dollars. The new bridge will have fewer but wider piers than the existing bridge. The piers are designed to have exposed pile foundations to be capped near the water surface. The two bascule piers that support the drawbridges will be protected from vessel impact by a fender system (Jones, 2000). Large dolphins were considered at one point.

The foundation of pier M1 which is one of the bascule piers is shown in Fig. 2. The dimensions of all the piers are shown with the scour result in Table 6. The foundation system for the replacement Woodrow Wilson bridge evolved continuously as design proceeded. The pier sizes, the dolphin diameter, and the deep foundation dimensions mentioned are the ones considered during this study but not necessarily those that will be finally retained.

THE SRICOS METHOD

The development of the scour depth in fine-grained soils is generally much slower than in coarse-grained soils. Applying the equations for coarse-grained soils to fine-grained soils regardless of time appears to be overly conservative. Therefore, a scour analysis method for fine-grained soils needs to consider the time effect as well as soil properties, hydraulic parameters, and pier size.

Because the soil at the site of the Woodrow Wilson bridge is fine-grained (cohesive), the SRICOS method (Briaud et al., 1999 (a), (b), Kwak, 2000 and Briaud et al. 2001 (a), (b)) was used. A brief summary of this method is described as a necessary background. The SRICOS method was developed to predict the scour depth z versus time t curve around a cylindrical bridge pier. This method has already been described in details in the references cited. The SRICOS method recognizes that the scour process is highly dependent on the shear stress τ imposed by the flowing water at the soil-water interface. Through tests performed on soil samples from the bridge site using the EFA (Erosion Function Apparatus, http://tti.tamu.edu/geotech/scour), the scour rate $\dot{z}$ versus the shear stress τ is obtained; this $\dot{z}$ vs. τ curve is the erosion function. Using this relationship and the maximum scour depth equation, a hyperbolic function describing the scour depth z versus time t curve can be developed. The SRICOS method was extended to include

a random velocity-time history and a multilayer soil stratigraphy; it is called the E-SRICOS method. The E-SRICOS method requires the use of a simple computer program and gives the scour depth versus time curve for a given hydrograph. The S-SRICOS which is a simplified version of the E-SRICOS method only requires simple hand calculations and gives the final scour depth at the end of the bridge life.

HYDROLOGIC DATA

The drainage basin at the Woodrow Wilson (WW) Bridge on the Potomac River has an area of 30,742 square kilometers. It is comprised of portions of Pennsylvania, West Virginia, Virginia, Maryland, and Washington, D.C. The nearest gaging station (Gage Station 01646500) was found at the USGS web site (www.usgs.gov). This gaging station is located on the Potomac River approximately 13 km upstream of the Woodrow Wilson Bridge near the Little Falls pump station and has a drainage area of 29,965 km^2. The discharge hydrograph was downloaded from the web site, multiplied by the drainage area ratio (30742/29965), and prepared as an input to the SRICOS program. The discharge hydrograph at the bridge site, calculated in such a way, is shown in Fig. 3. The maximum discharge occurred in 1972 and was 9850 m^3/s.

In this study, the computer program entitled Hydrologic Engineering Center's River Analysis System (HEC-RAS, 1997) developed by the United States Army Corps of Engineers was used for flood analysis. The input to this program is the average slope of the channel bed, the river bed cross-section profile, Manning's roughness coefficient and many selected discharges varying from 0 to the maximum discharge. The output of this program is the velocities and the water depths at the bridge pier location had the bridge not been there; the velocities and water depths correspond to the input discharges. The relationship between velocity and discharge and between water depth and discharge can then be obtained by regression. Using these relationships, the discharge hydrograph, which is the flow discharge versus time curve, is transformed into the water depth hydrograph and more importantly into the velocity hydrograph or velocity versus time curve used in the SRICOS program. The water depth history is needed for considering the water depth effect or wide pier effect. The water depth hydrographs for pier 1E and 27E of the existing Woodrow Wilson Bridge are shown in Fig. 4 over the length of the bridge from 1960 to 1999. Pier 1E is in the main channel and pier 27E in the secondary channel.

GEOTECHNICAL DATA

The Woodrow Wilson Bridge over the Potomac River in Washington D.C. is located within the Atlantic Coastal Plain Province which consists of a broad belt of flat-lying sediments over deep bedrock. Throughout the area, the ground surface has been altered in historic times by man-made fills especially in low lying areas and along rivers and streams. The soils below the main channel bed are mostly alluvial deposits, which consist of soft clay, silt, and silty sand, extending down to approximately 25 m over the layer of Pleistocene deposits which consist of dense sand, silt, and gravel.

For this study, soil samples were taken near the location of piers 1W, 2E, and 4E in the main channel, and piers 21E and 27E in the secondary channel by using thin-wall Shelby tubes with 76.2 mm outside diameter. The drilling locations are shown in Fig. 1 with the stratigraphy. The soil samples were tested using the EFA (http://tti.tamu.edu/geotech/scour). Before performing the EFA tests, basic soil properties were obtained by performing laboratory tests. All the soil property tests were conducted according to American Society for Testing and Materials (ASTM) standards. The undrained shear strength of the soil was measured at least twice using the vane test. The results of the soil property tests are shown in Table 2.

The purpose of the EFA test is to obtain the curve that relates the scour rate $\dot{z}$ to the shear stress τ induced by the flowing water. The water flows over the sample at a chosen velocity and the sample is advanced 1 mm as soon as it is eroded. These experiments are performed repeatedly for six or seven different velocities varying between 0.1 m/s and 5 m/s on each Shelby tube sample. The flowing water generates an average bed shear stress over the soil sample in the test section. The range of τ values imposed is approximately 0.1 N/m^2 to 100 N/m^2. The hydraulic shear stress imposed by the water on the soil is calculated by using Moody Chart (Moody, 1944). The critical shear stress is considered to be the shear stress when the scour rate is equal to 1 mm/hr. This number is used as a practical definition of the critical shear stress.

The erosion functions, scour rate $\dot{z}$ versus shear stress τ, were obtained for all the samples. Two examples are shown in Fig. 5 and 6. The soil at pier 27E (2.6 - 3.2 m depth) is a soft organic clay and the undrained shear strength is relatively low (22.0 kPa), however, the critical shear stress τ_c is relatively high (5.09 N/m^2, Fig. 5). The soil at pier 27E (11.2 - 11.7 m depth) is a hard mineral clay and the undrained shear strength is relatively high (130.0 kPa) however, the critical shear stress is relatively low (0.16 N/m^2, Fig. 6). In order to investigate the influence of cohesive soil properties on the erosion function, two erodibility parameters were defined: the critical shear stress τ_c and the initial erodibility S_i which is the initial slope of the erosion function. The two erodibility parameters τ_c and S_i were plotted against soil properties such as plasticity index, undrained shear strength, and percent passing sieve #200. All correlations were poor. In Fig. 7, the correlations between critical shear stress, initial erodibility, and undrained shear strength are shown with the data from a previous study (Briaud et al.,2001(a)). The poor correlations lead to think that obtaining these parameters by direct measurement in the EFA is more reliable than using correlations.

MEASURED SCOUR DEPTH

The existing Woodrow Wilson Bridge is approximately 1,800 m long and has 58 spans (57 piers). The piers are numbered beginning at the center of the bascule section in the main channel and increase as they approach each shore. Piers 1W through 26W are on the west side and piers 1E through 31E are on the east side. All the piers and abutments are made of reinforced concrete and are founded on piles. The junction between the pier and the piles is well below the current scour

depth. In other words, the width to be considered for scour analysis is the pier width not the piles width.

Some piers on the west side (4W to 26W) and some piers in the median area (6E to 22E) are not considered in the scour analysis because these piers are not over water. The parameters for the piers in water are shown in Table 1. The attack angle of the flow is 0° for all the piers.

The channel bed was monitored in 1998. The scour measurement results for each pier are shown in Table 1. The depth of local scour is defined here as the difference between the bed level at the pier and the bed level away from the pier. The bed level away from the pier is typically taken as the average of several points measured in the unscoured region around the obstruction. In this study, there was some ambiguity on the measured local scour depth because several interpretations of the scoured bed profile were possible. An example is shown in Fig. 8 for pier 5E. It was decided to use a range of possible values in all cases; Fig. 8 shows an example of minimum and maximum values. All values are listed in Table 1.

PREDICTED SCOUR DEPTH

The scour depth z versus time t curves were calculated for each pier of the existing bridge over the time period from 1960 to 1999. This period spans from the date the bridge was built to the date this study was performed. When soil samples were not taken from the exact pier location, the erosion function of the nearest soil samples was used as input to the SRICOS program. Examples for two representative piers of the existing bridge in the main and secondary channels (Pier 1E and 27E) are shown with the respective velocity hydrographs in Fig. 9 and 10.

In every case, the predicted final scour depth z does not reach the predicted maximum scour depth $z_{\max}$ even though the life of the existing bridge is about 39 years. The values of z and $z_{\max}$ are compared in Table 3. The ratio of the final scour depth over the maximum scour depth for all piers averages 66%.

The shape of the scour depth z versus time t curve depends on the scour rate of the soil as well as the shape and intensity of the hydrograph (Kwak, 2000). The scour depth at pier 1E increased gradually and the maximum velocity which occurred in 1972 did not greatly contribute to the scour depth because a certain amount of the scour had already developed when it occurred (Fig. 9). In the case of pier 27E, the maximum velocity in 1972 had a sudden influence on the scour depth because the low velocities prior to 1972 generated shear stresses below the critical shear stress of the soil and no scour developed before 1972 (Fig. 10).

The scour depth for each pier of the existing bridge is also calculated by using the S-SRICOS method. The length of the hydrograph t_{hydro}, the maximum velocity $v_{\max}$, and the initial scour rate $\dot{z}_i$ of the soil are used to calculate the equivalent time t_e. The parameters and the results are shown in Table 4.

Scour analyses for the 100-year and the 500-year floods were also performed for the replacement bridge by using the S-SRICOS method because the S-SRICOS only requires the peak velocity. The peak discharges for the recurrence intervals (100 and 500 years) were obtained from the Maryland State Highway

Administration and are shown in Table 5. They were transformed into peak velocity by using HEC-RAS as was done for the existing bridge. The equivalent pier width was taken as the sum of the projected widths of the piles obstructing the flow. It was used for these calculations because the piers of the replacement bridge are designed to have exposed pile foundations with the pile cap near the water surface. The SRICOS predictions are shown together with the HEC-18 results in Table 6 and 7. It is clear that the HEC-18 predicted scour depths are much higher than the SRICOS predicted scour depths.

COMPARISON

The predicted scour depths using the E-SRICOS and the S-SRICOS method are compared with the measured scour depths for the existing bridge in Fig. 11 and 12. The piers in the main channel (Pier 2W to Pier 3E) are excluded from the comparison because riprap was placed in the main channel in 1980 to prevent further scour.

As shown in Fig. 11 and 12, the E-SRICOS and S-SRICOS methods give reasonable predictions. The scatter in the predictions may be due to the fact that the erosion function for the soil was not always from samples taken at the scour location. Indeed the samples were taken near piers 4E and 27E. For those piers the coefficient of determination (R^2) is 0.79. For other piers the coefficient of determination (R^2) is 0.41. The scatter on Fig. 11 and 12 gives an idea of the factor of safety necessary to minimize the number of cases where the measured scour depth is much larger than the predicted scour depth. It is also very important to note that the larger the scour depth is, the more precise the prediction is.

CONCLUSION

The Woodrow Wilson Bridge across the Potomac River in Washington D.C. is being replaced due to the rapid growth of traffic. The scour depths were calculated for the existing Woodrow Wilson Bridge by using the E-SRICOS method and the S-SRICOS method and compared with measured scour depths. A scour analysis for the replacement bridge was also performed by using the S-SRICOS method for the design floods.

1. As shown by the results of the EFA tests, the scour rate of the soil samples taken from the bridge site is relatively high, however the critical shear stress is also relatively high. The EFA results confirm that the correlations between soil erodibility and soil properties are very weak at best.
2. In all cases, the measured and the predicted final scour depths did not reach the maximum predicted scour depth $z_{\max}$ even though the bridge life is about 39 years. The average predicted final scour depth for all piers was 66% of the average predicted maximum scour depth. This is an indication of the margin of safety that existed for that bridge.
3. A high velocity flood does not greatly contribute to the scour depth in erosion resistant cohesive soils when a certain amount of scour depth has already been developed. The scour depth development in cohesive soils tends to be much

more gradual than in cohesionless soils and therefore allows more time for inspection and maintenance.

4. Both of the E-SRICOS and the S-SRICOS methods gave reasonable predictions for the existing Woodrow Wilson Bridge. The simple SRICOS (S-SRICOS) method correlates well with the extended SRICOS (E-SRICOS) method.
5. The HEC-18 equation gave predicted scour depths larger than the final scour depths predicted by the SRICOS method.
6. A factor of safety should be used on the predicted scour depth to minimize the risk of having an actual scour depth much larger than the predicted one.

ACKNOWLEDGEMENTS

The SRICOS method and the EFA were developed under sponsorship by the Texas Department of Transportation (David Stopla). The EFA tests on the Woodrow Wilson bridge samples were performed as part of a project sponsored by the National Cooperative Highway Research Program of the U.S. Transportation Research Board (Tim Hess). The samples and the velocity hydrographs were provided by the Maryland State Highway Administration (Mark Wolcott, Dan Sajedi and Andrzej Kosicki). The scour measurements were provided by Hardesty-Hanover, LLP.

REFERENCES

Briaud, J.-L , Ting, F., Chen, H. C., Gudavalli, S. R., Perugu, S., and Wei, G. (1999 a). "SRICOS: Prediction of scour rate in cohesive soils at bridge piers", *Journal of Geotechnical and Geoenvironmental Engineering*, Vol. 125, No. 4, ASCE, Reston, Virginia, USA, pp.237-246.

Briaud, J.-L., Ting, F., Chen, H.C., Gudavalli, R., Kwak, K., Philogene, B., Han, S.-W., Perugu, S., Wei, G., Nurtjahyo, P., Cao, Y., Li, Y. (1999 b), "SRICOS: Prediction of scour rate at bridge piers", *Report No. 2937-1*, to the Texas Department of Transportation, Texas Transportation Institute, The Texas A&M University System, College Station, Texas, USA.

Briaud J.-L., Ting F., Chen H.-C., Cao Y., S.-W., Kwak K., (2001a), "Erosion Function Apparatus for Scour Rate Predictions,", *Journal of Geotechnical and Geoenvironmental Engineering*, Vol. 127, No. 2, pp. 105-113, Feb. 2001, ASCE, Reston, Virginia.

Briaud J.-L., Chen H.-C., Kwak K., Han S., Ting F., (2001b), "Multiflood and Multilayer Method for Scour Rate Prediction at Bridge Piers", *Journal of Geotechnical and Geoenvironmental Engineering*, Vol. 127, No. 2, pp. 114-125, Feb. 2001, ASCE, Reston, Virginia.

HEC-RAS River Analysis System (1997). *User's manual, Version 2.0*, Hydrologic Engineering Center, U.S. Army Corps of Engineers, Davis, California, USA.

Jones, J. S. (2000), "Hydraulic testing of Wilson Bridge designs", *Public Roads, March/April*, U.S. Department of Transportation, FHWA, Washington, DC, USA, pp.40-44.

Kwak, K. (2000), "Prediction of scour depth versus time for bridge piers in cohesive soils in the case of multi-flood and multi-layer soil systems", Ph.D. Dissertation, Texas A&M University, College Station, Texas, USA.

Kwak, K., Briaud J.-L., Chen H.-V., (2001), "SRICOS: Computer Program for Bridge Pier Scour", Proceedings of the 15th International Conference on Soil Mechanics and Geotechnical Engineering, held in Istanbul, Turkey on August 27-31, 2001, A.A. Balkema Publishers, Rotterdam, the Netherlands.

Melville, B. W. and Coleman, S. E. (1999), Bridge scour, Water Resource Publications, LLC, Highlands Ranch, Colorado, USA, pp.196-199.

Moody, L.F. (1994), "Friction factors for pipe flow", Transaction of the American Society of Mechanical Engineers, Vol. 66.

Richardson, E. V. and Davis, S. M. (1995). "Evaluating scour at bridges", *Pub. No. FWHA-IP-90-017, HEC No.18*, U.S. Department of Transportation, Washington, DC, USA.

Table 1 - Pier Parameters and Measured Scour Depths for the Existing Woodrow Wilson Bridge

Pier	Shape	Width (m)	Measured Scour Depth (m)	
			Min.	Max.
3W	Square	2.51	1.31	2.72
2W	Square	2.51	0.97	1.46
1W	Square	9.75	0.92	2.14
1E	Square	9.75	1.22	1.79
2E	Square	2.51	0.76	3.13
3E	Square	2.51	1.53	2.80
4E	Square	2.51	1.98	3.28
5E	Circle	1.68	0.77	1.72
23E	Circle	1.22	0.37	0.64
24E	Circle	1.22	0.37	0.60
25E	Circle	1.22	1.01	1.50
26E	Circle	1.22	0.76	0.88
27E	Circle	1.22	0.73	1.15
28E	Circle	1.22	0.61	0.73
29E	Circle	1.22	0.31	0.52

Table 2 - Soil Properties of the Soil Samples from the Woodrow Wilson Bridge Site

Sample Location	Depth (m)	Soil Type	Undrained Shear Strength (kPa)	Bulk Density (kN/m^3)	% Passing #200	Liquid Limit (%)	Plastic Limit (%)	Water Content (%)	Critical Shear Stress (N/m^2)	Initial Erodibility S_i
Pier 1W	4.0-4.6	Clay	11.5	18.1	57	53	12	56	3.90	4.0
Pier 1W	10.1-10.6	Clay	19.0	15.6	71	51	18	35	10.20	1.9
Pier 2E	5.5-6.1	Clay	14.0	18.5	48	47	14	29	1.30	182.9
Pier 4E	5.5-6.1	Sandy Clay	14.1	16.3	64	37	14	35	0.43	9.0
Pier 21E	2.1-2.7	Clay	6.1	15.4	86	68	13	47	1.92	2.7
Pier 27E	2.6-3.2	Organic	22.0	15.2	40	-	-	82	5.09	11.2
Pier 27E	5.2-5.6	Silt	-	15.2	73	43	39	66	3.80	91.0
Pier 27E	11.2-11.7	Clay	130.0	21.3	78	86	14	24	0.16	3.2
Pier 27E	11.9-12.5	Sand	12.0	17.1	9	-	-	59	0.025	1665.2

Table 3 - Predicted Scour Depths at the Existing Woodrow Wilson Bridge Using E-SRICOS Method

Pier	Final Scour Depth z (m)	Max. Scour Depth z_{max} (m)	$\frac{z}{z_{max}}$ (%)
3W	1.64	2.85	57.5
2W	2.92	3.66	79.8
1W	5.72	9.21	62.1
1E	6.14	9.51	64.6
2E	3.69	3.97	92.9
3E	3.34	3.57	93.6
4E	2.61	3.28	79.6
5E	1.07	1.89	56.6
23E	0.47	1.22	38.5
24E	0.52	1.25	41.6
25E	0.17	1.29	13.2
26E	1.07	1.54	69.5
27E	1.41	1.74	81.0
28E	1.40	1.74	80.5
29E	1.36	1.71	79.5

Table 5 - Peak Discharges for the Potomac River at the Woodrow Wilson Bridge

Recurrence Interval (years)	Peak Discharge (CMS)
100	13592
500	19822

Table 4 - Predicted Scour Depths at the Existing Woodrow Wilson Bridge Using S-SRICOS Method.

Pier No.	Length of Hydrograph t_{hydro} (yrs)	Max. Discharge $Q_{\max}$ (CMS)	Max. Velocity $v_{\max}$ (m/s)	Pier Width B (m)	Max. Scour Depth $z_{\max}$ (mm)	Shear Stress $\tau_{\max}$ (N/m^2)	Initial Scour Rate $\dot{z}_i$ (mm/hr)	Equivalent Time t_e (hrs)	Final Scour Depth z (m)
Pier 3W	39	9850.5	1.41	2.51	2852.4	9.85	25.77	108.6	1.48
Pier 2W	39	9850.5	2.09	2.51	3662.2	20.04	115.73	157.4	3.10
Pier 1W	39	9850.5	2.30	9.75	9212.6	17.92	90.88	194.5	6.25
Pier 1E	39	9850.5	2.42	9.75	9514.9	19.62	110.47	204.0	6.88
Pier 2E	39	9850.5	2.37	2.51	3966.6	25.14	696.67	136.2	3.82
Pier 3E	39	9850.5	2.01	2.51	3572.6	18.68	696.67	102.8	3.42
Pier 4E	39	9850.5	1.76	2.51	3283.6	14.70	163.50	109.6	2.81
Pier 5E	39	9850.5	1.28	1.68	1889.8	8.92	15.03	102.6	0.85
Pier 23E	39	9850.5	0.88	1.22	1215.8	4.79	5.88	65.3	0.29
Pier 24E	39	9850.5	0.92	1.22	1250.6	5.19	5.88	70.4	0.31
Pier 25E	39	9850.5	0.97	1.22	1293.3	5.72	5.88	77.1	0.34
Pier 26E	39	9850.5	1.28	1.22	1542.4	9.47	50.59	80.5	1.12
Pier 27E	39	9850.5	1.55	1.22	1741.7	13.40	79.16	102.0	1.43
Pier 28E	39	9850.5	1.55	1.22	1741.7	13.40	79.16	102.0	1.43
Pier 29E	39	9850.5	1.50	1.22	1705.8	12.62	75.78	97.3	1.39

Table 6 - Predicted Scour Depths at Replacement Woodrow Wilson Bridge Using S-SRICOS Method and HEC-18 (100 Year Flood)

Pier No.		M10	M9	M8	M7	M6	M5	M4	M3	M2	M1	Dolphin	V1	V2
Equivalent Pier Width (m)		6.4	6.4	6.4	6.4	6.4	6.4	6.4	6.9	6.9	9.6	13.7	9.6	6.9
Velocity (m/s)		1.80	1.80	1.80	1.80	1.16	1.16	1.16	2.80	2.80	2.80	2.80	2.80	2.80
Water Depth (m)		6.86	6.86	6.86	6.86	3.60	3.60	3.60	13.62	13.62	13.62	13.62	13.62	13.62
Scour Depth (m)	S-SRICOS	3.18	3.18	3.18	1.09	0.37	0.25	0.25	7.47	7.47	7.83	7.50	7.83	6.73
	HEC-18	17.07	17.07	17.07	17.07	17.07	12.31	12.31	26.64	26.64	33.10	17.68	33.10	26.64

Table 7 - Predicted Scour Depths at Replacement Woodrow Wilson Bridge Using S-SRICOS Method and HEC-18 (500 Year Flood)

Pier No.		M10	M9	M8	M7	M6	M5	M4	M3	M2	M1	Dolphin	V1	V2
Equivalent Pier Width (m)		6.4	6.4	6.4	6.4	6.4	6.4	6.4	6.9	6.9	9.6	13.7	9.6	6.9
Velocity (m/s)		2.38	2.38	2.38	2.38	1.65	1.65	1.65	3.60	3.60	3.60	3.60	3.60	3.60
Water Depth (m)		7.62	7.62	7.62	7.62	4.36	4.36	4.36	14.42	14.42	14.42	14.42	14.42	14.42
Scour Depth (m)	S-SRICOS	4.90	4.90	4.90	4.73	2.37	1.99	1.99	8.86	8.86	10.36	10.66	10.36	8.55
	HEC-18	19.29	19.29	19.29	19.29	19.29	14.51	14.51	29.50	29.50	36.67	19.57	36.67	29.50

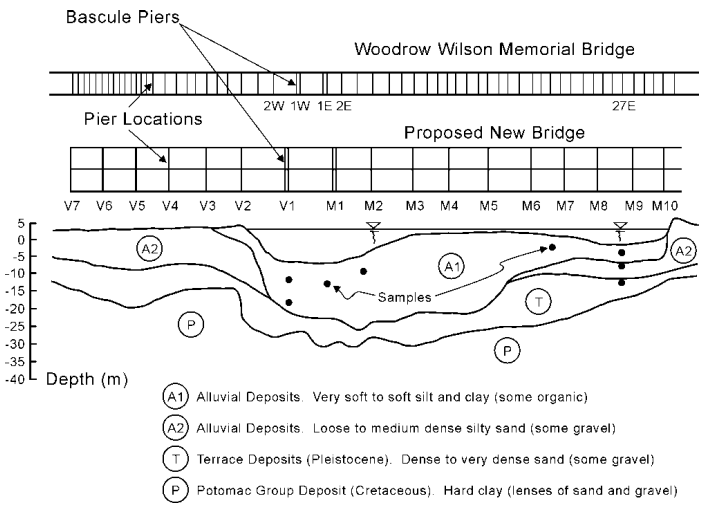

Fig. 1 Estimated Soil Stratigraphy at the Woodrow Wilson Bridge Location

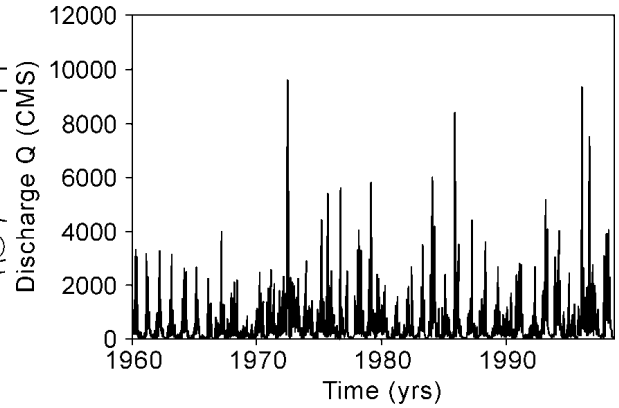

Fig. 3 Discharge Hydrograph at Woodrow Wilson Bridge (01/01/1960-09/31/1998)

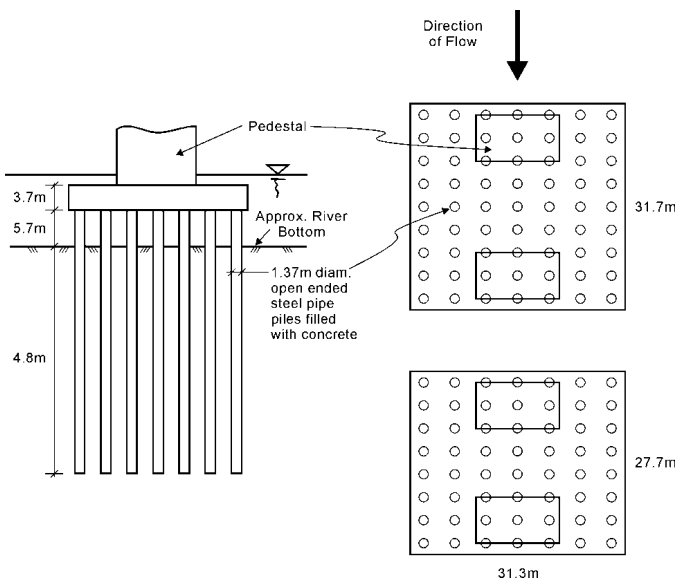

Fig. 2 Foundation of Pier M1 of the Replacement Woodrow Wilson Bridge Considered for Scour Calculations

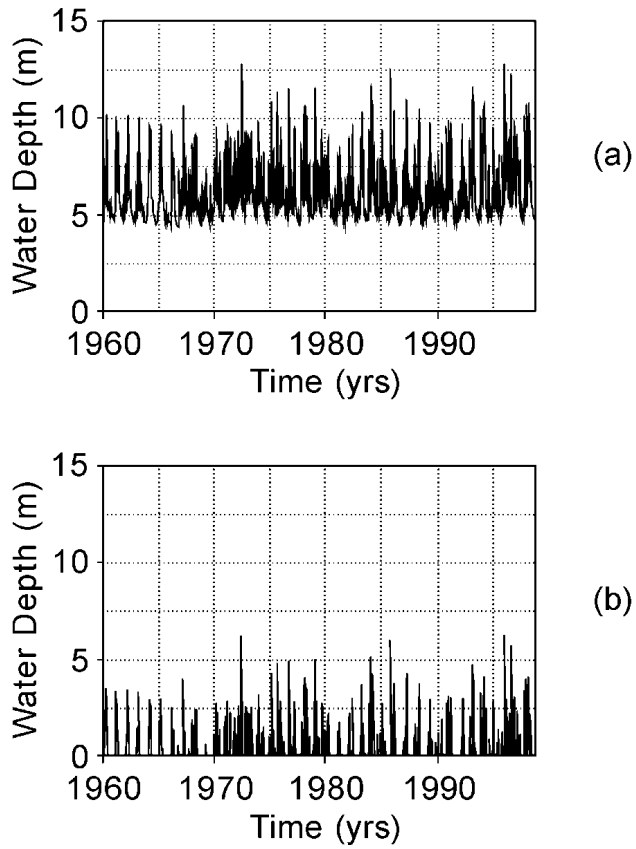

Fig. 4 Water Depth Hydrograph for the Existing Woodrow Wilson Bridge: (a) Pier 1E, (b) Pier 27E

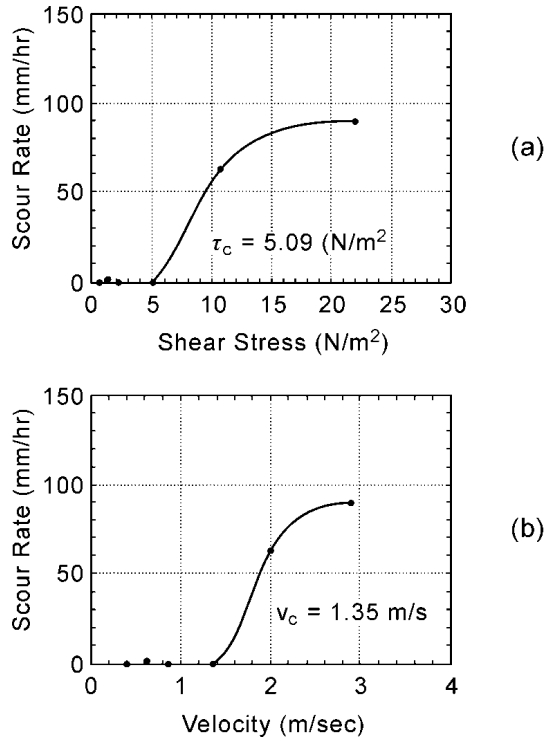

Fig. 5 Erosion Function for a soil sample taken near Pier 27E of the Existing Woodrow Wilson Bridge (2.6 – 3.2 meters depth): (a) Scour Rate vs. Shear Stress, (b) Scour Rate vs. Velocity

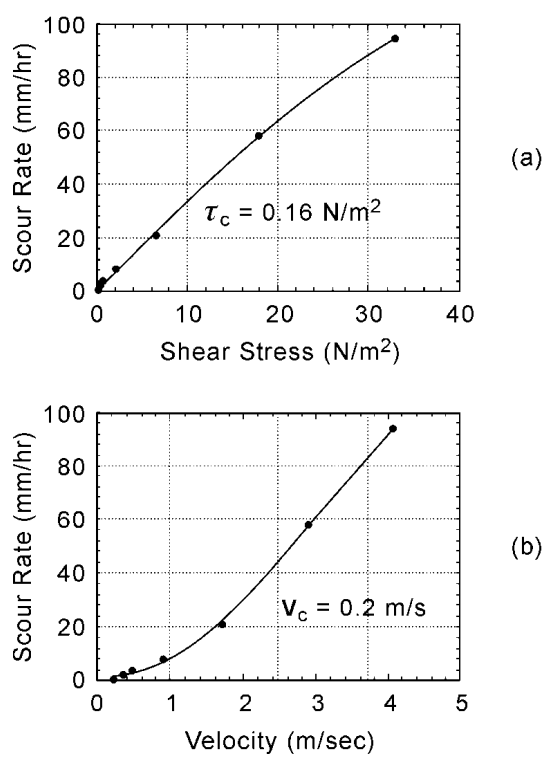

Fig. 6 Erosion Function for a soil sample taken near Pier 27E of the Existing Woodrow Wilson Bridge (11.2 – 11.7 meters depth) : a) Scour Rate vs.Shear Stress, b) Scour Rate vs. Velocity

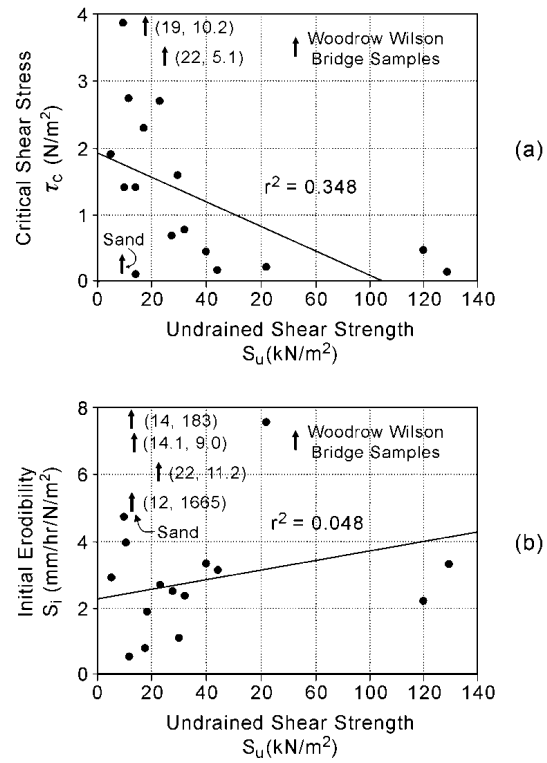

Fig. 7 Lack of Correlation Between Critical Shear Stress, Initial Erodibility, and Undrained Shear Stress (after Briaud et al. 1999 (b))

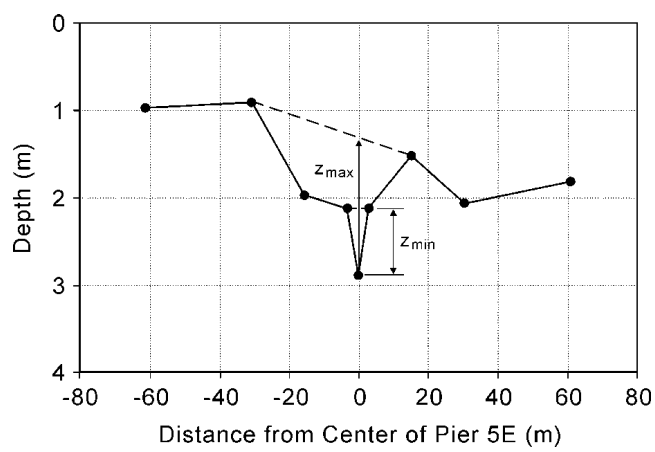

Fig. 8 Potomac River Bottom Profile Around Pier 5E of the Existing Woodrow Wilson Bridge

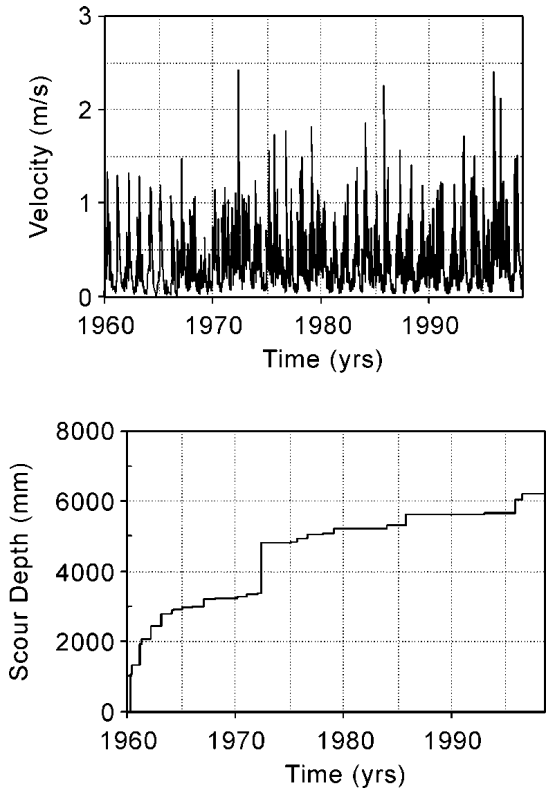

Fig. 9 Velocity Hydrograph and Predicted Scour Depth vs. Time Curve for Pier 1E of the Existing Woodrow Wilson Bridge

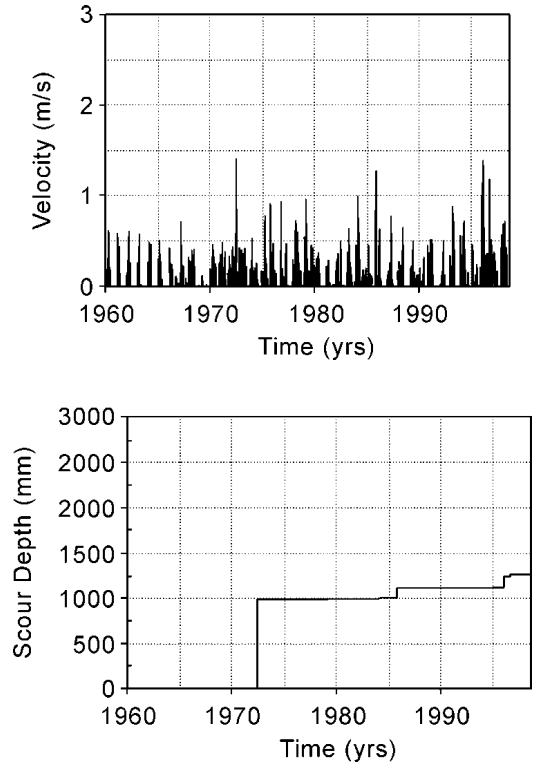

Fig. 10 Velocity Hydrograph and Predicted Scour Depth vs. Curve for Pier 27E of the Existing Woodrow Wilson Bridge

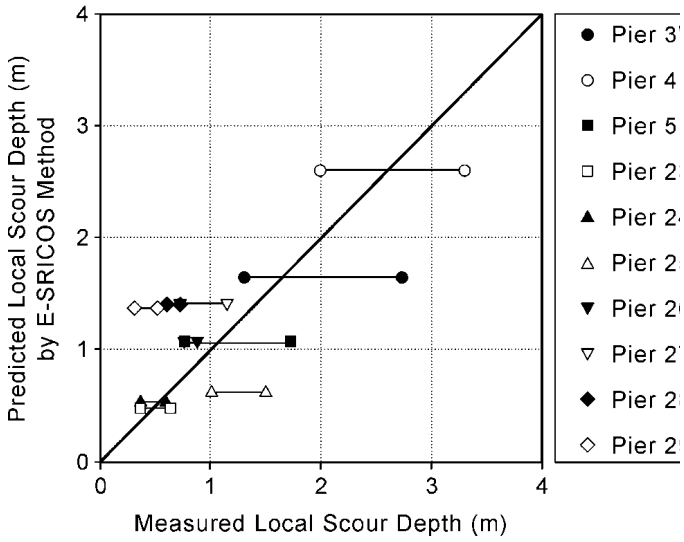

Fig. 11 Comparison of Measured and Predicted Scout Depth (E-SRICOS Method)

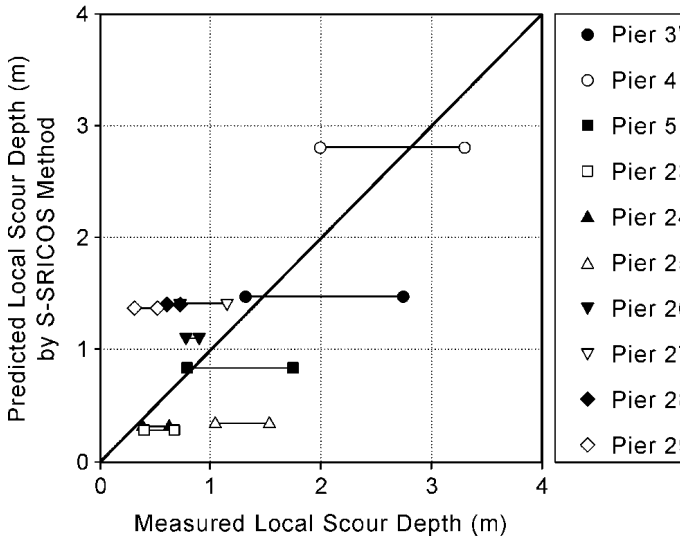

Fig. 12 Comparison of Measured and Predicted Scour Depths (S-SRICOS Method)

Bed Shear Stress Around Rectangular Pier: Numerical Approach

Prahoro Nurtjahyo[1], Hamn-Ching Chen[2], Jean-Louis Briaud[3], Ya Li[1], Jun Wang[1]

ABSTRACT

A Reynold-Averaged Navier-Stokes (RANS) method has been employed in conjunction with a chimera domain decomposition technique for time-domain simulation of flow around a rectangular pier. The main objective of the numerical model is to find the maximum shear stress which exists around the pier at the beginning of the scour process. It is found that for ratios of length (L) over width (B) greater than 1, the maximum shear stress remains constant. There is a significant influence of the effect of L/B on the maximum shear stress for L/B less than 1.

INTRODUCTION

In recent years, computational fluid dynamics (CFD) has quickly become one of the most popular and efficient methods to determine fluid flow behavior in industrial and environmental applications. In the scour research area, some numerical code have been used to simulate flow and scour around vertical pile.

BRIdge Stream Tube model for Alluvial River Simulation (BRI-STAR, Molinas, 1990) is a semi-two-dimensional code that is used to simulate laboratory bridge scour experiments. Hoffman and Booij (1993) applied Duct-model and Sustra-model to simulated the development of local scour holes behind the structure. Olsen and Melaaen (1993) simulated scour 3D around a cylinder by using finite volume SSIIM. The SSIIM model solves Reynold stresses by the $k-\varepsilon$ turbulence model. They observed and reported that there is agreement between the pattern of the vortices in front of the cylinder and the model. Wei et al. (1997) performed a numerical simulation of the scour process in cohesive soils around cylindrical bridge piers. A multi-block Chimera RANS method was incorporated with a scour rate equation to compute scour processes. A linear scour rate equation was assumed in which the scour rate was expressed as a linear function of the streambed shear stress. The simulation captured the important flow features such as the formation of horseshoe vortices ahead of the pier and the flow recirculation behind the pier. Comparison was showing an agreement with experimental data when the model simulated the time history of scour depth. Wei found out that the

[1] *Graduate Research Assistant, Department of Civil Engineering, Texas A&M University*
[2] *Professor, Ocean Engineering Program, Department of Civil Engineering, Texas A&M University*
[3] *Professor, Geotechnical Engineering, Department of Civil Engineering, Texas A&M University*

value of the critical shear stress has a significant influence on the scour process around a cylinder in cohesive soils. Xibing Dou (1997) simulated the development of scour holes around piers and abutments at bridge crossings. A stochastic turbulence closure model which includes an isotropic turbulence has been incorporated into a three-dimensional flow model, CCHE3D. Roulund et al (1998) present a comprehensive description on the flow around a circular pile and the development of the scour by use of a numerical study as well as an experimental study. The numerical model solves the three-dimensional Reynolds averaged Navier-Stokes equations with use of the k-ω turbulence closure model. The method implemented a fully three-dimensional bed load formulation including the effect of gravity.

Briaud et al (2001a, b) proposed a method to predict scour depth versus time curve around a cylindrical bridge pier of diameter D founded on cohesive soils, so called SRICOS-EFA. A series of numerical simulations were performed to develop an equation for the maximum shear stress $\tau_{\max}$ around the pier the scour start to develop. The method has been extended to cover complex single pier which include the effect of water depth, shape, group pier, and attack angle. This paper is part of the development of the new SRICOS-EFA method.

Bed shear stresses in cohesive soils around rectangular piers are presented in this research. The scour equation is incorporated with the 3-D RANS method (Wei et al., 1997) and the procedure of scour calculation will be coupled with the multi-block RANS flow solver (Chen and Chen 1998).

CHIMERA RANS METHOD

In the present study, the Chimera RANS method of Chen and Chen (1998) has been employed for a detailed resolution of the unsteady, viscous flow around a vertical pile. The method solves the Reynolds-Averaged Navier-Stokes equations for incompressible flow:

$$U^i_{,i} = 0 \tag{1}$$

$$\frac{\partial U^i}{\partial t} + U^j U^i_{,j} + \left(\overline{u^i u^j}\right)_{,j} = -g^{ij} p_{,j} + \frac{1}{\mathrm{Re}} U^i_{,jk} = 0 \tag{2}$$

where U^i and u^i represent the mean and fluctuating velocity components, and g^{ij} is conjugate metric tensor, p is pressure, and Re is the Reynolds number based on the pier diameter.

The present method solves the mean and turbulence quantities on embedded, overlapped or matched multiblock. Within each computational block, the finite analytic method of Chen, Patel and Ju (1990) was employed to solve the unsteady RANS equations in general curvilinear, body fitted coordinate system. Both the kinematic and dynamic boundary conditions were implemented on the exact free surface for accurate resolution of the effect of the free surface. The two-layer model of Chen and Patel (1988) was employed for an accurate resolution of the turbulence boundary layer flow including the laminar sublayer and buffer layer in the near wall region. A more detailed description of the chimera RANS method is given in Chen and Chen (1998).

RESULTS AND DISCUSSION

The scour process is highly influenced by the bed shear stress developed by the flowing water at the soil-water interface. When a cylinder obstructs the flow in an open channel with a flat bottom, the maximum shear stress τ_{max} is many times larger than the value given when there is no obstructions. Numerical simulation was performed (Wei et al., 1997) to obtain τ_{max}. It was found that for large water depth ($y/D > 2$), τ_{max} was dependent on the Reynolds number Re, the mean flow velocity V, and the mass density of water ρ. The equation is rewritten as:

$$\text{For a circular pier: } \tau_{\max} = 0.094\rho V^2\left[\frac{1}{\log Re} - \frac{1}{10}\right] \tag{3}$$

where the Reynolds number Re is defined as VD/ν where V is the mean flow velocity, D is the pier diameter, and ν is the kinematic viscosity of water (10^{-6} m^2/s at 20^0C). If this value of τ_{max} is larger than the critical shear stress τ_c that the soil can resist, scour is initiated. As the scour hole deepens around the cylinder the shear stress at the bottom of the hole decreases. Once the scour hole becomes deep enough, the bottom shear stress becomes equal to τ_c (the critical shear stress for the soil), the soil stops scouring, and the final depth of scour z_{max} is reached.

Wei's approach (equation 3) is developed based on the assumption of a single pier and a large water depth so that the effect of free surface on riverbed can be ignored. Further improvement of the code has been done to capture the effect of water depth, the effect of pier spacing, the effect of shape, and the effect of attack angle. A number of parametric studies were performed to determine the relationship between the maximum bed shear stress and the effect of water depth, the effect of spacing, the effect of shape, and the effect of attack angle. In this present study, the objective is to obtain the relationship between the maximum bed shear stress and various rectangular shapes.

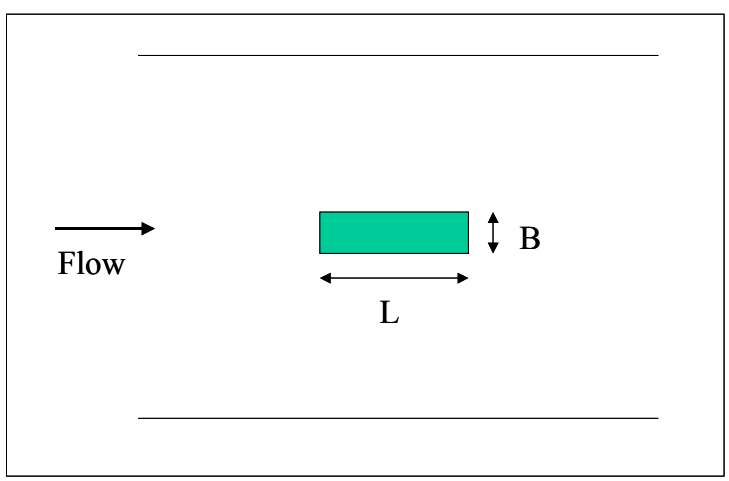

Figure 1. Problem definition

A rectangular pier with a width (B) of 0.061 meter was placed vertically in a 1.5 meter wide flume as shown in figure 1. The flow is a steady flow with a velocity of 0.33 m/s and the water depth is 0.375 meter. Four different pier length L/B=1, 4, 8, 12 are investigated. The value of Reynolds number is obtained based on the width of rectangular pier (Re=20130) and the Froude number based on the width of rectangular pier (Fr=0.4267). In order to reduce the amount of CPU time, a half domain is chosen because of the symmetry. The grid is constructed based on a half domain and divided into 4 blocks. Block#1 has dimensions 12x16x41 grid points in x, y and z direction respectively, Block#2 51x25x41, Block#3 32x16x41, and Block#4 61x7x41. In the case of L/B=1, the grid system is shown in figure 2.

The grid is very fine near the pier and riverbed to be able to apply the two-layer approach of the turbulence model. A few grid layers are placed within the viscous sublayer with the distance from the wall (i.e. pier and riverbed). The closest distance from the wall must satisfy $0.1 < y^+ < 1$, where $y^+ = \mathrm{Re}..u_\tau.y_n$, u_τ is the dimensionless friction velocity at the wall, and y_n is the dimensionless normal distance from the grid layer to the wall.

The velocity vector around pier is shown in figures 3, 4, 5 and 6. The horseshoe vortex system that develops at the base of the pier is the major feature of the flow around the upstream half of the pier. The term “horseshoe” is derived from the shape that the system takes as it wraps around the upstream base of the pier and tails downstream. Two other features to note is the velocity component downward on the front face of the pier and a boundary-layer separation upstream of the pier. The pier redistributes the vorticity normally present in the flow. Most of the vorticity is diffused to the boundaries - namely the bed and the pier surface.

Figure 7, 8, and 9 shows the pressure field induced by the pier. If the pressure field is sufficiently strong, it causes a three-dimensional separation of the boundary layer which in turn rolls up ahead of the pier to from the horseshoe vortex system. A blunt nosed pier is defined as being one which the pressure field induced by the pier is sufficiently strong to form the horseshoe vortex system.

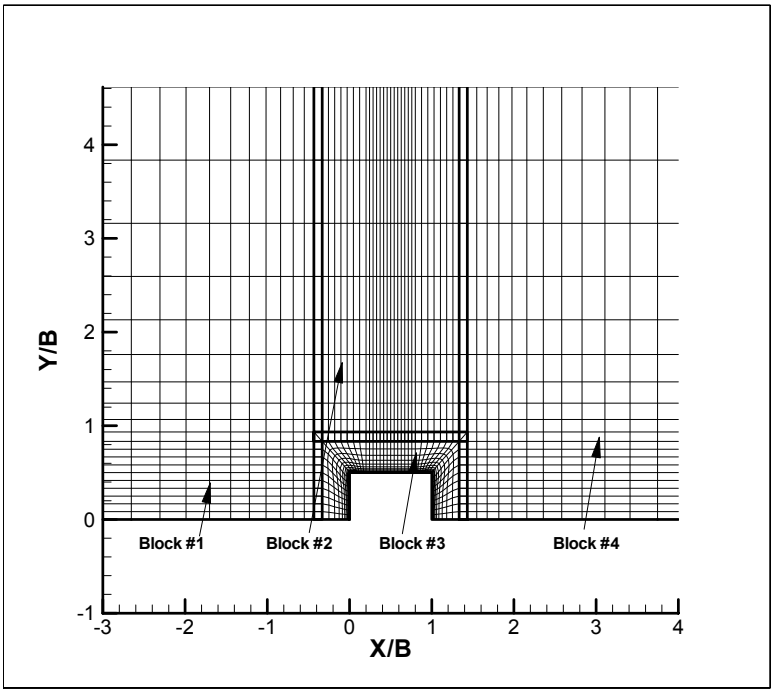

Figure 2. The Grid System for L/B=1

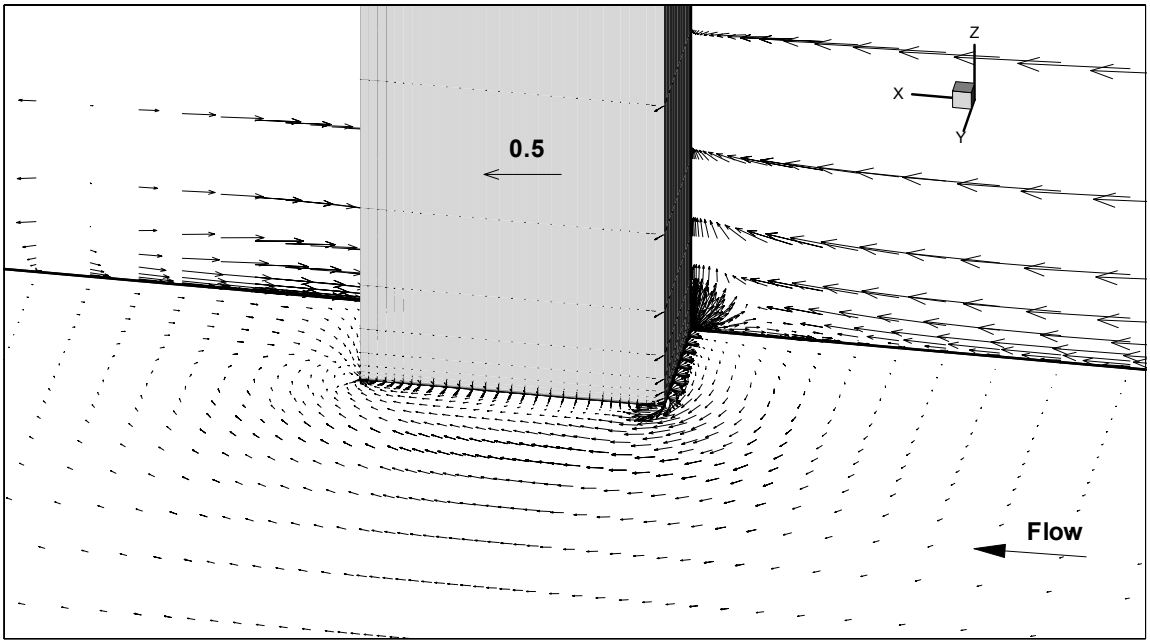

Figure 3. Velocity vector around rectangular pier (L/B=1) at initial condition

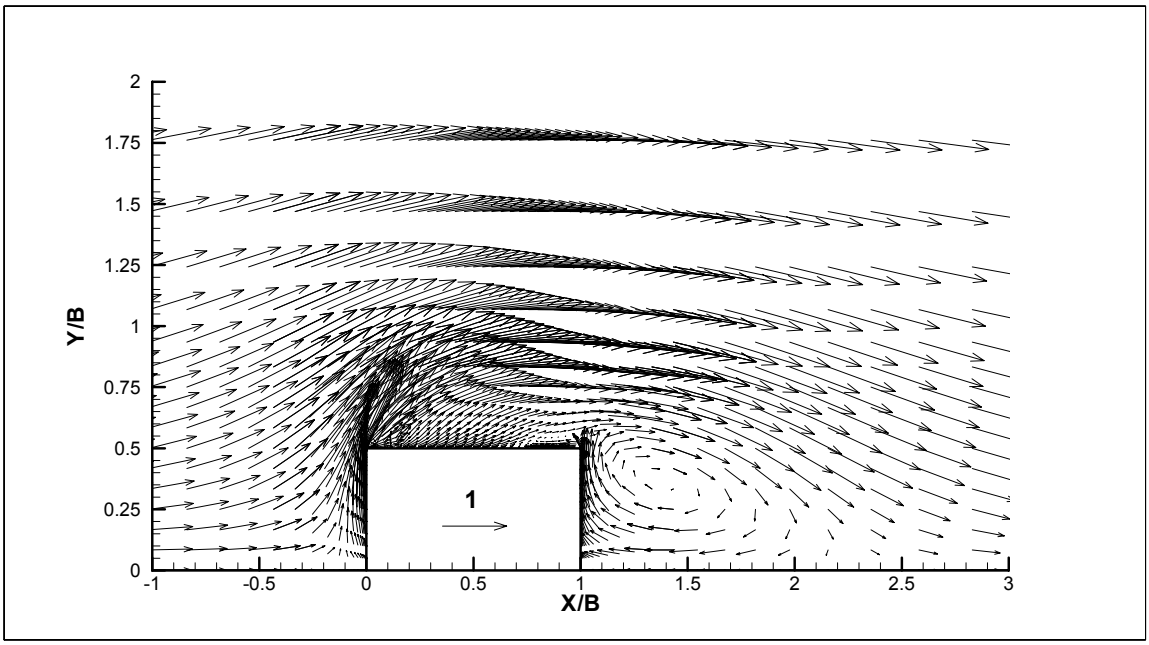

Figure 4. Velocity vector around rectangular pier at free surface (L/B=1)

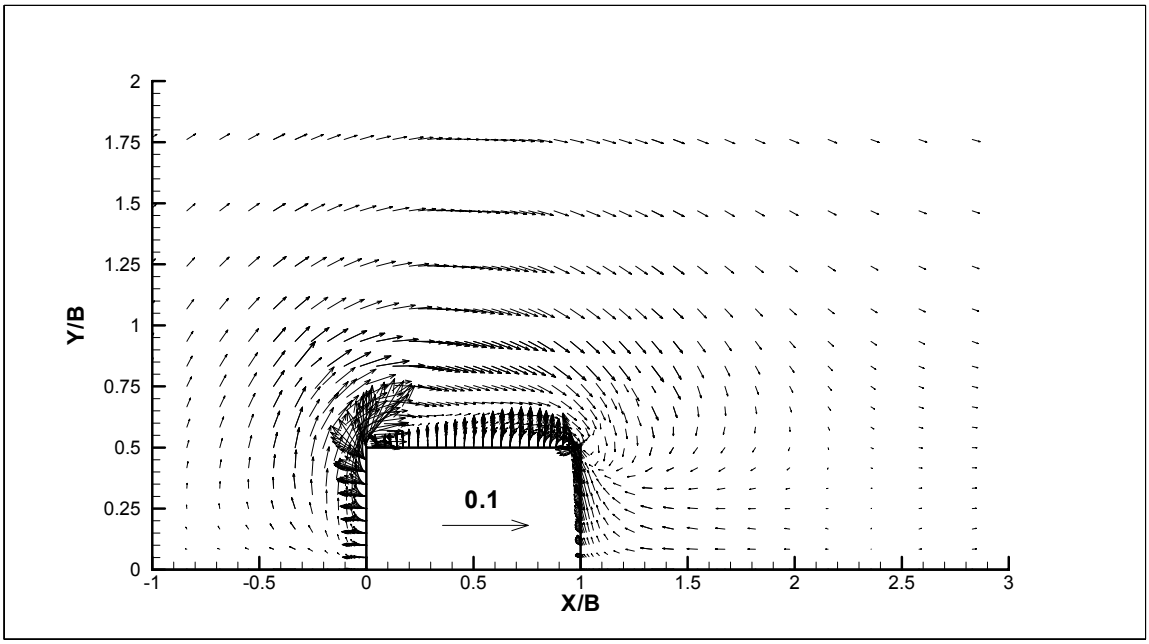

Figure 5. Velocity vector around rectangular pier at z/B=0.0001 above riverbed (L/B=1)

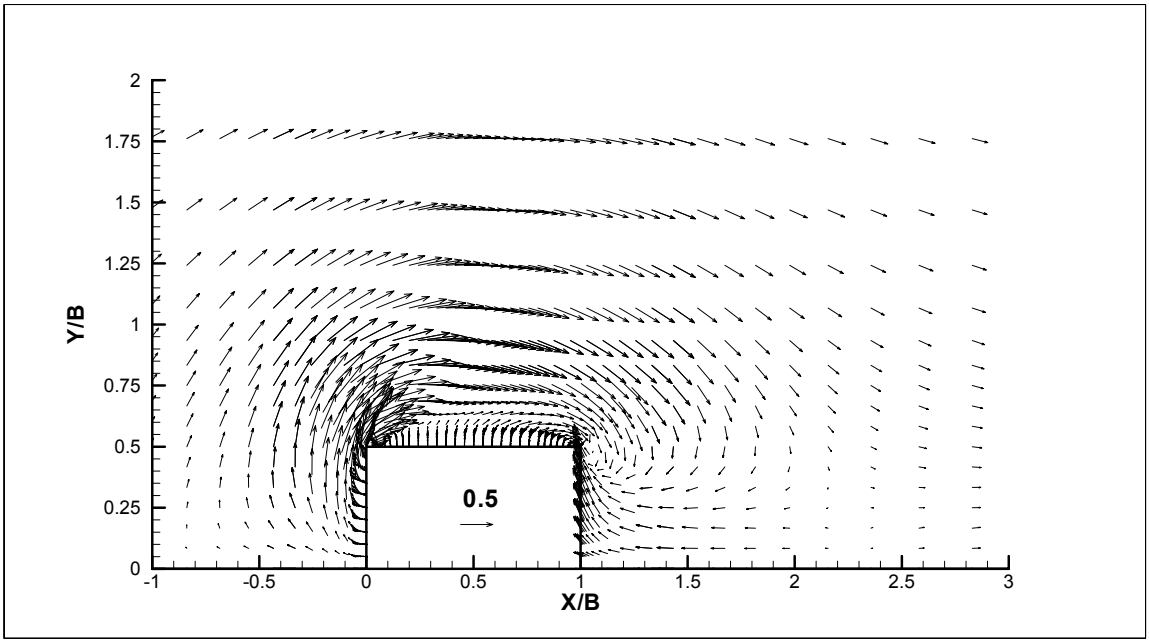

Figure 6. Velocity vector around rectangular pier at z/B=0.004 above riverbed (L/B=1)

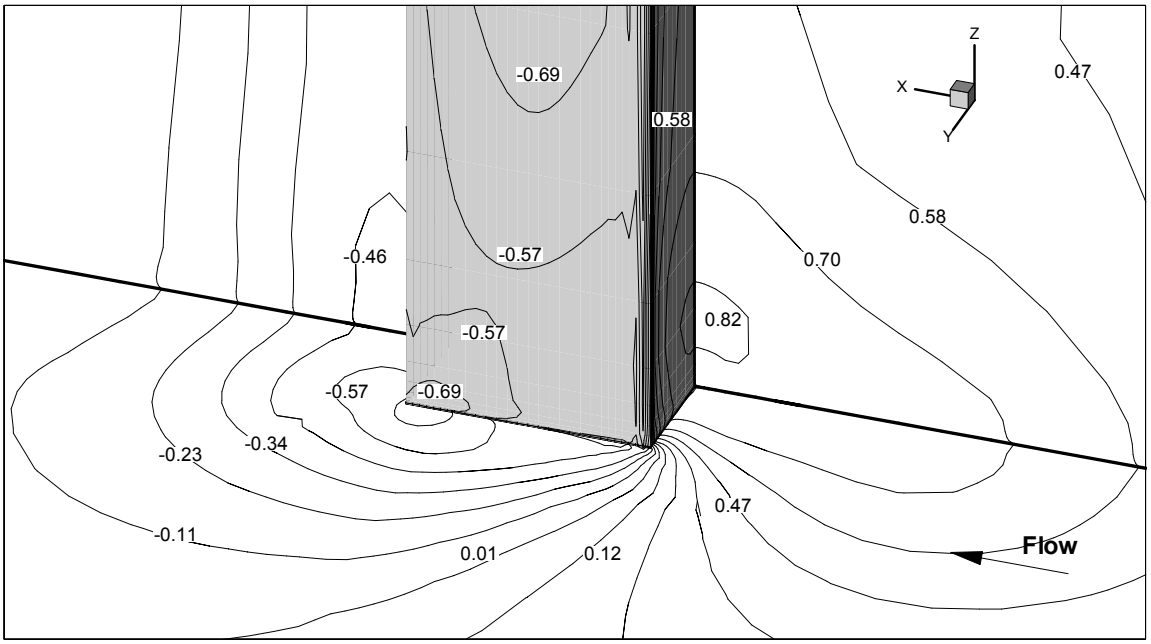

Figure 7. Pressure contour around rectangular pier (L/B=1) at initial condition

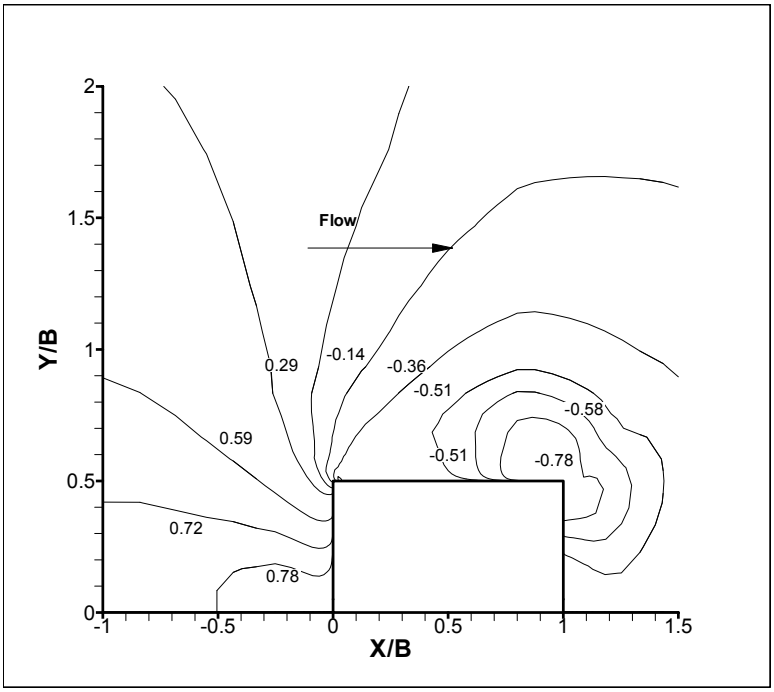

Figure 8. Pressure contour around rectangular pier (at bed) for L/B=1

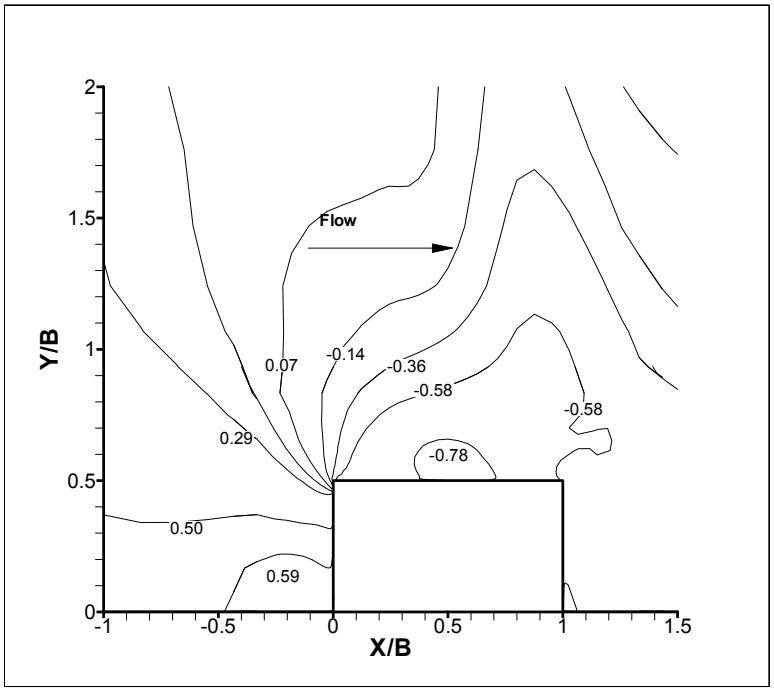

Figure 9. Pressure contour around rectangular pier (at free surface) for L/B=1

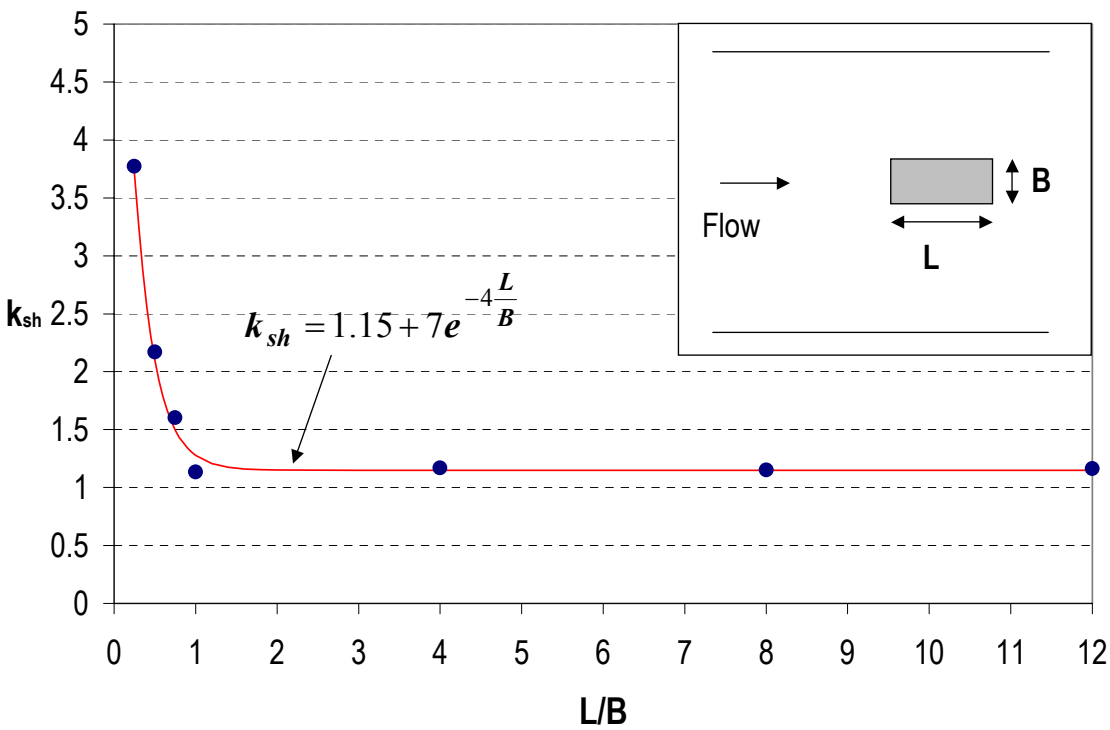

Figure 10. The relation between k_{sh} and **L/B** at deep water (y/D>2), $k_{sh} = \frac{\tau_{\max}}{\tau_{\max}(circle)}$

Figure 10 shows the relationship between the ratio of the maximum bed shear stress and rectangular pier for different L/B. It is found that the correction factor for shape (rectangular shape) is 1.15 only for L/B>1. The value is no longer valid when L/B is less than 1. The flow pattern around the rectangular pier for L/B=0.25 is quite different from the pattern for L/B=4. The flow is separating at the sharp corner. Since the length of pier (L) is smaller than the wide of pier (B), the case of L/B=0.25 allows the flow to go behind the pier while the flow for L/B=4 follows the length of the pier. In the case of L/B=4, the length of separated flow is about B hence we found similar flow behavior for L/B>1. Beyond the separated flow, the velocity remains uniform. On the contrary, for case of L/B<1, there is no region of separated flow and the decreasing pressure behind the pile may increase the velocity around the corner. Bed shear stress contours around the pier are shown in figure 11, 12, 13 and 14 for L/B = 0.25, 0.75, 1, and 4. The difference of flow pattern and pressure around the two rectangular pier (L/B=0.25 and L/B=4) are shown in figure 15, 16, 17 and 18.

The correction factor for the effect of pier shape is k_{sh} defined as $k_{sh} = \frac{\tau_{\max}(L/B)}{\tau_{\max}(circle)} = 1.15 + 7e^{-4\frac{L}{B}}$ for rectangular pier, and for circular pier $k_{sh} = 1$. The equation for maximum bed shear stress around rectangular pier can be written as:

$$\tau_{\max} = k_{sh} 0.094 \rho V^2 \left[\frac{1}{\log \mathrm{Re}} - \frac{1}{10} \right] \tag{4}$$

CONCLUSION

A chimera RANS method has been employed in conjunction for simulating bed shear stress in soils around rectangular pier. A smooth interface was assumed (cohesive soils). The method successfully resolved many important flow features for local scour around bridge piers including the formation of horseshoe vortices. The ratio of length of pier (L) over width of pier (B) may be ignored for L/B greater than 1. However, for L/B less than 1, the effect of L/B becomes significant. The correction factor is included into the equation of bed shear stress to capture the effect of a rectangular pier shape with different L/B ratio.

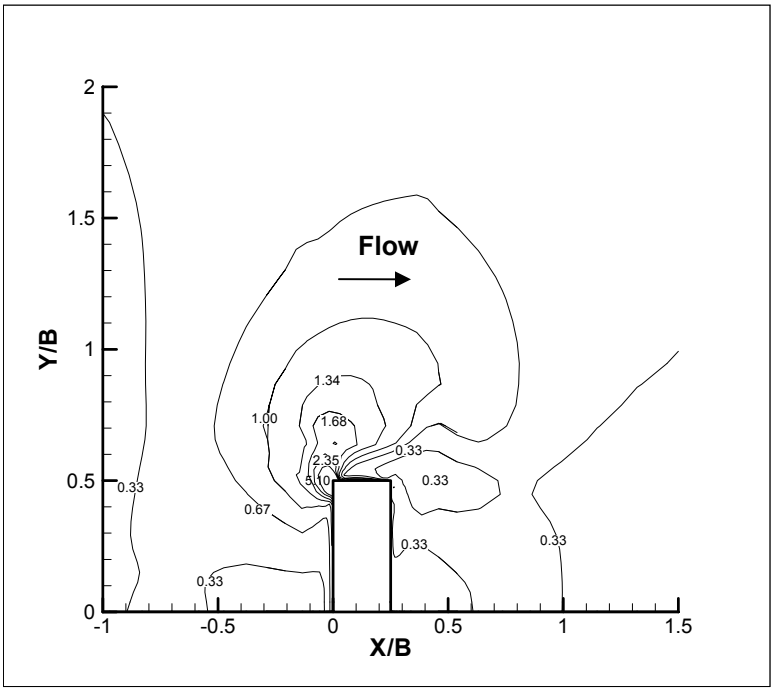

Figure 11. Bed shear stress contour (N/m^2) around rectangular pier for L/B=0.25

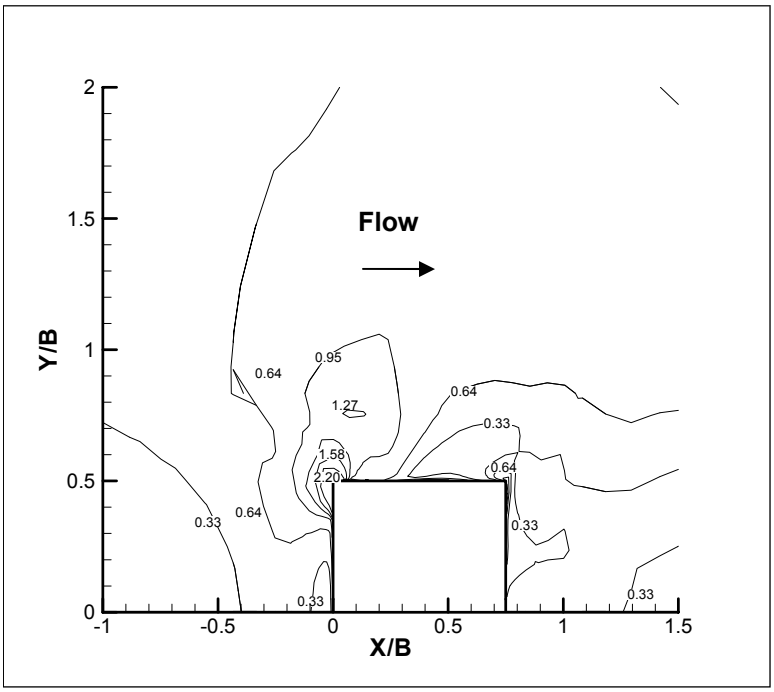

Figure 12. Bed shear stress contour (N/m^2) around rectangular pier for L/B=0.75

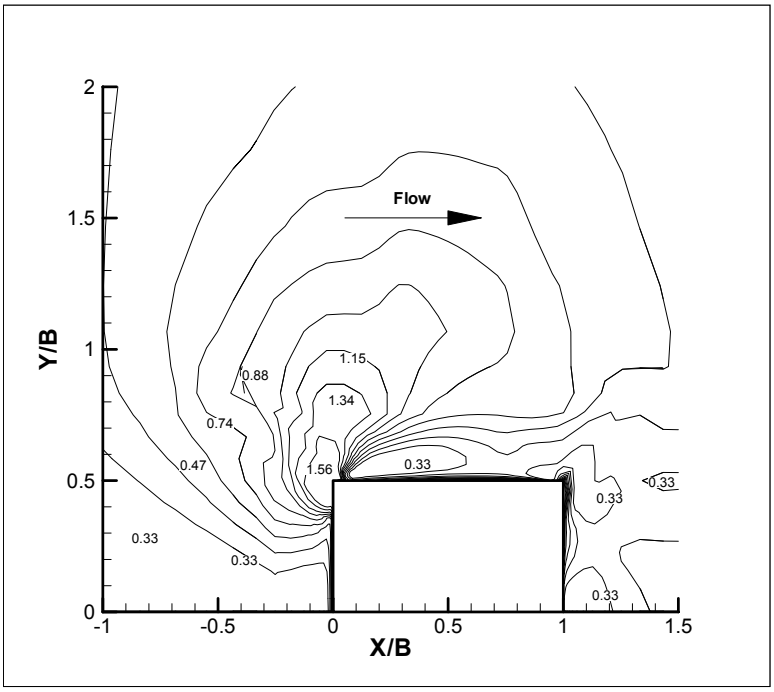

Figure 13. Bed shear stress contour (N/m^2) around rectangular pier for L/B=1

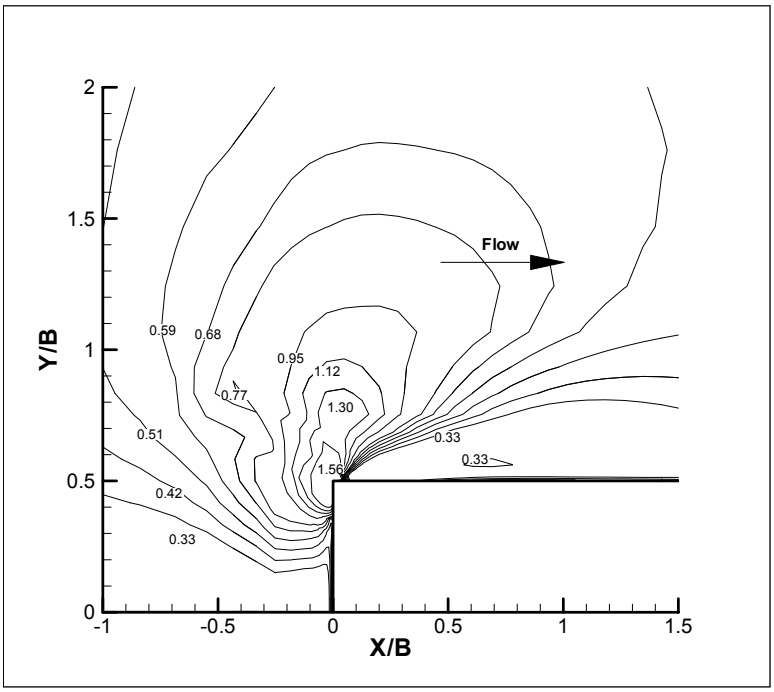

Figure 14. Bed shear stress contour (N/m^2) around rectangular pier for L/B=4

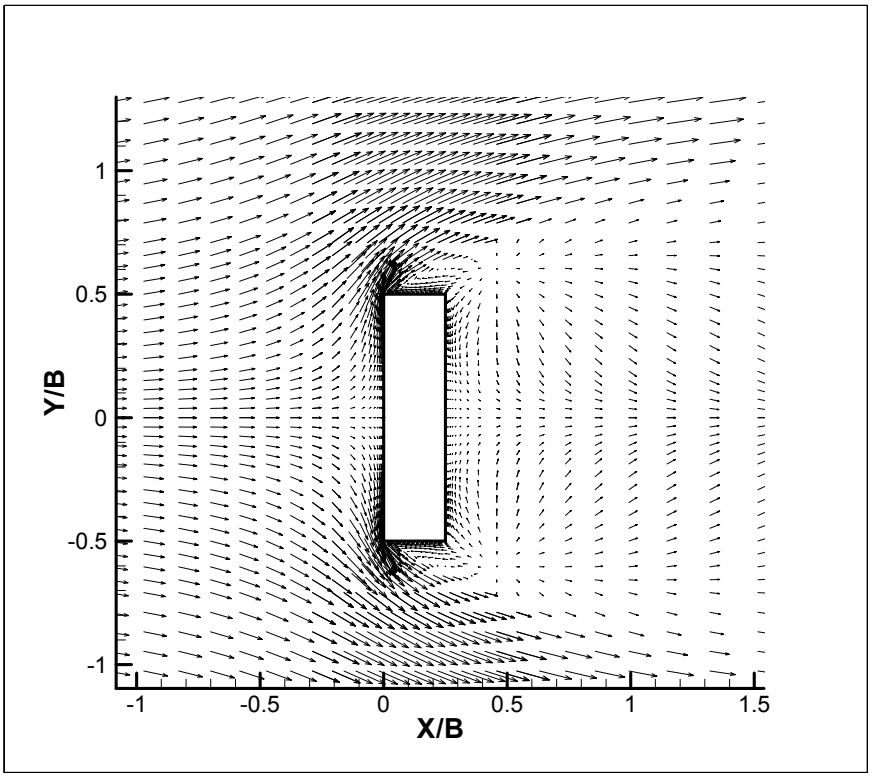

Figure 15. Velocity vector around rectangular pier for L/B=0.25

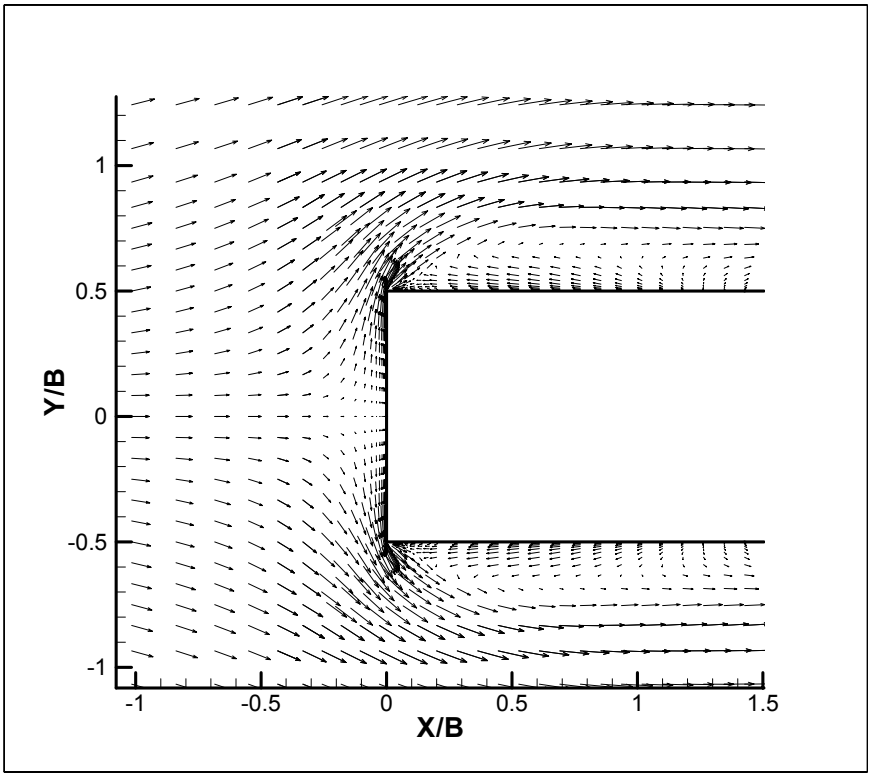

Figure 16. Velocity vector around rectangular pier for L/B=4

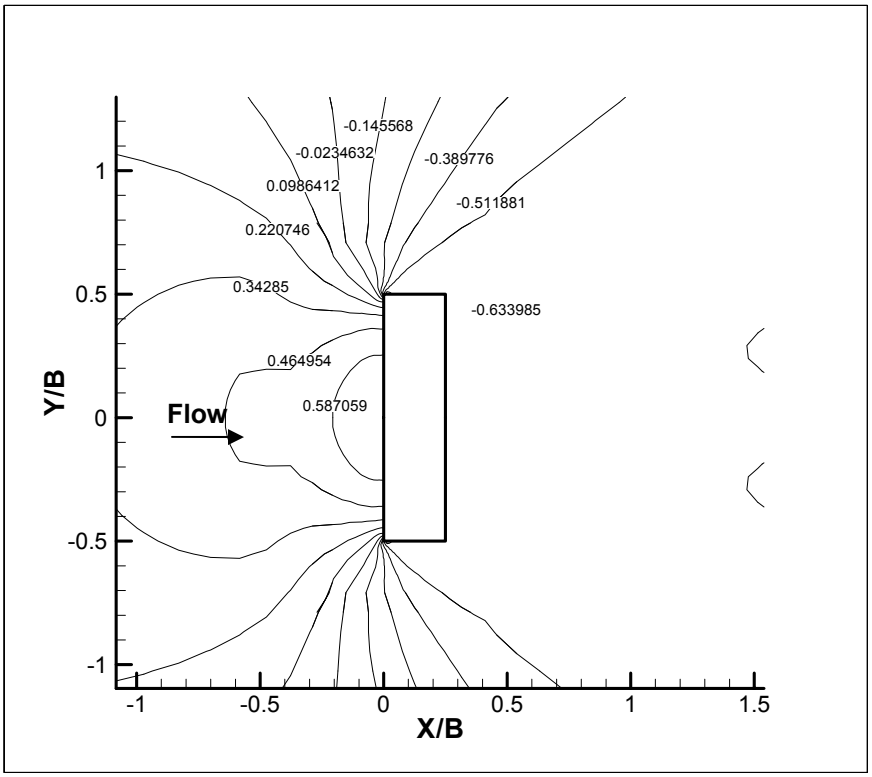

Figure 17. Normalized Pressure ( )contour around rectangular pier for L/B=0.25

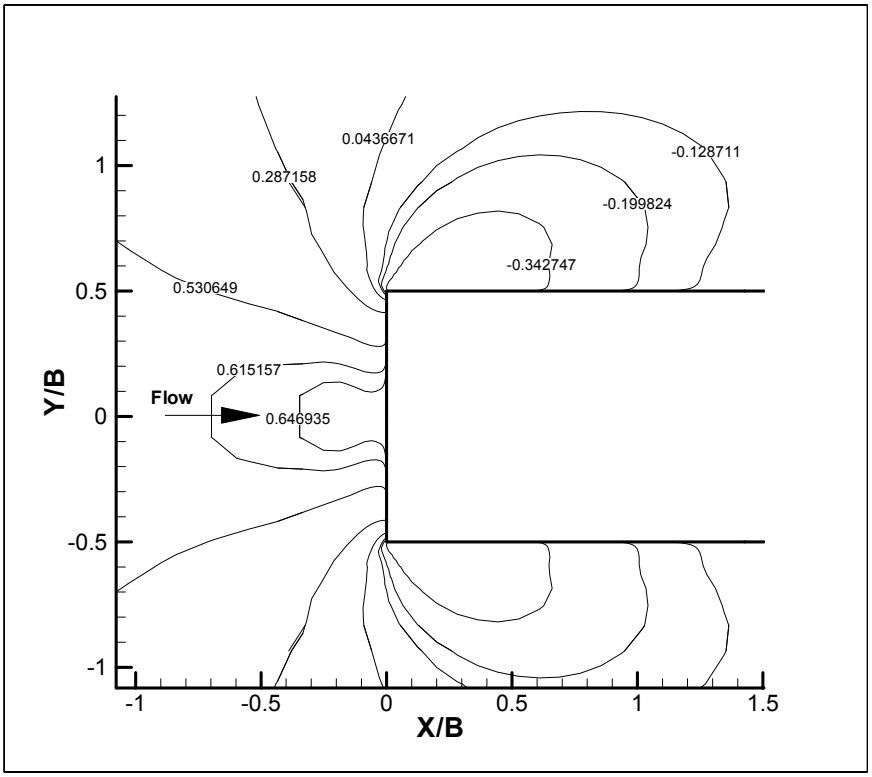

Figure 18. Pressure contour around rectangular pier for L/B=4

ACKNOWLEDGMENT
This work was supported by NCHRP-Project 24-15 where Mr. Tim Hess, the contact person, was very helpful.

REFERENCES

1. Briaud J.-L., Ting F., Chen H.C., Cao Y., Han S.-W., Kwak K., 2001a, "Erosion Function Apparatus for Scour Rate Predictions", Journal of Geotechnical and Geoenvironmental Engineering, Vol. 127, No.2, pp. 105-113, Feb. 2001, ASCE, Reston, Virginia.
2. Briaud J.-L., Chen H.-C., Kwak K., Han S., Ting F., 2001b, "Multiflood and Multilayer Method for Scour Rate Prediction at Bridge Piers", Journal of Geotechnical and Geoenvironmental Engineering, Vol. 127, No.2, pp. 114-125, Feb. 2001, ASCE, Reston, Virginia.
3. Chen, H. C. and Chen, M (1998),"Chimera RANS Simulation of a Berthing DDG-51 Ship in Translational and Rotational Motions." International Journal of Offshore and Polar Engineering, Vol. 8, No.3, pp. 182-191.
4. Chen, H. C. and Patel, V. C. (1988), " Near Wall Turbulence Models fro Complex Flows Including Separation, " AIAA Journal, Vol. 26, No. 6, pp. 641-648.
5. Chen, H. C., Patel , V. C. and Ju, S. (1990),"Solution of Reynolds-Averaged Navier-Stokes Equations for Three-Dimensional Incompressible Flows," Journal of Computational Physics, Vol. 88, No. 2, pp. 305-336.
6. Dou, X. "Numerical Simulation of Three-dimensional Flow Field and Local Scour at Bridge Crossings" Ph.D. Dissertation, 1997, The University of Mississippi.
7. Hoffmans, G. J. C. M. and Booij, R., "Two-dimensional Mathematical Modeling of Local Scour Holes", Journal of Hydraulic Research, Vol. 31, No.5, 1993.
8. Molinas, A. " Bridge Stream Tube Model for Alluvial River Simulation (BRI-STARS)", user's Manual, National Cooperative Highway Reaserch Program, Project No. HR 15-11, Transportation Research Board, 1990, Washington, D. C.
9. Olsen, N. R. B. and Melaaen, M. C. "Three-dimensional Calculation of Scour Around Cylinder", Journal of Hydraulic Engineering, Vol. 119, No. 9, 1993, pp.1048-1054.
10. Roulund, A., Sumer, B. M., Fredsoe, J., and Michelsen, J., "3D Mathematical Modeling of Scour Around A Circular Pile", ISRS 98, December 16-18, 1998, Hong Kong.
11. Wei, G., Chen, H. C., Ting, F, Briaud, J.-L, Gudavalli, S. R. and Perugu, S., "Numerical Simulation to study Scour Rate in Cohesive Soils" Research report to the Texas Department Transportation, 1997, Department of Civil Engineering, Texas A&M University, College Station, TX.

Analysis of Pier Scour Predictions and Real-Time Field Measurements

David S. Mueller and Chad R. Wagner[1]

ABSTRACT

The variability and complexity of site conditions make the development of methodology for predicting scour at bridge piers difficult. Laboratory investigations often oversimplify or ignore many of the complexities that are common in the field. The U.S. Geological Survey, in cooperation with the Federal Highway Administration and many State highway agencies, has collected and compiled 493 field measurements of local pier scour at 79 sites located in 17 States. The pier-scour measurements were used to evaluate 26 published pier scour equations. No single equation conclusively was better than the others, but the top six equations generally appear to be the Froehlich Design, HEC-18, HEC-18-K4, HEC-18-K4Mu, HEC-18-K4Mo (>2 mm), and Mississippi equations. However, comparison of the scour predicted from these equations with the observed scour clearly shows that there is variability in the field data that is not correctly accounted for in the equations. Analysis of laboratory and field data indicated the importance of bed-material characteristics as an explanatory variable in the predictive equations. A new correction to the HEC-18 equation to account for the relative bed-material size is presented.

INTRODUCTION

The lack of and need for reliable and complete field data on scour at bridges has been a recurring conclusion of many researchers (Shen and others, 1969; Melville and others, 1989; Richardson and Davis, 1995). Froehlich (1988), Zhuravljov (1978), Gao and others (1992), and others have compiled field measurements on local pier scour. These historical data sets contain valuable information, but most do not contain information on all of the major variables known to affect scour. Froehlich (1988) was unable to include the effect of sediment gradation in his analysis because many data sets did not include this information. Johnson (1995), in a comparison of seven published pier-scour equations with field data, assumed uniform sediment size because sediment-gradation information was not available for most of the data.

Cooperative research among the Federal Highway Administration (FHWA), State highway departments, and the U.S. Geological Survey (USGS) has allowed the collection of scour data at bridges during floods and has resulted in an extensive data base of local pier-scour measurements. This paper provides a summary of research completed for the FHWA (Mueller and Wagner, in press). A complete evaluation of all equations for the prediction of local scour around bridge piers is beyond the scope of this paper; however, 26 commonly cited pier-scour equations are compared with field measurements of scour to evaluate their potential to be used as

[1] U.S. Geological Survey, 9818 Bluegrass Parkway, Louisville, KY 40299, USA, (dmueller@usgs.gov and cwagner@usgs.gov)

design equations. A design equation should predict scour accurately; however, predicting sediment transport and scour accurately is difficult. If a design equation predicts too little scour the bridge could be under-designed and the traveling public put at risk. A good design equation should be as accurate as possible, but when in error, the equation should overpredict scour to ensure that the design always is safe. In addition, comparison of the field data with commonly published relations from laboratory investigations are presented. Finally, the importance of bed material properties on the depth of scour is shown and a new correction term introduced.

SUMMARY OF FIELD DATA

The 493 local pier-scour measurements in the Bridge Scour Data Management System (BSDMS) (Landers and others, 1996) were filtered, to ensure that the data were representative of the maximum scour that occurred for the recorded hydraulic conditions. The data collection techniques typically limited the data to cross sections along the upstream and downstream edges of the bridge. All measurements where the flow was not aligned with the pier were removed from the data set, because data were seldom collected along the sides of the piers. Where there were measurements along the upstream and downstream edges of the bridge, only the maximum depth of scour was used. All measurements where the effect of debris on the depth of scour was rated "substantial" were removed from the data set. Observations with scour in cohesive material also were removed from this analysis.

The hydraulic parameters measured should be the hydraulic conditions that caused the measured depth of scour. It is difficult to exactly associate hydraulics with a depth of scour because of the temporal development of the scour hole. Except at a few sites, the temporal development of the scour holes reported in the BSDMS is not available. It was rationalized that if the scour hole can be associated reasonably with the reported hydraulic conditions, the velocity at the pier must be competent to erode the bed material. Gao and others (1992) published an equation to compute the critical approach velocity for transport of the bed material at the pier. All measurements having an approach velocity (V_o) less than the critical approach velocity for transport at the pier (V_c') were removed from the data set.

Of the 493 pier scour measurements in the BSDMS, 266 were selected for this analysis. These 266 measurements represent 106 different piers at 53 bridges located in 15 States. A summary of the selected data and commonly used dimensionless variables are provided in Table 1. The maximum and minimum values of the data and of the dimensionless variables represent a range equal to or greater than most laboratory investigations. Unlike laboratory investigations, the distribution of the data cannot be precisely controlled in the field, and the data tend to be grouped near the low end of most of the variables.

DISCUSSION OF EQUATIONS

Local pier scour has been a popular topic of study by many laboratory researchers. A literature review by McIntosh (1989) found that more than 35 equations had been proposed for predicting the scour depth at a bridge pier. Most local-scour equations are based on research in laboratory flumes with noncohesive, uniform bed material and limited verification of results with field

Table 1 - Summary statistics for selected pier-scour measurements.

[D_x is the grain size for which x percent is finer; g is the acceleration of gravity; V_c is the velocity for incipient transport; -- is not applicable]

Variable	Units	Number of Points	Minimum	25th Quartile	Median	75th Quartile	Maximum	Mean	Standard Deviation	Coefficient of Variation	Skewness
Depth of scour (y_s)	m	266	0.00	0.43	0.61	1.19	7.65	1.06	1.19	1.13	2.68
Pier width (b)	m	266	0.38	0.88	1.13	1.52	5.52	1.53	1.11	0.73	1.88
Approach velocity (V_o)	m	266	0.18	0.66	1.14	1.89	4.48	1.36	0.90	0.66	0.94
Approach depth (y_o)	m	266	0.12	2.45	4.39	6.45	20.03	4.86	3.24	0.67	1.18
D_{16}	mm	262	0.03	0.20	0.35	3.78	68.00	5.48	13.26	2.42	3.45
D_{50}	mm	266	0.15	0.48	0.74	8.00	108.00	10.61	20.74	1.95	2.75
D_{84}	mm	262	0.26	1.30	2.35	29.00	233.00	22.36	39.71	1.78	2.91
D_{95}	mm	262	0.28	2.08	7.45	44.00	350.00	34.87	58.85	1.69	2.78
Gradation coefficient (σ_g)	--	262	1.20	2.03	2.30	3.65	21.80	3.21	2.27	0.71	3.17
Drainage area (DA)	km^2	192	166	1197	3680	9402	1805222	32706	135836	4.15	11.80
Slope (S)	m/m	219	0.00010	0.00016	0.00050	0.00105	0.00500	0.00090	0.00103	1.14	1.96
y_o / b	--	266	0.12	1.87	3.05	5.31	13.84	3.91	2.81	0.72	1.21
b / D_{50}	--	266	8.47	129.54	1024.54	1828.80	14224.00	2219.03	3401.47	1.53	2.33
y_s / b	--	266	0.00	0.40	0.58	0.88	2.09	0.68	0.41	0.61	1.01
V_o / V_c	--	266	0.43	0.75	1.14	1.53	4.92	1.32	0.84	0.64	2.15
$V_o / (gy_o)^{0.5}$	--	266	0.04	0.11	0.17	0.33	0.83	0.23	0.16	0.70	1.17

data (McIntosh, 1989). In evaluating and applying scour-prediction equations, it is valuable to know the limitations of the equations, the conditions for which they were developed, how the underlying data were interpreted, and the methods used to develop the equations. Such information about each equation has been published previously in Landers and Mueller (1996), Mueller (1996), and Pritsivelis (1999).

Three approaches have been used to develop equations that predict the maximum depth of scour at a pier. The first approach is to predict the maximum depth of scour that could occur at the bridge pier under any condition. The second approach is to predict, as accurately as possible, the maximum depth of scour for a given set of hydraulic and bed-material conditions. The equations from this approach often are developed by multiple regression analysis and, by definition, underpredict the depth of scour for about one-half of the observations used in the equation development. The third approach is to develop a design equation. A good design equation should predict accurately the scour depth for a given set of site and flood conditions, but when in error, always should error by predicting too much scour.

Analysis of how each equation addresses pier width, approach velocity, approach depth, and bed-material properties provides an indication of the effect of these variables on the depth of scour. The selected equations are formulated into two patterns. The regime equations are written to compute the total depth of flow including local scour. Nonregime equations are written to compute the depth of local scour only. The equation name, reference, and a summary of the basic variables included in the equation are listed in Table 2. The pier width is included in over 75 percent of the equations. The regime equations have an exponent on pier width between 0.2 and 0.25. The exponent on pier width ranges from 0.6 to 0.75 in over one-half of the nonregime equations when the pier width could be isolated. The smaller exponents on pier width for the regime equations are justified because pier width should have less effect on the total depth than on the depth of local pier scour. The exponents on approach velocity range from 0.2 to 0.68 (except for Shen-Maza with an exponent of 2) and on approach depth from 0.135 to 0.75. This variability indicates that there is a lack of agreement among the equations on the effect of approach depth and velocity on the scour depth. The median grain size only is included in 11 equations; it only can be isolated in four equations where it has a small negative exponent.

COMPARISON OF PREDICTIONS WITH FIELD DATA

This evaluation of the selected equations focuses primarily on the capability of the equations to be used as design equations for different site and flood conditions. The objective is to find an equation that accurately predicts the scour depth for the specified conditions, but when in error, overestimates the depth of scour. The capability of the equations to accurately predict the scour depth for the variety of field conditions represented in this data set varies greatly. Some of the equations (Ahmad, Breusers-Hancu, Chitale, Inglis-Poona I, Melville and Sutherland, and Shen-Maza) displayed trends away from the line of equality, indicating those equations do not properly represent the processes responsible for local pier scour in the field. Several equations (Arkansas, Blench-Inglis I, Blench-Inglis II, Froehlich, Shen, and Simplified Chinese) underpredict the scour depth for a large number of the observations and probably should not be considered for design equations. The other equations displayed some trend along the line of

Table 2 - Summary of exponents for variables used in selected equations.
[D_{50} is the median grain size, $\mathbf{F}_p$ is the pier Froude number]

Equation (Reference)	Pier Width	Approach		D_{50}	Other Bed Material
		Velocity	Depth		
Ahmad (1953)		0.667	0.667		
Arkansas (Southard, 1992)		0.684		-0.117	
Blench-Inglis I (Blench, 1962)*	0.25		0.75		
Blench-Inglis II (Blench, 1962)*	0.25	0.5	0.5	-0.125	
Breusers (1965)	1.0				
Breusers-Hancu (Pritsivelis, 1999)	X		X		
Chitale (1962)		X	X		
Froehlich (1988)	0.62	0.2	0.36	-0.08	
Froehlich Design (Froehlich, 1988)	X	0.2	0.36	-0.08	
HEC-18 (Richardson and others, 1993)	0.65	0.43	0.135		
HEC-18-K4 (Richardson and Davis, 1995)	X	X	X	X	X
HEC-18-K4Mo (Molinas, 2000)	X	X	X	X	X
HEC-18-K4Mu (Mueller, 1996)	X	X	X	X	X
Inglis-Poona I (Inglis, 1949)*	0.22	0.52	X		
Inglis-Poona II (Inglis, 1949)*	0.22		X		
Larras (1963)	0.75				
Laursen I (Neill, 1964)	0.7		0.3		
Laursen II (Laursen, 1962)	X		X		
Laursen-Callander (Melville, 1975)	0.5		0.5		
Melville and Sutherland (1988)	X	X	X	X	X
Mississippi (Wilson, 1995)	0.6		0.4		
Molinas (Molinas, 2000)	0.66	X	X	X	X
Shen (Shen and others, 1969)	0.62	0.62			
Shen-Maza $\mathbf{F}_p$<0.2		2.0			
$\mathbf{F}_p$>0.2 (Shen and others, 1969)	0.67	0.67			
Sheppard (Sheppard, University of Florida, written communication, 2001)	X	X	X	X	
Simplified Chinese (Gao and others, 1992)	X	X	X	X	

*Regime equation that in its original form computed total depth including pier scour and approach depth.

X - Equation uses this variable but the equation is complex, and this variable cannot be algebraically isolated.

equality with few underpredictions, but they display a broad scatter of data and often do not accurately predict the observed scour.

Ranking the performance of scour-prediction equations is difficult because of the tradeoff between accuracy and underpredictions. If only accuracy is considered, the sum of squared errors can be used to evaluate the equations performance (Table 3). This statistic shows the Froehlich equation to be the most accurate equation; however, the Froehlich equation is a regression equation and underpredicted the scour depth for 129 of 266 field observations. If the smallest number of underpredictions is used to evaluate the equations, the Froehlich Design equation is the best equation because it underestimated only four observations. The Froehlich Design equation, however, ranked 19th based on the sum of squared errors criteria. The magnitude of the underpredictions is just as important, if not more so, than the number of underpredictions; thus, the sum of squared errors for those observations that were underpredicted is another factor that should be considered in the analysis. The Melville and Sutherland equation had the lowest sum of squared errors for the underpredicted observations, but this equation ranked 26th in overall sum of squared errors. The Melville and Sutherland equation slightly underestimated scour in a few case, but grossly overestimated scour for many cases. The Froehlich Design, HEC-18-K4, HEC-18, HEC-18-K4Mu, and HEC-18-K4Mo (>2 mm) equations all had low sum of squared errors for the underpredicted observations. If all ranks for each equation are totaled, the Froehlich Design equation appears to be the best equation, followed by the HEC-18-K4Mu, HEC-18-K4, HEC-18, Mississippi, and HEC-18-K4Mo (>2 mm) equations; however, the Froehlich Design equation had the largest sum of squared errors for this group. If only the ranks based on the two sum of squared error categories are totaled for each equation, the HEC-18-K4Mu equation is favored and the Froehlich Design equation drops to a rank of 8.5. No single equation conclusively is better than the rest, but the top six equations generally appear to be the Froehlich Design, HEC-18, HEC-18-K4, HEC-18-K4Mu, HEC-18-K4Mo (>2 mm), and Mississippi equations.

Because no single equation was superior to the others and none of the equations accurately predicted the scour for all site and hydrologic conditions, it is important to assess where the equations failed. Residuals of selected equations were compared with Froude number ($V_o/(gy_0)^{0.5}$), relative velocity (V_c/V_o), median grain size (D_{50}), pier width (b), relative bed material size (b/D_{50}), and relative depth (y_o/b) to assess where the equations may fail to properly account for the scour processes (Mueller and Wagner, in press). The Froehlich equation displayed no clear patterns. The Froehlich equation, which is a regression equation, fit the data reasonably well; however, to convert the Froehlich equation from a regression equation to a design equation Froehlich added the pier width as a safety factor. The safety factor increases the scatter in the data. A comparison of residuals versus pier width showed that the safety factor became too large as the pier width increased. The HEC-18-K4 equation showed patterns of increasing overprediction as Froude number (0-0.4), median grain size, and pier width increased. The K_4, proposed by Mueller (1996), reduced the effect of the Froude number and median grain size, but patterns still were evident in the pier width. Only pier width displayed a pattern in the residuals of the Mississippi equation. Another revised HEC-18 equation, HEC-18-K4Mo, (Molinas, 2000) also showed patterns in the residuals with Froude number and median grain size, but the most dominant pattern was the bottom envelope on the pier width. Most underpredictions

Table 3 - Summary of the performance of the selected pier-scour equations.
[SSE, sum of squared errors]

				Number of Under Predictions				Summation of Ranks			
				Count		SSE		All Ranks		SSE Ranks	
Equation	**Number of Observations**	**SSE Magnitude**	**Rank**	**Number**	**Rank**	**Magnitude**	**Rank**	**Total**	**Rank**	**Total**	**Rank**
Ahmad	266	7536.86	27	61	14	159.48	22	63	23	49	25.5
Arkansas	266	239.52	4	74	20.5	165.61	23	47.5	20	27	16
Blench-Inglis I	266	265.83	5	74	20.5	52.14	17	42.5	18	22	11
Blench-Inglis II	266	954.55	17	174	27	824.60	27	71	25	44	23
Breusers	266	670.40	13	18	9.5	7.14	9	31.5	7.5	22	11
Breusers-Hancu	266	1205.60	21	77	22	201.18	25	68	24	46	24
Chitale	266	2299.40	25	90	23	169.37	24	72	26	49	25.5
Froehlich	266	160.67	1	129	26	98.24	21	48	21	22	11
Froehlich Design	266	1067.77	19	4	1	1.51	2	22	1	21	8.5
HEC-18	266	822.38	15	13	7	2.16	4	26	4.5	19	4.5
HEC-18-K4	262	791.54	14	15	8	1.93	3	25	3	17	2
HEC-18-K4Mo (All)	266	495.18	11	65	16	17.01	13	40	15.5	24	13
HEC-18-K4Mo (> 2 mm)	266	608.79	12	21	11	2.47	6	29	6	18	3
HEC-18-K4Mu	266	448.53	9	18	9.5	2.23	5	23.5	2	14	1
Inglis-Poona I	266	1758.81	24	119	25	597.74	26	75	27	50	27
Inglis-Poona II	266	229.68	3	72	19	45.67	16	38	12	19	4.5
Larras	266	311.13	7	48	13	72.09	20	40	15.5	27	16
Laursen I	266	1277.71	23	6	2	5.20	8	33	10	31	21
Laursen II	266	930.57	16	9	3.5	10.95	12	31.5	7.5	28	18
Laursen-Callendar	266	960.55	18	9	3.5	10.39	11	32.5	9	29	19.5
Melville & Sutherland	262	3092.08	26	28	12	1.45	1	39	13.5	27	14
Mississippi	266	465.05	10	12	6	7.90	10	26	4.5	20	6
Molinas	262	199.79	2	103	24	55.96	18	44	19	20	7
Shen	266	300.77	6	69	18	37.00	15	39	13.5	21	8.5
Shen-Maza	266	1133.23	20	67	17	36.90	14	51	22	34	22
Sheppard	262	1276.04	22	11	5	3.89	7	34	11	29	19.5
Simplified Chinese	254	344.46	8	62	15	56.21	19	42	17	27	16

occurred for grain sizes less than 2 mm. Two thirds of the under predictions by HEC-18-K4Mo occur at grain sizes less than 2 mm (Table 3). Limiting the K_i and K_4 bed material corrections to median grain sizes greater than 2 mm, improves the performance of the Molinas correction.

COMPARISON OF LABORATORY EXPERIMENTS WITH FIELD DATA

Laboratory research has been the primary tool in defining the relation among variables affecting the depth of pier scour. The validity of these relations has not been proven in the field. Landers and Mueller (1996) evaluated many relations developed in the laboratory by use of transformed data (to obtain a more normal distribution) and smoothing techniques to assess general trends in the data. They found only minimal agreement between the field data and laboratory-based relations. The assessment presented herein investigates the relations in the field data for variable combinations commonly reported by laboratory investigations. Unlike the data set used by Landers and Mueller (1996), all data at skewed piers were removed to prevent bias by these data, as previously discussed. No transformations were applied unless necessary for consistency with published relations. Whereas this lack of transformation results in a less uniform distribution of the data, this approach benefits from a more direct comparison with laboratory work.

Relative Velocity

Through a series of laboratory experiments, Chiew (1984) found relative scour depths (y_s/b) were less for ripple-forming sediments than for nonripple-forming sediments at relative velocities (V_o/V_c) ranging from 0.6 to 2. He determined that this reduction in scour depth was caused by the roughness and sediment transport associated with the formation of ripples near incipient motion. The upper envelope of the field data generally fit the curves developed by Chiew (1984) (Fig. 1). The maximum relative scour depth observed in the field does not appear to be strongly affected by whether the sediment is ripple forming or nonripple forming. The scatter of data below the envelope curves indicates that the relation between relative scour depth and relative velocity developed in the laboratory does not explain adequately the scour processes in the field.

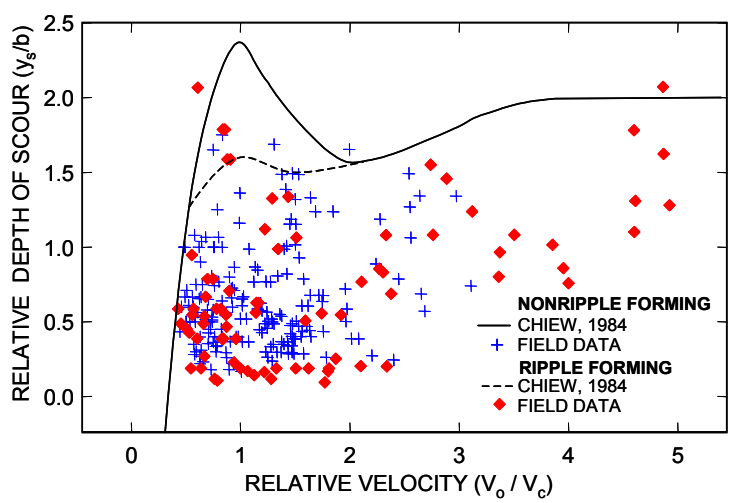

Fig. 1 - Comparison of field observations with the curves developed by Chiew (1984) showing the effect of sediment size and relative velocity on relative depth of scour.

Baker (1986) also investigated the effect of bed-material properties on the relation between relative scour depths and relative velocity, in the laboratory. Baker (1986) used nonuniform bed material characterized by the coefficient of gradation. He found that as the

coefficient of gradation increased, the relative scour depth was reduced and the maximum scour occurred at a relative velocity greater than one. The field data categorized by the coefficient of gradation are shown in Fig. 2 with hand-drawn envelope curves for the four categories of gradation. The effect of gradation has no consistent pattern in the relation between normalized scour depth and relative velocity for the field observations.

Baker (1986) changed the gradation while maintaining a constant D_{50} during his experiments. To simulate a constant D_{50} in the field data, Mueller (1996) used partial residuals to remove the effect of D_{50} from the field data. Mueller's approach did not improve the comparison between the field data and the laboratory observations by Baker (1986).

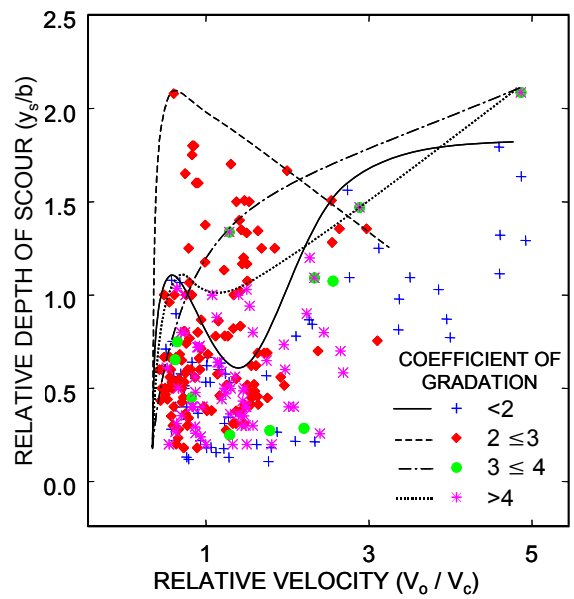

Fig. 2 - Effect of gradation and relative velocity on relative depth of pier scour for field data, with hand-drawn envelope curves for selected gradation classes.

Bed-Material Parameters

The scale of laboratory experiments prevents the effect of relative sediment size (b/D_{50}) on relative scour depth from being directly compared with field conditions. The maximum relative sediment size obtained in the laboratory was about 800. In the laboratory, ripple-forming sediments had lower relative scour depths than nonripple-forming sediments for relative sediment sizes ranging from 100 to 800. The field data do not contain ripple-forming sediments with a relative sediment size less than 900 (Fig. 3); therefore, there is insufficient overlap between laboratory and field data to make a valid comparison. The field data show a cluster of ripple-forming sediments near a relative sediment size of 1,000 that is below the maximum relative scour for nonripple-forming sediments; however, the maximum relative scour depth for ripple-forming sediments with relative sediment sizes of 4,000 exceeds the nonripple-forming sediments.

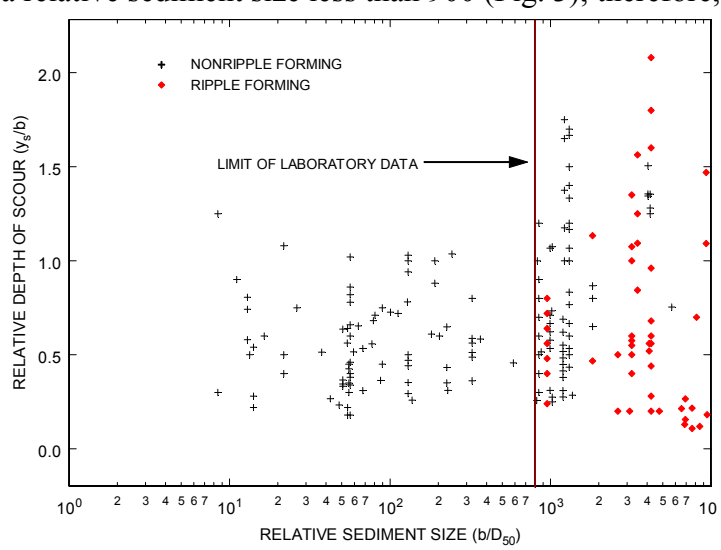

Fig. 3 - Effect of relative sediment size on relative depth of pier scour for field data.

Ettema (1980) recognized that although maximum scour depth was 2.4 times the pier width for uniform sediments; this maximum

depth was affected by the gradation of the bed material for nonuniform bed materials. Ettema used a series of laboratory experiments to develop a correction factor to account for the gradation of the bed material on the maximum scour depth. Hand-drawn envelope curves in Fig. 4 show that the relative scour depth for field data is greater for ripple-forming sediments than for nonripple-forming sediments when the gradation coefficient is less than about 2.5. For gradation coefficients greater than 2.5, there is a reduction in the relative scour depth for all observations. The reduction in the relative scour depth is larger for ripple-forming sediments than for nonripple-forming sediments. An increase in the coefficient of gradation for a constant median grain size results in an increase in the coarser size fractions of the bed material. An increase in the coarse size fractions of the bed material reduces the scour depth, thus, the scour depth is dependent on the size distribution of nonuniform bed material. The larger reduction in scour for ripple-forming sediments may be caused by armoring of the scour hole by the coarser size fractions; however, the small amount of ripple forming data for the larger gradations may make any conclusions questionable.

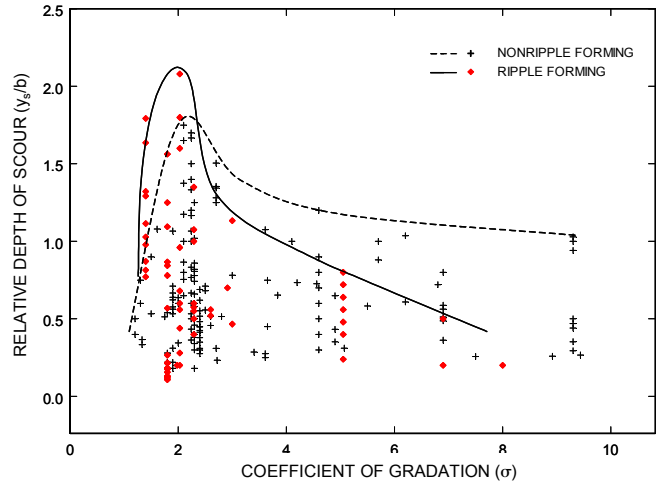

Fig. 4 - Effect of the coefficient of gradation on relative depth of pier scour for field data with hand-drawn envelope curves of ripple and nonripple forming sediments.

Depth of Approach Flow

Most researchers agree that for constant velocity intensity, local pier scour increases as depth of flow increases, but as the depth of flow continues to increase, the scour depth becomes almost independent of flow depth (Breusers and others, 1977; Ettema, 1980; Chiew, 1984). Chiew (1984) plotted data that he collected along with experimental data from Shen and others (1969), Ettema (1980), and Chee (1982) and concluded that the flow depth does not affect scour if the depth is greater than four times the pier width. From this research, Melville and Sutherland (1988) developed a correction factor for the relative depth of flow, $K_{y,}$. The relation between relative flow depth and relative scour depth for the field data is shown in Fig. 5. Although the curve for the K_y factor envelops the data to the right, the data do not follow the trend of the curve. Most laboratory data are collected at or near incipient motion. To better compare the field data with the laboratory data, sediment transport conditions near incipient motion ($0.8 < V_o/V_c < 1.2$) were selected and compared to the curve. Again, the field data did not follow the trend observed in the laboratory data; the data indicated that the relative scour depth tends to increase with increasing relative flow depth.

EVALUATION OF THE K_4 FACTOR

An evaluation of the performance of the HEC-18 equation for various sediment transport conditions and sediment sizes clearly show the need to provide a correction to the HEC-18 equation for coarse bed materials, K_4. An idealized K_4 was computed as the observed scour depth divided by the HEC-18 computed scour depth and compared to the armor potential, the sediment transport in the approach, and to the general size class of the median grain size (Fig. 6). The flow capacity to transport the D_{95} sediment size at the pier (estimated using Gao and others, 1992) was used to estimate armor potential. The armor potential was assumed to be high if the D_{95} sediment size could not be transported. It is clear that the HEC-18 equation tends to overpredict the scour depth for the larger size classes of sediment more than the sand-size class for which it originally was developed (Fig. 6). Therefore, the addition of a K_4 factor to account for grain size in the HEC-18 equation is justified.

The K_4 factor in the HEC-18-K4 equation was introduced in the third edition of HEC-18 (Richardson and Davis, 1995) to account for the bed material size characteristics that were missing from the original HEC-18 equation. The relation for that version of K_4 was derived by the FHWA from preliminary laboratory data provided by Molinas and it was intended as an interim adjustment factor until more detailed analyses were available. The sum of squared errors only was reduced from 822 to 791 (Table 3) by the inclusion of the K_4 term presented in the third edition of HEC-18.

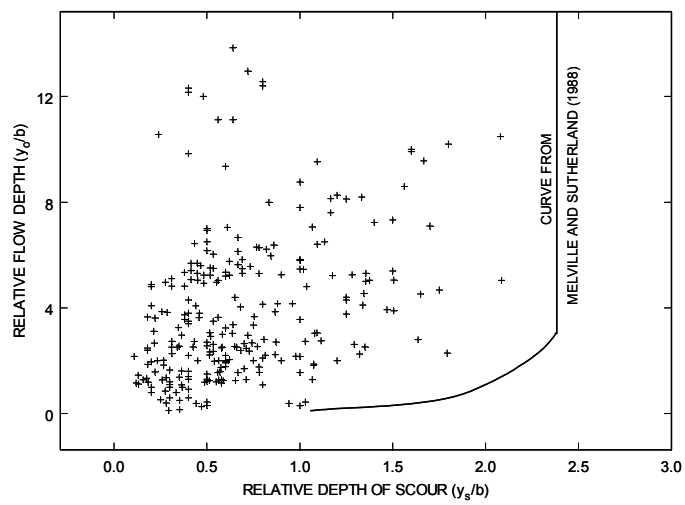

Fig. 5 - Effect of relative flow depth on relative depth of pier scour with field data compared to the relation presented by Melville and Sutherland (1988).

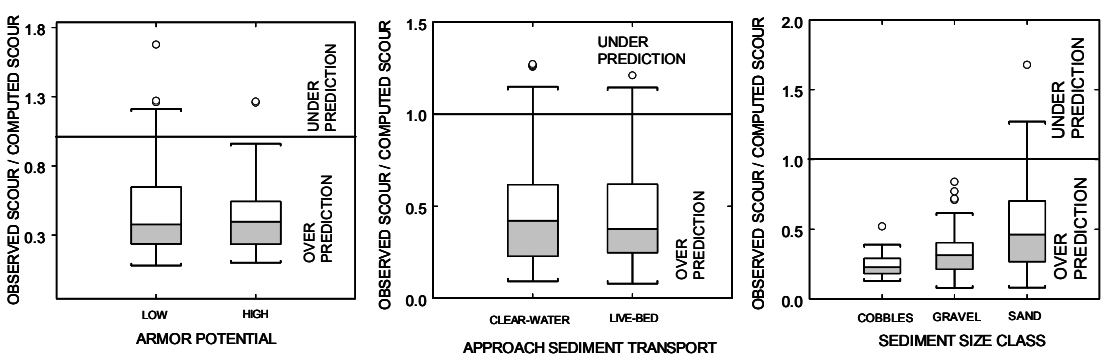

Fig. 6 - Box plot of the variation in the ratio of the observed scour to computed scour from the HEC-18 equation (idealized K4) for armor potential conditions, approach sediment transport conditions, and sediment size classes.

Molinas (2000) derived a new correction to the HEC-18 equation from his final laboratory data set (HEC-18-K4Mo equation). Although this new correction provided a significant decrease in the sum of squared errors (from 822 to 495), it also increased the number of observations that were underpredicted (from 13 to 65). Most of these underpredictions occurred at D_{50} less than 2 mm. If the correction developed by Molinas only is applied to D_{50} greater than 2 mm (HEC-18-K4Mo (>2 mm) equation), its performance was enhanced greatly. The sum of squared errors rose to 609 but the number of observations underpredicted dropped from 65 to 21 and the sum of squared errors for the underpredictions was reduced from 17 to 2.47.

Mueller (1996) developed a relationship for K_4 based on field data. The fourth edition of HEC-18 (Richardson and Davis, 2001) adopted Mueller's K_4 (HEC-18-K4Mu equation) but restricted the lower limit to 0.4 and required a value of 1 if D_{50} was less than 2 mm or D_{95} was less than 20 mm. These restrictions were applied to the evaluation of this factor in Table 3 (HEC-18-K4Mu). Table 3 indicates that Mueller's K_4 factor as adopted in the fourth edition of HEC-18 reduced the sum of squared errors significantly from 822 to 448 (Table 3). Although Mueller's 1996 K_4 factor worked well for the available field data, the formation of the equation causes it to be indeterminate for some situations and behave contrary to logic in others. The equation becomes indeterminate if the velocity for incipient motion of the D_{50} grain size is smaller than the approach velocity needed to scour the D_{95} grain size at the pier. The equation behaves contrary to logic if the D_{50} grain size is held constant and only the D_{95} is varied. In this situation, K_4 increases as D_{95} increases. In the field, variables tend to change together as a system, whereas in the laboratory selected variables can be held constant and other variables can be changed arbitrarily. For the field data used by Mueller (1996) to develop the K_4 factor, an increase in D_{95} always corresponded to an increase in D_{50}. Under these conditions, the relation for K_4 proposed by Mueller (1996) provides a reasonable envelope curve but it can produce illogical results caused by the arrangement of the variables.

In an attempt to better define a bed material correction factor, K_4, numerous combinations of variables were investigated to accurately describe the variation identified in the idealized K_4. Overall, the best correlation was found with the relative bed material size (b/D_{50}). The equation for the envelope curve using this variable combination is:

$$K_4 = 0.35\left(\frac{b}{D_{50}}\right)^{0.19}$$

The envelope curve for K_4 developed from the b/D_{50} ratio is shown in Fig. 7. This curve is applicable for all grain sizes and appears to explain some of the underprediction for the HEC-18 equation for the sand sizes. If this correction curve is applied to all observations, the 13 observations that HEC-18 originally

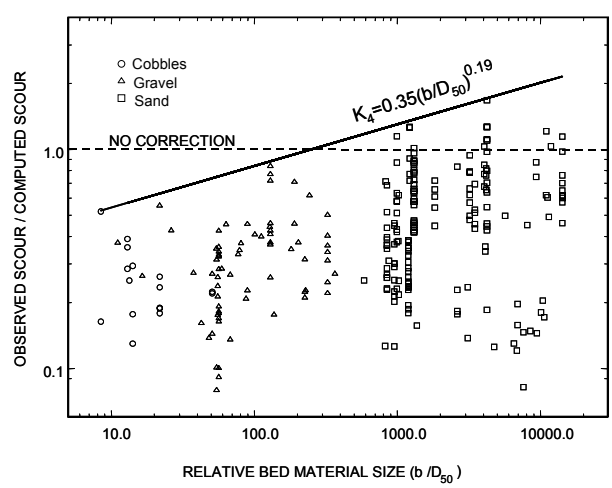

Fig.7 - Relation between relative errors in computed scour using the HEC-18 equation and relative bed material size.

underpredicted (Table 3) are corrected, but the sum of squared errors increases to over 2,800. The large increase in the sum of squared errors is caused by the large scatter below the curve for values of K_4 above 1. If the correction is limited to reducing the scour depth ($K_4 \leq 1$), the sum of squared errors is reduced to 611 but 14 observations are underpredicted. The sum of squared errors for the 14 observations underpredicted is 2.16, which is the same as the HEC-18 equation had prior to this correction (Table 3).

Although the K_4 based on b/D_{50} does not perform as well as the HEC-18-K4Mu equation in table 3, the basis for this new approach is supported to an extent by the work of Sheppard (University of Florida, written communication, 2001) and Ettema (1980) who found that b/D_{50} was an important parameter based on their laboratory research. In addition, although this new K_4 lacks the effect of the coarse size fraction, it does not behave illogically as does the HEC-18-K4Mu approach.

SUMMARY AND CONCLUSIONS

The USGS, in cooperation with the FHWA and State highway departments, has compiled and extensive data base of field measurements of local pier scour. These measurements contain bed-material parameters that have been missing from other previously compiled data sets. A comparison of these data with 26 pier-scour prediction equations showed that none accurately predicted the scour for all site and hydrologic conditions. No single equation conclusively was better than the rest, but the top six equations generally appear to be the Froehlich Design, HEC-18, HEC-18-K4, HEC-18-K4Mu, HEC-18-K4Mo (>2 mm), and Mississippi equations. These field measurements also were compared with the results of various laboratory investigations. This comparison showed that often the laboratory investigations do not cover the same range of variable combinations represented in the field data. Where comparisons between the laboratory investigations and the field data could be made, the laboratory experiments were able to envelope the field data but were unable to explain much of the variation in observed scour depths. The effect of bed-material properties on the scour depth was evident in both the laboratory and field data. Various equations for a bed-material correction (K_4) to the HEC-18 equation have been proposed. Evaluation of these K_4 equations showed that most of them improved the performance of the HEC-18 equation but none of them could fully explain all of the variation in the residuals of the HEC-18 equation. A new relation for K_4, based on the relative bed-material size, was introduced and shown to provide good corrections to the HEC-18 equation. However, much of the variation in the field data remains unexplained.

REFERENCES

1. Ahmad, M., 1953, Experiments on design and behavior of spur dikes, *in* Int. Hydr. Convention, Minneapolis, Minn., St. Anthony Falls Hydraulics Laboratory, p. 145-159.

2. Baker, R.E., 1986, Local scour at bridge piers in non-uniform sediment: University of Auckland Report, Report No. 402, 91 p.

3. Blench, T., 1962, Discussion of Scour at Bridge Crossings, by E.M. Laursen: Transactions of American Society of Civil Engineers, v. 127, p. 180-183.

4. Breusers, H.N.C., 1965, Scour around drilling platforms: Bulletin of Hydraulic Research, v. 19, p. 276.

5. Breusers, H.N.C., Nicollet, G., and Shen, H.W., 1977, Local scour around cylindrical piers: Journal of Hydraulic Research, v. 15, no. 3, p. 211-252.

6. Chee, R.K.W., 1982, Live-bed scour at bridge piers: University of Auckland, Report No. 290, 79 p.

7. Chiew, Y.M., 1984, Local scour at bridge piers: University of Auckland, Report No. 355, 200 p.

8. Chitale, S.V., 1962, Scour at bridge crossings: Transactions of the American Society of Civil Engineers, v. 127, no. 1, p. 191-196.

9. Ettema, R., 1980, Scour at bridge piers: New Zealand, University of Aukland, School of Engineering, Report No. 216.

10. Froehlich, D.C., 1988, Analysis of onsite measurements of scour at piers, *in* American Society of Civil Engineers National Conference on Hydraulic Engineering: Colorado Springs, Colo., American Society of Civil Engineers, p. 534-539.

11. Gao, D.G., Posada, L.G., and Nordin, C.F., 1992, Pier scour equations used in the People's Republic of China—review and summary: Fort Collins, Colo., Colorado State University, Department of Civil Engineering, Draft Report.

12. Inglis, S.C., 1949, Maximum depth of scour at heads of guide banks and groynes, pier noses, and downstream of bridges—The behavior and control of rivers and canals: Poona, India, Indian Waterways Experimental Station, p. 327-348.

13. Johnson, P.A., 1995, Comparison of pier-scour equations using field data: Journal of Hydraulic Engineering, v. 121, no. 8, p. 626-629.

14. Landers, M.N., and Mueller, D.S., 1996, Channel scour at bridges in the United States: Federal Highway Administration Research Report FHWA-RD-95-184, 140 p.

15. Landers, M.N., Mueller, D.S., and Martin, G.R., 1996, Bridge-scour data management system user's manual: U.S. Geological Survey Open-File Report 95-754, 65 p.

16. Larras, J., 1963, Profondeurs Maximales D'Erosion des Fonds Mobiles Autour des Piles en Riviere: Ann. Ponts et chaussees, v. 133, no. 4, p. 411-424.

17. Laursen, E.M., 1962, Scour at bridge crossings: Transactions of the American Society of Civil Engineers, v. 127, pt. 1, p. 166-209.

18. McIntosh, J.L., 1989, Use of scour prediction formulae, Proceedings of the Bridge Scour Symposium: McLean, Va., Federal Highway Administration Research Report FHWA-RD-90-035, p. 78-100.

19. Melville, M.W., 1975, Local scour at bridge sites: New Zealand, University of Aukland, School of Engineering, Project Report No. 117, 227 p.

20. Melville, B.W., Ettema, R., and Jain, S.C., 1989, Measurement of bridge scour, *in* Proceedings of the Bridge Scour Symposium: McLean, Va., Federal Highway Administration Research Report FHWA-RD-90-035, p. 183-194.

21. Melville, B.W., and Sutherland, A.J., 1988, Design method for local scour at bridge piers: Journal of the Hydraulics Division, v. 114, no. 10, p. 1210-1225.

22. Molinas, Albert, 2000, Bridge scour in non-uniform sediment mixtures and in cohesive materials: Federal Highway Administration Research Report FHWA-RD-99-189, 117 p.

23. Mueller, D.S., 1996, Local scour at bridge piers in nonuniform sediment under dynamic conditions: Fort Collins, Colo., Colorado State University, Ph.D. dissertation, 212 p.

24. Mueller, D.S., and Wagner, C.R., in press, Field observations and evaluations of streambed scour at bridges: Federal Highway Administration Research Report FHWA-RD-01-041, 116 p.

25. Neill, C.R., 1964, River-bed scour—a review for engineers: Canadian Good Roads Association Technical Publication No. 23.

26. Pritsivelis, A., 1999, Local sediment scour at large circular piles: Gainesville, Fla., University of Florida, M.S., 129 p.

27. Richardson, E.V., and Davis, S.R., 1995, Evaluating scour at bridges (3rd ed.): Federal Highway Administration Hydraulic Engineering Circular No. 18, FHWA-IP-90-017, 203 p.

28. Richardson, E.V., and Davis, S.R., 2001, Evaluating scour at bridges (4th ed.): Federal Highway Administration Hydraulic Engineering Circular No. 18, FHWA NHI 01-001, 378 p.

29. Richardson, E.V., Harrison, L.J., Richardson, J.R., and Davis, S.R., 1993, Evaluating scour at bridges (2d ed.): Federal Highway Administration Hydraulic Engineering Circular, April 1993 revision, FHWA-IP-90-017, 237 p.

30. Shen, H.W., Schneider, V.R., and Karaki, S., 1969, Local scour around bridge piers: Journal of the Hydraulics Division, v. 95, no. HY6, p. 1919-1940.

31. Southard, R.E., 1992, Scour around bridge piers on streams in Arkansas: U.S. Geological Survey Water-Resources Investigations Report 92-4126, 29 p.

32. Wilson, K.V., Jr., 1995, Scour at selected bridge sites in Mississippi: U.S. Geological Survey Water-Resources Investigations Report 94-4241, 44 p.

33. Zhuravljov, M.M., 1978, New method for estimation of local scour due to bridge piers and its substantiation: State All Union Scientific Research Institute on Roads, Transactions 109, 20 p.

Future Hydrographs and Scour Risk Analysis

Jean-Louis Briaud[1], Paolo D'Odorico[2], Eung Jin Jeon[3]

ABSTRACT

The SRICOS-EFA method is used to predict the scour depth versus time curve for bridge pier scour and/or contraction scour in soils. The input for this method consists of the velocity hydrograph to which the pier will be subjected, the geometry of the pier and the channel, and the soil erodibility function for the soils to be eroded. The velocity hydrograph required for the design of a new bridge describes the mean depth velocity of the water at the location of the pier as a function of time for the design life of the bridge, say 75 years. A new procedure is presented to generate possible future hydrographs. This new procedure makes it simple to give the scour depth results in terms of risk levels.

THE SRICOS-EFA METHOD

In cohesionless soils, it is usually sufficient to calculate the maximum scour depth due to the design flood. Indeed, the scour rate in cohesionless soils is fast enough that one flood is long enough to generate the maximum scour depth for that velocity. This is rarely the case in cohesive soils and in rocks where only a fraction of the maximum scour depth may occur during the design flood. In cohesive soils and in rocks it can be very advantageous to predict the scour depth vs. time curve because ignoring it can be very conservative and costly. Ignoring the rate of erosion effect in cohesive soils may lead to unnecessarily deeper and more expensive foundations. An example of the difference

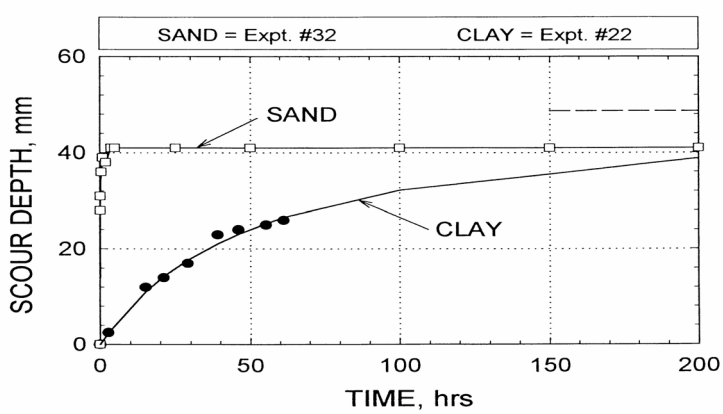

Fig. 1: Comparison between scour rate in sand and in clay for two flume experiments

1. Professor and Holder of the Spencer J. Buchanan Chair, Dpt. of Civil Engineering, Texas A&M University, College Station, Texas 77843-3136, USA (briaud@tamu.edu)
2. Professor, Dept. of Environmental Sciences, University of Virginia, Clark Hall,291 McCormick Road, Box 400123, Charlottesville, Virginia 22904-4123, USA
3. Graduate Student, Civil Engineering, Texas A&M University, College Station, Texas.

between a scour depth versus time curve in a cohesionless soil and a cohesive soil is shown in Figure 1.

Figure 1 shows the scour depth vs. time curve for a constant velocity; however in reality the mean depth velocity in a river (Figure 2) varies significantly during the life of a bridge. The SRICOS-EFA method (Briaud et al., 1999, 2001a, 2001b) was developed to predict the scour depth vs. time curve for bridges subjected to a varying velocity-time history in a layered soil or soft rock. The method can handle pier scour, contraction scour and the combination of the two occurring simultaneously. The solution for abutment scour is under development. The pier scour prediction includes circular and rectangular piers, shallow and deep water depth, different angles of attack, and the effect of pier spacing. The contraction scour prediction includes the effect of the contraction ratio, the length of the contracted channel, the water depth, and the transition angle.

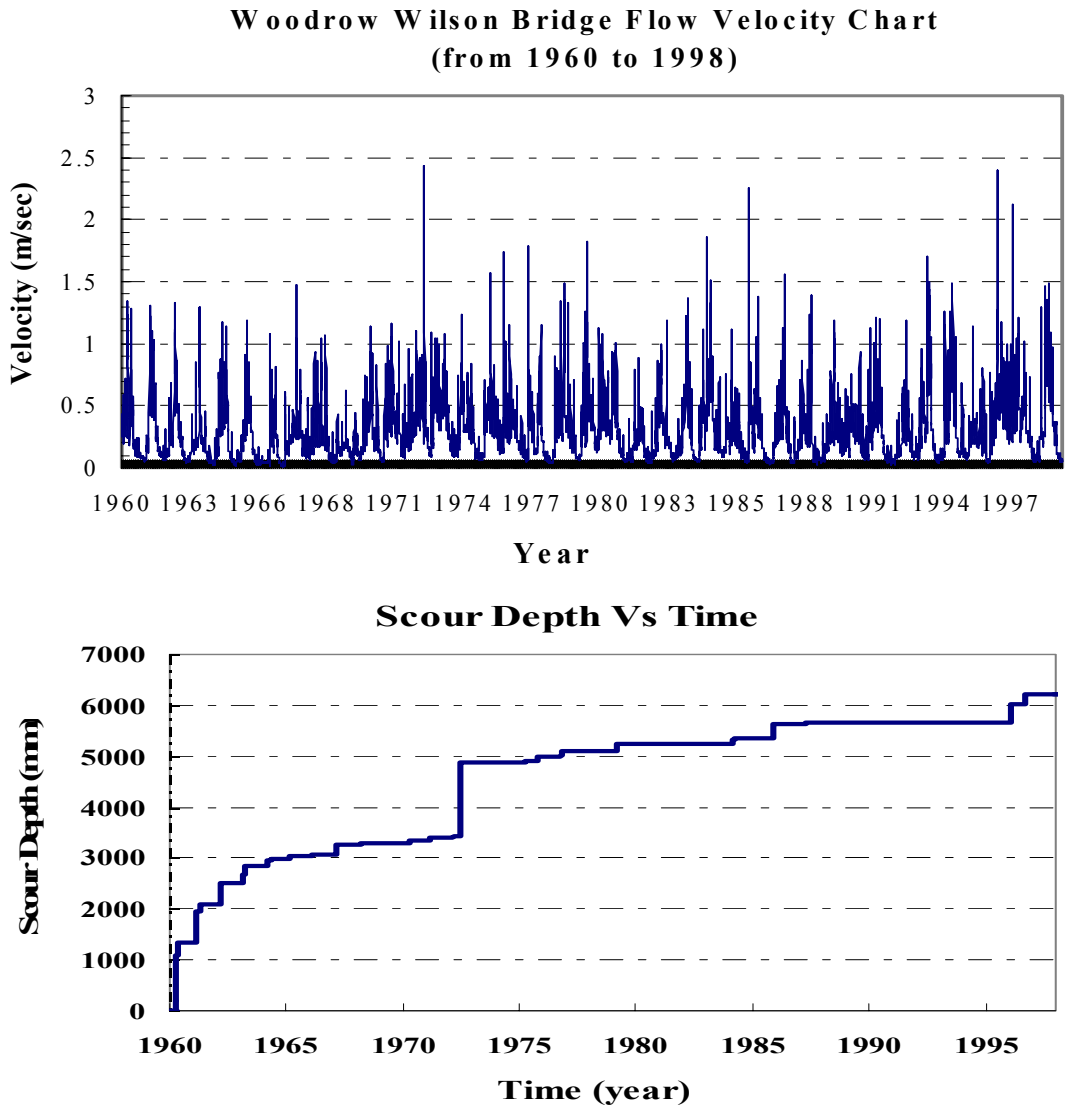

Fig. 2: Example of Output generated by the SRICOS-EFA Program.

The method consists of the following steps (Briaud et al., 2002):

1. Collect the input data: velocity and water depth hydrograph, geometry of the pier and of the contracted channel, erosion functions of the soil layers.
2. Calculate the maximum contraction scour depth for the ith velocity in the hydrograph.
3. Calculate the maximum complex pier scour depth using the ith velocity in the hydrograph at the pier location if there is no contraction scour in step 2, or the critical velocity for the soil if there is contraction scour in step 2.
4. Calculate the total pier scour depth as the total of step 2 and step 3.
5. Calculate the initial maximum shear stress for pier scour using the ith velocity in the hydrograph.
6. Read the initial scour rate corresponding to the initial maximum shear stress of step 5 on the erosion function of the soil layer corresponding to the current scour depth.
7. Use the results of steps 4 and 6 to construct the hyperbola describing the scour depth vs time for the pier.
8. Calculate the equivalent time for the given curve of step 7. The equivalent time is the time required for the ith velocity on the hydrograph to scour the soil to a depth equal to the depth scoured by all the velocities occurring prior to the ith velocity.
9. Read the additional scour generated by the ith velocity starting at the equivalent time and ending at the equivalent time plus the time increment.
10. Repeat steps 2 to 9 for the (i+1)th velocity and so on until the entire hydrograph is consumed.

The equations for the maximum scour depth values were developed on the basis of flume tests while the equations for the initial shear stress were developed from numerical simulations. The accumulation algorithms for velocity history and layering systems were constructed by using the concept of an equivalent time. Care was taken not to simply add the pier scour depth and the contraction scour depth. The details of the method as well as the manual for the SRICOS-EFA program can be found in Briaud et al. (2002).

USING AN EXISTING HYDROGRAPH

Since the SRICOS-EFA method predicts the scour depth as a function of time, one of the input is the velocity versus time curve or hydrograph at the foundation location. This hydrograph should cover the period over which the scour depth must be predicted. A typical bridge is designed for 75 years. Therefore the design for a new bridge requires the knowledge of the hydrograph from the year of construction until that year plus 75 years. The question is: how can one obtain the future hydrograph covering that long period of time? This requires predicting the future over a 75-year period! The uncertainty inherent to the climatic and hydrologic processes determining the hydrograph characteristics suggests using a statistical approach in the generation of plausible 75-year hydrographs.

One solution is to use a hydrograph recorded at a nearby gauge station over the last 75 years and assume that the future hydrograph will be equal to the past hydrograph. If the gauge is not at the future bridge location, the discharge can be multiplied by the ratio of

the drainage area at the bridge site over the drainage area at the gauge site. If the record at the gauge station is not 75 years long, one can simply repeat the recorded hydrograph until it covers the 75-year period. If the recorded hydrograph does not include the design flood (100 year flood or 500 year flood), one can spike the hydrograph with one or more of those floods before running the SRICOS program (Figure 3).

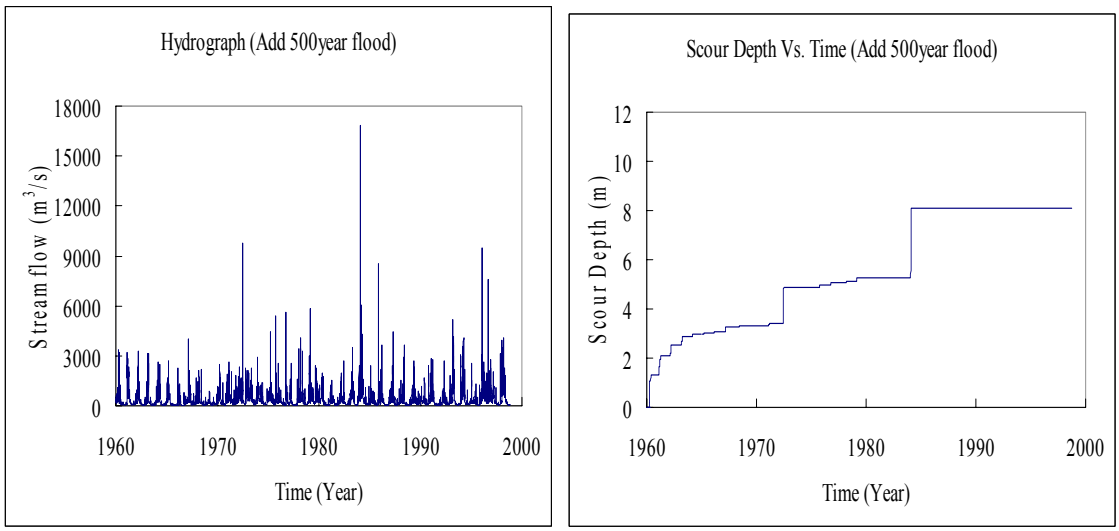

(a) Hydrograph (b) Scour Depth Vs. Time Curve

Fig.3: Woodrow Wilson Measured Hydrograph spiked with a 500-year Flood

RANDOMLY GENERATED FUTURE HYDROGRAPHS

Another solution is to use the new technique which is presented here. This technique consists of using a past hydrograph, preparing the frequency distribution plot for the floods within that hydrograph, sampling the distribution randomly and preparing a future hydrograph, for the required period, which has the same mean and standard deviation as the measured hydrograph. This process is repeated 10,000 times and, for each hydrograph, a final scour depth (the depth reached after 75 years of flow) is generated. These 10,000 final depths of scour are organized in a frequency distribution plot with a mean and a standard deviation. That plot can be used to quote a scour depth with a corresponding probability of occurrence, or better, to choose a risk level and quote the corresponding final depth of scour.

The SRICOS-EFA method determines the scour depth at the end of the bridge life as a progressive process driven by a given sequence of daily stream-flow values throughout the life, L_t, of the structure. The randomness of the hydrologic function suggests combining the scour model with some hydrological and statistical analyses. If the stream-flow sequence (or *hydrograph*) is modeled as a stochastic process, it is possible to set up a Monte Carlo procedure sampling from that process different realizations of the hydrograph (of length L_t), and estimating (SRICOS-EFA method) for each of them the scour depth, d, at the end of the bridge life. Thus, d is regarded as a random variable and

its statistics can be studied in detail to determine the risk of failure associated with different choices of the design value of the scour depth.

The modeling of daily stream-flow, *Q*, can be tackled using different approaches (e.g., Bras and Rodriguez-Iturbe, 1986; Montanari et al., 1997; 2000) corresponding to different levels of complexity. A first simple analysis suggested here considers *Q* as a random, uncorrelated variable. A suitable distribution is fitted to the data and the hydrographs are then generated as series of values sampled from such a distribution. Ongoing research is also applying other stochastic models to account for both the autocorrelation and the memory of the process and is assessing whether the temporal structure (i.e. both autocorrelation and memory) of the stream-flow sequences is able to affect the statistical properties of the scour-depth probability distribution.

The theoretical distribution used to model daily stream-flow observations needs to be defined only for positive values of *Q,* to have a positive skewness, and to be able to provide an accurate representation of the extreme values (i.e. good fit at the upper tail of the distribution). As expected, the extreme values are found to greatly affect the scour depth estimates and an imprecise modeling of stream-flow maxima could easily lead to unrealistic estimations of the scour depth statistics. Logarithmic transformations are frequently used to study stream-flow extremes (e.g., Chow et al., 1988; Benjamin and Cornell, 1970); therefore, a log-normal distribution can be a good candidate for modeling the daily stream-flows. The method of moments is used to determine the parameters of the distribution. As such, *Q* is expressed as the exponential of a normally distributed random variable, *y*, with mean

$$\mu_y = \frac{1}{2} Log\left[\frac{\mu_Q^{\,2}}{1+\left(\frac{\sigma_Q}{\mu_Q}\right)^2}\right] \tag{1}$$

and standard deviation

$$\sigma_y = \sqrt{Log\left[1+\left(\frac{\sigma_Q}{\mu_Q}\right)^2\right]} \tag{2}$$

with μ_Q and σ_Q being the mean and the standard deviation of daily stream flow, respectively.

In the case of the Woodrow Wilson Bridge, stream-flow data is available at the Little Falls station (USGS #01646500) on the Potomac River, approximately 13 km upstream from the bridge. Correction of the measured stream flow is applied by multiplying the values by the drainage area ratio. The correction is of the order of 3%. Figure 4 shows the original hydrograph and the corresponding prediction of scour depth history using the SRICOS-EFA method. The mean and standard deviation of *Q* in the period of record 1931-2000 are μ_Q=327 m^3s^{-1}, and σ_Q=467 m^3s^{-1}, respectively, while the maximum discharge in the 70-year-long record was 12,056 m^3s^{-1}. Synthetic hydrographs of the

same length generated by sampling from a lognormal distribution of mean μ_Q and standard deviation σ_Q have on the average a maximum value of about 12,000 m^3s^{-1}, suggesting that such a distribution gives an adequate representation of the extrema. Figure 5 shows an example of a generated future hydrograph and the associated scour depth history as predicted by the SRICOS-EFA method.

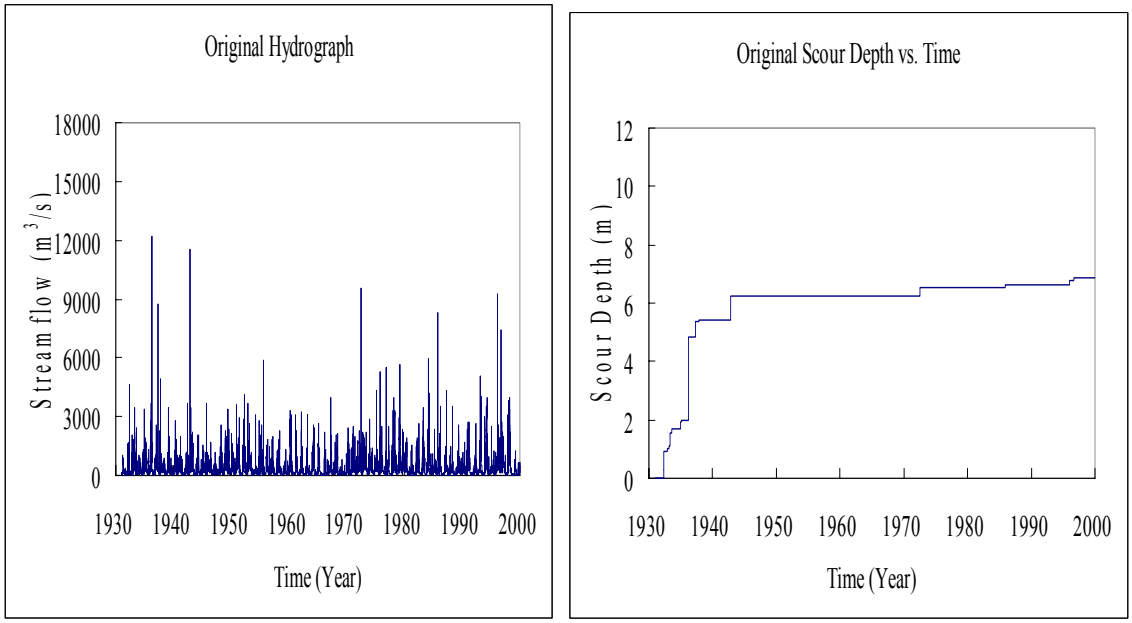

(a) Hydrograph (b) Scour Depth vs. Time

Fig.4: Original Hydrograph & Scour Depth vs. Time near Woodrow Wilson Bridge Site

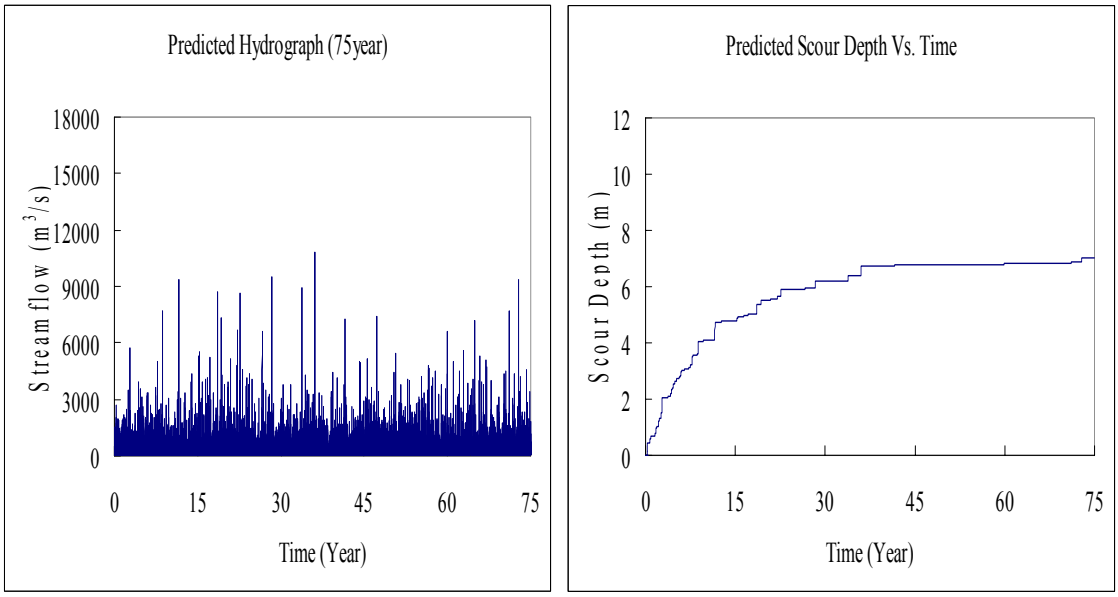

(a) Hydrograph (b) Scour Depth vs. Time

Fig.5: Predicted Hydrograph and Scour Depth vs. Time Curve near Woodrow Wilson Bridge Site (Project time = 75year)

RISK APPROACH TO SCOUR PREDICTIONS

Many equally possible future hydrographs such as the one in Figure 5 are generated by the random sampling process. For each hydrograph, the SRICOS program generates a scour depth history including a final depth of scour, d, at the end of the project life. These values of the final depth of scour can be organized in a frequency distribution. Figure 6 shows the probability distributions obtained for the example of the Woodrow Wilson bridge at the end of a chosen bridge life, L_t.

This analysis can be used to estimate the level of risk, R, associated with the choice of different design values of scour depth and project lives. By definition, the risk level is the probability that the design conditions are exceeded in the course of the life of the structure. Thus, from the probability distribution of d (Figure 6) it is possible to determine the cumulative distribution function (CDF) of d (Figure 7). The risk is then estimated as the probability of exceedence (Figure 7). Table 1 reports the risk level associated with different project lives and design values of d. It is observed that R is a non-linear function of d and L_t. This analysis provides a statistical framework that can be used in a cost-benefit study of bridge foundation design.

Commonly accepted methods of scour analysis in cohesionless soils refer to a single peak-flow value selected on the basis of its return period, T_r, as well as of the associated level of risk. Such an approach does not account for the contribution to bridge scour due to smaller (and more frequent) floods. The SRICOS-EFA method can be used to include the effect of the entire hydrograph. The Monte Carlo procedure outlined in this section represents a possible new probabilistic approach to scour analysis. Ongoing research is developing a extended version of this approach using different stochastic hydrologic models able to account for the daily-flow distribution, and for the autocorrelation of the stream-flow series. This study will show whether the scour depth is sensitive to the temporal structure of stream-flow sequences and will indicate the level of detail that is necessary to include in the hydrologic stochastic model.

OBSERVATIONS ON CURRENT RISK LEVELS

A direct comparison between the risk results obtained here with the SRICOS method (Table 1) and traditional approaches based on single peak-flow values is not easy. Nevertheless, an example is provided here. The peak flow value associated with a given return period can be determined through a flood-frequency analysis (e.g., Chow et al., 1988; pp 375-378). Figure 8 shows the result of such an analysis for the Woodrow Wilson measured hydrograph. As can be seen on that figure, the 100 year flood has a discharge of 12,600 m^3/s and the 500 year flood has a value of 16,600 m^3/s. If the design life of the bridge is L_t, the probability of exceedence or risk R for a flood having a return period T_r is given by:

$$R = 1 - (1 - 1/Tr)^{Lt} \quad (3)$$

If the design life of the bridge is 75 years, the probability that the flood with a return period of 100 year will be exceeded during the 75 year design life is 53% according to equation 3. The risk that the 100 year flood will be exceeded during the 75 years is 53%

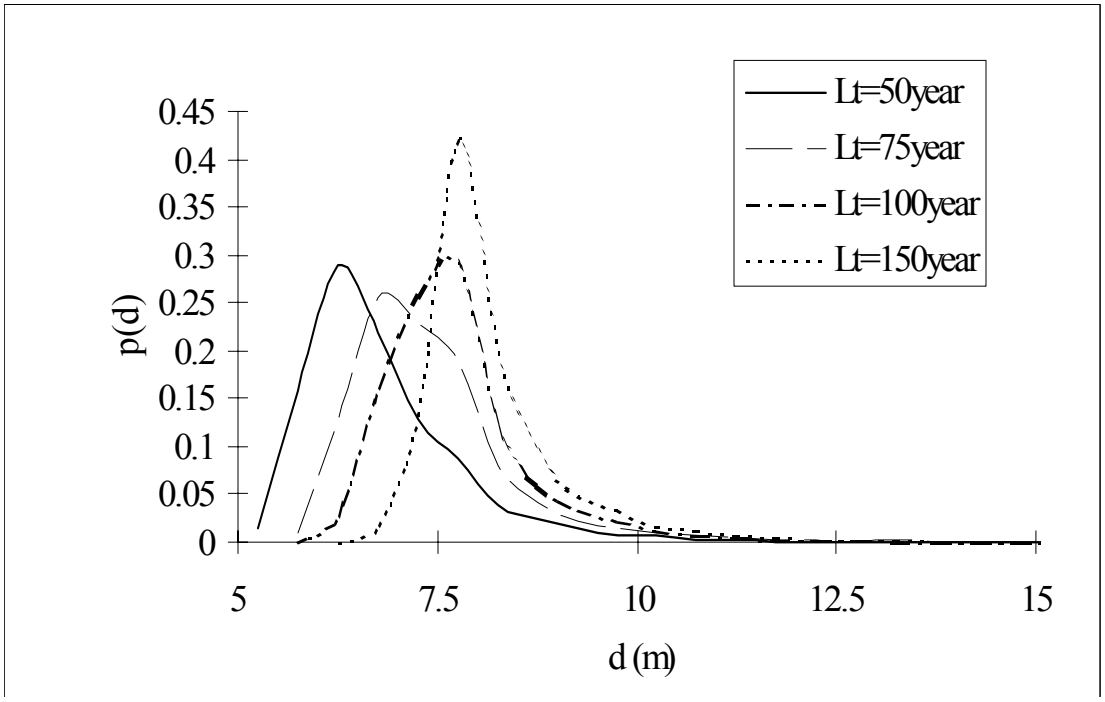

Fig.6: Probability distribution of scour depth, *d*, for different lengths of the project life, L_t

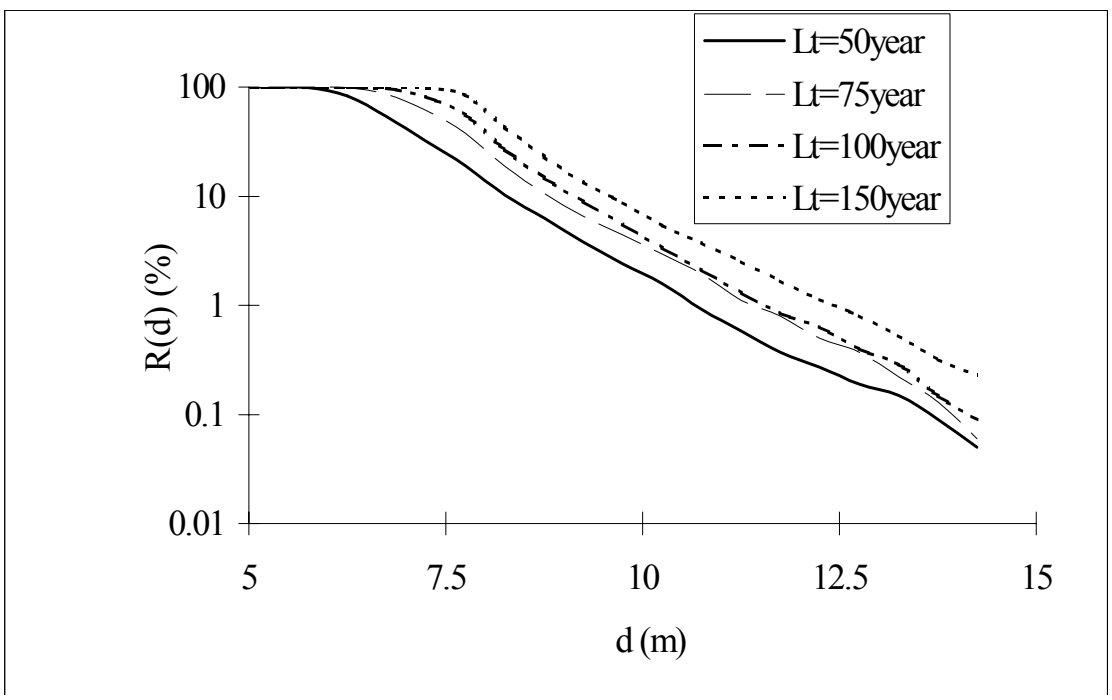

Fig.7: Risk associated with different design values of the final scour depth, *d*, and different lengths of the project life, L_t

Table 1: Risk of failure associated with different design values of scour depth and project lives

Design value of Scour depth (m)	Project Life			
	50 yrs	75 yrs	100 yrs	150 yrs
6.5	42%	74%	91%	99.8%
7.0	25%	48%	70%	93%
7.5	14%	27%	40%	65%

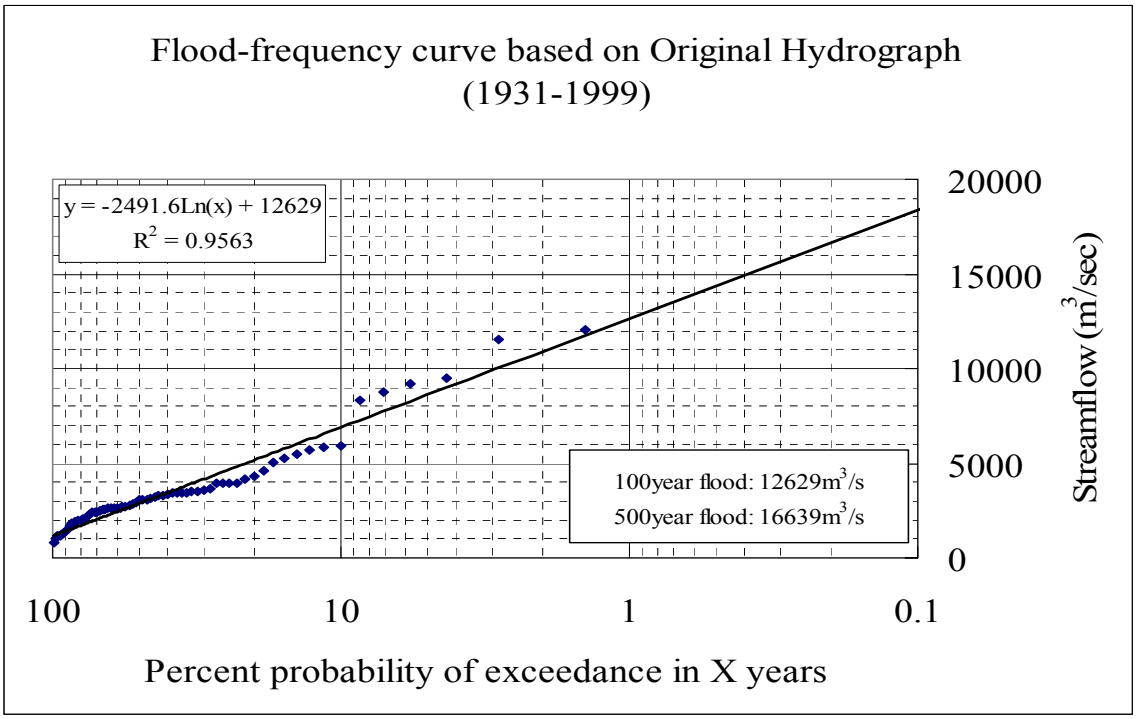

Fig.8: Flood-frequency curve for the Potomac River at the Woodrow Wilson Bridge

or about one chance out of two. For the 500 year flood, and for the same 75 year design life, the risk is 14% or one chance in about 7.

Even if a bridge designed for a 100 or 500 year flood experiences a 1000 year flood, this bridge may not collapse. Indeed collapse of the bridge is based on a different criterion than just exceedence of the design flood. There are numerous inherent redundancies in the design of a bridge and many design parameters have to be exceeded before collapse occurs. Nevertheless, the risk level associated with the floods used in everyday design appears very high compared to risk levels in other disciplines within Civil Engineering. For example the structural engineers have based their codes on a risk level of about 0.1%. The geotechnical engineers probably operate at about 1%. The scour engineers seem to operate at a much higher risk level. This is particularly worrisome since there is no factor of safety on the depth of scour passed on from the scour engineer to the geotechnical engineer for him to calculate the pile length.

CONCLUSIONS

The SRICOS-EFA method predicts the scour depth versus time curve for bridge piers. One of the input is the water velocity-time history or hydrograph covering the period over which the bridge is to be designed or evaluated. A new technique to obtain such hydrographs is presented. This technique consists of using a past hydrograph, preparing the frequency distribution plot for the floods within that hydrograph, sampling the distribution randomly and statistically modeling a future hydrograph, for the required period, which has the same mean and standard deviation as the measured hydrograph. This process is repeated 10,000 times and, for each hydrograph, a final scour depth (the depth reached after 75 years of flow) is generated. These 10,000 final depths of scour are organized in a frequency distribution plot with a mean and a standard deviation. That plot can be used to quote a scour depth with a corresponding probability of occurrence, or better, to choose a risk level and quote the corresponding final depth of scour.

ACKNOWLEDGEMENTS

Part of this work was sponsored by the Texas Department of Transportation in a project where Tom Dahl and David Stolpa are the technical contacts. At Texas A&M University, Eung-Jin Jeon, Jae-Chan Hoo, Hamn-Chin Chen, and Kuang-An Chang contributed to the development of the method. They are all thanked sincerely.

REFERENCES

1. Benjamin, J.R., and Cornell, C., A.,1970, “Probability, Statistics, and Decisions for Civil Engineers”, McGraw-Hill, New York, USA.
2. Bras, R. L., and Rodriguez-Iturbe, I., “Random Functions and Hydrology”, 1986. Dover.
3. Briaud, J.-L., Ting, F., Chen, H.C., Gudavalli, S.R., Perugu, S., and Wei, G.,1999, “SRICOS: Prediction of Scour Rate in Cohesive Soils at Bridge Piers”, Journal of Geotechnical Engineering, Vol.125, pp. 237-246, ASCE, Reston, Virginia, USA.
4. Briaud J.-L., Ting F., Chen H.C., Cao Y., Han S.-W., Kwak K., 2001a, “Erosion Function Apparatus for Scour Rate Predictions”. Journal of Geotechnical and Geoenvironmental Engineering, ASCE, Vol.127, No. 2, pp.105-113, ASCE, Reston, Virginia, USA.
5. Briaud, J. L., Chen, H. C. Kwak K., Han S-W., Ting F.,2001b, “Multiflood and Multilayer Method for Scour Rate Prediction at Bridge Piers”, Journal of Geotechnical and Geoenvironmental Engineering, Vol.127, No. 2, pp.105-113, ASCE, Reston, Virginia, USA.
6. Briaud J.-L., Chen H.-C., Li Y., Nurtjahyo P., Wang J., 2002, “Complex Pier Scour and Contraction Scour in Cohesive Soils”, Final Report for NCHRP Project 24-15, National Cooperative Highway Research Program, Transportation Research Board, Washington DC.
7. Chow V.T., Maidment, D.R., Mays L.W., 1988, “Applied Hydrology”, McGraw-Hill.

8. Montanari, A., Rosso, R., Taqqu, M.S., 1997. “Fractionally differenced ARIMA models applied to hydrologic time series: identification, estimation and simulation”, Water Resour. Res., Vol. 33, No. 4, pp 1035-1044, American Geophysical Union, Washington, D.C., USA.
9. Montanari, A., Rosso, R., Taqqu, M.S., 2000, A” seasonal fractional ARIMA model applied to the Nile River monthly flows at Aswan”, Water Resour. Res., Vol. 36, No. 5, pp 1249-1259, American Geophysical Union, Washington, D.C., USA.

Database Program for Highway Bridge-Scour Data

Khalid Farrag[1] and Mark Morvant [2]

ABSTRACT

A database management program was developed for the storage, retrieval, and display of scour data of highway bridges. The program is currently being used by the Louisiana Department of Transportation and Development (LA DOTD) to streamline the process of data entry and retrieval, and to detect scour and stream instability at any particular bridge. The quick analysis of the data has led LA DOTD to timely decision making with regard to remediation of scour critical locations.

The program tabulates and plots bridge information, pier data, and river cross-sections at the survey locations. It displays survey maps and soil boring data. The analysis of the scour data is performed using plots of the cross-sections, longitudinal sections and contour lines of the scour data. The history of the scour at any specific location is also plotted in time plots.

The compiled and plotted data from the program can be utilized in determining local scour at the piers and contraction scour at the bridge, analyzing the long-term changes in elevations, and in evaluating site conditions and soil properties for scour repair.

The use of the program by the LA DOTD replaced the tedious work of manual and visual retrieval and display of the monitored scour data. A case study of implementing the program to retrieve the scour data and evaluate scour potential of one of the bridges is presented.

INTRODUCTION

Field monitoring of scour at bridges that are susceptible to scour damage in Louisiana has been carried out since 1970's. LA DOTD monitors approximately one hundred and thirty bridges at a frequency of one to several times per year. Traditionally, in order to evaluate bridge scour, survey data had to be located, retrieved from central files, copied, and then manually plotted and analyzed. A database management program was developed in order to provide the means of retrieving the tremendous amount of scour data, plotting cross, and analyzing the changes in scour depth with time at any selected location near the bridge.

---

1 Manager, Geotechnical and Civil Research, GTI, 1700 S. Mount Prospect Road, Des Plaines, IL, 60018.
2 Manager, Geotechnical and Pavement Research, Louisiana Transportation Research Center, 4101 Gourrier Ave, Baton Rouge, LA 70803.

The paper presents the development of the database program, its use, and provides recommendations for the implementation of database systems for monitoring bridge scours.

DESCRIPTION OF THE BRIDGE-SCOUR DATABASE

The design of the database program was based on the LA DOTD need to electronically access the statewide fathometer data of all its surveyed bridges. The database was designed to provide the following capabilities:

- Electronic storage and retrieval of the bridge scour data, pier properties, hydrographic, and fathometer data collected since 1970.
- Graphical display and prints of the riverbed elevations, longitudinal sections, and cross sections at any selected location and survey date.
- Provide the main parameters required for proper prediction and repair of scour; such as bridge geometry, water levels, site characteristics, pier types and elevations, and soil properties from borings at pier locations.

The database was designed using Microsoft ACCESS software. Figure 1 shows the database tables and structure. A data management program was developed in Microsoft Visual Basic as a user front-end and it is connected remotely to the database in the server. The architecture implemented in the program consisted of two-tier client-server connection that enabled multi-users to access the database through the server. The program in the client side allowed sending queries, using Structured Query Language (SQL) commands, to retrieve the data from the server and to display the tables and graphs on the user's terminal.

a. Display of Bridge Information and Survey data

The first step in using the program is to select the bridge to analyze. The selection of the bridge is done using one or a combination of several indices such as bridge number, state project number, river name, route, parish name; or alternatively, by clicking on the screen on the selected district in the state map. Figure 2 shows the data search form.

The program displays the bridge information and pier data in a tabulated form. A typical bridge information data form is shown in figure 3. It also displays bridge plan and the locations of data collection (Figure 4).

The magnitude of scour depth primarily depends on site conditions, the hydraulic parameters at the bridge reach, and the properties of the bed material (1). Bed-material properties and soil classification at the locations of the soil borings were retrieved from construction drawings and are displayed in the 'Soil Boring' folder of the database. Figure 5 shows a schematic of the bridge structure and soil boring data.

b. Data Entry and Maintenance

Although the database is accessed through the LA DOTD Local Area Network (LAN), only the survey-section personnel can add or modify the data in the database. Data is added and edited in separate forms that are designed for easy and systematic data entry. The data entry consists mainly of: (i) Bridge Information, type, location, and geometry; (ii) Pier data, foundations types, their elevations, and coordinates; (iii) Fathometer data and coordinates. Figure 6 shows the pier data form. Data entry also includes scanned graphs and drawings of the bridge plans and soil borings. Figure 6 shows the data entry form for the Pier data.

USE OF THE DATABASE TO MONITOR BRIDGE SCOUR

Cross-section plots are one of the main functions that provide the user with the changes in scour depth at any location. The database includes the fathometer data at various locations at the approach sections. The user can plot the cross-sections at various locations at a specific survey date; or alternatively, plot the sections at various survey dates for the same location.

Figure 7 shows riverbed cross sections of a sample bridge at an upstream location near the pier for several survey dates. The distance from the baseline of the bridge is plotted in the x-axis. Plots of cross-sections at consecutive survey dates can be utilized in identifying local scour behind the piers. Pier local scour can be computed as the maximum vertical distance between an ambient bed elevation (an estimate of natural bed elevation without the pier in place) and the lowest elevation measured in the scour hole (2). The plots at two consecutive dates in figure 7 showed a change in the elevation near the middle pier. A detail plot at this location in Figure 8 shows a drop of an about 4 ft in the elevation at this location.

Long-term evaluation of the changes in riverbed scour at any location can also be performed using the time plots. Figure 9 shows historical change of riverbed elevation for the location plotted in figure 8. The figure shows the drop of elevation at the last survey dates.

The contours of the riverbed elevations at any selected survey date are also plotted from the data collected from various upstream and downstream locations. Although it is generally difficult to treat scour components separately, the changes in the contour elevations at two consecutive dates (commonly before and after flooding) provide means of evaluating overall scour components at the site. Figure 10 shows a sample of a contour plot of a bridge.

The database program also provides longitudinal cross sections of the riverbed elevations from field measurements. These plots define the changes of elevations at any selected survey date of along the water streamlines. References 3 and 4 provide more details about the capabilities and use of the database program.

CONCLUSIONS

The database scour program was developed to facilitate data retrieval and management of scour in Louisiana bridges. It provided the major parameters needed for an initial evaluation of scour potential from field data (e.g. riverbed elevations, water levels, bridge properties, pier types and elevations, and soil properties at the piers).

The evaluation of field scour data and developing a database for its management and analysis has been recognized as necessary to evaluate potential scour. For this purpose, a national Bridge Scour Data Management System (BSDMS) was developed to provide a description and analysis of the data required to assess scour process at a site (5). The database scour program for Louisiana bridges presents a model system that can be implemented for quick and comprehensive site assessment of and to provide most of the scour parameters needed for the implementation of the BSDMS.

Future development of the database systems can be achieved by including data needed for the estimation of scour values (e.g. hydraulic flood data, flow velocity, pier sizes and shapes, variations of water temperatures, and sediment gradations and properties). Ultimately, with the addition of these parameters, the output can be implemented in the theoretical analysis of scour management systems.

ACKNOWLEDGEMENT

The development of the database program for Louisiana bridge-sour data was supported by the Louisiana Department of Transportation and Development (LA DOTD) and Louisiana Transportation Research Center (LTRC).

REFERENCES

1. Richardson, E.V., Harrison, L.J., and Davis, S.R., "Evaluating Scour at Bridges", Federal Highway Administration Hydraulic Engineering Circular 18, FHWA-IP-90-017, 1991.
2. Jackson, K.S., "Evaluation of Bridge-Scour Data at Selected Sites in Ohio", U.S. Geological Survey, Water-Resources Investigations Report 97-4182, 1997.
3. Farrag, K., and Morvant. M. "Development of Database for Louisiana Highway Bridge Scour Data, A Program and Manual," LTRC, Report No. 331, October 1999.
4. Farrag, K. and Morvant, M., "Development of a Database for Louisiana Highway Bridge-Scour Data", Journal of Transportation Research, TRB, January 2001.
5. Landers, M., and Mueller, D., "Channel Scour at Bridges in the United States", Federal Highway Administration, Report FHWA-RD-95-184, 1995.

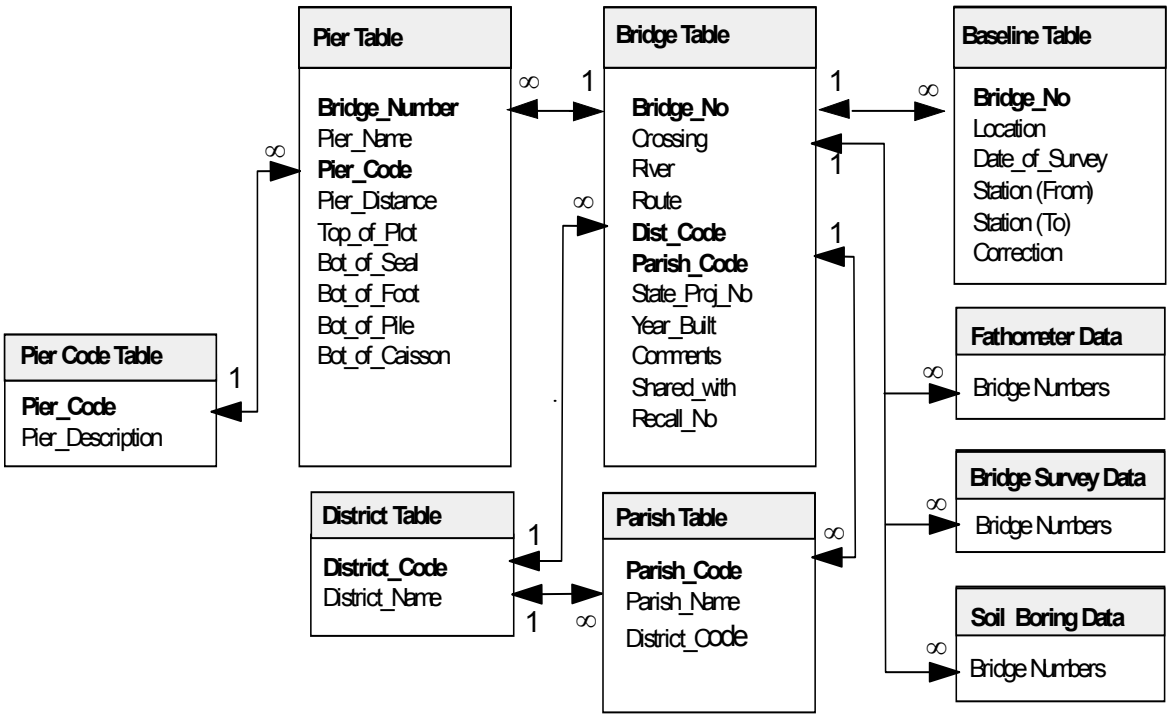

Figure 1. Data types and structure of the database

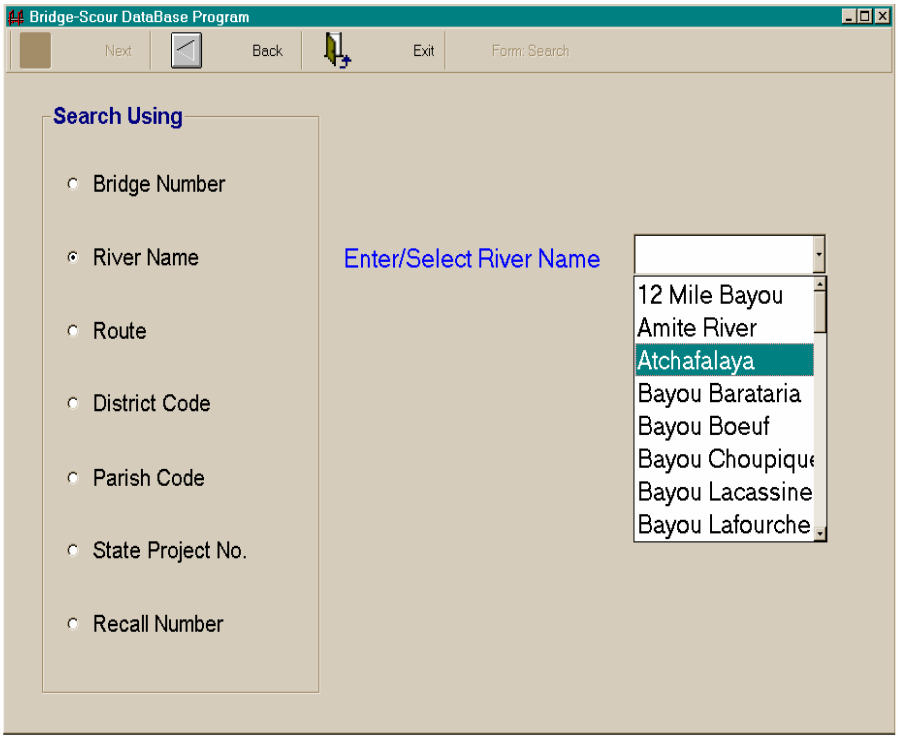

Figure 2. Use of Search Form to select a bridge using several search routines

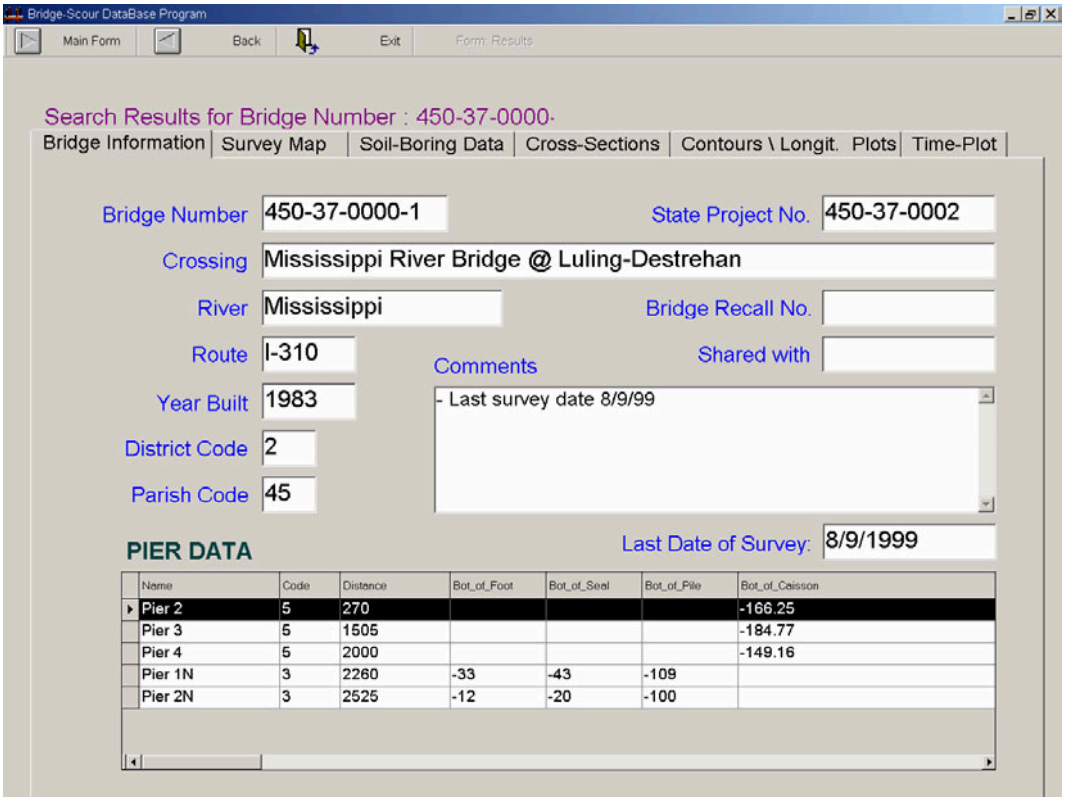

Figure 3. Bridge and pier data are shown in the Bridge Information Folder

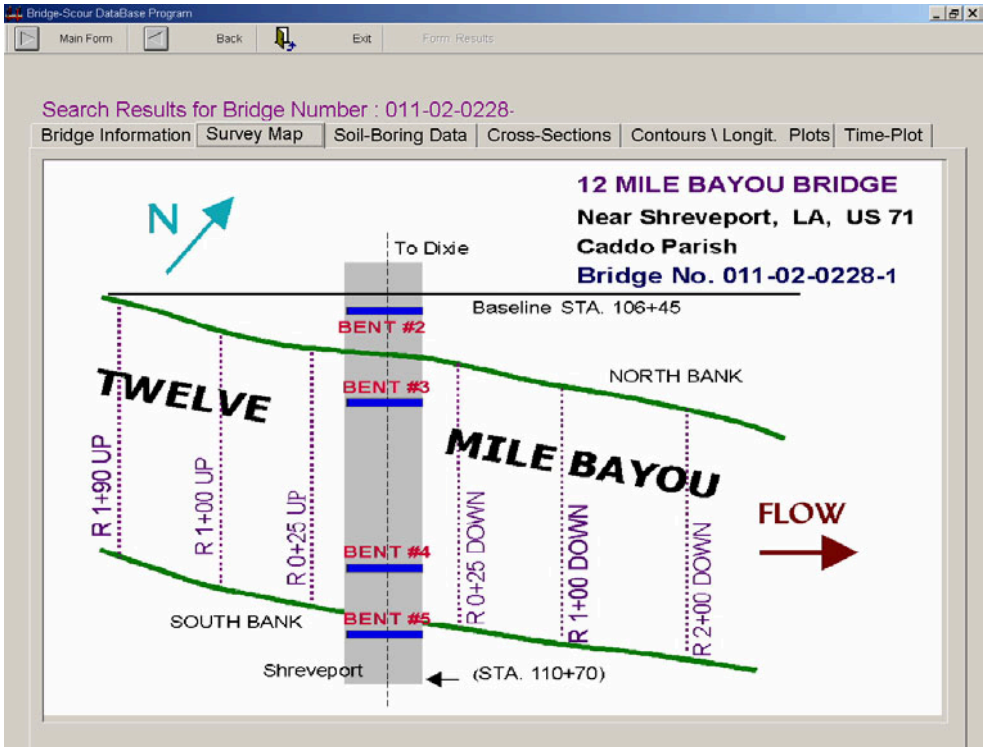

Figure 4. Survey map showing the locations of fathometer data-collection.

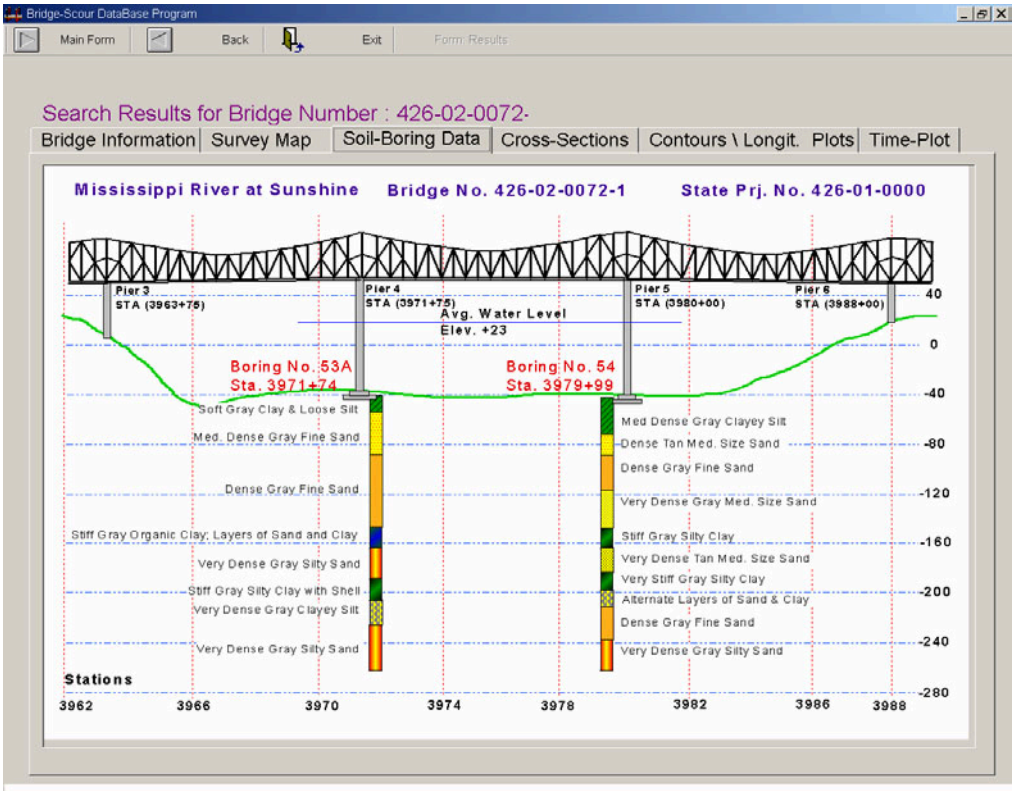

Figure 5. Schematic of the bridge structure showing soil boring locations and data

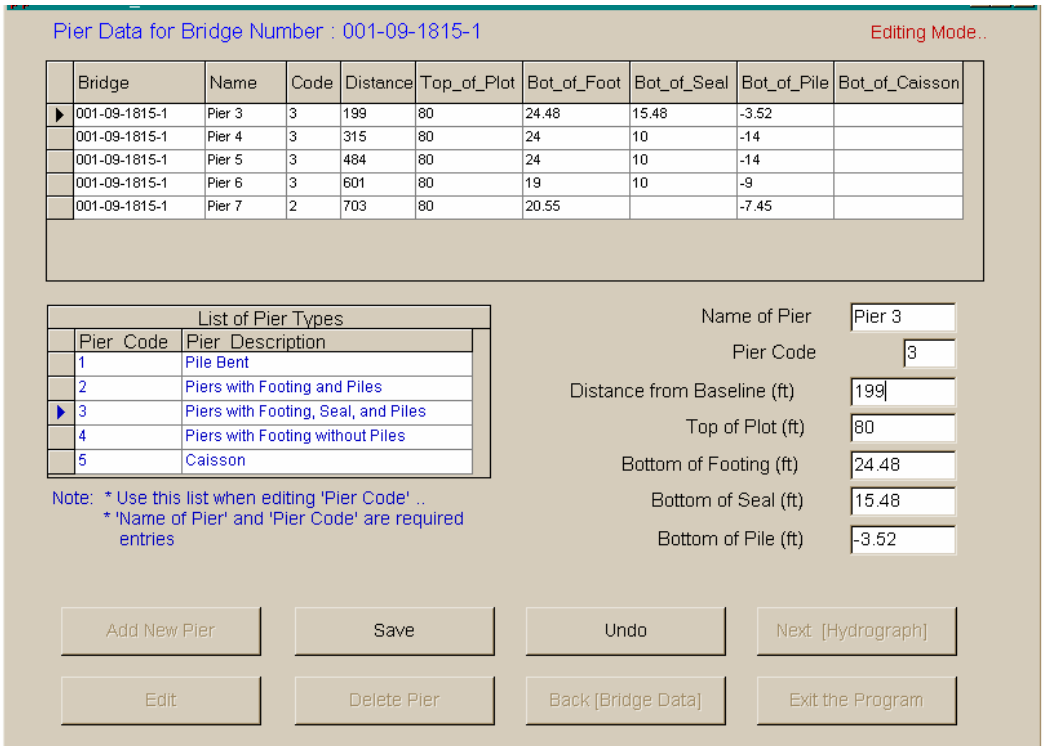

Bridge	Name	Code	Distance	Top_of_Plot	Bot_of_Foot	Bot_of_Seal	Bot_of_Pile	Bot_of_Caisson
001-09-1815-1	Pier 3	3	199	80	24.48	15.48	-3.52	
001-09-1815-1	Pier 4	3	315	80	24	10	-14	
001-09-1815-1	Pier 5	3	484	80	24	10	-14	
001-09-1815-1	Pier 6	3	601	80	19	10	-9	
001-09-1815-1	Pier 7	2	703	80	20.55		-7.45	

Pier Code	Pier Description
1	Pile Bent
2	Piers with Footing and Piles
3	Piers with Footing, Seal, and Piles
4	Piers with Footing without Piles
5	Caisson

Name of Pier	Pier 3
Pier Code	3
Distance from Baseline (ft)	199
Top of Plot (ft)	80
Bottom of Footing (ft)	24.48
Bottom of Seal (ft)	15.48
Bottom of Pile (ft)	-3.52

Figure 6. Data entry form of Pier data and elevations

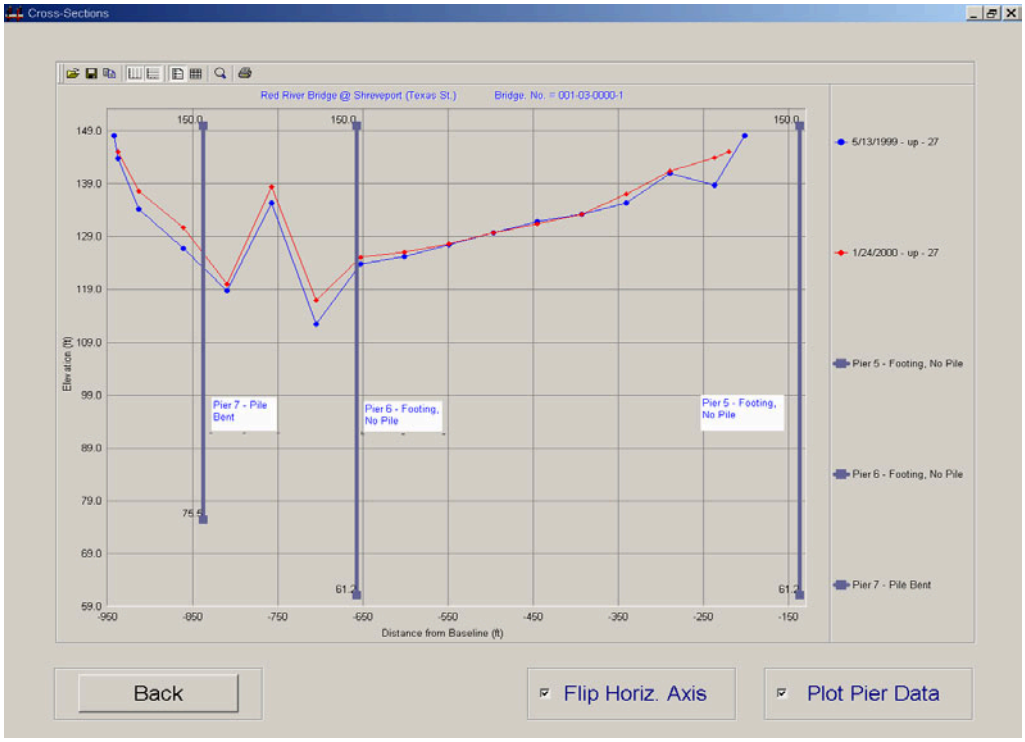

Figure 7 Cross-section plots for several dates at bridge downstream

Figure 8. Detail of Figure 7 showing elevation changes at two consecutive fathometer readings

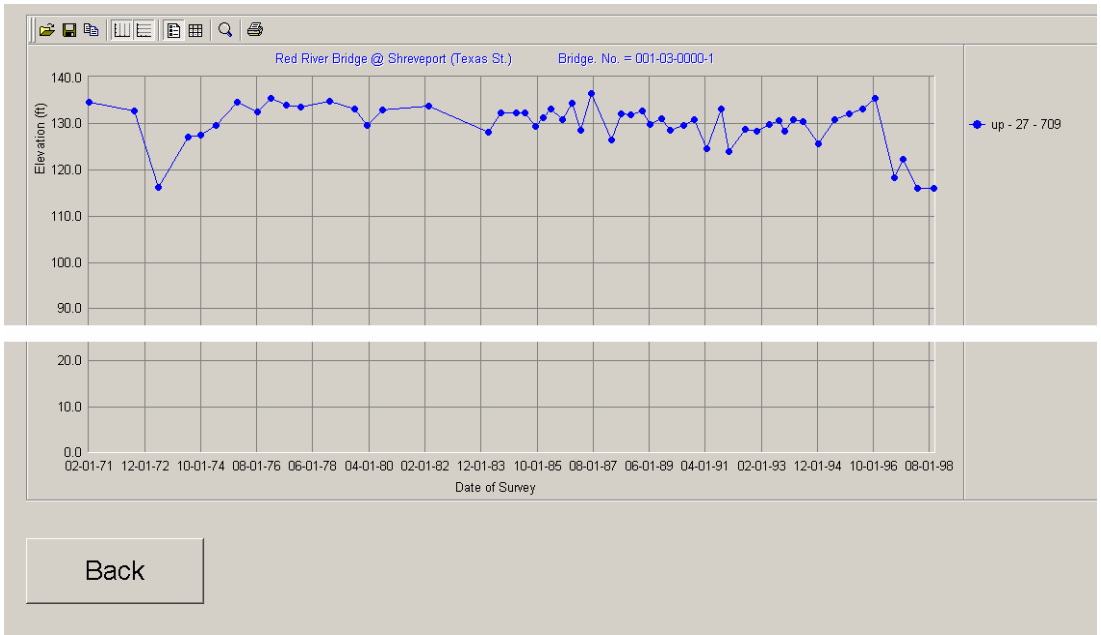

Figure 9. Tine plot showing the change of elevations near the pier at location shown in figure 8

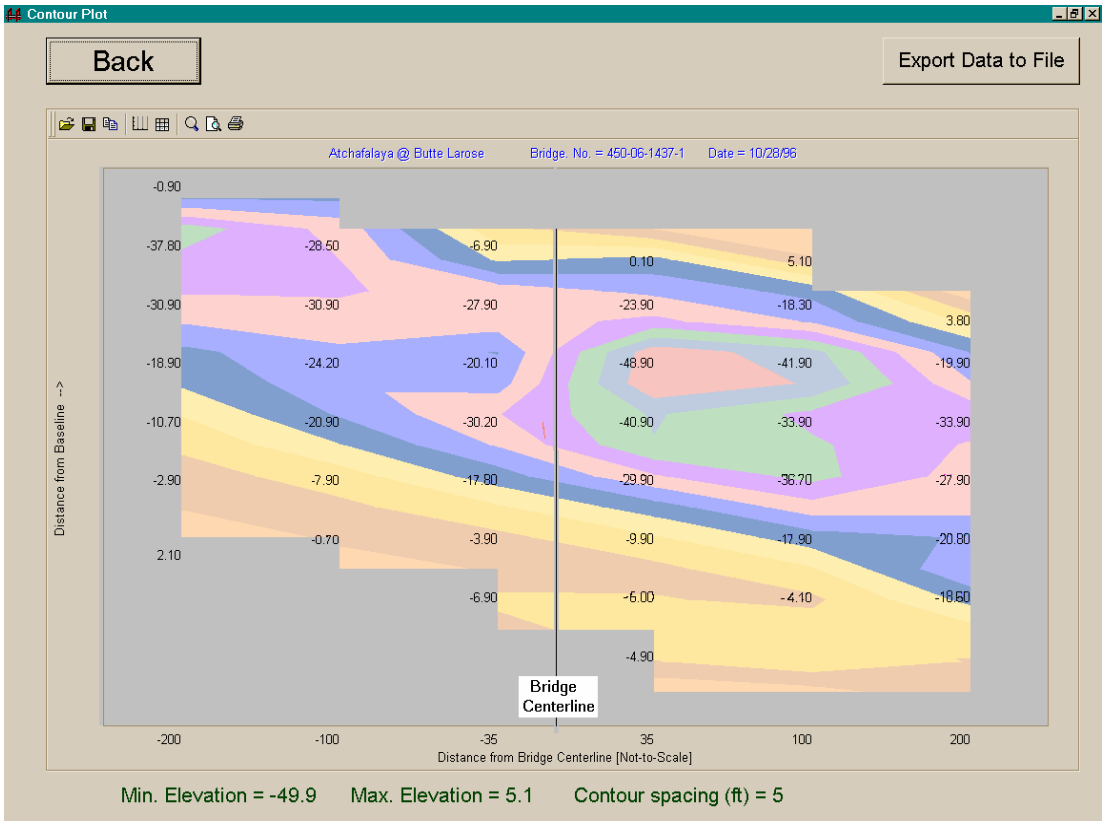

Figure 10. View of contour plot in the database program

Nondimensional Analysis of Clear-Water Scour at Bridge Contractions in Cohesive Soil

By

Oktay Güven[1], Joel G. Melville[2], and John E. Curry[3]

ABSTRACT

This paper presents a nondimensional formulation for the analysis of the time-dependent development of the depth of scour at bridge contractions in cohesive soils under clear-water conditions. The analysis is based on a new theory which is an extension of the clear-water scour theory for a long contraction that is currently used for noncohesive bed materials. The new theory is founded on the "scour rate in cohesive soils" (SRICOS) concepts introduced recently by Briaud and his colleagues at Texas A & M University. As part of the nondimensional formulation, two nondimensional scour time functions are introduced to facilitate calculation of the time-dependent scour depth in a contraction. An example is presented to illustrate the use of the nondimensional scour time functions.

INTRODUCTION

Recent studies by Briaud et al. (1999, 2001a and 2001b) have shown that the time-dependent development of foundation scour around bridge piers at stream crossings in cohesive soils may be estimated using erosion rate information obtained from erosion tests conducted on Shelby-tube samples of the bed soil by means of a new erosion function apparatus (EFA) developed by Briaud et al. (1999, 2001a). The EFA allows the measurement of the critical shear stress (minimum bed shear stress needed for erosion) of a sample of the bed soil and the erosion rate of the soil as a function of the bed shear stress imposed by the flowing stream (Briaud et al., 1999, 2001a). Briaud et al. (1999, 2001a, 2001b) have introduced a new method of analysis, called the "scour rate in cohesive soils" (SRICOS) method, based on the use of the EFA, to estimate the development of the depth of scour as a function of time around a circular cylindrical bridge pier, and have applied their method successfully to make predictions of the depth of scour at bridge piers in cohesive and very fine grained soils at several bridge sites (Briaud et al., 2001b). As also pointed out by Briaud et al. (2001b), at present the SRICOS method is limited to local pier scour around circular cylindrical piers, and additional work is needed to extend the method to other scour problems.

[1] Professor, Dept. of Civil Engineering, Auburn University, Auburn, Alabama, 36849-5337, U.S.A., (guven@eng.auburn.edu)
[2] Professor, Dept. of Civil Engineering, Auburn University, Auburn, Alabama, 36849-5337, U.S.A., (joel.melville@eng.auburn.edu)
[3] Hydraulic Engineer, Hydro-Engineering Solutions, LLC, Auburn, Alabama, 36831, U.S.A., (curryhes@bellsouth.net)

Encouraged by the availability of the EFA and building on the foundation provided by the recent studies of Briaud et al. (1999, 2001a, 2001b), G ven et al. (2001) have presented a new, simplified theory for the analysis of the time-dependent deve lopment of bed scour at a bridge contraction in a cohesive soil under clear-water conditions. This new theory is founded on the SRICOS concepts introduced by Briaud et al. (1999, 2001a, 2001b) and is an extension of the clear-water scour theory for a long contraction that is currently used for noncohesive bed materials (see, e.g., HEC-18 (Richardson and Davis, 1995)). The simplifying assumptions and limitations of the theory are described in detail by G ven et al. (2001); these include the assumptions that the flow in the contraction is subcritical, the flow rate is constant, the channel cross section is rectangular, the width of the contracted section remains constant throughout the time-dependent development of the scour, and the flow in the contracted reach is such that the bed shear stress may be related to the average flow velocity through an expression involving the Darcy-Weisbach friction factor for uniform flow in an open channel. While the theory has several limitations, and has not yet been tested completely with laboratory and field experiments, the theory does provide an estimate of an upper bound for the maximum flow depth for a given bed soil and a given flow rate at a bridge contraction under clear-water conditions, and allows the calculation of the development of the flow depth and the scour depth as a function of time for a constant, steady flow rate. Applications of the theory with actual EFA data for two different bed soils and several selected flow conditions have been presented by G ven et al. (2001)

The main purpose of this paper is to present a nondimensional formulation for the analysis of clear-water contraction scour based on the simplified theory presented by G ven et al. (2001). As part of the nondimensional formulation, two new nondimensional "scour time functions" are introduced to facilitate the calculation of the time-dependent development of the flow depth and the scour depth at a contraction for a given steady flow rate.

The next section includes an outline of the simplified theory presented by G ven et al. (2001). Following the outline of the theory, a description of the nondimensional formulation is presented, and the nondimensional scour time functions are introduced. An example application with actual EFA data for a particular soil and flow condition is included in the paper to illustrate the use of the nondimensional scour time functions.

THEORY

Clear-water scour in a contraction occurs when there is no bed material transport from the upstream reach or the bed material being transported from the upstream reach is transported through the contraction mostly in suspension (Richardson and Davis, 1995). With clear-water scour, the area of the contracted section increases until the bed shear stress, , becomes equal to the critical shear stress, $_c$, of the bed soil. As in most analyses (see, e.g., HEC-18 (Richardson and Davis, 1995)), it is assumed here that the width of the contracted section remains constant and the flow in the contraction is distributed uniformly along the width of the contraction, with a constant value of the flow rate per unit width, q, throughout the time-dependent development of the scour. This

means that, as the scour in the contraction progresses, the flow depth, y, increases and the average velocity, V = q/y, decreases with time until the depth of flow approaches its maximum value, y_{max}, corresponding to the limiting condition = $_c$.

Scour Depth

In a typical analysis of contraction scour at a bridge site, a flow model, such as HEC-RAS or WSPRO, is used to estimate the water surface elevation, the flow distribution, and the width and the average depth and velocity of flow in the main channel and overbank portions, if any, of the contracted section prior to the beginning of scour (see, e.g., HEC-18 (Richardson and Davis, 1995), and the references therein). The flow conditions at the contracted section at a bridge site are typically estimated (see, e.g., HEC-RAS (Brunner, 2001)) using the energy equation between the contracted section (section 2 in Fig. 1) and a section downstream from the bridge (section 1 in Fig. 1) at the end of the expansion reach. In current analyses of contraction scour with noncohesive materials, the time-dependent development of the flow depth is not considered, and assuming that the flow depth reaches its ultimate, maximum value, y_{max}, in a short period of time, the scour depth for a given flow condition is estimated as (Richardson and Davis, 1995)

$$y_s = y_{max} - y_i \tag{1}$$

where y_s is the estimate of the scour depth, and y_i is the initial flow depth at the contracted section before scour begins. It should be noted also that the scour depth estimate given by Equation 1 is based on the assumption that the elevation of the water surface in the contracted section remains constant during the development of the scour. As also indicated in HEC-18 (Richardson and Davis, 1995; page 13 of the original reference), this means that the velocity head, defined as $V^2/(2g)$ where g is the gravitational acceleration, is assumed to be negligible compared with the depth of flow, y, or that the Froude number, Fr, defined as $Fr = V/(gy)^{1/2}$ is nearly zero; furthermore, all possible head losses (h_L) which may occur in the expansion reach (Fig. 1) are assumed to be negligible.

If, as done in HEC-18 (Richard and Davis, 1995) to obtain Equation 1, it is assumed that the water surface elevation in the contraction remains constant during the development of the scour, the scour depth at any instant of time may be expressed as

$$s_1 = y_1 - y_i \tag{2}$$

where subscripted symbols have been used to denote the scour depth (s_1) and the flow depth (y_1) at the contracted section at any instant of time corresponding to the assumption of a constant water surface elevation.

If the velocity head is not negligible for a given flow condition, a possible assumption is that the total head remains constant during the development of the scour in the

contraction. This assumption leads to the following expression for the depth of scour at any instant of time:

$$s_2 = y_2 + \frac{q^2}{2gy_2^2} - \left(y_i + \frac{q^2}{2gy_i^2} \right) \tag{3}$$

where s_2, and y_2, are, respectively, the scour depth and the flow depth at the contracted section at any instant of time, corresponding to the assumption of a constant total head at the contraction. A definition sketch for the scour depth s_2 is given in Fig. 1.

The assumptions of a constant water surface elevation or a constant total head at the contraction during the development of scour are not entirely consistent with the energy principle, since the head loss, h_L, is expected to change as the scour develops. If the changes in h_L which occur during the development of the scour are taken into account, the scour depth at any instant of time may be expressed as:

$$s_3 = y_3 + \frac{q^2}{2gy_3^2} - \left(y_i + \frac{q^2}{2gy_i^2} \right) + \left(h_{Li} - h_L \right) \tag{4}$$

where s_3 and y_3 are, respectively, the scour depth and the flow depth at the contracted section which are consistent with the energy principle, and h_{Li} is the head loss at the initial instant before scour begins.

In this paper, we consider only the development of s_2, and as a special case, of s_1; the analysis of the development of s_3 is not included as the analysis of s_3 is somewhat more complicated due to the head loss terms appearing in Equation 4.

Bed Shear Stress

It is assumed here that the bed shear stress, , may be expressed as

$$\tau = f\frac{\rho V^2}{8} = f\frac{\rho q^2}{8y^2} \tag{5}$$

where f is the bed friction factor and is the fluid density. Following Henderson (1966), and Chow et al. (1988), and assuming that the contracted section is sufficiently wide so that the hydraulic radius is equal to the depth, the friction factor may be expressed as

$$\sqrt{f} = \frac{-1}{2\left[\log\left(\frac{k_r}{3} + \frac{2.5}{Re\sqrt{f}} \right) \right]} \tag{6}$$

where Re and k_r are, respectively, the Reynolds number and the relative roughness defined by

$$Re = \frac{V(4y)}{\nu} \tag{7}$$

$$k_r = \frac{k_s}{4y} \tag{8}$$

where k_s is the effect
viscosity. Using Equations 6 and 8, the friction factor may be expressed also as

$$f = \frac{0.25}{\left[\log\left(\frac{k_s}{12y} + \frac{2.5}{Re\sqrt{f}}\right)\right]^2} \tag{9}$$

Following Roberson and Crowe (1997), G ven et al. (2001) have used an explicit equation given by Swamee and Jain (1976) to approximate the dependence of f on Re and k_r instead of Equation 6. The approximate, explicit relation of Swamee and Jain (1976) is expressed as

$$f = \frac{0.25}{\left[\log\left(\frac{k_r}{3.7} + \frac{5.74}{Re^{0.9}}\right)\right]^2} \tag{10}$$

Strictly, Equation 10 was developed for pipe flow; however, it may also be used, as an approximation, for open channel flow as may be verified by comparison of the f values obtained with Equations 9 and 10.

It may be useful to note that since the unit discharge, q, in the contraction is assumed to be constant throughout the development of scour, the Reynolds number, Re = 4 q/í, is also constant. Regarding the effective roughness height of the bed material, Briaud et al. (2001a, 2001b) have suggested that $k_s = 0.5D_{50}$ for the cohesive soils which they studied, where D_{50} is the median soil size.

In the present study, one of the soils for which EFA data are available from Briaud et al. (2001a) is considered in the applications of the theory developed here. The soil considered here is a low plasticity clay soil from the Trinity River (Briaud et al., 2001a). As done by G ven et al. (2001), this soil will be referred to as Soil No. 1, for brevity. The median size, D_{50}, of the soil, is given as D_{50}=0.06 mm by Briaud et al. (2001a).
The erosion function of Soil No. 1 is linear (Briaud et al, 2001a). The linear erosion function of Soil No. 1 may be expressed as (G ven et al., 2001)

$$R(\tau) = S_i\left(\tau - \tau_c\right) \quad \text{for } \tau > \tau_c \tag{11}$$

where $_c$ = 2.74 N/m^2 and S_i = 0.51 (mm/hr)/(N/m^2), and R( ) = 0 for $_c$.

In general, the erosion function of a soil may be nonlinear (Briaud et al., 2001a). In the present study, it is assumed that any erosion function may be approximated as a piecewise linear function over specified ranges of the bed shear stress as follows:

$$R(\tau) = R_j + S_j(\tau - \tau_j) \text{ for } \tau_j \le \tau < \tau_k \tag{12}$$

where S_j is the slope of the erosion function over the range $_j$ < $_k$, and R_j is the erosion rate at = $_j$.

Limits of the Flow Depth

It is assumed in this study that the flow in the contraction is subcritical. Therefore, the lower limit of the flow depth is the critical depth, y_{cr}, corresponding to the unit discharge, q, in the contraction:

$$y_{cr} = \left(q^2 / g\right)^{1/3} \tag{13}$$

For subcritical flow, the Froude number, Fr, is less than one (Fr<1), and the flow depth, y, is greater than the critical depth ($y>y_{cr}$) (Henderson, 1966).

If there is scour in the contraction, the upper limit of the flow depth is the maximum flow depth, y_{max}, which occurs when the bed shear stress, , equals the critical shear stress, $_c$, for the bed soil. At this limit, using Equations 5, 6, 7 and 8, and rearranging, one obtains

$$y_{max} = \left(\frac{\rho q^2}{8\tau_c}\right)^{1/2} \sqrt{f} \tag{14}$$

where

$$\sqrt{f} = \frac{-1}{2\left[\log\left(\frac{k_s}{12y_{max}} + \frac{2.5}{Re\sqrt{f}}\right)\right]} \tag{15}$$

For known values of q, $_c$, Re and k_s, Equations 14 and 15 may be solved simultaneously for y_{max}.

Development of Scour with Time

The time-dependent behavior of scour depends on the rate of scour, ¿, of the bed soil. It is assumed here that the rate of scour is given by the erosion function determined from the EFA,

$$¿ = R(\ ) \tag{16}$$

where R( ) is the erosion function which gives the rate of scour as a function of the bed shear stress, , in the contraction. The development of scour depends furthermore on the particular assumptions and relation used for estimating the scour depth. In this paper, we consider only the development of the flow depth y_2, and as a special case, of y_1.

Starting with the definition of the scour depth, s_2, given by Equation 3 and taking the derivative of s_2 with respect to time, and rearranging, one obtains

$$\frac{ds_2}{dt} = \frac{dy_2}{dt}\left(1 - \frac{q^2}{gy_2^3}\right) \tag{17}$$

Dropping the subscript 2 from s_2 and y_2, for simplicity of notation, and also using Equation 13 $\left(q^2 = gy_{cr}^3\right)$, Equation 17 may be transformed as

$$\frac{ds}{dt} = \frac{dy}{dt}\left(1 - \frac{y_{cr}^3}{y^3}\right) \tag{18}$$

Since $ds/dt = \ = R(\tau)$, Equations (16) and (18) may be combined to obtain

$$\frac{dy}{dt} = \frac{R(\tau)}{1 - \left(y_{cr}^3 / y^3\right)} \tag{19}$$

or

$$dt = \frac{dy}{R(\tau)} - \frac{y_{cr}^3}{y^3}\frac{dy}{R(\tau)} \tag{20}$$

Since the shear stress, , is a function of the flow depth (Equation 5), the erosion rate, R( ), depends on the depth, y, also; hence, the right-hand side of Equation 19 is a function of y. Equation 19 may be solved to obtain y as a function of time, t, or equation 20 may be integrated to obtain time as a function of the flow depth. It may be useful to note also that the term y_{cr}^3 / y^3 which appears in Equations 18, 19, or 20 would be negligible if the velocity head is small compared to the depth. This means that solutions of Equations 19 or 20 which neglect this term give the development of y_1 with time, whereas solutions which do not neglect this term give the development of y_2 with time. Once the flow depth (y_2 or y_1) is obtained as a function of time, the corresponding scour depth (s_2 and s_1) may be determined using Equation 3 or 2 (G ven et al., 2001).

NONDIMENSIONAL FORMULATION

Various expressions obtained for the relations between the flow depth and the bed shear stress (Equation 5) or between the maximum flow depth and the critical shear stress (Equation 14), and for the time-dependent development of the flow depth (Equation 20) may be transformed into nondimensional forms if certain reference parameters and nondimensional variables are defined. The following parameters and nondimensional variables are introduced for this purpose:

$$y_{RJ} = \frac{1}{10}\left(\frac{\rho q^2}{8\tau_j}\right)^{1/2} \tag{21}$$

$$u = \frac{y}{y_{RJ}} = 10y\left(\frac{8\tau_j}{\rho q^2}\right)^{1/2} \tag{22}$$

$$u_{cr} = \frac{y_{cr}}{y_{RJ}} = \frac{\left(q^2/g\right)^{1/3}}{y_{RJ}} \tag{23}$$

$$t_{RJ} = \frac{y_{RJ}}{S_j\tau_j} \tag{24}$$

$$T = \frac{tS_j\tau_j}{y_{RJ}} = \frac{t}{t_{RJ}} \tag{25}$$

$$\kappa_j = 10k_s\left(\frac{8\tau_j}{\rho q^2}\right)^{1/2} = \frac{k_s}{y_{RJ}} \tag{26}$$

where y_{RJ} is a reference depth (length) based on $_j$; u is the nondimensional flow depth relative to the reference length, y_{RJ}; u_{cr} is the nondimensional critical flow depth; t_{RJ} is a reference time; T is the nondimensional time relative to the reference time, t_{RJ}; and $_j$ is the nondimensional roughness height relative to the reference length, y_{RJ}.

Time-Dependent Development of Scour

Using Equations 21, 22, 25 and 26, Equation 20 may be transformed as

$$dT = \frac{du}{g_R(u)} - u_{cr}^3\frac{du}{u^3 g_R(u)} \tag{27}$$

where

$$g_R(u) = \frac{R(\tau)}{S_j \tau_j} = a + \frac{100 f(Re, \kappa_j, u)}{u^2} \tag{28}$$

$$a = \frac{R_j}{S_j \tau_j} - 1 \tag{29}$$

$$f(Re, \kappa_j, u) = \frac{0.25}{\left[\log\left(\frac{\kappa_j}{12u} + \frac{2.5}{Re\sqrt{f}}\right)\right]^2} \tag{30}$$

Integration of Equation 27 gives

$$T_e - T_b = G(u_b, u_e) - u_{cr}^3 H(u_b, u_e) \tag{31}$$

where the subscripts b and e, respectively, denote the beginning and end of a time interval, $t = t_e - t_b$, and

$$G(u_b, u_e) = \int_{u_b}^{u_e} \frac{du}{g_R(u)} \tag{32}$$

$$H(u_b, u_e) = \int_{u_b}^{u_e} \frac{du}{u^3 g_R(u)} \tag{33}$$

$$u_b = \frac{y_b}{y_{RJ}} \tag{34}$$

$$u_e = \frac{y_e}{y_{RJ}} \tag{35}$$

The actual time difference, $\Delta t = t_e - t_b$, required for the flow depth to increase from y_b to y_e ($y_e > y_b$) may be obtained as

$$\Delta t = t_e - t_b = \frac{y_{RJ}}{S_j \tau_j}\left[T_e - T_b\right] = t_{RJ}\left[T_e - T_b\right] \tag{36}$$

or

$$\Delta t = t_{RJ}\left[G(u_b, u_e) - u_{cr}^3 H(u_b, u_e)\right] \tag{37}$$

NONDIMENSIONAL SCOUR TIME FUNCTIONS

The nondimensional functions $G(u_b, u_e)$ and $H(u_b, u_e)$ depend on the Reynolds number, Re, the roughness parameter, $_j$, and the nondimensional flow depths u_b and u_e. These functions, which may be called "scour time functions" may be evaluated by means of numerical integration for specified values of the Reynolds number and the roughness parameter. However, as several nondimensional parameters (Re, $_j$, u) are involved, numerical evaluation of the nondimensional integrals defined by Equations 32 and 33 may not provide any appreciable advantage over direct numerical solution of the original governing differential equations (Equation 19 or 20) on a computer.

The nondimensional formulation may still be quite useful in some cases. In cases where the Reynolds number and the roughness parameter are such that the bed behaves as a smooth boundary for the range of u, u_b u u_e, considered, closed-form expressions may be obtained for the integrals appearing in Equations 32 and 33. If the bed behaves as a smooth boundary, then the friction factor, f, depends only on the Reynolds number, Re. Since Re = 4q/í = constant throughout the development of the scour, the friction factor remains constant also, if the bed behaves as a smooth boundary. In such cases, the function $g_R(u)$ defined by Equation 28 may be expressed as

$$g_R(u) = a + \frac{c}{u^2} \tag{38}$$

where a is a constant defined by Equation 29

and

$$c = 100f = \text{ constant} > 0 \tag{39}$$

If the function $g_R(u)$ is given by Equation (38), closed-form expressions may be obtained for the integrals appearing in Equations (32) and (33), as follows:

$$IG = \frac{du}{g_R(u)} = \frac{u^2 du}{au^2 + c} \tag{40}$$

$$IH = \frac{du}{u^3 g_R(u)} = \frac{du}{u\left(au^2 + c\right)} \tag{41}$$

Since c > 0, the indefinite integrals IG and IH may be expressed as (Selby, 1972, pages 399, 400 of the original reference):

$$IG(u) = \frac{u}{a} - \frac{\sqrt{c/a}}{a} \tan^{-1}\left(\frac{u}{\sqrt{c/a}}\right) \quad \text{if } a > 0 \tag{42}$$

$$IG(u) = \frac{u^3}{3c} \qquad \text{if } a = 0 \tag{43}$$

$$IG(u) = \frac{u}{a} - \frac{1}{2a}\frac{\sqrt{c}}{\sqrt{-a}}\ln\left(\frac{\sqrt{c} + u\sqrt{-a}}{\sqrt{c} - u\sqrt{-a}}\right) \quad \text{if } a < 0 \tag{44}$$

$$IH(u) = \frac{1}{2c}\ln\left(\frac{u^2}{au^2 + c}\right) \tag{45}$$

In terms of the functions IG and IH, the nondimensional scour time functions G and H may be expressed as

$$G(u_b, u_e) = IG(u_e) - IG(u_b) \tag{46}$$

$$H(u_b, u_e) = IH(u_e) - IH(u_b) \tag{47}$$

so that (see Equation 41)

$$T_e - T_b = \left[IG(u_e) - IG(u_b)\right] - u_{cr}^3\left[IH(u_e) - IH(u_b)\right] \tag{48}$$

and

$$\Delta t = t_{RJ}\left(T_e - T_b\right) \tag{49}$$

The solution given by Equation 48 is an exact solution if f is constant. If f is not constant over the range of u considered (u_b u u_e), it is thought that the closed-form solution may still be useful to obtain an approximate estimate of t, provided that f does not vary excessively over the range of u (u_b to u_e) considered.

ILLUSTRATIVE EXAMPLE

G ven et al. (2001) have presented several applications with three different flow conditions and two different soils for which EFA data are available. In this section, an example is presented to illustrate the use of the nondimensional scour time functions for one case; namely, the case of flow condition FC1 and Soil No. 1 studied previously by G ven et al. (2001).

For this case, the unit discharge is q = 10.59 m^2/s, and the initial depth at the contraction is y_i = 2.84 m. The soil has a median size of D_{50} = 0.00006 m, a critical shear stress of $_c$ = 2.74 N/m^2, and a linear erosion function with R_j = 0, $_j$ = $_c$ = 2.74 N/m^2 and a slope of S_j = S_i = 0.51 (mm/hr)/(N/m^2) = 0.01244 (m/day)/(N/m^2). Using a density of = 1000 kg/m^3 and a kinematic viscosity of í = 10^{-6} m^2/s for the fluid (water), and assuming that

the roughness height is $k_s = 0.50D_{50} = 0.00003$ m, as suggested by Briaud et al. (2001a, 2001b), the values of various parameters are obtained as follows:

Reynolds number, Re = 4q/í = 4.236 x 10^7

Reference depth, $y_{RJ} = \frac{1}{10}\left(\frac{\rho q^2}{8\tau_c}\right)^{1/2} = 7.153\text{m}$

Nondimensional roughness, $_j = k_s/y_{RJ} = 4.2 \times 10^{-6}$

Nondimensional critical depth, $u_{cr} = \frac{\left(q^2/g\right)^{1/3}}{y_{RJ}} = 0.31493$

Nondimensional critical flow parameter, $u_{cr}^3 = 0.03124$

Reference time, $t_{RJ} = y_{RJ}/(S_j\ _j) = 213.3$ days

Nondimensional erosion parameter, $a = R_j/(S_j\ _j) - 1 = -1$

Since a = – 1, the forms of the nondimensional functions IG(u) and IH(u) for this case are as follows:

$$IG(u) = -u + \frac{\sqrt{c}}{2}\ln\left(\frac{\sqrt{c}+u}{\sqrt{c}-u}\right) \tag{50}$$

$$IH(u) = \frac{1}{2c}\ln\left(\frac{u^2}{c-u^2}\right) \tag{51}$$

Using the Swamee-Jain equation (Equation 10) for the friction factor, f, G ven et al. (2001) obtained y_{max} = 6.01 m. Using the Henderson equation (Equation 9) for f, one obtains y_{max} = 6.01 m, again. At this depth, both equations give f = 0.00706, for this case.

G ven et al. (2001) studied the time-dependent development of the flow depths y_2 and y_1, and the scour depths s_2 and s_1 for this case, and several other cases, by direct numerical integration of the governing differential equation. Here, we focus only on the development of y_2, for brevity.

Table 1 shows the results obtained for the development of the flow depth y_2 for the flow condition FC1 and Soil No. 1. Table 1 includes several flow depths and the corresponding scour times obtained by various means, for comparison. In Table 1, t_A is the scour time calculated by G ven et al. (2001) by direct numerical integration using the Swamee-Jain equation for f, t_B is the scour time obtained by means of the present closed-form nondimensional scour functions using the Swamee-Jain equation for f, and t_C is the scour time obtained by means of the closed-form scour functions using the Henderson equation for f. It may be seen from Table 1 that the scour times (t_B and t_C) obtained with

the closed-form scour time functions differ from the times (t_A) obtained by direct numerical integration; this is because the friction factor f is not constant and varies with the depth of flow for this case (see Table 2). However, the results indicate that the closed-form nondimensional scour time functions may be useful even when the friction factor f is not constant. A tabulation of the actual calculations performed to obtain the scour times t_C presented in Table 1 is shown in Table 2. All the calculations shown in Table 2 were performed using a hand-held calculator. For brevity, details of the calculations for the scour time, t_B, obtained with the Swamee-Jain equation for f are not shown in this paper.

Table 1. Scour times for various flow depths for flow condition FC1 and Soil No.1

Flow Depth y (m)	Remark	Time(1) t_A (days)	Time(2) t_B (days)	Time(3) t_C (days)
2.84	y_i	0	0	0
3.02	y_2	1.00	0.90	0.90
3.33	y_2	3.00	3.20	3.19
3.53	y_2	5.00	5.25	5.22
5.95	y_2	250	262	266
6.01	y_{max}			

(1)Obtained by direct numerical integration, using the Swamee-Jain equation for f (G ven et al., 2001).
(2)Obtained by means of the closed-form scour time functions, using the Swamee-Jain equation for f.
(3)Obtained by means of the closed-form scour time functions, using the Henderson equation for f.

Table 2. Calculations table for scour time t_C

Flow Depth y (m)	u(1)	f(2)	c(3)	IG(u)(4)	IH(u)(5)	T(u)(6)	Time t_C(7) (days)
2.84	0.397	0.00742	0.742	0.03234	–0.88305	0.05993	0
3.02	0.422	0.00738	0.738	0.03990	–0.77611	0.06415	0.90
3.33	0.466	0.00733	0.733	0.05646	–0.59017	0.07490	3.19
3.53	0.494	0.00730	0.730	0.06967	–0.47179	0.08441	5.22
5.95	0.832	0.007063	0.7063	1.39167	2.75764	1.30552	266

(1) $u = y / y_{RJ};\ y_{RJ} = 7.153\text{m}$

(2) $f = \dfrac{0.25}{\left[\log\left(\dfrac{\kappa_j}{12u} + \dfrac{2.5}{Re\sqrt{f}}\right)\right]^2};\ \kappa_j = 4.2 \text{ x } 10^{-6}$

(3) $c = 100f$

(4) $IG(u) = -u + \dfrac{\sqrt{c}}{2}\ln\left(\dfrac{\sqrt{c}+u}{\sqrt{c}-u}\right)$

(5) $IH(u) = \dfrac{1}{2c}\ln\left(\dfrac{u^2}{c-u^2}\right)$

(6) $T(u) = IG(u) - u_{cr}^3 IH(u);\ u_{cr}^3 = 0.03124$

(7) $t_C = t_{RJ}\left[T(u) - T(u_i)\right];\ u_i = y_i / y_{RJ} = 0.397;\ t_{RJ} = 213.3\text{days}$

CONCLUSION

The results indicate that the nondimensional scour time functions introduced here may be useful to obtain estimates of the scour time for clear-water scour at bridge contractions in cohesive soils.

ACKNOWLEDGEMENTS

This study was supported by the Alabama Department of Transportation (Research Project No. 930-490) and administered by the Highway Research Center of Auburn University. The authors thank Dr. Frazier Parker for his support as Director of the Highway Research Center. The authors also thank Ms. Priscilla Clark who typed this paper.

REFERENCES

1. Briaud, J.L., F.C.K. Ting, H.C. Chen, R. Gudavalli, S. Perugu, and G. Wei, 1999, "SRICOS: Prediction of Scour Rate in Cohesive Soils at Bridge Piers", *Journal of Geotechnical and Geoenvironmental Engineering*, Vol. 125, No. 4, April 1999, pp. 237-246, American Society of Civil Engineers, Reston, Virginia, U.S.A.

2. Briaud, J.L., F.C.K. Ting, H.C. Chen, Y. Cao, S.W. Han, and K.W. Kwak, 2001a, "Erosion Function Apparatus for Scour Rate Predictions", *Journal of Geotechnical and Geoenvironmental Engineering*, Vol. 127, No. 2, February 2001, pp. 105-113, American Society of Civil Engineers, Reston, Virginia, U.S.A.

3. Briaud, J.L., H.C. Chen, K.W. Kwak, S.W. Han, and F.C. Ting, 2001b, "Multiflood and Multilayer Method for Scour Rate Prediction at Bridge Piers", *Journal of Geotechnical and Geoenvironmental Engineering*, Vol. 127, No. 2, February 2001, pp. 114-125, American Society of Civil Engineers, Reston, Virginia, U.S.A.

4. Brunner, G.W., 2001, *HEC-RAS, River Analysis System Hydraulic Reference Manual, Version 3.0*, Hydrologic Engineering Center, U.S. Army Corps of Engineers, Davis, California, January 2001.

5. Chow, V.T., D.R. Maidment, and L.W. Mays, 1988, *Applied Hydrology.* McGraw-Hill, Inc., New York.

6. Güven, O., J.G., Melville, and J.E. Curry, 2001, *Analysis of Clear-Water Scour at Bridge Contractions in Cohesive Soils*, Interim Report No. 930-490, Highway Research Center, Auburn University, Alabama.

7. Henderson, F.M., 1966, *Open Channel Flow*. MacMillan Co., New York.

8. Richardson, E.V., and S.R. Davis, 1999, *Evaluating Scour at Bridges*, 3rd Edition. Report FHWA-IP-90-017, Hydraulic Engineering Circular No. 18 (HEC-18), FHWA, U.S. Department of Transportation, 1995.

9. Roberson, J.A., and C.T. Crowe, 1997, *Engineering Fluid Mechanics*, 6th Edition. John Wiley and Sons, Inc., New York.

10. Selby, S.M., 1972, *Standard Mathematical Tables*, 20th Edition. CRC Press, Cleveland, Ohio.

11. Swamee, P.K., and A.K. Jain, 1976, "Explicit Equations for Pipe-Flow Problems", *Journal of the Hydraulics Division*, ASCE, Vol. 102, No. HY5, May 1976, American Society of Civil Engineers, Reston, Virginia, U.S.A.

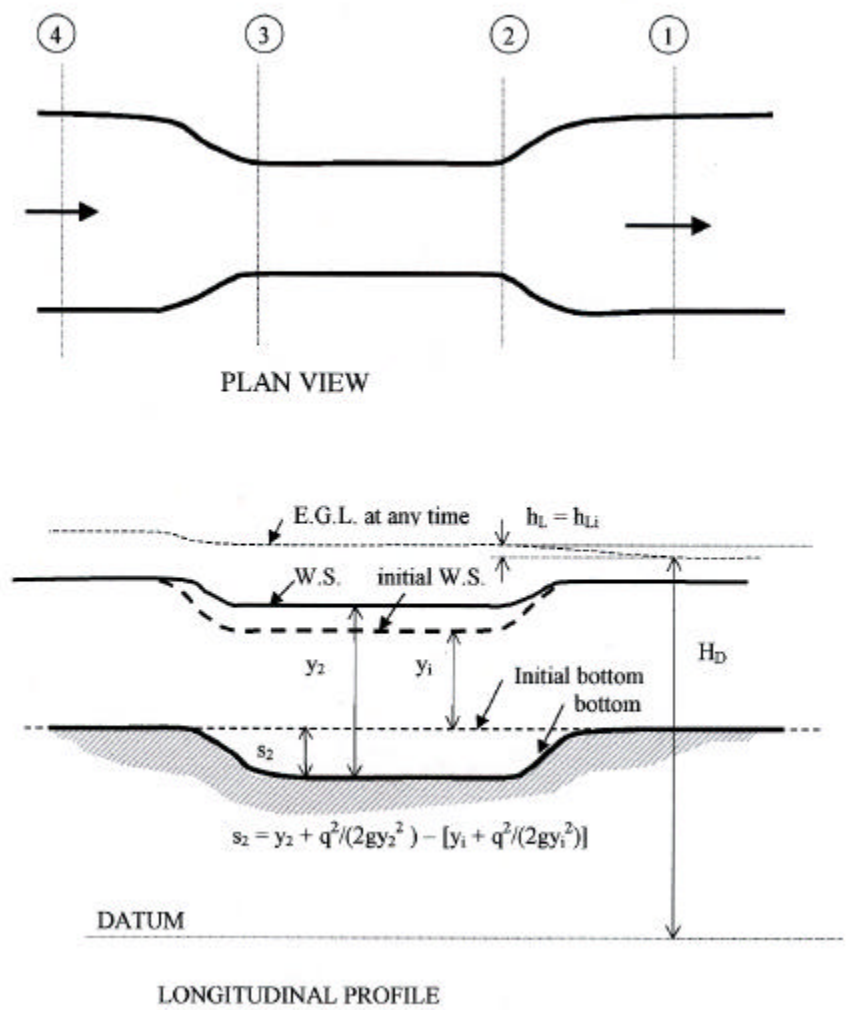

Fig. 1 – Schematic diagram of flow at a bridge contraction and definition sketch for contraction scour depth s_2 (E.G.L. denotes the "energy grade line"; W.S. denotes the "water surface"; H_D is the total head at section 1).

FE Analysis of Coastal Cliff Erosion due to Ocean Wave Assailing

By

Kazuya Yasuhara[1], Satoshi Murakami[2], Yashunori Kanno[3], Zishien Wu[4],

ABSTRACT

The coastal erosion is divided into two categories : (i) sand erosion, (ii) cliff erosion. The mechanism and countermeasures for those two have mainly been pursued from coastal engineering point of view. Unfortunately, less attention has been paid to the cliff erosion from a viewpoint of geotechnical engineering. Rather, much attention has been directed from the standpoint of geology and geomorphology. Based on the extensive achievements on the problem in Japan which had been carried out by Sunamura (1992) using the methodology of the geomorphology, further investigation by the authors has been performed by the authors (2002) from a viewpoint of geotechnical engineering. The results by the authors include the mechanism, prediction and countermeasure with a special emphasis being placed on the cliff erosion of rocky coasts at Ibaraki Prefecture, Japan. Among them, the current paper aims at describing the successful results of prediction from the finite element analysis combined with the crack propagation theory involved in the field of fracture mechanics. This analysis requires unit volume weight, compressive strength, tensile strength, and Young's modulus of rocks consisting of the coastal cliff. It is indicated from analysis that:

1) Coastal cliffs consisting of soft rocks become unstable depending on increase in the eroded distance of the toe of cliffs. The failure of rocky coasts is more sensitive to tensile strength than to compressive strength of rocks.

2) The FE analysis considering the crack propagation in rocks can predict of the progress of failure in rocky coasts. The results from the FE analysis lead to construction of a design chart for roughly predicting the possibility of collapse when the geographical conditions at a given site and the geotechnical properties of a rock are given.

INTRODUCTION

The erosion at the coast has become chronic in Japan. The coastal erosion is generally

[1] Professor, Department of Urban and Civil Engineering, Ibaraki University, Hitachi, Ibaraki, 316-8511, Japan.

[2] Research Assistant, Department of Urban and Civil Engineering, Ibaraki University, Hitachi, Ibaraki, 316-8511, Japan.

[3] Graduate Student, Department of Urban and Civil Engineering, Ibaraki University, Hitachi, Ibaraki, 316-8511, Japan..

[4] Professor, Department of Urban and Civil Engineering, Ibaraki University, Hitachi, Ibaraki, 316-8511,Japan.

divided into the beach erosion and the cliff erosion. Less attention has been paid to the cliff erosion than to the beach erosion. In addition, the researches on the cliff erosion have mainly been limited to the fields of coastal engineering, geology and geomorphology, and have scarcely included the geotechnical aspects. Even in the extensive achievements for the erosion of rocky coasts in Japan which have been carried out by Sunamura (1992), less information has been described from the geotechnical point of view. Authors (1995, 1997, 1999) have been investigating the mechanism, proposing the prediction and exploring the countermeasures in the past few years. Based on the previous studies, the current paper aims to propose the design charts and the predictive manual through the results from the numerical analysis by using the finite element method incorporating the crack propagation theory. Photo.2-Izura Coast

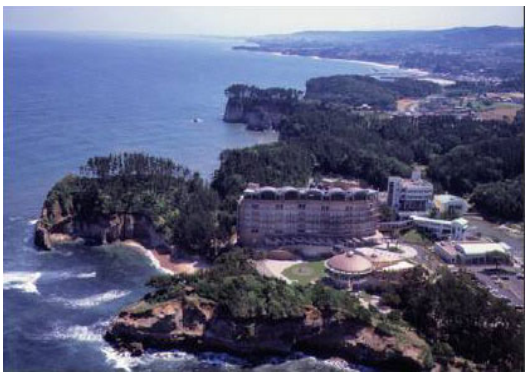

Photo.1-Unomiaki Coast

Photo.2-Izura Coast

MECHANISM OF COASTAL CLIFF EROSION

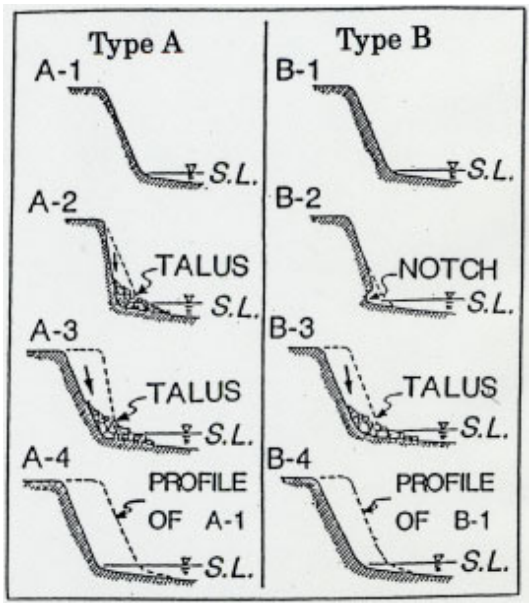

Fig.1-The process of Coastal Cliff Erosion (Sunamura)

Fig. 1 shows a typical result of the profile changes of laboratory cliffs caused by breaking waves. According to the investigation by Sunamura, the Japanese style of cliff erosions pertains to the type-B from the two types in Fig. 1. In this type, the toe of the cliff is eroded due to assailing ocean waves and the notch is formed. The rocky coast collapses when a certain distance of this notch formed due to wave actions is attained. However, the mechanism of the collapse has remained unknown. For example, no method has been found to determine whether the failure mode must be in the compressive failure or in the tensile failure. It is therefore required for taking countermeasures to deal with the situation to predict when and how the collapse initiates.

CRACK PROPAGATION ANALYSIS USING FINITE ELEMENT METHOD

The crack propagation analysis is based on the idea of the biaxial principal failure method that the crack occurs when the tensile major principal stress exceeds the tensile strength used in the analysis by considering the self-weight in whole the objective area. The analysis is characterized by:

1) the elements that undergo the crack are taken off by postulating that they are assumed not to retain their strength.
2) the analysis in the new area is repeated until the computation is converged. The

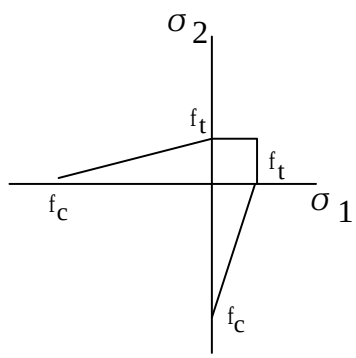

Fig.2-The Crack Generation Criteria

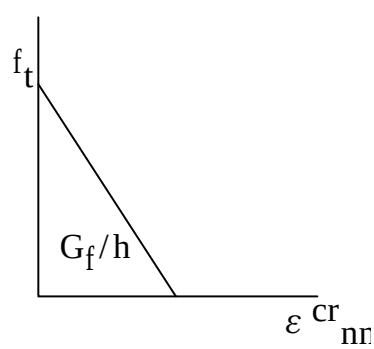

Fig.3-Tensile Softening Criteria

collapse possibility is estimated by means of the propagation condition of cracks that occur in the cliff due to the formation and development of notches.

The distributed crack model is employed in predicting the crack occurrence phenomena by means of the finite element analysis that incorporate the following:

1) The crack generation condition : this is governed by the condition as shown in Fig. 2.

2) As the softening of the material after the occurrence of the cracks, the linear tensile softening is adopted as shown in Fig. 3. The ultimate crack strain necessary to meet this condition is given by:

$$\varepsilon^{cr}{}_{nn.ult} = \frac{1}{\alpha}\frac{G_f{}^{I}}{h} \tag{1}$$

where α : angle of gradient of the cliff, G_f^I : failure energy, h : equivalent converted distance of one element.

3) The shear retention after the occurrence of tension cracks is assumed to be constant, that is, β is kept constant during shearing which is equal to 0.05.

OBJECTIVE MODEL FOR TWO DIMENSIONAL ANALYSIS

Analytical Procedure

The crack propagation analysis by using a FE analysis for exploring stability of rocky coasts is performed by following the procedure as (Fig. 4):

i)Self-weight analysis for the objective rocky coast undergoing erosion at the toe of the cliff due to assailing ocean waves was conducted to find the elements where cracks occur.

ii)By assuming that the rock elements with cracks lose strength leading to failure, the new region in which the elements with cracks are eliminated is set for the successive analysis.

iii) Self-weight analysis was carried out again for the new analytical region without elements where cracks take place.

iv) This procedure from (i) to (iii) is repeated until the analytical solution is diverged.

The divergence of the solution in this procedure indicates the condition that the some elements with cracks being taken place suffer from collapse. Accordingly, the collapse seems to occur and propagate from the bottom to the top of the cliff, as is shown in Fig. 5.

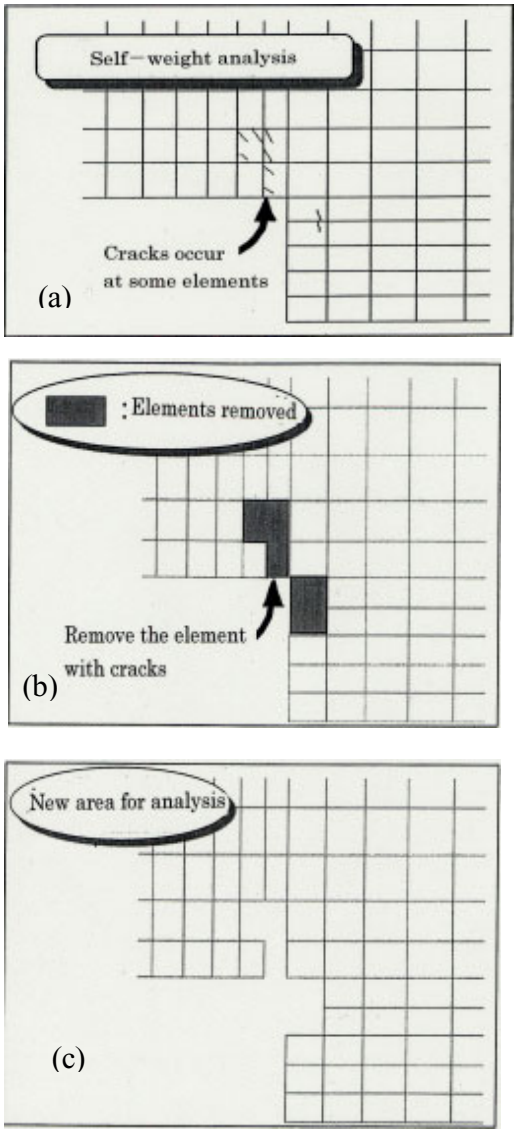

Fig.4-Analytical Procedure

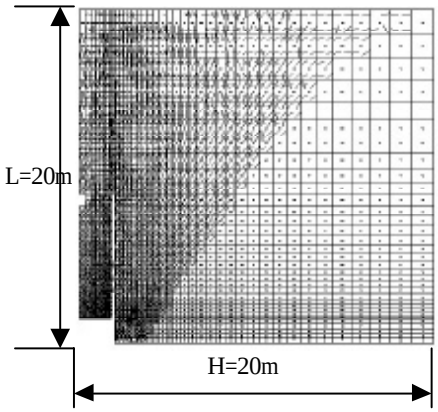

Fig.5-An Example for FE Analysis

Two-dimensional Modeling of the Objective Ground for Finite Element Analysis

For modeling the coastal cliff whose typical configuration is shown in Fig. 6, the following assumptions are employed:

i) The coastal cliff is formed by the homogeneous rock and deformation of rocky coasts occurs under the plane strain condition.

ii) Base foundations supporting the cliff consist of the extremely hard rocks.

iii) The base is constrained with the vertical and the horizontal directions, while the back face is constrained at the vertical direction only.

The two-dimensional FE analysis was conducted by changing the height of rocky

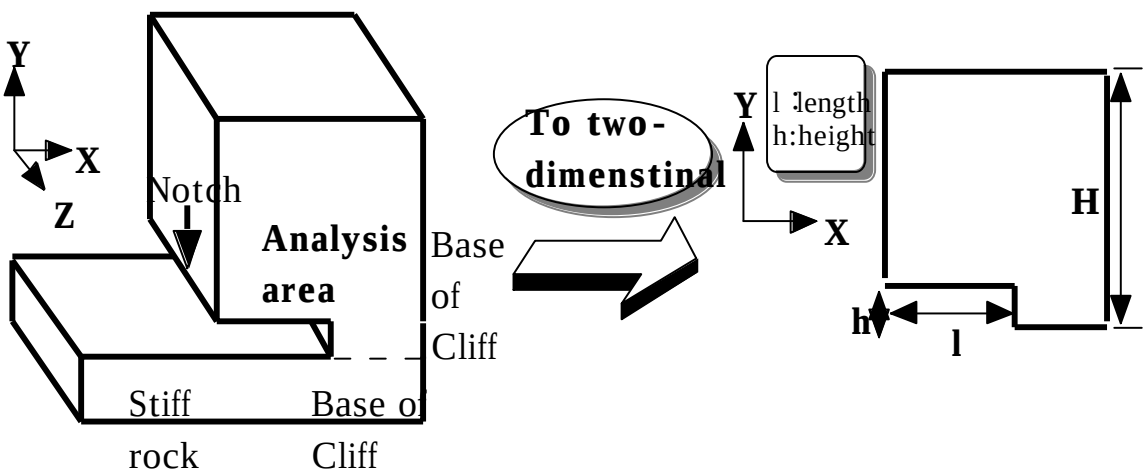

Fig6-Model for FE Analysis

coast, the gradient of the slope, and the width as is shown in Fig. 6. The width and height of the notch formed by erosion are also assumed 1m and 1m, respectively.

SELECTION OF PRAMETERS NECESSARY FOR ANALYSIS

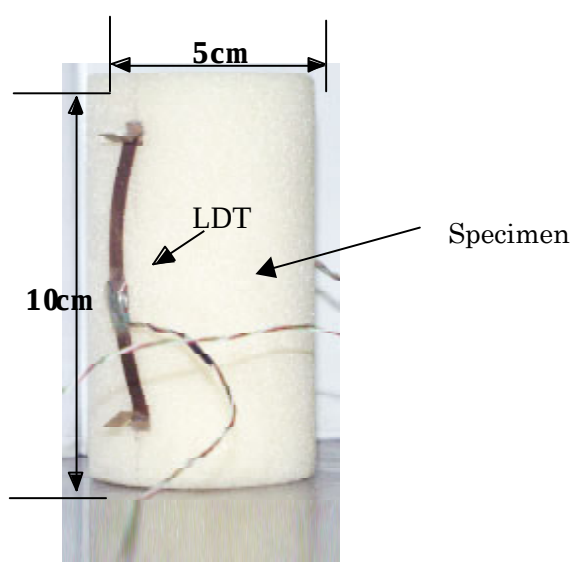

Fig.7-Specimen attached by LDT

The parameters necessary for CPA-FE analysis are : unit volume weight, compression and tensile strengths, and elastic modulus. The compressive and tensile strengths, f_c, f_t were obtained from unconfined compression and Brazilian tests, respectively, at laboratory on rock samples. The elastic modulus, E, was determined from small strain which was measured using the local displacement transducer (LDT) attached at the specimen in unconfined compression tests as shown in Fig. 7. The typical examples of the results from unconfined compression and Brazilian tests on a mud rock that was taken at the coastal cliff of the Northern Ibaraki, Japan are presented in Figs. 8a, b. A considerable difference in the elastic modulus determined from the results using the outer displacement meter and the LDT was observed. This gives the results from numerical computation based on the crack propagation analysis (CPA) as will be described in the later part of the paper.

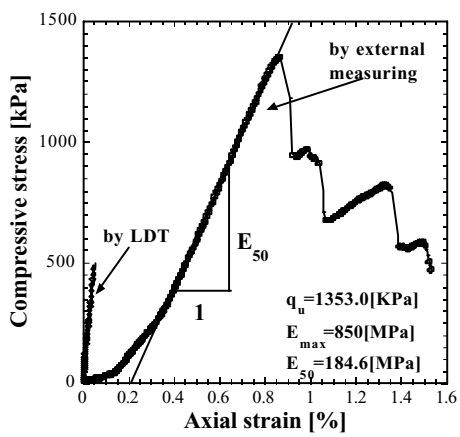

Fig.8a-Results from Unconfined Compression Test

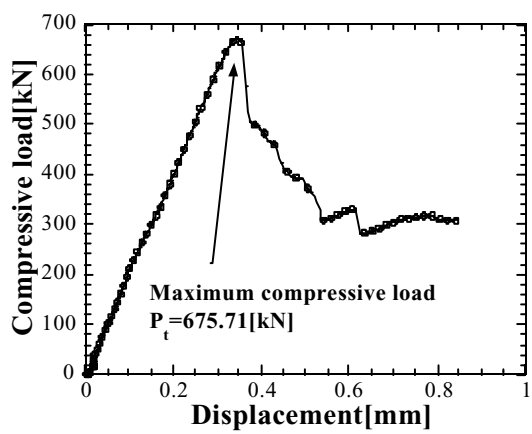

Fig.8b-Results from Brazilian Tests

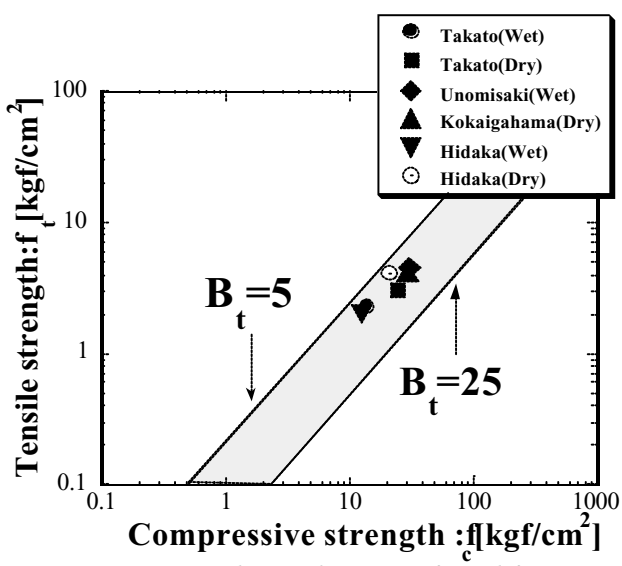

Fig.9-Relation between f_t and f_c

Among the mechanical properties, a correlation between compressive and tensile strength

is presented in Fig. 9. Thus, the brittleness index, B_t, is defined by:

$$B_t = f_c/f_t \quad (2)$$

where f_c and f_t are compressive and tensile strengths, respectively. Fig. 9 shows the tensile strength plotted against the unconfined compression strength for the mud rocks together with the data on saturated rock samples collated by Sunamura (1991). There is a clear tendency for tensile strength, f_t, to increase with increasing compression strength, f_c. It is also found that the brittleness index, B_t, ranges from 5 to 25.

PREDICTION OF COLLAPSIBLE RISK USING CRACK PROPAGATION ANALYSIS

Results from FE Analysis

A typical result from finite element analysis using the crack propagation theory is shown in Fig. 10 which present the effects of Young's modulus on manners of crack propagation in coastal cliff and distribution of principal stresses. Those two values of Young's modulus correspond to those measured using an outer displacement indicator and a LDT. Although there is not a considerable difference in distribution of crack propagation between both values of Young's modulus, time required for computation is different with each other, three times being required for the larger Young' modulus than the smaller one. In other words, the coastal cliff with the larger Young's modulus is more stable for cliff erosion than with the smaller one.

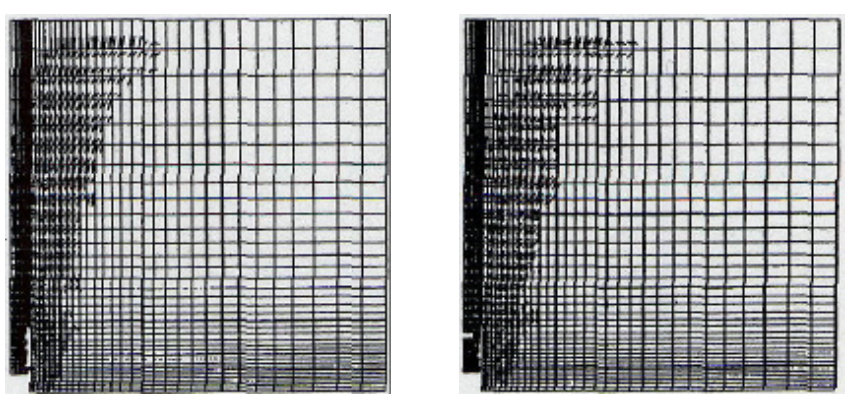

(a)E=250[MPa] (b)E=850[MPa]

Fig.10- Effects of Young's Module on Results from FEM

Definition of Safety Factor

The safety factor for evaluating a possibility of collapse of the cliff at rocky coasts is given by:

$$D = \frac{f_{ta}}{f_t} \quad (3a) \quad or \quad F_s = \frac{1}{D} = \frac{f_t}{f_{ta}} \quad (3b)$$

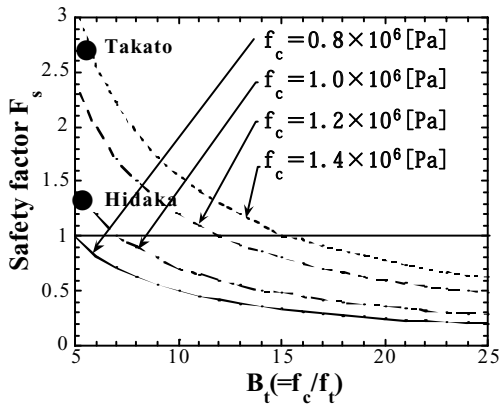

Fig.11-Relation between F_s and B_t

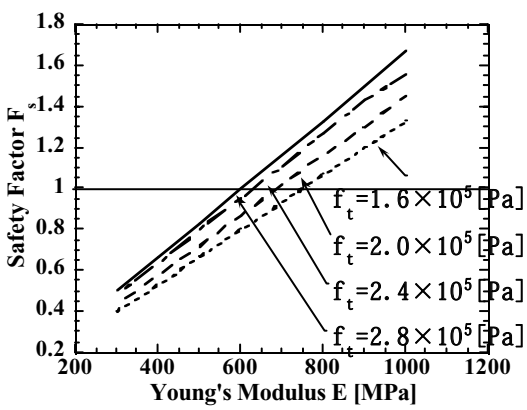

Fig.12-Relation between F_s and E

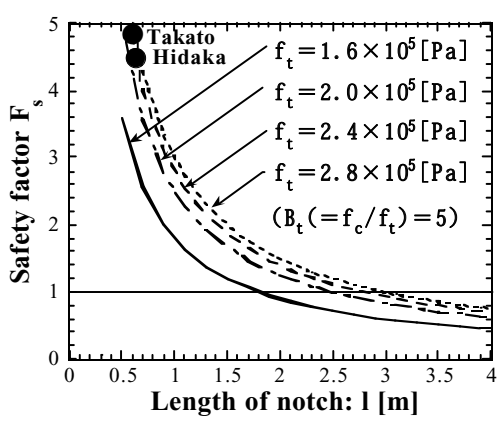

Fig.13-Effect of B_t on the Relation between F_s and the Length of Notch

where f_t: tensile strength at a given condition, f_{ta}: allowable tensile strength of rocks

which constituting of cliffs, which do not lead to collapse, D : failure potential. The results from FE analysis are given in the form of the safety factor, F_s, being plotted against the given parameters of the configuration of cliffs and the properties of rocks.

Effects of Mechanical Properties of Rocks Constituting Coastal Cliffs

Fig. 11 shows the influence of the brittleness, B_t, on the safety factor, F_s, calculated as a parameter of the compression strength, f_c. It is indicated that the safety factor decreases with increasing the brittleness and with decreasing the compression strength.

Effects of Young's Modulus of Rocks

As was previously described, the Young's modulus is an important factor influencing on the stability of coastal cliffs. The results from FE analysis are given in Fig. 12 as the relations between the safety factor and the Young's modulus.

Effects of Configuration of Coastal Cliffs

Among the effects of configuration of coastal cliffs, the eroded distance to form notch is taken as the most important one. Fig. 13 shows the relation of the safety factor plotted against the maximum eroded distance measured at laboratory tests. As far as the present situation of the eroded distance at the two coastal sites, the Takato and Hitachi coasts in the Northern Ibaraki which have suffered from severe cliff erosion is concerned, they are not situated under the serious condition to collapse of rock slope due to breaking waves.

COLLAPSE FUNCTION IN TERMS OF FE ANALYSIS

In terms of the results from the afore-mentioned FE analysis, the authors have proposed the following "collapse function" which enables us to predict quantitatively the possibility of collapse of rocky coasts under assailing ocean waves:

$$F = F(H, \alpha, f_c, f_t, l) \qquad (4)$$

where H : height of cliff, a : inclination of rock slope, and L : horizontal length of notch. The possibility of collapse depends on whether F is larger or smaller than unity. Here, if the collapse function monotonically increases or decreases with increasing the values of B_t, H and L, Eq. (4) is converted into:

$$F = F(H, \alpha, f_c^{-1}, B_t, l) \quad (5)$$

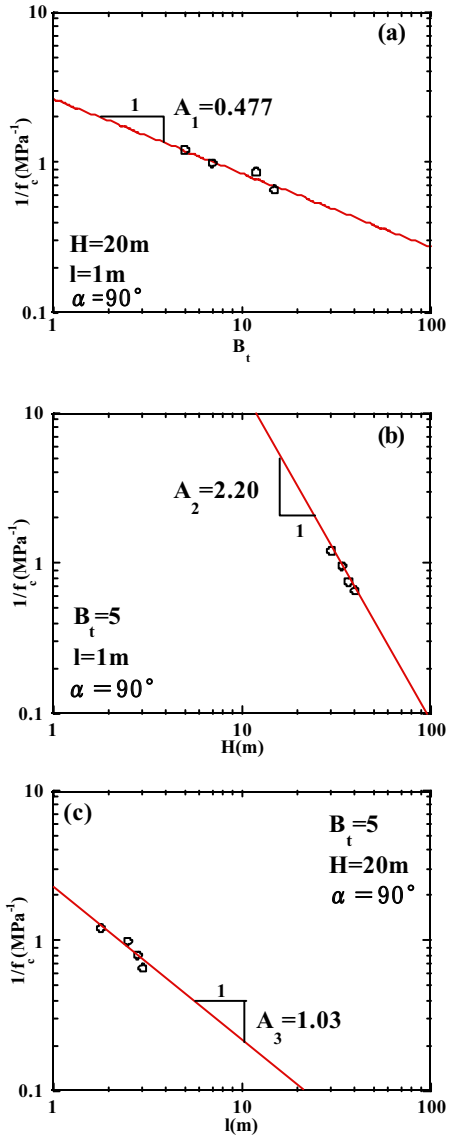

Fig.14-Effects of influencing factors on ($1/f_c$)

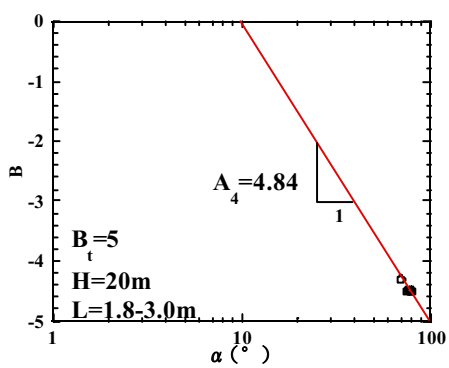

Fig.15-Relation between B and α

Fig. 14 represents the interrelations between $1/f_c$ and one of other three parameters, B_t, H and L. If we postulate that the projection to the two parameters plane can be approximated by the curves with the same gradient when the other conditions get changed, the collapse function towards the cliff with the gradient of 90 degree for slope can be expressed by:

$$F_{90} = \ln(f_c^{-1}) + A_1 \ln(B_t) + A_2 \ln(H) + A_3 \ln(L) + A_4 \ln(a) + C_{90} \quad (6)$$

$$F = \ln(f_c^{-1}) + A_1 \ln(B_t) + A_2 \ln(H) + A_3 \ln(L) + A_4 \ln(a) + C \quad (7)$$

Where A_4 and C are determined from the relation between B_t and a as shown in Fig. 15. Eq. (7) can be converted into:

$$l_f = f_c\ B_t H\ \alpha\ C \quad (8)$$

When we assume the values for the Takakdo Coast, 1.2 MPa for f_c, 5 for B_t, 20m for H and 90 for $_a$, then we have $L_f = 3.81$ corresponding to $F_s = 1$. This is in good agreement with the value for the allowable length of notch, L equal to 3.35m as can be read out from Fig. 13.

When the erosion rate is designated by l (= dl/dt), the collapsible period, T_f, is defined by:

$$T_f = \frac{l_f}{d} \quad (9)$$

By inserting Eq. (8) into Eq. (9), Eq. (9) leads to:

$$T_f = \frac{f_c\ B\ H\ \alpha\ C}{d} \quad (10)$$

Accordingly, the collapsible period, N_T, at a certain period, T is given by:

$$N_T = \langle T,\ T_f \rangle \quad (11)$$

where the symbol, <A, B> implies the quotient in which A is divided by B. Therefore, the retarding distance D_T of cliffs can be given by:

$$D_T = l_f N_T \quad (12)$$

Using the parameters, compression strength and tensile strength, for the five coasts in

Northern Ibaraki, the collapse frequency, T_f, collapsed cycle, N_{100}, and retarding distance, D_{100} in coming 100 years are calculated and listed in Table 1.

Table 1 Results from Calculation for 5 Coasts

	T_f(y)	N_{100}	D_{100}(m)
Izura	5.45	18	60.85
Takato	3.13	31	45.58
Kokaiga-hama	24.84	4	32.80
Hidaka	6.33	15	94.96
Ohmika	26.28	3	18.14

COCLUSIONS

1) It is verified that the collapse of coastal rocky cliffs is the tension failure mode that is governed by the tension toughness.
2) The failure potential increases with increasing the brittleness, f_c/f_t, in which f_c and f_t are compression and tensile strengths.
3) The crack propagation analysis using the finite element method can predict this failure mode. Based on the numerical analysis, the design charts are established.
4) The collapse frequency and the collapse period can be predicted using the collapse function that is defined by the results from FE analysis.

REFERENCES

1. Japan Information Proceeding : DIANA, Release 7.1, Basic Course, 1998.

2. Sunamura, T.: Geomorphology of Rocky Coast, John Wiley & Sons LTD, 1992.

3. Research Committee : Report of the Technical Research Committee on Large-scaled Collapse in Large-scaled Rock Slope, p. 2, JSCE, 1997.

4. Yasuhara, K., Murakami, S., Kanno, Y., Wu, Z-S. and Kanazawa, H.: Crack propagation analysis of rock collapse due to coastal cliff erosion, Memoir of Faculty of Engineering, Ibaraki University, Vol. 49, pp.32-43, 2002 (in Japanese).

Local Scour Around Structures in Tidal Flows

By

Richard W P May[1] and Manuela Escarameia[2]

ABSTRACT

An experimental study was carried out to investigate the development of local scour around structures in tidally-reversing flows. Tests were made in a laboratory flume with square, circular and rectangular structures (aspect ratio = 2) for a range of water depths and with two sizes of bed sediment. Two types of tidal profile were studied: a square-wave profile with a constant velocity in each direction and a profile in which the velocity was varied sinusoidally so as to be representative of conditions in astronomical tides. Tests were made with a range of different tidal durations and peak velocities. After a sufficient number of cycles, the scour depths at either end of a structure reached an equilibrium value. In most of the tests with clear-water scour, the equilibrium depth was significantly less than the maximum depth that would have been produced by a unidirectional current of the same magnitude. However, in the case of live-bed scour, the equilibrium scour depth was found to be similar to the corresponding unidirectional value. Based on an analysis of the results, a method of predicting the equilibrium scour depth was developed using existing data on unidirectional scour and the ratio between the half-cycle duration of the tide and a characteristic time of the scouring process.

1. INTRODUCTION

Structures located in channels or rivers produce local changes in flow velocity and turbulence that can give rise to scouring of the bed or nearby banks. Although there has been considerable research on local scour around structures in unidirectional flows, much less is known about how the depth of erosion is influenced by tidal conditions that produce periodic reversals of flow direction. The development of tidal scour around a structure can be envisaged as passing through the following stages, assuming for convenience that scouring starts from an initially flat bed condition.

- In the first half-cycle of the tide, a scour hole will develop around the upstream face of the structure, but due to the limited tidal period the scour depth will normally be much less than the maximum value associated with an equivalent unidirectional current of long duration.

[1] Technical Director, Water & Industry Group, HR Wallingford, Howbery Park, Wallingford, Oxfordshire, OX10 8BA, United Kingdom.
[2] Principal Engineer, Water & Industry Group, HR Wallingford, Howbery Park, Wallingford, Oxfordshire, OX10 8BA, United Kingdom.

- When the flow reverses in the second half-cycle, scour will start to occur at the opposite end of the structure and some of the eroded sediment will be carried downstream into the first scour hole and thereby begin to fill it up again.

- In the next half-cycle, the process is reversed again with the newly-deposited sediment in the first scour hole being eroded and with, possibly, some additional scour taking place in the time remaining before the tide reverses.

- This process will continue until a state of quasi-equilibrium is reached in which the amount of sediment eroded from a scour hole in one-half cycle is, on average, equal to the amount of sediment deposited in the hole in the following cycle. In most cases, the resulting equilibrium depth of scour will be less than the equivalent value that would occur with an equivalent unidirectional flow. This can be appreciated by considering two limiting cases: if the half-cycle duration of the tide is extremely short, no significant amount of erosion will be able to occur before the flow direction reverses; at the other extreme, if the duration is very long, the scour depth will almost reach the maximum value for unidirectional flow.

Another point of difference for tidal flows is the profile of the bed upstream of the structure. Even if the peak tidal velocity does not exceed the critical threshold velocity needed to erode sediment from an initially flat bed, the areas of erosion and deposition around the structure will locally disturb the flow conditions near the bed and cause dunes to propagate outwards from the structure. The final shape of the sediment bed is therefore likely to be highly complex and very different from the flat bed case that often applies in laboratory studies of unidirectional scour.

2. BASIC APPROACH TO STUDY

Previous research on local scour at structures in unidirectional flow (see for example Breusers & Raudkivi, 1991 and Melville & Coleman, 2000) has shown that the ultimate depth of scour, S_∞ , at a structure (occurring after a time $t \rightarrow \infty$) depends on the following factors:

$$\frac{S_\infty}{B} = \text{function}_1\,(\text{shape of structure}) \times \text{function}_2\,(Y/B) \times \text{function}_3\,(U/U_c) \times \text{function}_4\,(\text{angle of incidence of flow}) \qquad (1)$$

where:

S_∞ = ultimate depth of scour below mean upstream bed level
Y = depth of water above mean upstream bed level
B = width of structure transverse to the flow
U = depth-averaged flow velocity upstream of structure
U_c = critical value of U at threshold of movement of sediment in bed.

For non-cohesive bed sediments, the mean size, d_{50}, of the material does not normally need to be considered directly because studies have shown that its effect can be satisfactorily allowed for by the value of its critical flow velocity, U_c.

In the case of tidal flows, the equilibrium scour depth, S_{eq}, that is reached after a sufficient number of tidal cycles can be expected to be related to S_∞ for unidirectional flow by the following additional factors:

$$\frac{S_{eq}}{S_\infty} = \text{function}_5\,(R/Y_m) \times \text{function}_6\,(D_T/T_C) \times \text{function}_7\,(\text{shape of tide curve, e.g. } U_p/U_{av}) \qquad (2)$$

where:

- R = tidal range (i.e. difference between high and low water levels during tide)
- Y_m = value of Y at mean tide level
- D_T = duration of tidal half-cycle (e.g. ≅ 6.2 hours for astronomical tides)
- T_C = characteristic scouring time of sediment
- U_p = peak velocity during tide
- U_{av} = average velocity during half-cycle.

The characteristic scouring time, T_C, is related to the rate at which the scouring process occurs and needs to be defined in a way that enables it to be reliably assessed from experimental data.

It is apparent from Equation (2) that tidal conditions introduce a significant number of extra variables to the scouring process and make it difficult to obtain general results from a limited number of laboratory experiments. Apart from the effects caused by reversals in flow direction, it is apparent that the rate of scouring will vary continuously with time due to the variations in flow velocity and water depth. At some points in the cycle, the velocity may be well above the critical velocity of the bed and therefore produce high rates of bedload transport, while at other times during the cycle the velocity may be too low to produce any erosion at all.

For these reasons, it was decided to make some simplifications to the way in which the tides were represented in the experiments described in Section 4. Since for astronomical tides the maximum velocity in either direction normally occurs around mean tide level, it can be argued that the equilibrium scour depth, S_{eq}, is likely to be best characterised by the flow velocities and water depth occurring at this level. The experiments were therefore carried out at different constant water depths but with the flow speed and direction varied with time to simulate two different types of tidal cycle:

(a) <u>Square-wave cycle</u> – i.e. constant velocity U in one direction for one half-cycle time D_T, then velocity U in opposite direction for an equal time, and so on.

(b) <u>Sinusoidal cycle</u> – with instantaneous velocity at time t given by :

$$u = U_p \sin(\pi t / D_T) \qquad (3)$$

Although case (a) is not realistic in comparison with astronomical tides, it was considered that it was important to understand this simpler case before attempting to analyse data for sinusoidal tides in case (b).

When seeking to derive general methods that can be applicable to both model results and possible prototype situations, it is important to ensure that time factors, such as the ratio D_T/T_C specified in Equation (2), are correctly evaluated. Since T_C depends on the rate of sediment erosion from the scour hole, simple Froudian scaling of D_T between the astronomical tide and the model tide (based on the square root of the length scale) cannot be assumed. For this reason, the experiments were made with a wide range of D_T values to enable time-dependent effects to be evaluated from the data.

A final factor that influenced the design of the experimental programme was the wish to produce a prediction method for tidal conditions that was consistent with other generally accepted results for local scour at structures. Therefore, in the limiting case of a tide with an extremely long duration, the method should predict a scour depth similar to that given by previous studies on scour in unidirectional flows.

3. TEMPORAL DEVELOPMENT OF SCOUR

The first step in the study was to develop a suitable definition of the characteristic scouring time, T_C. For this purpose, data from a previous study by May & Willoughby (1990) on the rate of increase of scour depth with time were analysed.

This study was principally concerned with determining the ultimate scour depth occurring in steady unidirectional flows for structures such as cofferdams that are large in relation to the water depth. The tests were made with square and circular piers with transverse widths of B = 0.10 m, 0.20 m and 0.40 m, and with relative water depths between Y/B = 4.0 and 0.125. The bed sediment was sand with a mean size of d_{50} = 0.145 mm, and the tests were carried out in a 2.4 m wide flume at flow velocities up to and including the critical threshold velocity, U_c, for the sediment bed upstream of the pier. The following best-fit equations for the ultimate scour depth occurring in unidirectional flows were obtained from the experimental data:

- For circular piers of diameter B:

$$\frac{S_\infty}{B} = 2.4\left[0.44\left(\frac{Y}{B}\right)^{0.67}\right]\left[1 - 3.66\left(1 - \frac{U}{U_c}\right)^{1.76}\right] \qquad (4)$$

for $Y/B \le 3.4$ and $0.522 \le U/U_c \le 1.0$.

When $Y/B > 3.4$, the first square bracket is replaced by a constant value of 1.0. Similarly, when $U > U_c$, the second square bracket is assumed to have a maximum value of 1.0; when $U < 0.522\ U_c$, no scouring occurs and $S_\infty = 0$.

- For square piers of transverse width B (at zero angle of incidence to the flow):

$$\frac{S_\infty}{B} = 3.2\left[0.44\left(\frac{Y}{B}\right)^{0.67}\right]\left[0.6\left(\frac{2.67\,U}{U_c} - 1\right)\right] \tag{5}$$

  for $Y/B \le 3.4$ and $0.375 \le U/U_c \le 1.0$.

  As with Equation (4), the first square bracket is replaced by a constant value of 1.0 when $Y/B > 3.4$. When $U > U_c$, the second square bracket has a maximum value of 1.0; when $U < 0.375\ U_c$, no scouring occurs and $S_\infty = 0$.

As part of this study, measurements were also made of the change in scour depth with time up to the point at which the ultimate value was effectively reached. Initial attempts were made to fit the data to an equation of the form:

$$\frac{S}{S_\infty} = 1 - \exp\left[-\left(\frac{t}{T_c}\right)^p\right] \tag{6}$$

where S is the scour depth at time t. However, problems were encountered in obtaining stable estimates of S_∞, the factor p and the characteristic time, T_c. A simpler approach was therefore adopted using the equation:

$$\frac{S}{S_\infty} = \left(\frac{t}{T_E}\right)^\alpha \quad , \text{ for } 0 \le t \le T_E \tag{7}$$

where S_∞ is the ultimate scour depth obtained by May & Willoughby (1990) and T_E is the time at which the value was reached in the experiments. Nine tests on circular piers gave values of α between 0.21 and 0.41, with an average of $\alpha = 0.327$. The twelve tests on square piers gave values between 0.10 and 0.18, with an average of $\alpha = 0.165$. The difference in the values of α for the two types of structure reflects the fact that the initial rate of scour development at the square piers was proportionately greater than at the circular piers, possibly because the flow separation at the sharp corners created stronger flow separation and more turbulence.

On the basis of these results, it is convenient to define a new characteristic time, T_{50}, which is defined as the time taken for the scour depth to reach 50% of the final equilibrium scour value. From Equation (7) it follows that:

$$\frac{S}{S_\infty} = \frac{1}{2}\left(\frac{t}{T_{50}}\right)^\alpha \tag{8}$$

where it can be assumed that $\alpha = 0.165$ for square structures and $\alpha = 0.327$ for circular structures.

T_{50} can be considered as having some similarities to the “half-life” used for describing the decay rate of radioactive materials. The major advantage of using T_{50} as the

characteristic time factor for the erosion process is that it can be found quite precisely from data on the rate of scour development, whereas the time T_E to final equilibrium can be much more difficult to determine with certainty. Also, T_{50} is more relevant to practical problems of tidal scour because the half-cycle duration of the tide will usually be much closer to T_{50} than to T_E.

The characteristic time, T_{50} , can be expected to become shorter as the flow velocity increases and to be greater for larger structures than for small ones. Various non-dimensional groupings of the variables were investigated using the data from the 21 unidirectional flow tests, and it was found that the best correlation was obtained using the quantity:

$$X = \frac{(\beta U - U_c)\, T_{50}}{B} \tag{9}$$

The coefficient β is the local velocity intensification factor due to the presence of the structure. Thus βU is the effective flow velocity occurring at the structure when the upstream flow velocity is U. Values of β can be determined by assuming that local scouring of the bed will start to occur if $\beta U = U_c$. For circular structures, it follows from Equation (4) that $\beta = 1/0.522 = 1.92$; for square (and rectangular) structures in line with the flow, it can be seen from Equation (5) that $\beta = 2.67$.

Analysis of the data from the unidirectional flow tests showed that the value of X was reasonably constant (given the scatter inherent in sediment erosion studies) and that it did not have any dependence on the relative flow depth, Y/B. The mean value was found to be X = 5500 with a standard deviation equivalent to 36% of the mean (see Escarameia & May, 1999, for more details). A reasonable estimate of the characteristic time, T_{50}, can therefore be obtained from Equation (9) in the form:

$$T_{50} = \frac{5500\, B}{(\beta U - U_c)} \tag{10}$$

where consistent units must be used (e.g. B in m, U and U_c in m/s, and T_{50} in s). It should be noted that this result was obtained from tests in which the flow velocity U did not exceed the critical threshold velocity U_c. Additional data from tests with higher flow velocities are needed to extend the range of application of this approach.

4. EXPERIMENTS WITH TIDAL FLOWS

Full details of the scour measurements with tidal flows are given in Escarameia (1998) and Escarameia & May (1999) and are summarised in Table 1. The tests were made in a 24 m long reversing flume having a width of 0.605 m, depth of 0.440 m and pump capacity of 60 l/s. The main experiments were carried out with two different sands as bed material (with mean sizes of d_{50} = 0.75 mm and 0.44 mm) and with three shapes of structure:

- Circular pier of 75 mm diameter
- Square pier measuring 75 mm × 75 mm in plan

- Rectangular pier with transverse width of 75 mm and length of 150 mm.

Each tidal test was continued until the maximum depths of scour occurring at either end of the structure were effectively the same at the end of each tidal cycle; the average value of this equilibrium scour depth is given as S_{eq} in Table 1. However, during the development of the scour holes, greater depths of erosion sometimes occurred in individual cycles; the maximum depth of scour recorded in each test is given as S_{max} in Table 1. Separate tests were also made to investigate requirements for the extent of bed protection necessary to prevent local scour; full details are given in the above two references.

Before starting the tidal experiments, two tests were made with unidirectional flows (see Tests A.1 and J.1 in Table 1) to ensure that the facility gave consistent results relative to the earlier study by May & Willoughby (1990), which was carried out in a larger flume and with a different size of sediment.

In order to investigate the relative effects of the square-wave and sinusoidal tidal cycles on the equilibrium depth of scour, results were compared on the basis of the volume of tidal flow, Δ_T , per unit width occurring in each half-cycle. For the square-wave profile with a constant velocity U and half-cycle duration, D_T :

$$\Delta_T = Y\,U\,D_T \tag{11}$$

For the sinusoidal profile with a peak velocity, U_p , and half-cycle duration, D, the equivalent result is:

$$\Delta_T = Y \int_0^D U_p \sin(\pi t / D)\,dt = \frac{2}{\pi} Y\,U_p\,D \tag{12}$$

If the unit tidal volume is made equal for the two types of profile, it follows that:

$$U\,D_T = \frac{2}{\pi} U_p\,D \tag{13}$$

Two alternatives were studied in the tests:

Option I – U_p in sinusoidal profile = U in square-wave profile
– Duration (D) of sinusoidal half-cycle = $\pi/2 \times$ duration (D_T) of square-wave half-cycle.

Option II – U_p in sinusoidal profile = $\pi/2 \times$ U in square-wave profile
– Duration (D) of sinusoidal half-cycle = duration (D_T) of square-wave half-cycle.

Thus, as an example, Tests B.1, C.1 and D.1 in Table 1 can be compared as having the same unit tidal volume but different profiles of tidal cycle.

Most of the tests were carried out with the velocity, U, upstream of the piers just equal to the threshold velocity, U_c , of the sediment so that there was no general bed-load

movement. The conditions were therefore equivalent to the limit between what is termed “clear-water” scour (with no bed-load transport) and live-bed” scour (with bed-load transport). In unidirectional flows with uniformly graded sediment, this limiting condition usually produces the maximum possible scour depth (see, for example, Breusers & Raudkivi, 1991). However, a limited number of tests were also carried out in this study with $U > U_c$ to study the live-bed condition.

5. RESULTS FROM EXPERIMENTS

The key results from the experiments were as follows.

(a) In the case of the square-wave tidal cycles carried out with the flow velocity equal to the critical threshold velocity (i.e. $U = U_c$), the final equilibrium scour depth, S_{eq} , was always intermediate between the ultimate scour depth, S_∞ , occurring with unidirectional flow and the scour depth, S_D , achieved at the end of the first half-cycle (i.e. at time $t = D_T$). These findings are illustrated by Figure 1, which shows how the scour depth varied with time at the square pier for the case of unidirectional flow and for a square-wave tide having a half-cycle duration of $D_T = 2.0$ hours. The data for the tidal test are shown as two sets of points, with those for the “flood” condition corresponding to the scour depths measured at the end of the pier that was facing the flow in the first half-cycle of the test. Similarly, the data for the “ebb” condition correspond to the depths at the opposite end of the pier that was facing the flow in the second half-cycle.

(b) For a given set of conditions, increasing the duration of the tidal cycle increased the value of the equilibrium scour depth. This applied both for square-wave and sinusoidal tidal cycles, as illustrated by Figure 2 for the case of the square pier with a relative water depth of $Y/B = 1$.

(c) For unidirectional flows, previous studies have shown that scour depths at circular structures are typically about 75% of those at square piers for the same transverse width and flow conditions (cf Equations (4) and (5)). However, in the present tests, there was very little difference between the equilibrium scour depths for the circular and square piers under similar tidal conditions. Corresponding scour depths around the rectangular pier (aspect ratio = 2) were about 90% of those for the square and circular piers. This may have been because the greater length of the rectangular structure reduced the degree of interaction between the scour holes at either end.

(d) The equilibrium scour depths produced by the sinusoidal tidal cycles were about 88% of those produced by the square-wave cycles when compared on the basis of Option I in Section 4 (i.e. with $U_p = U_c$ and a longer tidal duration). However, Option II (with $U_p = 1.57\ U_c$ and the same duration) gave scour depths that were on average 1.73 times those occurring with the square-wave cycles. With Option II, live-bed scour occurred around the peak of each cycle and this caused the erosion to develop much more rapidly, with the values of the equilibrium scour depth, S_{eq} , being close to the value of S_∞ that was obtained in the unidirectional flow test with $U = U_c$ (see Figure 2).

6. ANALYSIS OF DATA

As explained in item (a) of Section 5, the value of the equilibrium depth of scour, S_{eq}, in tidal conditions will normally lie between the scour depth, S_D, achieved after the first half-cycle of the tide (starting from a flat bed condition) and the ultimate depth, S_∞, produced by an equivalent unidirectional current. If the half-tidal duration, D_T or D, is small in relation to the characteristic time, T_{50}, of the scouring process, then S_{eq} is likely to be closer to S_D than to S_∞, and vice versa.

Experimental data on values of S_∞ are now available for many types of hydraulic structure, and the type of approach suggested in Section 3 provides a method of estimating the first half-cycle scour depth, S_D. This enables the value of equilibrium scour depth to be assessed taking into account the relative magnitudes of D_T and T_{50}.

The suitability of the proposed method for estimating S_D was checked using the data from the experiments with square-wave tidal profiles and $U = U_c$ (i.e. the limiting case of clear-water scour). The characteristic scouring time, T_{50}, for each test was calculated from Equation (10) and then substituted in Equation (8) to give:

$$S_D = \frac{S_\infty}{2}\left(\frac{D_T}{T_{50}}\right)^\alpha \tag{14}$$

where $\alpha = 0.327$ for circular piers and $\alpha = 0.165$ for square piers. Estimates of S_∞ for the two shapes of structure were determined from Equation (4) for circular piers or Equation (5) for square piers. The predicted values of S_D are compared in Figure 3 with the values of S_D that were actually measured in the experiments after the first half-cycle of each tidal test. The overall agreement is satisfactory and shows no major discrepancies for the range of tidal durations studied or for the two structure shapes and two sediment sizes. It should be noted that the prediction method was developed independently using only data from the earlier study on unidirectional scour by May & Willoughby (1990). As mentioned above, the pier sizes, water depths and sediment size in that study were significantly different from those in the present tidal tests.

The effect of the time ratio D_T/T_{50} on the scour ratio S_{eq}/S_D is shown in Figure 4 for the case of square-wave tidal cycles. In the case of the results for the square piers with $U = U_c$ (which cover three different water depths and two sediment sizes), the values of S_{eq}/S_D vary between about 0.9 and 1.2 with an average of about 1.1, but with no clear dependence on the value of D_T/T_{50}. For conservative estimates, it is recommended to assume:

$$S_{eq} = 1.2\,S_D \quad , \quad \text{for } D_T / T_{50} \le 8 \tag{15}$$

In the case of the circular piers, the expected dependency of S_{eq}/S_D on D_T/T_{50} is more apparent, and it is recommended to use the following estimation formulae:

$$S_{eq} = \left[2.0 - 0.267\left(\frac{D_T}{T_{50}}\right)\right]S_D \quad , \quad \text{for } D_T / T_{50} \le 3 \tag{16}$$

$$S_{eq} = 1.2 S_D \quad , \quad \text{for } 3 < D_T / T_{50} \leq 8 \tag{17}$$

For a sinusoidal profile with $U_p = U_c$ and a duration equal to 1.57 × the duration of an equivalent square-wave tide (Option I in Section 4), the equilibrium scour depth could be expected to be about 90% of that predicted from the above equations. For the case of a sinusoidal profile with $U_p = 1.57\ U_c$ and duration equal to that of the square-wave tide (Option II), insufficient data are available from these tests to define an equivalent prediction method. However, the results suggest that if a significant degree of live-bed scour occurs (e.g. U or $U_p > 1.5\ U_c$) both square-wave and sinusoidal tides will tend to produce equilibrium scour depths, S_{eq}, that are close to the ultimate value, S_∞, that would be produced by a unidirectional current of $U = U_c$. This conclusion is in accordance with results of Sumer et al (1992, 1993) who studied wave-induced scour at structures. In the present tests, equivalent values of the Keulegan-Carpenter number (defined here as $KC \equiv 2\ U\ D_T / B$) range from about 6000 to 52 000. In their wave tests, Sumer et al found that when the value of KC reached about 5000 the equilibrium scour depth was similar to that produced by an equivalent unidirectional current

7. SUGGESTED DESIGN PROCEDURE

Based on the results of this initial study, the following procedure is tentatively proposed for estimating the equilibrium depth, S_{eq}, at a structure in tidal conditions.

(1) Determine the variation in tidal velocity with time at the site being considered and calculate the average tidal volume, Δ_T, in one half-cycle of the tide. Calculate the half-cycle duration, D_T, of an equivalent square-wave tide with a flow velocity U equal to the peak velocity, U_p, in the actual tide, i.e. $D_T = \Delta_T / (U_P\ Y)$, where Y is the water depth at mean tide level.

(2) For the values of U and Y, estimate the ultimate depth of scour, S_∞, that would be produced by a unidirectional current, e.g. using Equations (4) or (5) or other formulae suitable for the type of structure and flow conditions being considered.

(3) If $U > 1.5\ U_c$, where U_c is the critical threshold velocity for the bed sediment, it is likely that the equilibrium scour depth, S_{eq}, under tidal conditions will not be significantly less than S_∞.

(4) If $U \leq 1.0$, estimate the characteristic scouring time, T_{50}, from Equation (10).

(5) Determine the scour depth, S_D, that would occur after one half-cycle of the equivalent square-wave tide using Equation (14).

(6) Calculate the equilibrium scour depth, S_{eq}, produced after successive tidal cycles from Equations (15), (16) or (17) depending on the shape of the structure (i.e. sharp-edged or rounded) and the value of D_T / T_{50}.

(7) An astronomical tide will produce somewhat less scour than the equivalent square-wave tide defined in step (1). Therefore, the actual equilibrium scour depth at the structure should be estimated as equal to 90 % of the value of S_{eq} obtained from step (6).

(8) For rectangular structures having an aspect ratio (length / transverse width) ≥ 2, the equilibrium scour depth is likely to be about 90 % of the value for a square pier of the same transverse width (assuming that in both cases they are in-line with the flow).

(9) No data are yet available for the intermediate case in which $1.0 < U/U_c < 1.5$. An approximate value of the equilibrium scour depth may be calculated on a pro-rata basis using the value of S_{eq} from step (3) for $U = 1.5\ U_c$ and the value from step (7) or (8) for $U = U_c$.

8. CONCLUSIONS

The study has shown that, in the case of clear-water scour (with $U \leq U_c$), the equilibrium scour depths at hydraulic structures in tidal flows can be significantly less than can occur with equivalent unidirectional currents. However, in the live-bed scour case, the equilibrium depths are likely to be close to the unidirectional flow values due to the faster development of the scour holes in each tidal cycle and due to the formation around the structure of a duned bed of complex shape.

The analysis of the data for the clear-water case suggests that a non-dimensional formulation based on the ratio between the tidal duration and a characteristic scouring time is useful in predicting the value of the equilibrium scour depth in tidal conditions. Further experimental study is needed to extend the analysis to the case of live-bed scour.

9. ACKNOWLEDGEMENTS

This study was partially funded by the Construction Directorate of the UK Department of Trade and Industry under its Partners in Innovation programme. The authors are grateful for the assistance of Ms Ruth Cano who carried out many of the experimental measurements.

10. REFERENCES

Breusers H N C & Raudkivi A J (1991). “Scouring”. International Association for Hydraulic Research. A.A. Balkema/Rotterdam/Brookfield, The Netherlands. ISBN 90 6191 983 5.

Escarameia M (1998). Laboratory investigation of scour around large structures in tidal waters. 3rd International Conference on Advances in Hydro-Science and – Engineering, Cottbus, Germany, Vol III.

Escarameia M & May R W P (1999). Scour around structures in tidal flows. Report SR 521, HR Wallingford, England.

May R W P & Willoughby I R (1990). Local scour around large obstructions. Report SR 240, HR Wallingford, England.

Melville B W & Coleman S E (2000). “Bridge scour”. Water Resources Publications, LLC (Colorado).

Sumer B M, Fredsoe J & Christiansen N (1992). Scour around a vertical pile in waves. Journal of Waterway, Port, Coastal and Ocean Engineeering, ASCE, Vol 118, No 1, pp 15-31.

Sumer B M, Christiansen N & Fredsoe J (1993). Cross section influence on wave scour around piles. Journal of Waterway, Port, Coastal and Ocean Engineeering, ASCE, Vol 119, No 5, pp 477-495.

Table 1 Summary of test data

Test No	Structure type	Sediment size d_{50} (mm)	Water depth Y (m)	Critical velocity U_c (m/s)	Characteristics of tidal cycle				Predicted characteristic scour time T_{50} (h)	Equilibrium scour depth S_{eq} (m)	Maximum scour depth S_{max} (m)
					Peak velocity in cycle U (m/s)			Duration of half-cycle D or D_T (h)			
					Unidirectional	Square-wave	Sinusoidal				
A.1	Square	0.75	0.075	0.274	$U = U_c$			–	0.250	0.116	–
B.1	Square	0.75	0.075	0.274		$U = U_c$		0.250	0.250	0.057	0.057
B.2	Square	0.75	0.075	0.274		$U = U_c$		0.500	0.250	0.064	0.067
B.3	Square	0.75	0.075	0.274		$U = U_c$		1.000	0.250	0.066	0.070
B.4	Square	0.75	0.075	0.274		$U = U_c$		2.000	0.250	0.079	0.088
C.1	Square	0.75	0.075	0.274			$U_{max} = \pi U_c/2$	0.250	0.131	0.100	0.102
C.2	Square	0.75	0.075	0.274			$U_{max} = \pi U_c/2$	0.500	0.131	0.105	0.109
C.3	Square	0.75	0.075	0.274			$U_{max} = \pi U_c/2$	1.000	0.131	0.118	0.120
D.1	Square	0.75	0.075	0.274			$U = U_c$	0.390	0.250	0.049	0.052
D.2	Square	0.75	0.075	0.274			$U = U_c$	0.785	0.250	0.057	0.057
D.3	Square	0.75	0.075	0.274			$U = U_c$	1.570	0.250	0.059	0.059
D.4	Square	0.75	0.075	0.274			$U = U_c$	3.140	0.250	0.068	0.070
E.1	Square	0.75	0.075	0.274		$U = \pi U_c/2$		0.250	0.131	0.110	0.111
E.2	Square	0.75	0.075	0.274		$U = \pi U_c/2$		0.500	0.131	0.120	0.122
F.1	Square	0.75	0.056	0.259		$U = U_c$		0.250	0.265	0.049	0.049
F.2	Square	0.75	0.056	0.259		$U = U_c$		0.500	0.265	0.050	0.053
F.3	Square	0.75	0.056	0.259		$U = U_c$		2.000	0.265	0.068	0.071
G.1	Square	0.75	0.0375	0.239		$U = U_c$		0.250	0.287	0.032	0.041
G.2	Square	0.75	0.0375	0.239		$U = U_c$		0.500	0.287	0.035	0.039
G.3	Square	0.75	0.0375	0.239		$U = U_c$		2.000	0.287	0.042	0. 044
H.1	Circular	0.75	0.075	0.274		$U = U_c$		0.250	0.455	0.057	0.060
H.2	Circular	0.75	0.075	0.274		$U = U_c$		0.500	0.455	0.064	0.065
H.3	Circular	0.75	0.075	0.274		$U = U_c$		1.000	0.455	0.068	0.070
H.4	Circular	0.75	0.075	0.274		$U = U_c$		2.000	0.455	0.072	0.073
I.1	Rectangular	0.75	0.075	0.274		$U = U_c$		0.250	0.250	0.050	0.056
I.2	Rectangular	0.75	0.075	0.274		$U = U_c$		1.000	0.250	0.060	0.070
I.3	Rectangular	0.75	0.075	0.274		$U = U_c$		2.000	0.250	0.070	0.075
J.1	Square	0.44	0.075	0.253	$U = U_c$			–	0.271	0.112	–
J.2	Square	0.44	0.075	0.253		$U = U_c$		0.250	0.271	0.051	0.056
J.3	Square	0.44	0.075	0.253		$U = U_c$		1.000	0.271	0.072	0.075
J.4	Square	0.44	0.075	0.253		$U = U_c$		2.000	0.271	0.081	0.087

Figure 1 Development of scour in unidirectional and tidal flows

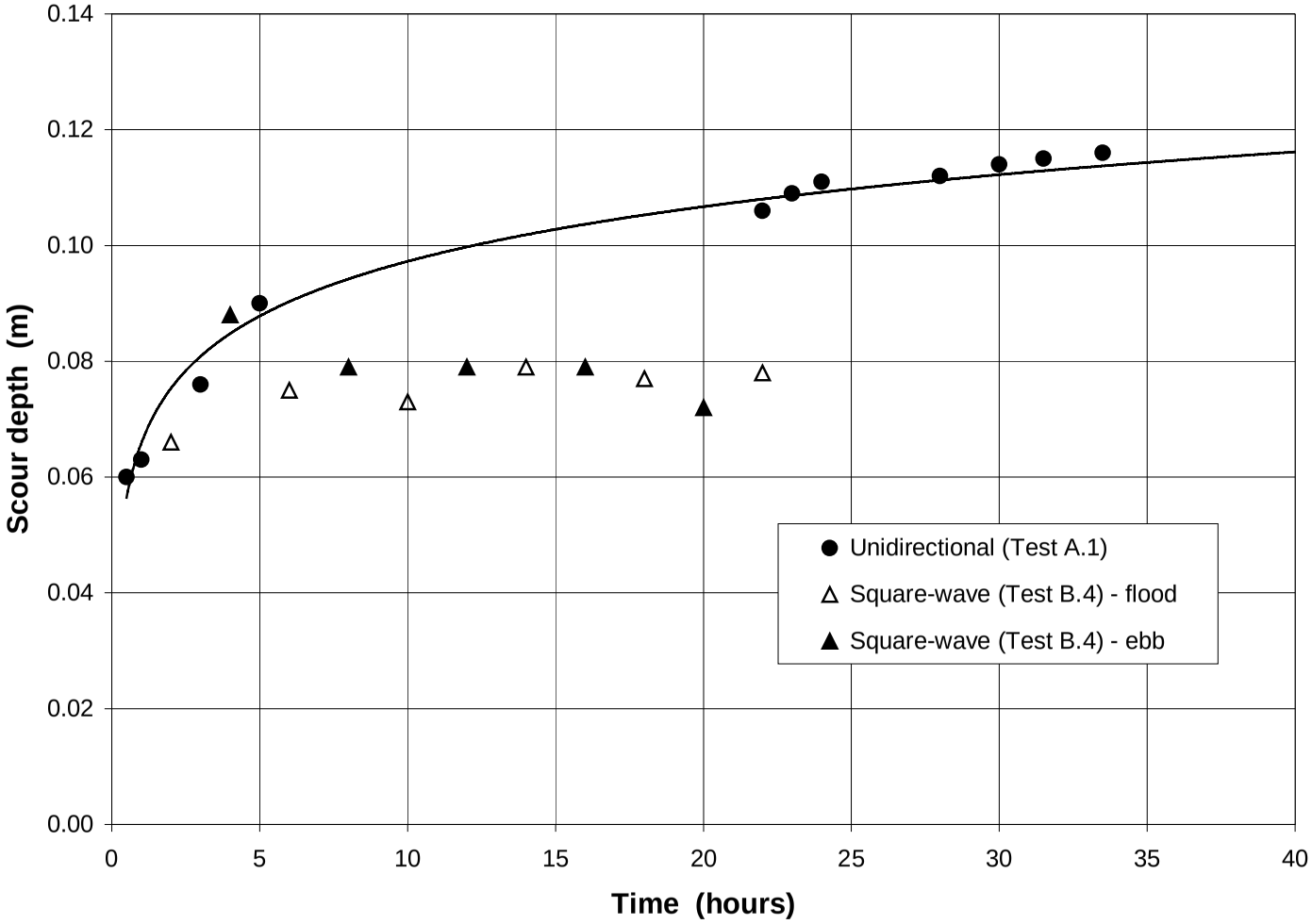

Figure 2 Variation of equilibrium scour depth with half-cycle duration

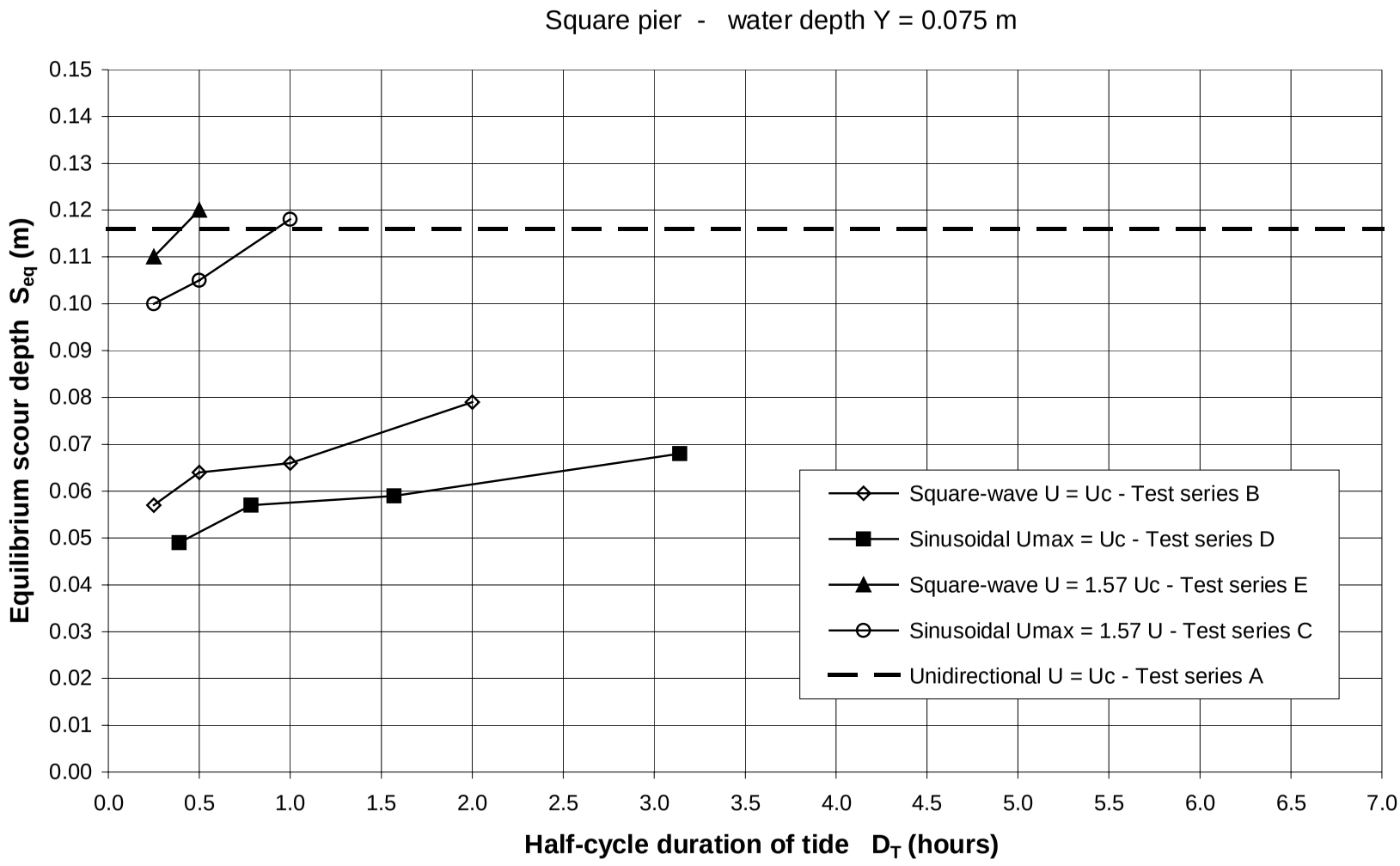

Figure 3 Comparison of predicted and measured scour depths after first half-cycle of square wave tides (with $U = U_c$)

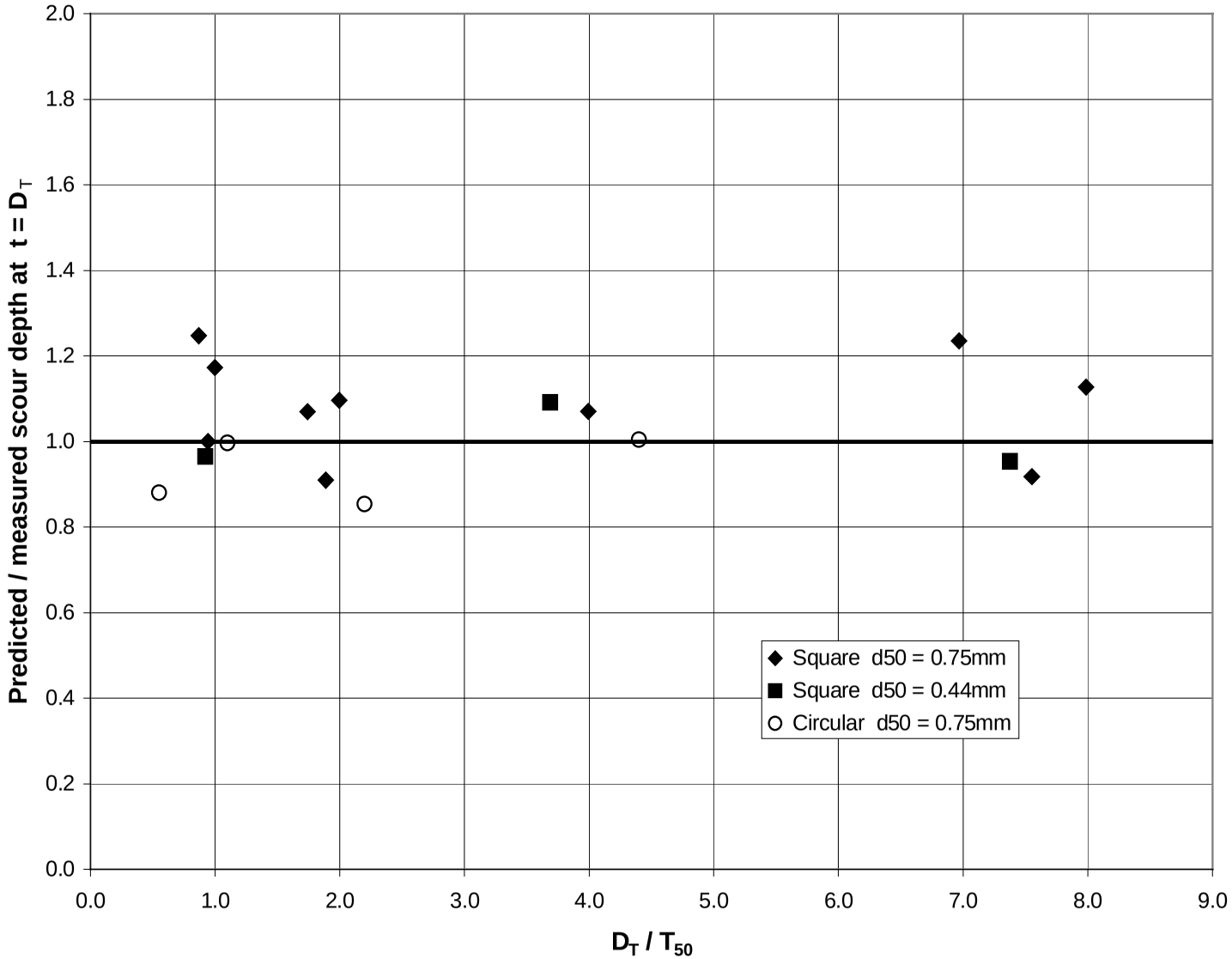

Figure 4 Relationship between equilibrium scour depth and predicted scour depth after first half cycle of square-wave tides

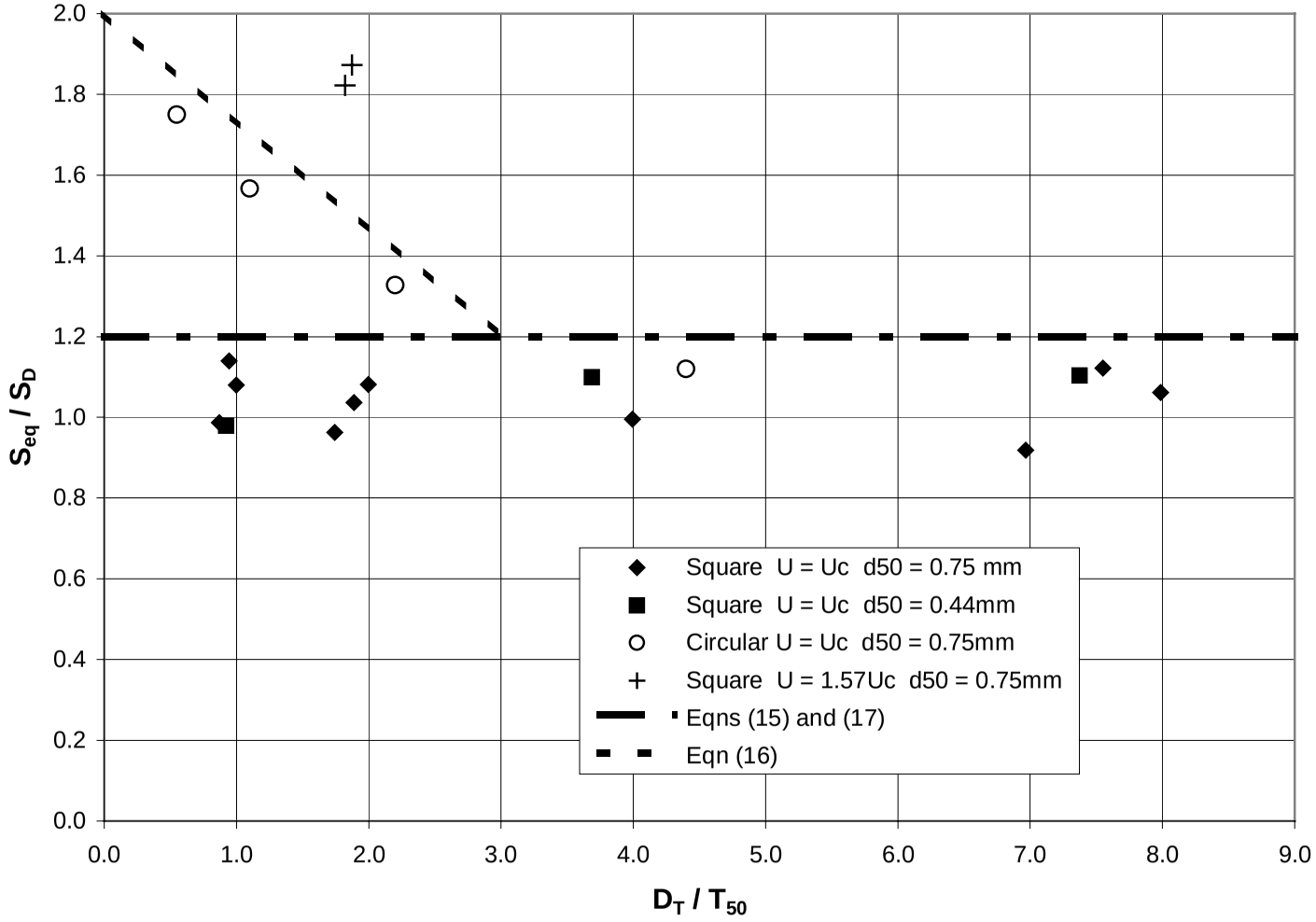

Movement of Bridge Pier by Water Flow Under Flood Condition

By

Kunihiro Ogihara[1], Hisasshi Muraishi [2]
Samizo Masahiko[3], Daisuke Nakajima[4]

ABSTRACT

The foundation of bridge pier is scoured by water flow at the flood condition and this condition makes some changes on the support system of bridge foundation by soil mechanics. Namely some parts of soil foundation are scoured by water flow and the support force for bridge pier by this part is diminished at flood condition.
In this report, the authors show the results of model test on the vibration phenomenon by water flow under the flood condition to compare the feature of vibration between at flood condition and at non flood condition. The natural vibration of bridge pier is so different not only scored effects but also the surrounded water such as the frequency of locking motion of bridge pier becomes lower by added mass of water to compare the one at the non flood condition. Furthermore the vibration under the water flow shows some periodic motion combining the natural vibration motion of locking. The several results by different support condition of foundation are shown by changing the flow condition.

PREFACE

Bridge piers have potentially possibility that there happened harmful alteration such as inclination or settlement during flood time(J.Tanak et al, 2000). Main causes of those pier damages are considered by scour around the base due to strong stream flow. However, it is very difficult to evaluate the soundness of bridge pier, because nobody could confirm the base ground directly during flood. Because piers are normally supported by the rigid base ground, the change of supporting condition would affect to the vibration feature of the pier itself, that is, a dynamic characteristic(O. Suzuki et al, 2000).
Therefore, if supporting condition can be quantitatively observed by any measurement equipment, the running safety of the train on the railway bridges after and/or during the flood will be remarkably improved. However, few research papers treat the problem on the vibration properties of the bridge pier by flood condition especially related to the damage of pier. Therefore, we have performed fundamental hydraulic experiments to study the vibration of a cylindrical model pier supported by different steel springs.

[1] Dr. and Prof. of Toyo University, Civil and Environmental Engineering Department, 2100 Kujirai, Kawagoe Saitama, Japan, (oguhara@toyonet.toyo.ac.jp)
[2] Chief Research Engineer, Geological Hazards Prevention Group, RTRI, 2-8-38 Hikaricho, Kokubunji-city, Tokyo, Japan, (muraishi@rtri.or.jp)
[3] Chief Research Engineer, Geological Hazards Prevention Group, RTRI, (samizo@rtri.or.jp)
[4] Research Engineer, Geological Hazards Prevention Group, RTRI, (nakaji01@rtri.or.jp)

MODEL OF BRIDGE PIER

Bridge pier is usually constructed on hard ground basement or on the base which is supported on piles and is considered to be supported by elastic base such as locks and piles. As the ground materials around pier are removed by water flow at flood condition, the supported condition becomes to be changed and elastic supported system is also changed. The model bridge pier is made by spring supported system to be considered by similarity on field's pier and the change of basement by flood is adapted by the strength of spring plate. In model test, authors used two different plate spring and two different supporting length and also two different supporting systems such as four points support and three points support.

The vibration systems in model are three freedoms as vertical motion and rotation motion in two directions which are perpendicular to each other. And the vertical motion is very smaller than rotation motion by the deformation of plate springs, the analysis on model test data is mainly done to the rotational motion.

Model bridge piers are shown in figure 1 as four points support is the left hand side and three points support is right side, and dimensions of pier are as follows.

Height L is 30.7cm, diameter d is 8.8cm and distance of support by plate spring d1 is 5cm. Plate springs are used in two type as A (length is 103mm and width is 16mm) and B (length is 103mm and width is 26mm).

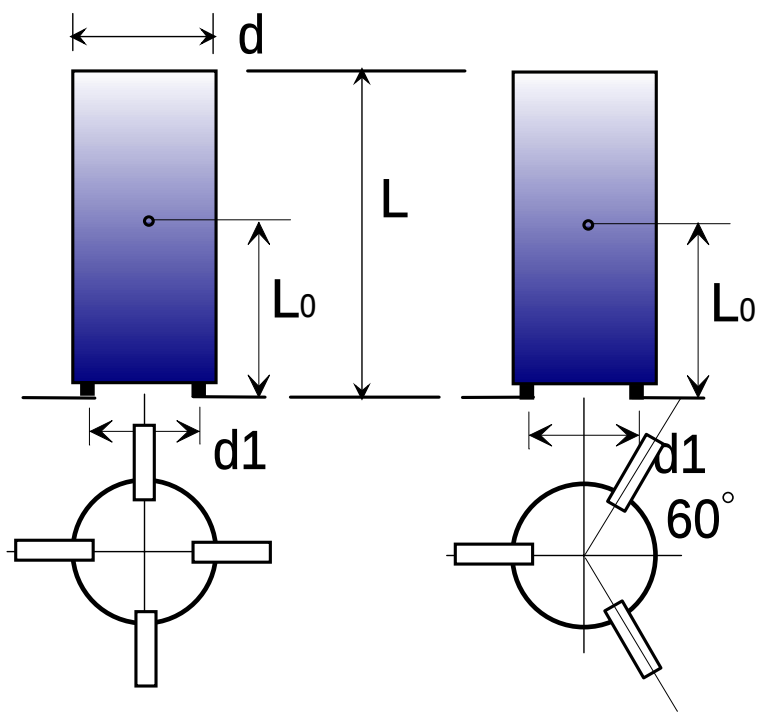

Fig.1 - Model Pier and Support System

THEORETICAL MODEL

As shown in figure 1, model piers are arranged two support systems as four points support and three points support, so the equations of motion must be made for these two support

systems. When the pier moves in the water, it affects on the water movement and pier is also affected by velocity of water. Generally when the body makes accelerated motion in water, it must be considered added mass by surrounded water of body. This phenomenon is very familiar of hydrodynamic pressure on dam surface in reservoir at the earthquake conditions.

Coordinate system in model pier is shown in figure 2 for experimental model shown in figure 1. The equations for vibration is made under the water depth is h from the base of plate spring is fixed.

The rotational vibration in experimental model pier is larger than vertical movement, so the equation of vibration is shown only for rotational motions here.

At first added mass around the pier in water is written as equation (1) by distributed on pier surface with length dz.

$$dM_w = \rho C_w A dz \qquad \cdots\cdots(1)$$

Here C_w is coefficient of added mass, A is horizontal section of pier and ρ is density of water. So the moment of inertia I_w by this added mass at origin o is derived as equation (2).

$$I_w = \int_0^h z^2 dM_w = \int_0^h \rho C_w A z^2 dz = \rho C_w A \frac{h^3}{3} \qquad \cdots\cdots(2)$$

And moment of inertia by mass of pier is given as equation (3) when the mass of pier is M and its gravity center is laying at height L_0 from the base of plate spring.

$$I = M L_0^{\,2} \qquad \cdots\cdots(3)$$

For four points support system, plate springs are arranged with two different stiffness for x and y directions respectively. But in three point support system, it is arranged with same stiffness at three points.

The basic equations of vibration for model pier are shown from equation (4) to (6).

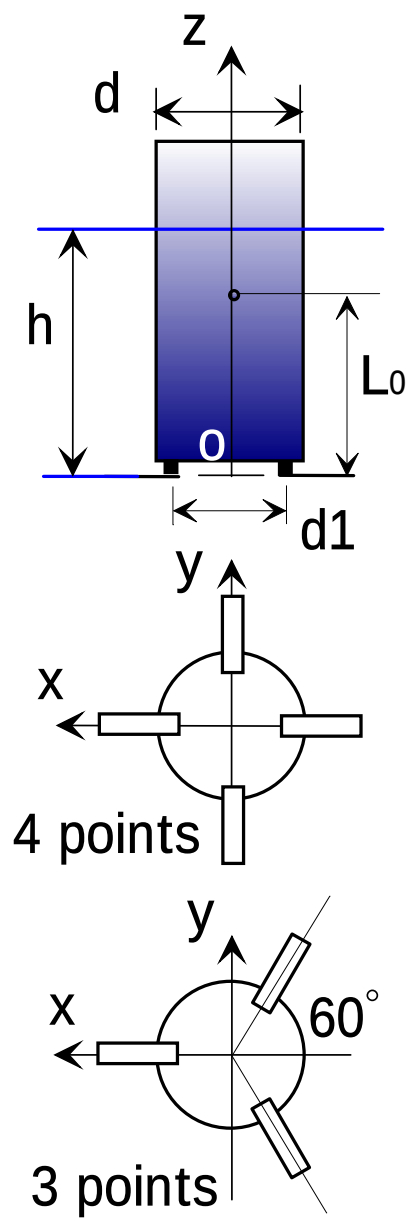

Fig.2 - Coordinate System

For four points support system, equation (4) and (5) are given for rotational motion of x and y direction.

$$\left(M L_0^{\,2} + \rho C_w A \frac{h^3}{3}\right)\frac{d^2\theta_x}{dt^2} + R_{2x}\frac{d\theta_x}{dt} + 2k\left(\frac{d_1}{2}\right)^2 \theta_x = F_{\theta_x} \qquad \cdots\cdots(4)$$

$$\left(M L_0^{\,2} + \rho C_w A \frac{h^3}{3}\right)\frac{d^2\theta_y}{dt^2} + R_{2y}\frac{d\theta_y}{dt} + 2k\left(\frac{d_1}{2}\right)^2 \theta_y = F_{\theta_y} \qquad \cdots\cdots(5)$$

Here θ_x and θ_y are movement of angle for direction x and y respectively at origin o and $F\theta_x$ and $F\theta_y$ are external force for each directions. For three points support system, equation (6) gives basic vibration equation for ax and y directions in same expression.

$$\left(M L_0^{\ 2} + \rho C_w A \frac{h^3}{3}\right)\frac{d^2\theta}{d\,t^2} + R\frac{d\theta}{d\,t} + \frac{3k}{2}\left(\frac{d_1}{2}\right)^2\theta = F_\theta \qquad \cdots\cdots(6)$$

In these equations, R, R_x and R_y are damping constants for vibration in each direction. When the external force does not act on the pier, these equations show the natural damping conditions. Natural frequencies for these equations are written as equation (7) and (8).

$$f = \frac{1}{2\pi}\frac{d_1}{2L_0}\sqrt{\frac{2k_i}{M}}\frac{1}{\sqrt{1+\frac{\rho C_w A h}{3M}\left(\frac{h}{L_0}\right)^2}}, \quad i = x, y \qquad \cdots\cdots(7)$$

$$f = \frac{1}{2\pi}\frac{d_1}{2L_0}\sqrt{\frac{3k_i}{2M}}\frac{1}{\sqrt{1+\frac{\rho C_w A h}{3M}\left(\frac{h}{L_0}\right)^2}} \qquad \cdots\cdots(8)$$

It is very interesting that the effect of water depth on natural frequency is given by three power term of h. This means that pier under flood condition has decreasing of natural frequency in three power term of h and has some difficulty for the response of pressure change by water flow under the flood.

EXPERIMENTAL RESULTS

Experiments in model pier are made two types such as using the vibration table and using water flow channel. Test by vibration table has done by model pier is fixed in the box that supporting spring plate are arranged and this box is placed in water tank.

Fig.3 - Pier Box

Fig.4 - Four Point Plate Spring

The figure 3 and 4 are shown pier box and four points plate spring with pier model and vibration table and water tank which placed on vibration table are shown in figure 5 and 6.

Pier box as shown figure 3 is fixed in the water tank when vibration in water is measured.

Fig.5 - Vibration Table

Fig.6 - Water Tank

Test by Vibration Table

Vibration table can be operated continuously to be varied frequency from 5 Hz to 20 Hz in 10 minuets intervals under constant output power. Movement of pier is measured at three points by accelerometer which are attached on the top of pier for x and y directions and base at vibration table for x direction. Data are collected by data logar which can take the data in 0.01 second intervals and treated by Excel Soft in personal computer.
Experiment has been done both in air and in water by using two type spring plates under four and three supporting system. Here the typical results by test are shown.

1) Three points support system
The natural frequency for x and y directions are same in theoretical analysis and this is confirmed by experimental test as follows. Response curves in frequency and amplitude of acceleration are shown in figure 7 and 8 for x and y direction in air and the peak value of channel 2 has almost same value in these two graphs as 11.1Hz and 10.9Hz. The difference of these is only 0.2Hz and 2% of value. This result shows good relations for theoretical analysis. But when the amplitude becomes larger for vibration direction, the motion of perpendicular direction for this also becomes larger. This feature is different from the response of four points support system, because an irregularity in fixed point of spring may affect on this motion.

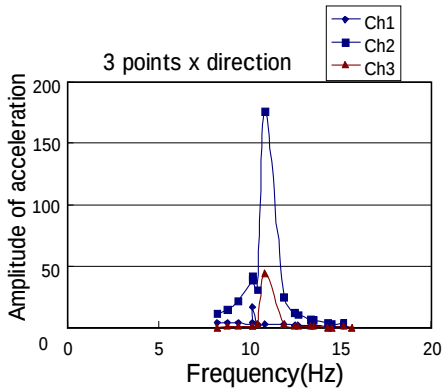

Fig.7 - Three Points x Direction

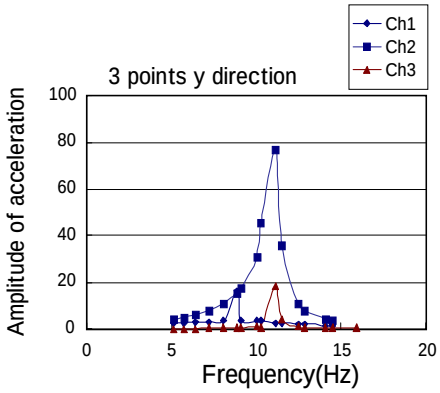

Fig.8 - Three Points y Direction

2) Four point support system

Response curves in four points support system are shown in figures 9 and 10 in the case that the stiffness supporting plate is different as the one of x direction is stronger than y direction. The natural frequencies for x and y directions are10.5 and 8.25 Hz respectively can be found as peak point in figure 9 and 10.

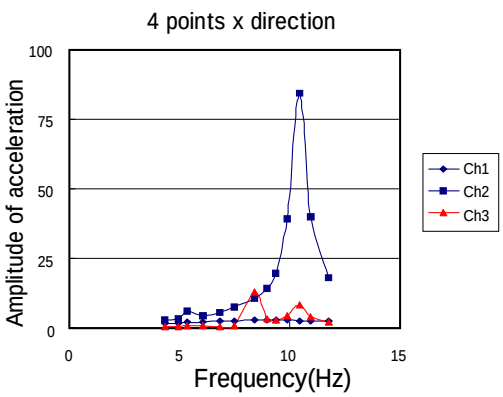

Fig.9 - Four Points x Direction

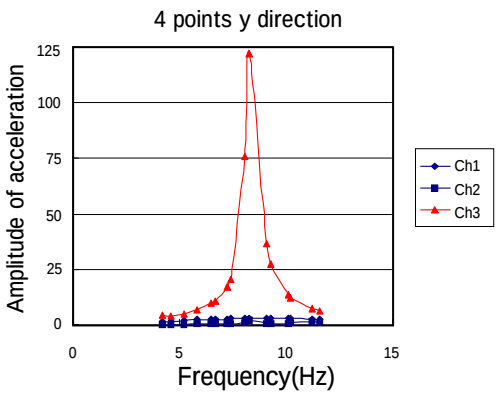

Fig.10 - Four Points y Direction

In these graphs there is a difference in figure 9 compared to figure 10 as that response of y direction arises at natural frequency of y direction and also at natural frequency of x direction. In the case of weak spring constant, motion can occur easily by some irregular support conditions same as three point support system.

3) Response in water

The response in water for four point support is shown as an example and analysis on this result is treated with the data of test in water flow channel. When water depth is changed from 0 to 19cm in step 10, 15 and 19 cm, natural frequency is decreasing and its results are shown in figure 11.

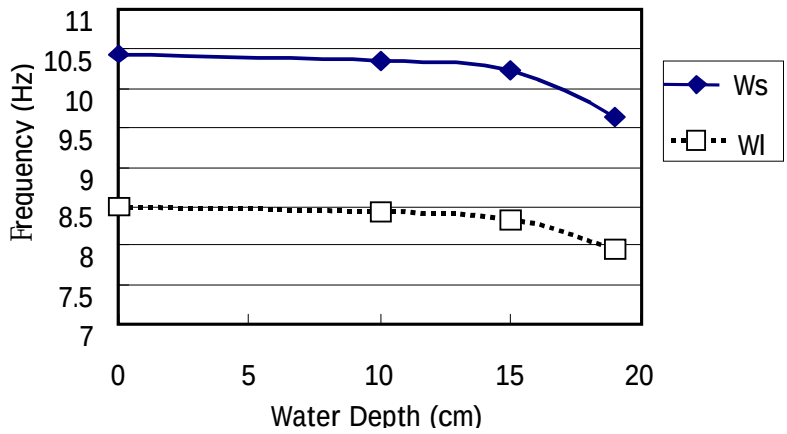

Fig.11 - Frequency Change with Water Depth

Frequency is decreasing about 10% from in air to 19cm water depth in figure 11, and this feature has good correlations to the theoretical analysis.

Test in Water Flow Channel

In water channel, two type data are collected as natural frequency by damping vibration and vibration in flow. In this report, authors focus on the variation of natural vibration in water especially, so the data on how the natural frequency in the water is changed is summarized in this chapter.

The test has been done in several cases combining the stiffness of plate spring, mass of bridge pier with sand or without sand and water depth. The typical record of damping vibration is shown in figure 12; the natural frequency and damping ratio are calculated from this record.

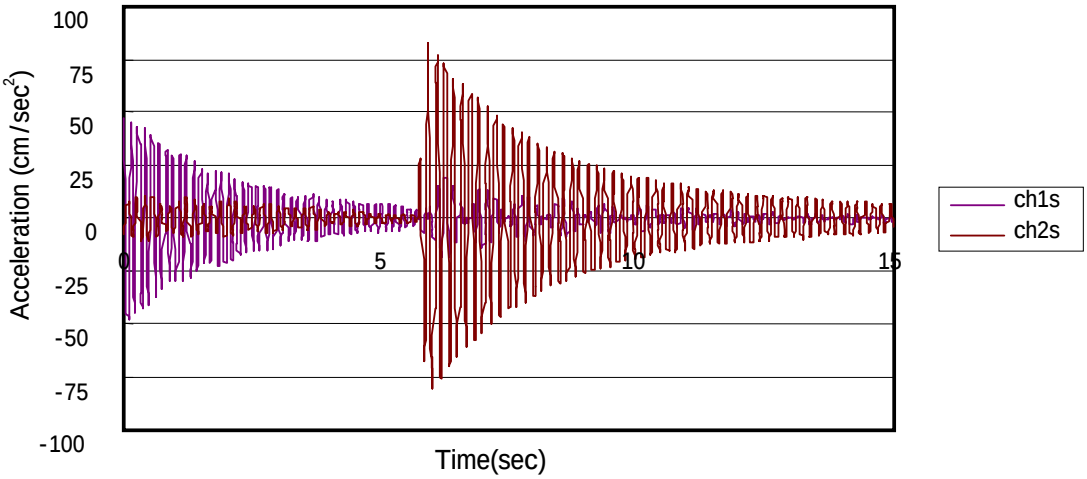

Fig.12 - Damping Vibration in Water Flow Channel

In this figure, channel 1 shows the vibration of x direction and channel 2 shows the one of y directions. They show very fine damping vibration curves. From these observation data, natural frequency and damping ratio are collected in two direction x and y which are flow direction and perpendicular direction of flow and those values are different with the amount of water depth.

1) Spring constant

Spring constant can be derived from the data in air by using data of mass and inertia of pier from three points support and four points support conditions and the results are 1800 N/cm in long span and 2600 N/cm in short span fixed case in both support systems with B type plate (width is 26mm). A type spring plate has 1650 N/cm and 890 N/cm for short and log span fixed case respectively.

2) Natural frequency in water flow and added inertia in water flow

Experiments in flow are carried in variation of mass of pier and stiffness of spring constant as shown in Table 1.

Table 1 - Cases in Water Flow

Case	Spring type	Mass g	X N/cm	Y N/cm
N	B	1220	1800	2600
S	B	3000	1800	2600
F	B	3000	2600	1800
A	A	1220	1650	890
B	A	3000	1650	890
C	A	3000	890	1650

Experimental data in these cases gives many results on natural frequency and damping ratio. The main interest is the variation of natural frequency by water depth changes and an example of case N is shown in figure 13.

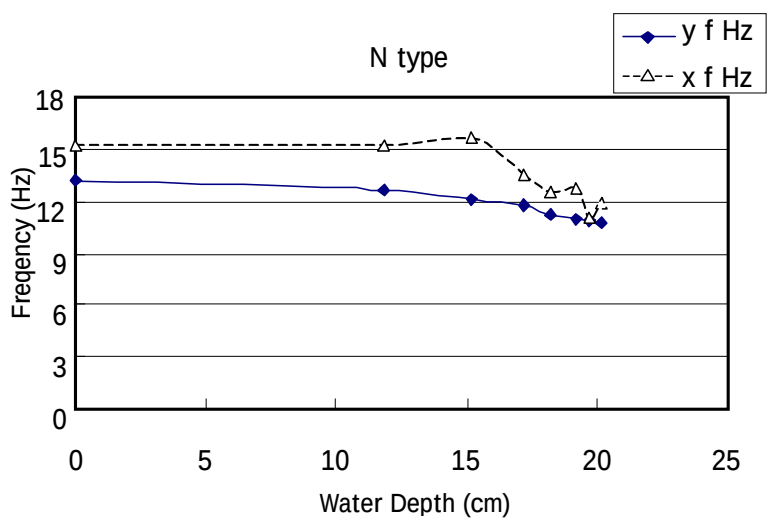

Fig.13 - Natural Frequency in Water Flow

As shown in figure 13, natural frequency decreases with the water depth is increasing, this means that the inertia of pier must be increased because the spring constant does not changed. This change is derived from the term in equation (7).

$$dM = \frac{\rho C_w A h}{3}\left(\frac{h}{L_0}\right)^2 \qquad \cdots\cdots(9)$$

The value of dM can be calculated from data by using the equation (7) and after that, the evaluation for equation (9) has been done. An example of the relation between natural frequency and added mass is shown in figure 14 as the case A.

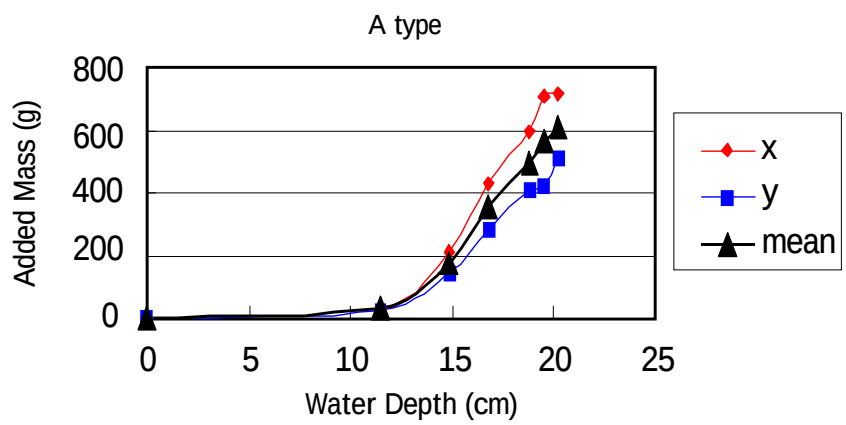

Fig.14 - Added Mass Inertia in Water Flow

Inertia by added mass is increasing great with water depth is increasing as shown in figure 14 and the values of x and y direction are different is different. These features can be seen in the cases A, B and C without the cases N, S and F. This main difference may be a stiffness of plate spring in this stage.

3) Consideration on added inertia

There is a difference in added inertia between cases N, S and F and cases A, B and C as mentioned above, such the value of dM has a difference of value in directions X and Y in cases A, B and C. But it is almost same value in cases N, S and F. This relation is clearly understood in figures 16 and 17 as there can be seen two different area in cases A, B and C. In these graphs, the most fitted line is drawn by calculating the value C_w in equation (9) from the data. The value of C_w is shown in table 2 with the value of spring constant k.

Table 2 - Value of C_w

Case	k N/cm	Cw
N,F,S	2700	1.591
N,F,S	1800	1.568
A,B,C hard	1650	1.109
A,B,C soft	890	0.8112

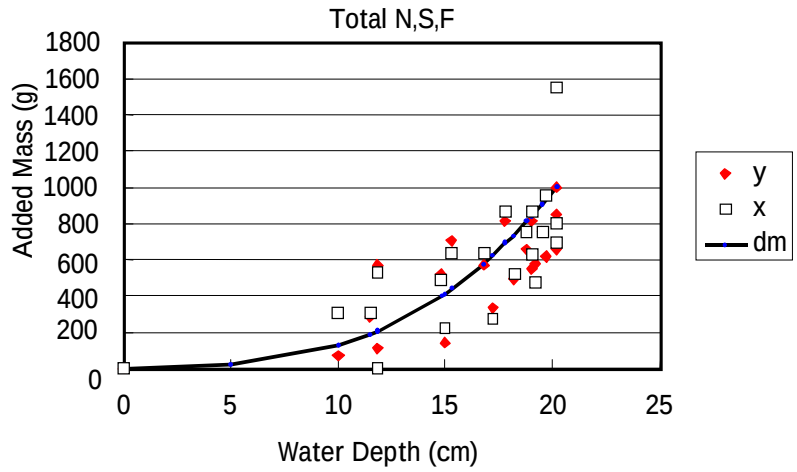

Fig. 15 - Cases N, S and F

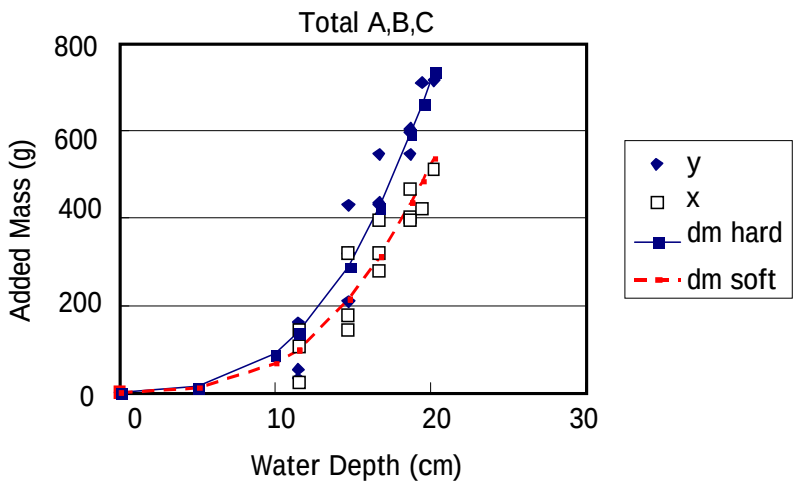

Fig. 16 - Cases A, B and C

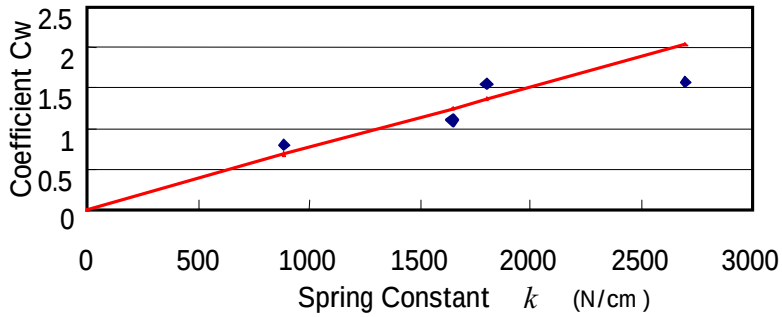

Fig. 17 - Relation between C_w and k

The value of C_w is not constant in all cases but it is related to the spring constant as it becomes greater with the spring constant as shown in table 2 and figure 17. It is not clear why it becomes greater in this stage, it must be made to be clear in next model test.

4) Damping ratio in water flow

There can be seen a difference in damping ratio with the difference of direction as flow direction or perpendicular direction of flow. The typical example is case C as shown in figure 18.

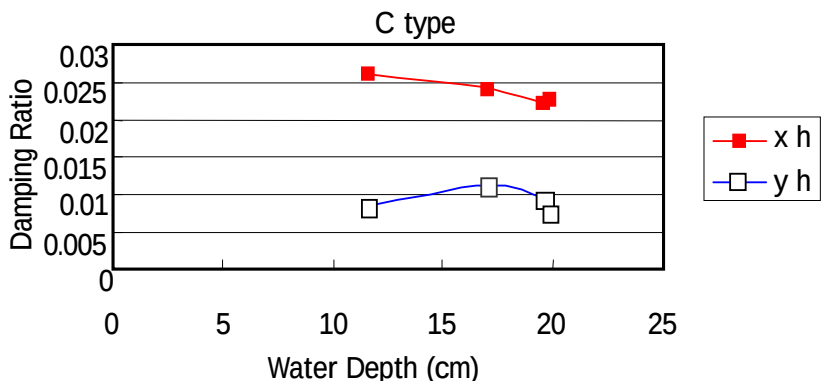

Fig.18 - Damping Ratio in Case C

Direction x in this figure is corresponding to water flow direction and y is perpendicular direction of flow. The value of y direction has 1/2.5 of value of x direction and this shows the possibility of continuous vibration by water flow. This point also gives the interests on vibration of pier under the flood conditions.

CONCLUSION

The model test of bridge pier related to the flood condition has developed without the similarity between fields bridge pier, but the very interesting results can be derived on the added inertia under the water. It has three power terms of water depth h and has good correlations between theoretical analysis and the results from model test.

There remains many interesting problems in this phenomenon such as the relations to water velocity and flow pattern around the pier and the similitude the phenomenon to fields bridge pier especially under the flood condition. This research work is two years program between JR and Toyo University from 2001 to 2002. These remained problems are studying in model test and theoretical analysis in this year.

REFERENCES

1. J.Tanak, M. Mikami: ”Setting Train Suspension Rules on the Bridges Prone to Scour in Consideration with Riverbed Characteristics”, International Symposium on Scour of Foundations, Melbourne, Australia, Nov.19
2. O.Suzuki, M. Shimamura: “Development of New Scour Monitoring Devices for Railway Bridges”, International Symposium on Scour of Foundations, Melbourne, Australia, Nov.19

3-Dimensional Measured and Simulated Flow for Scour Near Spur Dikes

Roger Kuhnle[1], Yafei Jia[2], and Carlos Alonso[3]

ABSTRACT

To improve understanding of the flow and scour processes associated with spur dikes more fully, 3-dimensional flow velocities were measured using an acoustic Doppler velocimeter at a closely spaced grid over a fixed flat bed with a submerged spur dike. Some 2592 three-dimensional velocities around a trapezoidal shaped submerged spur dike were measured. General velocity distribution and detailed near field flow structures were revealed by the measurement. Some important differences between the flow fields measured in this study and those measured for non-submerged vertical obstructions were observed in this study. Numerical simulation was performed using the free surface turbulent flow model, CCHE3D. The numerical simulation of the flow showed very good agreement between the computation results and the measurements. The numerical simulation results indicate the CCHE3D model can be used to predict near-field flows around hydraulic structures.

Keywords: *submerged spur dike, 3-dimensional flow, velocity measurements, 3-dimensional modeling, free surface flow, hydraulic structure*

INTRODUCTION

A spur dike may be defined as a structure extending outward from the bank of a stream for the purpose of deflecting the current away from the bank to protect it from erosion. Where the bank material is erodible, streams and rivers often erode the banks and move laterally, resulting in land loss, channel change, excessive sediment yield and degradation of the water quality. The use of a series of spur dikes is one of the most effective means of stabilizing or realigning channel banks. For economic reasons, spur dikes are often constructed of riprap and are commonly designed to be submerged during high flows. The pools formed from the local scour associated with spur dikes have been used successfully to enhance aquatic habitat in unstable streams (Shields et al., 1995). Despite the widespread use of spur dikes, many aspects of their design are based on prior experience and are only applicable to streams of a similar nature (e. g. Copeland, 1983). An improved understanding of the complicated 3-D flow in the vicinity of spur dikes and its interaction with the entrainment and transport of sediment is needed.

[1] Research Hydraulic Engineer, National Sedimentation Laboratory, USDA, Agricultural Research Service, P. O. Box 1157, Oxford, Mississippi 38655, USA. Email: rkuhnle@ars.usda.gov.
[2] Research Associate Professor, National Center for Computational Hydroscience and Engineering, The University of Mississippi 38677, USA. Email: jia@ncche.olemiss.edu.
[3]Research Leader, Channel and Watershed Processes Research Unit, National Sedimentation Laboratory, USDA, Agricultural Research Service, P. O. Box 1157, Oxford, Mississippi 38655, USA. Email: calonso@ars.usda.gov.

There have been few previous studies of the flow in the vicinity of spur dikes. Rajaratnam and Nwachukwu (1983) studied the flow in a laboratory flume near groin-like structures represented by an aluminum plate which projected above the water surface. A pitot-static tube was used to measure the flow in regions of undisturbed flow and a three-tube yaw probe was used in regions of skewed flow. They found that the bed shear stresses at the upstream corner of the plate were up to five times the bed shear stresses in the approach flow section. The initiation of local scour is associated with the increase in shear stress caused by the accelerating flow around the obstruction. For cylindrical bridge piers, scour has been observed to be dominated by a strong downflow on the upstream side of the pier and a horseshoe vortex which surrounds the upstream and lateral sides of the pier (e.g. Mellville and Raudkivi, 1977; Graf and Yulistiyanto, 1998; Istiyato and Graf, 2001). For bridge abutments, which are in many ways similar to spur dikes, flow features resembling those observed around one-half of a cylindrical bridge pier have been measured, including the primary vortex (essentially one half of the horse-shoe vortex), which forms around the structure and contributes to the development of scour (Kwan and Melville, 1994). These investigators have determined that the flow structures around a model wingwall abutment are dominated by the large primary vortex and an associated downflow.

Detailed velocity measurements around a submerged spur dike with a trapezoidal shape are rare. Flow around this structure would be expected to vary from that of flat plates and abutments due to the over-topping flow and 3-dimensional shape of the structure. The over-topping flow and trapezoidal shape would be expected to affect the characteristics of the primary vortex and make the recirculation zone behind the spur dike more three-dimensional. Because the flow is the key to understanding the performance of a submerged spur dike, the velocity field around the spur dike was measured in a laboratory flume at the National Sedimentation Laboratory. This data set of 2592 point measurements was compared to flow simulations calculated using the 3-dimensional numerical flow model (CCHE3D) developed at the National Center for Computational Hydroscience and Engineering, University of Mississippi.

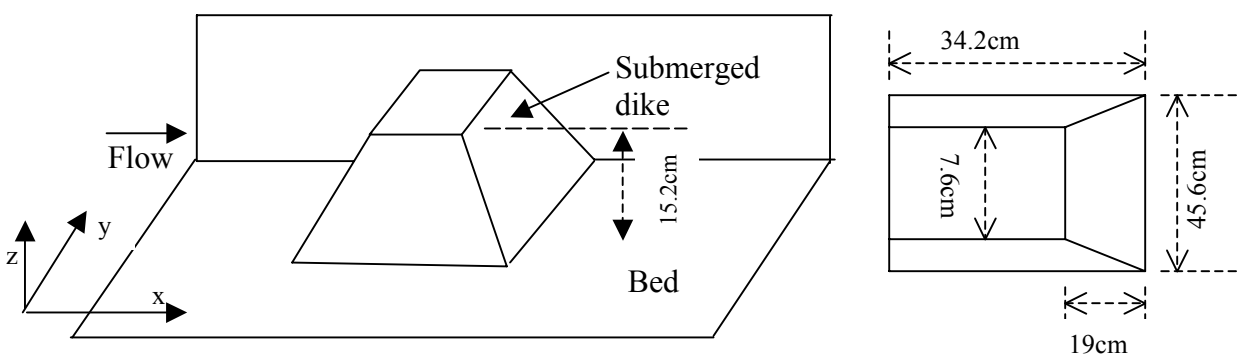

Fig. 1. Sketch of the model spur dike (not to scale) used in the experiments.

PHYSICAL MODEL AND VELOCITY DATA

All of the flow measurements were collected in a recirculating flume with a test channel 30 m long, 1.2 m wide, and 0.6 m deep located at the National Sedimentation Laboratory. Flow rate in the flume was measured using a pressure transducer connected to a Venturi meter in the return

Table 1. Flow condition of the flume experiments.

Exp. Run	Flow rate (m^3/s)	Flow depth (m)	Mean Flow velocity (m/s)	Froude Number
Flat fixed bed	0.129	0.3048	0.347	0.201

pipe. Flow depth was controlled by the amount of water in the flume and measured by taking the difference in elevation between 12-m long bed and water surface transects in the approach flow section. The bed of the approach flow section was covered with sediment (D_{50} = 0.8 mm, $[D_{84}/D_{16}]^{1/2}$ =1.35). The bed sediment was immobilized with a thin layer of cement from 21.9 m downstream of the channel inlet to the tail box to prevent the bed from changing. The zero location of the *x* (streamwise) coordinate was located 22.6 m downstream of the channel inlet and the center of the spur dike model was located 1.19 m downstream from the zero coordinate. The spur dike model (Fig. 1) was located on the left wall of the channel facing downstream. Flow conditions were very similar to those used in one experiment from Kuhnle, et al. (1999) and are summarized in Table 1. The ratio of the flow shear stress to the critical shear stress of the bed material sediment obtained from the Shields (1936) curve was 0.7 in the approach flow section.

The velocity data was collected using a commercially available Acoustic Doppler Velocimeter (ADV). The measurement head of the ADV is mounted on a stainless steel mast 60 cm long and 1 cm in diameter. The measurement head has three sensors mounted at a spacing of 120° around a circle approximately 7 cm in diameter. The sampling volume of the ADV is a cylinder 6 mm in height and 6 mm in diameter (170 mm^3) located 5 cm away from the head of the ADV. Flow velocity data at each point was collected at 50 Hz for 5 minutes. The 5 minute sample duration was determined empirically as the optimum length of time to capture the mean velocity at the sampling location within a reasonable time frame. The relatively large measurement volume and low rate of data acquisition of ADVs when compared to laser Doppler anemometers, indicate that the higher frequency and smaller scales of flow turbulence cannot be adequately measured using an ADV.

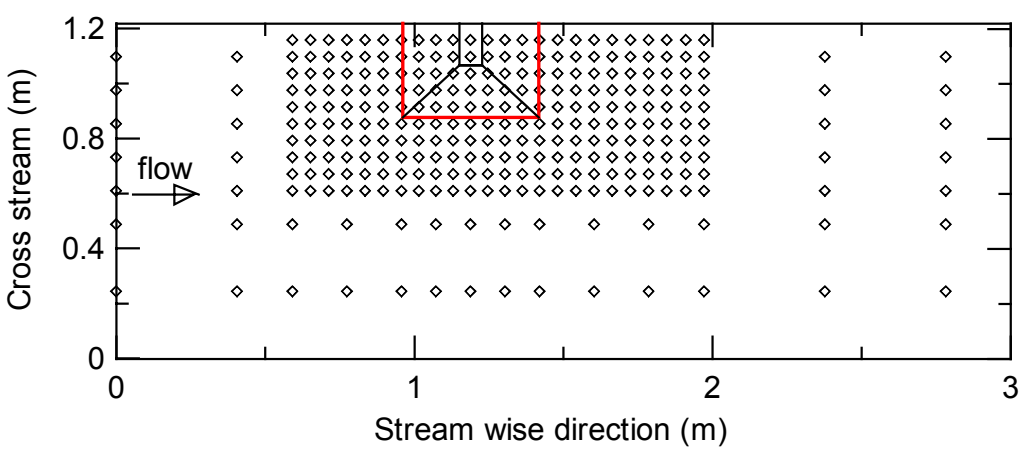

Fig. 2. Plan view of experimental flume with measurement locations indicated by diamond symbols. Outline of base of spur dike shown in red.

Flow velocities were measured at 288 locations as shown in Figure 2. At each location the flow was measured at 9 vertical positions: 0.0100, 0.0225, 0.0350, 0.0475, 0.0600, 0.1000, 0.1400,

0.1800, and 0.2200 m from the bed. The vertical measurement positions were adjusted accordingly at the locations above the spur dike to arrive at nine measurement positions. A total of 2592 velocity vectors were measured. All velocity records were processed using the public domain program, WinADV. Measurements were filtered using WinADV to reject points with a correlation coefficient less than 0.7. In most files 90% or more of the data was above 0.7.

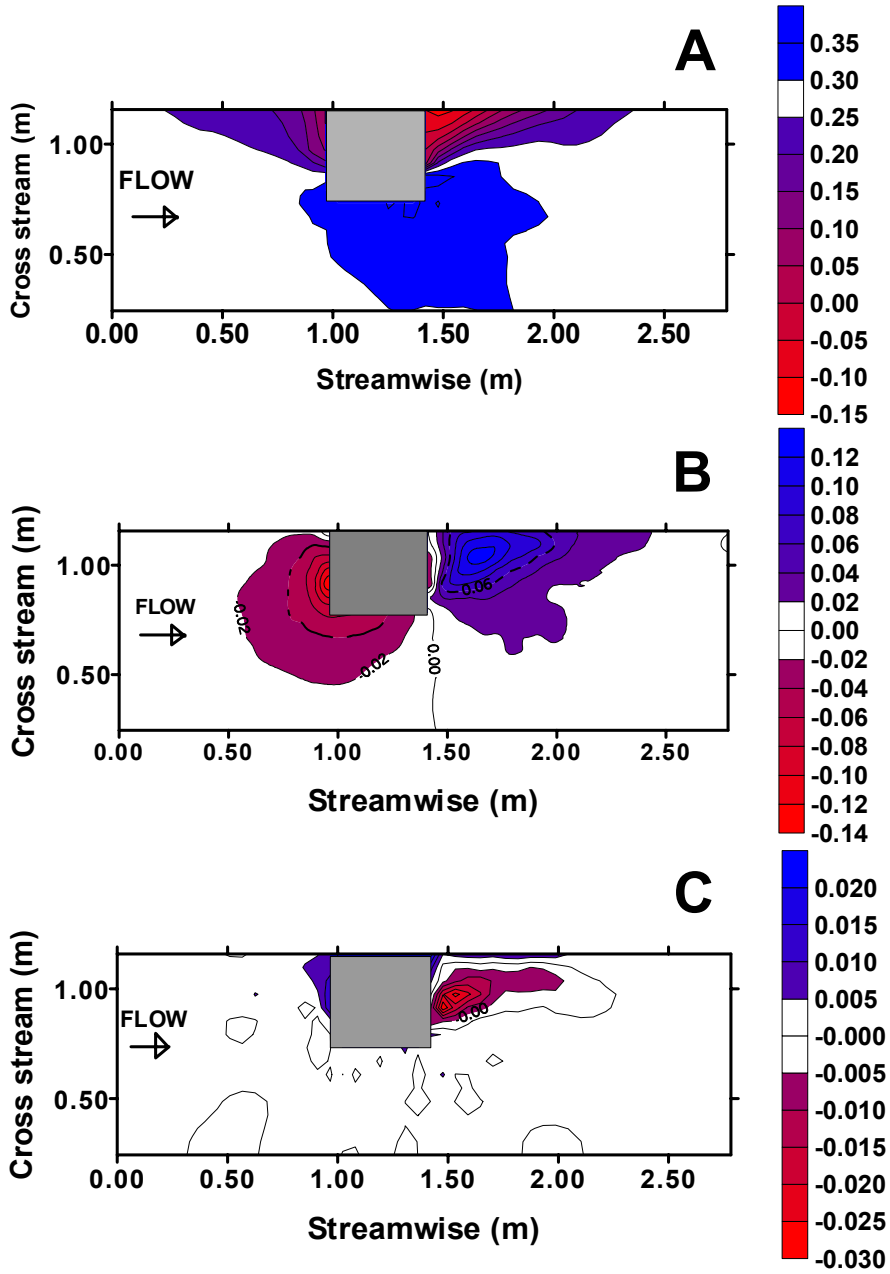

Fig. 3. Contours of flow velocity (m/s) for the plane 0.01 m above the bed, (A) u - streamwise velocity, (B) v - cross-stream velocity, and (C) w - vertical velocity. Gray area represents the outline of the model spur dike at the bed.

GENERALIZED VELOCITY DATA

The general trends of flow velocities in the plane 0.01 m from the bed are shown in Figure 3. Streamwise velocity is shown to increase in magnitude on the right side of the spur dike while decreasing and becoming negative upstream of and in the lee of the structure. Cross-stream velocity is directed around and over the structure (Fig. 3B), and vertical velocity (Fig. 3C) is affected upstream and downstream of the structure as the flow converges and diverges over the top of the structure. In Figure 4 the root mean square of the deviations in *u* are shown to decrease as the flow accelerates around the structure, and to be the greatest in the region downstream of the structure where the flow separates from the boundary. Contour plots for *v*- and *w*-fluctuations were similar to Figure 4. A salient aspect of these results stems from the fact that the structure being trapezoidal in shape and submerged generates a flow pattern that does not "pile up" on the upstream edge of the structure, and the separation zone is more complicated because flow is converging from more than one direction as compared with other studies (Rajaratnam and Nwachukwu, 1983; Kwan and Melville, 1994).

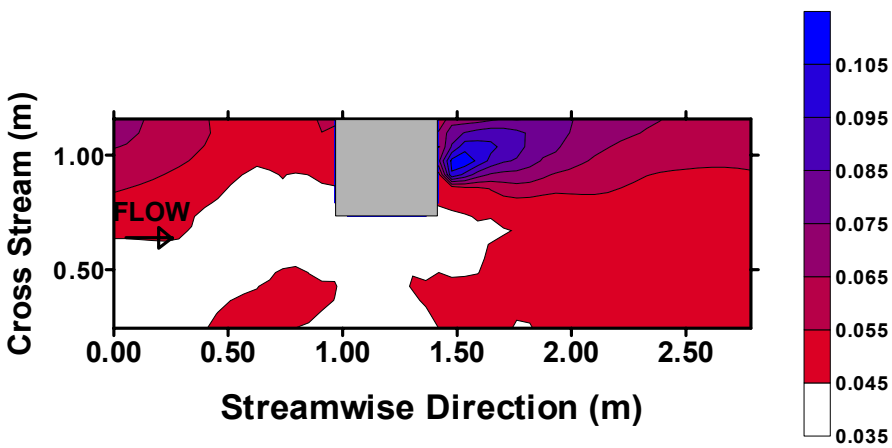

Fig. 4. Contours of root mean square of deviations in u, at plane 0.01 m above the bed.

NUMERICAL SIMULATION MODEL

Numerical simulations of three-dimensional free surface flow around hydraulic structures have been attempted with reasonable success (Jia and Wang 1996, 1999, Richardson, and Punchang, 1998). The three-dimensional, unsteady, turbulent free surface flow model, CCHE3D, has been applied to simulate the flow around submerged spur dikes in this study. This model has been applied (Jia and Wang, 2000) to simulate a similar experimental case conducted by Kuhnle et al. (1997), to study flow field and local scouring without measured velocity data. This model uses the finite element method to solve the following governing equations.

The Reynolds stress equations:

$$u_{i,t} + u_j u_{i,j} - (-\overline{u_i u_j})_{,j} + \frac{p_i}{\rho} + f_i = 0 \tag{1}$$

$$u_{j,j} = 0 \tag{2}$$

where u represents the mean velocity, u' represents the turbulent velocity fluctuation, p is the mean pressure, ρ is the density of the water, and f is the gravitational force.

The free surface kinematic equation:

$$\frac{\partial \eta}{\partial t} + u_\eta \frac{\partial \eta}{\partial x} + v_\eta \frac{\partial \eta}{\partial y} + w_\eta = 0 \tag{3}$$

where η denotes the free surface elevation.

The k-ε turbulence closure scheme:

$$k_{,t} + u_j k_{,j} - (\frac{\nu_k}{\sigma_k} k_{,j})_{,j} = P - \varepsilon \tag{4}$$

$$\varepsilon_{,t} + u_j \varepsilon_{,j} - (\frac{\nu_k}{\sigma_\varepsilon} \varepsilon_{,j})_{,j} = c_{\varepsilon 1} P \frac{\varepsilon}{k} - c_{\varepsilon 2} \frac{\varepsilon}{k^2} \tag{5}$$

where k represents the turbulent kinetic energy $u_i' u_i'/2$, ε represents the rate of dissipation of turbulent kinetic energy, ν_t denotes the turbulent viscosity given by:

$$\nu_t = c_\mu \frac{k^2}{\varepsilon} \tag{6}$$

and P is the production of turbulent kinetic energy computed from:

$$P = \nu_t (u_{,j} + u_{,i}) u_{,i} \tag{7}$$

The values of empirical coefficients appearing in the preceding equations were assigned c_μ=0.09, σ_k=1.0, σ_ε=1.3, $c_{\varepsilon 1}$=1.44, $c_{\varepsilon 2}$=1.92.

The velocity correction method was used to solve the momentum equations (Jia et al, 2001). A Poisson's equation formulated with the velocity correction terms and the continuity equation was solved on a staggered grid to obtain the dynamic pressure and force the flow to satisfy the divergence free condition. Wall boundary conditions were used for the momentum equations and the k-ε closure model. The shape of the spur dike is trapezoidal in cross-sectional and longitudinal directions with very steep slopes, a body fitted 3D grid was generated over the dike. The system of equations was solved implicitly by using the SIP method with the first order Euler's scheme.

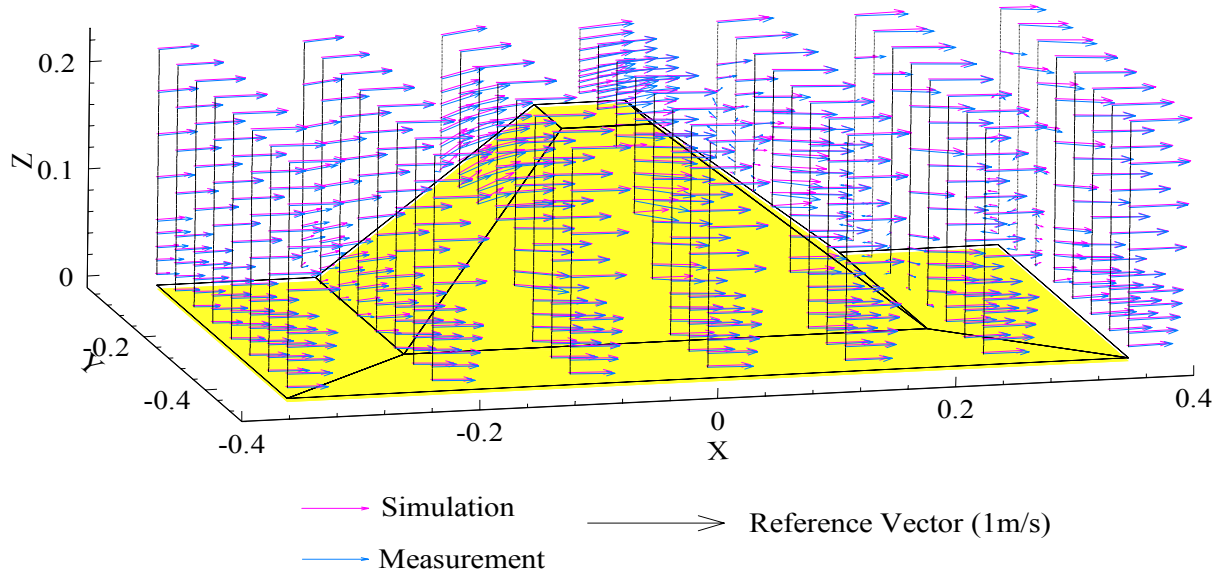

Fig. 5. A perspective view of simulated and measured flow field around the submerged spur dike.

SIMULATION RESULTS

Figure 5 shows a perspective view of the trapezoidal-shaped spur dike and the simulated and measured velocities in this study. The far side (Y=0) is where the vertical wall of the flume is, and the horizontal plane is the channel bed. To focus attention and make the comparison clear, the area shown in the figure is only the close vicinity of the spur dike, and all other measured locations are ignored. The spur dike (Fig. 5) is surrounded by a field of measured and computed velocity vectors, with all the data in the seven cross sections displayed. Two velocity vectors are drawn at each point along a vertical line. The vectors in blue represent measured velocities and those in red represent the simulated velocities at the same location. Because the spatial locations of measuring points differ from mesh points of the computation, linear interpolation was applied to estimate the simulated velocity at the measuring locations. Generally, the flow field of the physical model is well reproduced by the numerical simulation. The velocity magnitude and direction of most simulated vectors agree with those measured. It is noted though, larger differences appear at several places: the corner near the wall and bed in the upstream side; in the recirculation zone downstream of the spur dike, and on the upper part of the spur dike slopes. For vectors of smaller magnitude, the relative differences appear larger.

Figure 6 shows the comparison of the computed and measured total velocity magnitude. The diagonal line represents the perfect agreement. It can be seen that the numerical prediction reproduced the physical model data with very little systematic error (r^2=0.97). The error norm for the total velocity

$$\sigma = \frac{1}{N}\sum\sqrt{\left|U_s^2 - U_m^2\right|} \approx 0.0825 \tag{8}$$

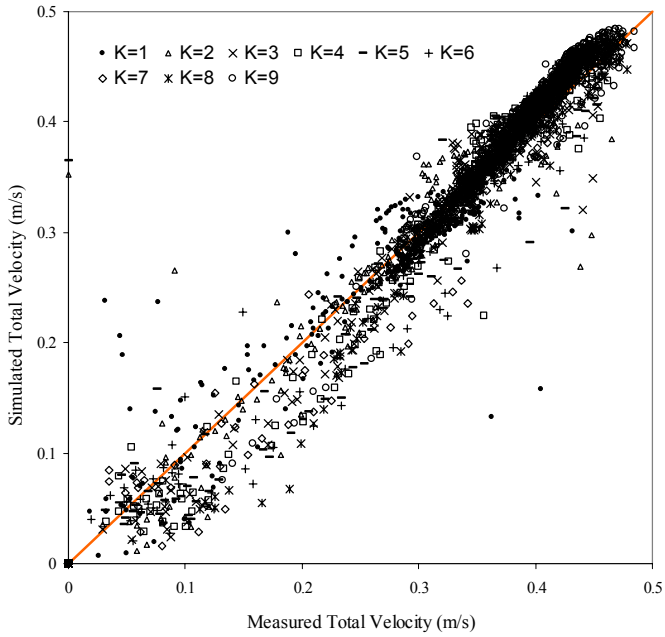

Fig. 6. Comparison of the simulated and measured total velocity magnitude. K=1, K=2, … K=9 indicate the vertical level of measurement with K=1 represents the level near the bed and K=9 represents the level near the surface.

is reasonably small with U_s and U_m representing simulated and measured total velocity and N=2592. The point scattering is slightly higher for smaller velocities (<0.3m/s). Most of the points which scatter farther away from the diagonal line are those close to the bed or spur dike surface. This scattering reflects the difficulty of measuring acoustic data close to a solid surface.

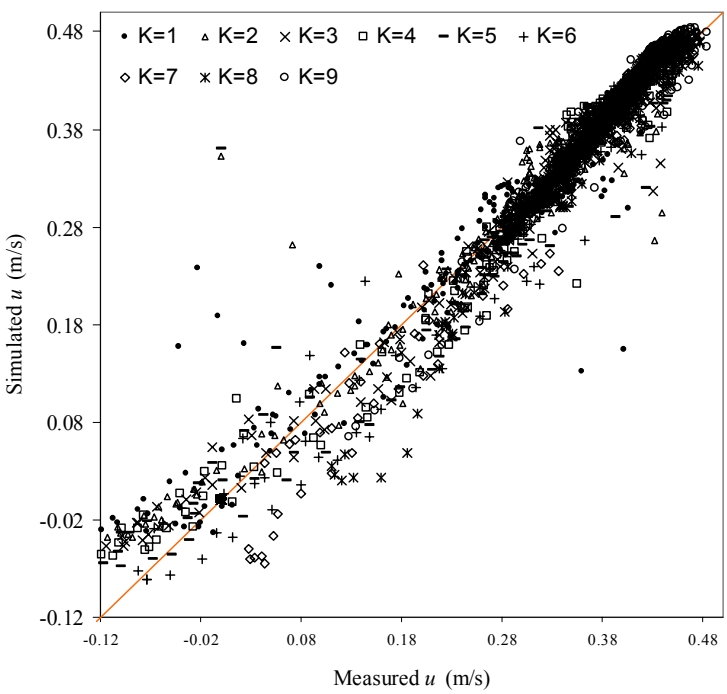

Fig. 7. Comparison of simulated and measured *u* velocity component (R^2=0.970). K=1, K=2, … K=9 indicate the vertical level of measurement with K=1 represents the level near the bed and K=9 represents the level near the surface.

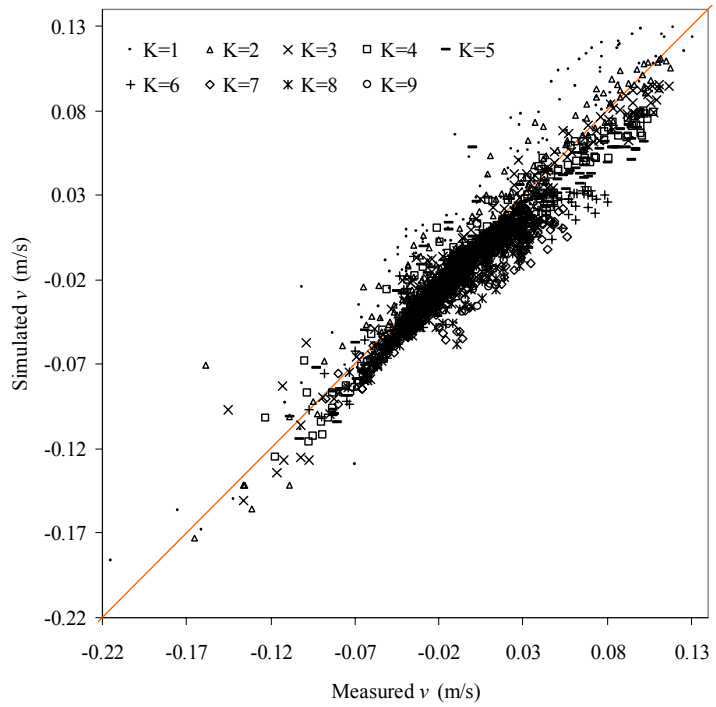

Fig. 8. Comparison of simulated and measured *v* velocity component (R^2=0.886). K=1, K=2, … K=9 indicate the vertical level of measurement with K=1 represents the level near the bed and K=9 represents the level near the surface.

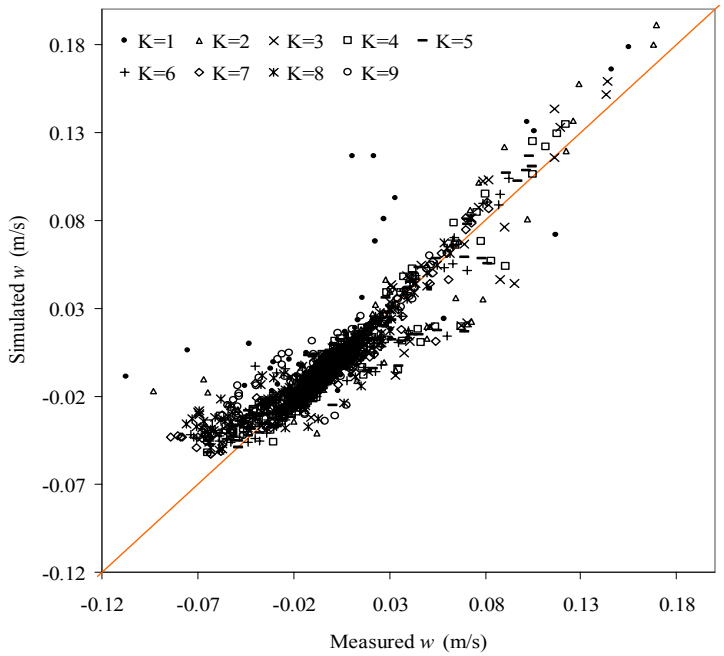

Fig. 9. Comparison of simulated and measured *w* velocity component (R^2=0.834). K=1, K=2, … K=9 indicate the vertical level of measurement with K=1 represents the level near the bed and K=9 represents the level near the surface.

Figures 7, 8, and 9 show comparisons of simulated velocity components *u, v*, and *w* individually. As shown in Figure 1, *u, v* and *w* are the longitudinal, transverse and vertical components, respectively. The *v* component is seen to be distributed along the diagonal without skew but scattering is wider for the range $v>0$ (Fig. 8). *u* and *w* components are a little under predicted when they have negative values (Fig. 7 and 9).

Since the *u* component is negative, *v* component is positive only in the recirculation zone, and the negative *w* component values distribute mainly behind the spur dike, these differences therefore are mainly in the recirculation zone. At other locations the prediction and the measurement are consistent without obvious systematic errors.

The comparisons of simulated and measured transverse velocity (secondary currents) in cross-sections around the spur dike are shown in Figure 10. To facilitate the visual comparisons, alternate sections are plotted separately in two plots. Although differences between the simulations and measurements can be observed, the general patterns of secondary flows agree very well. The agreement in the front and middle sections is better than behind the spur dike. In the recirculation zone, the general directions and magnitude of the secondary flow vectors are simulated quite well, however, the magnitude of vertical velocity components away from the bed are under-estimated, and, thus the angles between the simulation and measured vectors are relatively large.

Velocities projected on longitudinal sections (*u*-*w*) are plotted in Figure 11. To enhance clarity, alternate sections are drawn in separate plots (a) and (b). The perspective view is from outside the wall attaching the spur dike and from downstream to upstream. The comparisons in the figure indicate that the re-circulation downstream of the spur dike, driven by the overtop shear flow, is simulated very well, although reverse flow velocities are weaker than those measured. The simulated velocity vectors in these sections in general exhibit little differences from the measured ones. In the front corner near the wall and bed, the predicted velocity is smaller than the measured, and the primary vortex that has been observed in spur dikes with vertical front wall and abutment models is not observed in this case. This is why the skews appear at the lower end of Figures 7 and 9.

The flow direction and general pattern are illustrated by velocity vectors and particle path lines in Figure 12. The secondary flows around the spur dike include a small vortex in the front corner and a larger recirculation cell behind the spur dike. The high shear stress zone on the channel bed indicates the potential location of the scour hole. Unlike the flow around obstructions with vertical walls, the flow around the submerged trapezoidal spur dike has a fully three-dimensional recirculation cell. For structures with a vertical front, the blockage to the oncoming flow usually creates a strong down-flow and primary or horseshoe vortex. This has been observed in studies of cylindrical piers and bridge abutments (Melville and Raudkivi, 1977; Kwan and Melville, 1994; Graf and Yulistiyanto, 1998). The down-flow in front of this trapezoidal shaped submerged spur dike, however, is almost not present as the flow instead moves upwards along the surface of the spur dike, except close to the bed and near the corner of the wall where a small vortex is generated. The primary vortex measured and recognized by Kwan and Melville (1994) was not observed in this study.

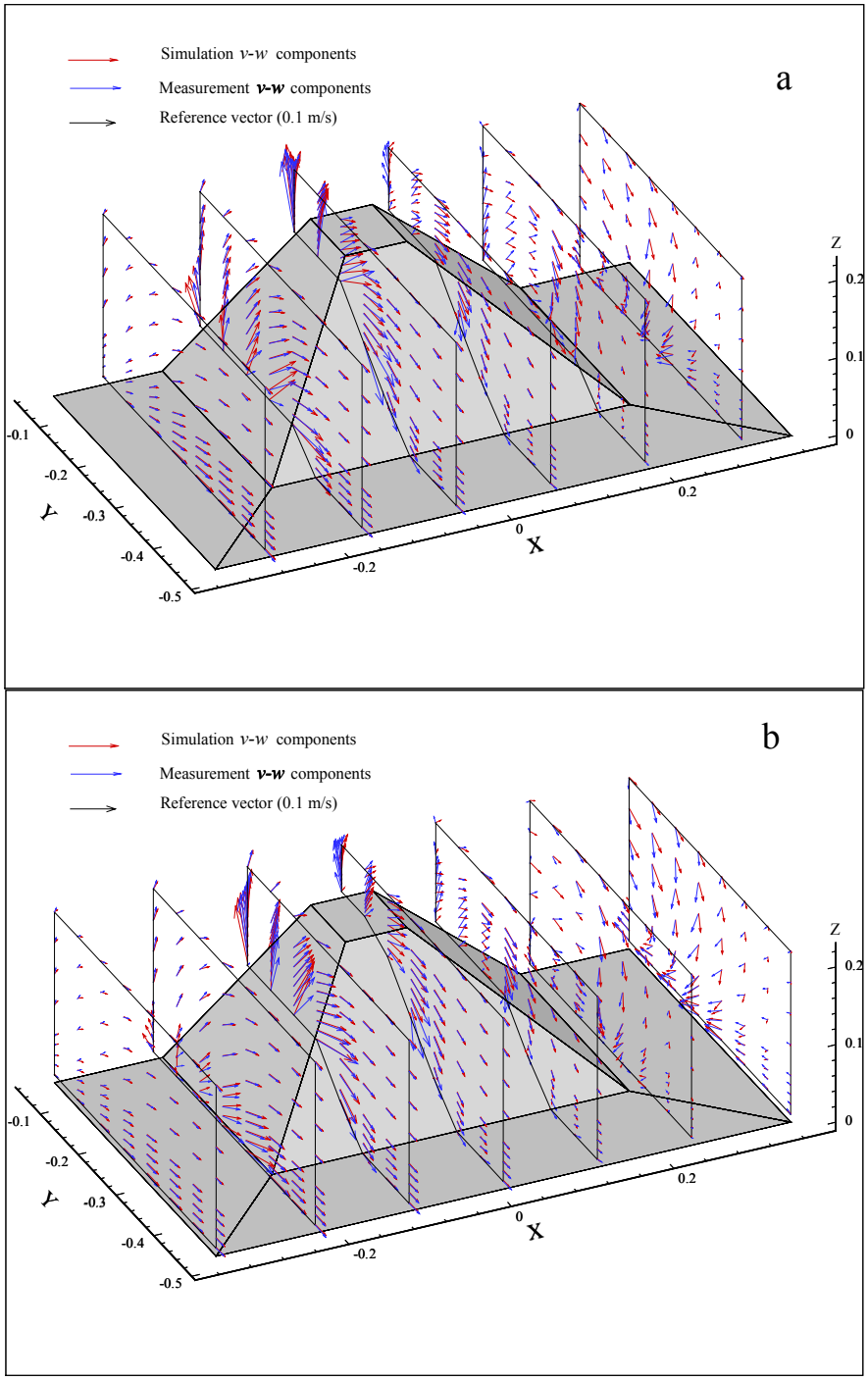

Fig. 10. Comparison of simulated and measured transverse velocity (*v*-*w*) components in cross-sections around the spur dike at the locations (a) x = 0.8961, 1.0150, 1.1308, 1.2466, 1.3625, 1.4813 m; (b) x = 0.8352, 0.9571, 1.0729, 1.1887, 1.3045, 1.4204, 1.5423 m, shown in Fig. 2.

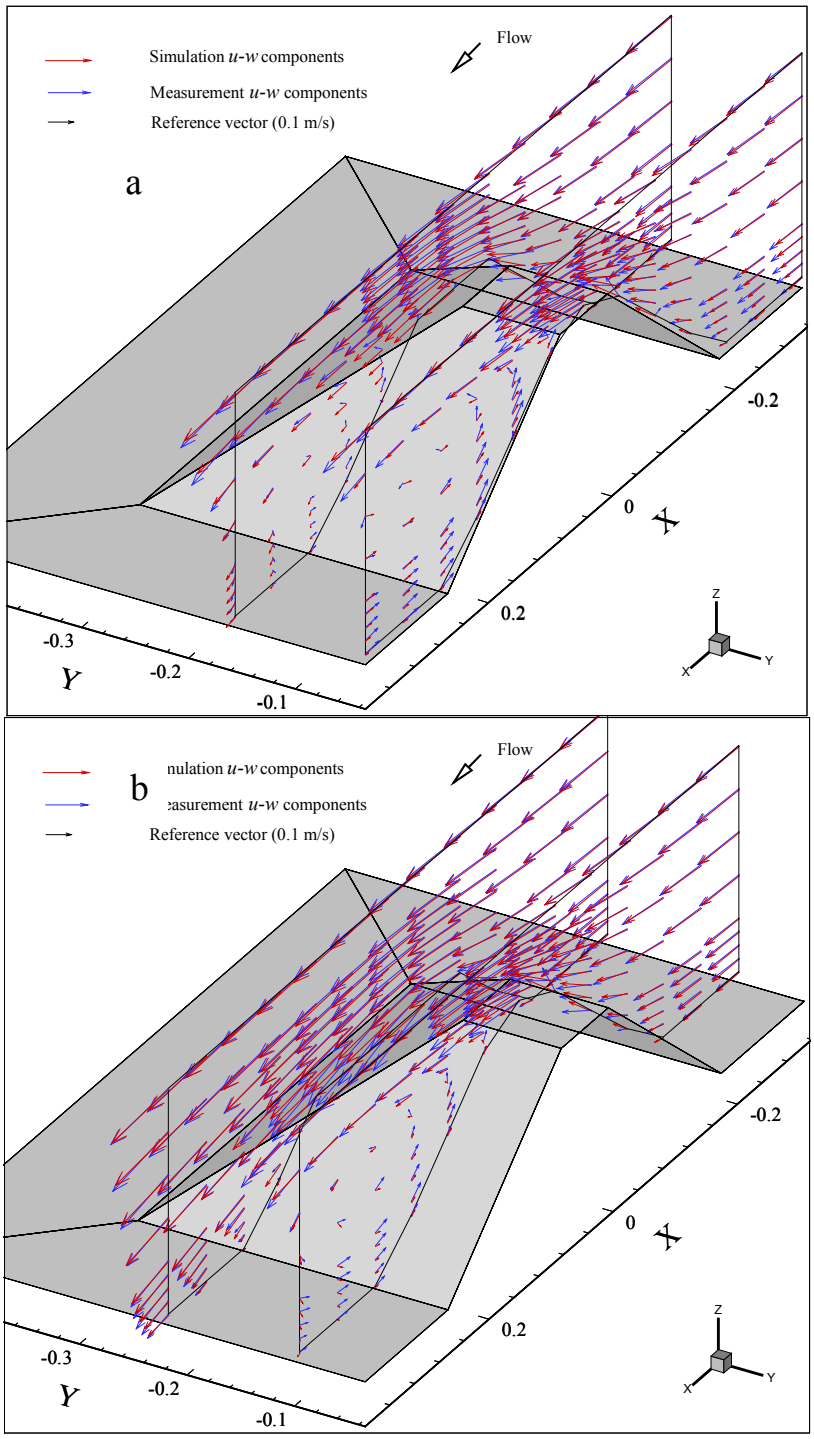

Fig. 11. Comparisons of simulated and measured flow pattern (*u-w*) in longitudinal sections: (a) y = 1.1582, 1.0363 m; (b) y = 1.0973, 0.9754 m, shown in Figure 2.

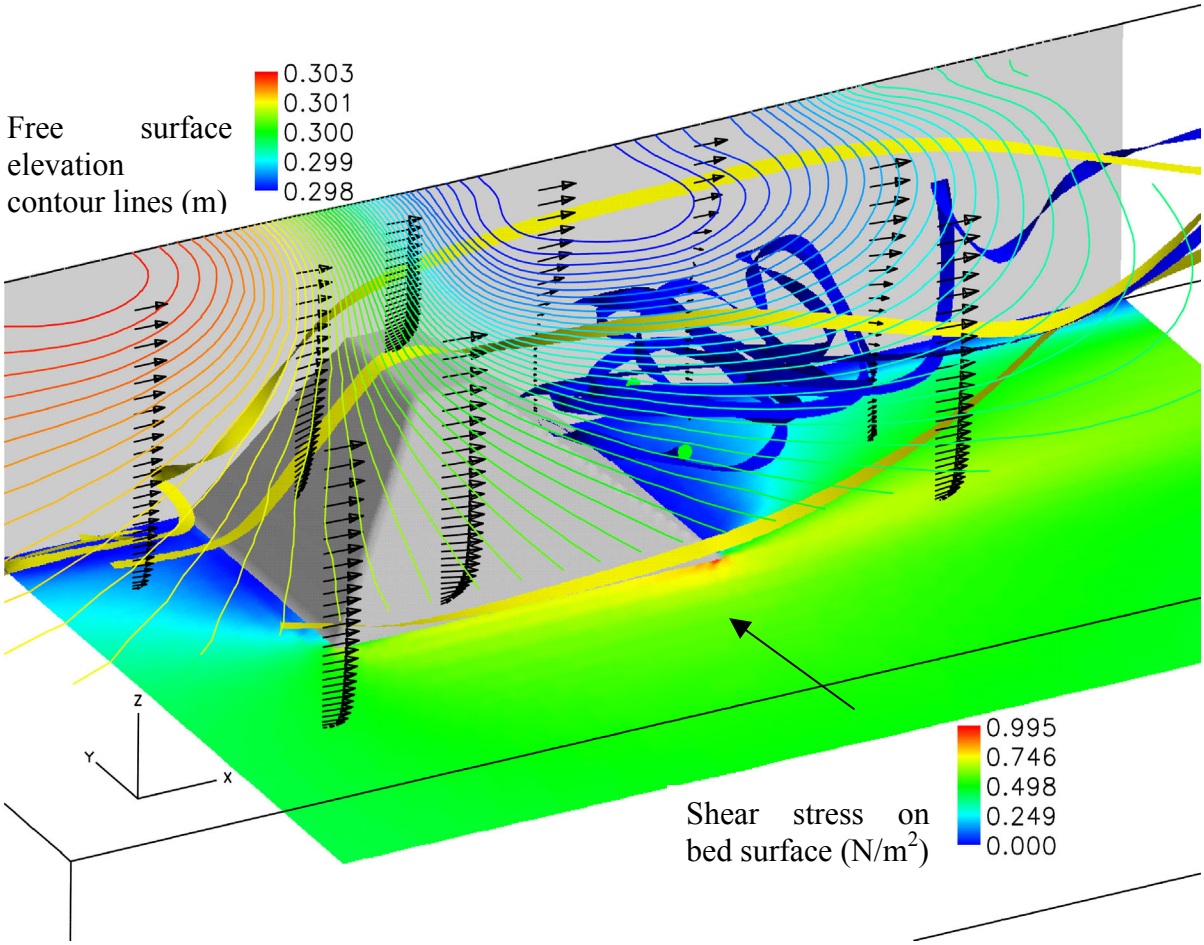

Fig. 12. Simulated near field flow pattern around the submerged spur dike. Yellow ribbons are released in front of the spur dike, blue ones are released from behind. The shear stress distribution on the bed is shown by color shading (red – high; yellow – low).

CONCLUSIONS

Three dimensional flow measurements around a model spur dike with a stationary bed showed little or no evidence for a strong downflow on the upstream side or a primary vortex. These features have been described in other studies of piers, dikes and abutments. The differences in flow features observed is believed to be the result of the 3-dimensional shape of the model spur dike and the over-topping flow used in this study.

The three-dimensional finite element model for free-surface and turbulent flow (CCHE3D) was used to simulate the flow around the submerged spur dike. The agreement between the simulation results and the observations is very good, although some discrepancy is noted downstream of the spur dike in the recirculation zone. The error norm of the comparison for the whole data set is 8.25%. These results indicate that the CCHE3D model can yield robust simulations of velocity flow patterns around hydraulic structures of complex shape such as the

trapezoidal submerged spur dike used in this study. Use of computational models, such as CCHE3D, have the potential to improve the design of spur dikes for erosion control projects.

ACKNOWLEDGMENTS

This work is a result of research supported in part by the USDA Agriculture Research Service under Specific Research Agreement No. 58-6408-7-035 (monitored by the USDA-ARS National Sedimentation Laboratory) and The University of Mississippi. Research Assistant, T.T. Zhu, helped to produce many of the figures. John Cox and Emery Sayre collected the flow data that was used in this paper. John Cox carried out the initial processing of the flow data.

REFERENCES

Copeland, R. R., 1983, "Bank protection techniques using spur dikes." Miscellaneous Paper HL-83-1, U. S. Army Waterways Experiment Station, Vicksburg, Mississippi, 32 pp.

Graf, W.H., and Yulistiyanto, B., 1998, "Experiments on flow around a cylinder; the velocity and vorticity fields", Journal of Hydraulic Research, IAHR, 36(4), 637-653.

Istiyato, I., Graf, W.H., 2001, "Experiments on flow around a cylinder in a scoured channel bed", International Journal of Sediment Research, Vol. 16, No. 4, pp431-444.

Jia, Y., and Wang, S.S.Y., 1996, "A modeling approach to predict local scour around spur dike-like structures", Proceedings of the Sixth Federal Interagency Sedimentation Conference, p. II-90-97.

Jia, Y., and Wang, S.S.Y., 1999, "Simulation of horse-shoe vortex around a bridge pier", Proceedings of the International Water Resources Engineering Conference". CD-ROM, 10 pp.

Jia, Y., and Wang, S.S.Y., 2000, "Numerical Study of Turbulent Flow around Submerged Spur Dikes", 4th International Conference for Hydroscience and Engineering, 2000, Seoul, Korea.

Jia, Y., Kitamura, T., and Wang, S.S.Y., 2001, "Simulation scour process in a plunge pool with loose material", ASCE, *Journal of Hydraulic Engineering*, Vol. 127, No. 3, pp219-229.

Kuhnle, R., Alonso, C.V., and Shields, F.D., 1997, "Geometry of scour holes around spur dikes, and experimental study", Wang, S.S.Y., Langendoen, E.J., and Shields, F.D., (ed.) Proceedings of the Conference on Management of Landscapes Disturbed by Channel Incision, Center for Computational Hydroscience and Engineering, School of Engineering, The University of Mississippi, p. 283-287.

Kuhnle, R., Alonso, C.V., and Shields, F.D., 1999,"Geometry of scour holes associated with 90° spur dikes", Journal of Hydraulic Engineering, ASCE, 125(9), 972-978.

Kwan, T.F., and Melville, B.W., 1994, "Local scour and flow measurements at bridge abutments", Journal of Hydraulic Research, IAHR, 32(5), 661-673.

Melville, B.M., and Raudkivi, A., 1977, "Flow characteristics in local scour at bridge piers", Journal of Hydraulic Research, IAHR, 15(4), 373-380.

Rajaratnam, N., and Nwachukwu, B. A. 1983. "Flow near groin-like structures." Journal of Hydraulic Engineering, ASCE, 109(3), 463-480.

Richardson, J.E., and Punchang, V.G., 1998, "Three dimensional simulation of scour-induced flow at bridge piers", Journal of Hydraulic Engineering, ASCE, 124(5), 530-540.

Shields, A., 1936, Anwendung der Aenlichkeitsmechanik und der Turbulenzforschung auf die Geschiebebewegung, Mitteilungen der Preussischen Versuchsanstalt fur Wasserbau und Schiffbau, Berlin, Germany, translated to English for W.P. Ott and J.C. van Uchelen, California Institute of Technology, Pasadena, CA.

Shields, F. D., Jr., Cooper, C. M., Knight, S. S., 1995, "Experiment in stream restoration." Journal of Hydraulic Engineering, ASCE, 121(6), 494-502.

Scour Experiments on Dike Angle, Porosity, and Hook for a Thin Dike

By

Emilio Martinez[1], Robert Ettema[2], and Ahmed Lachhab[3]
Iowa Institute of Hydraulic Research
The University of Iowa
Iowa City, IA 52242

ABSTRACT

This paper presents preliminary results from laboratory experiments conducted to determine how dike angle, porosity, and hook-length influence local scour at a thin dike (possibly constructed from sheet-pile) for use in deflecting debris and ice away from a water intake for a thermal power station. The experiments involved straight dikes and dikes fitted with an end hook, directed downstream and upstream. The results from the experiments usefully reveal trends between equilibrium scour depth and these aspects of dike design. The relationships may aid in the design of porous dikes. They show how dike angle and porosity may reduce local scour. Additionally, they show that dike hook-length exerts only a minor influence on scour depth. The results also include information on the extent of sediment deposition downstream of a dike.

INTRODUCTION

The present study was prompted by the need to design a flow-guidance dike that would deflect debris and ice away from a water intake located on a riverbank along a mid-size alluvial channel, minimize local scour depth as well as sediment accumulation. Scour was a concern for the foundation depths required for the dike. Sediment deposition was a concern, as it is intended that the dike should not aggravate alluvial-sediment ingestion by the water intake; sediment potentially could accumulate in the flow separation zone behind the dike and thereby move readily into the intake. Two ways to mitigate the two concerns is to make the dike sufficiently porous so as to weaken the stagnation pressure heads associated with the local flow field around the dike, and to enable flushing flow to pass through the dike. To determine how dike porosity and angle influence local scour, series of flume experiments were conducted.

Additional experiments were conducted to determine whether hook length, for a dike perpendicular to the flow, influences scour depth. These experiments also entailed exploring the merits of modifying the flow field at the end of the dike so as to reduce the turbulence generated by flow passing around a dike.

[1] emilio-martinez@uiowa.edu
[2] robert-ettema@uiowa.edu, ph 319-384-0596
[3] ahmed-lachhab@uiowa.edu

A considerable number of prior experiments have been conducted to determine dike/wall/abutment angle effects on local scour. Melville and Coleman (2000) usefully summarize the effects. It is noteworthy, though, to mention that the prior studies seem to have been conducted for conditions of clear-water scour, and that the influence of pier or dike width has not been considered in deciphering the data.

Though some prior investigation has been conducted regarding the influence on scour depth of dike porosity, the results of those studies are not widely disseminated, and require further confirmation. Notable studies are those by Subramanya and Gangadharaih (1989) and Juyal (2002), both of whom provide data from laboratory flumes. To date the literature seems to have lacked information concerning the influences on scour of dike angle and dike-spur geometry.

A further novel aspect of the present experiments is the measurement of maximum equilibrium height for the sediment deposited immediately downstream of the dike. Information on deposition height and extent is sometimes needed for assessing the influence that a dike may have on the channel bank downstream of the dike.

As the experiments were underway when this paper was prepared, the results presented are preliminary, and are subject to some conjecture. Further work is underway to confirm the trends revealed by the data obtained to date.

HYDRAULIC MODEL

The layout of the hydraulic model is given in Figure 1. Water flow through the model was circulated by means of a pump, which also re-circulated the sediment forming the model's bed. Similitude was based on a shear-velocity-excess criterion whereby the channel's sand bed was fully mobilized in a dune regime. The hydraulic model discharge was 0.057 cumecs at an average flow depth of 0.15m. Model flow rate was measured using a side-contraction orifice placed in the 0.25m diameter pipe. The median diameter of the prototype bed sediment is in the coarse-sand range, with a medium particle diameter of about 1.5 mm.

Experiments were conducted to determine the maximum scour depth (ds_e) produced by a dike subject to several modifications (Figure 2):

1. Dike porosity (0% to 79%)
2. Dike angled to the flow (15° to 150°; with dike pointing upstream when angle exceeds 90°)
3. Dike hook directed downstream or upstream (hook length = 0 to 3L)

Here, L is the length that a dike protrudes perpendicularly into the flow.

Except for the first set of experiments in which dike porosity was varied, the subsequent experiments were conducted with solid dikes (porosity = 0). The model did not include simulation of the intake flow. The variables measured were the equilibrium depth of bed scour, ds_e, and the maximum height of sediment deposition, d_D, immediately downstream of the dike. These variables were measured relative to average bed level.

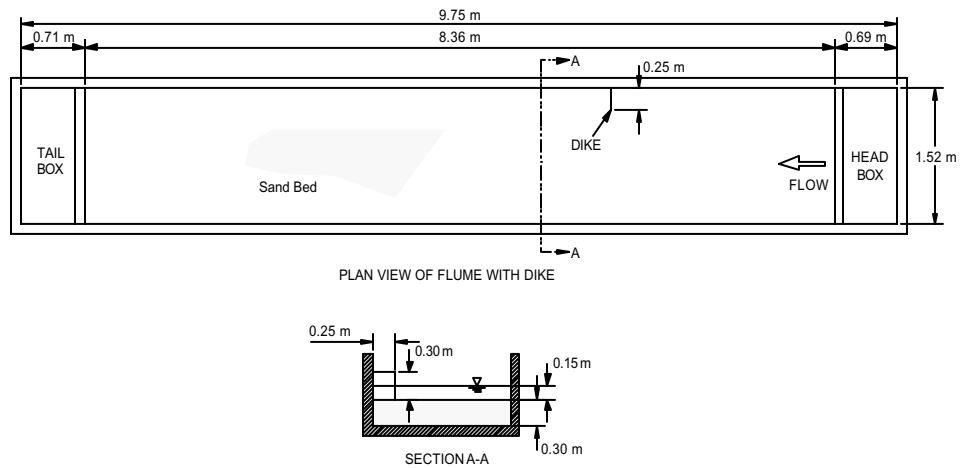

Figure 1. Layout of flume and model dike.

The model dike projected a length into the flow, for all dike angles, equal to 0.254m. Each test was run for a 24-hour period, which proved sufficient to attain equilibrium conditions of sediment accumulation and scour. The same water discharge (0.057 m^3/s) was used for all tests. The geometric features of dike investigated are illustrated in Figure 2.

RESULTS

Figures 3a-e provides views of the scour holes observed during the experiments. The scour data presented in this paper are for the deepest scour, which invariably occurred at the end of each dike.

The data resulting from the experiments provide trends indicating how scour depth decreases with increasing dike porosity and with diminishing dike angle to the flow. The experiments also show that dike width did not exert a significant influence on scour depth. Additionally, they show that an upstream spur does not significantly reduce scour depth. Figures 4 and 5 show the trends for scour depth versus dike angle and porosity. The data for ds_e and d_D are presented below in normalized format, whereby the values of ds_e and d_D resulting with the modified dike are normalized using their values as obtained for the baseline case for which the non-porous dike was at 90° to the bank (ds_{e-o} *or* d_{D-0}).

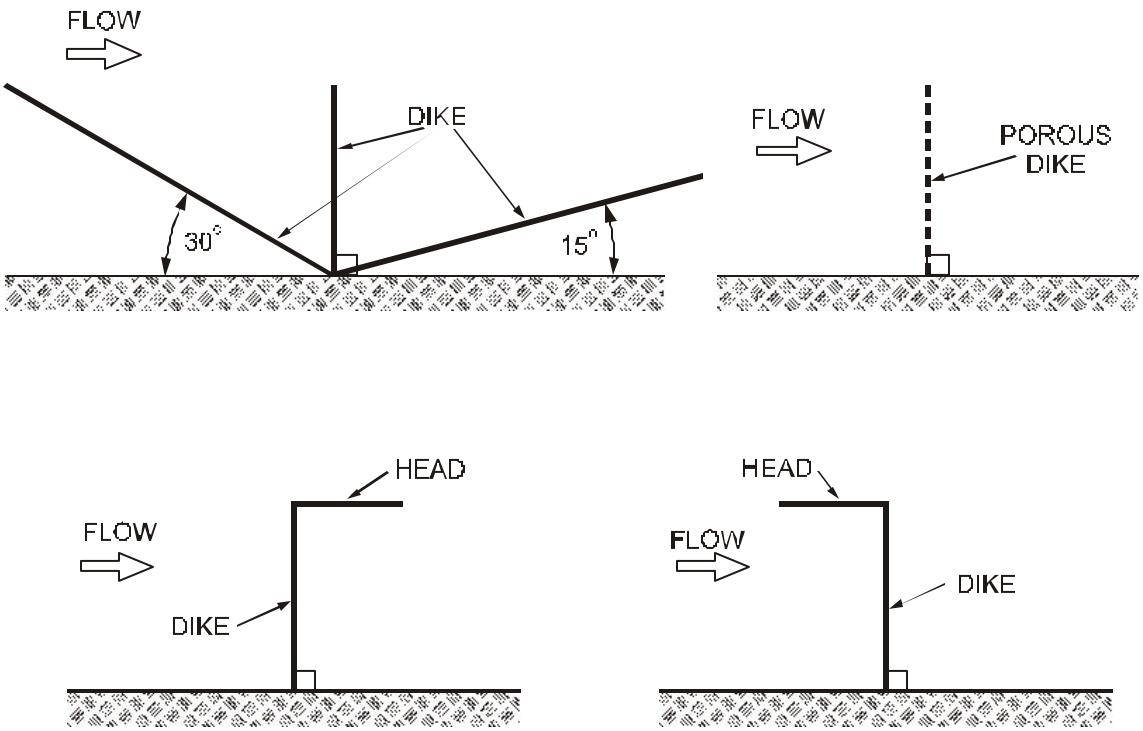

Figure 2. Variations of dike layout investigated. Dike orientation was varied from 15° to 150°; dike porosity was varied from 0 to 79%; the dike hook was varied in length and direction.

Dike Angle

Figure 4 shows how depth of local scour varied as dike angle changed from +15° to 90° (dike normal to the flow), and from 90° to 150°. As the dike swung from pointing upstream to pointing downstream, ds_e increased, attaining a maximum at 90°, then decreased. It is interesting to note that the variation of ds_e with angle is appears to be almost symmetrical for the dike oriented upstream or downstream. As mentioned above, for all angles, the deepest scour occurred at the end of the dike. The trend shown in Figure 4, however, differs from that indicated by Melville and Coleman (2000). They provide an upper-bound curve enveloping data from several studies. Their upper bound curve shows ds_e to increase with angle beyond 90°, and to decrease less steeply as angle diminishes below 90°. However, data obtained by T.F Kwan (1984) showed a trend similar of scour variations to figure 4. As of the time this paper was written, the writers are planning further diagnostic experiments to determine why their data show different trends to the data from prior studies. Factors being considered are that the present study was conducted with a very thin dike placed in a mobile bed.

(a) Wall 90^0 with 0% porosity

(b) Wall 90^0.L_{headt}/L=1,downstream

(c) Wall 30^0 with 0% porosity

(d) Wall 30^0 with 79% porosity

(e) Wall 30^0 with 50% porosity

Figure 3. View of the experiments

Observations from the present experiment indicate that the downflow and horseshoe vortex decreased in strength as the thin dike pointed upstream, as they did when the dike pointed downstream. Additionally, the presence of dunes affected local orientation of flow toward the dike.

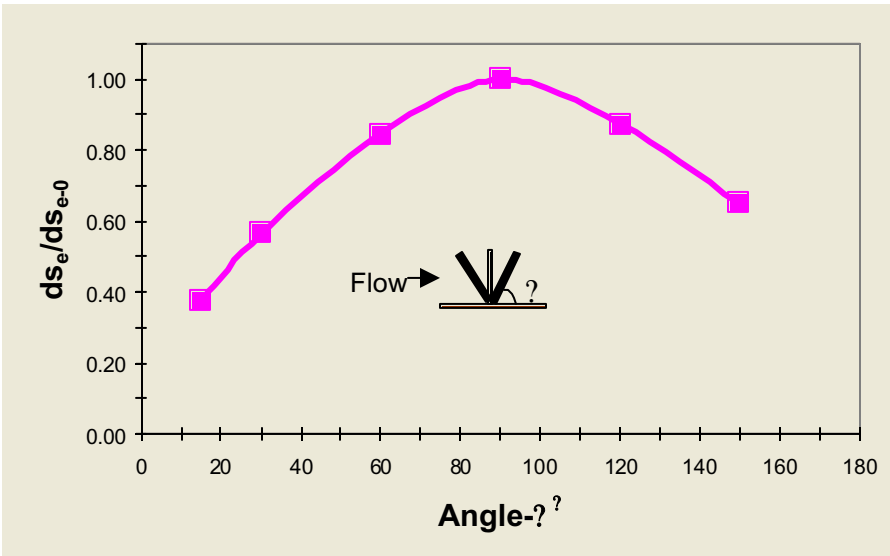

Figure 4. Variation of ds_e/ds_{e-0} with dike angle.

Porosity

Dike porosity significantly affects scour depth. Figure 5 shows the ratio *(ds_e/ds_{e0})* versus dike porosity. The figure shows that the scour depth decreases with the porosity; a porosity in excess of about 44% reduced scour depth by more than 50%. A practical difficulty, however, is that the dike porosity may diminish owing to blockage by debris and possibly ice. This consideration is being considered further.

The combination of dike angle and dike porosity substantially reduces sediment accumulation behind a dike, as well as reducing scour depth. Figure 6 shows the variation of sediment accumulation height when a thin porous dike is set at 90° and 30°. In the case of 90^0 dike setting, ds_e is 20% larger than 30^0 case, and porosities are effective up to the 75% porosity dike. Above this porosity it is tedious to make a difference between the natural riverbed oscillations and the induced scouring and accumulation due to the dike implementation. The average height of the bedforms is presented in both plots by a horizontal straight line. In the case of accumulation, the 90^0 dike appears to be ineffective beyond 50% porosity.

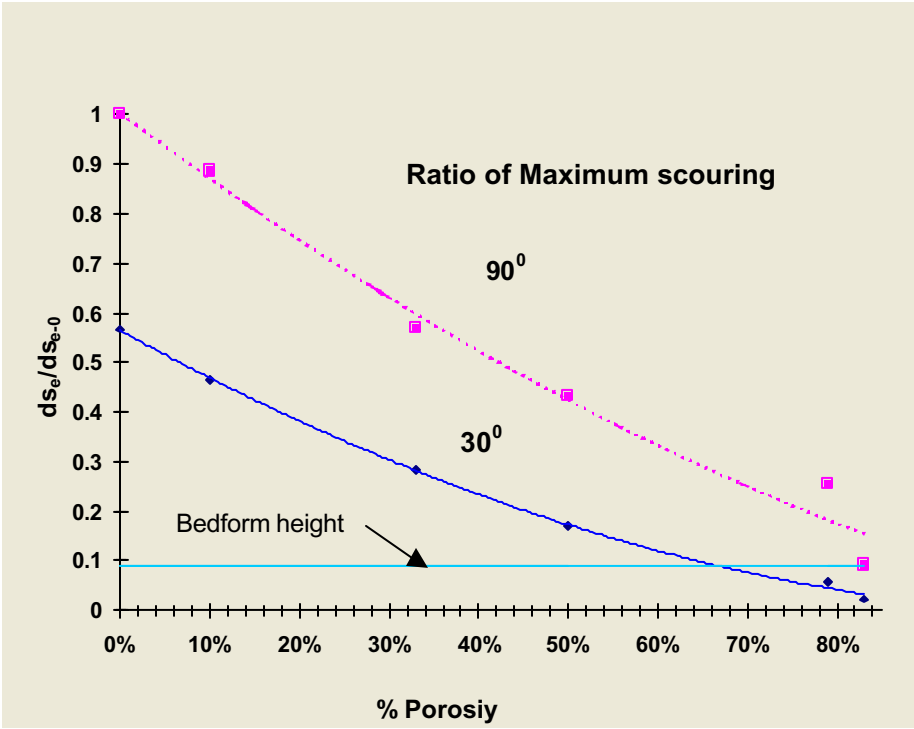

Figure 5. Variation of ds_e/ds_{e-0} with dike porosity; de_{s-0} was 0.22m.

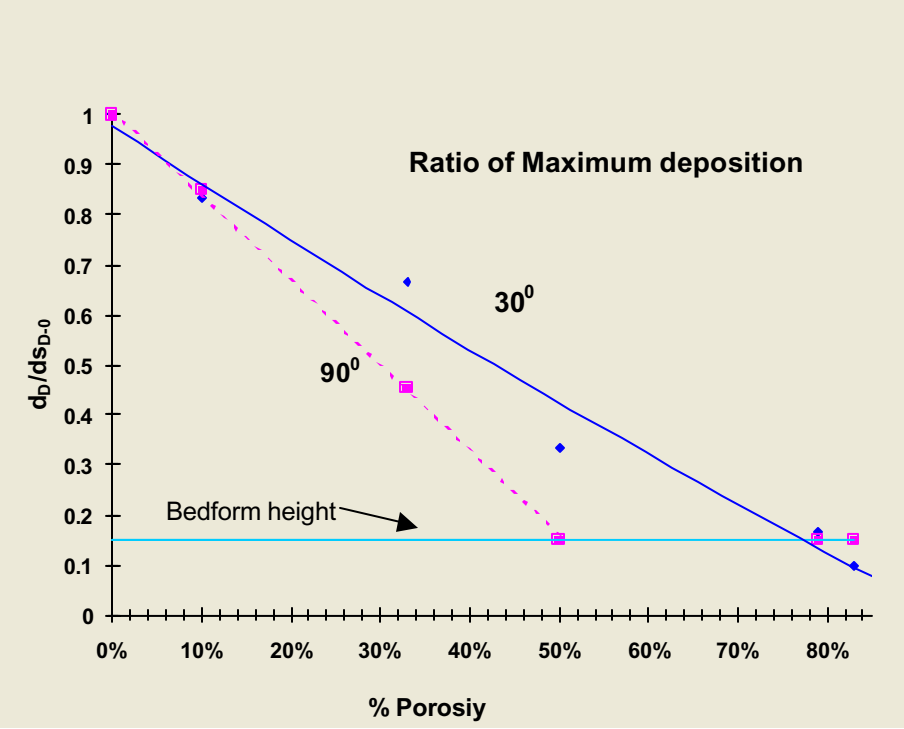

Figure 6. Variation of d_D/ds_{D-0} with dike porosity.

Dike Hook

The downstream-directed dike in effect acted to increase dike width. The experiments show that dike thickness (for a dike at 90°) had a minor influence on scour depth. Figure 7 shows that a hook pointing downstream slightly increased scour depth ($ds_{e/}ds_{e-0}$ = 1.1).

Widening the dike appeared to strengthen the horseshoe vortex around the dike's upstream face and side. Also, it seemed to strengthen the down flow into the scour hole at the end of the dike. It also moved the wake vortex downstream from the face of the dike. The net effect on scour was a mild (10%) increase in scour depth, as shown in Figure 7.

A hook pointing upstream of the dike decreased scour slightly, as shown in Figure 7. An upstream pointing hook appeared to weaken the horseshoe vortex and the down flow into the scour hole. Additionally, turbulence generated by the

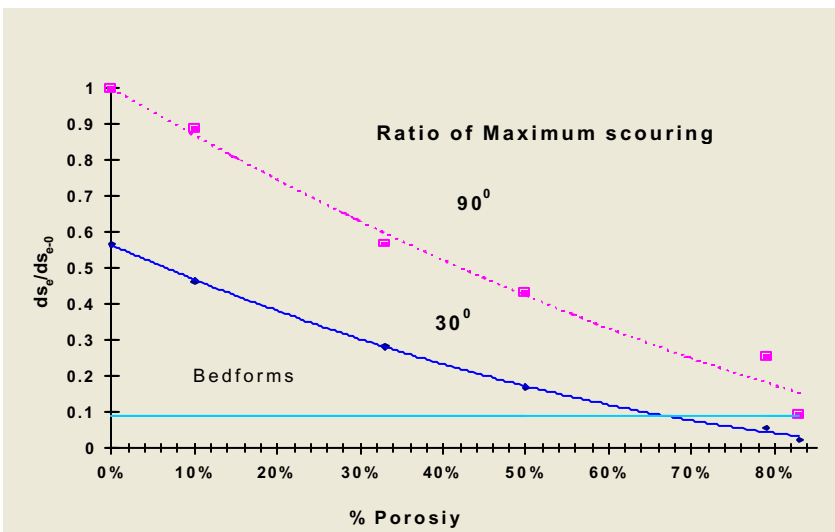

Figure 7. Variation of ds_e/ds_{e-0} vs. Dike Thickness and Upstream Hook

wake vortex was shifted downstream away from the front of the scour hole. The net effect was a mild (10%) decrease in scour depth.

CONCLUSIONS

The data in hand enable some preliminary conclusions to be drawn. Further experiments are underway to confirm and explain some of the results obtained.

Dike angle and porosity significantly influence scour depth. Widening the dike, or the addition of an upstream-pointing hook, did little to reduce scour depth. The relative insensitivity of scour depth to dike width and hook presence is attributable to the consideration that the flow still was forced to pass around the

dike, which extended a constant distance into the flow. Once a scour hole formed, the major factor influencing scour development appears to be the overall distance that the dike extends into the channel.

The mild decrease in scour depth observed for the upstream-pointing hook agrees qualitatively with the decrease in scour depth observed when the dike was angled upstream. In both cases, the flow, though still contracting around the dike, essentially impinged against a narrower body (dike).

The experiments showed that porosities of about 50% reduced scour and sediment accumulation downstream of a dike. Moreover, porosity higher than 75% does not modify channel bathymetry.

REFERENCES

1. Juyal, G.P.(2002). "Scour Around Permeable Spurs." PhD Thesis, University of Roorkee, Roorkee, India.

2. Melville, B.W. and Coleman, S., (2000). Bridge Scour. Water Resources Publications Ltd. Littelton, CO.

3. Subramanya, K. and Gangadharaih, T., (1989). "Flow Around Slotted Spurs," Third International Workshop on Alluvial River Problems, University of Roorkee, Roorkee, India, 1989.

4. T.F. Kwan,. Report No. 328: Study of Abutment Scour. University of Auckland. School of Engineering. Department of Civil Engineering. January 1984. Auckland, New Zealand.

Shallow Water Effect on Pier Scour in Clays

Ya Li[1], J.-L. Briaud[2], H.C. Chen[2], Prahoro Nurtjahyo[1], Jun Wang[1]

ABSTRACT

Shallow water effect is a common phenomenon in pier scour evaluation. While extensive studies have been carried out on the shallow water effect in sands, studies in clays are practically inexistent. Systematic flume tests were conducted on porcelain clay to explore the shallow water effect. Test results indicate that pier scour in clays has a very similar discount factor for shallow water scour depth to that in sands. The results also show that a faster scour rate can be caused by shallow flow. Therefore in clays, the shallow water effect leads to a shallower scour depth which occurs faster than in deep water.

INTRODUCTION

Shallow water effect on pier scour is also called wide pier effect. It happens when the flowing water depth, H, is relatively small compared to the pier size, B. Observations show that the scour depth increases with the depth of flow until the deep-water case is reached, where the scour depth is almost independent of water depth. However no fixed value exists to define the shallow water range. Bonasoundas (1973) concluded that the effects of flow depth became insignificant when H/B > 1 to 3 for clear-water scour, where H is the water depth and B is the pier diameter. Ettema (1980) stated that the shallow water effect was affected by the relative size of the pier and sediment and that H/B<3 was a good range to define shallow water in coarse sands. Ettema also stated that, as summarized by Johnson (1999), three reasons accounted for the shallow water affect: (1) the portion of the approach flow available to be diverted into the scour hole diminishes, (2) the development of the scour hole is influenced by the formation of a sediment bar behind the pier, (3) the formation of a surface roller in opposite direction to the rotation of the horseshoe vortex and the down flow into the scour hole.

Consideration of the shallow water effect is important because it has an economic impact on the final depth of the foundation. In Lander and Mueller's (1992) bridge pier scour database, if only the 234 cases of single pier with 0° attack angle are counted, there are 57.7% piers with H/B<3, 15.4% the piers with H/B<1, and 8.1% for H/B<0.5. It should be also noted that even though some pier scour prediction equations have a water depth term embedded in the formula such as HEC-18 (Richardson and Davis, 2001), the shallow water effect may not be fully represented because the original equation may have been based on flume tests performed in relatively deep water cases. Furthermore, previous research on shallow water effect has been concentrated on sand beds and there is

[1] Graduate student, Dept. of Civil Engineering, Texas A&M Univ., College Station, TX, USA 77843-3136

[2] Professor, Dept. of Civil Engineering, Texas A&M Univ., College Station, TX, USA77843-3136

no corresponding study on clay beds. Due to the difference between clay and sand, it was the primary goal of this research to investigate the shallow water effect in clay.

CORRECTION FACTOR FOR SHALLOW WATER EFFECT IN SANDS

Research on shallow water effects in sand can provide a background to clay scouring. Among the well-known studies on shallow water effect in sands are the studies by Melville (1999) and Johnson (1999). Both of them considered shallow water effects in the form of a correction factor Kw. It was calculated as the ratio of the shallow-water maximum scour depth to the deep-water maximum scour depth, which is defined as the reference case in this study. Johnson (1999) defined shallow water as H/B<0.8 and low velocity as Fr<0.8 where Fr is the Froude number. She isolated the data that met these conditions in the original data set from CSU used in the HEC-18 equation and added data from other sources to derive a new equation for wide pier using the same parameters. The new equation accounting for shallow water effect in the HEC-18 equation is:

$$Kw = 1.04\left(\frac{H}{B}\right)^{0.15} Fr^{0.21} \qquad \textbf{(1)}$$

Water depth was already included in the HEC-18 equation which can be written:

$$Z_{\max} = 2.0K_1 K_2 K_3 K_4 H^{0.135} B^{0.65}\left(\frac{V}{\sqrt{g}}\right)^{0.43} \qquad \textbf{(2)}$$

So, the total term for water depth effect in Johnson's equation should be a combination of (1) and (2) as:

$$K_w = 1.04\left(\frac{H}{B}\right)^{0.15} Fr^{0.21} H^{0.135} \qquad \textbf{(1. A)}$$

Melville(1999) defined the water depth effect on scour depth by using data published by Chabert and Engeldinger(1956), Lausen and Toch(1956), Hancu(1971), Bonasoundas(1973), Basak(1975), Jain and Fisher(1979), Chee(1982), Chiew (1984), and Ettema(1980). He proposed that piers be classified according to H/B: narrow pier (deep-water), intermediate pier (intermediate-water), and wide pier (shallow-water). The maximum scour depth for narrow piers is controlled by pier width, for wide piers by water depth and for intermediate piers by both water depth and pier width. The corresponding correction factor is:

$$Kw = \begin{cases} 0.53(B/H) & B/H < 0.7 \\ 0.44\sqrt{B/H} & 0.7 < B/H < 5 \\ 1 & B/H > 5 \end{cases} \qquad \textbf{(3)}$$

FLUME TESTS

Systematic flume tests were conducted at Texas A&M University to investigate the shallow water effect on clay soils. The flume is a 1.5 m wide concrete tank and the water is circulated in a close system by pumps. Two different sizes of PVC piers were used: B=273mm and B=160mm. They were installed in a 1.2m×1.5m soil tank filled with porcelain clay. The soil properties of the porcelain clay are listed in Table 1. During each test, velocity and water depth were kept constant. The velocity was measured as the

depth-average velocity with an ADV placed upstream of the pier where the pier had no influence on the velocity distribution. The instant scour depth z(t) (maximum depth of the scour hole at a given time) was recorded as a function of time t with a precise point gage without interrupting the flow. The primary parameters for each test are listed in Table 2.

Table 1: Soil Properties of Porcelain Clay

NO.	Property	Porcelain
1	Liquid Limit, %	40.23
2	Plastic Limit, %	19.17
3	Plastic Index (PI), %	21.06
4	Bulk Unit Weight (KN/m^3)	19.65
5	Water Content, %	27.35
6	Sand Content, %	0.0
7	Clay Content, %	100.0
8	Shear Strength, KPa	10.7

Table 2: Parameters and Major Results of Flume Tests (*bold one is the reference case in each group*)

Test No.	H (mm)	B (mm)	V (m/s)	H/B	Time Lasting (hr)	$\dot{z}_i$ (mm/hr)	Zmax (mm)
Sh-1	**683.00**	**273.00**	**0.30**	**2.502**	**-----**	**----**	**112.94**
Sh-2	546.00	273.00	0.30	2.000	515.75	1.06	129.62
Sh-3	258.00	273.00	0.30	0.945	262.33	1.57	79.37
Sh-4	137.00	273.00	0.30	0.502	237.42	1.39	57.80
Sh-5	60.00	273.00	0.30	0.220	164.08	1.71	81.30
Sh-6	60.00	273.00	0.30	0.220	111.03	4.49	61.35
Sh-7	25.80	273.00	0.30	0.095	30.50	38.91	35.59
Sh-8	**400.00**	**160.00**	**0.40**	**2.500**	**191.33**	**1.50**	**76.92**
Sh-9	320.00	160.00	0.40	2.000	129.67	1.82	109.67
Sh-10	170.00	160.00	0.40	1.063	117.17	1.98	77.73
Sh-11	85.00	160.00	0.40	0.531	64.50	2.62	53.48

MAXIMUM SCOUR DEPTH AND INITIAL SHEAR STRESS CALCULATION

Clay scouring is really a time dependant process due to its extremely low erosion rate. Generally it takes several months to reach the equilibrium scour depth, Zmax, which is too time-consuming for a flume test. So in the current research, all the flume tests were terminated after a limited time, as shown in Fig 2, and a hyperbolic model (Briaud, 1999, 2001) was used to fit the data. The hyperbola model is:

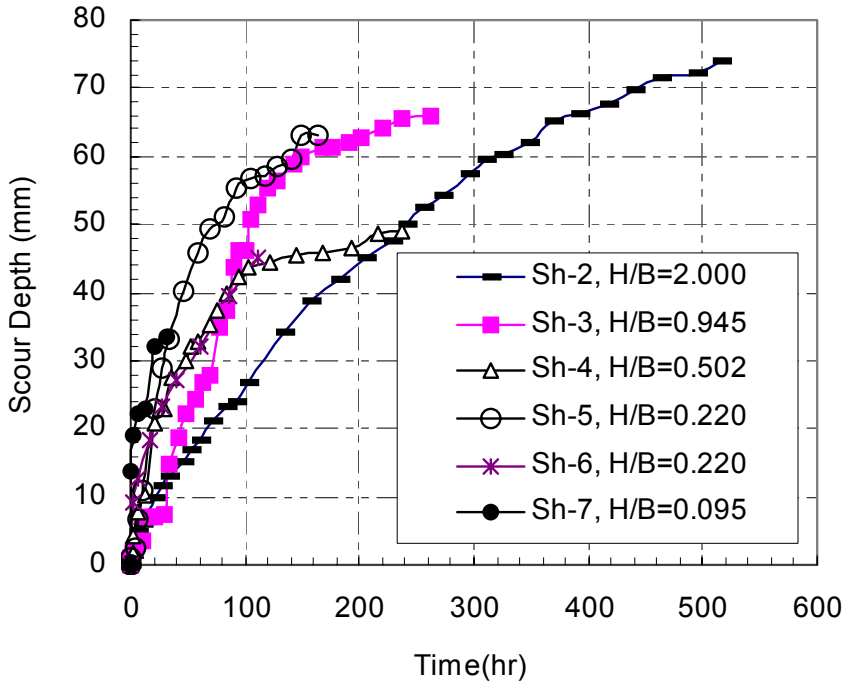

(Pier: B=0.273m and V=0.3m/s)

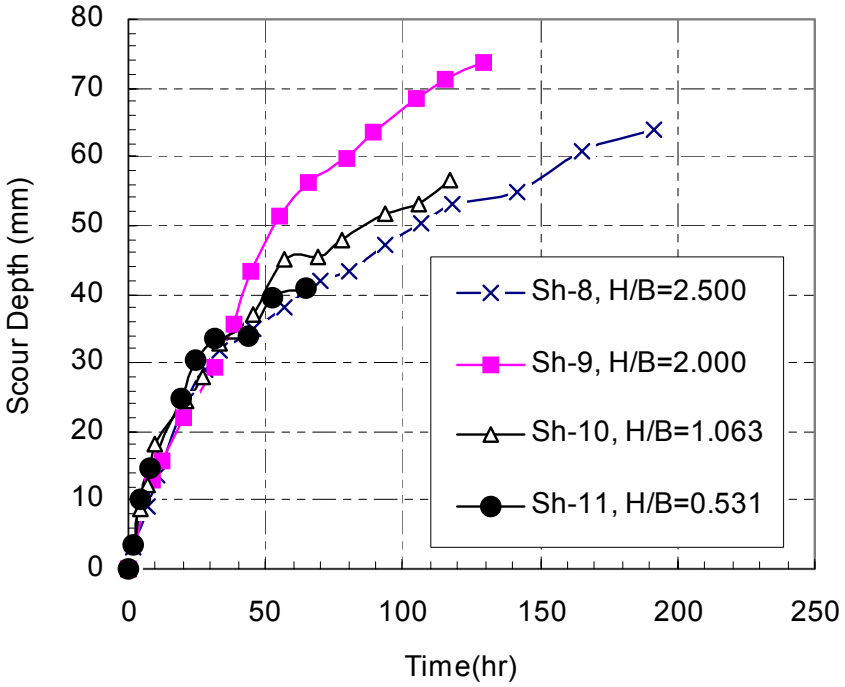

(Pier: B=0.160m and V=0.4m/s)

FIG 1 Scour Development in Shallow Water Case

$$z(t) = \frac{t}{at + b} \tag{4}$$

Where a is the inverse of the initial scour rate, $\dot{z}_i$, and b is the inverse of the maximum scour depth, Z_{max}. The hyperbola model can be written as:

$$\frac{t}{z(t)} = at + b \tag{5}$$

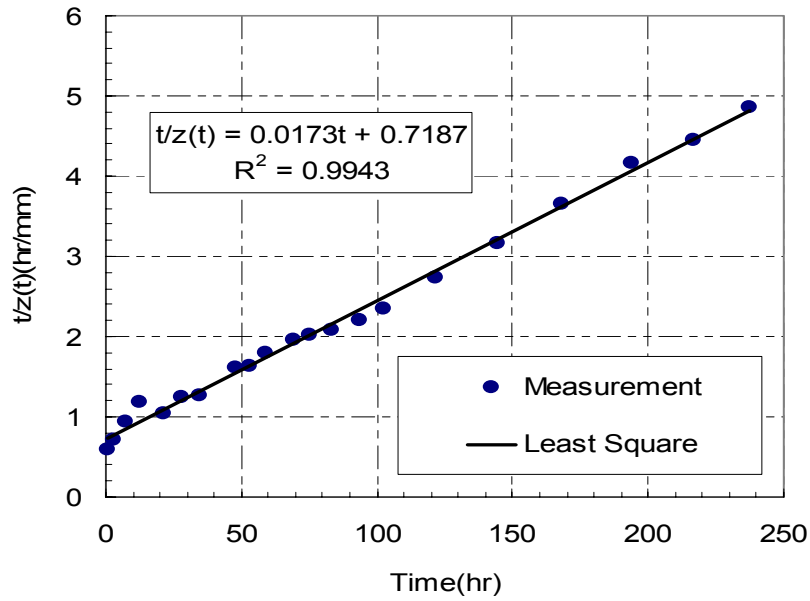

Fig 3 Least Square Method to determine a and b for Test Sh-4

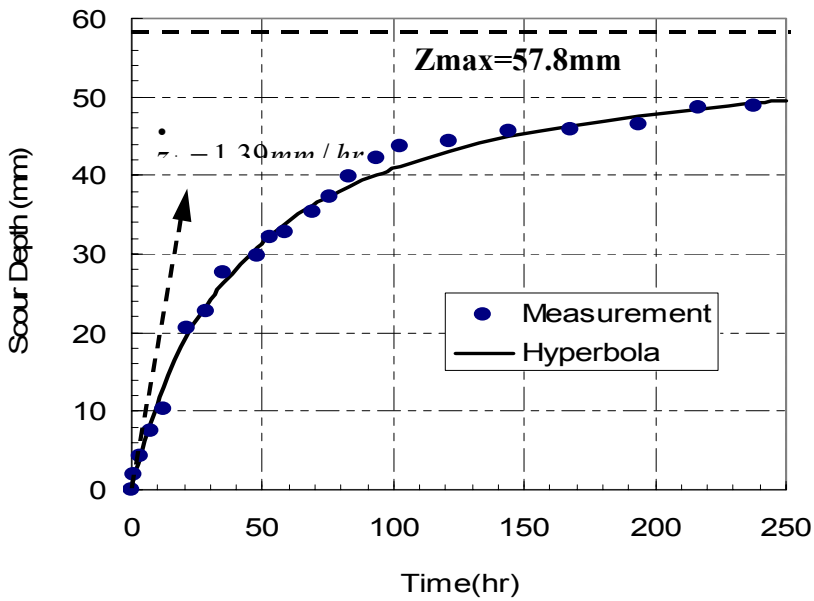

Fig 4 Comparison between Hyperbola Model and Measurement for Test Sh-4

Both a and b can be determined by a least square regression on the data z(t) and t. Test Sh-4 is used as an example to explain the above approach in Fig 4 and the scour depth vs. time curves obtained from the hyperbolic model and the measurement are compared in Fig 5.

Note that the hyperbolic approach gives not only the maximum scour depth Zmax but also the initial scour rate $\dot{z}_i$. For a given flume test, if one single hyperbola could not simulate the initial section and the final section of the scour curve with satisfactory precision at the same time, two separate hyperbolas were used: $\dot{z}_i$ was obtained by a hyperbola simulating the initial part while Zmax by simulating the final part of the measurements. The calculated results of Zmax and $\dot{z}_i$ are summarized in Table 2.

SHALLOW WATER EFFECT ON PIER SCOUR DEPTH

To compare the shallow water effect between these flume tests and other research results in sands, two approaches were taken based on different normalization methods.

Zmax/B vs. H/B

When both scour depth and water depth were normalized with respect to pier size, the relative scour depth, Zmax/B, increases with increasing relative water depth, H/B, in the shallow water range. Even though the tendency of the curve in Fig 5 is consistent with the result in sands, there is some variation in the magnitude of the Zmax/B for a given value of H/B. This is possibly because the shallow water effect depends on the soil properties and on the water velocity. For example, Zmax/B can be 0.7 to 2 when the soil bed changes from medium sand to coarse sand under the corresponding critical velocity (Melville and Colleman, 1999). It indicates that this kind of normalization is not a good way to get a unique solution for shallow water effect.

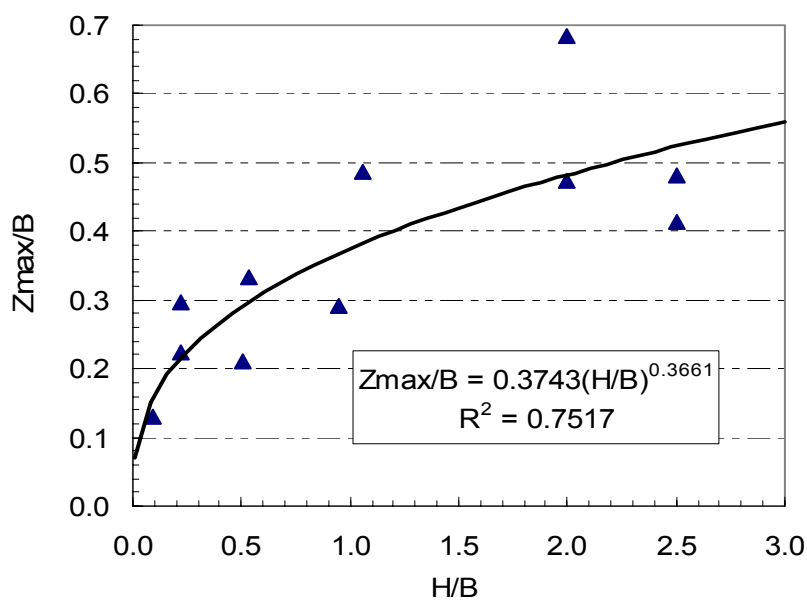

Fig 5 Influence of Flow Shallowness on Pier Scour Depth

Correction Factor Kw vs. H/B

The correction factor, Kw, is calculated as the ratio of the shallow water scour depth to the scour depth for a reference case where the water depth has no longer any noticeable influence on the scour depth. In this research, the maximum scour depth under the deepest relative water depth, H/B=2.5, was used as the reference case. Test Sh-1 was used as the reference for the tests where B=0.273m and V=0.3m/s, and test Sh-9 was used as the reference for the tests where B=0.160m and V=0.4 m/s. In Fig 6, the Kw values obtained in this study are compared with Melville and Johnson's results. Johnson's correction factor depends on both pier size and velocity. So "Johnson 0.273/0.3, Equ (1)" represents the correction factor for the condition of B=0.273m and V=0.3m/s according to Equation (1), and ditto for "Johnson 0.160/0.4, Equ (1)". Because Johnson did not provide the equation for very shallow water, a straight line connects the origin to the first point on Johnson's curve. As mentioned previously, the combined effect of Johnson's Kw and the water depth effect included in the HEC-18 equation is represented by Equation (1.A). The Kw for Equation (1.A) is plotted in Figure 6 under the label "0.273/0.3, Equ (1.A)" and "0.160/0.4, Equ (1.A)" with H/B =2.5 as the reference cases for B=0.273m, V=0.3m/s and B=0.160V=0.4m/s respectively.

The water effect factor for the cohesive soil of this study is very close to the one for sand (Fig. 6). The correction factor for clay is somewhat smaller than Melville's result at very shallow water depth when H/B<1.12 and reaches 1.0 for H/B=1.62. For H/B> 1.62, the flow in clay is treated as a deep water flow and the correction factor is truncated at 1.0. By regression, the expression of the current correction factor is:

$$Kw = \begin{cases} 0.85\left(\dfrac{H}{B}\right)^{0.34} & H/B < 1.62 \\ 1 & H/B > 1.62 \end{cases} \tag{6}$$

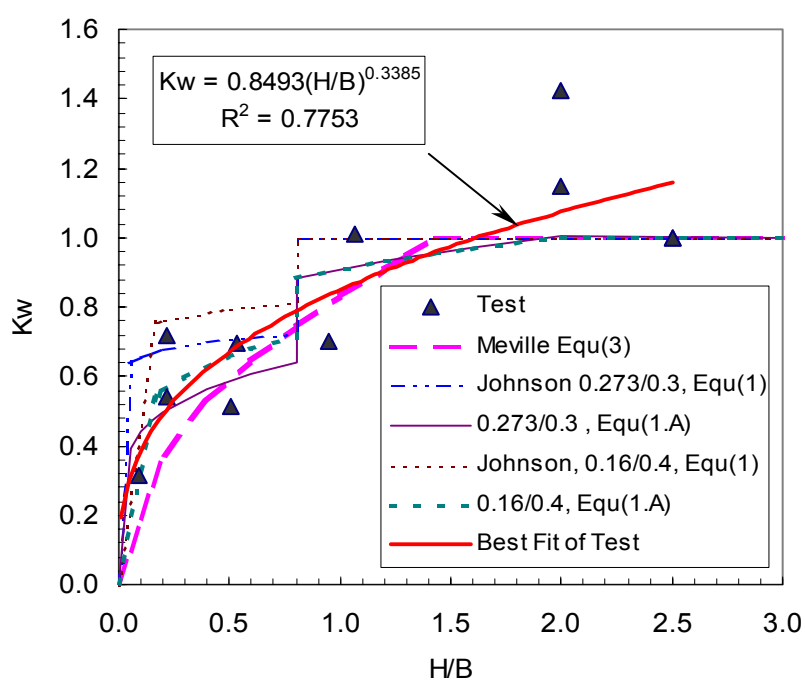

Fig 6 Correction Factor for Shallow Water Effect on Pier Scour Depth

SHALLOW WATER EFFECT ON INITIAL SHEAR STRESS

Scouring in clays is a time-dependant process compared to scouring in sands, so the scour rate becomes a critical issue. For a given scour flume test, the initial scour rate

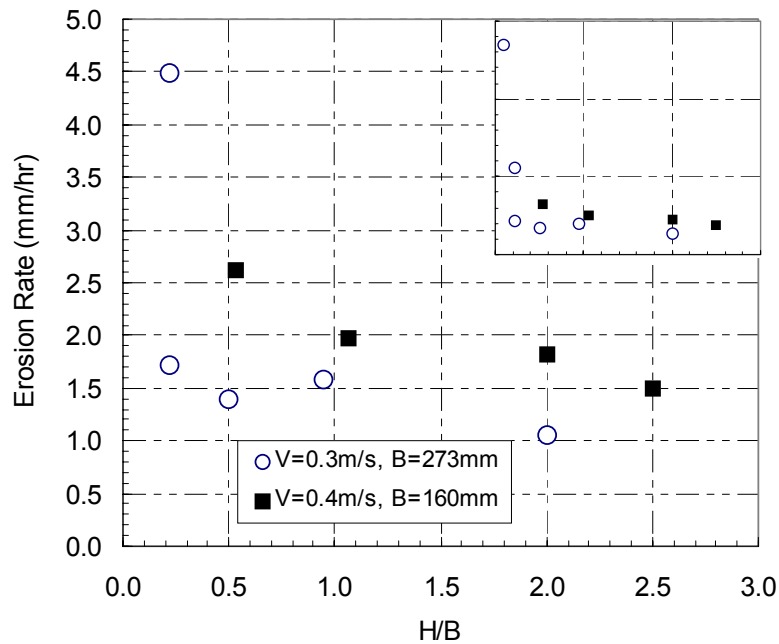

Fig7 Initial Scour Rate for Shallow Water Effect on Pier Scour

is one of the two parameters obtained from the hyperbolic model. The two groups of initial scour rates are plotted in Fig 7. Because Test Sh-8 has a much higher initial scour rate, the data including Test Sh-8 are plotted in the small upright figure. Fig.7 indicates that the initial scour rate decreases as the water depth increases within the shallow water range. There is a more pronounced increase in the initial scour rate when H/B< 0.5. The scour rates for the pier with B=0.273m are smaller than the ones for the pier with B=0.160m because the larger pier induces a smaller shear stress.

SCOUR MODEL FOR SHALLOW WATER EFFECT

Based on the above experiments and data analysis of shallow water effect on the maximum scour depth and initial scour rate in clay, a summarized scour model is developed in Fig 8. For a pier under shallow water flow such as C, the scour depth develops more rapidly than in the deep-water case and results in a deeper scour depth at the beginning. But the scour rate decays quickly and converges to the maximum scour depth, which is smaller than deep water one. This trend increases with the shallowness of the flow as A→B→C in Fig 8.

This model demonstrates that it is important for cohesive soils to include time effects in scour depth calculations.

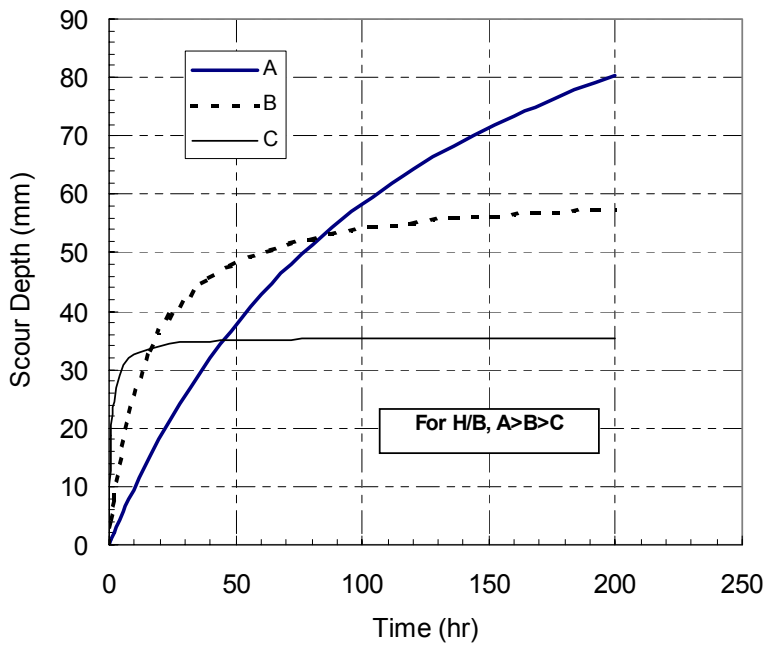

Fig 8 Scour Model for Shallow Water Case

SUMMARY

A correction factor for scour depth was developed for clay scouring under shallow water conditions. The value is close to the correction factors given by Melville and Johnson in sands. The water depth limit for the shallow water effect in clay is around 1.6 times the pier size.

The initial scour rate decreases with increasing water depth within the shallow water range. A summary scour model shows that the scour depth in shallow water may be larger at first but smaller in the long term than the deep water case.

ACKNOWLEDGEMENTS

This work was part of a project sponsored by the National Cooperative Highway Research Program (NCHRP 24-15). Tim Hess was the technical contact at NCHRP and Stephen Smith was the chairman of the NCHRP panel.

SYMBOL INDEX

a	Parameter in hyperbola model, inverse of maximum scour depth Zmax (1/mm)
b	Parameter in hyperbola model, inverse of initial scour rate $\dot{z}_i$ (hr/mm)
B	Pier diameter, m
Fr	Froude number $=V/\sqrt{gH}$
g	Gravity acceleration, 9.81m/s^2

Kw	Correction for scour depth under shallow water case
V	Upstream depth-average velocity (m/s)
$\dot{z}_i$	Initial scour rate (mm/hr)
Z_{max}	Maximum scour depth or equilibrium scour depth (mm)

REFERENCES:

1. Basak, V. (1975), " Scour at square piers," Devlet su isteri genel mudulugu, Report No. 583, Ankara.
2. Bonasoundas, M., (1973), " Non-stationary hydromorphological phenomena and modeling of scour processes," Proc. 16th Congress I.A.H.R., Sao Paulo, Brazil, Vol2, PP. 9-16.
3. Briaud, J.-L., Ting, F., Chen, H.C., Gudavalli, S.R., Perugu, S., and Wei, G., (1999), "SRICOS: Prediction of Scour Rate in Cohesive Soils at Bridge Piers", Journal of Geotechnical and Geoenvironmental Engineering, Vol.125, pp. 237-246, ASCE, Reston, Virginia, USA.
4. Briaud J.-L., Ting F., Chen H.C., Cao Y., Han S.-W., Kwak K., 2001a, "Erosion Function Apparatus for Scour Rate Predictions". Journal of Geotechnical and Geoenvironmental Engineering, Vol.127, No. 2, pp.105-113, ASCE, Reston, Virginia, USA.
5. Chee, R.K., (1982), "Live-bed scour at bridge piers," University of Auckland, School of Engineering, Report No. 290.
6. Chiew, Y.M., (1984), "Local scour at bridge piers," University of Auckland, School of Engineering, Report No. 355.
7. Ettema, R. (1980) " Scour at bridge piers," University of Auckland, Scholl of Engineering, Report No.355.
8. Hancu, S., (1971), "sur le Calcul des Affouillements Lcaux dans la Zane des Piles due Pont," Proceedings of the 14th Congress, IAHR, Vol. 3, P299-306.
9. Jain, S.C., and Fisher, E.E., (1979), "Scour around circular bridge piers at high Founde numbers," FHWA, Report No. FHWA-RD-79-104, Washington D.C.
10. Johnson, P. A. (1999), "Scour at wide piers relative to flow depth," Stream Stability and Scour Highway Bridges, Compendium of ASCE conference, PP. 280-287.
11. Lausen, E. M. and Toch, A. (1956) , "Scour around Bridge piers and Abutments," Bulletin No.4, Iowa Highways Research Board, Ames, Iowa, U.S.A
12. Landers, M.N. and Mueller, D.S., (1996), "Channel scour at bridges in the Unite States," Rep. No. FHWA-RD95-184 (HEC-18), U.S. Department of Transportation, Federal Highway Administration, Washington, D.C.
13. Melville, B.W and Coleman, S.E (1999), " Bridge Scour, " P173-186, Water Resources Publications, LLC
14. Richardson, E.V. and Davis, S.R. (2001), "Evaluating scour at bridges," Rep. No. FHWA-IP-90-017 (HEC-18), Federal Highway Administration, Washington, D.C.

Flume Experiments on Abutment Scour: Confronting Complexities in Process and Similitude

by

Robert Ettema
IIHR ~ Hydroscience and Engineering
The University of Iowa, Iowa City, USA

ABSTRACT
The paper addresses the extensive complexities confronting laboratory flume experiments on scour at bridge abutments. The complexities complicate the development of reliable scour-prediction relationships, and in a practical sense imply that such relationships can only be of approximate accuracy. The complexities stem from the nature of the approach flow–field, the soil and sediment conditions at typical abutments, and thereby from the mix of scour and slope-stability failure processes potentially at play in the vicinity of bridge abutments. The full set of failure processes has yet to be determined and documented, and inevitably entails extensive investigative experiments using laboratory flumes. However, flume experiments on abutment scour are fraught with their own significant complexities of process and similitude; some failure processes are difficult to replicate directly in flumes, and certain scale effects prevail. Arguably, the mix of complexities has muddled perceptions of scour extents observed at bridge sites. The paper attempts to somewhat clarify the muddle, and it floats for comment a plan of flume experiments aimed at addressing, and working around, the complexities.

INTRODUCTION
Few situations of flow and boundary erosion are potentially more complex than those associated with scour of alluvial channels at bridge crossings, especially in the vicinity of bridge abutments located in compound channels. The complexities arise from considerations of the flow field, the varied sediments and soils, as well as from the mix of failure modes that may occur at and near abutments. Additionally, some of the complexities inevitably are difficult to replicate in a laboratory flume, and pose issues of hydraulic-modeling scale and similitude. It is small wonder that these complexities raise a concern that, relative to approach-flow depth or abutment dimensions, values of local-scour depths observed in laboratory flume studies seem not to coincide values observed at actual abutments.

The present paper discusses the complexities in broad terms, addressing itself to the mix of scour processes that may occur at bridge abutments, and to the scale and similitude considerations attendant to hydraulic-modeling of scour. The complexities are under close consideration in a project the writer and colleagues currently are conducting at IIHR; the project is NCHRP 24-20 Prediction of Scour at Abutments. This project aims at producing reliable predictive relationships for scour estimation at bridge abutments. The relationships inevitably must be derived in large part from laboratory flume experiments. However, in planning and conducting such experiments, the writer and his

colleagues immediately are confronted with the nettlesome issues incurred with reducing complex abutment situations to simplified, relatively tractable, yet practically meaningful flume experiments.

The first complexity confronting flume experiments is replication of a complex flow field. A further complexity is replication of the variable nature of the sediments and soils found at most abutment sites. These complexities combine to create the possibility of a number of abutment-failure processes, of which several involve both geotechnical slope-stability and hydraulic erosion concerns.

The sequence of figures given as Figs 1 and 2 illustrate the complexities faced when attempting flume experiments aimed at producing reasonably general and acceptably reliable prediction relations for estimating scour at abutments. Factors characterizing abutment-site morphology and sediment (and soil) conditions influence the flow field in the vicinity of an abutment the abutment site; producing a range of flow conditions. In turn, the flow field influences the type and extent of abutment failure that may occur.

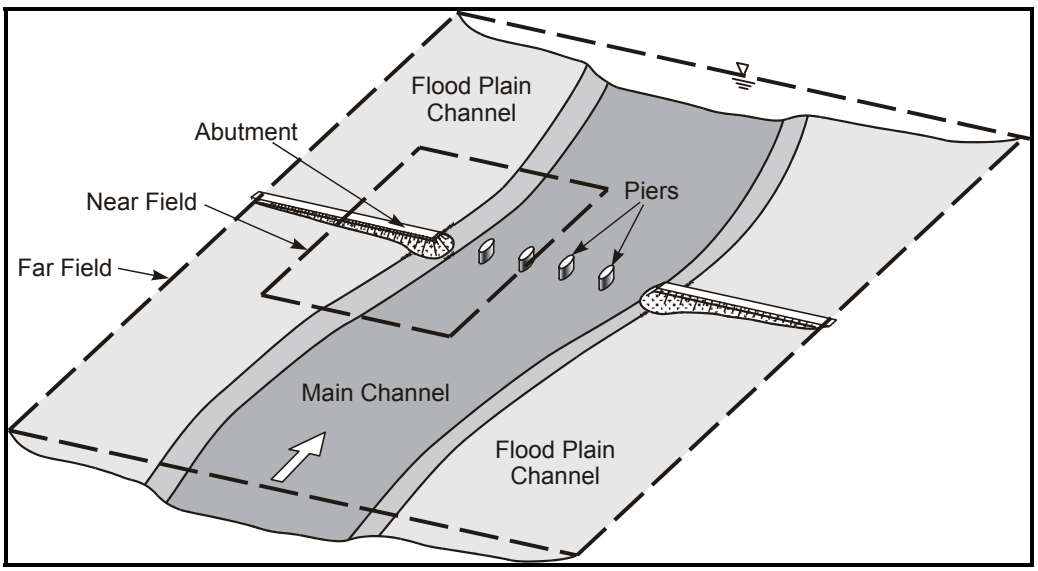

Fig. 1. Overview of far-field and near-field of flow in abutment vicinity.

FLOW FIELD

To varying extents, most channels, natural or built, are compound in shape and/or roughness. As depicted in Figs 1 and 2, they comprise a central deeper portion flanked by side portions (floodplains) formed to aid conveyance of larger flows. Though substantial information exists regarding the flow field around an abutment in rectangular channel without a floodplain, little is known about the flow field formed at a floodplain abutment that is in close proximity to the main channel, as sketched in Figs 1 and 2. It is clear, though, that the near field of flow at an abutment is significantly influenced by the far field of flow.

Additionally, it is important to observe that, besides the overall complexity of flow field in compound channels, turbulence (its generation, dispersion, and decay) at a variety of scales is a prominent feature of the flow field, not only in the immediate vicinity of the abutment, but also at in the approach flow to the bridge. This flow feature poses a similitude difficulty for hydraulic modeling.

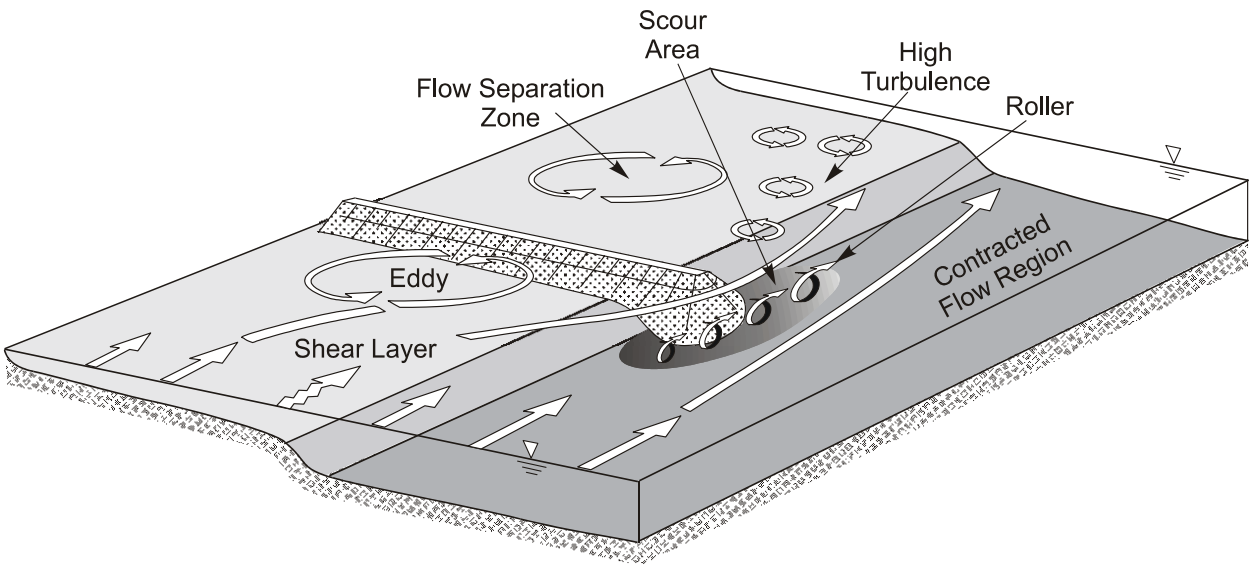

Fig. 2. Schematic of near-field flow around an abutment.

Fascinating composite flow interactions can occur between the floodplain and the main channel of a compound channels. The interactions involve exchange of flow between portions. They also involve the formation of large-scale turbulence and eddies in the shear layer developed in the flow region between the channel portions. By virtue of their protrusion into a compound-channel flow, abutments significantly increase local complexity of flow field, as sketched in Fig. 2, developed from flume experiments at IIHR. The flow field in the vicinity of an abutment is sensitive to circumstances of abutment geometry and setting in a compound channel. Additionally, the flow field evolves as the flow substantially scours the channel around the abutment. To date, there exists little information on the local flow field at an abutment for a situation such as shown schematically in Fig. 2.

The flow field at an abutment typically comprises an acceleration of flow from the upstream approach to the most contracted cross section somewhere at or just downstream of the head of the abutment, followed by a deceleration of flow. A flow-separation region forms immediately downstream of the abutment, and flow expands around the flow separation region until it fully re-establishes across the compound channel. Just upstream of the abutment, a flow-separation point and a small eddy may develop (Fig. 2). The size of the upstream eddy depends on the length and alignment of the abutment. The curvature of the flow along the interface between the stagnation region and the flow causes a secondary current that, together with the flow leads to a spiral motion or vortex

motion like flow through a channel bend. The vortex in flow around an abutment head is more localized and it has a strong scouring action. The vortex erodes a groove along its path and it also induces a complex system of secondary vortices. At abutments with wing walls (Fig. 3), the flow impinging on the wall may create a downflow (similar at a bridge pier), which excavates a locally deepened scour hole at the wall. The effect of downflow is potentially reduced for spill-through abutments.

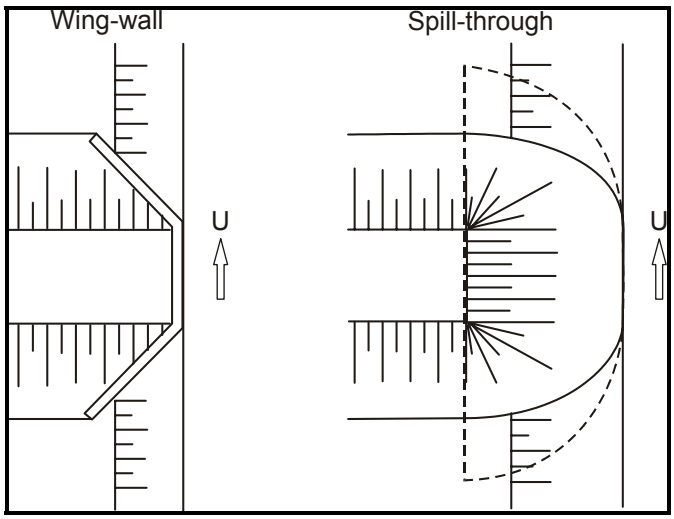

Fig. 3. Two common basic shapes of abutment; wing-wall; and, spill-through. This paper focuses on the latter shape.

SEDIMENT AND SOILS

Abutment sites may comprise sediment and soils quite varied in their constitution and erosion behavior. For compound channels, such as those sketched in Figs 1 through 3, the soils comprising the floodplain likely differ in erosive behavior from the sediment forming the bed of the main channel. Floodplain soils likely contain greater amounts of fine sediment (silts and clays), and likely are more cohesive in character than main-channel sediment. The same may be said for soils forming the embankment and the abutment. The banks flanking the main channel attest to the greater strength of floodplain soils.

Much of the complexity confronting flume experiments aimed at replicating abutment situations as in Figs 1 and 2 revolves around simulating erosion of cohesive (or somewhat cohesive) soils forming the floodplain, simulating the geotechnical slope stability of the main-channel bank and the embankment, as well as simulating scour of the non-cohesive sediment comprising the bed of the main channel.

SCOUR TYPE(S)

Consequent to the variably complex nature of abutment flow fields and sediments and soils, several types of scour may lead to abutment failure. Field observations show that all have occurred. Figs 4 through 8 illustrate several scour-related processes that may occur at spill-through abutments (possibly, a parallel set of figures could be prepared for

wing-wall abutments, though such abutments are more common for small rivers and streams). The scour types can be summarized as follow:

-- Type I, abutment in single channel (no floodplain)

- (I-a) Abutment threatened by local scour of main-channel bed (Fig. 4); and,
- (I-b). Abutment threatened by local scour and constriction scour of main-channel bed (not illustrated).

-- Type II, abutment on floodplain (to varying extents)

- (II-a) Abutment threatened directly by scour (local and constriction) of main channel (Fig. 5);
- (II-b) Abutment threatened by collapse of main-channel bank consequent to scour (local and constriction) of main-channel bed (Fig. 6);
- (II-c) Abutment threatened by scour of floodplain (Fig. 7); and,
- (III-d) Abutment threatened by embankment erosion (Fig 8).

The scour types may result from several flow conditions:

1. General scour of the main channel bed. It occurs in response to an overall propensity of the main-channel flow to degrade should an imbalance of sediment supply along the channel occur.
2. Change in main channel alignment and morphology, which adversely affects abutment location and orientation relative to flow in the main channel (e.g., a meander-loop migration may direct flow adversely towards an abutment);
3. Constriction scour of the main channel (and possibly a part of the floodplain channel) at the abutment site. Flow, constricted at the abutment site, locally scours the site, until a new balance is established between flow and bed. Constriction scour can be severe in situations where a long embankment to a bridge abutment intercepts flow over a floodplain; the intercepted flow is funneled through the abutment site;
4. Local scour attributable to the local flow field at an abutment; and,
5. Constriction scour of the floodplain at the abutment. Flow on the floodplain adversely impinges against the approach embankment.

A complication for flume studies and for developing reliable predictive relationships, is that these scour processes may occur at the same time, and therefore be difficult to estimate reliably (notably Types I-a and –b, and II-a and –b). Additional factors, such as variable vegetation cover and roughness of the floodplain, complicate the flow conditions.

For scour Types I-a and –b (Fig. 4), abutments are threatened by scour of the main-channel bed, and by direct entrainment of material from the abutment face. The deepening scour hole may pose a slope-stability problem for the abutment. Failure, to varying degrees, relates to extent of abutment-slope failure and washout. The scour may be attributed (depending on abutment length and channel width) to the combined effects of local and constriction scour processes. So far, most flume experiments have investigated this category. The simplest (relatively speaking) sub-category of this scour

type is that for a rectangular abutment, or a wing-wall abutment, sited in a uniformly deep alluvial channel. In that case, abutment failure occurs when scour undermines, or reduces support for, the abutment's foundation. Most flume experiments so far have investigated this condition (e.g., as summarized in Melville and Coleman 2000).

One or more of several possible scour types may occur for abutments on, or protruding from, floodplains. Type II-a (Fig. 5), illustrates essentially the same scour process as in category I-a, except that the presence of a floodplain may alter the flow field at the abutment.

Scour Type II-b (Fig. 6) has received little attention, but may be common for bridges. Here, the abutment is threatened by a geotechnical failure of the main-channel bank. The failure is triggered by scour of the main channel bed at the bank. The scour could be caused by a combination of local as well as constriction scour processes, and by main-channel shifting.

Type II-c (Fig. 7) is scour of the floodplain immediately at the abutment. And, Type II-d (Fig. 8) is erosion of the embankment approach to the abutment.

The gallery of scour processes illustrated in Figs 4 through 7 poses considerable modeling complexities for laboratory flume investigation of abutment scour. Note that these figures depict abutment circumstances uncluttered by the additional ad-hoc complications attributable to variable vegetation, or presence of an adjacent pier or an entire other bridge, or other features (e.g., debris) influencing the abutment flow field.

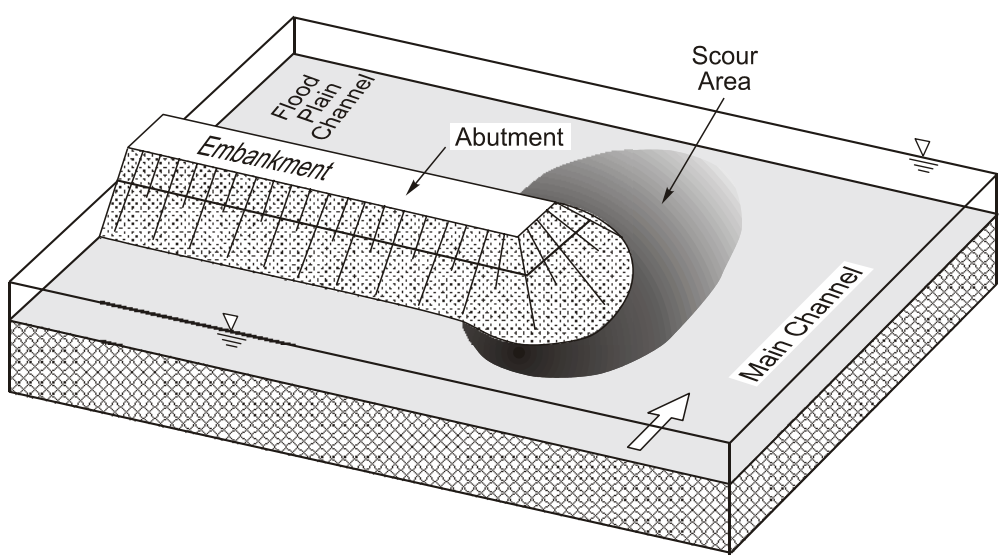

Fig. 4. Scour Type I-a, abutment threatened by scour of main-channel bed. Note, scour Type I-b includes additional effect of constriction scour.

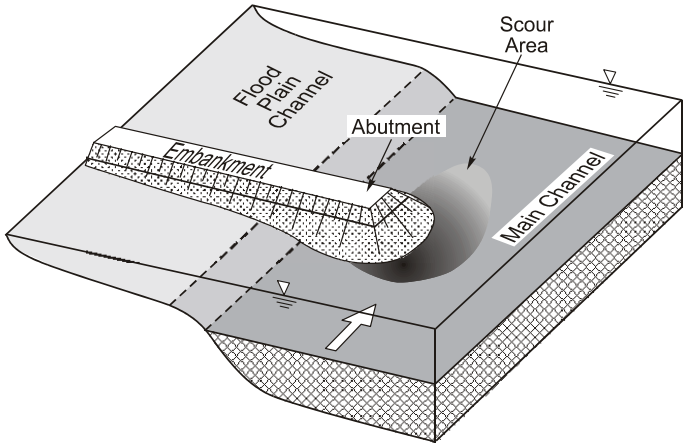

Fig. 5. Scour Type II-a, abutment threatened by scour of main-channel bed.

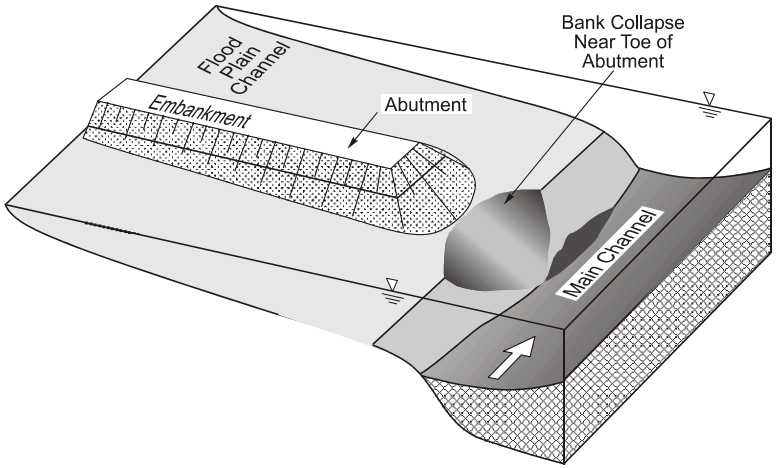

Fig. 6. Scour Type II-b, abutment threatened by collapse of main-channel bank consequent to scour (local and constriction) of main-channel bed

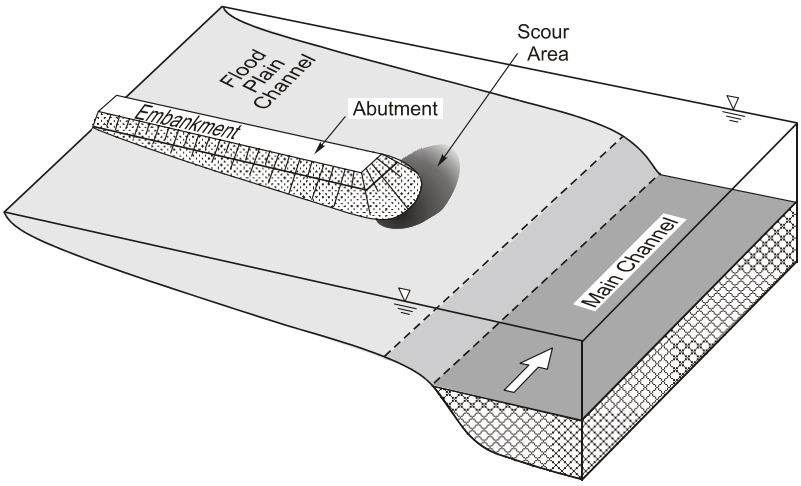

Fig. 7. Scour Type II-c, abutment threatened by scour of floodplain.

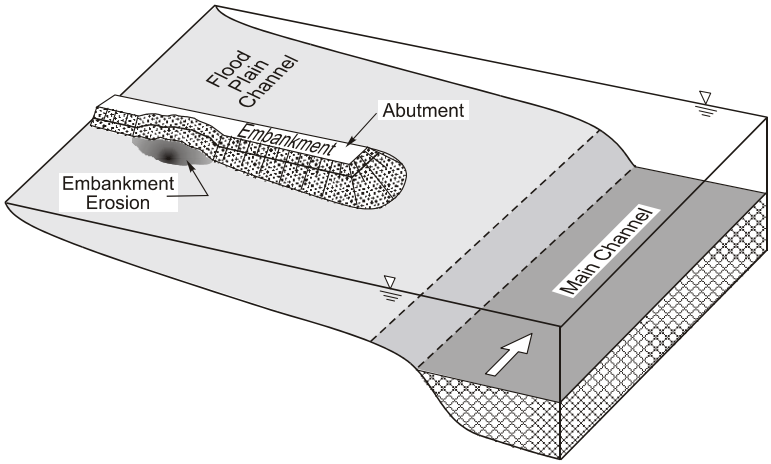

Fig. 8. Scour Type II-d, abutment threatened by scour of embankment.

SIMILITUDE LIMITATIONS

Limitations in hydraulic-model similitude hamper the capacity of flume experiments to directly replicate many of the complexities of soil/sediment and flow conditions at abutment sites, and thereby to reproduce the abutment-failure processes shown in Figs 4 through 8. The similitude limitations stem directly from the material properties of water as well as sediment and soils. The limitations must be recognized then worked around.

Sediments and Soils

The essential difficulties concern simulating scour of cohesive sediment and simulating slope stabilities (of main-channel bank, and of abutment and approach embankment). These difficulties especially face flume experiments intended for investigating abutments prone to Type II failures; though, actually they face all experiments on spill-through abutments, because failure of those abutments seems predominantly to occur as slope instability and collapse consequent to scour of the main channel or floodplain at the base of the abutment.

The practical limitations in simulating cohesive sediment also limit direct hydraulic modeling of slope failure (unless the slope is formed of non-cohesive sediment). Those limitations greatly complicate flume investigation of scour category Types II.

Flow-Field

Two not unrelated considerations complicate flume experiments of abutment scour. One consideration concerns the extent of far-field flow to be encompassed in the experiment setup. The other, a more fundamental issue, concerns flow-field similitude, notably simulation of shear stresses as well as pressures.

Flume experiments must balance considerations of extent of flow-field to be simulated, and the balance of forces acting on the flow. A difficulty is that abutment layout and size, as well as the pertinent extent of approach-channel bathymetry together with the

non-uniform and the complexly turbulent nature of the approach flow (e.g., as sketched in Fig. 2), and similitude constraints, require that hydraulic models of abutments practically be far-field models that encompass a substantial area of the approach channel, yet also be large enough in size as to facilitate accurate replication of flow forces. This composite requirement confronts investigators with the need to use a large (especially wide) flume for investigating Type II scour categories.

Recent work (Ettema et al. 1998, Ettema 2001) infers that a substantial scale effect occurs in loose-bed modeling whose similitude primarily is based on intensity of bed sediment movement is used as the primary criterion for similitude, as elaborated briefly below. It is useful to digress momentarily to explain the effect. For the simplest (still complicated enough) case of scour at a vertical wall placed in a straight rectangular channel with a bed of uniform sediment, the key variables typically involved can be discussed in terms of

$$\rho, \sigma, \mu, S_0, y_0, g, d, u_{*c}, L, K_S, \beta$$

where, ρ, σ, and μ = fluid density, surface tension, and dynamic viscosity, respectively; g = gravitational acceleration; d = representative particle diameter; u_{*C} = the critical value of shear velocity associated with entrainment of bed sediment; L = abutment length, K_S = abutment shape factor, and β = abutment angle to flow. The ensuing quick analysis drops σ, because surface-tension effects are neglible in flume experiments of scour.

The variables correspond to the following set of independent parameters developed using y_0, S_0, and ρ as the normalizing variables (and writing $u_{*0} = (gS_0 y_0)^{0.5}$, $U_0 = u_{*0}(8/f)^{0.5}$, with Darcy-Weisbach resistance coefficient $f = F_1(d/y_0)$ in fully turbulent flow):

$$\frac{u_{*0}}{u_{*c}}, \frac{(U_0)^2}{g y_0 f}, \frac{\rho U_0 L}{\mu f^{0.5}}, \frac{y_0}{d}, \frac{L}{y_0}, K_S, \beta$$

Scour depth (below average ambient bed level), y_s, can be functionally related to these parameters:

$$\frac{y_S}{y_0} = F_2\left(\frac{u_{*0}}{u_{*c}}, \frac{(U_0)^2}{g y_0 f}, \frac{\rho U_0 L}{\mu f^{0.5}}, \frac{y_0}{d}, \frac{L}{y_0}, K_S, \beta\right) \tag{1}$$

To date, however, laboratory studies (e.g., as described in books by Neill 1973, Breusers and Raudkivi 1991, Hoffmans and Verheij 1994, Raudkivi 1999, Lagasse and Richardson 1999, Melville and Coleman 2000; and in Federal Highway Administration reports [e.g., Richarson and Davis 1995]) essentially use the functional relationship

$$\frac{y_S}{y_0} = F_3\left(\frac{u_{*0}}{u_{*c}}, \frac{y_0}{d}, \frac{L}{y_0}, K_S, \beta\right) \tag{2}$$

to interpret results from laboratory studies. Work by Ettema and Muste (2002) shows that neglect of the Froude-number parameter $\frac{(U_0)^2}{gy_0 f}$ (actually a parameter expressing ratio of flow inertia to flow resistance) leads substantial distortion of the flow field and strength of turbulence around structures (e.g., dikes and abutments) in alluvial channels. While not significant for long constrictions (Ettema (2001)), the distortion would amplify scour depths in small-scale models. The extent of scour amplification still needs to be defined. Melville and Coleman (2000) mention this parameter, but also argue that it be discarded because doing so is conservative. The writer suggests that doing so is overly conservative, especially for scour at abutments.

Ettema and Muste (2002) also show that elevated levels of turbulence in models significantly affect flow distributions in small-scale models of dikes and wingdams. Not only does exaggerated Froude number result in increased stagnation-pressure heads, it amplifies the effect of centrifugal acceleration in regions of curved flow.

CONFRONTING THE COMPLEXITIES

The complexities discussed above presently face the writer and his IIHR colleagues embarked on NCHRP Project 24-20, whose objectives are to improve reliability of abutment-scour prediction, especially for abutments straddling floodplains. The complexities have been faced in a few prior abutment-scour studies; e.g., Sturn (1998) and Sturm and Chrisochoides (1997). The writer and his colleagues are configuring a plan of study that aims to address, and to work around, the complexities. Early issues in preparing the plan, which involves extensive flume experiments, are –

1. What scour processes are pertinent?
2. How to design effective experiments for elucidating the pertinent scour processes?
3. What levels of scour-prediction accuracy are practical and even meaningful?

Preparation of the plan has involved the following series of tasks:

1. Select the most important and common scour types for spill-through and wing-wall abutments;
2. Design experiment setups for replicating the selected scour types;
3. Define the flow-field associated with each scour type;
4. Conduct parametric investigation of scour depths and extents incurred with each scour type.

Floated below for audience/reader comment are the scour types selected and the commensurate flume experiments contemplated. The experiments will be conducted in two flumes, one being 5m wide, and the other 2.5m wide.

Scour Types
The scour types identified to be of highest importance are Types II-a & -b (Figs 5 and 6). Also important, but somewhat less so, is Type I (Fig. 4). These scour types should be investigated for through-flow and wing-wall abutment forms.

Flume-Experiments
Three basic series of experiments are planned. Of them, Type I scour (Fig. 4), is relatively straightforward to set up in a flume, and for which quite a few prior studies have been conducted. This series can be conducted at a range of scales, and used to ascertain scale effects.

Flume experiments on Types II-a and -b scour can be investigated using a flume fitted with a fully rigid floodplain with an alluvial (erodible) main channel. The simplifying assumption used here is that the floodplain is much less erodible than the bed of the main channel. The experiments would seek to determine the extent of scour in the main channel adjacent to the abutment, but would not go so far as to replicate bank failure. The objective of the experiments would be to provide a predictive relationship for maximum depth of main channel scour. Predictions of scour depth would be given to a geotechnical engineer, who then would estimate the stability of the main-channel bank. The experiments should entail varying abutment-head location relative to the edge of the main channel. Additionally, they may entail varying abutment orientation relative to the main channel.

A variation of flume setup involving a rigid floodplain is to fit an erodible sediment recess around abutment head. The remainder of the floodplain could still be kept rigid. This setup would be used to investigate possible interaction between scour in the main channel and scour on the floodplain around the abutment.

As the flow field for scour type illustrated in Figs 5 and 6 is not adequately known, flow-field delineation is a necessary precursor task before determining predictive relationships. It is especially necessary for abutments situated on floodplains. Of prime interest in this respect are situations where the abutment is in close proximity to the main channel. In these situations, scour likely results as the combined impact of flow constriction and the flow features generated by the abutment itself.

CONCLUDING COMMENTS
Many bridge abutments are located in compound channels whose morphology (alignment, bathymetry) is fairly complex. Additionally, many bridge abutments are located in situations where the channel is formed of various materials, occupying different locations within a bridge site. Non-cohesive sediments may form the bed of a main channel; silts and clay may predominate in riverbanks and underlying floodplains; and rocks may have been placed as riprap protection for the abutment, as well sometimes along adjoining riverbanks. Scour-estimation relationships and guidelines presently available do not adequately take into account the complexities of channel morphology and sediment/soil disposition. Given the complexities described in this paper, the writer believes that scour-prediction relationships should aim at a level of practical

approximation, whereby bridge designers may estimate reasonable upper-bound extents of scour produced by overall general (and somewhat simplified) conditions of scour; e.g., as illustrated in Figs 4 through 8. Bridge designers should be aware of the influences on scour of additional important factors such as proximity of other structures and of, say, floodplain vegetation. To include many of those factors in a predictive relationship is an unfinalizeable task.

The flume experiments outlined above aim at investigating several general, though simplified, conditions of scour at abutments. The experiments directly confront some scour complexities (e.g., influence of similitude), and hopefully sidesteps others (e.g., slope stability). The writer is curious to learn if the conference audience concurs with the flume-experiment approach outlined herein.

REFERENCES

Breusers, H.N.C. and Raudkivi, A.J. (1991). "Scouring." *IAHR Hydraulic Structures Design Manuel 2*, IAHR.

Ettema, R. (2001). "A framework for investigating micro-models." IIHR Limited Distribution Rept 210, IIHR, The University of Iowa, Iowa City.

Ettema, R., Melville, B.W., and Barkdoll, B.D. (1998). "Scale effect in pier-scour experiments*." J. Hydraulic Engrg*., Vol. 124, No. 6, ASCE, p. 639.

Hoffmans, G.J.C, and Verheij, H.J., (1997). Scour Manual. A. A. Balkema, Rotterdam, Netherlands.

Melville, B.W. and Coleman, S.E. (2000). *Bridge Scour* ,Water Resources Publications.

Molinas, A., Read, N.G.Y., and Jones, S. (1998). "Effect of cohesion on abutment scour." *Conf. Proc. Water Resources Engrg*, 1998, ASCE p. 252.

Ettema, R., and Muste, M. (2002). "Flume study of scale effects in hydraulic models of flow around dikes." IIHR Report 342, submitted to US Army Corps of Engineers, Waterways Experiment Station, Vicksburg.

Neill, C.R. (1973). Guide to bridge hydraulics. Roads and Transportation Assoc. of Canada, Univ. of Toronto Press, Toronto, Canada.

Raudkivi, A. J., (1999). Loose Boundary Hydraulics, A A. Balkema, Rotterdam, The Netherlands.

Richardson, E.V. and Davis, S.R. (1995). "Evaluating Scour at Bridges." *Publication No. FHWA HI-96-031, HEC 18, FHWA.*

Richardson, E.V., Harrison, L.J., and Davis, S.R. (1991). "Evaluating scour at bridges." *Report No. FHWA-IP-90-017 HEC 18*, Federal Highway Administration (FHWA), Washington, D.C.

Richardson and Richardson (1993a), "The fallacy of local abutment scour equations." *Conf. Proc. Hydraulic Engng*, 1993, ASCE, p. 749.

Richardson, J.R. and Richardson, E.V. (1993b) "Determining constriction scour." *Stream Stability and Scour at Highway Bridges*, ASCE Reston, VA pp. 483-91.

Richardson, J.R. and Roberts, D.L. (1998). "Non-structural method to reduce local pier scour." *Proc. 1998 Int. Water Resources Engrg Conf.* Part 1 (of 2) Aug 3-7 1998 v 1 1998 Memphis, TN ASCE p 768

Richardson, E.V. and Simons, D.B. (1984). "Use of spurs and guidebanks for highway crossing.: *Proc. Transportation Research Record 2nd Bridge Engrg. Conf.* v2 p.184.

Sturm, T.W. (1998). "Abutment scour in compound channels." *Stream Stability and Scour at Highway Bridges*, ASCE Reston, VA, pp. 443.

Sturm, T.W. and Chrisochoides, A. (1997). "Local scaling of bridge abutment scour in compound channels." *Conf. Proc. Hydraulic Engnrng*, 1997, ASCE p. 196.

Scouring Downstream of Sluice Gate

By

Siow-Yong Lim[1] and Guoliang Yu[2]

ABSTRACT

This paper presents the results of an extensive experimental study on local scour caused by high velocity jets issuing from submerged sluice gates or 2-D jet outlets. 84 sets of experiments have been conducted, out of which 63 sets were under deeply submerged jet conditions. Dimensional analysis is used to delineate the characteristic parameters affecting the maximum scour depth downstream of the structure. Under certain hydraulic conditions, the study discovered a cyclical jet-flipping phenomenon whereby the jet action would flip from the bed to the water surface and vice versa.

The erosion at the interface between the solid apron and the sand bed, i.e., at the brink of the apron was measured. The maximum brink scour depth, d_b, immediately at the downstream end of the apron was found to be about 0.44 times the maximum scour depth. For the prediction of the maximum scour depth, an empirical formula has been proposed, based on a database of 163 experiments from the present study and various other researchers. The formula takes into account the jet size and velocity, median sediment size, sediment density and gradation and the length of the protective apron. The formulation directly takes into account the effect of the apron length, which is a key parameter in the design of scour countermeasure for this type of problem. The range of applicability of the formula, and its uses and limitations has been discussed. The formula was used to estimate the scour caused by the high jet velocity issuing from the sluice gate of the Shimen Arch Dam in China and the prediction was close to the measured scour in the field.

INTRODUCTION

Water releases at high flow velocity through hydraulic structures, such as sluice gates or spillways, may cause stability problem of the riverbed downstream of the structure. To protect the structures, a typical engineering solution is to build a solid apron downstream of the structures in order to minimize the effect of erosion from the structures. However, local scour downstream of the apron may still occur even though most of the flow energy has been appropriately dissipated over the length of the apron. The scour depth not only depends on the impinging flow velocity, characteristics of bed material, but also the apron length and apron surface roughness. The optimum apron length is a key parameter in the design of this type of scour countermeasures. It is therefore necessary to study the effect of apron on the scour depth. Since the initial investigation of water jet scouring by Rouse (1939) and Laursen (1952), numerous experiments have been carried out to study

[1] Associate Professor, School of Civil & Environmental Engineering, Nanyang Technological University, Nanyang Avenue, Singapore 639798. csylim@ntu.edu.sg
[2] Research Fellow, School of Civil & Environmental Engineering, Nanyang Technological University, Nanyang Avenue, Singapore 639798.cglyu@ntu.edu.sg

the scouring phenomenon. For 2-D jets without an apron, these include the works by Tarapore (1956), Valentin (1967), Basmaci (1971), and Rajaratnam (1981), Ali and Lim (1986). Other investigators have studied the influence of a rigid protective apron on the bed scouring, such as Iwagaki et al (1965), Hassan and Narayanan (1985), Chatterjee et al (1994), Li (1993), Aderibigbe and Rajaratnam (1998).

A few empirical models have been proposed for the prediction of the maximum scour depth for jet scour phenomena. These models were mainly based on the densimetric particle Froude number, opening size of the jet, and uniform sediment size. Aderibigbe and Rajaratnam (1998) found that the non-uniformity of the sediment has a significant effect on the size of the scour hole produced by the jet.

The primary objective of this study is to investigate the bed scouring caused by flow issuing from a sluice gate or 2-D horizontal water jets from a nozzle. The flow may or may not initially flow over a protective apron before reaching the erodible bed. Extensive experimental investigations have been carried out to study the jet flow characteristics and the bed scouring using different apron lengths and bed material sizes under varying flow conditions. Dimensional analysis is used to delineate the characteristic parameters affecting the flow patterns and the maximum scour dimensions of the hole created by the jet flow.

EXPERIMENTS

The experiments were conducted in the Hydraulics Laboratory at NTU. Two flumes were used and the experimental set up is shown in Figs. 1a and 1b. The large glass-wall flume (Fig. 1a) measures 20m long, 0.494m wide and 0.688m deep and the water is released from a well-rounded vertical sluice gate installed near the upstream end of the flume. The small glass-wall flume (Fig. 1b) measures 8m long, 0.2m wide and 0.3m deep. In the small flume, in addition to using the sluice gate, a specially designed shoe-shaped nozzle made of stainless steel was also used to issue a 2-D horizontal wall jet. The rational behind using the nozzle was to overcome the physical constraint of the small flume. The flume is only 0.3 m deep; hence, it is difficult to produce a jet of high velocity from the small difference in head upstream and downstream of the sluice.

In both flumes, a solid Perspex platform approximately 4m long was constructed to simulate a rigid apron. The sluice gate or nozzle can be installed at any location on the apron. This arrangement facilitates the study of the effect of apron length on the scouring downstream of the gate.

A sediment recess area followed the end of the apron. This was filled with the bed material and flushed level with the apron. In the small flume, the sediment bed was 10cm deep and 2m in length, while in the large flume, the sediment bed was 25cm deep and 5m in length. The arrangements assured that each equilibrium scour hole formed would not hit the bottom of the flume. Seven different types of uniform quartz sediments were used as bed material. The median size of the sediments varies from 0.68 mm to 4.92 mm. The geometric standard deviation of the sediments varies from 1.17 to 1.33.

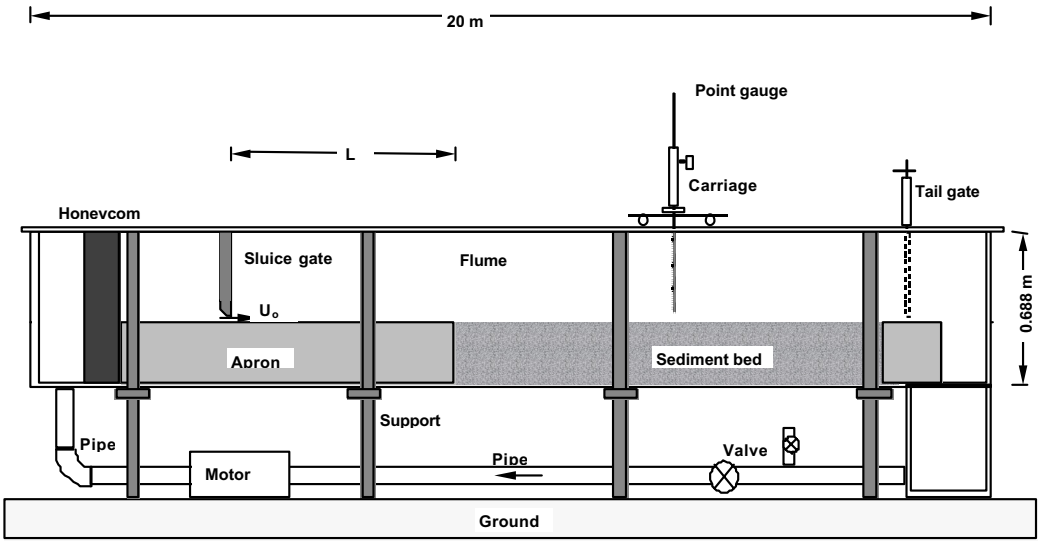

Figure 1a. Layout of experimental set-up in the big flume

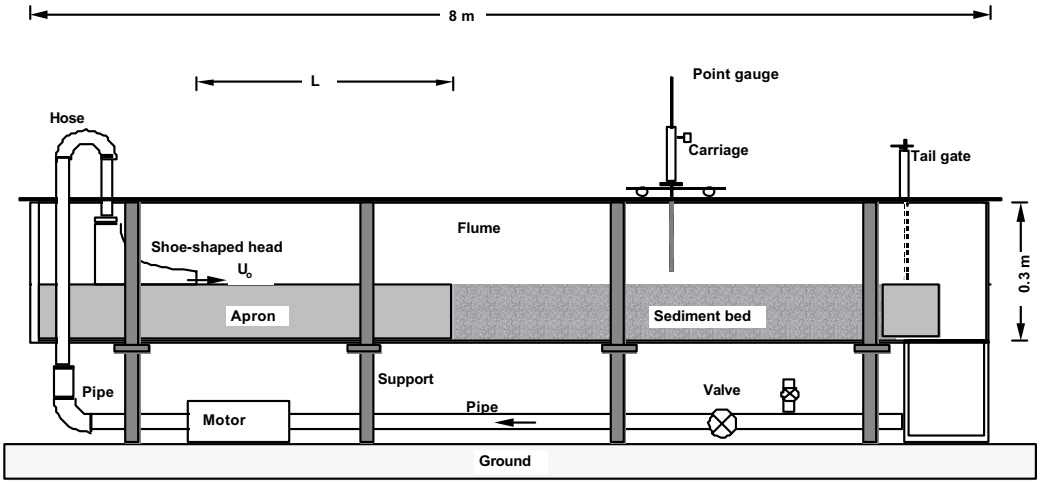

Figure 1b. Layout of experimental set-up in the small flume

Altogether, 84 sets of experiments were conducted, out of which 63 sets were under deeply submerged jet conditions, i.e., the tailwater depths were larger than 10 times the size of the jet opening. The experiments covered a wide range of jet velocities, apron lengths and sediment sizes and the range of the test conditions are listed in Table 1.

Table 1 Summary of the experimental conditions for the present study

No of Runs	d_o (mm)	d_{50} (mm)	σ_g	L (mm)	U_o (m/s)	S	F_o	d_{se} (mm)
14	3	0.68-4.92	1.17-1.24	0-180	0.92-1.37	2.65	3.26-10.58	14.5-61.0
48	10	0.82-2.94	1.14-1.33	0-900	0.34-2.45	2.65	2.95-11.23	6-185
7	20	2.66	1.34	0	0.71-1.77	2.66	3.41-8.50	62-210
15	26	1.82	1.22	0-1040	0.42-1.31	2.65	2.45-7.66	37-143.5

The procedure for each run is similar. Before each run was started, the sediment bed was leveled so that it was flushed with the rigid apron. The sluice gate or nozzle was installed by shifting to the desired distance from the sediment bed. The pump was turned on and the flow was adjusted to a pre-determined flow rate using a flow meter connected in the supply pipeline. The flow rates were checked regularly to ensure the consistency of the flow. At the end of the flume, a tailgate was adjusted so that the tailwater depth was maintained at a high level to achieve a 2-D fully submerged horizontal jet. The experiments were usually conducted for days or even several weeks until no significant changes in the scour profile were observed. During the run, the scour profiles along the centerline were measured at regular time interval using a point gauge attached to a traversing carriage that could slide along the two rails on the top of the flume. The time evolution of the scour profiles along the sidewall was also recorded on transparencies pasted on the glass wall.

SCOURING PROCESSES

Fig. 2 shows a definition sketch of the scour hole formation downstream of the apron. In general, the scouring process is such that once the jet discharging from the sluice gate or nozzle comes into contact with the erodible bed, a lot of sand particles are eroded and transported downstream. During the process a scour hole and a crest are formed. During the initial stage, the rate of scouring is very rapid. As time increases, the rate would decrease and eventually approaches zero as the equilibrium scour hole is reached. For a typical scouring process, the three observable stages of scouring are: (i) an initial stage with rapid rate of scouring; (ii) a development or erosion stage which has a relatively slower rate of scouring; (iii) an equilibrium stage where there are no observable changes in the scour depth after a long scouring time.

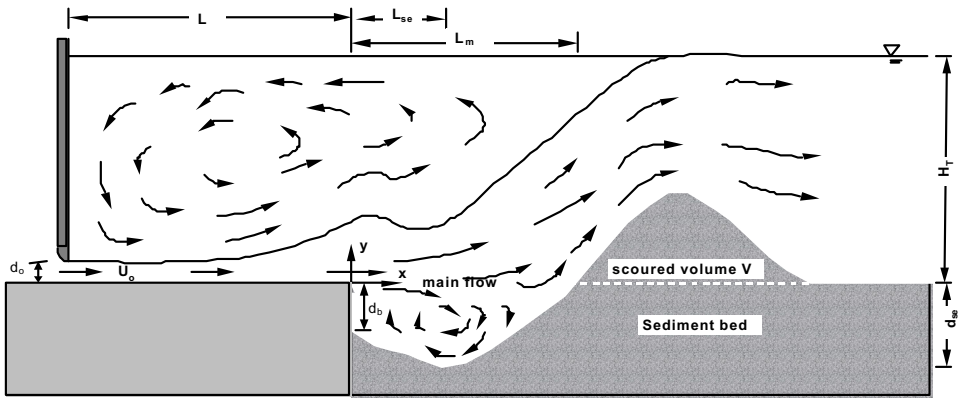

Fig. 2. Definition sketch of scour below a sluice with an apron

At the equilibrium stage, the scour hole would have attained its maximum depth. Though there were no observable changes in depth, the scour hole continued to lengthen and simultaneously shifting the crest further downstream. At the same time, the sand particles around the region of the maximum scour depth would roll to and forth without causing any deepening of the scour hole. At the end of the experiment, it was observed that, even for the uniform sediment used, the crest was covered by a layer of relatively finer particles and upstream of the crest, the particles were coarser. The coarsest particles were located around the region of the maximum scour depth. While proceeding further upstream towards the rigid apron, the particle sizes were finer again.

In some experiments, it was observed that the discharging jet from the sluice gate was unstable during the scouring process. The jet axis was observed to be 'oscillating' between a position along the bottom of the scouring bed and a position in the horizontal direction. Figs. 3 to 5 show these jet positions and the interaction of the jet with the erodible bed. The oscillation period was generally between 5 to 10 seconds.

When the jet was attached to the bed (Fig. 3), it eroded and transported a lot of particles, some of which (mainly finer particles) were transported over the dune or while others were swept upstream by the reverse flow. The coarser particles were mainly deposited and piled at the downstream end of the scour hole, resulting in the thickening of the coarser layer and the steepening of the bed slope, which was supported by the jet. Once the steepness of the bed exceeded a certain limit, the jet could no longer support the bed and it was forced to impinge on a section of the scour hole. While doing so, it strongly eroded the bed and generated a sediment cloud immediately downstream of it.

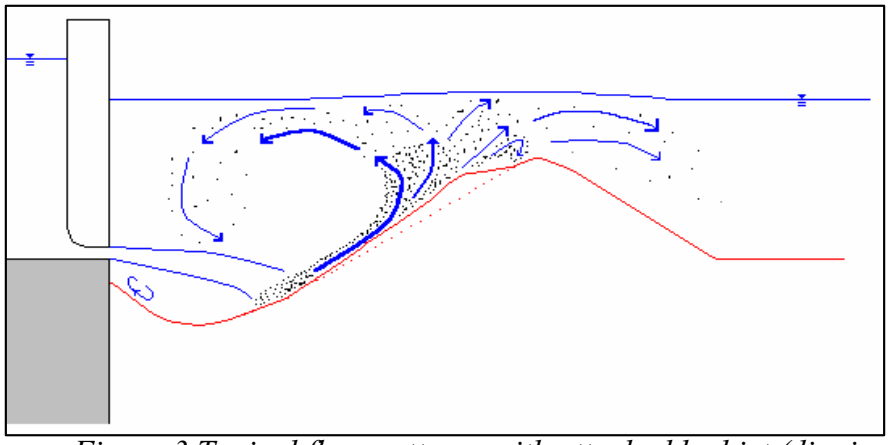

Figure 3 Typical flow patterns with attached bed jet (digging phase)

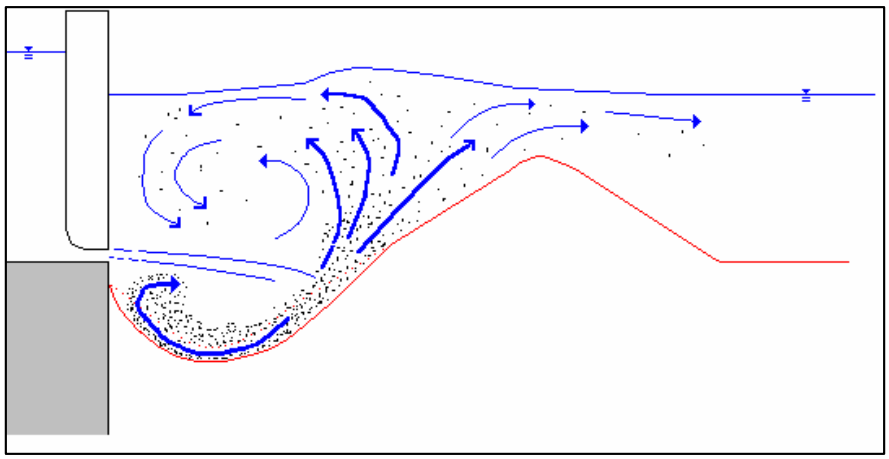

Figure 4. Typical flow patterns with the jet rising to the surface

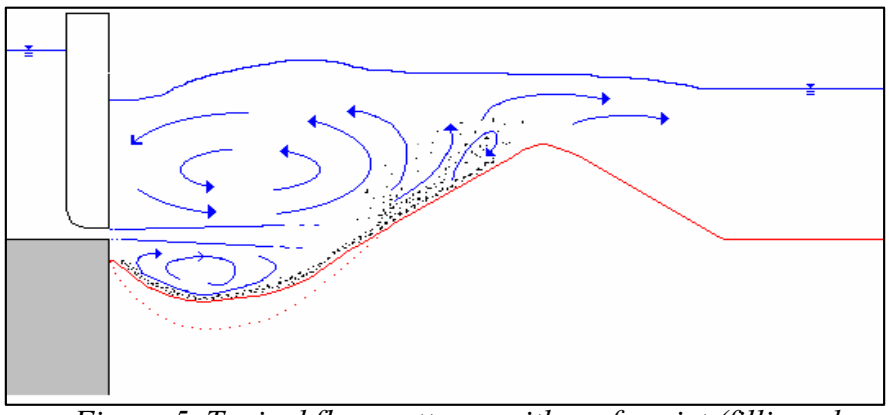

Figure 5. Typical flow patterns with surface jet (filling phase)

The maximum scour depth occurred during the jet impingement (Fig. 3) and it was referred to as the deeper dynamic scour depth (digging phase). A sediment-laden vortex was formed upstream between the bed and the jet. The jet then started to rise (Fig. 4) towards the horizontal position, causing the impingement area to move downstream into the sediment deposits which at the same time were being transported along the bed and

back into the mid section of the scour hole. By the time the impingement area had reached the end of the scour hole, that is, when the jet path was horizontal, all the sediment deposits were back in the mid-section of the scour hole (filling phase). The maximum scour depth at this point was referred to as the shallower dynamic scour depth (Fig. 5). This process was continuously repeated, resulting in a scour hole with mainly coarser particles and a dune covered by finer particles. Though the armor layer was never stable, the scouring process was assumed to reach equilibrium state when the scour hole did not show any significant change in depth during the digging phase.

The water surface profile also changed during the two phases. During the digging phase the water surface was very calm (Fig. 3), whereas during the filling phase the water surface was characterized by rippling profile as though the water was boiling (Fig. 4). As a result of the filling and digging actions at the scour hole zone, a shallower dynamic scour depth and a deeper dynamic scour depth were produced, respectively. When the jet was stopped the static profile of the eroded bed lay in between the two dynamic scour depths and this is recorded as the equilibrium scour depth.

CENTERLINE SCOUR PROFILES

Fig. 6 shows a typical time development of the centerline scour profiles caused by the submerged wall jet with an apron length 30 times the jet opening size. The scour profiles show that the scour patterns are rather similar in shape. In the past, Laursen (1952), Tarapore (1956), Rajaratnam (1981), Hassan and Narayanan, (1985) Ali and Lim (1986) and Chatterjee et al (1994) have shown that the scour patterns caused by jets were similar in shape as the scour progressed.

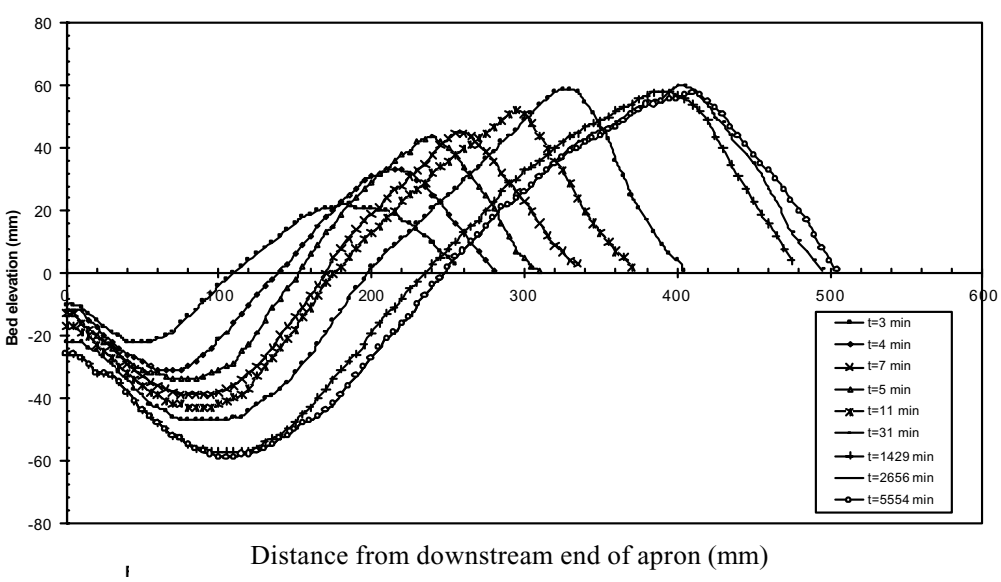

Figure 6 Centerline scour profiles, L = 300mm, d_o = 10 mm, U_o = 1.18 m/s, d_{50} = 2.94mm, H_t/d_o = 24.3 (Run SPB 4)

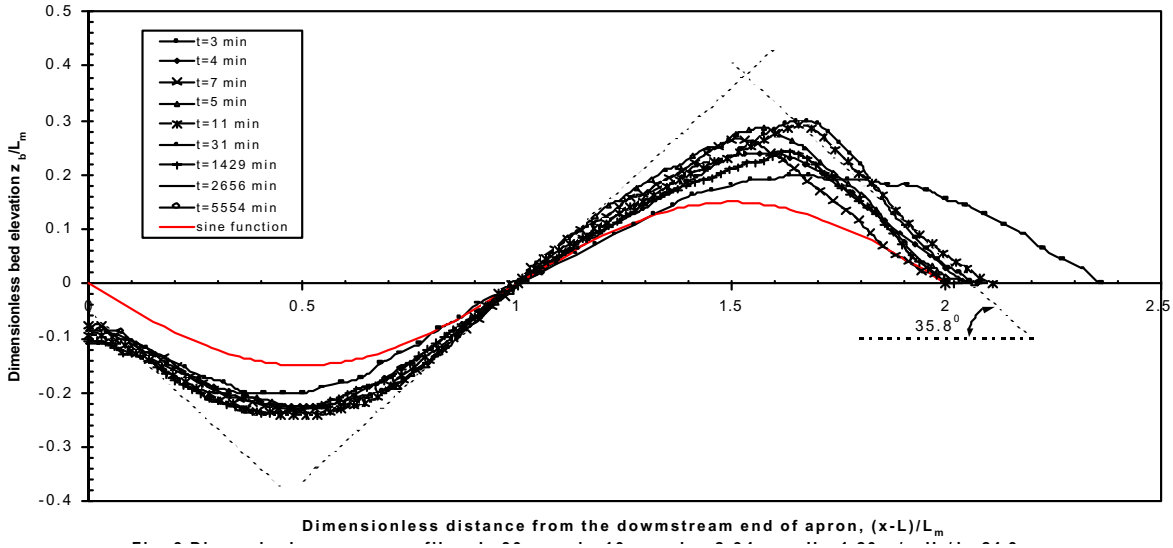

Figure 7 Similarity of centerline scour profiles, L = 30mm, d_o = 10 mm, U_o = 1.18 m/s, d_{50} = 2.94mm, H_t/d_o = 24.3 (Run SPB 4)

This means that using the proper scaling lengths; the scour profiles could be described by a single parameter. The scaling parameters used were different for different researchers. In this study, the scaling length used is L_m, which is the temporal length of the scour hole (see Fig. 2). Fig. 7 shows the dimensionless plot of z_b/L_m versus $(x-L)/L_m$ for the profiles in Fig. 6, where z_b is the scour depth at any x-distance in the scour hole. Except for the profiles in the first few minutes of scouring action, the figure shows that the plotted data could satisfactorily be represented by one curve, especially for the scour hole part of the eroded bed profiles. The profile resembles that of a sine function, which is superimposed on the figure.

The angle of repose for the sediment (=35.8^0) used was also calculated and superimposed on the figure. Generally, it can be seen that the upstream slope of the scour hole is slightly steeper than the downstream one. However, the downstream slope of the scour hole and the upstream slope of the ridge were quite close to the angle of repose.

MAXIMUM EQUILIBRIUM SCOUR DEPTH

There are a number of parameters that will affect jet scour in an alluvial bed, listed as follows,

$$d_{se} = f_1(\nu, \rho, \rho_s, d_{50}, \sigma_g, H_t, k_e, U_o, L, d_o, g) \qquad (1)$$

where d_{se} = maximum equilibrium scour depth, U_o = mean jet velocity at the efflux section, L = length of apron, d_o = jet opening size, H_t = tailwater depth, d_{50} = median sediment diameter, k_e = roughness height of the apron, ? = kinematic viscosity of fluid, ρ = fluid density, ρ_s = sediment density, σ_g = standard deviation of particle size distribution, g = gravitational acceleration. Using dimensional analysis, Eq. (1) becomes

$$\frac{d_{se}}{d_o} = f_2\left(Re = \frac{U_o d_o}{\nu}, \frac{d_{50}}{d_o}, \frac{k_e}{d_o}, S = \frac{\rho_s}{\rho}, \sigma_g, \frac{H_t}{d_o}, Fr = \frac{U_o}{\sqrt{g d_{50}}}, \frac{L}{d_o}\right) \quad (2)$$

Some of the terms in Eq. (2) may be dropped or combined with the following reasoning. First, the jet velocity is usually relatively high and the corresponding Reynolds number will therefore be much greater than a few thousands. This means the effect of the viscosity on the jet hydraulics and its scouring should be insignificant. Second, the apron roughness parameter, k_e/d_o may be neglected since the apron surface is relatively smooth and the apron length is also comparatively short in terms of energy dissipation on the apron surface compared to the energy lost due to the vortices generated. Third, the flow Froude number Fr and specific gravity of sediment S can be combined to form a sediment densimetric Froude number, F_o. Fourth, only data with deep tailwater submergence will be used in the analysis, i.e., with H_t/d_0 greater than 10. Hence, Eq. (2) becomes

$$\frac{d_{se}}{d_o} = f_3\left(\frac{d_{50}}{d_o}, \frac{H_t}{d_o}, F_o = \frac{U_o}{\sqrt{(S-1) g d_{50}}}, \frac{L}{d_o}, \sigma_g\right) \quad (3)$$

To evaluate the function, a database of 163 sets of flume data have been collected, out of which 63 data sets were from the present study and 100 sets were from other researchers. A summary of the experimental conditions is listed in Table 2. The data cover a wide range of flow and sediment conditions, and there are 61 sets of experiments with the installation of an apron downstream of the jet exit. Using regression technique, the dimensionless maximum scour depth is obtained as follows:

$$\frac{d_{se}}{d_o} = 1.04\, \sigma_g^{-0.69}\, F_o^{1.47} \left(\frac{d_o}{d_{50}}\right)^{-0.33} e^{-0.04\,\beta\left(\frac{L}{d_o}\right)^{1.4}} \quad (4)$$

where $\beta = \sigma_g^{-0.5} F_o^{-0.35} \left(\frac{d_o}{d_{50}}\right)^{0.5}$. Fig. 8 shows comparisons between the calculated and measured d_{se}/d_o. The comparison indicates that 76% of the data were within the ± 20% error band and 91% were within ± 30% error band. Eq. (4) includes the effects of the flow, jet size, sediment characteristics, and length of the protective apron. For example, for the same sediment size, the scour depth would decrease by about 50% if σ_g were increased from 1.2 to 3.13. This is consistent with the findings of Aderibigbe and Rajaratnam (1998).

Eq. (4) also indicates that the scour depth would decrease rapidly as the protective apron length increases. However, the deduction of the scour depth vis-à-vis the apron length is not a simple function of the latter. It is also associated with the jet size, flow and sediment characteristics as indicated by the factor β in Eq. (4).

Table 2 Summary of data from present study and other sources

Researchers	No of Run	d_o (mm)	d_{50} (mm)	σ_g	d_o/d_{50}	L/d_o (mm)	U_o (m/s)	S	F_o	d_{se}/d_o
Present Study	63	3-20	0.68-4.92	1.17-1.34	0.61-11.2	0-90	0.34-2.45	2.65	2.95-11.2	0.6-19.5
Rajaratnam (1981)	14	3.56-24.9	1.2-2.38	1.2*	1.5-10.5	0	0.87-2.22	2.65	4.43-14.0	3.34-31.29
Basmaci (1971)	13	3.74-12.62	1.3-6.50	1.2*	0.95-9.71	0	0.55-1.92	1.30-2.60	3.85-13.3	3.57-29.26
Iwagaki et al (1965)	19	5-20	1.85-3.75	1.2*	2.7-5.41	8-16	0.5-3.32	2.61	2.93-13.74	2.65-27.04
Tarapore (1956)	7	3.18	0.70-4.4	1.2*	0.72-4.54	0	0.85-1.86	2.65	6.97-12.16	11.72-28.48
Aderibigbe & Rajaratnam (1998)	32	5-25	1.15-6.75	1.32-3.13	0.74-31.7	0	0.58-4.77	2.65	2.78-29.46	1.32-32.74
Chatterjee et al**, (1994)	15	20-50	0.76-4.3	1.22-1.43	4.65-39.5	22-33	0.4-2.125	2.63-2.65	2.38-11.68	0.882-4.205

** σ_g is assumed to be 1.2 because the value was not given in the original source, but the bed material was mentioned as uniform;*

*** Efflux velocities were calculated from the discharges per meter width and the height of jet, given in Table 2 of Chatterjee et al (1994).*

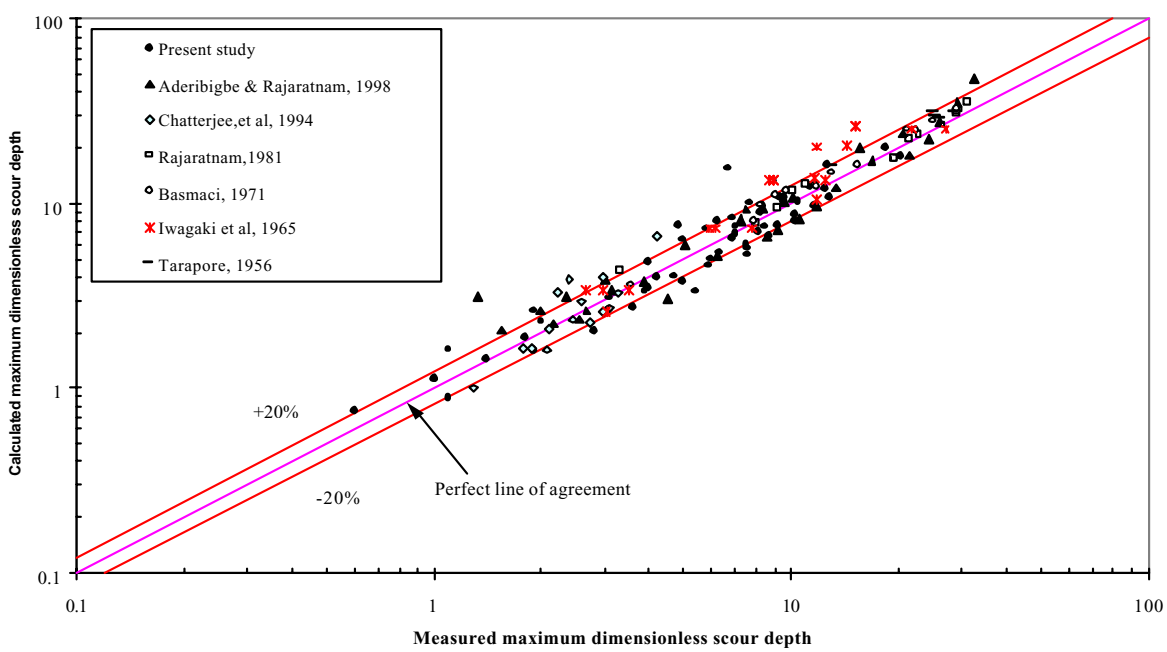

Figure 8 Comparison between calculated and measured dimensionless maximum scour depth, d_{se}/d_o for cases with and without aprons

When there is no apron installation after the jet opening, i.e., $L/d_o = 0$, Eq. (4) becomes

$$\frac{d_{se}}{d_o} = 1.04\ \sigma_g^{-0.69}\ F_o^{1.47} \left(\frac{d_o}{d_{50}}\right)^{-0.33} \tag{5}$$

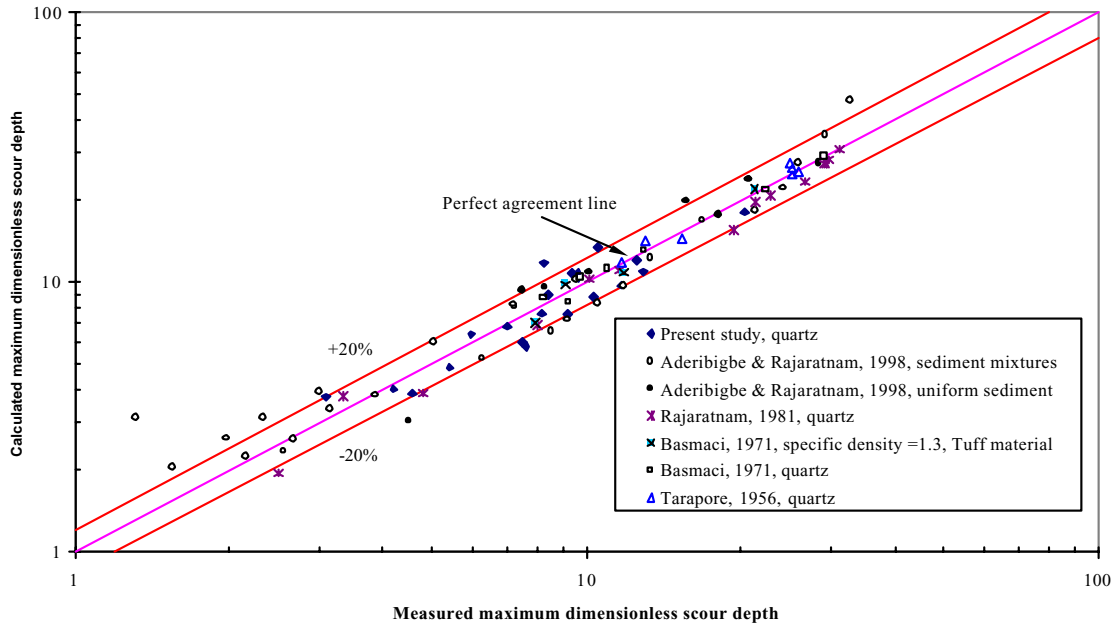

Figure 9 Comparison between calculated and measured dimensionless maximum scour depth, d_{se}/d_o for cases without apron

Fig. 9 shows the good agreement between the measured scour depth data without apron installation compared to the computed values using Eq. (5). 79.5% of the data tested were within the ± 20% error band and 94.4% of data tested were within the ± 30% error band. Note that the database used for Fig. 9 includes experiments conducted with tuff material where the specific gravity is equals to 1.3.

MAXIMUM BRINK SCOUR DEPTH

The erosion at the interface between the solid apron and the sand bed, i.e., at the brink of the apron is also of concern to the engineers. The reverse flow in the toe region immediately downstream or brink of the apron causes this to occur. The maximum brink or backwater scour depth, d_b, (see Fig. 2) at the downstream end of the apron base is also measured and evaluated in this study. As shown in Fig. 10, the maximum brink or backwater scour depth, d_b, is linearly related to the maximum scour depth, i.e.,

$$d_b = 0.44\, d_{se} \tag{6}$$

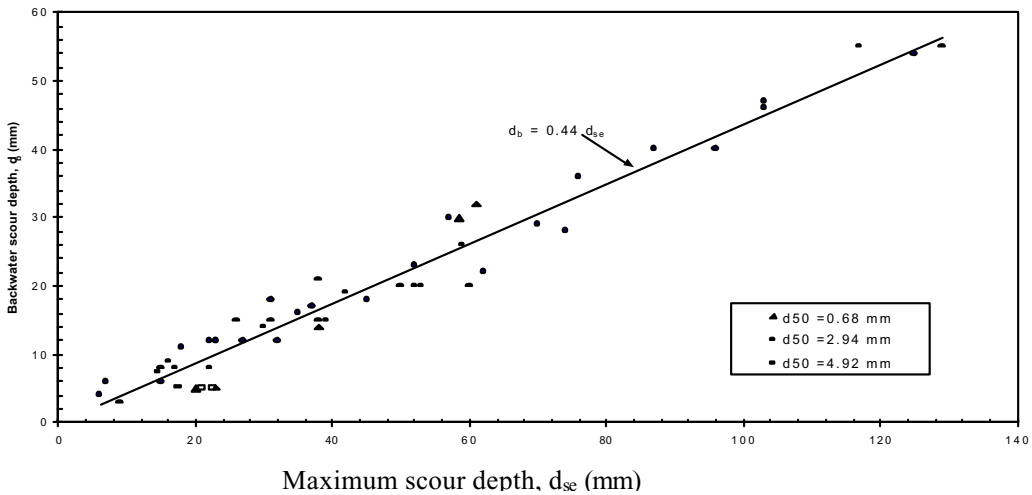

Figure 10 Relationship between maximum brink or backwater depth with maximum scour depth

FIELD APPLICATION

It is important to check if the proposed equation is applicable to field condition. An interesting field study on the Shimen Arch Dam by Li and Li (1999) provided the opportunity to test the formula. The Shimen Arch Dam was built in China along the Bao River in 1973. The structure has a 20m apron downstream of the six sluice gates (each with dimensions of 7m wide × 8m high) as shown in Fig. 11. In 1978 the apron protection was extended by 30 m to give a total apron length of 50m. The average slope of the apron floor is 7.6%, starting at elevation 535.8m and ending with an elevation of 530.0m. The head of water from the bottom of the sluice gates is about 22m.

In the period from 14 to 25 August 1981, the river was inundated with a one in 300 years flood flow and the water released from the 6 gates was as high as 4,840 m^3/s. Scouring occurred downstream of the sluice gates and the maximum scour depth recorded was about 13.6m, below the original bed level of the downstream channel. The mean efflux jet velocity at the entrance to the apron floor was estimated to be about 20.8-25.4 m/s, based on the head of water upstream of the sluice gates. This is consistent with the physical model measurements by Li and Li (1999). The mean flow field and the near bed velocities in bracket at three locations along the apron are also shown in Fig. 11. The mean efflux flow depth was estimated to be 4.03m, based on the flood discharge and the apron width. With a downstream water depth of about 53 m, the efflux flow can be considered as a deeply submerged jet.

The bed material downstream of the dam consists of layers of cipolin or quartzite. Each layer is less than 10 m thick. The high-speed flow destroyed the rocky layers into loose pieces of rock blocks. Some of these rocks were flushed out by the flow and formed the scour hole during the floods. According to the survey on the bed material in the scour hole, it was found that the rock blocks have a volume varying between 24 to 26 m^3. Taking the mean of 25 m^3 and assuming it to be spherical would give the bed material size a value of 3.62 m in diameter. We further assumed the bed material in the scour hole was quite uniform with $\sigma_g = 1.2$. With the above considerations and using Eq. (4), we obtained the computed maximum scour depths of between 12.9m to 17.0m for the velocity range of 20.8 to 25.4 m/s at the entrance section to the apron. Hence, the mean

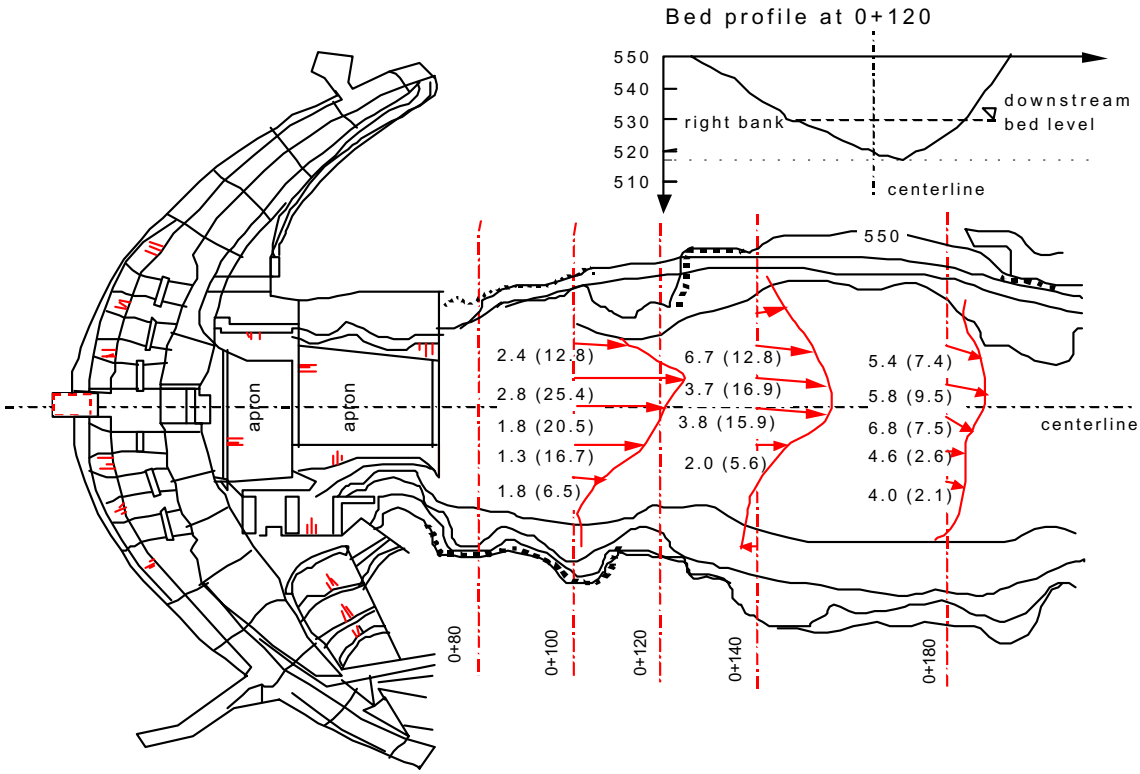

Figure 11 Structural layout of Shimen Arch Dam, the flow field and bed profile at maximum scour location (after Li and Li, 1999)

scour depth is 14.95m, and this value compares favorably with the measured maximum scour depth of 13.6m in the field.

RANGE OF APPLICABILITY

In this study, a formula (Eq. 4) has been proposed for the prediction of the maximum scour depth downstream of a submerged sluice gate or two-dimensional jet with an apron. The formula has considered most of the major factors affecting the formation of the scour

hole, such as the jet opening size, velocity, sediment size and gradation, and length of apron. The ranges of the pertinent parameters are: $2.38 \leq F_o \leq 29.46$, $0 \leq L/d_o \leq 90$, $0.61 \leq d_o/d_{50} \leq 39.5$, $1.3 \leq S \leq 2.65$, $1.17 \leq \sigma_g \leq 3.13$. Nevertheless, some aspects need to be discussed for future study and application.

First, the influence of the non-uniformity of bed material on the scour depth needs to be studied because the range of the geometric standard gradation of the bed material used in the database is not extensive. The second aspect to consider is the sediment size. The database is limited to jet scour with median sand size larger than 0.68 mm. The third is the influence of the tailwater depth. In the present analysis, this effect is neglected and the database considers only cases where the jet is fully submerged with tailwater depths greater or equal to 10 times the jet opening size. The proposed equation is therefore applicable to deeply submerged jets. In addition, Eq. (4) assumes the roughness on the rigid apron surface is smooth and would not affect the subsequent scour formation. However, if the apron surface is very rough, for example, with baffles on the apron floor for energy dissipation, Eq. (4) may give an over estimation of the scour depth.

Finally, the scattering of the experimental data in Fig. 8 may be due to systematic errors. As discussed earlier, the jet-flipping phenomenon causes the bed to be in a state of dynamic equilibrium between the filling and the digging phase. For these experiments, the largest scour depth is during the dynamic digging phase and this value is used in the analysis. This is consistent with the data provided by Aderibigbe and Rajaratnam (1998) where the dynamic maximum scour depths were measured at the end of the bed digging action. It should be mentioned that most of the other researchers adopted the time-averaged maximum scour depths. Using the data from the present work and Aderibigbe and Rajaratnam (1998), it is estimated that the two different measuring methods of the maximum scour depth may have contributed about ±15% of the systematic errors. From the viewpoint of engineering safety, we suggest that a safety factor of 1.3 should be considered when applying Eqs. (4) or (5) into field practices.

CONCLUSIONS

1. Generally, the bed scouring progress can be characterized into the three different stages, i.e., an initial stage where the scour rate is very rapid, a developing stage, and an equilibrium stage whence the maximum scour depth is attained. The time to achieve the equilibrium stage typically takes a few days to reach.
2. Under certain hydraulic conditions, a jet-flipping phenomenon was discovered in the present study. The process is cyclical. The jet would first act as an attached bed jet digging at the bed and creating a scour hole. When the hole had attained a certain depth, the bed jet would abruptly flip towards the water surface and transforms into a surface jet. At this instant, the digging action stopped abruptly and the sediment was observed to be back-filling from the ridge region into the scour hole. When the scour hole was almost leveled, the surface jet would transform into a bed jet again. The cyclical process of jet flipping from the bed (digging action with a calm water surface) and to the free surface (back-filling action with "boiling" water surface) was observed throughout the full duration of the experiment.

3. The time development of centerline scour profiles was found to be similar using the length of the scour hole as the scaling parameter.
4. The maximum brink scour depth at the toe of the apron was evaluated and found to be about 0.44 times the maximum scour depth.
5. Using a database consisting of 163 data sets from the present study and various researchers, an empirical formula (Eq. 4) has been proposed for the prediction of the maximum scour depth downstream of a submerged sluice gate or 2-D wall jets with or without a protective apron. The formula takes into account the jet size and velocity, median sediment size, sediment density and gradation and the length of the apron.
6. The formula was used to estimate the scour downstream of the sluice gate of the Shimen Arch Dam in China and the prediction was close to the measured scour in the field.

REFERENCES

1. Ade, F. and Rajaratnam, N. (1998). "Generalized study of erosion by circular horizontal turbulent jets." *J. Hydr. Res.*, IAHR, 36 (4), 613-635.
2. Aderibigbe, O. and Rajaratnam, N. (1998). "Effect of Sediment Gradation on Erosion by Plane Turbulent Wall Jets." *J. Hydr. Engrg.*, ASCE, 124 (10), 1034-1042.
3. Ali, K.H.M. and Lim, S.Y. (1986). "Local scour caused by submerged wall jets." *Proc. Instn. Civ. Engrs*, Part 2, 81, 607-645.
4. Basmaci, Y. (1971). "Localised scour under vertical gates by submerged jets." MSc Thesis, Middle East Tech. Univ., Turkey.
5. Chatterjee, S.S., S. N. Ghosh, and M. Chatterjee (1994). "Local scour due to submerged horizontal jet."*J. Hydr. Engrg.* ASCE, 120 (8), 973-992.
6. Hassan, N. M. K. and Narayanan, R (1985). "Local Scour Downstream of an Apron." *J. Hydr. Engrg*, ASCE, 111 (11), 1371-1385.
7. Iwagaki, Y., Tsuchiya, Y., and Imamura, M. (1965). "Studies of the Local Scour from Flows Downstream of an Outlet (1)." *Disaster Prevention Research Institute*, Annuals No. 8, Kyoto University, Japan, 363-377.
8. Laursen, E.M. (1952). "Observations on the Nature of Scour." *Proc. Fifth Hydr. Conf.*, Bulletin 34, University of Iowa, USA, 179-197.
9. Li, B.H. and Li, Z. (1999). "Three Dimensional Flow and Scour in the Energy Dissipation Zone of Shimen Arch Dam." *Journal of Water Power*, No. 12 (in Chinese).
10. Li, W. (1993). "Scour of Fine Sediment by a Turbulent Wall Jet*" Ph D Thesis*, Lamar University, Texas, USA.
11. Rajaratnam, N. (1981). "Erosion by plane turbulent wall jets" *J. Hydr. Research,* IAHR, Vol. 19, No. 4, 339-357.
12. Rouse, H. (1939), "Criteria for similarity in transportation of sediment." State University of Iowa Bulletin, 20, 33-39.
13. Tarapore, Z.S. (1956). "Scour below a submerged sluice gate." M Sc Thesis, University of Minnesota, USA.
14. Valentin, F. (1967). "Considerations Concerning Scour in the case of Flow under Gates." *Proc.12th Congress*, IAHR, Vol.3, 92-96.

Development of the New Inspection Method on Scour Condition Around Existing Bridge Foundations

by

Jiro Fukui[1] and Masahiro Otuka[2]

ABSTRACT

In the past, investigation on the scour condition around bridge foundations in Japan has been conducted by the traditional method which is to measure a depth from water surface to streambed by using a standing bar on a boat. However, it has been difficult to measure the precise depth through this method. Then, PWRI has newly developed such the method that depth is measured by a radio-controlled boat with an acoustic analysis device and a personal computer analyzing data collected in combination with its location. According to the method, ups and downs of streambed around a pier can be two-dimensionally and precisely measured. The method based on the relatively simple principle for survey of the progressive condition at streambed during floods has also been developed.

1. INTRODUCTION

There has been a large amount of bridge stock in Japan as roads improvement has advanced positively. We should keep bridges in good condition for a long period in the future, which means that the operation and maintenance for bridges will become more important.

There are many kinds of causes such as major earthquake, floods scouring, ground movement and the others in terms of main damage of bridge foundations in Japan. We can point out that floods scouring is distinguished among these factors causing bridge failures or severe damages, and the most common cause which requires the repair or strengthening of bridge foundations is also from floods scouring. Consequently, it is absolutely necessary to investigate the scour condition as early and accurate as possible and to estimate the soundness of bridges in terms of keeping bridge foundations in good condition. The problem is, however, that it is generally hard to make a cost-effective investigation since scours occur under water.

[1] Team Leader, Structures Research Group, Public Works Research Institute, Independent Administrative Institute, 1-6 Minamihara, Tsukuba, Ibaraki, 305-8516, Japan
[2] Senior Researcher, ditto

In this paper, the authors present current situation of scour investigation and innovative investigation techniques and monitoring equipments for scour developed by Public Works Research Institute (PWRI).

2. CURRENT INVESTIGATION FOR SCOUR

Scour investigation currently used for bridge foundations is shown in Photos 1 and 2 indicating a primitive technique in a manner using sounding poles or staffs to measure a streambed depth from a footing or a boat above water surface. This technique is not only in poor degree of accuracy, but also a dangerous work by itself. In the case that detailed investigation under water is required a visual inspection by divers is used together as shown in Photo 3. However, the combined method has a problem such that (1) investigations are hard and dangerous if flow velocity is so fast, and (2) they generally take much time and cost.

In order to solve these problems we should develop innovative techniques with safety and readiness for investigating scour condition

3. TECHNIQUES FOR INNOVATIVE SCOUR INVESTIGATION

First, the authors selected some sensors which were highly possible devices to be able to precisely measure the location of streambed as shown in Table 1, and then conducted applicability testings in advance of development of techniques for innovative scour investigation.

The result of applicability testings is shown in Table 2. Based on the result, we chose a fathometer instrument which can surely measure the location of streambed and require no professional knowledge on the interpretation of data collected. As the methods to investigate the location of streambed through sensors we decided to choose the following two techniques:

(1) a technique for wider investigation around piers

(2) a technique for simplified narrower investigation limited to vicinity of piers

With regard to an instrument of moving and holding a sensor, the former is the technique using a radio-controlled boat with a sensor and the latter, on the other hand, is the technique using a sounding rod with a sensor at its edge from a bridge deck.

3.1 Technique using RC boat

This technique consists of hardware and software for data storage and image processing as shown in Figure 1. The radio-controlled boat (hereafter RC boat) is

1.5 m long, 0.8 m wide and 20 kgf weight and is a hydrospace screw type using a gasoline engine (Photo 4).

The digital fathometer instrument and a telemeter which transmits to a receiver mounted near river by radio are on the boat. A laser-type total station is installed at the bank of a river and follows up the location of the RC boat (Photo 5). The data of the water depth and location of the RC boat are input automatically into a personal computer (PC) on which a trail figure usually is mapped out. Consequently, we can measure a wider range around piers.

When the data of the water depth and its location are input there may happen some troubles such as electronic noises due to unknown reasons and/or tracing errors of the RC boat, although these are repairable at an editorial stage. The investigation result shows us precise streambed condition around bridge piers using processing through PC, and the furthermore can draw figures of a two-dimensional contour line and a birds-eye view as shown in Figures 2 and 3.

We can conduct wider investigation of streambed condition around piers and estimate the soundness of bridge foundations against scour based on the location of piers and streambed conditions using these techniques.

3.2 Technique from bridge deck

This technique is to measure through a supersonic sensor mounted on the edge of a sounding rod from pavement of a bridge deck or an inspection scaffold on a bridge inspection vehicle and to investigate a limited area around piers different from RC boat investigation for wide area.

In the case of selecting devices we considered that they should be with a compact and light weight instrument and capability to deal promptly with investigation since the work is conducted from the bridge deck or the inspection scaffold on the bridge inspection vehicle. Furthermore, we tried to find configuration of streambed easily with display of an investigation result on a monitor screen with color image.

A brief introduction of a supersonic sensor (or a color-imaged sonar) which is selected based on the applicability testing is as follows.

Figures 4 and 5 shows an outline of the color-imaged sonar. First, a sonar head attached to the edge of a sounding rod is brought down from the bridge deck or the inspection scaffold on the bridge inspection vehicle until about 1 m under water, and then we can measure through going into a 360-degree roll of the sonar head.

An example of streambed profile displayed on the monitor screen is shown in Photo 6. By reason that the color-imaged sonar can measure one topographic profile only in every measurement, the investigation should be conducted measuring streambed conditions around piers using rotating the sonar around

horizontally in every 30 degrees. If there may be dead angles due to pier's location we should measure with the location of a sonar moving. This system can draw a birds-eye view compiled by the software of image processing for RC boat technique. In the case of focusing on limited area of near pier the color-imaged sonar can collect more condensed data than other techniques.

4. SCOUR MONITORING EQUIPMENT

It becomes possible to precisely investigate scour conditions of streambed around bridge piers using two techniques above. However, these investigation techniques are useful only for normal flow condition and are useless in the case of a rapid current during floods condition causing scour. Furthermore, nobody can measure a maximum scour depth through investigation during normal floods condition since scour holes can be filled back with secondary sediments after floods. On this context, the authors developed another device which can measure degradation of streambed even during floods and also the maximum scour depth eliminated the effect of secondary sediments, and conducted its applicability-proved testing as well.

Figures 6 and 7 show outlines of two techniques indicating investigation manners at the testing as follows:

(a)Ring type
First, a supporting pipe is driven into streambed and then a ring with magnet are attached to the outside of the pipe on the streambed. The ring also can slide to the bottom as the level of streambed degrades downward due to scour. Maximum scour depth can be investigated through measuring a location of the ring using a movable magnet sensor inside the pipe.

(b) Electromagnetic type
A supporting pipe is driven into streambed and then sensors which can perceive the existence of magnet are attached to the inside of the pipe while magnets are arranged outside. If the magnets are destroyed by a flood, the sensor can recognize their location lost. The measured time-depending variation figure indicates the maximum scour depth.

With regard to scour monitoring equipments (Ring type and Electromagnetic type), it is necessary to confirm movability of sensing element, maintainability and reliability since they should be installed under water for a long period. Accordingly, applicability testings in laboratories were first conducted, and then they were installed at in situ bridge piers constructed near the center of stream after small improvements based on the testing. The investigation result on degradation conditions of streambed during flood are shown in Figure 8, which indicate that the progressive condition of the rapid streambed degradation more

prompt than expected and deeply accumulated secondary sediments can be observed.

5. CONCLUDING REMARKS

In this paper, the authors propose several kinds of investigation techniques based on the office survey related to existing technologies and in situ applicability testing in order to develop techniques with safety and readiness for investigating scour conditions around bridge foundations.

All bridges in every country have the possibility of the occurrences of scour damages while there are many countries in which we don't need to pay attention to the effect of major earthquakes in bridge design unlike Japan or America in the world. The authors wish that investigation techniques and monitoring equipments proposed by them are put to practical use and to contribute to the cost-effective operation and maintenance for bridge foundations.

REFERENCES

1. M. Okoshi & J. Fukui, Present state of investigation technique for scouring, The Foundation Engineering & Equipment, pp19-21, vol.29, No.9, 2001.9.
2. Cooperative research report on development of measurement & diagnoses technique for bridge substructures, Public Works Research Institute, No.157, 1997.1.

Photo 1 - Conventional investigation technique for scour from a footing

Photo 2 - Conventional investigation technique for scour from a boat

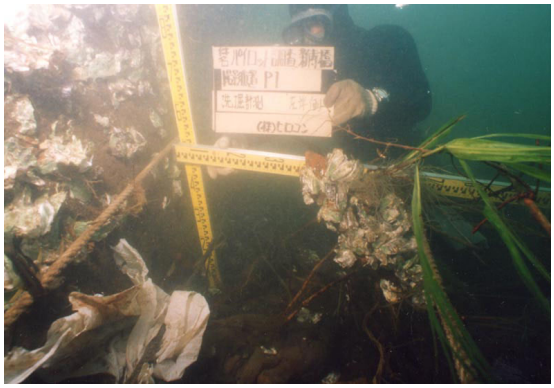

Photo 3 - Scour investigation technique by divers

Photo 4 - Outline of investigation using a RC boat

Photo 5 - Measurement of RC boat's location by total station

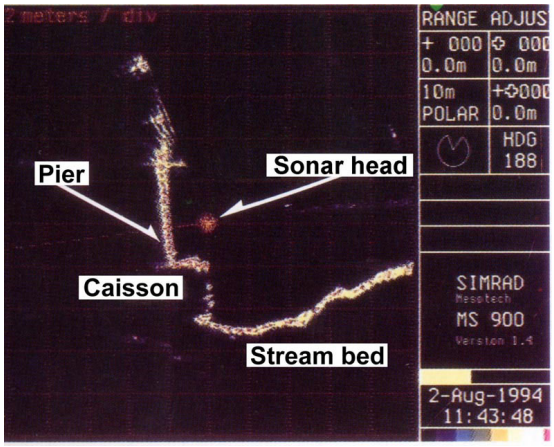

Photo 6 - Streambed profile measured by color-imaged sonar

Table 1 - Conventional Sensors

Principle	Sensor
Supersonic	Fathometer
Acoustic wave	Acoustic exploration
Electromagnetic wave	Underground radar
Non-confrontational	Electric exploration
Elastic wave	Seismic exploration
Resistance	Sounding
Magnetism	Magnetic logging
Light	Underwater camera

Table 2 - Applicability Testing

Sensor	Advantage	Disadvantage
Supersonic	• can measure the distance to streambed immediately. • can repair data destroyed easily	shall be moved because the sensor can measure forward only.
Underwater camera	Visual inspection of structural members underwater and streambed condition	Scope is limited. Result depends on the turbidity of a river.
Acoustic wave	can investigate the secondary sedimentation layer and geological structure.	Energy damping becomes large in the certain river condition.
Elastic wave	(ditto)	(ditto)
Electromagnetic waves	(ditto)	(ditto) Impossibility at a tidal area

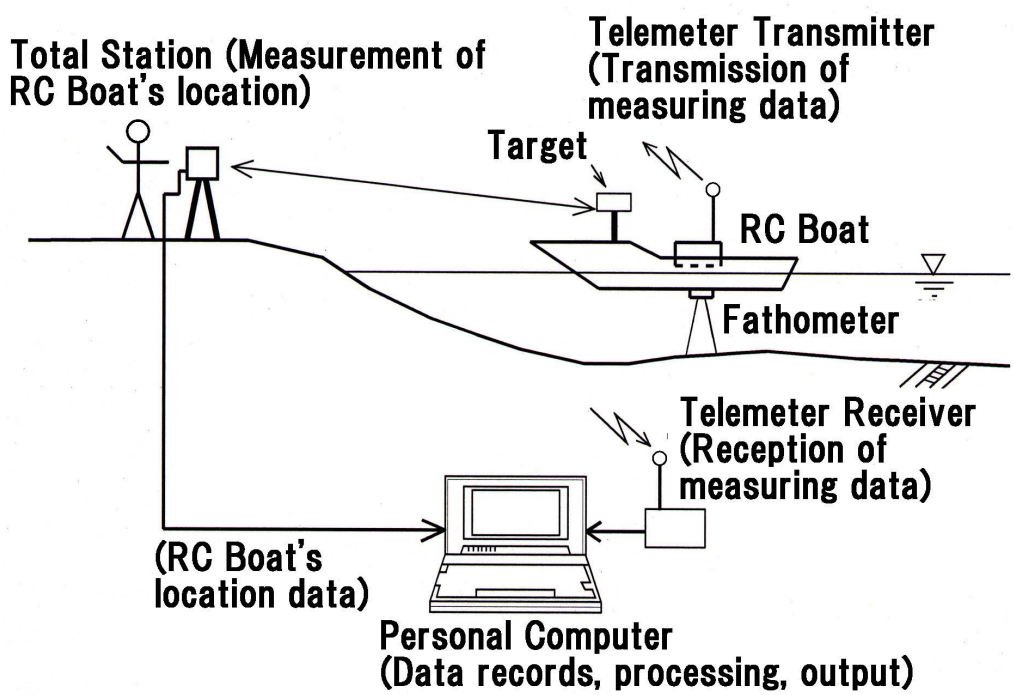

Fig. 1 - Outline of RC boat system

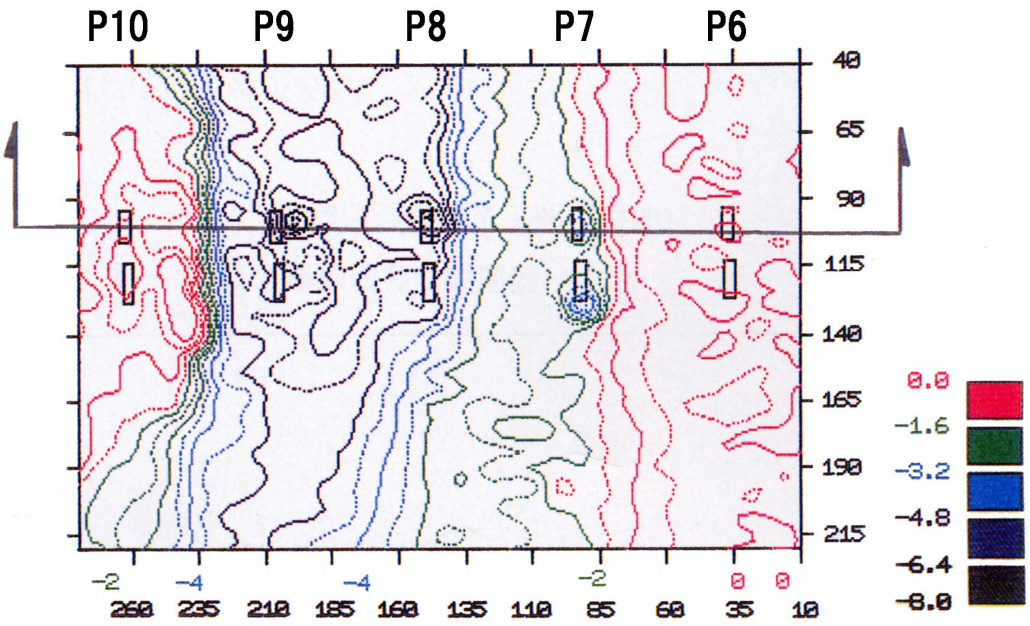

Fig. 2 - Two-dimensional contour line

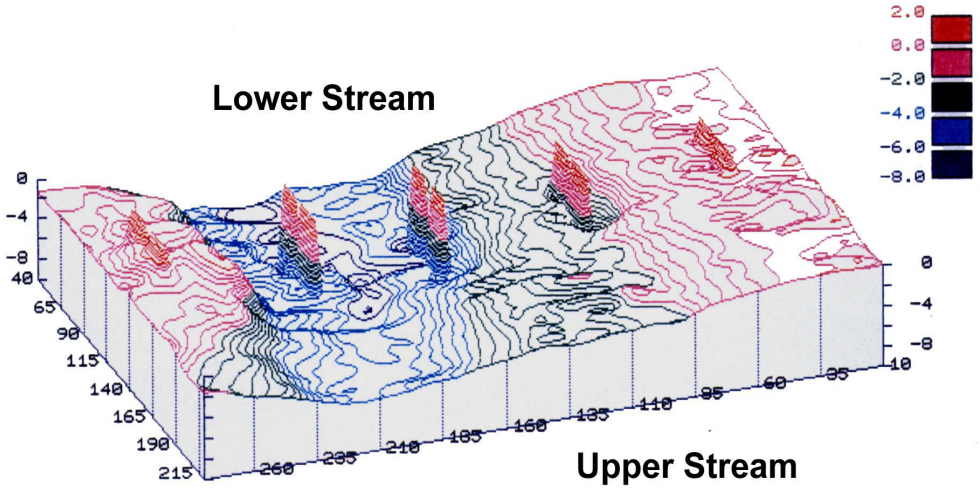

Fig. 3 - Birds-eye view of streambed
(three-dimensional contour line)

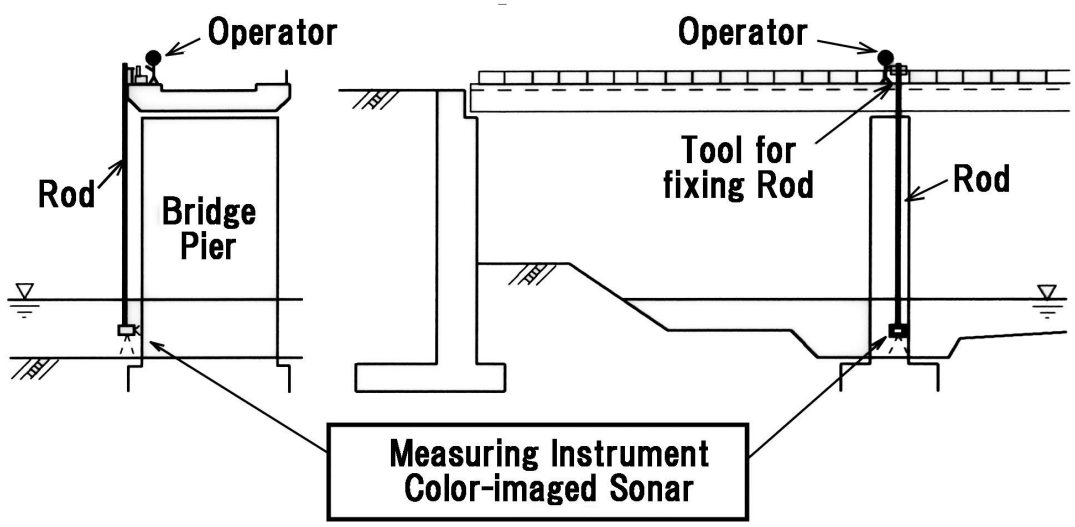

Fig. 4 - Outline of the Color-imaged sonar

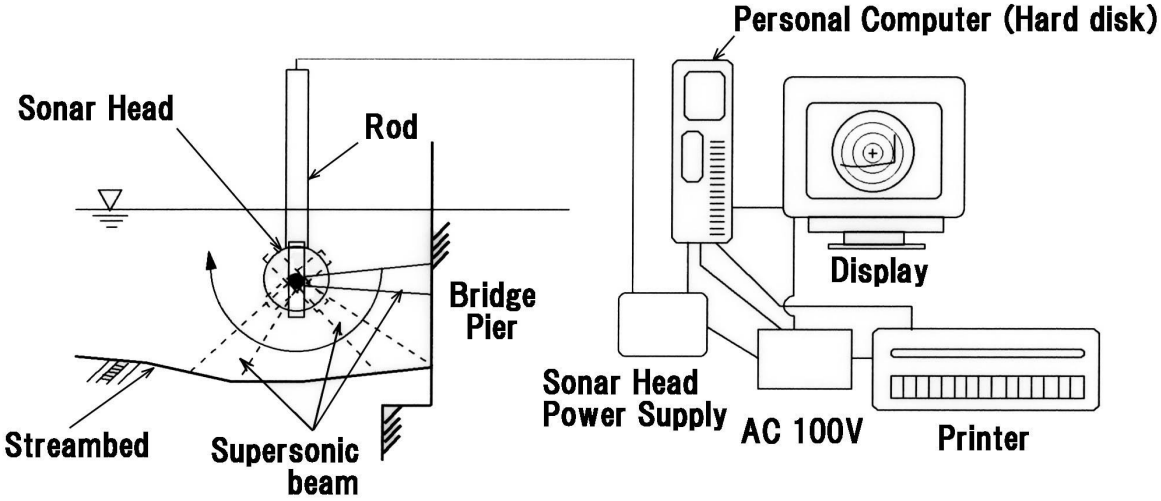

Fig. 5 - Outline of the Color-imaged sonar

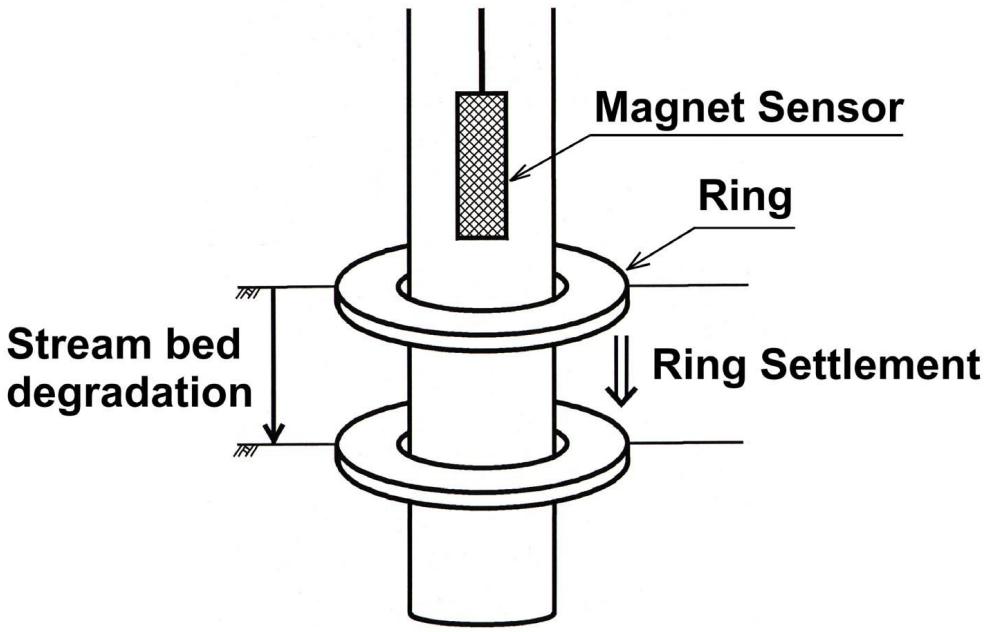

Fig. 6 - Outline of ring type equipment

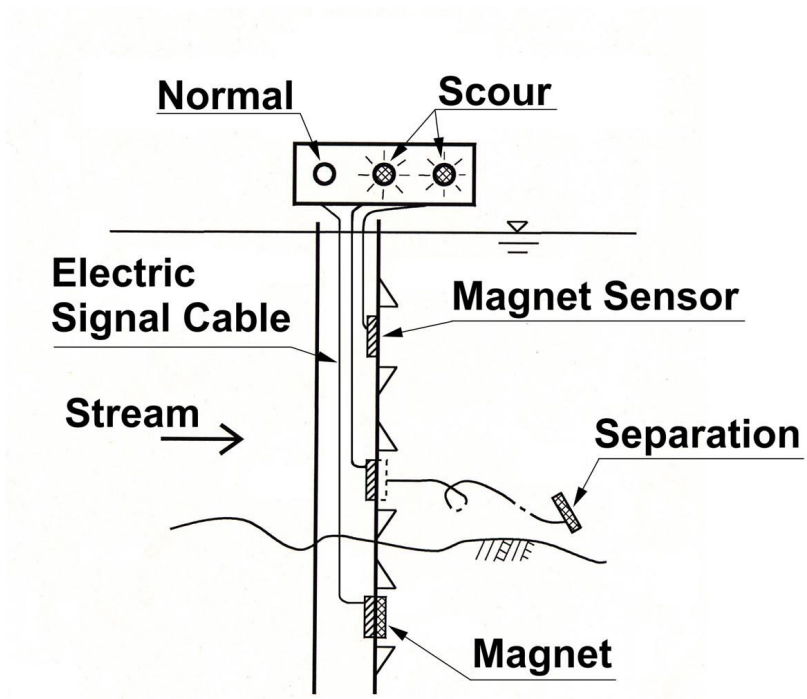

Fig. 7 - Outline of electromagnetic type equipment

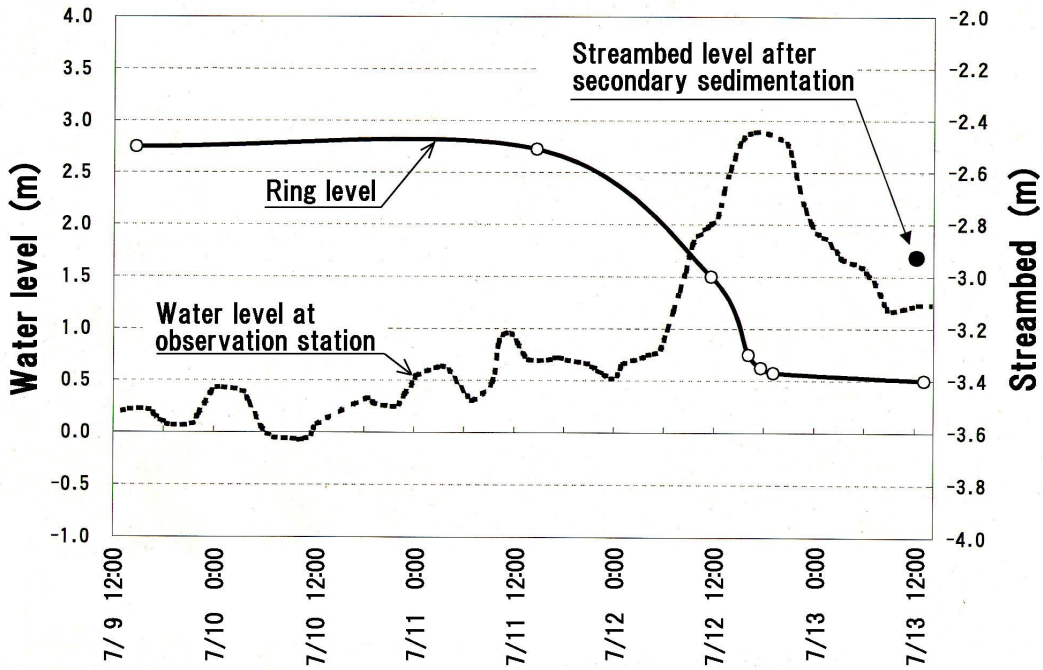

Fig. 8 - Degradation conditions of streambed

Experimental Study on Toe Scour of Seawall Covered with Armor Units Due to Waves

By

Tsutomu Sakakiyama[1] and Ryoichi Kajima[2]

ABSTRACT

Toe scouring in front of a seawall covered with armor units was investigated using large- and small-scale physical model tests with large wave-flume (205m long, 6.0m deep and 3.4m wide) and small one (51m long, 1.2m deep and 0.9m wide). Topography, velocity, surface displacement, pore pressure in the sand layer, and overtopping volume were measured at several time stages. Topography changes were compared between results of large- and small-scale tests using irregular waves to discuss scale effects on the scour. The difference is not significant except just in front of the toe. Topography changes due to irregular and regular waves were investigated at the small-scale tests. The difference of the time averaged velocity between the irregular and regular waves correspond to types of the topography change. A relationship between the topography change and wave overtopping was also investigated. The wave overtopping increases as sand was deposited near the toe.

INTRODUCTION

Scouring near toe of armor layer can cause failure of wave dissipating works and extend to damage of caissons. Both regular wave and irregular wave tests were carried out by Xie (1981). Irie and Nadaoka (1984) classified pattern of topography change due to standing waves into the N-type and L-type scour. Oumeraci (1994) reviewed problems on scour in front of vertical breakwaters. Field investigations on failures of wave-dissipating works were carried out by Gomyoh *et al.* (1996). Three dimensional experiments were performed by Sutherland *et al.* (1999).

Although the resultant profiles of the damaged armor layer were obtained through the above field measurements, relationship between the scouring and driving force was not examined yet. In this work, included was the velocity field near the toe of

---

[1]Senior Researcher, Central Research Institute of Electric Power Industry, 1646 Abiko, Abiko-city, Chiba, 270-1194, Japan (sakaki@criepi.denken.or.jp).
[2] Vice-president, Central Research Service CO. LTD, 2-11-23 Shibakidai, Abiko, Chiba, 270-1176, Japan (ryoichi.kajima@nifty.ne.jp)

wave dissipating work to explain the topography change. Pore pressure in sand layer was also measured to examine a possibility of liquefaction of the sand bed at both small- and large-scale tests. A relationship between the topography change near the toe of armor layer and mean overtopping rate was also investigated.

EXPERIMENTS

Experiments were carried out using a large wave-flume (205m long, 6.0m deep and 3.4m wide) and a small one (51m long, 1.2m deep and 0.9m wide). Fig.1 shows a cross section of experimental set-up in a full-size scale. A scale factor of the large-scale test is 1/22.7 and that of small-scale one 1/60. Armor units placed in front of the caisson were models of 80-t Tetrapod. Back-filling stone and sand were also placed to model reclaimed land. Sheet was placed between them to prevent sand flow-out through the back-filling stones. A bottom slope in front of the structure was 1/40. Sand bed was made from x=-450m to x=100m, where x is the horizontal coordinate defined as shown in Fig.-1. The san bottom from x=-450m offshore was impermeable.

Sand diameters used at both small and large-scale experiments were 0.2mm. Another set of experiments were carried out at small-scale tests using finer sand with 0.16mm diameter. Free surface displacement in front of the structure was measured using capacitance-type wave gages at ten positions on irregular wave tests and at nineteen positions on regular wave tests. Number of waves at one test run of irregular wave was 250. That of regular wave was 30 waves. Tests were repeated with those wave numbers to make less contaminated multi-reflected wave conditions. Horizontal and vertical components of velocity were measured using two electromagnetic current meters. They can provide time histories of velocity induced by wave but not turbulence components.

Wave pressure acting on the caisson was measured at sixteen positions and pore pressure in the sand layer at six positions as shown in Fig.-1.

Topography change was obtained by using two wheel-type depth meters. Profiles of the sand bottom were measured along four lines, every 1.0cm at the large-scale

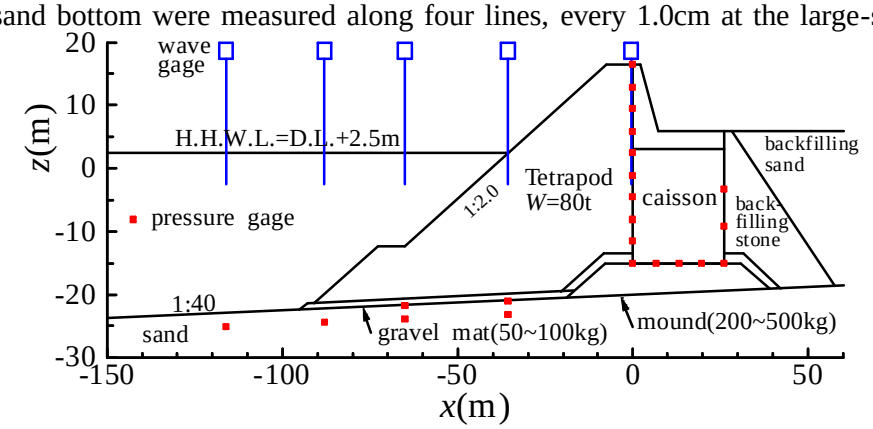

Fig.-1 Cross-section of seawall covered with armor units

tests and every 0.5cm at the small-scale ones. Averaged profile of four profiles was used in the following discussions. Those measurements were done at several time stages, for example, $t/T_{1/3}$=0, 500, 1000, 2000, 3000, 6000, 9000, 12000.

The overtopping volume at the large-scale tests was measured using water depth meter in the tank settled behind the caisson. That at the small-scale test was measured using a tank behind the caisson suspended to four load cells to weigh its weight.

Table 1 shows wave conditions of the full-size, the large-scale test (scale factor λ= 1/22.7) and the small-scale one (λ=1/60). The wave height was 10.3m and 12.8m. The former one is design basic wave height (D.B.W.) taking 100 year as a return period against which the structure should be stable according to a conventional design concept. The latter one has higher wave height than D.B.W., which is applied to confirm durability of the structure against the higher wave than D.B.W. It is named as a functional check wave (F.C.W.) based on the new design concept for very important coastal structure for power plants (Kajima, 1994).

Table 2 shows non-dimensional total time of wave duration for topography measurement. The waves concerned here are design waves for stability of structure. Its return period is 100 years or longer than that. The duration time of wave was at beginning one storm term about 10 hours. But scour near the toe of structure was not observed; therefore the duration time was extended up to 72000 waves (320 hours) at a certain case.

Table-1 Wave conditions

Scale factor λ	D.B.W. $H_{1/3}$(m)	F.C.W. $H_{1/3}$(m)	wave period $T_{1/3}$(s)	water depth h(m)
1.0	10.3	12.8	16.0	22.5
1/22.7	0.452	0.563	3.36	0.991
1/60	0.172	0.213	2.07	0.375

Table 2 Non-dimensional wave duration time $t/T_{1/3}$ (hours in prototype scale)

sand diameter d_{50}(mm)	test scale factor λ=1/22.7		test scale factor λ=1/60	
	D.B.W.	F.C.W.	D.B.W.	F.C.W.
0.20	6000 (26.7)	12000 (53.3)	24000 (106.7)	24000 (106.7)
0.16	no test	No test	72000 (320)	3000 (13.3)

Table 3 Regular wave test for scour protection (hours in prototype scale)

H=0.258m T=2.06s	Scale factor 1/60	
	Without protection	With protection
d_{50} 0.16mm	12000 (53.3)	12000 (53.3)

Table 3 shows non-dimensional total time of wave duration of regular wave tests for scour protections test.

Figures 2 and 3 are pictures taken at the large- and small-scale experiments, respectively. Wheels seen in these pictures are the depth-meters. Both profiles of armor layer and sand bed were measured using the same wheels. The diameter of the wheels was chosen to be able to measure both surfaces of the armor layer and sand bed. Small structure of sand bed, e.g., ripple was not exactly obtained at the large-scale tests which was not an interest of the present work but does at the small-scale tests. As seen in Fig.2, wave overtopping was also measured by collecting water into a tank with a full width of wave flume.

Fig.-2 Large wave flume test (205m long, 3.4m wide and 6.0m deep)

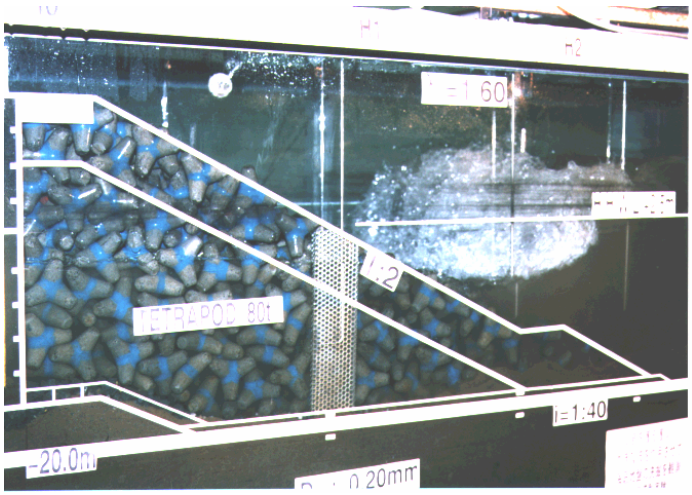

Fig.-3 Laboratory wave flume test (51m long, 0.90m wide and 1.2m deep)

EXPERIMENTAL RESULTS

Comparison of results between large- and small-scale tests

Fig.4 shows comparisons of topography changes between the large- and small-scale tests using irregular waves. Fig.4 (a) shows a comparison measured at $t/T_{1/3}$=6000 under the wave condition of $H_{1/3}$=10.3m and $T_{1/3}$=16s ($H_{1/3}$=0.452m, $T_{1/3}$=3.36s at the large-scale test and $H_{1/3}$=0.172m, $T_{1/3}$=2.07s at the small-scale one) and Fig.4 (b) was at $t/T_{1/3}$=12000 under the wave condition of $H_{1/3}$=12.8m and $T_{1/3}$=16s

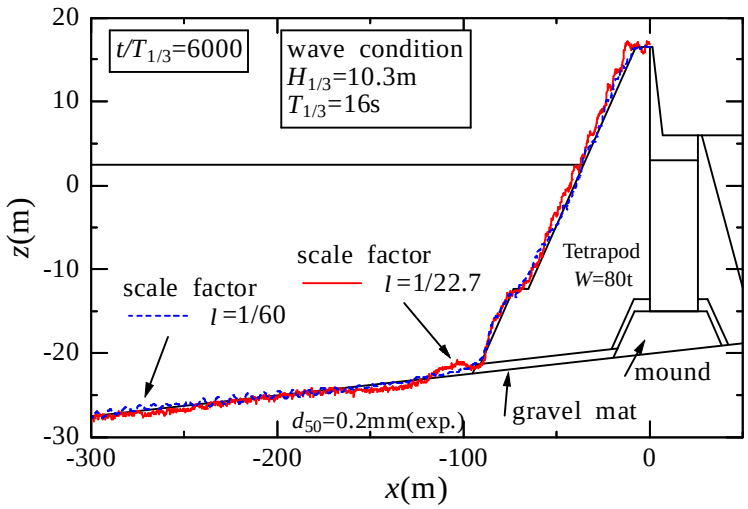

(a) H=10.3m (D.B.W.)

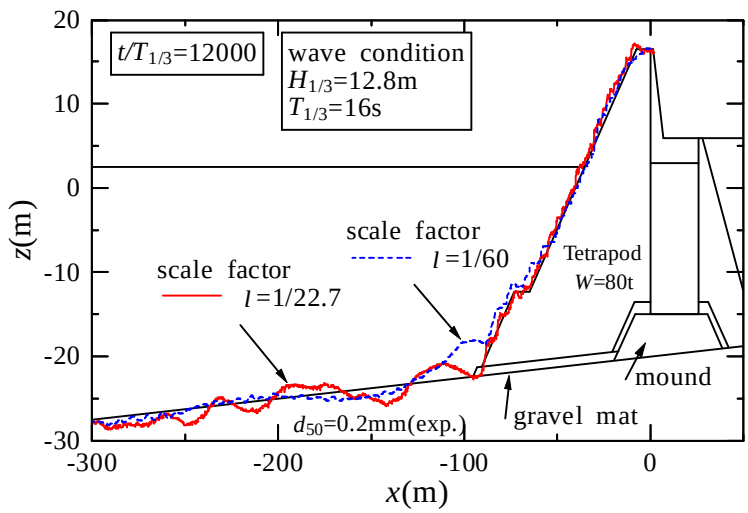

(b) H=12.8m (F.C.W.)

Fig.-4 Comparison of seabed change between large- and small-scale ($H_{1/3}$=0.563m, $T_{1/3}$=3.36s at the large-scale test and $H_{1/3}$=0.213m, $T_{1/3}$=2.07s at the

small-scale one).
It seems that the water depth h=22.5m is relatively deep for sand movement. However, the ratio of the water depth to the wave length is h/L =1/10 (h=22.5m and L=223.5m). That means this condition is shallow water. Reference velocity as progressive wave water particle at seabed level is u_w=3.0m/s in case of wave height H=10.3m. That at large-scale test is 0.68m/s and 0.39m/s at small-scale test.
As seen in Fig.4 (a) difference of the topography is not significant between two scale tests and accretion at the toe was recognized. Sand transport of the large-scale test is bigger than that of the small-scale one. At the small-scale test two–dimensional (long-crested) ripples were generated.
Fig.4 (b) with a higher wave height and longer wave duration time tendency of bed profile change is seen more clearly. Small-scale test result denoted with dashed line shows accretion at the toe and erosion far from there. This is same as lower wave height as shown in Fig.4 (a). The large-scale test in Fig.4 (b) shows a fluctuated bed profile. It is not related with velocity field of a partial standing wave (the wave length L is 223m long).
In those experimental results, scour or erosion is not observed near the toe. At the small-scale experiment, accretion near the toe was clearly observed. It should be noted that sand with the same diameter was used at both scale tests although the Froude law for similarity was applied for scaling. Therefore, at the small-scale test, relatively larger sand was supposed to be used.
Fig.5 shows sand bed near the toe of the structure at the large-scale test under the wave condition $H_{1/3}$=0.563m and $T_{1/3}$=3.36s. As seen lunate ripple was generated very close to and ripples become three-dimensional far from the breakwater.
Fig.6 shows buried Tetrapod at the small steps of the armor layer after removing several ones. Some of Tetrapod settled into the sand bed through gravel mat. Settled depth in to the sand bed is about one-third of the height of Tetrapod.

LABORATRY TESTS

As described above, comparison of the profile changes between the large- and small-scale tests shows that there is not scour at the of the armor layer. We investigated under what condition scour was observed instead of accretion. Using available smaller sand (d_{50}=0.16mm), tests applying both irregular and regular waves were carried out in a laboratory wave flume.

Irregular wave tests

Profile changes of bottom topography and armor layer due to irregular wave were investigated using finer sand ($H_{1/3}$=0.17m, $T_{1/3}$=2.07s, d_{50}=0.16mm) at the small-scale experiment. Fig.7 (a) shows topography changes of sand bed in front of the structure. At this test, wave duration time was 72000 times the significant wave period $T_{1/3,}$ which is longer than 12000 in addition to the use of finer sand compared with the previous experiments.

Fig.5 Large wave flume test (3.4m wide). $H_{1/3}$=0.56m, $T_{1/3}$=3.36s and d_{50}=0.2mm

Fig.6 Several Tetrapods are buried in sand bed under gravel mat.

The sand was transported onshore and accretion occurred at the toe of wave dissipating works. Long-crested ripples are shown in Fig.7 (a). Fig.7 (b) shows the enlarged one of Fig.7 (a) near the wave dissipating work. It was observed that sand was transported as both bed load and suspended load. Especially, suspended load was transported into the rubble mound through the armor layer resulting in quite small transmitted waves behind the caisson. Rubble mound was filled with sand and pressure acting on wall facing back filling stone became quite small.

Gomyoh *et al*. (1996) reported in the filed observations that toe scour casing armor units damage at the water depth from *h*=5.6 up to 19.4m.

We did additional experiments to observe sand transport under the various irregular wave conditions ranging from water depth *h*=2.5m to 16.5m and *H*=6.0m to 12.8m, wave period *T*=12s to 16s in full-size scale. Although the sand movement was investigated in a wide range of such wave conditions, erosion was not confirmed. Direction of the sand transport was onshore. Experimental result on bed profile change by Sutherland *et al.* (1999) also showed deposition in front of a detached breakwater due to a normal incident irregular wave.

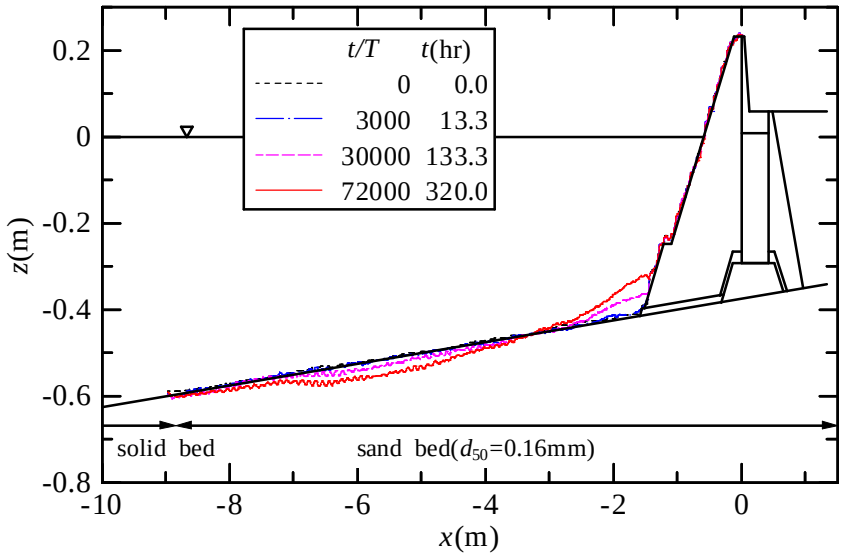

(a) whole region of sand bed

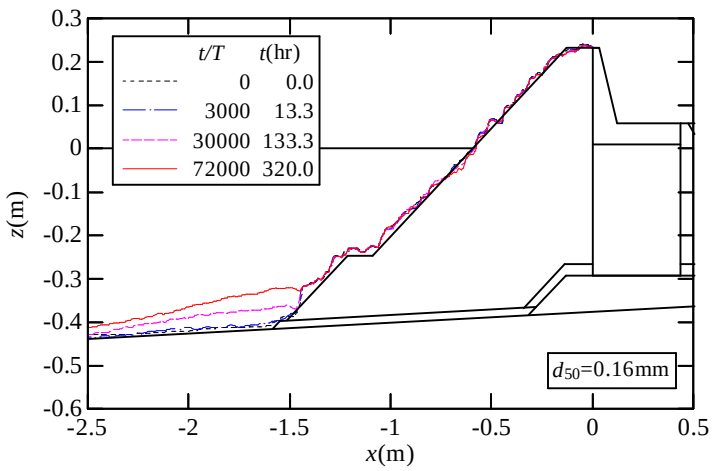

(b) near toe of armor layer

Fig.7 Profile change in case of accretion due to irregular wave

It was reported by Gomyoh *et al*. (1996) that scouring was reproduced using regular waves. Tests using regular waves were performed to investigate countermeasure. Firstly, to reproduce scour at toe of structure, we carried out an experiment using regular wave. Wave conditions are wave height H=0.274m at h=0.375m and T=2.07s (H=16.4m at h=22.5m and T=16s in full scale). Duration time was 12000 waves (53.3 hours in full scale).

Fig.8 (a) shows profile change over whole region of the sand bed and Fig.8 (b) scouring at the toe of armor layer. As seen in Fig.8 (a), sand was transported

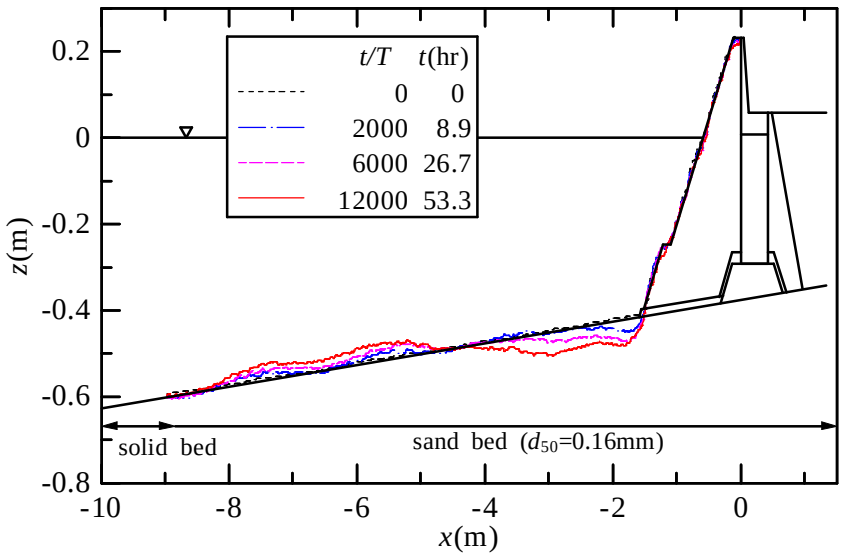

(a) whole region of sand bed

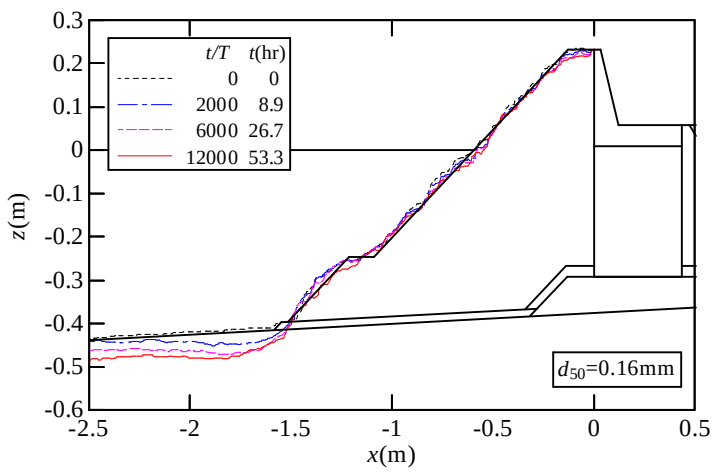

(b) near toe of armor layer

Fig.8 Profile change in case of erosion due to regular wave

offshore and deposited offshore within the region of the sand bed. Maximum water depth of scour is about 0.55m (33m in full size scale). Although there is toe scour, damage of the armor layer was not significant. Crest level of armor layer and its surface near the still water level were decreased. These are not related to the toe scour. The related is visible at an edge of gravel mat where the slight damage of the grave mat resulted in settlement of armor units at the shoulder of toe step.

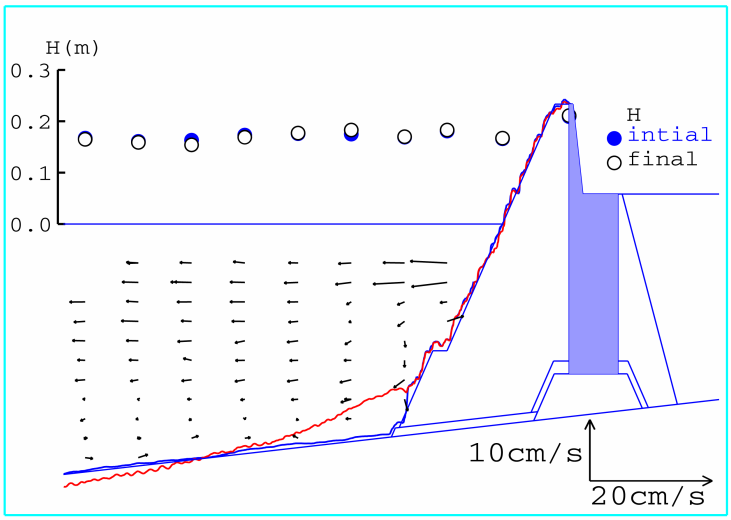

Fig.-9 Time average velocity due to irregular waves causing accession

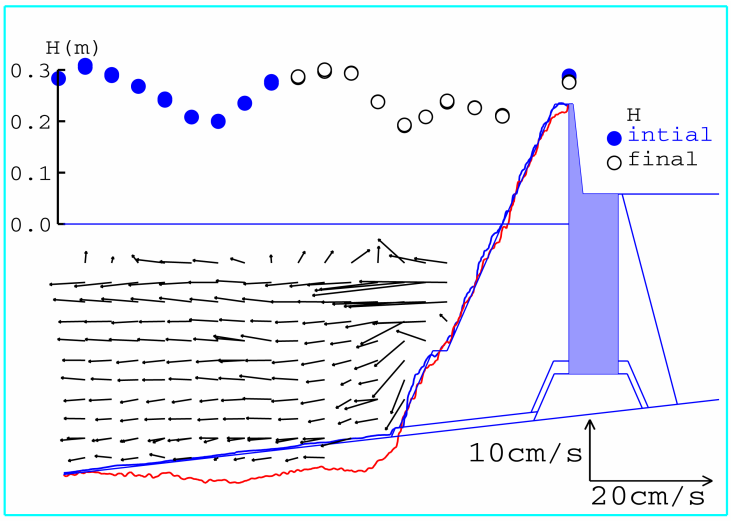

Fig.-10 Time average velocity due to regular wave causing erosion

So far, topography change was mainly discussed in previous work but driving force to understand the mechanism of scour or accretion was not described. In the present work velocity filed was obtained as well as wave height change.

Fig.9 shows the time averaged velocity field of the irregular wave. The direction of time averaged velocity is offshore except that near the bottom. In the case of the regular wave as shown in Fig.10, the direction of the time averaged velocity is offshore over the depth under the wave trough elevation. The difference of the

time averaged velocity between the irregular and regular waves corresponds to types of the bottom profile changes. The latter case is familiar as compensate velocity field for Stokes' drift. Because an electromagnetic current meter is used in the present work, the velocity could not be measured over the wave trough level. Sakakiyama and Liu (2000) obtained turbulent velocity field using LDV as well as mean and time- averaged velocity in front of a breakwater covered with armor units. Wave height change is also shown in those figures. Partial standing wave was seen in case of regular wave but the sand bed topography does not match with the wave height change. In case of irregular wave, wave height is somewhat uniform, or can be described that very weak standing wave occurs. Bed topographies in both cases do not follow the wave height changes.

Countermeasure test using regular wave test

As described previous sections, scour was not reproduced in the tests using irregular waves at both large- and small-scale tests. However, damage of armor layer which was seemed to be due to scour was observed. In this work, countermeasure was also one of topics included.

Significant damage was not observed using regular wave even there is scour at toe of the breakwater. Observed was damage of the gravel mat. Gomyoh *et al.* (1996) also proposed the protection method to toe scouring. They proposed as the following equation:

$$\frac{st}{LH_{1/3}} > 0.04$$

where, s: width of gravel mat, t: thickness of gravel mat, L:wave length and $H_{1/3}$ wave height. The present condition without a protection, $st/LH_{1/3}$=0.0007. To satisfy the above condition, we need roughly 60 times volume (0.04/0.0007=57) for a toe protection. According to the method, width of gravel mat is extended and thickness is increased. However, significant damage is not recognized by the regular test. A half volume required by the above equation is placed and experiment was carried out.

Fig.11 (a) shows the resultant profile change in whole region of sand bed. Fig11 (b) shows comparison of profiles between without and with scour protection. Profiles of sand bed meet but due to gravel mat enlargement, the structure itself does not take damage.

Wave overtopping rate due to bottom topography change

Design of wave overtopping is usually performed considering wave transformation on a uniform slope or fixed bed topography. It is not taken into account of sea bed change, e.g. scouring or accretion near the structure. In the present work, wave overtopping associated with the sand bed change was investigated.

Fig. 12 shows the time histories of the mean overtopping rate due to irregular waves. The mean overtopping rate q was obtained by averaging the collected water volume for 250 waves. At the beginning, the overtopping rate decreases rapidly. It is caused

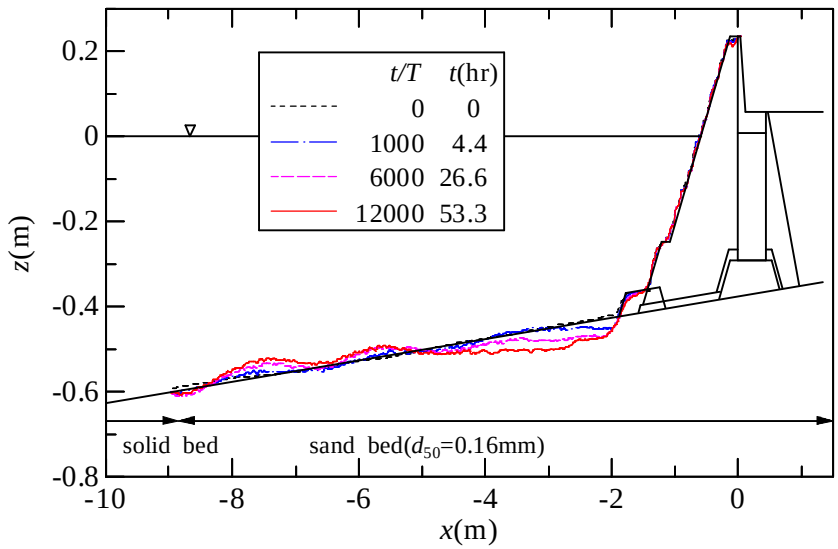

(a) whole region of sand bed

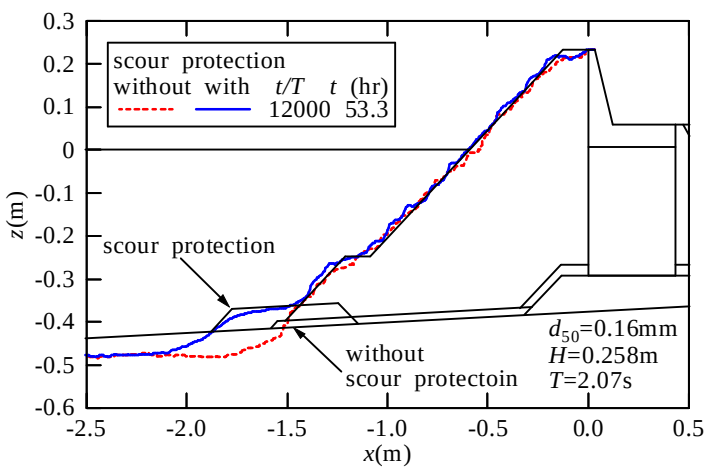

(b) comparison near toe of armor layer

Fig.11 Profile changes with countermeasure

by the settlement of armor units to lower the crest level of the wave dissipating work. After settlement was completed, the overtopping rate increases as the topography changed. The water depth near the toe decreases. Although the accretion occurred near the toe due to the irregular waves and the armor layer is stable, the mean overtopping increases.

On the other hand, Fig.13 shows that the mean overtopping rate decreases due to the toe scouring. In this case, regular waves applied. However, if there is scour due to irregular waves, the same situation is true. This is not serious problem except that

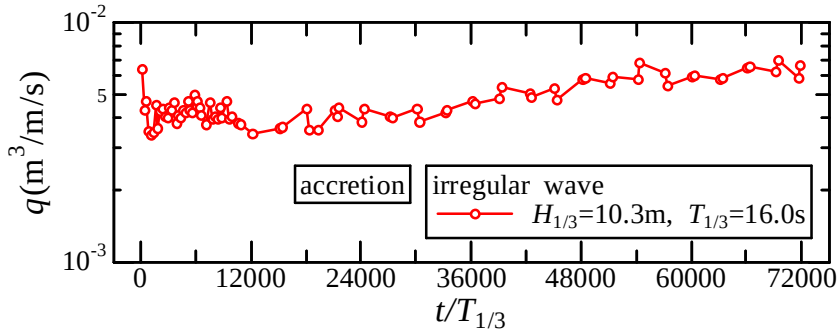

Fig.12 Overtopping rate change due to toe scouring by irregular wave

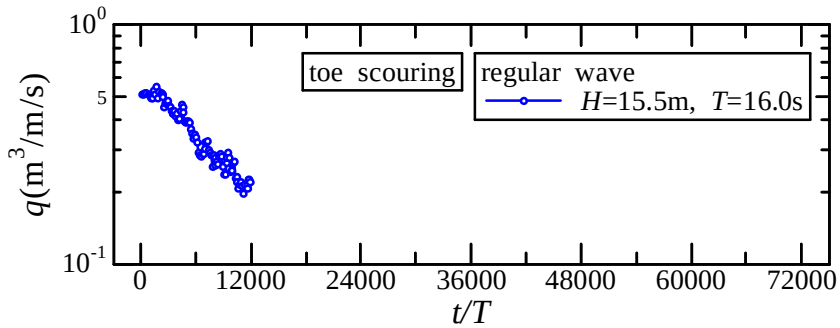

Fig.13 Overtopping rate change due to accretion at toe by regular wave

scour causes settlement of armor units. The former situation is dangerous. It is noted that the overtopping rate can increase due to the topography change by applying irregular waves even when the armor units are stable.

Pour pressure

Settlement of armor units at toe of breakwater is caused by scouring and/or wave-induced liquefaction. Pore pressure was measured at six positions in sand bed at both large- and small-scale tests.

Fig.14 shows the time histories of pore pressure in sand bed obtained at the small-scale test (z=-25.2m in full scale) and free surface displacement at the same position (x=-116m in full scale). Figures 15 and 16 are those in sand bed under gravel mat obtained at small- and large-scale tests, respectively. As shown in Fig.14, pore pressure in the sand bed follows the free surface displacement compared with those in Figures 15 and 16. It means that the pore pressure under the gravel mat was dissipated. The settlement of armor units into sand bed as shown in Fig.6 is not due to the liquefaction.

Comparison between Fig.15 and Fig.16 shows that dissipation of pore pressure of the large-scale test is significant compared with that of the small-scale one. The same sand was used in both experiments. Therefore, the sand is relatively larger at the small-scale test than the large-scale test. It is hard to reproduce liquefaction in a

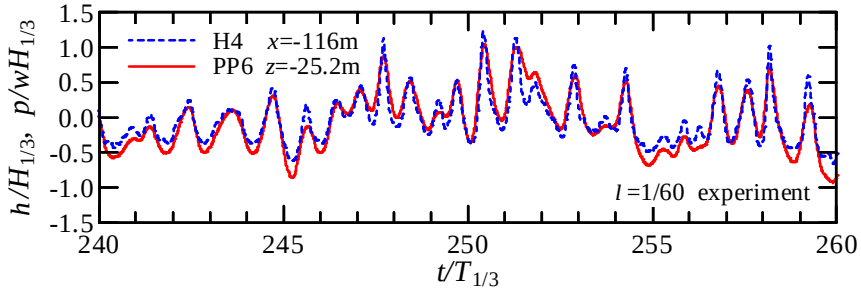

Fig.14 Free surface displacement and pour pressure in sand bed, λ=1/60

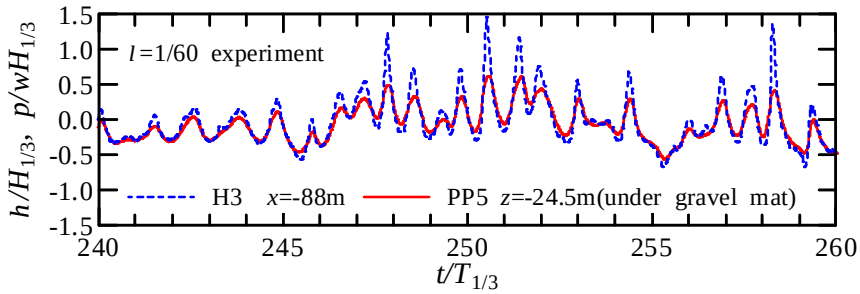

Fig.15 Free surface displacement and pour pressure in sand bed under gravel mat, λ=1/60

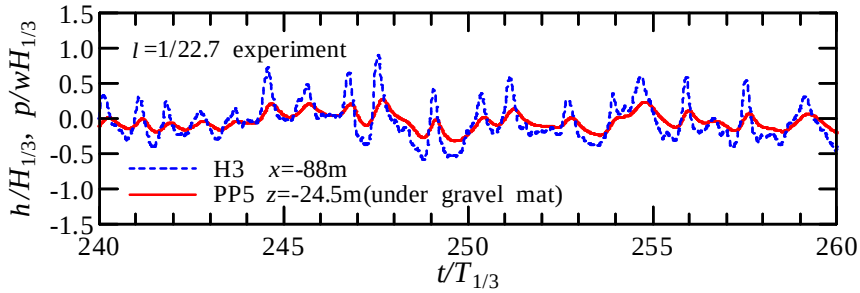

Fig.16 Free surface displacement and pour pressure in sand bed under gravel mat, λ=1/22.7

small-scale test. Phase-lag between the free surface and the pore pressure is visible in the large-scale test but not in the small-scale one. It means that using the sand with same diameter works as coarser sand in the small-scale test.

Fig.17 shows moving-averaged pore pressure at the last stage of the wave action to investigate change of excessive pore pressure. If the excessive pore pressure increases, there is a possibility of liquefaction of the sand bed. However, it is not confirmed from the results of Fig.17 in both small- and large-scale tests.

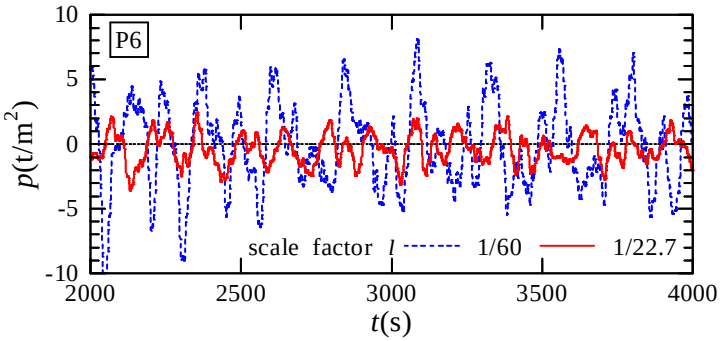

Fig.17 Moving-averaged pour pressure in sand bed

CONCLUSIONS

The followings are main results obtained in this work.

1) Large- and small-scale experiments on sand bed change near toe of armor layer was carried out under irregular wave conditions. Scour was not observed in both experiments.

2) Under various wave conditions of irregular waves, scour near toe was not confirmed. Under regular wave condition, there is scour. The time-averaged velocity fields of irregular and regular wave correspond to the sand transport resulting in scour and accretion.

3) Stability of the armor units covering the caisson against the toe scouring was maintained if toe scour is protected. Gravel mat works well to protect sand out-lift through rubble mound.

4) Wave overtopping change related to topography change in front of structure was investigated. The overtopping increases due to accretion and it decreases due to scour.

REFERENCES

Gomyoh, M., K. Sakai, T. Takayama, K. Suzuki and S. Takahashi (1996): Field investigations on wave-dissipating concrete blocks covering vertical wall breakwater, 25-th ICCE, pp.1652-1664.

Irie, I and K.Naoka (1984): Laboratory reproduction of seabed scour in front of breakwaters, Proceedings of International Conference of Coastal Engineering, ASCE, pp.1715-1731.

Kajima, R.(1994): A new method of structurally resistive design of very important seawalls against wave action, Proceedings of international workshop on Wave barriers in deepwater, Port and Harbour Research Institute, pp.518-536.

Oumeraci, H.(1994): Scour in front of vertical breakwaters -Review of problems-, Proceedings of International Workshop on Wave Barriers in Deepwater, Port and Harbour Research Institute, pp.281-307.

Sakakiyama, T. and P.L.-F. Liu (2000): Laboratory experiments for wave motion and turbulence flows in front of a breakwater, Coastal Engineering, 44, pp.117-139.
Sutherland, J., R.J.S. Whitehouse and B. Chapman (1999): Scour and deposition around a detached rubble mound breakwaters, Proceedings of International Conference Coastal Structure '99, pp.897-904.

Scour Around Rubble-Mound Breakwater Head of Cheju Outer Port

By

Hyoseob Kim[1], Byung Chul Oh[2], Byung-Soon Jung[3], Suk Zun Youn[3]

ABSTRACT

Scour due to waves and wave-driven current around two breakwater heads at Cheju Harbour, Korea was described in this paper. The scour at the site is believed to be mainly caused by waves. The scour at the head of the West Breakwater of the Outer Port was predicted by two numerical model systems, a two-dimensional, and one-dimensional horizontal model systems. The model experiment suggested that an additional step is needed to prevent scour near the breakwater foot for a typical storm wave condition at the site.

INTRODUCTION

Scour was frequently reported around breakwater heads over the world. When the scour develops, it threatens the stability of the main structure bodies, especially for rubble-mound structures. The main causes of the scour can be waves, wave-driven currents, or tidal currents. This paper concerns the scour due to waves and wave-driven currents. Even if we take the main driving forces as waves, and wave-induced currents only, inherent process of the scour seems complicated, since it is linked with bed shear stress, bed form, and pore pressure. Therefore, it is recommended to use numerical models to predict the scour due to waves and wave induced current.

Cheju Inner Port was built on the north coast of Cheju Island. To enlarge its capacity a development scheme was planned at the port. The scheme is basically attaching another port, called Outer Port, to the east side of the existing Inner Port.

Around the breakwater heads the waves are concentrated, and wave-breaking becomes more violent than at other straight parts. However, the scour cannot

[1] Dept. of Civil & Env. Engineering, Kookmin Univ., 861-1, Chungnung-Dong, Sungbook-Goo, Seoul, 136-702, Korea, hkim@kookmin.ac.kr
[2] Korea Ocean Research & Development Institute, Ansan, Korea
[3] Dept. of Civil & Env. Engineering, Kookmin Univ., 861-1, Chungnung-Dong, Sungbook-Goo, Seoul, 136-702, Korea

happen unless any transport of sediment is enabled. The wave-driven currents or tidal currents can transport the disturbed sediment particles. The head of the west breakwater of the Inner Port was built at elevation of -11.2 m with reference to the mean sea level, while the head of the west breakwater of the Outer Port will be built at elevation of -22 m. Around the Cheju Ports the wave heights of the NE, NW waves are relatively strong. The significant design waves in the 2 directions are 4.7 m, 6.0 m, respectively, and the wave periods of the 2 design waves are 9.0 s, 12.0 s, respectively. The mean tidal range at the site is about 1.4 m, and the mean spring tidal range is about 2.0 m. The maximum speed of the tidal current outside the port is about 20 cm/s. The effect of the tidal current was not studied in this paper. The bed material at the site is mainly sand, and silt. The median diameter of the sediment at the site varies between 0.016 and 0.406 mm depending on the water depth.

Scour has developed around the head of the west breakwater of the Inner Port since it was built in 1994. The scour hole is about 2 m deep at the moment. The scour hole shape was measured by a video camera, and the measurements are under analysis, see Fig. 2. The tetrapods are inserted into the sea bed. The scour may develop further when extreme wave conditions attack. The analysis about the stability of the rubble-mound foundation itself of the west breakwater of the Inner Port is beyond the scope of the present work. A development scheme was recently organized by the Korean Government to enlarge the capacity of the Cheju Inner Port. It is the time to diagnose the possibility of the scour around the new breakwater to be built in the near future at this design stage. Numerical techniques for prediction of scour improved rapidly in recent years. A numerical model system, KU-BATH-01 was developed in 2001 by the coastal research group at Kookmin University, Seoul, Korea. The system considers wave, wave-driven current, steady or tidal current, and final scour around near-shore or submerged structures. The model system was verified at Chukpyon site, Korea (Kim, 1993), and used to predict bathymetric changes at several coastal sites in Korea, the United Kingdom, and Portugal (Kim et al., 2002; O'Connor et al., 1998; Kim et al., 2000). The governing equations, and other details of the two model systems will be described in the following sections.

PLAN NUMERICAL MODEL SYSTEM

The plan numerical model system is composed of 3 modules; wave module (KU-IWPH-02), wave-driven current module (KU-WIFLOW-01), and sediment transport module (KU-SEDTRAN-01). The wave module solves Copeland's (1985) intra-wave-period, split, hyperbolic, mild-slope wave equations. The module includes a sponge technique for treatment of absorbing boundary condition (Kim, 1999). A simple breaking criteria was adopted for the wave module, see Galvin (1972). The variables of the wave module were defined either

on grid centres or on grid border lines.

The wave-driven current module of the model system solves typical non-linear, depth-integrated, horizontal, two-dimensional, long wave equations in two horizontal directions. The dependent variables of the current module are also defined either on grid centers or on the grid border lines.

The governing equation of motion in the x direction is (Copeland, 1985):

$$\frac{\partial Ud}{\partial t}+\frac{\partial}{\partial x}dU^2+\frac{\partial}{\partial y}dUV=-\frac{1}{\rho}(\frac{\partial S_{xx}}{\partial x}+\frac{\partial S_{yx}}{\partial y})+gd\frac{\partial \eta}{\partial x}+\frac{\partial}{\partial x}[dK_x\frac{\partial U}{\partial x}]+\frac{\partial}{\partial y}[dK_y\frac{\partial U}{\partial y}]-\frac{1}{\rho}\overline{\tau_{b,x}}$$

where

$$S_{xx}=\overline{Q_x^2\Omega^2}\cdot A-\overline{[\frac{\partial}{\partial x}(Q_x\Omega)+\frac{\partial}{\partial y}(Q_y\Omega)]^2B}$$
$$+\overline{\frac{\partial}{\partial x}\{Q_x\Omega[\frac{\partial}{\partial x}(Q_x\Omega)+\frac{\partial}{\partial y}(Q_y\Omega)]D\}}+\overline{\frac{\partial}{\partial y}\{Q_y\Omega[\frac{\partial}{\partial x}(Q_x\Omega)+\frac{\partial}{\partial y}(Q_y\Omega)]D\}}$$
$$+\frac{1}{2}\rho g\overline{\eta^2}$$
$$S_{xy}=\overline{\Omega_x\Omega_y}\cdot\Omega^2\cdot A$$
$$A=\frac{\rho k}{4\sinh^2 kh}[\sinh 2kh+2kh]$$
$$B=\frac{\rho}{4k\sinh^2 kh}[\sinh 2kh-2kh]$$
$$D=\frac{\rho k}{4\sinh^2 kh}[\frac{1}{2kh}\sinh 2kh-\cosh 2kh]$$

where t = time, x = cartesian horizontal coordinate, y = cartesian horizontal coordinate perpendicular to axis, U = depth-mean velocity in the direction, V = depth-mean velocity in the direction, d = total depth, ρ = fluid density, g = acceleration due to gravity, S_{xx} = normal radiation stress in the direction, S_{yx} = tangential radiation stress in the direction, K_x = dispersion coefficient in the direction, K_y = dispersion coefficient in the direction, $\tau_{b,x}$ = bottom shear stress, Q_x = fluid flux in the direction, Q_y = fluid flux in the direction, Ω = wave celerity over group wave celerity, Ω_x,Ω_y = defined on gid border lines, h = water depth, k = wave number, η = water surface level from still water level, and $\bar{}$ (overbar) = wave-period average.

The sediment transport module was proposed by Kim (1993). The module solves the bed load, and three-dimensional suspended sediment transport. The finite difference forms for the terms in the above equations were proposed by Kim

(1993), and Kim et al. (2002).

LINE NUMERICAL MODEL SYSTEM

The line scour model system, KU-SCOUR-01, is composed of two modules, the wave module and erosion module. Firstly, short period waves propagate from offshore to on-shore or the breakwater slope. The waves are reflected at the wall with the slope of 1:1.5. The reflection of the waves is quite complicated due to the non-vertical wall slope. The waves are not only nonlinearly transformed, but also broken depending on the wave and structural conditions. In the present work wave breaking was considered, but the nonlinear wave transformation was ignored. In order to obtain precise information of the superimposed waves of incident and reflected waves, Copeland's (1985) time-dependent mild-slope wave equation system derived from Berkhoff's (1972) elliptic mild-slope equation was adopted for the governing equation of the present model. Suh and Lee (1995) suggested that even steeper slope than 1:3 can be modelled by the mild-slope equation with tolerable errors.

The governing equations of the wave model are as follows:

$$\nabla Q + \frac{c_g}{c}\frac{\partial \eta}{\partial t} = 0$$

$$\frac{\partial Q}{\partial t} + c c_g \nabla \eta = 0$$

where t is time, Q is the flux, c is the phase velocity, c_g is the group velocity, and η is the water level disturbance from the mean sea level.

At the open boundary, a radiation condition was used to allow outgoing waves to go out through the boundary line using the following equation:

$$\frac{\partial Q}{\partial t} = \pm c \frac{\partial Q}{\partial x}$$

where the sign is dependent on the direction of the open boundary. At the land boundary, the zero-flux condition ($Q = 0$) was used. The governing equations were transformed to finite difference equations. A first order accurate explicit scheme (time forward, space centred) was adopted for the equations as was done by Copeland (1985).

Secondly, when the wave information is obtained at every calculation point by the above method, the bathymetric change can be calculated by using a sediment entrainment model. The seabed entrainment was modeled by modifying a typical empirical equation suggested by Nielsen (1992) as:

$$E = C(\tau_b - \tau_{b,cri})^n$$

where E is the entrainment rate of the seabed material to the water column due to seabed erosion, τ_b is the instantaneous bed shear stress, $\tau_{b,cri}$ is the critical bed shear stress for erosion, and C and n are empirical coefficients for a specific bed material. A sufficiently small number was assigned to the empirical coefficient C for stability of computation, and 1.5 was assigned to n. The instantaneous seabed shear stress (τ) can be calculated from the following equation:

$$\tau_b = \frac{1}{2}\rho f_w U_\infty^2$$

where ρ is the fluid density, f_w is the wave friction coefficient, and U_∞ is the instantaneous seabed wave orbital velocity at the top of the wave boundary layer near the bed. The wave friction coefficient was obtained by the equation proposed by Kim (1993):

$$f_w = 0.000684 \exp\left(7.80\left(\frac{A}{Z_0}\right)^{-0.106}\right)$$

where A is the excursion length amplitude, and Z_0 is the bed roughness over 30. The calculations of the wave transformation and seabed profile evolution are interactively proceeded until the final solution is obtained.

MODEL RESULTS

The breakwater head of the Outer Port will have the geometry in Fig. 3. The first tentative section of the breakwater is shown in Fig. 4.

Firstly, the plan model system was applied to an incident wave condition. The significant wave height of the incident wave was 4.0 m, mean wave period was 9.0 s, and wave direction was parallel to the breakwater (close to NE). The computed wave-driven current field is shown in Fig. 5. The wave-driven current develops around the structure slope due to wave breaking. The computed wave-driven current away from the structure looks negligible. The computed erosion or deposition per hour for the given wave condition is shown in Fig. 6. The computed erosion on the rubble-mound slope does not mean true erosion, since the bed material was assumed to be uniform during computation. The scour extends from the foot of the breakwater to about 6 m away.

Then, the plan model system was applied to the second wave condition. The computed wave-driven current field for the second wave direction is shown in Fig. 7. The significant wave height was 6.0 m, mean wave period was 12.0 s, and the wave direction was normal to the breakwater centre line. The computed wave-driven current is strong over the structure slope compared to other areas in the computation domain. The computed scour or deposition rate per hour is shown in

Fig. 8. The scour happens, from the structure foot to about 10 m outside from the structure.

The second line numerical model system examines the possibility of scour due to wave reflection. The computed possible largest scour hole is shown in Fig. 9. The scour hole develops as the computation time goes by. Eventually, the scour hole reaches the final stage, and does not grow any more after that. The computed scour depth for the given profile is about 1.4 m. When a step of 7 m width is added to the original profile, the scour hole does not appear for the same wave condition, see Fig. 10. It should be noted that the waves at the site may vary from time to time, so that the additional step could not perfectly protect scour.

CONCLUSIONS

The present plan model system results seem to describe the scour around the breakwater head well. The model results show that the waves rapidly transform at the breakwater head, and quite strong wave-induced currents develop around the head, and the scour also develops near the structure foot. The computed wave-induced current around the head was strong enough to erode the sea bed material. The system could be used for prediction of scours at other similar structures caused by waves and wave-driven current. The computation results present the area boundary which needs protection scheme. The one-dimensional horizontal model results for wave reflection also suggest that a protection scheme is required in front of the breakwater. A step of 7 m width will perform the protection function well according to the model results.

ACKNOWLEDGEMENT

The present work was supported by KOSEF under contract no. I-99-005.

REFERENCES

1. Copeland, G.J.M., 1985. A practical alternative to the “mild-slope” wave equation. Coastal Engineering, Vol. 9, pp. 125-149.
2. Kim, H., 1993. Three-dimensional sediment transport model. Ph.D. Thesis, The University of Liverpool, Liverpool, UK.
3. Moon, Y., Lee, S. and Kim, H., 1998. Comparison of absorption coefficients of sponge layers. Annual Meeting of Korea Water Resources Association, Muju, Korea.
4. Kim, H., Oh, B.C. and Jung, B.S., 2002. Numerical model system KU-IWPH-02 for wave-driven current with wave reflection. Proceeding of China-Korea Joint Seminar on Coastal Sediment Transport 2002, Quindao, China.

5. O'Connor, B.A. et al., 1998. INDIA Project, Third Marine Science and Technology Conference, (Eds) K.-G. Barthel et al., EU (Brussels, 1998), pp. 601-609.
6. Kim, H., Kim, T.H. and O'Connor, B.A., 2000. Application of WIBATH-00 to wave-induced currents with tide at Algarve, Portugal. HYDROSOFT 2000, Lisbon, Portugal, Vol. 8, pp. 227-239.
7. Suh, K.D. and Lee, C., 1995. Time-dependent wave equations on bottom with substantial depth variation. Proc. Annual Meeting Korean Society of Coastal and Ocean Engrs., Sung Kyun Kwan Univ. pp. 75-80 (in Korean)
8. Berkhoff, J.C.W., 1972. Computation of combined refraction-diffraction. ICCE, ASCE, pp. 471-490
9. Galvin, C.J., 1972. Wave breaking in shallow water, Waves on beaches and resulting sediment transport, Academic Press Inc., 413-455
10. Nielsen, P., 1992. Coastal bottom boundary layers and sediment transport., World Scientific

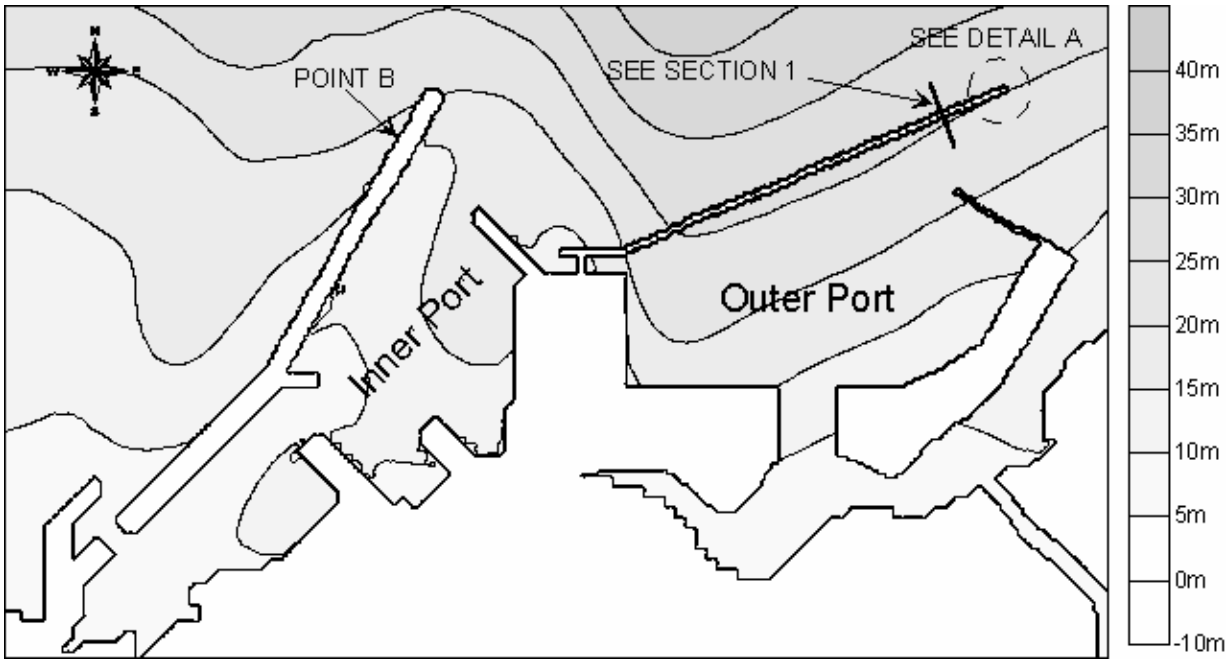

Fig. 1 - Study site bathymetry

Fig. 2 - Video-captured scour hole

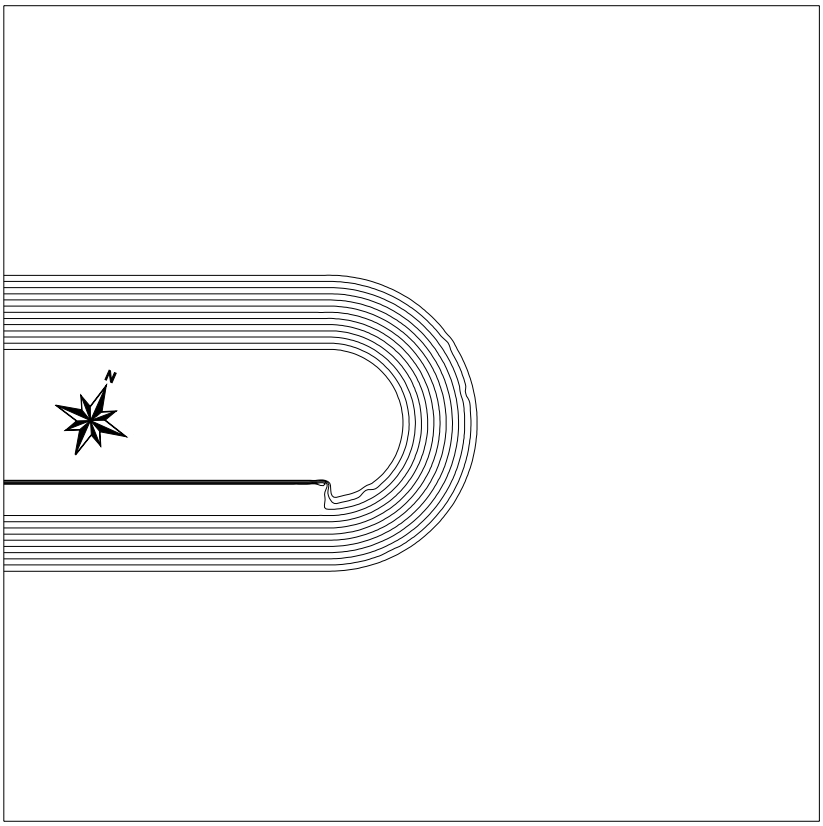

Fig. 3 - West Breakwater head geometry of Cheju Outer Port

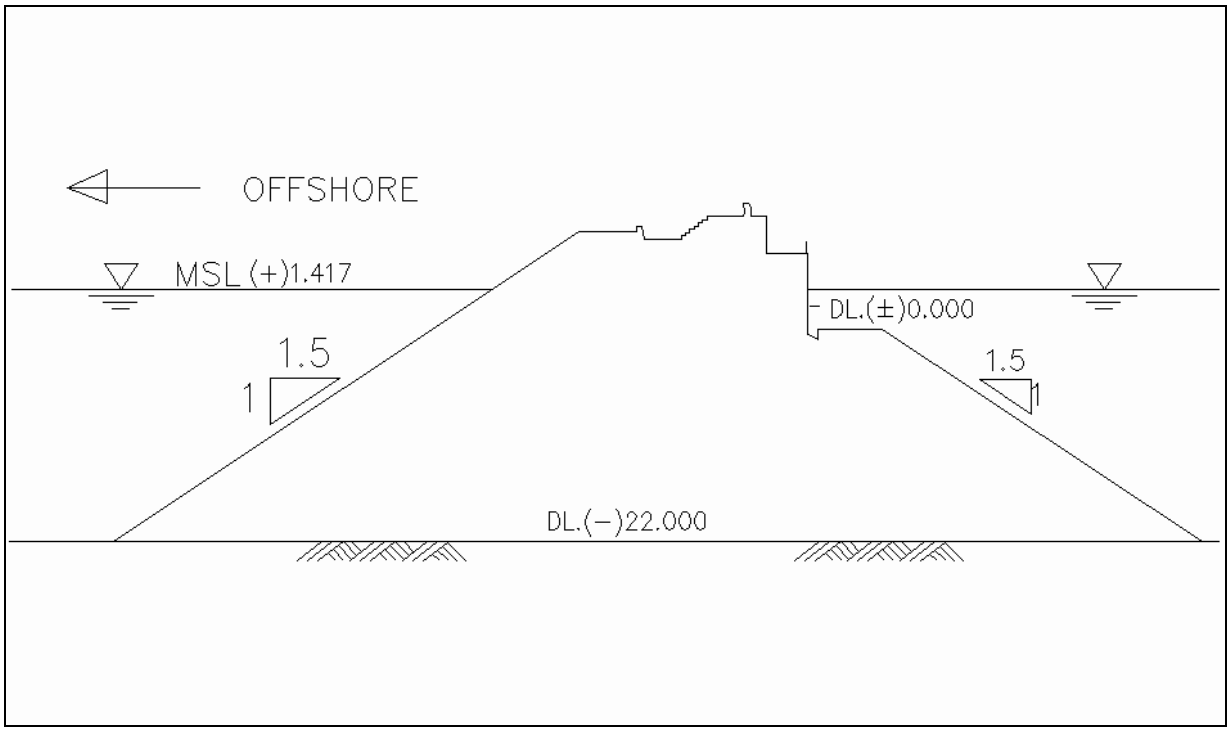

Fig. 4 – Section of West Breakwater of Cheju Outer Port

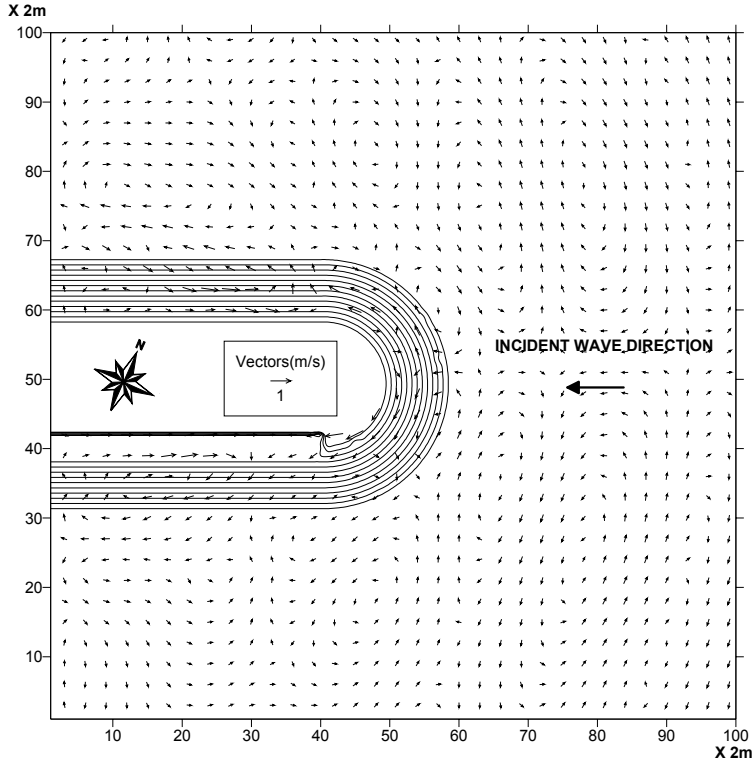

Fig. 5 - Computed wave-driven current for NE wave

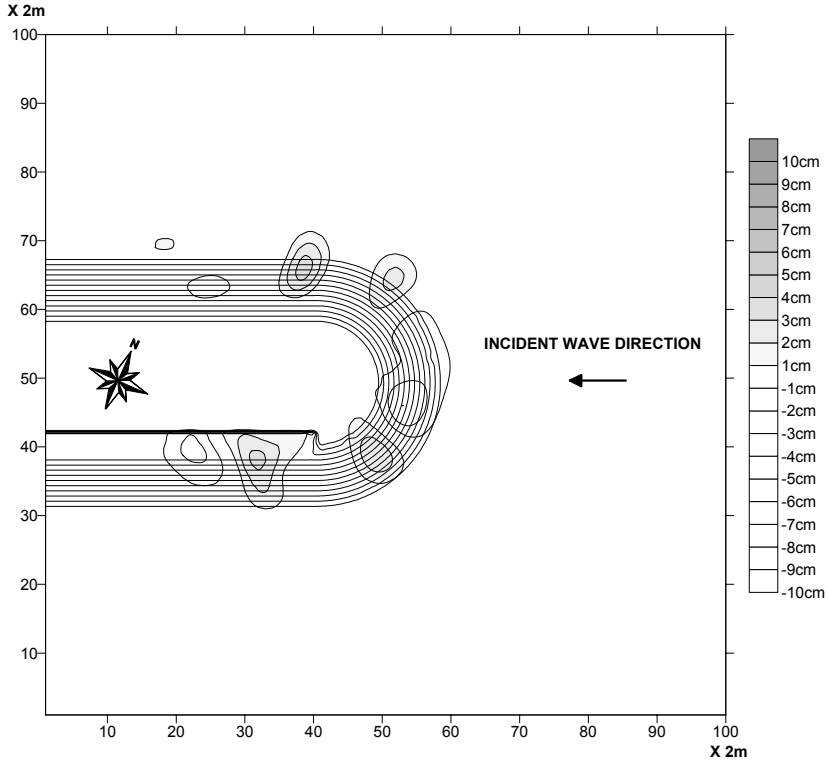

Fig. 6 - Computed scour depth contours for NE wave

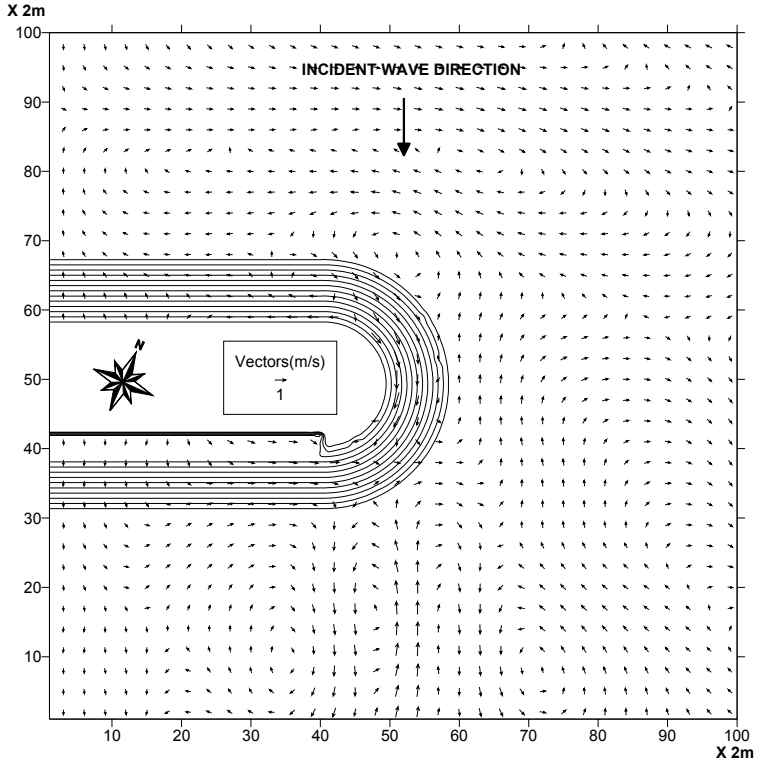

Fig. 7 - Computed wave-driven current for NW wave

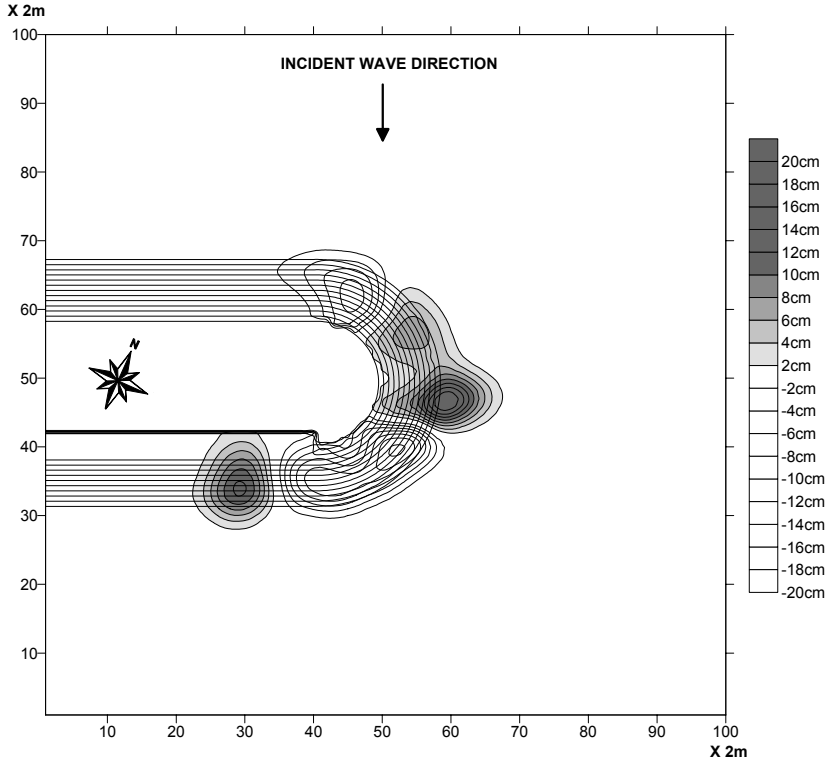

Fig. 8 - Computed scour depth contours for NW wave

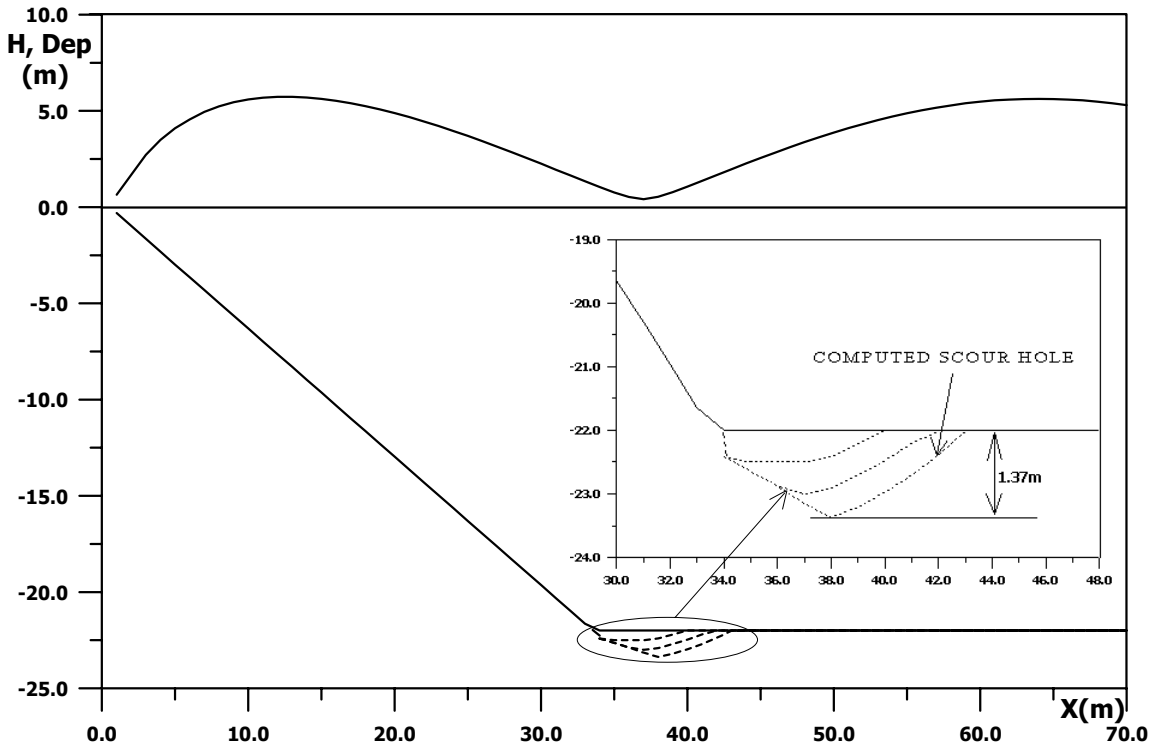

Fig. 9 - Computed scour hole for straight slope

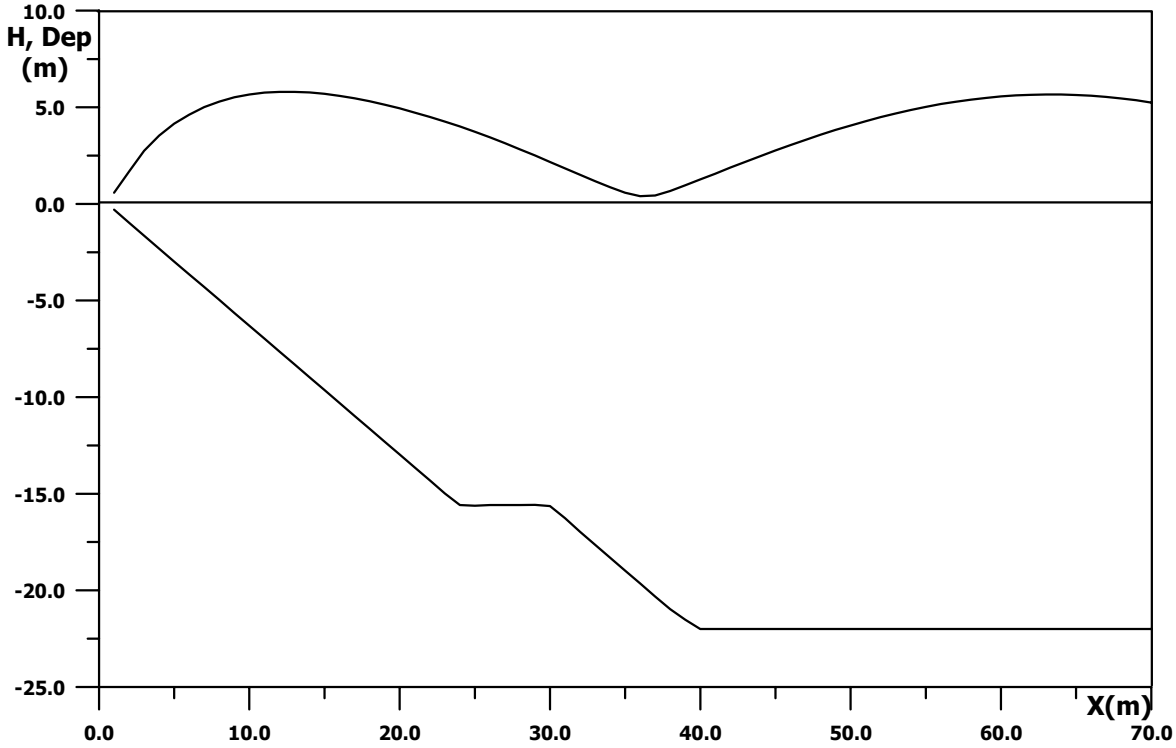

Fig. 10 - Computed Zero scour hole with scour protection step

Theoretical and Practice Aspects of Rock Scour Prediction

By

George W. Annandale[1], Erik Bollaert[2] and Anton Schleiss[3]

ABSTRACT

Annandale's Erodibility Index Method (Annandale 1995) is a semi-empirical technique that is used to assess the erodibility of a wide variety of earth materials under varying flow conditions. The method is based on the premise that the erosive power of water is highly dependent on pressure fluctuations, and that the relative ability of rock and other earth materials to resist scour is dependent on the unconfined compressive strength of the material, the shear strength between blocks of rock or soil particles, and geometric properties like block or particle size, and shape and orientation of the same. Detailed research by Bollaert (2002) on the nature of pressure fluctuations in rock fissures and discontinuities, and application of fracture mechanics to describe the failure of rock confirms the premises used to develop Annandale's method.

INTRODUCTION

Simulation of rock scour can be accomplished by detailed constitutive modeling, semi-empirical modeling or simplistic empirical correlation. Bollaert's (2002) research results form the basis for constitutive modeling of rock scour subject to plunging jets. Annandale's (1995) Erodibility Index Method allows semi-empirical simulation of scour of earth materials, including rock. The methods of Mason and Arumugam (1985) and Yildiz and Üzücek (1994) are examples of procedures that use pure empirical correlation to estimate plunge pool scour resulting from plunging jets.

Rock scours when the erosive power of water exceeds its relative ability to resist scour. The erosive power of water is determined by pressure fluctuations that originate from turbulence in flowing water. Amplified pressures in rock fissures and discontinuities result in breakup of the rock mass, and scour of the same.

The resistance that rock offers to the fluctuating pressures within close ended fissures is largely dependent on its mass strength and the shape and size of the fissures. Once

[1] George W. Annandale, *Engineering & Hydrosystems Inc., P.O. Box 260-555, Highlands Ranch, Colorado 80126, USA.*
[2] Erik Bollaert, *Laboratory of Hydraulic Constructions, Swiss Federal Institute of Technology, Lausanne, Switzerland.*
[3] Anton Schleiss, *Laboratory of HydraulicConstructions, Swiss Federal Institute of Technology, Lausanne, Switzerland.*

fissured rock has cracked, it is similar to rock with discontinuities. Scour of such rock is largely dependent on the weight of rock blocks, and friction between the blocks. Rock weight is a function of block size and shape.

This paper outlines elements of Bollaert's (2002) work, which entails detailed research into the nature of pressure fluctuations in rock fissures and fracture mechanics of rock, and relates it to Annandale's (1995) Erodibility Index Method, which is a semi-empirical method relating the erosive power of water to the relative ability of earth material, including rock, to resist scour. The paper illustrates that the conceptual model that Annandale (1995) used to explain the role that pressure fluctuations play in rock scour is consistent with the findings of Bollaert (2002), as are the variables that were used to quantify the relative ability of rock to resist scour.

EROSIVE POWER

Erosive Power

Annandale (1995) used the conceptual model shown in Figure 1 as the basis for explaining the role that pressure fluctuations play in scour of rock. As water flows over rock, some of the water penetrates the rock discontinuities that act as conduits for transferring pressure fluctuations originating at the interface between the rock and the flowing water. Pressure fluctuations are considered to originate from the turbulence in the flowing water. The resultant of the pressure fluctuations over the rock blocks jacks them out of their position of rest (Figure 1a). Once dislodged (Figure 1b), the blocks of rock are finally displaced from the dislodged position to a downstream location by the sediment carrying capacity of the water (Figure 1c).

By relating the rate of energy dissipation in flowing water to the standard deviation of pressure fluctuations within the water (Figure 2) Annandale (1995) argued that estimates of the rate of energy dissipation of flowing water could be used to represent the relative magnitude of pressure fluctuations, and thus the relative magnitude of the erosive power of water. The rate of energy dissipation in flowing water is also known as stream power. A simple expression that can be used to estimate the rate of energy dissipation is

$$P = \gamma \,.\, Q \,.\, \Delta E \qquad (1)$$

Where γ = unit weight of water; Q = discharge of water; ΔE = energy loss.

Using this point of view Bohrer and Abt (1996) developed an equation that can be used to estimate the change in flow velocity in plunge pools subject to plunging jets:

$$-\ln\left(\frac{v}{V_i}\right) = -0.5812\ln\left[\left(\frac{\rho_i}{\rho_w}\right)\left(\frac{V_i^2}{gL}\right)\right] + 2.107 \qquad (2)$$

$$-0.29 < \ln\left[\left(\frac{\rho_i}{\rho_w}\right)\left(\frac{V_i^2}{gL}\right)\right] < 2.6.$$

$$L = \frac{z_1 - z_2}{\cos\alpha} \tag{3}$$

where v = flow velocity in plunge pool; V_i = flow velocity at location where the jet enters the pool; ρ_i and ρ_w = density of air and water respectively; g = acceleration due to gravity; L = distance along centerline of jet within the plunge pool; α = impingement angle between jet and water surface at point of contact; z = elevation.

The rate of energy dissipation in the plunge pool is a discretized function of the total head at various elevations along the centerline of the submerged jet. Equation 4 shows a discrete calculation for the change in head between points j and j+1. As the velocity decays with decreasing elevation, or increasing displacement along the jet centerline, the total head decreases. Equation 5 yields the corresponding available power per unit area,

$$\Delta E_j = \frac{v_j^2}{2g} - \frac{v_{j+1}^2}{2g} + \frac{P_j}{\gamma} - \frac{P_{j+1}}{\gamma} + z_j - z_{j+1} \tag{4}$$

$$p_{A_j} = \left(\gamma v_j \Delta E_j\right) \tag{5}$$

Equation (5) is used to estimate the rate of energy dissipation (relative magnitude of the erosive power of water) at any elevation within a plunge pool. Scour potential and extent of scour is determined by comparing the magnitude of the rate of energy dissipation at the interface between the bottom of the plunge pool and the water. Scour occurs when the rate of energy dissipation (stream power) is greater than the ability of the rock to resist scour (the stream power required to cause scour).

Bollaert (2002) conducted detailed research into the nature of pressure fluctuations, as summarized in what follows.

Pressure Fluctuations

Bollaert (2002) performed experiments to investigate the nature of pressure fluctuations in rock fissures by discharging a high velocity jet into a container with a simulated fissure at its base (Figure 3). The high, near-prototype jet velocity caused significant turbulence in the container, resulting in fluctuating pressures at the entrance to the fissure located in the base of the container. Pressure fluctuations at the entrance to and within the simulated fissure were measured with high frequency pressure transducers.

Measuring pressures at such high frequencies within the fissure lead Bollaert (2002) to the discovery that the fissure acts like resonance chambers, significantly amplifying

maximum pressures in closed fissures. He furthermore discovered that open discontinuities also amplify pressure fluctuations, although to a lesser degree than close-ended fissures. The use of a near-prototype scale jets in the experiments furthermore lead to the discovery that substantial energy still subsist at frequencies of several hundreds of Hz. This **contradicts** generally held beliefs that the spectral energy content in macro-turbulent flows in plunge pools occurred mainly within the 25 Hz range (Toso & Bowers 1988).

Bollaert (2002) also showed that air entrainment in the water entering the fissures played an important role in amplifying the pressures. As increased air concentrations decrease the celerity of the water the conditions for resonance improve, resulting in significant pressure amplifications within the fissures. An example of a time series showing pressures amplification within a fissure is shown in Figures 4. The graph shows pressure fluctuations at the entrance to the fissure (pool bottom) and at the end of the fissure. In open-ended discontinuities the pressure amplification was as high as 1.6 times the incoming kinetic energy.

SCOUR RESISTANCE

Rock Scour Mechanics

Bollaert (2002) developed a Comprehensive Fracture Mechanics (CFM) model that can be used to simulate fracturing of rock with close-ended fissures and open-ended discontinuities. The concept is based on the theoretical framework that is outlined in Bollaert (2002) and Bollaert & Schleiss (2001). As such, the model is completely physically based and represents a comprehensive assessment of the two major physical processes that govern break-up of rock: 1) hydrodynamic fracturing of rock joints, and 2) dynamic uplift of rock blocks. Two failure criteria are relevant:

- Failure of closed-end rock joints by *propagation* of the joints. This propagation can be instantaneous or time-dependent. The latter case involves failure by fatigue.
- Failure of open-ended rock joints by *dynamic uplift* or displacement of the rock blocks out of their surrounding mass.

Fracture Mechanics theory transforms the hydrodynamic loading into is a stress intensity factor K_I, and then compares this factor with the corresponding resistance of the material, which is expressed by the fracture toughness value K_{Ic}. If $K_I > K_{Ic}$ instantaneous failure occurs. In cases when $K_I < K_{Ic}$, time-dependent failure by fatigue can occur. Failure by fatigue depends on the number and the amplitude of the load cycles. The fracture toughness K_{Ic}, representing the strength of good quality rock with few fissures can be related to the Unconfined Compressive Strength (UCS) of the rock by the equation:

$$K_{I,\,UCS} = (0.010) \cdot UCS + (0.054 \cdot \sigma_c) + 0.42 \qquad (6)$$

Where σ_c = in-situ horizontal stress field.

Bollaert (2002) also showed that removal of rock surrounded by open discontinuities can be simulated by calculating the net force over blocks of rock. Figure 5 illustrates that although the uplift pressure on the blocks for the three scenarios shown in the figure could be the same it would be easier to remove the rock blocks shown in Figure 5 (c) than those shown in Figure 5(a). In addition the friction between the blocks of rock will also affect the ease with which blocks of rock could be removed. The Erodibility Index used by Annandale (1995) uses the same variables to quantify the relative ability of rock to resist scour.

Quantification of Scour Resistance

The Erodibility Index, a geomechanical index that can be used to empirically quantify the relative ability of earth material to resist scour is expressed as (Annandale 1995)

$$K = M_s \,.\, K_b .\, K_d .\, J_s \qquad (7)$$

Where M_s = intact mass strength number; K_b = block size number; K_d = inter-block bond shear strength number; J_s = ground structure number.

The intact mass strength number (M_s) represents the strength of a homogenous, "perfect" sample of earth material. In order to acknowledge the roles of discontinuities and imperfections for determining the earth material's relative ability to resist scour, the intact mass strength number is multiplied by other parameters. The value of the intact mass strength number is adjusted by multiplying it with the block / particle size number (K_b), the discontinuity / inter-particle bond shear strength number (K_d) and the relative ground structure number (J_s).

Ways to quantify each of these numbers are presented in Annandale (1995). The mass strength number M_s is directly proportional to the Unconfined Compressive Strength of the rock. The block size and orientation numbers are functions of the geometry of the rock blocks. The inter-block shear strength number is dependent on the joint roughness and gouge in the discontinuities between the rocks.

EROSION THRESHOLD

The erosion threshold established by the Erodibility Index Method relates the erosive power of water to the relative ability of earth material to resist scour (Figure 6). The relative magnitude of the erosive power of water is quantified by the stream power of the water, and the relative ability of earth material to resist scour is quantified by the Erodibility Index. The threshold relationship is based on analysis of a large number of field observations pertaining to scour of rock and other earth materials.

Bollaert (2002) conducted sensibility studies comparing the CFM model with the Erodibility Index Method, which indicated a reasonable correlation (Figure 7). The figure shows that the trend relating fracture dimension and time to scour are similar for

the CFM model and the Erodibility Index Method. In Figure 7 the ratio a/B = relationship between the depth of fracture and thickness of rock block; c/W = ratio between fracture width and width of rock block; a/c = depth to width ratio of fracture; H = pressure head.

CONCLUSION

Bollaert's (2002) research pertaining to the nature of pressure fluctuations in rock fractures and discontinuities, and his constitutive CFM model confirm the conceptual model used by Annandale (1995) in the development of the Erodibility Index Method.

Annandale's (1995) use of stream power (rate of energy dissipation) to quantify the relative magnitude of the erosive power of water is based on the concept that net pressure fluctuations acting on fractures and rock blocks lead to scour. The nature of such pressure fluctuations, investigated in detail by Bollaert (2002), confirms their pivotal role in scour of rock.

The variables used to express the ability of rock to resist scour are similar in both the semi-empirical and constitutive modeling. The Unconfined Compressive Strength of the rock quantifies the ability of "perfect" rock to resist scour. Once rock contains open-ended discontinuities, the geometric properties of the rock and friction (shear strength) between blocks of rock play an important role in determining its resistance to scour. The Erodibility Index uses the concept of "perfect" rock as a base for quantifying its relative ability to resist scour, and then multiplies the mass strength number with other values to account for the impact of discontinuities that lead to "less perfect" rock, usually accounted in practice.

A comparison between constitutive modeling (the CFM model) and semi-empirical modeling (the Erodibility Index Method) indicates that the trends defining the relationship between scour and the erosive power of water are similar.

REFERENCES

1. Annandale, G. W. 1995. "Erodibility", Journal of Hydraulic Research, Vol.
2. Bollaert, E. 2002. "Transient Water Pressures in Joints and Formations of Rock Scour due to High-Velocity Jet Impact", PhD Thesis, Ecole Polytechnique Federale de Lausanne, Switzerland.
3. Bollaert, E. & Schleiss, A. 2001. "A new approach for better assessment of rock scouring due to high velocity jets at dam spillways", *Proceedings of the 5th ICOLD European Symposium*, Geiranger, Norway.
4. Mason, P.J., Arumugam, K., "Free Jet Scour Below Dams and Flip Buckets." Journal of Hydraulic Engineering, Vol. 111, No. 2, ASCE, February 1985.
5. Toso, J. and Bowers, E.C. 1988. "Extreme pressures in hydraulic jump stilling basin", Journal of Hydraulic Engineering, ASCE, Vol. 114, No. HY8, pp. 829-843.
6. Yildiz, D., Üzücek, E., "Prediction of Scour Depth From Free Falling Flip Bucket Jets", Intl. Water Power and Dam Construction, November, 1994.

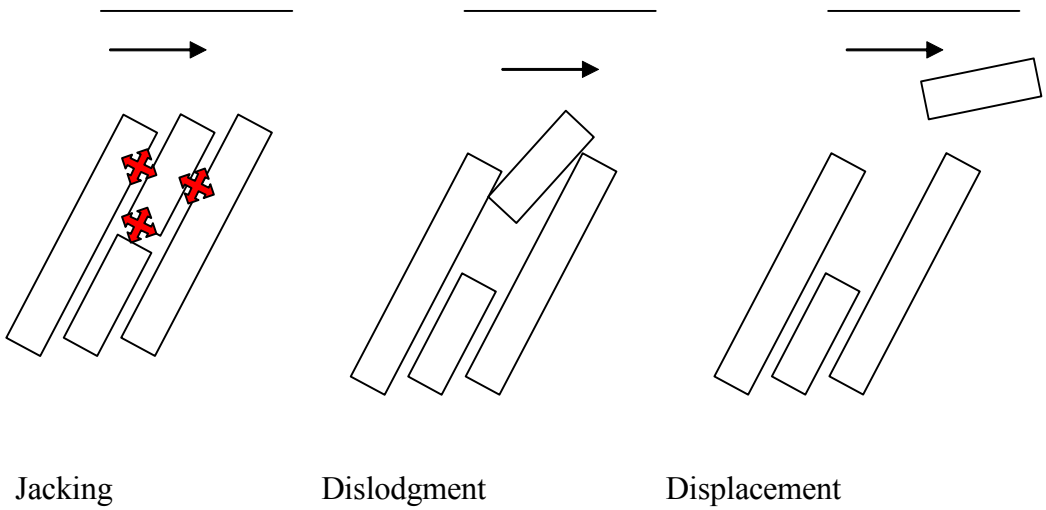

Fig. 1 - Three stages of erosion of rock (Annandale 1995)

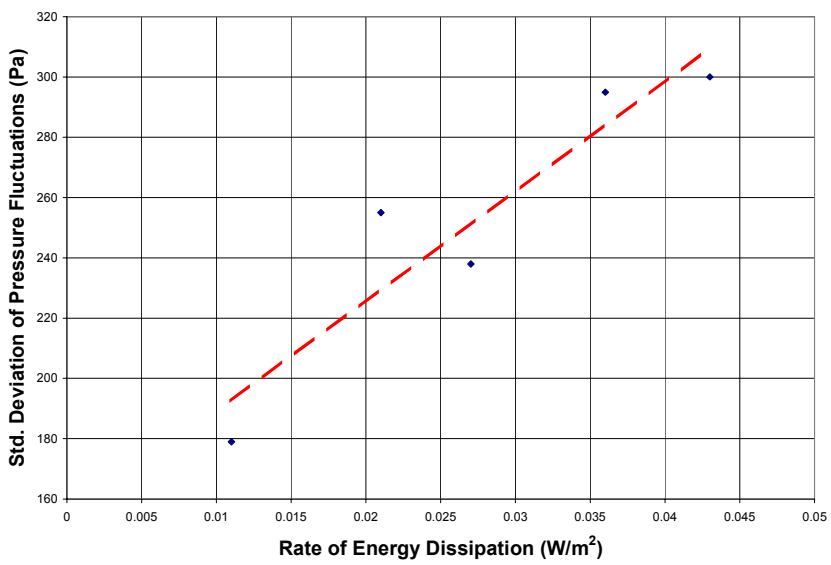

Fig. 2 - Relationship between rate of energy dissipation and standard deviation of fluctuating pressures (Annandale 1995).

Fig. 3 - Experimental facility for measuring pressure fluctuations in simulated rock fissures

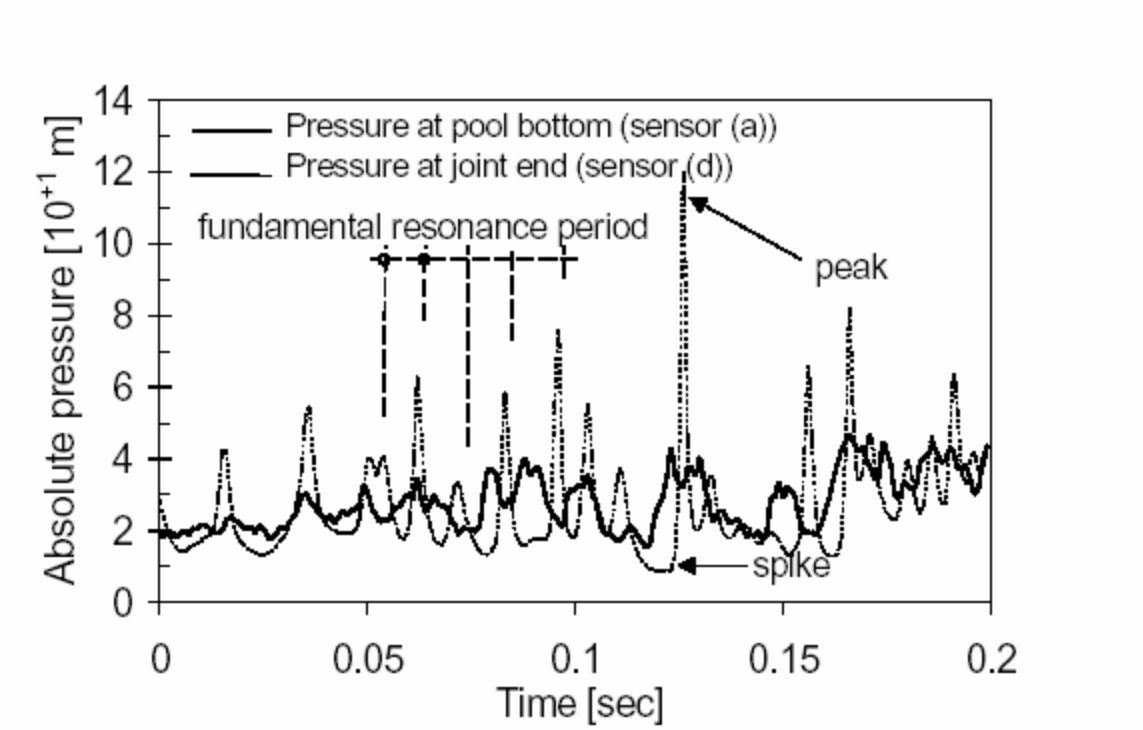

Fig. 4 - Pressure amplification in artificial, close-ended fissure (Bollaert 2002)

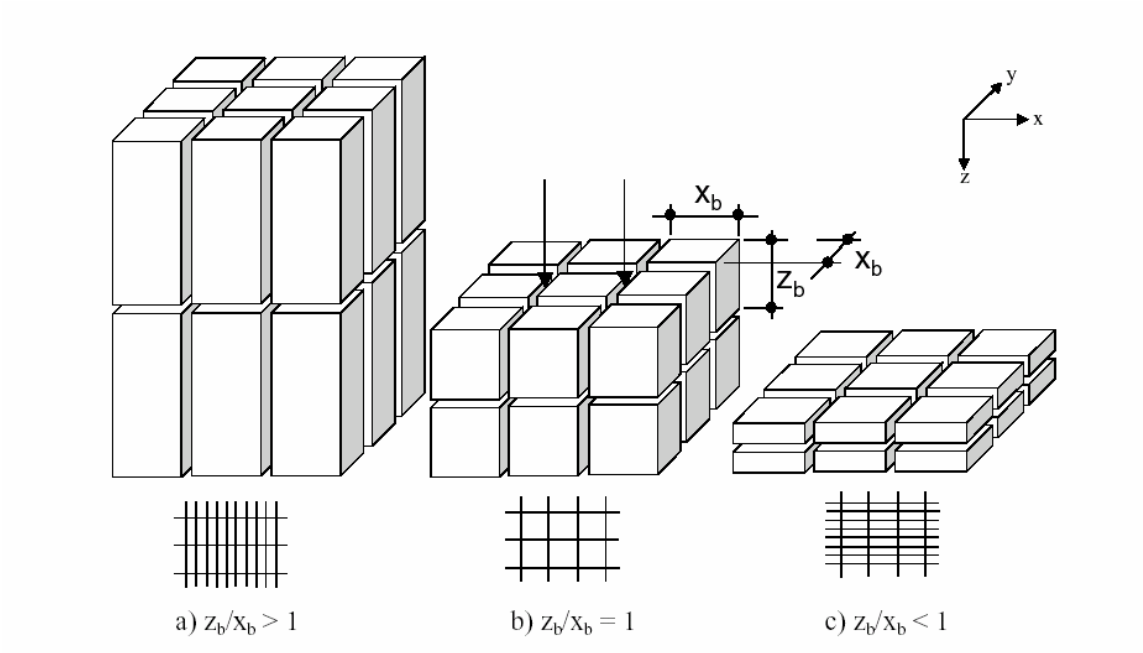

Fig. 5 - Rock with open discontinuities (Bollaert 2002)

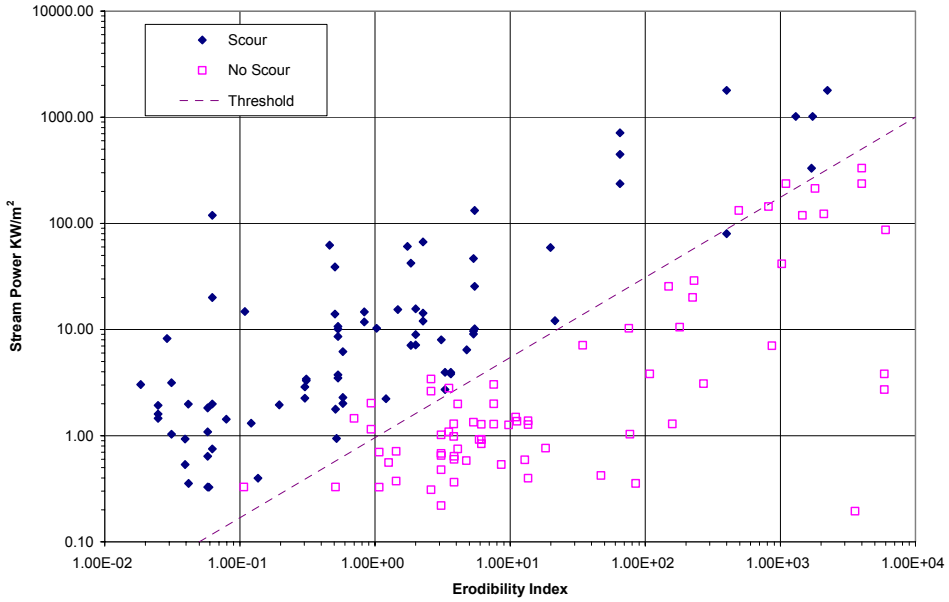

Fig. 6 - Erosion threshold for rock and other earth materials (Annandale 1995)

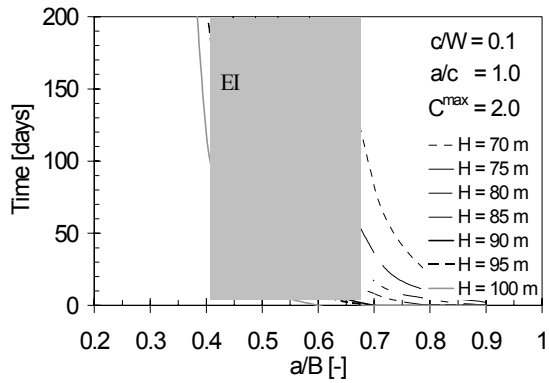

Fig. 7 - Comparison between CFM simulation and Erodibility Index Method (Bollaert 2002)

Erosion Function Apparatus Overview and Discussion of Influence Factors on Cohesive Soil Erosion Rate in EFA Test

Y. Cao[1], J. Wang[1], J.L. Briaud[2], H.C. Chen[2], Y. Li[1], and P. Nurtjahyo[1]

Abstract: The EFA (Erosion Function Apparatus) is a new device used to measure the erodibility function of soils and soft rocks. Samples are taken from the bridge site in a thin wall steel tube which is then fitted through a tight opening at the bottom of a pipe with a rectangular cross section. Water flows over the soil or soft rock sample. The erosion rate of the soil or soft rock is recorded and the hydraulic shear stress applied at the interface is calculated by using Moody Chart. The advantages and limitations of the EFA are discussed in this paper. The results of tests using water with different pH and salinity show that both factors influence the erodibility function. An attempt is made to find a correlation between the critical shear stress, and the initial slope of the erodibility function on one hand and the water content, the undrained shear strength, the plasticity index and the percentage passing the #200 sieve on the other. This attempt is unsuccessful.

INTRODUCTION

Bridge scour is an important factor which can cause the failure of a bridge. One thousand bridges have collapsed between 1961 and 1991 in the United States and 60% of the failures are due to the scour (Shirole and Holt, 1991). Only 2% of the bridge failures in that database were due to earthquakes. A new method called SRICOS (Scour Rate in Cohesive Soil) was published (Briaud et al., 1999). This method was proposed to predict the scour depth versus time around a bridge pier. One essential part of SRICOS method is to test the soil samples collected at the site in the EFA (Erosion Function Apparatus) to obtain the scour rate versus hydraulic shear stress applied curve or erodibility function (Briaud et al, 1999). The EFA test gives

- The erosion rate versus shear stress curve
- The critical shear stress at which erosion starts

These two results are used in the SRICOS method to predict bridge scour.

This paper presents the EFA, the EFA test and gives some EFA test results including some tests to quantify the influence of the pH and salinity of the water eroding the cohesive soil.

EFA (EROSION FUNCTION APPARATUS) OVERVIEW

The EFA was designed, developed, patented, and licensed at Texas A&M University starting in 1991 (Briaud et al., 1999). Humboldt is now manufacturing the device which is in its third generation of evolution.

Basic Principle

The EFA is used to measure the erosion rate of different types of soils and soft rocks, ranging from clay to gravel, and from soft soils to soft rocks. The conceptual

[1] Graduate student, Department of Civil Engineering, Texas A&M University, College Station, TX, USA
[2] Professor, Department of Civil Engineering, Texas A&M University, College Station, TX, USA

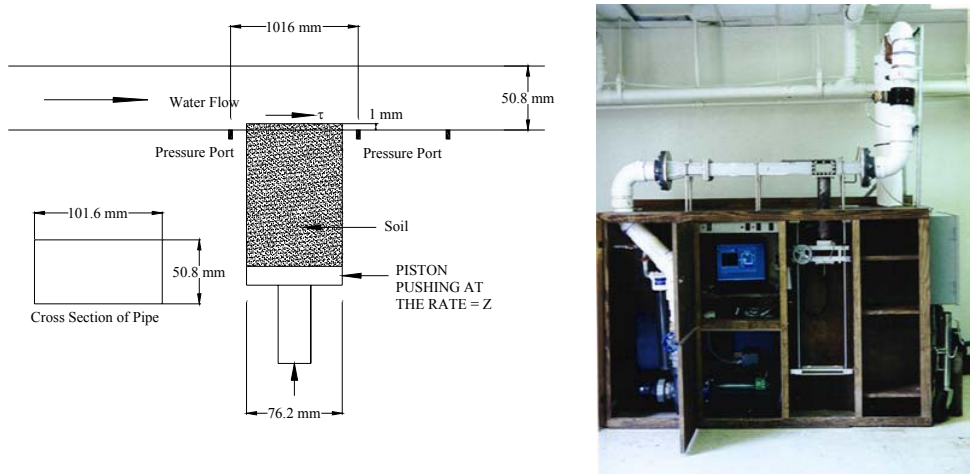

(a) **(b)**

Figure 1: (a) Conceptual Diagram; (b) Photograph of EFA

diagram and photograph of the EFA are shown in Figure 1. The soil sample is taken from the bridge site by pushing an ASTM standard Shelby tube with a 76.2 mm outside diameter (ASTM 1999a). If the tested material is a soft rock, a core sample can be obtained and placed in the Shelby tube. The Shelby tube will be put into the rectangular cross section pipe through a circular opening in the bottom of the pipe. The dimension of the rectangular cross section of the pipe is 101.6 × 50.8 mm. The length of the horizontal pipe is approximately 1.2 m. The water is driven through the pipe by a pump. A valve is used to adjust and regulate the flow velocity and a flow meter is installed to measure the flow rate. The end of the Shelby tube is kept flush with the bottom of the rectangular pipe. A piston pushes the soil sample until it protrudes 1mm into the rectangular pipe. This 1mm protrusion of the soil sample will be eroded with time.

General Procedure of EFA Test

The general procedure of the EFA test is as follows: (Briaud et al., 2001)

1. Place the sample in the EFA, fill the pipe with water, and wait one hour.
2. Set the initial water velocity, say 0.2 m/s.
3. Push 1mm of soil sample out of the steel tube into the test section
4. Pushing the soil sample when necessary during the erosion process to maintain a soil or soft rock protrusion between 0 mm and 1 mm into the flow until a 50 mm length of soil is eroded or 1 hour has been reached, whichever comes first. The scour rate corresponding to that velocity is calculated as the total soil push divided by the time required for the erosion process.
5. Stop the pump, take out the Shelby tube, trim the surface to be flush with the bottom of the rectangular pipe and then repeat Step 2 to 4 with another water velocity.
6. Once 6 to 8 velocities have been tested, the scour rate vs. velocity curve is

obtained, and is converted into the scour rate vs. shear stress curve or erodibility function.

EFA Test Results

The test result consists of the erosion rate $\dot{z}$ versus shear stress τ curve (Figure 2) also called erodibility function. For each flow velocity, the erosion rate (mm/hr) is simply obtained by dividing the length of sample eroded by the time required to do so. After several attempts at measuring the shear stress τ in the apparatus it was found that the best way to obtain τ was by using the Moody Chart (Moody, 1944) for pipe flows.

$$\tau = \frac{1}{8} f \rho \upsilon^2$$

Where τ is the shear stress on the wall of the pipe, f is the friction factor obtained from Moody Chart (Figure 3), ρ is the mass density of water (1000 kg/m3) and υ is the mean flow velocity in the pipe. The details of the calculations can be found in Briaud et al. (2001).

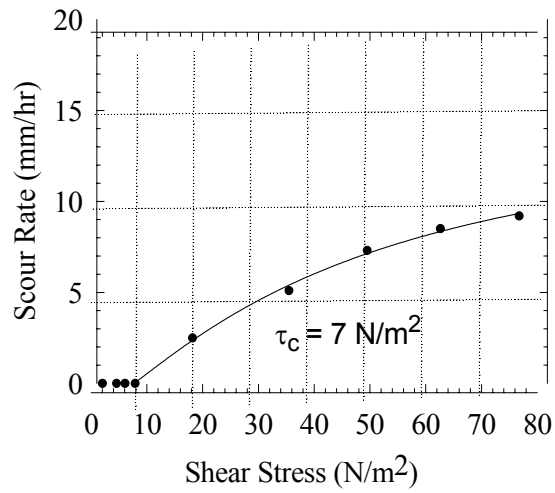

Figure 2: Typical EFA Test Result

Advantages of the EFA

1. Minimum sample disturbance.
2. Direct site specific measurement of the erosion rate vs. shear stress curve (erodibility founction) including the critical shear stress for the soil or soft rock.
3. Test results incorporated in a scour prediction method (SRICOS) which may save foundation depth.

Drawbacks of the EFA

1. Requires samples from the site.
2. Test takes about one hour per velocity.
3. Size of particles that can be tested limited by size of sample.

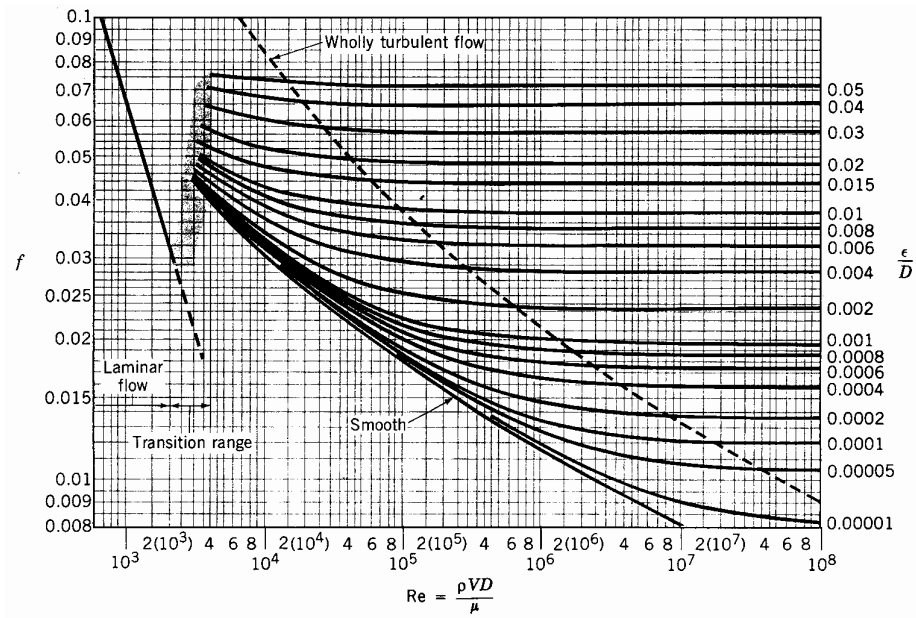

Figure 3: Moody Chart [Reprinted with Permission from Munson et al. (1990)]

INFLUENCE OF WATER pH ON ERODIBILITY FUNCTION

The erosion of cohesive soils is a very complicated process. Gravitation and friction laws control the scour process of cohesionless soils while physicochemical laws control the scour process in cohesive soil. The scour process is a soil-water interaction, which involves a large number of factors. The erodibility of a cohesive soil is characterized by the erodibility function, which is the $\dot{z}$ versus τ curve. It requires a number of curve-fitting parameters to describe the nonlinear relationship between $\dot{z}$ and τ (Briaud et al., 2001). One of the curve-fitting parameters is the critical shear stress τ_c, the shear stress at which erosion begins. For sands, HEC-18 gives some equations to calculate the critical shear stress by using the size of the grains represented by D_{50}. For clay, it is difficult to use a formula to get the τ_c value directly because of the large number of factors influencing it. Briaud et al. (1999) summarized the influence factors for τ_c: soil water content, soil unit weight, soil plasticity, soil shear strength, soil void ratio, soil swell, soil mean grain size, soil percentage passing the No. 200 sieve, soil clay mineral, soil dispersion ratio, soil cation exchange capacity, soil sodium absorption ratio, soil pH, soil temperature and water chemical composition. In order to evaluate the influence of this last factor on the erodibility function of a cohesive soil, two major water chemistry factors (water pH and salinity) were selected and a series of tests were run in the EFA for this purpose.

Introduction

The purpose of the pH tests was to study the possible influence of the pH on the erodibility of clays. The clay tested was a porcelain clay. Many researchers have studied the influence of the water pH value or the soil pH value on the erodibility of a

cohesive soil. Alizadeh (1970) found that the pH value in the eroding water and the pH value in the soil influences significantly the erodibility of a cohesive soil. Arulanandan et al. (1980) also mention that the pH value of the eroding fluid and the soil pH value were critical factors for the erodibility of a cohesive soil. Sherard et al. (1976) found that the erodibility of a Ca-Montmorillonite in an embankment, which was severely damaged by rainfall, could be reduced by using sodium salt, such as Na_2CO_3. Shaikh et al. (1988) used a series of flume tests with three different types of clay. Their results showed that the soil pore water chemistry is the most important parameter affecting the erodibility of unsaturated compacted clays. The pore water chemistry was characterized by the SAR (Sodium Absorption Ratio) and the TDS (Total Dissolved Salts). The SAR is the ratio of the dissolved sodium ions to other main basic cations, such as Ca and Mg in the pore water; and the TDS is the total dissolved salt, or total dissolved solids concentration. The erosion rate of the Ca-Montmorillonte with a TDS=7.8 and an SAR=0.4 was 300 times greater than that of the Na-Montmorillonite with a TDS=20.5 and an SAR=19.8.

Experimental Parameters

The soil used was the Armadillo Porcelain Clay. The predominant component of this commercial clay is Kaolinite. The chemical formula for Kaolinite is $Si_2Al_2O_5(OH)_4$. The layers of Kaolinite are composed of one silica tetrahedral sheet and one alumina octahedral sheet (gibbsite). Kaolinite is the most prominent member of this group, which also includes halloysite, nacrite and dickite. Tap water was used as the eroding water. The chemical material used to bring the pH value down was sodium bisulfate ($NaHSO_3$). It is the main component of the product named pH minus, which contains 94.5% of $NaHSO_3$ and 5.5% of other ingredients. The chemical material used to raise the pH value is soda ash or sodium carbonate (Na_2CO_3). It is the main component of the product called pH plus. It contains 99.6% of Na_2CO_3 and 0.4 % of the inter ingredients. Before the tests started, the water tank was filled with tap water. Then the pH plus or pH minus products were gradually added into the tank. A pH probe (OAKTON pH Tester 3) was used to measure the pH value when the chemical material was absolutely dissolved into the water. Once the desired pH value was reached, the EFA tests were started immediately. During the tests, there was neither fresh water filled in nor water pumped out. The following table shows some chemical properties of the eroding water.

Properties	Tap water	Acid Condition	Alkalinity Condition
Molar Concentration (M/L)	N/A	0.0077	0.463
pH Value	8.39	5	10.79
TDS (mg/L)	536	1210	>19900
SAR (ppm)	500	1200	44300
Conductivity (millisiements)	1.1	2.4	65.40

General Procedures for pH Tests in the EFA

1. Push a standard Shelby tube (ASTM) with a perpendicular direction into a porcelain clay block to get the soil sample. Then label the tube properly.
2. Fill the water tank and gradually add pH minus or pH plus into water. Make sure that the desired pH value of water has been reached before the test start.

3. Start the pump and achieve an initial low water velocity in the flume. The water flows over the sample at the chosen velocity and 1mm of soil sample is pushed into the flow.
4. Keep pushing the soil sample in Shelby tube to maintain the protrusion of soil sample between 0mm and 1mm in the flow until a 50mm height of soil has been eroded or 1 hour is reached, whichever comes first. The scour rate can be calculated as the total soil push divided by the time it takes to erode it.
5. Stop the pump, take out the tube and trim the clay surface to be flush with the edge of the Shelby tube. Then repeat Step 2 to Step 4 with a higher flow velocity.
6. Once 6 to 8 velocities have been performed, the scour rate vs. velocity curve is obtained. Then the scour rate vs. shear stress curve can be calculated by using Moody Chart.

Test Results:

The results of the pH tests are shown on figure 4. They indicate that whenever the pH value was away from neutral, the scour rate of the porcelain clay decreased and the critical shear stress τc increased. The initial slope Si of the scour rate vs. shear stress curve did not change much when the pH value changed. The surface charges of some soil are dependent on the soil properties (Brady, 1990). Porcelain clay belongs to this type of soil. As the pH value increases, the cation concentration changes and affects the resistance to erosion.

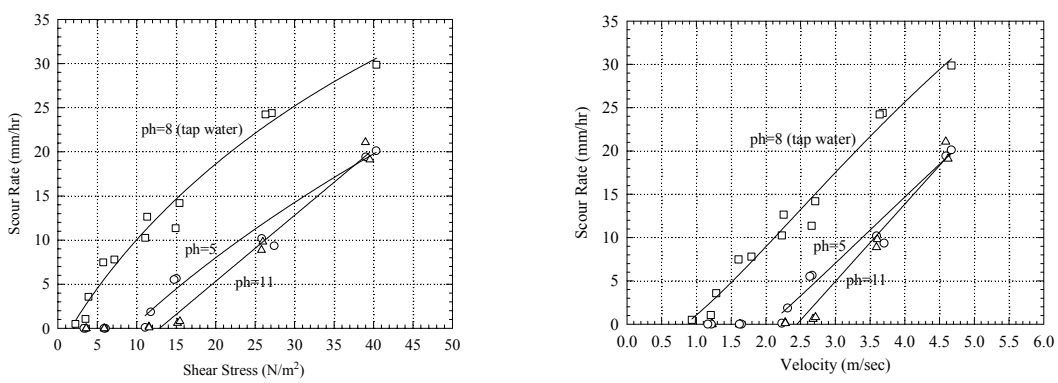

Figure 4: Relationship between Erosion Rate and Shear Stress & Velocity for different pH Values

INFLUENCE OF WATER SALINITY ON ERODIBILITY FUNCTION

Introduction

In delta areas, where the river flows into the sea or bridges cross an inlet, the salt concentration in the water under the bridge can range from 0 to 35,000 ppm (part per million). EFA tests using water at the right salinity can simulate the real condition.

Sherard et al. (1972) carried out extensive research work on piping in earth dams of

dispersive clay in Australia. It was found that two major factors would influence the erosion rate of dispersive clays: SAR and TDS. Sherard reported that smaller TDS concentrations in the eroding water lead to higher erosion rates in clay soils. Arulanandan (1975) performed a series of erosion tests in Yolo Loam using a rotating cylinder apparatus with different concentrations of NaCl in the eroding water: distilled water, 0.001N NaCl and 0.005N NaCl. Figure 5 shows the results of the tests and indicates that the critical shear stress increases with the salt concentration and so does the erosion rate.

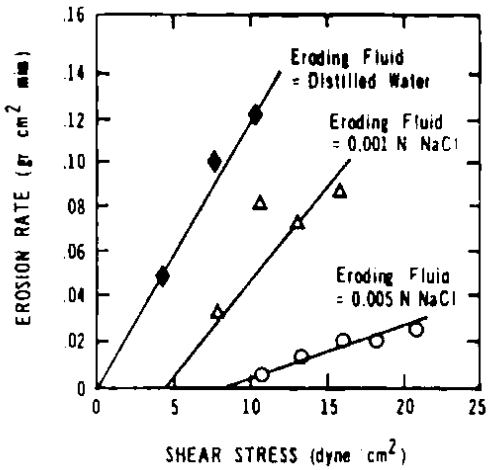

Figure 5: Relationship Between Erosion Rate and Shear Stress for Different Concentration of Eroding Fluid (After K. Arulanandan)

Liou (1970), Sherard et al. (1972, 1976) and Sargunan et al. (1973) also studied the effect of the chemical composition of the pore water on the soil erosion rate. They concluded that the presence of cations in the pore water tends to make the soil more scour resistant because they reduce the repulsive electric force between clay particles.

Experimental Parameters:

The porcelain clay used for the pH tests was also used for the salinity tests in the EFA. Tap water was used as the eroding water and mixed with salt to reach the following concentrations: 500ppm salinity (tap water), 17500ppm salinity (50% seawater), 35000ppm salinity (100% seawater). The salt used in the salinity tests was table salt, 99% of which was NaCl. Before the test, table salt was gradually added into the water with mechanical agitation. A salinity probe (ORION Model 115) was used to measure and monitor the change in salt concentration. As in the pH tests, there was neither salt nor water added or withdrawn during the EFA test. The following table shows the selected chemical properties of eroding water for the salinity test.

Properties	Tap water	50% seawater	100% seawater
Salinity (ppm)	500	17500	35000
TDS (mg/l)	536	15900	>19900
PH Values	8.39	8.12	7.96
Conductivity (millisiements)	1.15	28.3	52.9

General Procedure for Salinity Tests in the EFA:

The procedure for the salinity tests was similar to the procedure for the pH tests. Please refer to the corresponding section in the pH test and just replace table salt with pH plus or pH minus at the appropriate places.

Experimental Results

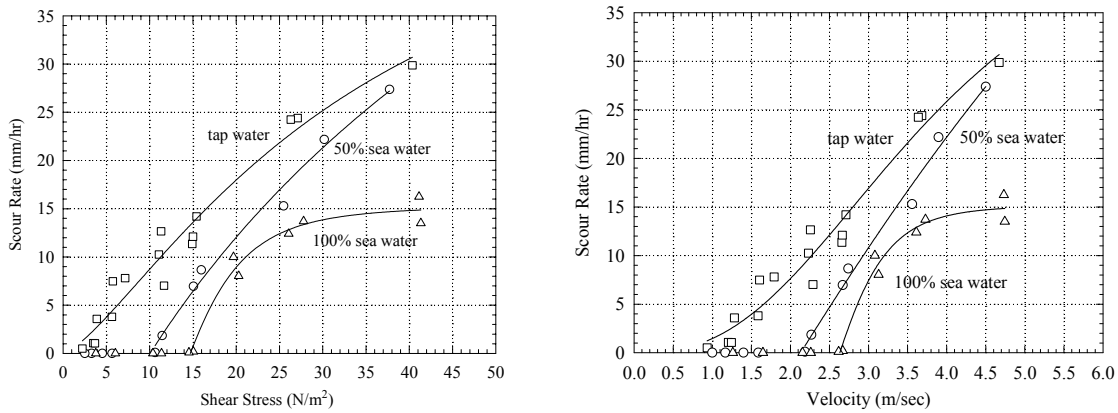

Figure 5: Relationship Between Erosion Rate and Shear Stress & Velocity for Different Concentration of Salinity of Eroding Fluid

Data Analysis:

The results of the salinity tests are similar to the tests by Arulanandan (1975). They show that the scour rate decreases with increasing salinity, while the critical shear stress increases with increasing salinity. The influence of salinity on the scour rate and the critical shear stress seems to be significant. Some differences with Arulanandan's work were also found. First, the initial slope of the scour rate vs. shear stress curve in Arulanandan's tests decreased with increasing salinity, while it was the opposite in the EFA salinity tests. Second, at high salinity concentration in EFA tests, the scour rate vs. shear stress curves lost linearity and converged to a maximum value. While the curves from Arulanandan's tests were linear. A possible explanation is that the shear stress level in Arulanandan's tests is quite low compared to the EFA tests. The maximum shear stress for Arulanandan's tests is about 2 N/m^2; compared to 40 N/m^2.in the EFA tests.

INFLUENCE OF SOIL PROPERTIES ON ERODIBILITY FUNCTION

More than 100 EFA tests have been performed at Texas A&M University on different soils. Based on the data accumulated, a scour database has been organized. Using this database, the potential relationship between on one hand the critical shear stress and the initial slope of scour rate vs. shear stress curve and on the other hand the water content (w%), the undrained shear strength (Su), the plastic index (PI), and the percentage passing sieve no. 200. The following figures show the results.

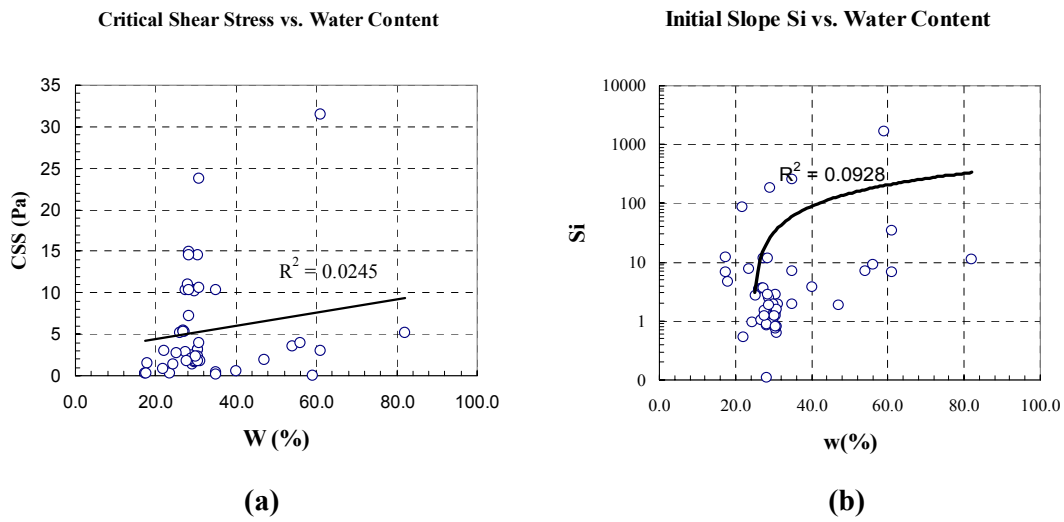

Figure 7: (a) Relationship Between Critical Shear Stress vs. Water Content; (b) Relationship Between Initial Slope Si vs. Water Content

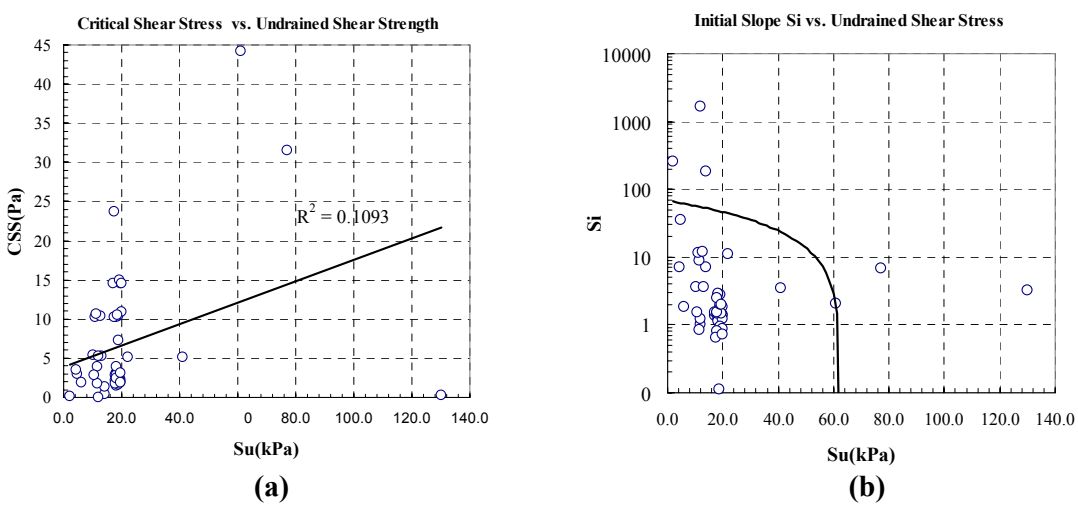

Figure 8: (a) Relationship Between Critical Shear Stress vs. Undrained Shear Strength; (b) Relationship Between Initial Slope Si vs. Undrained Shear Strength

Each figure also indicates the R^2 value obtained from various regressions. It is clear that no satisfactory relationship could be found. The fact that no relationship could be found between the critical shear stress or the initial slope of the erodibility function on one hand and common soil properties on the other seems to be at odds with the accepted idea that different cohesive soils erode at different rates. Indeed if different clays erode at different rates then the erodibility function and therefore its parameters should be

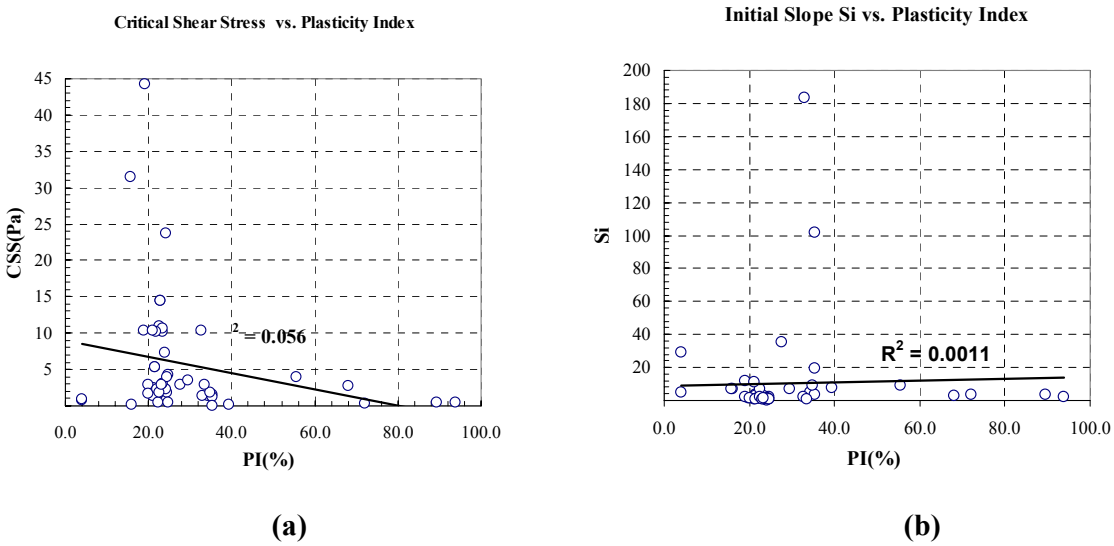

Figure 9: (a) Relationship Between Critical Shear Stress vs. Plasticity Index; (b) Relationship Between Initial Slope Si vs. Plasticity Index

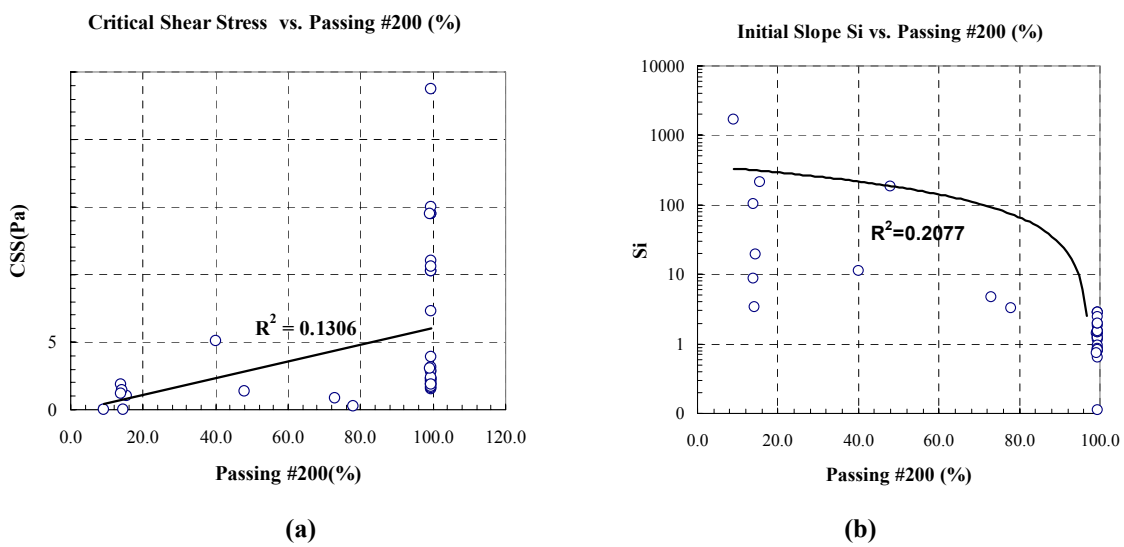

Figure 10: (a) Relationship Between Critical Shear Stress vs. Percentage Passing #200 Sieve; (b) Relationship Between Initial Slope Si vs. Percentage Passing #200 Sieve

functions of the soils properties. The likely explanation is that there is a relationship between erodibility and soils properties but that this relationship is quite complicated, involves advanced soil properties, and has not be found within the budget and time of the research projects undertaken by various researchers. Instead, it was found much easier to develop an apparatus which could measure the erodibility function on any sample of cohesive soil from a site. This apparatus is the erosion function apparatus or EFA.

CONCLUSIONS

The EFA has proven to be a simple and reliable device to study the erosion function of different soils and soft rocks. In this paper, the influence of the pH and salinity of the water were investigated and a database of EFA test results was used to try to develop a correlation between the erodibility function and various soil properties.

1. **pH tests:** the pH value of the eroding water affects the erosion process. The erosion rate was largest and the critical shear stress lowest when the water was neutral (pH = 7). The erosion rate decreased and the critical shear stress increased when the pH became acidic and when the pH became alkaline. It is suggested that the total dissolved salts content is the factor which influences the erodibility of the soil through the pH. If tap water is used as the eroding water (pH ~ 7), it will be more conservative compared to using water with a low pH or a high pH value.
2. **Salinity tests:** the salinity of the eroding water affects the erosion process. The erosion rate decreases and the critical shear stress increases when the salt content increases. The cations in the eroding water tend to neutralize the surface electronegativity of clay particles thereby making the clay more erosion resistant. If tap water is used as the eroding water, it will be more conservative compared to using water with a higher salt content.
3. **Correlations to soil properties:** a database of about 100 EFA tests was organized. For each soil tested, the following soil properties were measured: water content, undrained shear strength, plasticity index, percent passing sieve number 200. All attempted correlations lead to very poor R^2 values; therefore the conclusion is that there is no simple correlation between erodibility parameters and the chosen soil properties. On the other hand it is well accepted that different soils erode at different rates. The apparent contradiction between the last two statements suggests that a relationship exists but that it is complex and involves many soil properties. If this is the case then, rather than measuring all those soil properties, it is much easier to measure the erodibility function directly with the EFA for example.

ACKNOWLEDGMENTS

This work was part of two projects: one sponsored by the Texas Department of Transportation and one by the National Cooperative Highway Research Program.

REFERENCES

1. Yiwen Cao, 2001, “The Influence of Certain Factors on the Erosion Functions of Cohesive Soil”, Master Thesis, Texas A&M University, College Station, Texas 77843, USA
2. Arulanandan, K., Loganathan, P. and Krone, R.B., 1975, Pore and Eroding Fluid Influences on Surface Erosion of Soil”, Journal of Geotechnical Engineering, Vol.101, No.GT1, pp.51-66
3. Donald L.Sparks, 1986, “Soil Physical Chemistry”, CRC Press, 2000 Corporate Blvd., N.W., Boca Raton, Florida 33431, pp.308

4. Hinrich L,Bohn, Brian L, Mcneal, George A. O'Connor, 1985, "Soil Chemistry", John Wiley & Sons, Inc., 605 Third Avenue, New York, NY 10158-0012, pp.341
5. J.L. Briaud, H.C.Chen, P.Nurtjahyo, K.Kwak, S.W. Han, 1999, "Bridge Scour in Cohesive Materials", Interim Report NCHRP 24-15, Texas Transportation Institute, College Station, Texas 77843-3135
6. J.L. Sherard, R.S. Decker, 1977, "Dispersive Clays, Related Piping, and Erosion in Geotechnical Project", American Society for Testing and Material, 1916 Race Street, Philadelphia, PA.19103, pp.486
7. James K. Mitchell, 1993, "Fundamentals of Soil Behavior", 2nd edition, John Wiley & Sons, Inc, 605 Third Avenue, New York, NY 10158-0012, pp. 437
8. Malcolm Cresser, Ken Killham, Tony Edwards, 1993, "Soil Chemistry and its Applications", the Press Syndicate of the University of Cambridge, 40 West 20th Street, New York, NY 10011-4211, USA, pp.192
9. Nyle C. Brady, 1990, "The Nature and Properties of Soil", 10th edition, Macmillan Publishing Company, 866 Third Avenue, New York, New York 10022, pp. 621
10. Quirk, J.P., and Schofield, R.K., "the Effect of Electrolyte Concentration on Soil Permeability", Journal of Soil Science, Vol.6, 1955, p.163
11. Sargunan, A, Riley, P., Arulanandan, K., and Krone, R.B., March 1973, "Physico-Chemical Factors in Erosion of Cohesive Soils", Journal of Hydraulics Division, ASCE, Vol.99, No.HY3, Proceedings Paper 9606, pp.555-558
12. SeungWoon Han, 1999, "Effect of Soil Properties on Scour", master of engineering report, Department of Civil Engineering, Texas A&M University, College Station, TX 77843-3136, USA, pp.67
13. Shaikh, A., Ruff, J.F. and Abt, S.R., March 1988, "Erosion Rate of Compacted Na-Montmorillonite Soils", Journal of Geotechnical Engineering, Vol.114, No.3, pp.296-305
14. Shaikh, A., Ruff, J.F. Charlie, W.A., and Abt, S.R., 1988, "Closure to the article Erosion Rate of Dispersive and Non-Dispersive Clays", Journal of Geotechnical Engineering, Vol.114, No.x, pp.1826
15. Shaikh, A., Ruff, J.F. Charlie, W.A., and Abt, S.R., May 1988, "Erosion Rate of Dispersive and Non-Dispersive Clays", Journal of Geotechnical Engineering, Vol.114, No.5, pp.589-600
16. Sherard, J.L., Decker, R.S., and Ryka, N.L., "Piping in Earth Dams of Dispersive Clay", presented at June 12-14, 1972, ASCE Soil Mechanics and Foundation Conference Held at Purdue University, Lafayette, Indiana

Identification of Dispersive Clays in Gaza Strip Area; and Filter Effects on Dam Safety

Mohamed A. Awad*, Member of ASCE

Abstract:

Some clay soils disperse in the presence of flowing water, therefore laboratory testing has been carried out on eight soils from different places of Gaza Strip. The testing program consisted of pinhole, double hydrometer, crumb, soil security tests, chemical analysis at the saturation extract and classification tests, in order to investigate their dispersion characteristics. The effects of presence of granular zones on erosion were also investigated using soil security test. Laboratory tests to obtain the basic properties of the used soils has been performed. A comparison between chemical and physical soil properties under different conditions is studied. Presence of granular zones in the up and down side of water increased time-to-failure in the soil security test for all samples. A study was conducted to determine the effect of using ash (3%) in the soil security test.

Introduction:

Internal erosion have been recognized for decades as problems of embankments and foundations subjected to seepage forces. Hjeldnes and Lavania (1980) showed that erosion depends on water content and soil type. Foster et al. (2000 a) presented that dams constructed on dispersive clays are particularly susceptible to internal erosion and piping failures. Internal erosion induced instability problems in many different geological setting and in a variety of materials; that can be realized by dragging induced by seeping water and enlargement of cracks or holes (Crosta and di Prisco 1999).

A number of check dams is planned for Wadi Gaza area. The suggested core of dams made of clay would resist erosion along any cracks which could be developed. Soil security and pinhole tests are the most reliable laboratory test for identifying dispersive clays by direct measurements (Statton, C.T. et al. 1977, and Tuncer et al 1989). It is observed that an average water content with 2 percent on the wet side of optimum water content is the maximum stability water content in

*Assoc. Prof., Dept. of Civ. Engrg., Islamic University of Gaza, Palestine.

performing the soil security test (Tadanier, R. et al. 1985). Distilled water is used in performing all tests. In general, the flow coming out from the soil specimen of dispersive clays is cloudy, and the cracks/holes enlarge rapidly. The discharge for non-dispersive clays is clear and the cracks/hole does not increase or enlarge. These tests was developed to identify the dispersive clays and are not intended to be a scaled model of an actual prototype structure. Quantitative data are not obtained on quantity of flow through the hole, amount of soil erosion, or rate of soil erosion.

This paper presents the results of the case studies conducted in the soil Laboratory, the Islamic University-Gaza 1999-2000. Eight different clays for the core of dams representing a wide range of geographic locations of Gaza Strip are obtained; That was carried out to examine the clay dispersion characteristics. The effect of filter on time-to-failure of the soil security test, and the presence of granular zones as filters was investigated.

Sites of Clay:

The location of the soil specimens is shown in Figure 1. The clay soils are inorganic of low to medium plasticity (CL) from eight sites. Standard laboratory tests were performed on soil samples to obtain plasticity index and activity values. The soils are classified according to the Unified soil classification system (USCS). Table 1 shows the standard soil index properties.

Table 1: Soil Index Properties:

Sample	LL %	PL %	PI %	LSL %	G_S	GRAIN SIZE DISTRIBUTION(%)				A	W_{NAT} %	W_{OPT} %	ρ_d g/cm^3	USCS
						G	S	M	C					
Rafah-AL-Jenina	25	18.57	6.43	7.5	2.64	1	43.5	34	21.5	0.299	5.75	13	1.875	CL-ML
Rafah-AL-Salam	31.59	19.17	12.42	8.57	2.65	1.5	34	38	26.5	0.469	12.19	15.8	1.771	CL
Abassan-1	41.4	22.07	19.33	10	2.75	0	20	44.5	35.5	0.545	5.95	17.6	1.569	CL
Abassan-2	21.15	16.83	4.32	4.29	2.67	1.5	56.5	28.4	13.6	0.318	0.77	13.5	1.88	CL-ML
AL-Nusirat	29.05	17.68	11.37	8.93	2.62	2.2	30.4	41.7	25.7	0.442	2.47	15.7	1.76	CL
AL-Shajaiah	32.55	20.96	11.59	11.29	2.7	1	45	29	25	0.464	3.68	13	1.875	CL
Bit Lahia	41	16.62	24.38	12.14	2.57	1.4	40.4	39.1	19.1	1.276	17.85	16.6	1.797	CL
Industrial Zone	47.58	30.68	16.9	12.5	2.72	1.1	32.9	31	35	0.483	20.62	24.3	1.505	ML or OL

LL: LIQUID LIMIT, PL: PLASTIC LIMIT, PI: PLASTISTY INDEX, LSL: LINIAR SHRENK. LIMIT, G_S: SPESIFIC GRAVIT, G: GRAVEL (>2 mm) %, S: SAND (0.06-2mm, M: SILT (2μm-60μm) %, C: CLAY (<2μm) %, A: ACTIVITY, W_{NAT}: NATURAL WATER CONTENT, W_{OPT}: OPTIMUM WATER CONTENT, ρ_d: MAXIMUM DRY DENSITY (g/cm^3), CL: Inorganic clay of low plasticity, ML: Inorganic silts with slight plasticity, OL: Organic silty clay of low plasticity

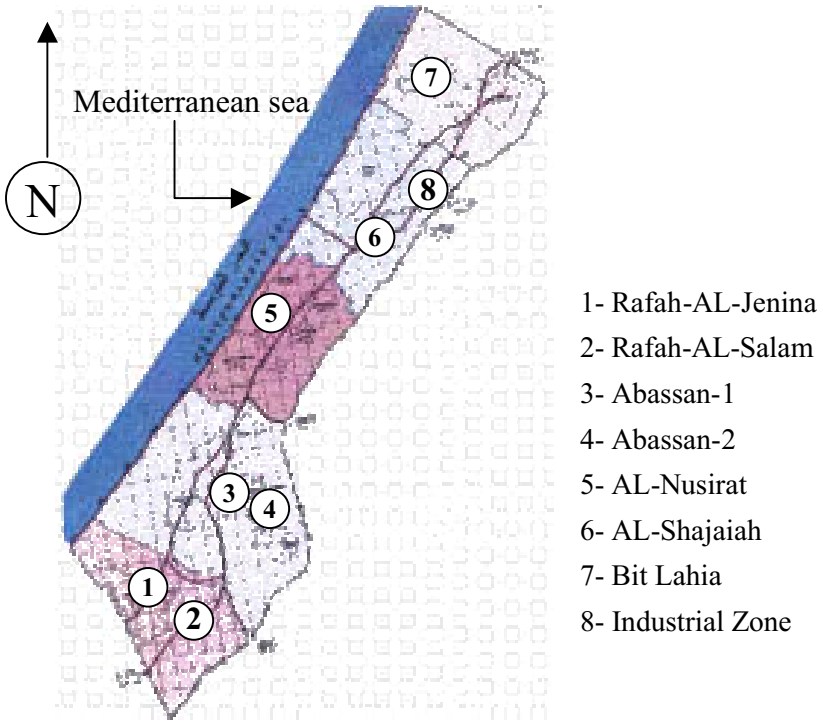

Figure 1: Gaza Strip Map, Location of Soil Samples.

Testing Program:

Dispersive clays are particular types of soils in which the clay fraction erodes in the presence of water by a process of deflocculation. (Sherard et al 1972). Sherard et al. (1976 "b") concluded that dispersive clays cannot be identified by conventional index tests such as particle size distribution, Atterberg limits, compaction characteristics, particle size distribution, and activity. Resendiz (1977) presented a disagreement showing that clays with activity between 0.3 to 1 seemed to be a necessary condition, but not sufficient for indicating dispersive state.
Tadanier (1985) Showed that the clay samples with activity between 0.3 to 1 can be either dispersive or non-dispersive.

Chemical Tests:

Chemical analyses of the eight soils samples were carried out to determine the chemical parameters which identify the dispersion characteristics. The saturated soil pastes were prepared by adding distilled water to the soil specimen while stirring with a spatula. The soil-water mixture was occasionally consolidated during the stirring process by tapping the container on the workbench. At the saturation point, the soil paste glistens as it reflects light and flows slightly when the container is tipped. After mixing, the specimens were allowed to stand for more than an hour, and then the saturation point was rechecked. Then, the specimens were

filtered using a vacuum pump to obtain a clear extract. Soluble cations in saturation extract were first measured. Then using these known values, the total dissolved salts in saturation extract (TDS), exchangeable sodium percentage (ESP), sodium adsorption ratio (SAR) and percent of sodium (PS) were calculated. Based on the criterion established by sherard et. al. (1976 b), the soils were classified in the manner shown in Figure 2. The results of various chemical tests carried out on the eight specimens are listed in Table 2. The lowest ion concentration of dissolved salts occurs at Bit Lahia.

Table 2: Chemical Properties of Soil:

Sample	EC µS/cm	PH	CL mg/L	O %	SOLUBLE SALT IN SATURATION EXRTACT			SAR	TDS Meq/l	%Na	ESP
					Na^+ meq/l	$Ca^{++} + Mg^{++}$ meq/l	K^+ meq/l				
Rafah-AL-Jenina	3240	7.19	875	2.2	33.88	12.53	0.26	13.54	46.67	72.59	15.76
Rafah-AL-Salam	1177	7.8	300	2.36	16.52	10.78	0.33	7.12	27.63	59.79	8.46
Abassan-1	942	8.46	50	2.53	13.91	3.74	0.31	10.17	17.96	77.47	12.09
Abassan-2	1007	8.37	140	2.01	9.72	5.12	0.05	6.08	14.89	65.28	7.15
AL-Nusirat	1000	8.1	150	1.75	7.71	6.23	0.53	4.37	14.47	53.30	4.93
AL-Shajaiah	2600	7.92	850	2.62	31.84	22.13	0.36	9.57	54.33	58.61	11.40
Bit Lahia	376	7.1	50	2.38	2.00	6.59	0.17	1.10	8.76	22.82	0.36
Industrial Zone	2060	8.04	600	2.62	15.30	17.41	0.43	5.19	33.15	46.17	6.01

O: Organic mater, meq= milliequivalent; **µS**= micro siemens.

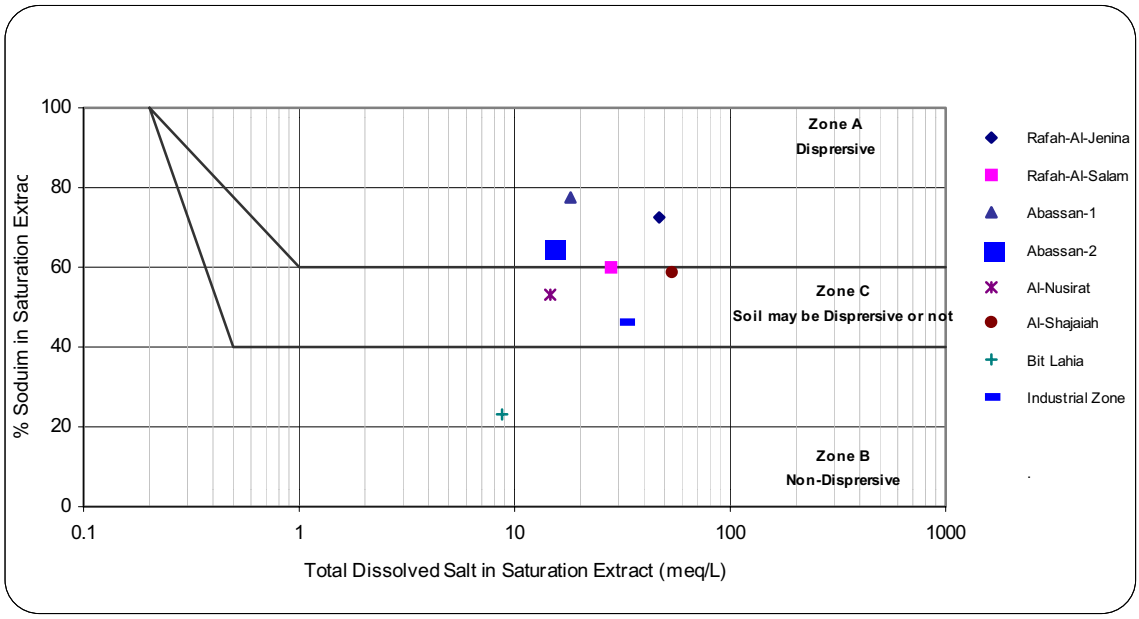

Figure 2: Result of Pore Water Salinity Test

All specimens exhibited a slightly alkaline pH (average 7.87). The predominance of sodium in the saturation extract of clay samples classifies them in dispersive zone and intermediate zone, The lower sodium percent of Bit Lahia clay classifies it in nondispersive zone.

Crumb Test:

Crumb test is used to determine dispersion potential qualitatively. A natural piece of soil is placed in water and the tendency of the clay particles to go into colloidal suspension is observed as a degree of muddiness of the water, using the interpretative guide proposed by sherard et. al. (1976 b). The suggested Grades are; grade 1- No reaction, 2- Slight reaction, 3- Moderate reaction, and 4- Strong reaction. The crumb test were applied for the eight soils. Electrical conductivity (EC) and (pH) of the test water were measured at the beginning and at the end of the test. The results of these test are listed in Table 3.

The measured pH of the soil specimens which were slightly below 7 in acidic environment could result in electrostatic attraction between particles and consequently less dispersion. (Landau and Altschaeffl 1977).

Table 3: Crumb Test Results:

SAMPLE	WATER CONTENT %	2 min		15 min		60 min		24 hr		pH	EC µS/cm	COMMENTS
		GRADE	TEMP.C	GRADE	TEMP.C	GRADE	TEMP.C	GRADE	TEMP.C			
Rafah-AL-Jenina	Dry	1	14.5	1	14.5	1	14.5	1	14.6	6.60	883	Nondispersive
	14.81	1	15	1	15	1	15	1	15	6.39	601	Nondispersive
Rafah-AL-Salam	Dry	1	14.5	1	14.5	1	14.5	1	14.6	6.40	176.2	Nondispersive
	9.01	1	15	1	15	1	15	1	15	6.80	236	Nondispersive
Abassan-1	Dry	3	14.5	2	14.5	2	14.5	1	14.6	7.11	219	Nondispersive
	6.2	2	15	1	15	1	15	1	15	6.74	148	Nondispersive
Abassan-2	Dry	1	14.5	1	14.5	1	14.5	1	14.5	6.90	229	Nondispersive
	2.55	1	15	1	15	1	15	1	15	6.84	197	Nondispersive
AL-Nusirat	Dry	2	14.2	2	14.5	1	14.5	1	14.6	6.95	210	Nondispersive
	3.8	2	15	2	15	2	15	1	15	6.85	430	Nondispersive
AL-Shajaiah	Dry	1	14.5	1	14.5	1	14.5	1	14.6	7.05	492	Nondispersive
	2.99	1	15	1	15	1	15	1	15	7.00	400	Nondispersive
Bit Lahia	Dry	1	14.5	1	14.5	1	14.5	1	14.6	6.20	75.6	Nondispersive
	3.71	1	15	1	15	1	15	1	15	6.64	150	Nondispersive
Industeial Zone	Dry	2	14.5	2	14.5	1	14.5	1	14.6	6.00	147.7	Nondispersive
	7.51	2	15	2	15	2	15	1	15	6.71	177.8	Nondispersive

Initial temperature: 15°C, Initial pH=6.8, Initial EC=10µS/cm

In general, crumb test classified all soils as nondispersive in the dry and natural water content states.

Double Hydrometer Test:

In this test, the soil is subjected to hydrometer analysis twice. The results of the regular hydrometer test are compared with one which done without dispersing agent and mechanical agitation. According to U.S. Soil Conservation Service, the percent dispersion is calculated as the ratio of percentage of material less than 5 μm without dispersing agent and mechanical agitation to that measured with dispersing agent and mechanical agitation. Soils with percent dispersion values greater than 50 were classified as dispersive, less than 30 as nondispersive, and between 30 to 50 as intermediate. Percent dispersion values and grading of all soils are given in Table 4 which compare the outcome of all dispersion tests.

Table 4: Double hydrometer test results

Sample	A Particles smaller than 0.005 mm In the modified test %	B Particles smaller than 0.005 mm In the Standard test %	Percent Dispersion (A/B)*100	COMMENTS
Rafah-AL-Jenina	4.44	22.68	19.58	Nondispersive
Rafah-AL-Salam	5.83	24.97	23.34	Nondispersive
Abassan-1	6.29	37.86	16.61	Nondispersive
Abassan-2	3.48	17.11	20.34	Nondispersive
AL-Nusirat	11.91	26.59	44.79	Intermediate
AL-Shajaiah	2.13	24.81	8.59	Nondispersive
Bit Lahia	4.14	24.53	16.88	Nondispersive
Industrial Zone	10.08	41.92	24.05	Nondispersive

Using the criteria for dispersion, seven specimens are classified as nondispersive and one as intermediate (Al-Nusirat).

Pinhole Test:

Water flows through a pinhole in a clay specimen at varying heads. Pinhole test was carried out on all eight soils, using the procedure described by U.S. Bureau of Reclamation. In this method, flow rates can be evaluated quantitatively to classify the soils as dispersive (D1, D2), intermediate (ND3, ND4), nondispersive (ND1, ND2), (Sherard et al 1976 a). A grading of soils in terms of flow rates obtained in pinhole tests are shown in Table 5.

Table 5: Pinhole test results

Sample	FLOW RATE (ml/sec)								Percent Erosion %	Comment
	Head (50 mm)		Head (180 mm)		Head (380 mm)		Head (1020 mm)			
	Minimum	Maximum	Minimum	Maximum	Minimum	Maximum	Minimum	Maximum		
Rafah-AL-Jenina	0.03	0.06	0.05	0.08	0.08	0.33	0.41	0.88	0.156	Nondispersive
Rafah-AL-Salam	0.06	0.1	0.2	0.233	0.333	0.4	0.683	0.92	0.146	Nondispersive
Abassan-1	0.02	0.09	0.04	0.07	0.06	0.14	0.433	0.433	1.103	Nondispersive
Abassan-2	0.08	0.16	0.16	0.26	0.41	0.46	0.55	0.66	1.086	Nondispersive
AL-Nusirat	0.01	0.03	0.03	0.1	0.1	0.27	0.25	0.27	0.656	Nondispersive
AL-Shajaiah	0.01	0.05	0.06	0.08	0.08	0.25	0.78	0.91	0.35	Nondispersive
Bit Lahia	0.04	0.08	0.1	0.15	0.2	0.36	0.6	0.91	0.07	Nondispersive
Industrial Zone	0.02	0.03	0.03	0.09	0.09	0.2	0.2	0.33	0.015	Nondispersive

ND1=Nondispersive soil: no collaidal erosion under 380 or 1020mm, flow rate <5.ml/sec

Pinholes test results indicated no erosion occurred through the pinhole in the soil specimen under all stages of the test . This indicates considerable resistance of the intact soil to erosion and piping.

Soil Security Test:

Soil security test, developed by Tadanier and Ingles (1985), is performed by filling a central hole in a compacted soil cylinder with distilled water and determining the failure time as suggested by Geomechanics Laboratory of the New South Wales Public Work Department. Compacted samples are cored axially to a depth of 85 mm using a sampling tube of 50 mm in external diameter. The test enables to grade the soils qualitatively according to the color of the flowing water. If the flowing water is visibly cloudy and does not become clearer with time, the soil is dispersive; with a slight cloudiness, it is intermediate; and in case of clear water without any noticeable erosion, it is nondispersive. Eight samples were compacted on the wet side with 2 percent above the optimum water content and the soil security test were carried out on them.

Tuncer B.R. et al. (1989) made an attempt to quantify the soil security test, using the experimental data represented by Tadanier and Ingles (1985). The results of each test can be categorized into one of the three categories shown below Tabl e 6. Results showed five samples have

intermediate dispersion, and one dispersive, while the rest are nondispersive.

Powder ash with specific gravity equals to 2.57, percent smaller than 300μm is 92.4% and specific surface area (the total surface area of all grains per unit weight) equals to 397.2 m^2/kg was added to the samples in ratio of 3% of the dry soil by weight and mixed thoroughly before preparing the compacted specimens. In general, the ash is nonplastic and cohesionless material. Time-to-failure of all specimens was decreased after adding ash. This addition of ash transforms the highly nondispersive clay to intermediate or dispersive clay. Hausmann, M.R. (1990) mentions that the lack of cohesion in ash makes it highly erodible that agrees with the above results.

Table 6: Soil Security test results:

Sample	OPTIM. WATER CONTENT (%)	MAXIMUM DRY DENSITY (g/cm^3)	TIME TO FAILURE T_f (minutes)	
			NO FILTER	ASH (3%)
Rafah-AL-Jenina	13.0	1.875	165	25
Rafah-AL-Salam	15.8	1.771	100	70
Abassan-1	17.6	1.569	36	23
Abassan-2	13.5	1.880	> 420	123
AL-Nusirat	15.7	1.760	159	40
AL-Shajaiah	13.0	1.875	> 420	108
Bit Lahia	16.5	1.797	62	26
Industrial Zone	24.3	1.505	139	46

Note: Time to failure Category

$T_f < 45$	Dispersive;
$45 < T_f < 420$	Intermediate;
$T_f > 420$	Non-Dispersive

Relationship Among Individual Tests:

The relationship among the individual tests can be developed using the results of the tests where all five tests were performed on each of eight clay samples. The dispersive category indicated by each test is listed in Table 7. The last right column of Table 7 lists the common agreement of the five tests, determined by averaging the individual results from the five tests with equal weight given to each test.

Table 7: Comparison of test results.

Sample	Chemical	Crumb	Double Hydrometer	Pinhole	Soil Security	consensus
Rafah-AL-Jenina	D	ND	ND	ND	ND	ND
Rafah-AL-Salam	I	ND	ND	ND	ND	ND
Abassan-1	D	ND	ND	ND	I	ND
Abassan-2	D	ND	ND	ND	ND	ND
AL-Nusirat	I	ND	I	ND	ND	ND
AL-Shajaiah	I	ND	ND	ND	ND	ND
Bit Lahia	ND	ND	ND	ND	ND	ND
Industrial Zone	I	ND	ND	ND	ND	ND

ND: nondispersive, I: Intermediate.

In general, all tests agree with each other in predicting nondispersive clays, except the chemical test results. In contrast, the chemical test indicated that only Bit Lahia specimen was nondispersive. On the other hand, the rest results of the chemical analysis were in considerable disagreement on clays of high sodium content; this result indicated an agreement with Marshall and Workman (1977).

It is important to observe that the activity coefficient of eight samples ranges from 0.299 to 1.276 and the clays are nondispersive, which disagrees with Resendiz (1977).

Modified Soil Security Test:

Erosion in the dams is a function of the interaction of several variables. The author believes that, to fully explain the internal erosion process, the factors that measure the water-retention performance in situ must be considered. The principal difference in the erosion environment of the soil security test is that transition zones (up stream and down stream) are not used to control the clay particles migration in the soil security test, whereas it probably is a major factor in controlling a crack enlargement in an earth dam. The modified soil security test is an attempt to simulate the field conditions. Arulanandan, et al (1983) concluded "Even if the clay is erodible, it is possible to prevent dam failure if adequate protective filters are provided". Foster et al (2000 b) presented

that statistically there have been no failures for dams with good quality filters in downstream of the core. Well-designed and well-constructed graded filters are effective in preventing internal erosion and sealing concentrated leaks (Sherard and Dunnigan 1989, Peck 1990, Ripley 1983,1984,1986, quoted from Foster et al. 2000 b).

To study the influence of having granular zones in dispersion, the model suggested by Oud 1987 for future research is used. The filter thickness should be sufficient to allow a filtration zone to be developed, to retain the soil particles from eroding away. The standard filter thickness ranges from 2.5cm to 3.7cm. (Tomlinson and Vaid 2000). For each sample, three modified soil security tests were performed using pea gravel (6.7mm to 9.5mm size) as filter. A sketch of the modified soil security test is shown in Figure 3. The soil security test includes (i). Placing filter in the central hole only, (ii). Placing filter around the compacted soil cylinder only and, (iii). Placing filter in the central hole and around the compacted soil cylinder (modified test). The results of the testing could be used to determine quantitatively the variation in the clay classification.

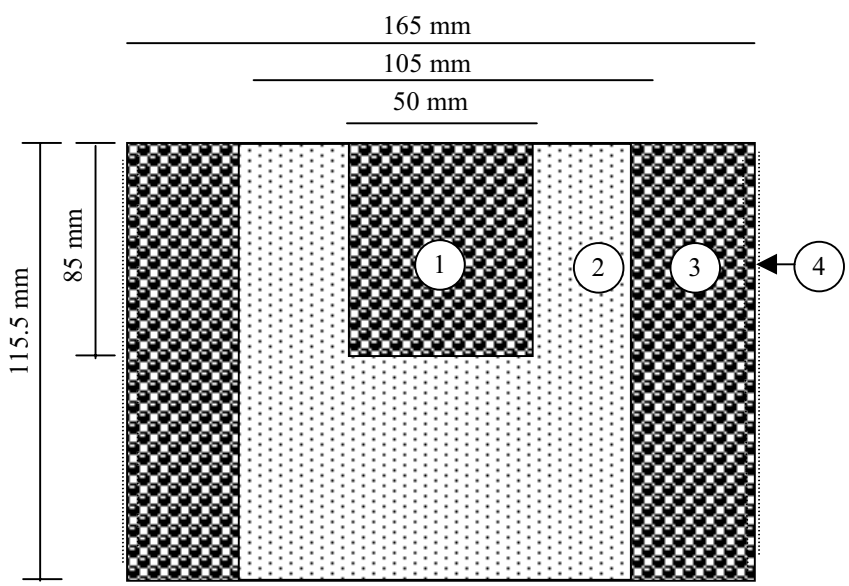

1) Axial hole 50mm diam., 85mm depth. With filter material.

2) Soil Sample. , (3) Filter Material., (4) Screen.

Figure 3: Modified Soil Security Test.

Test results and grading the dispersibilty of soils in terms of time-to-failure under the presence of granular zones presented in Table 8.

Table 8: Modified Soil Security test results.

Sample	TIME TO FAILURE T_f(minutes)			Quantitative		Qualitative	
	INTERNAL FILTER	EXTERNAL FILTER	COMBINED FILTER	SST	MSST	SST	MSST
Rafah-AL-Jenina	301	258	> 420	I	ND	ND	ND
Rafah-AL-Salam	116	150	201	I	I	ND	ND
Abassan-1	48	133	151	D	I	I	ND
Abassan-2	> 420	> 420	> 420	ND	ND	ND	ND
AL-Nusirat	> 420	> 420	> 420	I	ND	ND	ND
AL-Shajaiah	> 420	> 420	> 420	ND	ND	ND	ND
Bit Lahia	88	75	98	I	I	ND	ND
Industrial Zone	183	157	259	I	I	ND	ND

SST: soil Security Test; MSST: Modified Soil Security Test.

It is interesting to recognize that T_f in the case of modified test is increased with an average of 150% compared to the regular soil security test. The results of each modified soil security test are further compared in Table 8. It can be seen that qualitatively the classification of dispersive clays by the modified soil security test is not strongly influenced, only Abssan-1 transformed from intermediate to nondispersive. The qualitative results of modified soil security tests are also in excellent agreement with crumb and pinhole tests; that provided additional confidence in this test.

The quantitative results of the modified test are in good agreement with qualitative results of overall tests, which shows better agreement than the soil security test.

Conclusions:

The main conclusions of this study are:

1. To classify the erosion potential of a given soil, the effect of interactions between several variables, should be considered. Soil type, chemical composition of soil and water content, well-designed and well-constructed filter are of primary important factors.

2. It is confirmed that filter effectively increases the time-to-failure and controls the migration of the clay particles.
3. It seems that ash can't be used as stabilizing materials to reduce the erosion potential of a soil. Any soil additives should be examined before use in dam construction.
4. Four physical tests were found to be in excellent agreement for nondispersive clays.
5. Considerable disagreement was found among the chemical analysis and the physical one.
6. Soil classifications showed no relationship with soil dispersivity or time-to-failure.
7. Practical recommendations for the control of internal erosion failure should be based on theoretical results, and practical testing.
8. It appears that the general boundary of change between dispersive and nondispersive behaviour for a given clay needs to be studied for modified soil security test.

Acknowledgments:

The author is grateful to IUG. Soil Mech. Laboratory and Eng. Astal, K., AL-Jazzar, T., Farra, S. and Isliem, A. who assisted in Test performing as part of their graduate project. Personal thanks go to Eng. Kurd, A. and Hamad, A.

References:

1. Arulanandan, K. and Perry, E. B., 1983 "Erosion in Relation to filter Desian Criteria in Earth Dams' J. of Geotech. Eng. ASCE, Vol. 109, No. 5, pp. 682-698.
2. Crosta, G., and di Prisco, C., 1999 "On Slope instability induced by seepage erosion" Can. Geotech. J. 36: 1056-1073.
3. Foster, M., Fell, R., and Spannagle, M. 2000 (a) "The statistics of embankment dam failures and accidents" Can. Geotech. J. 37: 1000-1024.

4. Foster, M., Fell, R., and Spannagle, M. 2000 (b) "A method for assessing the relative likelihood of failure of embankment dams by piping" Can. Geotech. J. 37: 1025-1061.
5. Hjeldnes, E. I., and Lavania, B.V.K., 1980. "Cracking, Leakage and Erosion of Earth Dam Materials", Journal of Geotechnical Engineering Division, American Society of Civil Engineers, Vol. 106, No GT2, pp. 117-135.
6. Hausmann, M. R., 1990. "Engineering Principles of Ground Modification" McGrow-Hill Publishing Company pp. 318-324.
7. Landau, H.G., and Altschaeffl, A.G., 1977. "Conditions Causing Piping in Compacted Clay". Dispersive Clays, Related Piping and Erosion in Geotechnical Projects, ASTM, STP 623, J.L. Sherard and R.S. Decker, Eds., American Society for Testing and Materials, pp. 240-259.
8. Marshall, A.F., and Workman, J.P, 1977. "Identification of Dispersive Clays in the Texas Gulf Coast Area", Dispersive Clays, Related Piping and Erosion in Geotechnical Projects, ASTM, STP 623, J.L. Sherard and R.S. Decker. Eds., American Society for Testing and Materials, pp. 274-288.
9. Oud, M. 1987, " Internal Erosion in Earth Structures" Master of Science Thesis, Middle East Technical University, Ankara.
10. Resendiz, D., 1977. "Relevance of Atterberg Limits in Evaluating Piping and Breaching Potential", Dispersive Clays, Related Piping and Erosion in Geotechnical Projects, ASTM, STP 623, J.L. Sherard and R.S. Decker. Eds., American Society for Testing and Materials, pp. 341-353.
11. Sherard, J.L., Decker, R.S., and Ryker, N.L., 1972. "Piping in Earth Dams of Dispersive Clay", Proceedings, Specialty Conference on Performance of Earth and Earth Supported Structures, American Society of Civil Engineers, Vol. 1, Part 1, pp. 589-626.
12. Sherard, J.L., Dunnigan, L.P., Decker, R.S., and Steels, E.F., 1976 (a). "Pinhole Test for Identifying Dispersive Soils",

Journal of Geotechnical Engineering Division, American Society of Civil Engineers, Vol. 102, No. GT1, pp. 69-85.

13. Sherard, J.L., Dunnigan, L.P., Decker, R.S., and Steels, E.F., 1976 (b). "Identification and Nature of Dispersive Soils", Journal of Geotechnical Engineering Division, American Society of Civil Engineers, Vol. 102, No. GT1, pp. 287-301.
14. Statton, C.T., and Mitchell, J.K. 1977 "Influence of Eroding Solution Composition on Dispersive Behavior of a Compacted Clay Shale", Journal of Geotechnical Engineering Division, American Society of Civil Engineers, Vol. 102, No. GT1, pp.398-407.
15. Tadanier, R., and Ingles, O.G., 1985. "Soil Security Test for Water Retaining Structures", Journal of Geotechnical Engineering, American Society of Civil Engineers, Vol. 111, No. 3, pp. 289-301.
16. Tomlinson, S.S., and Vaid, 4. P. 2000. "Seepage forces and Confining Pressure Effects on Piping Erosion" Can. Geotech. J. Num. 1. Pp. 1-13.
17. Tuncer, E.R., Ordemir, I.M., and Oud M. 1989 "Soil Suceptibility to dispersion", Proceedings, of the Twelfth International Conference on Soil Mech. And Found. Engineering, pp. 2115-2118.

Effects of Cohesion on Bridge Scour

By

Albert Molinas[1], Sterling J. Jones[2]

ABSTRACT

This paper summarizes the comprehensive experimental study that was carried out at the Colorado State University Hydraulic Laboratory for the Federal Highway Administration to investigate effects of cohesion on bridge scour. In general, cohesive bridge scour experiments are classified as low clay content and high clay content experiments. In the presence of low clay contents, scour taking place around bridge piers and abutments exhibits characteristics observed in non-cohesive materials. In this case, the clay content is accounted for by the introduction of a scour reduction factor. As the clay content increases beyond a certain limit, cohesive material properties such as compaction, shear strength, initial water content, clay mineralogy, etc. dominate the scour process. For each class of experiments, results are summarized by equations using commonly measured parameters. The experimental study shows that for flows falling within the clear-water scour range, effects of cohesion may play a significant role in the magnitude of scour.

INTRODUCTION

In this paper effects of cohesion on local pier and abutment scour are investigated experimentally for Montmorillonitic and Kaolinitic clay mixtures using larger scale, 1.2 m, 2.4 m, and 5 m wide test flumes at the Colorado State University Hydraulics Laboratory housed in the Engineering Research Center. For low clay content soil mixtures with up to 12 percent clayey material, pier and abutment scour experiments show that the presence of a small amount of cohesive material may reduce scour considerably. To quantify the impact of clay content, scour in clayey sands is expressed as a fraction of scour measured in non-cohesive materials through a clay content reduction factor (K_{cc}). It is shown that K_{cc} is a function of clay content. It is also shown that different clay minerals have varying impacts on reducing bridge scour. For cohesive soils with significant clay content (30 percent for the present mixtures), soil parameters such as compaction, initial water content, degree of saturation, shear strength, and type of clay mineral dominate the abutment scour. In this study these effects are

[1] President, Hydrau-Tech, Inc., 333 West Drake Road, Suite 40, Ft Collins, CO 80526 (molinas@hydrau-tech.com).
[2] Hydraulic Research Engineer, Federal Highway Administration, 6300 Georgetown Pike, McLean, VA 22101 (Sterling.Jones@igate.fhwa.dot.gov).

quantified for flow conditions with Froude numbers ranging from 0.2 to 0.9. Equations relating flow and selected cohesive soil parameters to bridge pier and abutment scour were developed to explain the variability of abutment scour with cohesion properties. These equations express bridge scour in cohesive soils relative to clear-water scour in non-cohesive material for the same flow and geometry conditions. Under the same geometric and flow conditions, measured scour in cohesive materials varies from 7 percent to 140 percent of that measured in medium sand.

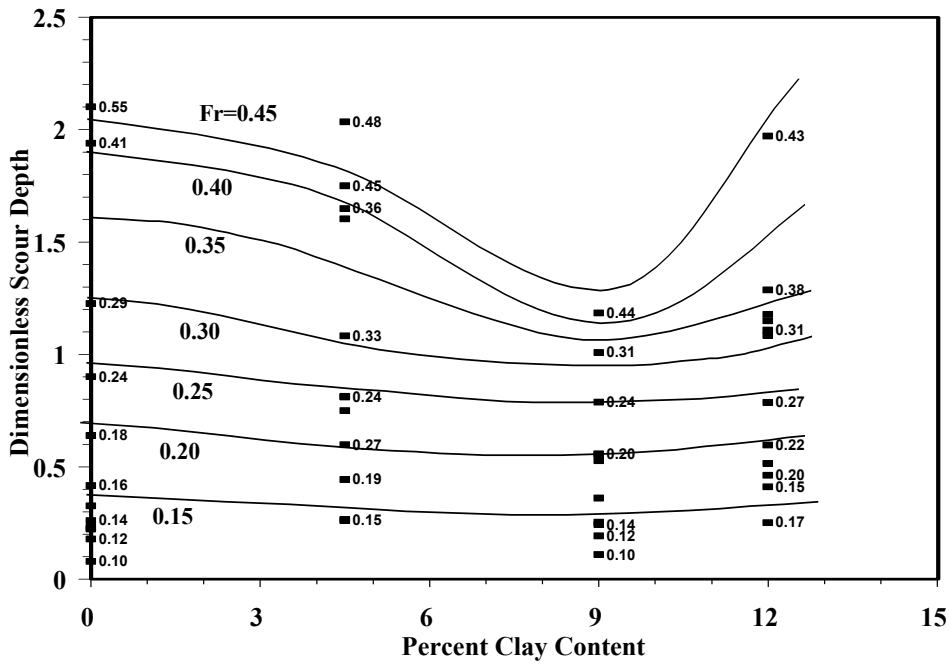

Fig. 1. Effect of clay content on abutment scour

LOW CLAY CONTENT EXPERIMENTS

Scour at bridges has been studied extensively in the past for non-cohesive sediments. The currently adopted scour estimation methodologies are developed from laboratory experiments conducted in sand or gravel beds. No expression for scour depth estimation is available to account for the presence of cohesive materials in cases where bridges are founded in clayey sands. Figure 1 illustrates the effect of varying cohesive material content on abutment scour. As shown in this figure, as the cohesive material content is increased, the depth of scour is reduced. However, beyond a certain threshold this behavior is reversed. The ultimate scour depth computations for the sandy clay materials are further

complicated by the presence of different clay minerals. This section presents the results of experiments to quantify the presence of small amounts of clay on bridge scour. Results of these experiments are presented in terms of empirical relationships that relate scour in cohesive material to that observed in the non-cohesive material that was used in preparing the mixtures for the same flow and geometric conditions. The sand used in mixing with clayey soils had a median diameter of 0.55 mm and a gradation coefficient σ_g of 2.43. The properties of clays used in the mixtures are elaborated in the following section.

Pier Scour

Results of pier scour experiments in clayey sands are presented in figure 2. In deriving this figure, scour depths observed in Montmorillonitic clayey sand were normalized with the sand scour observed under similar flow and geometry conditions. In figure 2, pier scour results are expressed in terms of a reduction factor, K_{cc} , whose value ranges between 0 and 1; K_{cc} equal to unity denotes the depth of scour being equal to that observed in sand. Since the pier shape and width, flow depth, and sand properties were kept near constant, it was possible to identify the effects of clay content under various flow conditions. Figure 2 shows that for a given clay content, the clay content reduction factor (K_{cc}) is independent of approach flow conditions. The expression that best fits the data is given by:

$$K_{cc} = \frac{1}{1 + (\frac{CC}{11})^{0.9}}; \qquad 0 \le CC \le 11 \tag{1}$$

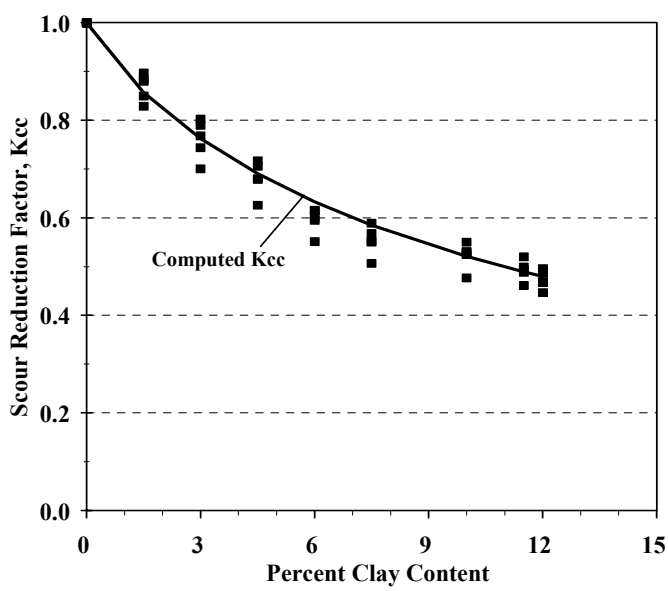

Fig. 2. Pier scour reduction factor for Montmorillonite clay mixtures.

Abutment Scour

Results of abutment experiments in clayey sands are summarized in figures 3 and 4. Similar to pier scour experiments, in deriving these figures scour depths observed in clayey sand were normalized with the scour observed in sand under similar flow and geometry conditions. In figures 3 and 4, abutment scour results are expressed in terms of a reduction factor K_{cc} whose value ranges between 0 and 1; K_{cc} equal to unity denotes the depth of scour being equal to that observed in sand. Since the abutment size and shape, flow depth, and sand properties were kept near constant, it was possible to identify the effects of clay content under various flow conditions. Figures 3 and 4 show that for a given clay content, the clay content reduction factor (K_{cc}) is independent of approach flow conditions. The expression that best fits the data for Montmorillonite clay mixtures is given by:

$$K_{cc} = \frac{1}{1 + (\frac{CC}{\alpha})^{\beta}}; \qquad 0 \le CC \le 11 \tag{2}$$

$\alpha, \beta =$ 16 and 1.5 for the best-fit line; and 22 and 1.8 for the envelop line that can be used as a design equation, respectively.

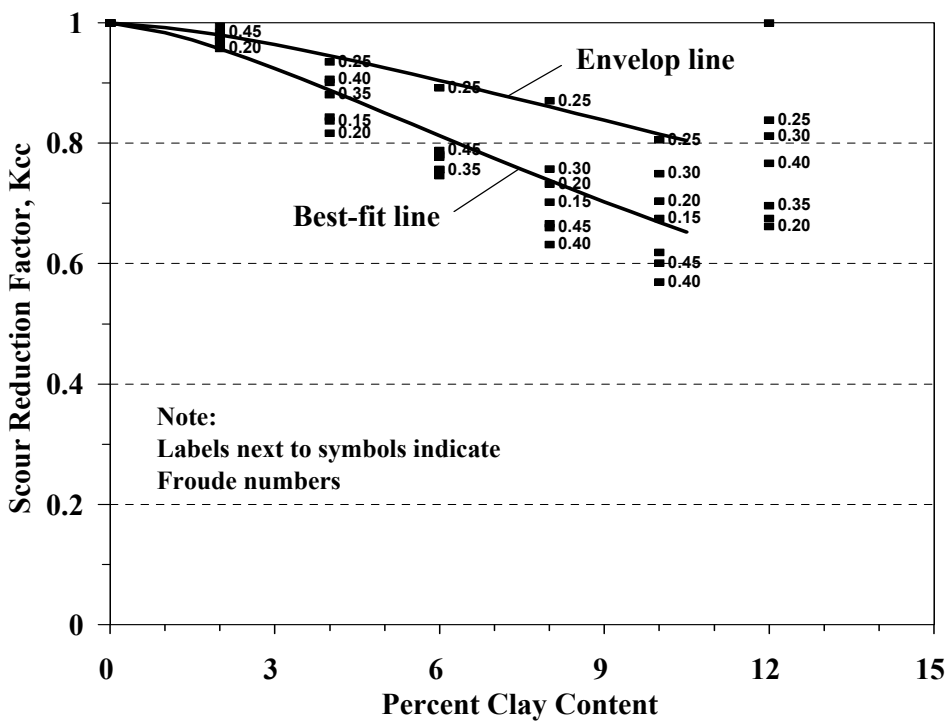

Fig. 3. Abutment scour reduction factor for Montmorillonite clay mixtures.

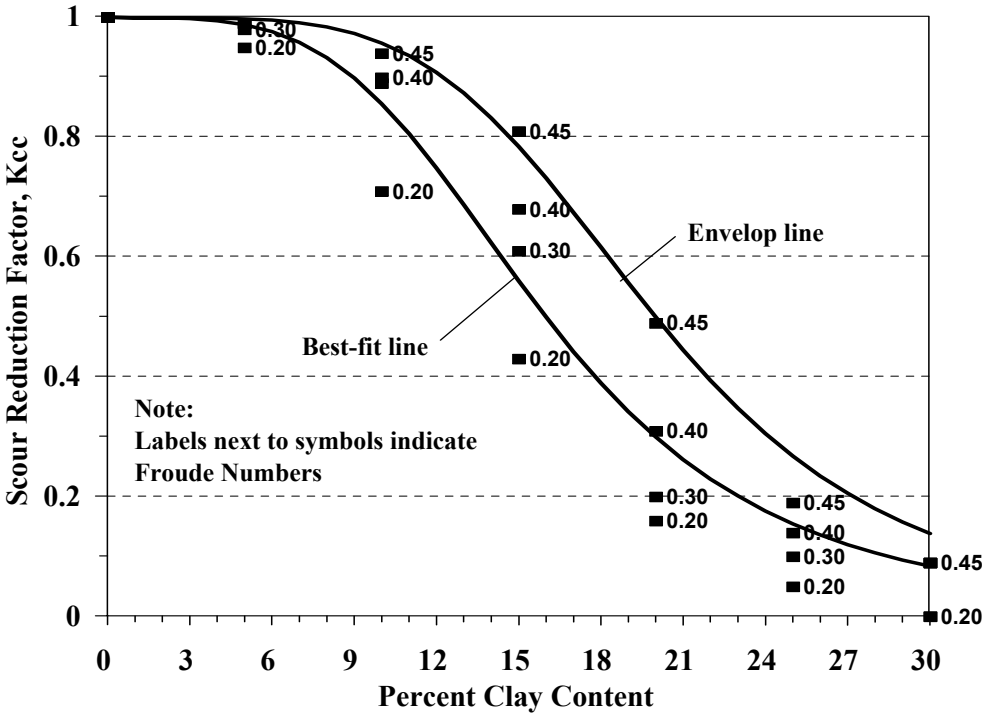

Fig. 4. Abutment scour reduction factor for Kaolonite clay mixtures.

For the Kaolinite clay mixtures the expression that best fits the data is:

$$K_{cc} = \frac{1}{1 + (\frac{CC}{\alpha})^{\beta}}; \qquad 0 \le CC \le 30 \tag{3}$$

where α,β = 16 and 3.8 for the best-fit line and 20 and 4.5 for the envelop line, respectively.

HIGH CLAY CONTENT EXPERIMENTS

Flow structure around bridge piers and abutments and the resulting local scour were studied in the past by numerous experimental, numerical, and analytical investigations for non-cohesive materials. As a result, series of empirical and semi-empirical prediction equations were developed to relate the local scour depth at bridge piers and abutments to different approach flow conditions, sediment size and gradations, and different structural types and size characteristics.

The mechanism of cohesive-material scour is significantly different from scouring of alluvial non-cohesive materials. The process involves not only the balancing of flow-induced shear stresses and the shear strength of soils to withstand scour, but also the chemical and physical bonding of individual particles and the properties of the eroding fluid. Cohesive materials, once eroded, remain in suspension. As a result, the phenomenon identified as clear-water local scour in

non-cohesive materials always prevails. Along with the eroding fluid properties, the scour process in cohesive soils is strongly affected by the amount of cohesive material present in the soil mixture as well as the type of mineral clay, initial water content, soil shear strength, and compaction of the clay. The objectives of this paper are to apply the knowledge gained in the past in cohesive material scour to study local scour around piers and abutments and to analyze effects of compaction, initial water content, soil shear strength, and the approach flow conditions on local bridge scour. For this purpose two different types of clay mixtures were used. The first cohesive mixture was a naturally occurring soil that contained 32 percent Montmorillonite mineral clay with almost the same amounts of fine sand and silt. The second cohesive mixture was prepared by blending 30 percent pure Kaolinite clay with medium sand.

Details of experiments, tabulated results, and the initial analysis of data are presented by Molinas and Hosni (1998), Molinas and Reiad (1998), Molinas and Abdeldayem(1998), Molinas, Jones and Hosni (1999). In general terms, the pier and abutment scour experiments using Montmorillonite clay mixtures are classified as unsaturated and saturated clay experiments. The Kaolinite clay scour experiments were conducted under unsaturated conditions where compaction and initial water content of the mixture were varied.

Flumes

Experiments were conducted in two different larger scale test flumes housed at the Engineering Research Center at Colorado State University to achieve desired flow intensities. These flumes are identified as the Sediment Transport Flume and the Steep Flume. The Sediment Transport Flume is 2.4 m wide by 60 m long and the Steep Flume is 1.2 m wide by 12 m long. The flow depths used in the experiments varied between 0.12 m and 0.3 m, and approach Froude numbers ranged from 0.1 to 0.9.

Measurements

Flow and sediment parameters measured in experiments were velocity distribution (vertical, longitudinal, and lateral), depth of flow, depth of scour, initial water content of soil, Torvane shear strength, and degree of compaction. Velocity measurements were carried out by the use of a magnetic flowmeter. In the experiments, approach velocity to each pier and abutment was determined by depth- and width-integrated average of 7 vertical velocity profiles. Similarly, the approach depth was determined from a width- and length-averaged value of water surface and bed elevation measurements. The bed elevations were measured along flumes across the flow channel before and after each experiment. The depth of abutment scour was measured during and at the end of each experiment; it was determined by the difference between the minimum bottom elevation at the nose region of abutment and the maximum elevation away from the structure.

Cohesive Soil Types

In this study two cohesive soil mixtures were used. The first is a naturally occurring homogeneous soil containing 32 percent clay, 30 silt, and 38 percent fine sand particles. Utilizing the X-Ray Diffraction Test, the dominant clay mineral was found to be Montmorillonite. According to the USCS, the cohesive soil is classified as medium plasticity clay and the texture as clay loam. The second cohesive soil mixture was prepared by blending commercially obtained pure Kaolinite clay with medium sand. This mixture was composed of 30 percent clay and 70 percent sand.

Piers and Abutments

In pier scour experiments, 1-m-long cylindrical piers made of clear Plexiglas with 0.152-m and 0.102-m diameters were used. The scour depth development was measured against time utilizing three measuring tapes attached to the interior wall of each pier and a periscope manufactured by the use of a small inclined mirror.
In abutment scour experiments rectangular vertical-wall abutments constructed of clear Plexiglas with protrusion lengths of 0.22 m and 0.11 m were used. Lengths of these abutments in the direction of flow were 0.44 m and 0.22 m, respectively. The scour depth development was measured against time utilizing three measuring tapes attached to the interior wall of each abutment and by the use of a small inclined mirror.

Analysis

(a) Pier Scour

In pier-scour experiments, the effects of compaction on unsaturated cohesive soils were studied by compacting the material around piers at 58, 65, 73, 80, 87, and 93 percent degree of compaction; and the effects of initial water content on saturated cohesive soil erosion were examined by saturating the soils at initial water contents of 32, 35, 40, and 45 percent.
Dimensional analysis that has been used for correlating the variables affecting the local scour depth at bridge piers has been extended to include cohesive soil properties in order to account for the cohesive bed material. The variables used in the analysis are parameters defining the soil, the fluid, and the geometry of the modeled system. Depth of pier scour, D_s, which is the dependent variable in this analysis, can be expressed as a function of the following independent variables:

$$D_{sc} = f(Y, b, V, D_{50}, \sigma_g, \phi, \rho, t, g, \upsilon, S, CC, Mn, C, IWC) \qquad (4)$$

in which D_{sc} = depth of scour; Y = depth of approach flow; b = pier width; V = velocity of approach flow; D_{50} = mean sediment diameter; σ_g = standard deviation of sediment size; ϕ = pier shape factor; t = time; g = gravitational acceleration; ρ = fluid density; υ = fluid kinematic viscosity; S = soil shear strength; CC = clay

content; *Mn* = origin of clay minerals (e.g. Kaolinite, Illite, Montmorillonite); *C* = degree of compaction; and *IWC* = initial water content.

Applying the dimensional analysis using b, V, and ρ as repeating variables, and using appropriate simplifications, the following set of dimensionless parameters can be obtained:

$$\frac{D_{sc}}{b} = f\left(F_r, IWC, \frac{S}{\rho V^2}, C \right) \tag{5}$$

in which F_r is the approach Froude number.

In the derivation of equation 5, the clay content (*CC*) was eliminated as a variable since the effects of this parameter was found to be an independent factor up to 12 percent clay content. In the pier scour experiments using Montmorillonite-clay mixtures, clay content was kept constant at 32 percent. In these experiments, the variation of scour with time was measured. This relationship was shown to be an asymptotic function with a sharp initial scour development followed by a gradual increase (Molinas, Jones, and Hosni, 1999). The initial rate of scour hole development is generally controlled by the nature of the clay mineral and other cohesive material parameters such as compaction, initial water content, etc. Past experimental and theoretical studies have shown that the velocity at the nose region of a circular pier is amplified by a factor of 1.6 to 1.7 times the approach velocity, *V*. Accordingly, the bottom shear stresses that are related to V^2 are also amplified and cause local scour in the affected zone. If approach velocities are increased beyond a threshold value, defined as critical velocity, the entire approach channel bottom becomes subject to general scour in addition to the local scour. Under these conditions, the scour hole development process continues until equilibrium slopes are attained for the entire reach and may last indefinitely. The experimental study presented in this report limited itself to conditions in which the oncoming flows do not scour the approach reach (clear water conditions). Under these conditions, as soon as the scour hole reaches a depth where the shear stresses within the hole become equal to the critical shear stress of the cohesive material, local scouring ceases. The duration of experiments in the study were long enough to maintain the equilibrium condition for at least 4 hours. The final scour depth values obtained under these conditions are independent of time, and therefore in deriving equation 5 the time parameter, *t*, is eliminated.

Pier scour analysis in this study was conducted under two major categories: 1) unsaturated Montmorillonite clay scour and 2) saturated Montmorillonite clay scour. The distinction is made since for saturated cohesive materials, parameters such as Torvane shear strength and compaction have no physical significance; whereas these parameters are important in unsaturated cohesive material scour.

UNSATURATED CONDITIONS

The measured values of (D_s /b) were regressed against the remaining dimensionless groups in equation 5. The best-fit regression equation resulting from the statistical analysis of experimental data is:

$$\frac{D_{sc}}{b} = 24715.49\ (IWC)^{-0.36}\ F_r^{\ 1.92}\ C^{-1.62} \tag{6}$$

where the initial water content (IWC) and compaction (C) are in percent. In deriving this expression, the initial water content ranged from 15 to 50 percent, and compaction ranged from 50 to 100 percent. The development of equation 6 is based on laboratory tests in which Froude numbers ranged from 0.18 to 0.37 and soil shear strength values ranged from 0.1 to 0.45 kg/cm^2. The higher value of the correlation coefficient, $R^2 = 0.95$, between the observed and predicted scour ratio indicates the strong correlation between measured scour depths and the parameters selected for defining flow and sediment properties. The plot of equation 6 with observed data is presented in figure 4. Pier scour corresponding to Froude numbers less than 0.2 and for compaction ratios higher than 85 percent is zero (scour threshold conditions).

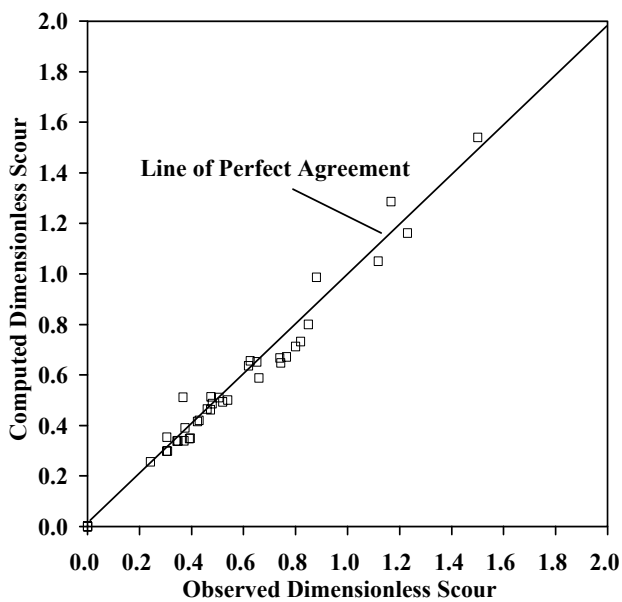

Fig. 4. Computed vs. measured dimensionless pier scour depth for unsaturated Montmorillonite clay.

SATURATED CONDITIONS

For saturated Montmorillonite clay soils, equation 5 can be further simplified by eliminating the dimensionless soil shear strength parameter, ($S/\rho V^2$), since this term has no physical meaning for saturated clays at high initial water contents (it approaches to 0). Also, for saturated conditions the compaction of cohesive soils, C, is mainly related to the water content and can therefore be removed from the list of independent variables. Introducing the pier scour initiating Froude number, F_i, to define threshold conditions for pier scour and replacing F_r by $(F_r\text{-}F_i)$, equation 5 becomes:

$$\frac{D_{sc}}{b} = f(IWC, F_r - F_i) \tag{7}$$

Using the results of experimental study, F_i and D_s/b are determined as:

$$F_i = \frac{350}{(IWC^2)} \tag{8}$$

$$\frac{D_{sc}}{b} = \begin{cases} 0 & for \quad F_r < F_i \\ 0.0288(IWC)^{1.14}(F_r - F_i)^{0.6} & for \quad F_r < F_i \end{cases} \tag{9}$$

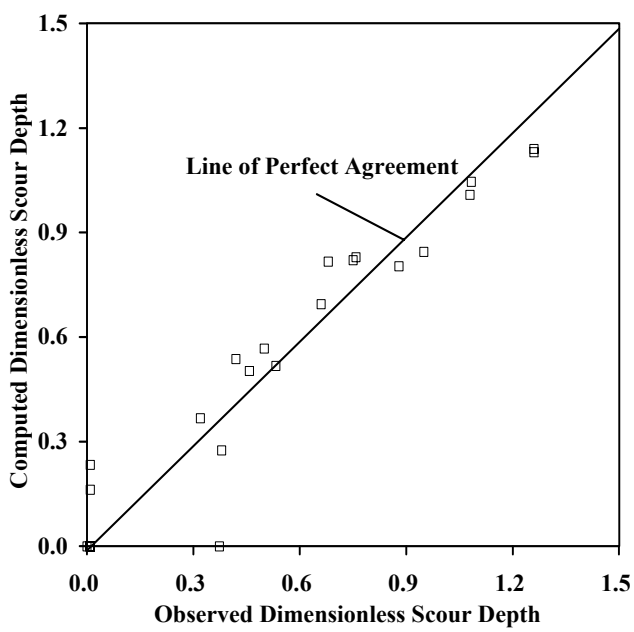

Fig. 5. Computed and measured dimensionless pier scour depth for saturated Montmorillonite clay.

For supercritical approach conditions, the value of experimental coefficient 0.0288 was found to be 0.0131. The plot of equation 9 with observed data is presented in figure 5.

(b) Abutment Scour

The functional relationship between the maximum depth of abutment scour and the parameters defining the soil, fluid, and the geometry of the abutment is derived through dimensional analysis. The depth of abutment scour in cohesive material (D_{sc}) can be expressed as a function of the following independent variables:

$$D_{sc} = f(D_s, Y, a, L, V, IWC, C, CC, S, Mn, T, t, g, \alpha, \phi, \rho, \upsilon) \quad (10)$$

in which D_s = depth of abutment scour in noncohesive material for conditions corresponding to D_{sc}; Y = depth of approach flow; a = abutment protrusion length; L = length of abutment in the direction of flow; V = velocity of approach flow; IWC = initial water content; C = compaction related to the optimum compaction; CC = clay content; S = Torvane shear stress, Mn = type of clay (e.g., Kaolinite, Illite, Montmorillonite); T = water temperature; t = duration of experiment; g = gravitational acceleration, α = angle of attack; ϕ = pier shape factor; ρ = fluid density; and υ = fluid kinematic viscosity.

Applying the dimensional analysis using D_s, V, and ρ as repeating variables, and using appropriate simplifications, the following set of dimensionless parameters can be obtained:

$$\frac{D_{sc}}{D_s} = f\left(IWC, \frac{S}{\rho V^2}, C, Mn \right) \quad (11)$$

In the derivation of equation 11, the clay content (CC) was eliminated as a variable since the effects of this parameter was found to be an independent factor up to 12 percent clay content. In cohesive bridge-scour experiments, the clay content was kept above 30 percent. In local scour experiments, the variation of scour with time was measured. This relationship was shown to be an asymptotic function with a sharp initial scour development followed by a gradual increase (Molinas and Reiad, 1998). The initial rate of scour hole development is generally controlled by the nature of the clay mineral and other cohesive material parameters such as compaction, initial water content, etc. Experimental and theoretical studies have shown that the velocity at the nose region of a vertical wall abutment is amplified by a factor of 1.2 to 1.8 times the approach velocity, V. Accordingly, the bottom shear stresses that are related to V^2 are also amplified (by up to 11 times) and cause local scour in the affected zone (Molinas, Kheireldin, and Wu, 1998). If approach velocities are increased beyond a threshold value,

defined as critical velocity, the entire approach channel bottom becomes subject to general scour in addition to the local scour. Under these conditions, the scour hole development process continues until equilibrium slopes are attained for the entire reach and may last indefinitely. The experimental study presented in this report limited itself to conditions in which the oncoming flows do not scour the approach reach (clear water conditions). Under these conditions, as soon as the scour hole reaches a depth where the shear stresses within the base become equal to the critical shear stress of the cohesive material, local scouring ceases. The duration of experiments in the study were long enough to maintain the equilibrium condition for at least 4 hours. The final scour depth values obtained under these conditions are independent of time, and therefore in deriving equation 11 the time parameter, *t*, can be eliminated. Additionally, the dimensionless shear strength, *S*, can be related to *C* and *IWC*, further reducing the number of parameters. The local abutment scour analysis in this study was conducted separately for the two clay types. This distinction is made since the type of clay mineral (*Mn*) was found to have a dominant effect on the scour resistance of bed material.

MONTMORILLONITE SCOUR

Montmorillonite-clay mixture experiments studied the effects of compaction, initial water content, and shear strength for unsaturated and saturated soil conditions. This was achieved by compacting the cohesive material placed around the abutments at various degrees of compaction and by using soils of different initial water content. The measured values of (D_{sc}/D_s) were regressed against the remaining dimensionless groups in equation 11 using nonlinear multiple regression analysis through the use of a commercially available SAS computer package. The best-fit regression equations resulting from the statistical analysis of experimental data are:

For **unsaturated** clays with initial water content less than 25 percent:

$$\frac{D_{sc}}{D_s} = (2.186 - 0.05342\ IWC)(15.407 - 0.522\ C + 0.006087\ C^2 - 0.0000235\ C^3) \quad (12)$$

where initial water content (*IWC*) and compaction (*C*) are in percent.

For **saturated** clays with initial water content in the range of 28 to 45 percent:

$$\frac{D_{sc}}{D_s} = (4.76 - 0.451\ IWC + 0.01361\ IWC^2 - 0.000126\ IWC^3)(-0.339 + 0.01744\ C) \quad (13)$$

In deriving equations 12 and 13, IWC ranged from 12 to 45 percent, and C ranged from 58 to 89 percent. Equations 12 and 13 were developed based on laboratory tests in which Froude numbers ranged from 0.1 to 0.6 and soil shear strength values ranged from 0.1 to 0.63 kg/cm^2. The plot of equations 12 and 13 with observed data is presented in figure 6.

KAOLINITE SCOUR

Kaolinite-clay experiments investigated the effects of initial water content on unsaturated clay erosion by preparing mixtures with varying initial water contents. In these experiments compaction was varied over a narrow range of conditions.

For **unsaturated** Kaolinite clay soils, the basic form of equation 13 was retained. For the cohesive soil consisting of 30 percent Kaolinite clay and 70 percent medium sand with a median diameter of 0.81 mm, the best-fit regression equation from the statistical analysis of experimental data is:

$$\frac{D_{sc}}{D_s} = (0.12 + 0.014\ IWC - 0.00205\ IWC^2 - 0.000057\ IWC^3)(-0.4 + 0.017\ C) \qquad (14)$$

Scour initiating velocities for the Kaolinite clay mixture were experimentally determined to be 0.6 m/s. For velocities smaller than this value, the scour ratio is zero. The plot of equation 14 with observed data is presented in figure 7.

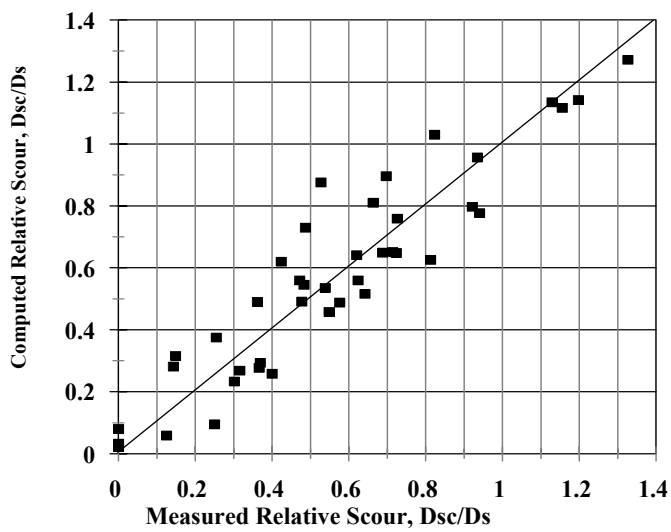

Fig. 6. Computed vs. measured relative abutment scour for Montmorillonite clay.

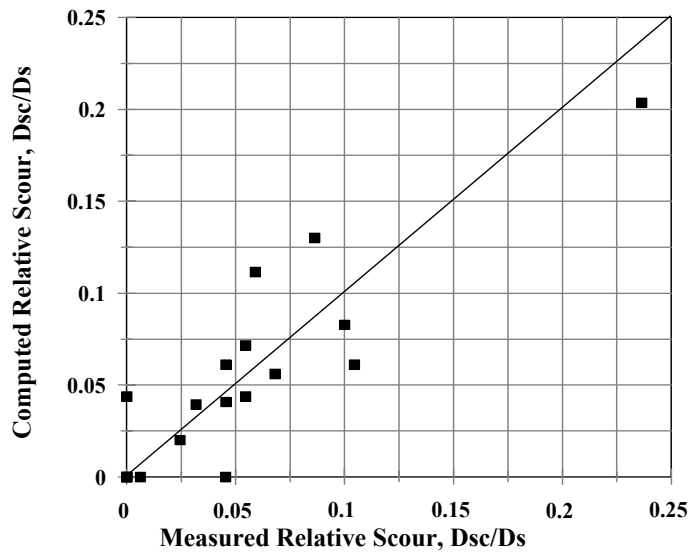

Fig. 7. Computed vs. measured relative abutment scour for Kaolinite clay.

CONCLUSIONS

Conclusions from the study can be listed as:

1. Bed material mixtures that are predominately sand with low clay content can be analyzed using the traditional non-cohesive soil parameters for scour with a reduction factor to account for the cohesive effects from the clay fraction. The experimentally determined reduction coefficients found from the present study are given by equations 1 through 3 for Montmorillonite and Kaolinite clays, respectively. Two sets of coefficients are given for equations 2 and 3 to represent the best-fit line through the data and the envelop-line that can be used as a design equation. Bed material mixtures with high clay contents are governed by cohesive soil properties. There is no clear clay content percentage that determines where the shift occurs from non-cohesive to cohesive properties. For the present study this limit was found to be around 12% and was affected by the clay mineralogy.
2. There is a distinction between pier scour taking place in unsaturated compacted clayey soils and saturated clayey soils. This differentiation affects parameters controlling local pier scour. For unsaturated compacted Montmorillonite clay soils, a new scour depth predictor is proposed in terms of initial water content, Froude number, soil shear strength, and degree of compaction. The pier scour depth and volume decrease as the compaction of cohesive soils increases. For saturated cohesive soils, the scour depth can be expressed as a function of initial water content and excess Froude number,

(F_r-F_i). Under saturated conditions, the scour depth is directly proportional to excess Froude number and is inversely proportional to initial water content.

3. Abutment scour in cohesive soils shows a wide range of variability depending on properties of soils. In the present experiments, under the same geometric and flow conditions, measured scour in cohesive materials varied anywhere from 7 percent to 140 percent of that measured in medium sand. This is due to initial water content, soil shear strength, degree of compaction, and type of clay mineral present in the soil. For Montmorillonite-clay soils, the relative scour depth is expressed in terms of initial water content and degree of compaction. For unsaturated Montmorillonite-clay mixtures, abutment scour depth decreases as the compaction and initial water content increases. For saturated cohesive soils, however, the scour depth is mainly a function of the initial water content and is inversely proportional to initial water content. For unsaturated Kaolinite-clay mixtures, the initiation of scour takes place under higher flow intensities, and under same flow conditions the total scour is up to a factor of five times smaller.

ACKNOWLEDGEMENT

Authors wish to acknowledge Federal Highway Administration for the support of this study and Drs. Ahmad Abdeldayem, Magdi Hosni, and Nagy Reiad for collecting and analyzing the data used in this paper.

REFERENCES

1. Molinas, A., and Abdeldayem. A. W. (1998). *Effects of Gradation and Cohesion on Bridge Scour*, *Vol. 3, Abutment Scour for Nonuniform Mixtures*, Federal Highway Administration, FHWA-RD-99-185.
2. Molinas, A., and Hosni, M. (1998). *Effects of Gradation and Cohesion on Bridge Scour, Vol. 4, Experimental Study of Scour Around Circular Piers in Cohesive Soils*, Federal Highway Administration, FHWA-RD-99-186.
3. Molinas, A., and Reiad, N. Y. (1998). *Effects of Gradation and Cohesion on Bridge Scour, Vol. 5, Effect of Cohesion on Bridge Scour*, Federal Highway Administration, FHWA-RD-99-187.
4. Molinas, A., and Noshi, M. H. (1998). *Effects of Gradation and Cohesion on Bridge Scour, Vol. 6, Abutment Scour in Uniform and Stratified Sand Mixtures*, Federal Highway Administration, FHWA-RD-99-188.
5. Molinas, A., Jones, S. and Hosni, M. (1999). *Effects of Cohesive Material Properties on Local Scour Around Piers,* Journal of the Transportation Research Board, Transportation Research Record, No. 1690, National Academy Press, pp. 164-175.
6. Molinas, A., Kheireldin, K., and Wu, B. (1998). *Shear Stress Around Vertical Wall Abutments*, Journal of Hydraulic Engineering, ASCE, Vol. 124, No. 8, pp 822830.

Scour Around Submarine Pipeline in Clayey Soil

By

Neelamani, S. [1], Vijaya kumar, A. [2], Narasimha Rao, S[3].

ABSTRACT

Experimental investigations on scour due to waves under the submarine pipeline resting on the clay soil bed for different consistency index of the soil were carried out. Based on the scour measurements for few hours of wave action, the ultimate scour depth is estimated using hyperbolic model. The equilibrium scour depth below the pipeline is estimated as 45% of the pipe diameter for consistency index of 0.17 and is 35% of the pipe diameter for consistency index of 0.23. Investigations on wave pressures around the submarine pipeline (exposed, half buried and fully buried) are also carried out. It is found that the pressure is reduced by about 40%, if the pipeline is just buried in clay soil. It is also found that the consistency index of the soil significantly affects the wave-induced pressure.

[**Key words**: Submarine pipeline, Scour, Ocean waves, Wave pressure, Clayey soil, Consistency index, Pipe burial**]**

INTRODUCTION

The search for oil under deep-sea bed has led into extensive theoretical and experimental investigations in the field of offshore oil exploration and exploitation. The discovery of large deposits of oil and gas in many deep-water offshore regions has resulted in the construction of large production and drilling platforms. Since 1940's, the tendency to build the fixed offshore structures in deep waters has progressed steadily. Once the production platforms are erected in the sea, the next immediate task is to transport the oil and natural gas from the production site to onshore terminal facilities. Submarine pipeline offers an efficient mode of transportation of oil and gas continuously from offshore to onshore. Though the pipeline appears as a simple structure, interaction of submarine pipeline with waves is a complex phenomenon. Many foundations of water front structures built on sandy soils have suffered extensive damage due to scour. Even the foundations built in clayey soil beds are not free from scour effects. There are many thick under-consolidated marine clayey deposits located in several coastal areas and the scouring of foundations in such soft cohesive sediments can be quite significant. The review of existing literature reveals that studies on wave induced scour, pressures and uplift forces on submarine pipeline, **especially in cohesive soils** is in the developing stage as compared to the studies in sandy soils. Therefore, the present study has been focused on wave-induced scour and pressures around submarine pipeline in soft marine clayey soil. One of the important questions in the selection of burial of a submarine

[1]Associate Professor, Department of Ocean Engineering. IT Madras, Chennai-600 036, India, Phone: 0091-44-445 8639, Fax : 0091-44-235 0509, E-mail: sneel@iitm.ac.in
[2] Research scholar, Department of Ocean Engineering, IIT Madras,India
[3] Professor, Department of Ocean Engineering, IIT Madras, India

pipeline is "WHAT IS THE OPTIMUM DEPTH OF BURIAL FOR ACHIEVING SUFFICIENT STABILITY AGAINST SCOUR?". The effect of consistency index of the clayey soil on wave induced scour and pressures are also not known clearly and this aspect also is considered in the present investigation. Scour around the submarine pipeline results in spanning problems, flow induced vibrations and resonance, which leads to failure of pipelines.

LITERATURE REVIEW

Comparatively, not much of work is carried out on structures resting on cohesive soils. In most of the previous investigations, the resistance of the soil to erosion was related to soil and hydraulic properties. Some of the important investigations are mentioned in the following:-

Partheniades (1965) investigated the influence of shear stress, suspended cohesive sediments concentration and shear strength of bed on the erosion rate of cohesive bed in an open channel. From the flume experiments, it was found that the erosion rates were independent of the bed shear strength. **Kamphusis and Hall (1983)** studied the initiation of motion of consolidated cohesive sediments under a unidirectional flow (up to a velocity of 3.5 m/s) for clear water conditions in a flume-tunnel. It was found that critical shear stress and critical velocity were found to increase with compressive strength, vane shear strength, plasticity index, clay content and consolidation pressure. **Mitchener and Torfs (1996)** attempted to characterise the erosion behaviour of mixed sediments. It was found that the critical shear stress for erosion increased and erosion rates decreased when mud was added to sand and a maximum value had reached at a sand content in the ratio of 50% - 70 % by weight. **Civik and Yiiksel (1999)** carried out experimental investigation on scour around submarine pipeline in cohesionless soil due to regular wave actions. Based on the experimental data it was found that the relative scour depth increased with increase in wave height, wave period and pipe diameter.

Macpherson (1978) derived an analytical solution from the potential theory for the wave induced pressure distribution in the sandy soil bed surrounding a buried pipeline and the dynamic seepage force exerted on the pipeline was computed. **McDougal et. al. (1988)** developed an analytical model for estimating the pore water pressure in the sandy soil and the resulting pressure force on the submarine pipelines. The analytical solutions were compared with the results of both small and large-scale tests. Reasonable agreement is obtained for the small-scale tests. **Magda (1997)** performed comprehensive numerical studies of the hydrodynamic force acting on a submarine pipeline buried in compressible seabed sediments by using the Boundary Integral Equation method.

In cohesionless sediments, the submerged density of the soil and gravity forces provides the main resistance to erosion, but in clays essentially the physico-chemical properties plays a dominant role. The scour rate in cohesive soil is much lower than the sandy soil. Due to laboratory mechanical limitations, it could not be possible to run the wave maker continuously for long duration. Because of this reason, tests were conducted for few hours in the present study. Since the scour depth obtained at the end of the test is not the ultimate value, there is a necessity to use theoretical models like the "Hyperbolic model" to extrapolate the observed data to arrive at the ultimate scour depth.

EXPERIMENTAL INVESIGATIONS

Test Facility

The present experimental investigations were carried out in a 30m long, 2.0m wide and 1.7m deep wave flume in the Department of Ocean Engineering, Indian Institute of Technology Madras, Chennai, INDIA. Piston type wave maker is used for generation of waves. The wave height and period to be generated are controlled by a personal computer. The other end of the flume is provided with a rubble mound absorber to effectively dissipate the incident wave energy. The details of the flume, position of the model and the wave gauges used to register the wave elevations in front of the model are shown in **Fig.1.**

Experimental Set-Up

The sizes and materials for the model pipes were chosen on the considerations of normal sizes of pipeline adopted in the field and surface characteristics of field pipeline. It has been brought by **Summer et. al. (1993)** that the hydrodynamically smooth surface can contribute a good amount of scouring. **PVC** (Poly vinyl chloride) pipes can be considered as fairly smooth and hence, PVC pipe of 160 mm outer diameter and 1.96 m length were selected. The submarine pipeline model is fitted with three numbers of inductive type pressure transducers placed with equal angular spacing of 120° on the circumference of the pipe. The measuring ranges of two pressure transducers are of 0.5 bar and one with 0.2 bar. A test section of silty clay bed of size, 2.0 m×2.0 m×0.6 m is formed at a distance of 13m from the wave maker. Uplift force are measured by using bellow type load cell of 20 kg capacity, which is connected to the model by angle section at one end and another end is fixed to the rigid frame which is placed at the top of the flume. But in this paper only the results of scour and some aspects of the wave pressures around submarine pipeline is provided. The detailed results of wave pressures and forces can be obtained from **Vijayakumar et. al. (2002).** The water depth, 'd' of 0.3m and consistency indices of the soil, I_c of 0.17 and 0.23 and pipeline resting on soil bed is adopted for scour measurement around pipeline. The clay bed is meticulously prepared to achieve these consistency indices. For scour measurement, a scale is used whose least count is 1 mm. The (x, y) co-ordinates on the scour bed are identified by using steel mesh of size 2.0 m × 1.2 m with grids of size of size 50 mm × 50 mm. Wave height of 0.2 m and wave period of 1.5 sec was used for scour study. The co-ordinate detail of scour measurements is shown in **Fig.2**.

For wave pressures around the submarine pipeline, regular waves with wave height, H ranging from 0.05m to 0.25m with an interval of 0.05m is used. For each wave height, six different wave periods, T ranging from 1.0 sec to 2.25 sec with an interval of 0.25 sec is used. The water depths, 'd' adopted for the tests are 0.3m, 0.4m and 0.5m. The consistency index of the cohesive soil, I_c used was 0.18, 0.24 and 0.33. Tests were carried out for 3 different conditions based on the position of model with reference to the bed:

1. Pipeline resting on the bed
2. Pipeline Half buried and
3. Pipeline fully buried.

Scour Measurement

The clay bed was prepared for the required consistency and initial bed level was measured. For the purpose of reference, four concrete cubes of size 150 mm are placed at

four corners of the pit and two-channel section of 2.5 m length is placed over the concrete cubes. Now steel mesh was placed over the channel section to measure the level of bed by using scale with 1 mm as least count. After taking all the measurements, the above set up was removed and the model was placed over the soil bed. The water level was raised to a depth of 0.3 m. The scour testing was carried out for a total of about 7200 wave cycles (about 3 hours) to ensure a good progressive rate of scour at the end of the tests. It may be noted that to reach ultimate conditions of scouring in this type of soil, it has been established earlier **(Rambabu (2000)**) in this laboratory that it is required to continue the testing for more than three days. Due to the limitations in the wave maker equipment, it was not possible to extend this testing beyond 3 – 4 hours. In view of this, the test duration was limited to 3 hours for about 7200 cycles of waves. At this stage, a good progressive rate of scouring was observed. After every 1 hour test run, the water level was lowered and the magnitude of scour depth (clay bed topography) was measured around the submarine pipeline by following the same procedure as explained above. This measurement at a particular point, after subtraction from the initial measurement gives the scour depth at that particular co-ordinate.

Test Bed And Soil Placement

A test section with soil bed of size 2.0 m × 2.0 m × 0.6 m was formed at distance of 13m from wave maker. The fine-grained soil, silty clay from a local deposit was brought and used in this investigation. Fairly homogeneous and saturated clay bed was formed using the technique adopted by the earlier investigators **(Mallikarjuna Rao, 1992)**. The soil brought was first air dried and mixed with water to get the desired water content and this soil was placed layer by layer in the test pit. The index property tests like liquid limit (LL) and plastic limit (PL) were conducted as per IS 2720 (part 5) - 1985. The grain size distribution of the soil was established through hydrometer test conducted as per IS 2720 (part 4)-1985. The different properties of the soil measured were presented in **Table. 1.** It is generally known that the fine-grained soil is less prone for scouring. However, if these soils are deposited with higher moisture contents, significant scouring in these deposits is possible. In order to get in to these conditions, soil bed was formed at higher moisture contents. Moisture content can be expressed in terms of consistency index, I_c. As the soil bed was formed at higher moisture contents, there was no difficulty in the formation of homogeneous bed **(Prasad and Narasimha Rao, 1994)**.

RESULTS AND DISCUSSIONS

Scour Around Submarine Pipeline

The stability of many structures in ocean environment is very much controlled by wave activity. In the first instance, waves can cause significant amount of scouring around these structures, which are founded on / in seabed, affecting seriously the stability of foundations. In few cases, along with the scour, the increase in the magnitude of forces on the structures leads to structural failures. From the results presented in the previous sections, it is clear that with change in burial depth of submarine pipeline, there are enormous difference in the forces and pressures. It is known that pipeline resting on the seabed induces significant scour compared to buried pipeline (Sumer & Fredsoe, 1990) in sandy soil. In view of this an attempt has been made to get the spatial and temporal variation of scour depth for submarine pipelines resting on the seabed. From the limited measured scour depth data, ultimate

values are predicted using an established observational hyperbolic method (Kondner (1963)).

Hyperbolic Model

According to this model by Kondner (1963), the scour depth (S) can be expressed as function of time 't' as

$$S = t / (A + B\,t) \quad (1)$$

$$S_u = \lim_{t \to \alpha} S = (1/B) \quad (2)$$

The constant 'A' and 'B' depends on soil and hydraulic conditions. The slope of the best line fit i.e.'1/B' gives the ultimate scour depth. This is essentially the model suggested by **Kondner (1963)** to validate stress-strain relationship in soils. The following example illustrates the estimation of the ultimate scour depth from the data of measured scour depth and time duration. The time development of scour depth for a particular diameter (D=160 mm) at different locations around pipeline with two different consistency index of soil is shown in **Table 2**. The effect of time of wave action, t on development of scour depth, S at four different relative locations at the upstream side of the pipeline (y/D = -0.31, -0.62, -0.94 and –1.25) for two different consistency index of the soil (I_c = 0.17 and 0.23) is brought out in **Figs.3.** A similar plot for the down streamside of the submarine pipe for y/D = 0.0, 0.31, 0.62 and 0.94 is provided in **Fig.4**. Here 'y' is the distance of the scour measurement point upstream (-ve) or downstream (+ve) from the centre of pipe. The scour measurement was carried out after every 1 hour wave action on the submarine pipe-clay bed. From these plots it is observed that the scour rate is higher in the initial stages. It is observed that the time development of scour depth reduces with increase in consistency index of soil. This is due to the fact that the increase in the consistency index of the soil is associated with increase in the strength of the soil. It is generally established in the field of geotechnical engineering that as the consistency index of the clay soil changes from a very soft to soft one, there is a tendency for the reduction in the scour depth. At the end of 3 hours of wave action, the measured scour for I_c = 0.17 below the centre of the pipe (y/D=0.0) was 34 mm, which is not the ultimate scour depth for these conditions. The plots of scour depth "S_i" with time "t" appears to resemble the rectangular hyperbolae and if this is valid, the transformed plots between 't/S_i' and 't' should be of linear fits.

The variation of the ratio of time to the scour depth (t/S_i) with the time 't' for the different experimental conditions is shown in **Figs.5 and 6** for the above refered experimental conditions. The best line fit suggest linear plots, thereby confirms the application of hyperbolic model. In view of this, it is possible to predict the ultimate scour depth from the measured slope of the linear fit. The predicted values of ultimate scour depth by using the hyperbolic model are given in **Table 3**. For the tests with I_c = 0.17 and for y/D = 0.0 (below the centre of the pipe), the ultimate scour depth is found to be 72 mm.

A typical spatial variation of normalised ultimate scour depth, S_{uc} for Ic of 0.17 and 0.23 for both upstream and downstream side of the pipeline is shown in **Fig.7.** It is found that the maximum S_{uc}/D below the centre of the pipeline is 0.45 and 0.35 for Ic=0.17 and 0.23 respectively. For similar hydrodynamic conditions, the S_{uc}/D for sandy soil is about 0.67 (Sumar and Fredsoe (1990)). From the limited results available it is clear that I_c significantly influences the scour depth below the pipeline resting on the seabed in clayey soil.

Wave Induced Pressure Around Submarine Pipeline

In the field, selection of minimum burial depth of the submarine pipeline is one of the important factors from stability point of view. Deeper the burial, expensive is the pipeline installation. The optimum depth of burial depends on the stability of pipe from scour, floatation and hence on pressures and uplift forces. Due to the variation of moisture content in clay, the consistency index of the soil also varies. In many places the consistency index of marine clay is generally very much less than the values observed for clays on land. At several places on the West Coast of India (Kandla and Cochin) and in East Coast of India (Krishna – Godavari basins), large tracts of marine clays are found with I_c = 0.1 to 0.3. The effect of burial of the pipeline and consistency index of the soil on local water particle velocity and hence the wave induced pressure around submarine pipeline is required. The variation of pressure around submarine pipeline is indirectly an influencing parameter on the magnitudes of scour under the submarine pipeline.

The variation of wave pressure for different consistency index of the soil around submarine pipeline at different location for e/D = 1.0 (i.e. fully buried), d/a = 6.25 and ka = 0.148 is shown in **Fig.8.** It is observed that, when the pipeline is fully buried, the pressure at point P_3 is high as compared to other two points. This marginal difference in pressure is due to the damping effect of soil. The variation of pressure around submarine pipeline for I_c = 0.24, d/a = 6.25, H/D = 0.64 and for different burial depths is given in **Fig.9.** It is observed that the normalised pressure is decreased, when the pipeline is buried in to the seabed.

The effect of relative burial depth, e/D on the variation of normalised wave induced pressures {P/[ρg(H/2)(1/cosh kd)]} on the submarine pipeline for H/D = 0.64 & 0.94 are presented for d/a = 5.0 and I_c = 0.33 in **Fig.10.** The results show that the increase in e/D results in a general decrease in the normalised pressure. This plot also indicates that the normalised pressure at point P_1 and P_2 are reduced by about 45% and at point P_3 it is reduced by about 26%, when the pipe is just fully buried compared to the pipeline resting on the seabed. Due to the limitation in the experimental set up, tests could not be conducted with pipeline buried at greater depths of embedment. It is observed that, when the pipeline is resting on the seabed, the pressure at point P_2 facing to waves is high as compared to other two points. This marginal difference in pressure is due to difference in the levels of the still water at that instance due to stagnation effects. Further, it can be observed from the above figures that the normalised pressure increases with increase in wave height ratio, H/D.

The effect of consistency index of soil, I_c on the variation of normalised pore water pressure {P/[ρg(H/2)(1/cosh kd)]} around the submarine pipeline for d/a of 5.0 and 6.25 for e/D = 1.0 with constant H/D of 0.94 is shown in **Fig.11.** In any parametric study, it is normally considered to be satisfactory, if the investigation is carried out for more values of that parameter. But with the clay kept in contact with water, it is very difficult to keep the I_c at a value greater than 0.35. In view of this, the variation in Ic is considered not much. From these plots it is observed that the normalised pore water pressure decrease by about 26% when the consistency of the soil increases from 0.18 to 0.33. The increase in the consistency index of the soil is associated with increase in the strength of the soil. It is generally established in the field of geotechnical engineering that as the consistency index of the clay soil changes from a very soft to soft one, there is a tendency for the reduction in the pore water pressure **(Bishop and Henkel, 1962)** with a consequent increase in effective stress and this accounts for improved strength.

CONCLUSIONS

Based on the present experimental investigations on scour and wave pressures around the submarine pipelines in clayey soil, the following conclusions can be drawn: -

1. The maximum scour depth under the submarine pipeline resting on the cohesive seabed is 45% D for I_c = 0.17 and 35.4% D for I_c = 0.23. For similar hydrodynamic condition, for sandy bed, the value of S_{uc}/D is about 0.67 (Sumer and Fredsoe (1990)).
2. The normalised significant wave induced pressure around the submarine pipeline is decreased by 30% to 52%, when the position of the submarine pipeline is shifted from e/D=0.0 (resting on the bed) to e/D=1.0 (just fully buried) in clayey soil.
3. The normalised significant wave induced pressure around submarine pipeline in clayey soil is decreased by 20% to 30%, when the consistency index of the soil is increased from 0.18 to 0.33.

REFERENCES

Bishop, A.W. and Henkel, D.J. (1962). The measurements of soil properties in Triaxial test. Eedward Annold Limited, London. (2nd Edition).

Civik, E. and Yiiksel, Y. (1999). "Scour under submarine pipelines in waves in shoaling conditions". Journal of Waterway, Port, Coastal and Ocean Engineering, ASCE, 125(1), 9-18.

Kamphuis, J.W. and Kevin, R.H. (1983). Cohesive material erosion by unidirectional current. Journal of Hydraulic Engineering, Vol. 109, No.1, January, pp. 50-61.

Kondner, R.L. (1963). "Hyperbolic stress-strain response: Cohesive soil". Journal of Soil Mech. and Found.Div., ASCE, 89(1), 115-143.

MacPherson, H. (1978). "Wave forces o pipeline buried in permeable seabed". Journal of Waterways, Port, Coastal and Ocean Engrg, ASCE, 104(3), 407-419.

McDougal, W.G., Davidson, S.H., Mokmeyer, P.L. and Solltt, C.K. (1988). "Wave-induced forces on buried pipelines". Journal of Waterways, Port, Coastal and Ocean Engrg, ASCE, 114,220-236.

Magda, W. (1997). Wave- induced cyclic pore-pressure perturbation effects in hydrodynamic uplift force acting on submarine pipeline buried in seabed sediments. Coastal Engineering, Vol.39, pp.243-272.

Mitchener, H.J., Torfs, H. and Whitehouse, R.J.S. (1996). Erosion of mud/sand mixtures, Coastal Engg, Vol.29, pp.1-25.

Partheniades, E. (1965). "Erosion and deposition of cohesive soils". Journal of the Hydraulic division, ASCE, 91(HY1), 105-139.

Prasad, Y.V.S.N. and Narasimha Rao, S. (1994). "Pullout behaviour of model piles and helical pile anchors subjected to lateral cyclic loading". Canadian Geotechnical Journal, 31, 110-119.

Sumer, B.M., and Fredsoe, J. (1990). Scour below pipeline in waves. Journal of Waterways, Harbours and Coastal Engg Div., ASCE, Vol.116, No.3, pp.307-322.

Sumer, B.M., Christiansen, N. and Fredsoe, J. (1993). "Influence of cross section on wave scour around piles". Proc. AM. Soc. Civ. Engrs, Journal of Waterway, Port, Coastal and Ocean Engrg., 119(5), 477-495.

Vijayakumar, A., Neelamani, S. and Narasimha Rao,S. (2002). "Wave Pressures and Uplift Forces on and Scour around Submarine Pipelines in Clayey Soil". Accepted for publication in Ocean Engineering.

Table:1. Properties of soil used for the present study

S.No	Property	Magnitude
1	Clay fraction(<0.002mm)	57%
2	Silt fraction (0.002 to 0.075mm)	35%
3	Sand fraction (0.075 to 4.75mm)	8%
4	Liquid Limit(LL)	52%
5	Plastic Limit(PL)	32%
6	Plasticity Index(PI)	20%

Table:2. Spatial variation of scour depth measurements (mm) w.r.t time

Co-ordinates (0,y/D)	$I_c = 0.17$			$I_c = 0.23$		
	1 hour	2 hour	3 hour	1 hour	2 hour	3 hour
(0,0)	17	29	34	15	25	29
(0,-0.31)	15	24	29	13	22	25
(0,-0.63)	13	21	24	11	18	20
(0,-0.93)	10	16	19	9	15	17
(0,-1.25)	7	11	14	6	10	12
(0,0.31)	13	20	25	11	19	22
(0,0.63)	11	18	21	9	16	18
(0,0.93)	8	14	16	7	12	14

Table:3. Spatial variation of ultimate scour depth (mm w.r.t consistency index of the soil, I_c

Co-ordinates (0,y/D)	$I_c = 0.17$	$I_c = 0.23$
(0,0)	71.4	55.5
(0,-0.31)	55.5	45.4
(0,-0.63)	41.6	35.7
(0,-0.93)	35.7	28.6
(0,-1.25)	28.6	24.4
(0,0.31)	50	38.4
(0,0.63)	40	32.3
(0,0.93)	33.3	28.6

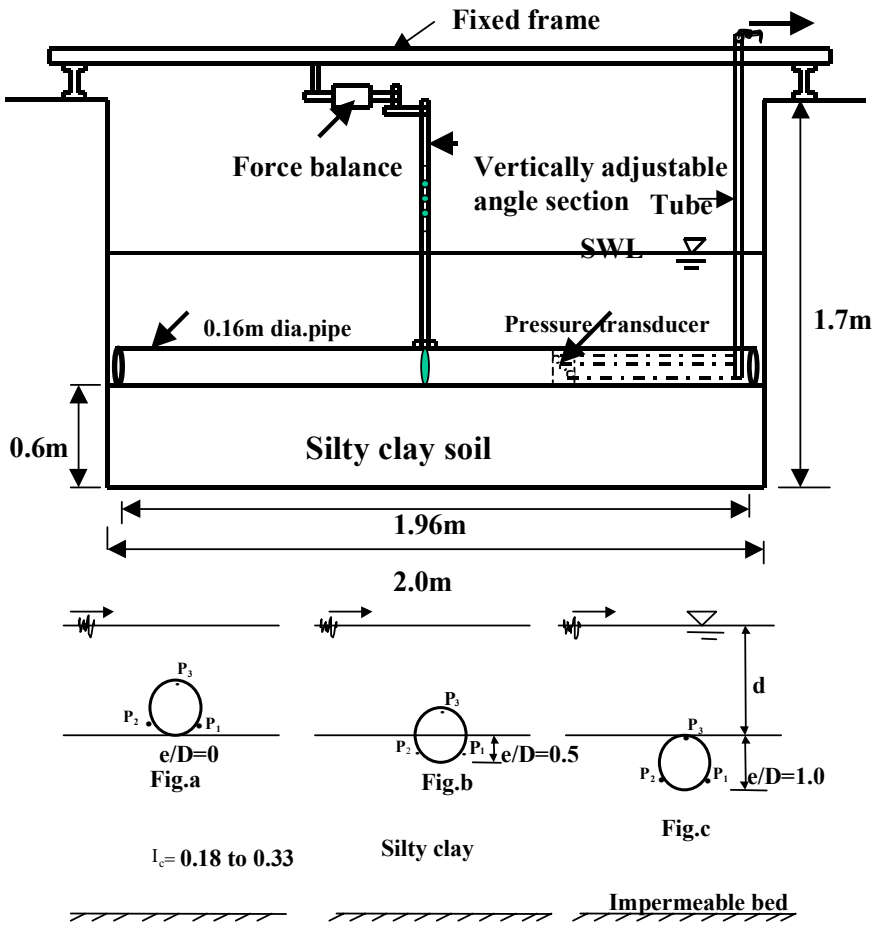

Fig.1 Experimental set-up for the present study

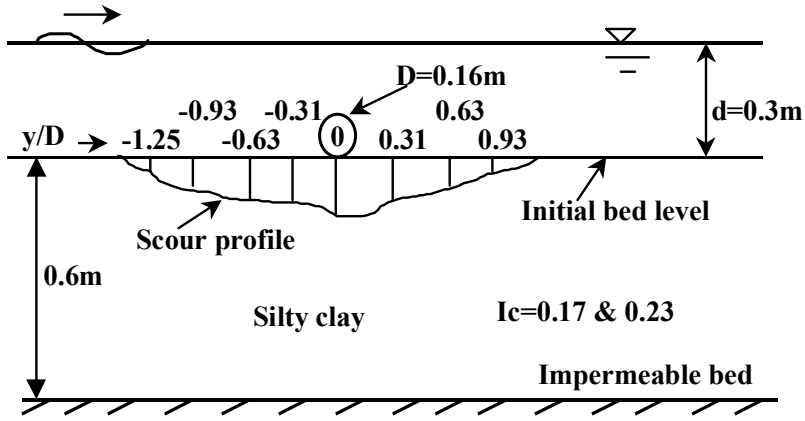

Fig.2 Scour measurements

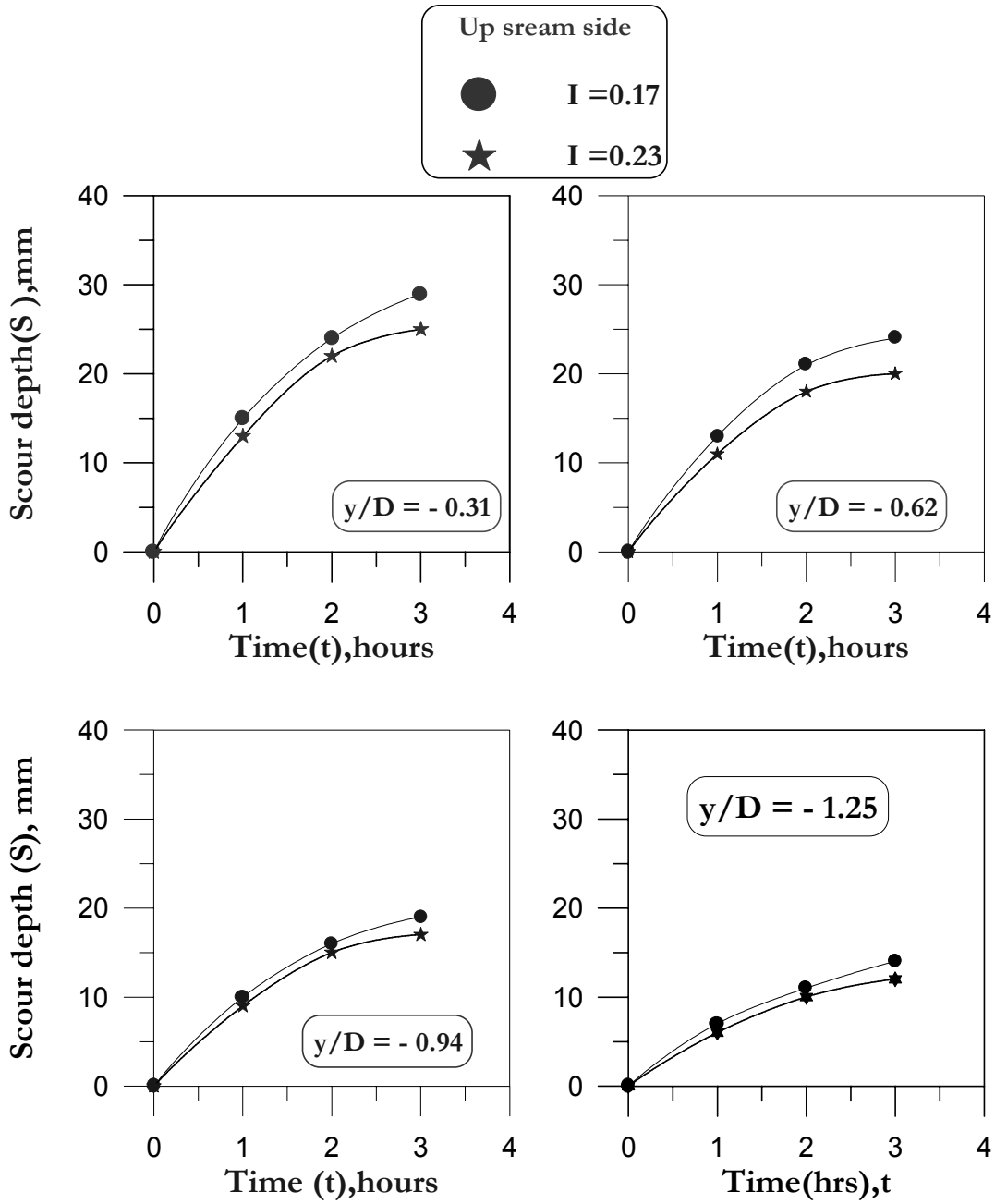

Fig.3 Effect of I_c on the variation of time development of scour depth on the upstream side of the pipeline.

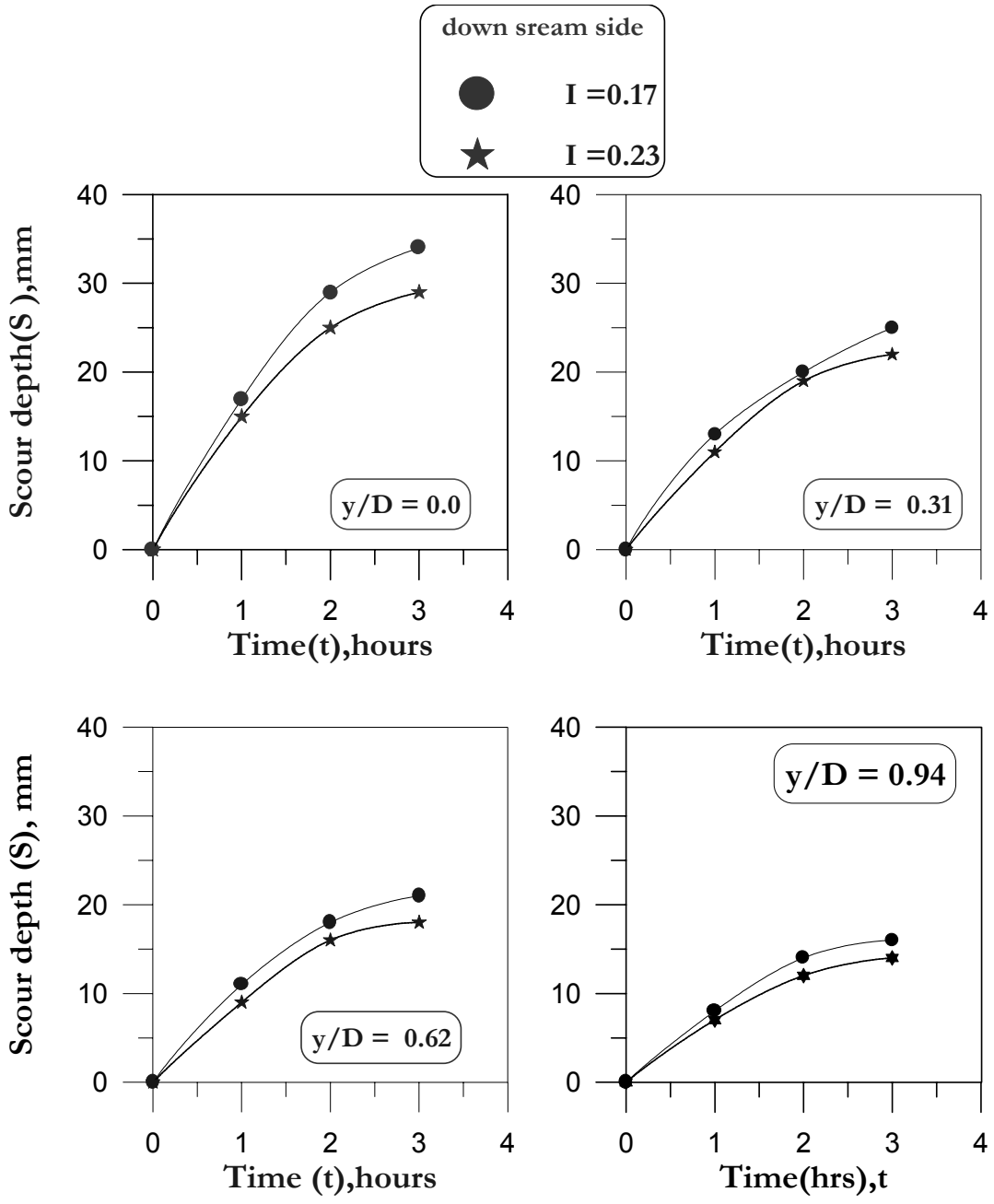

Fig.4 Effect of I_c on the variation of time development of scour depth on the down stream side of the pipeline.

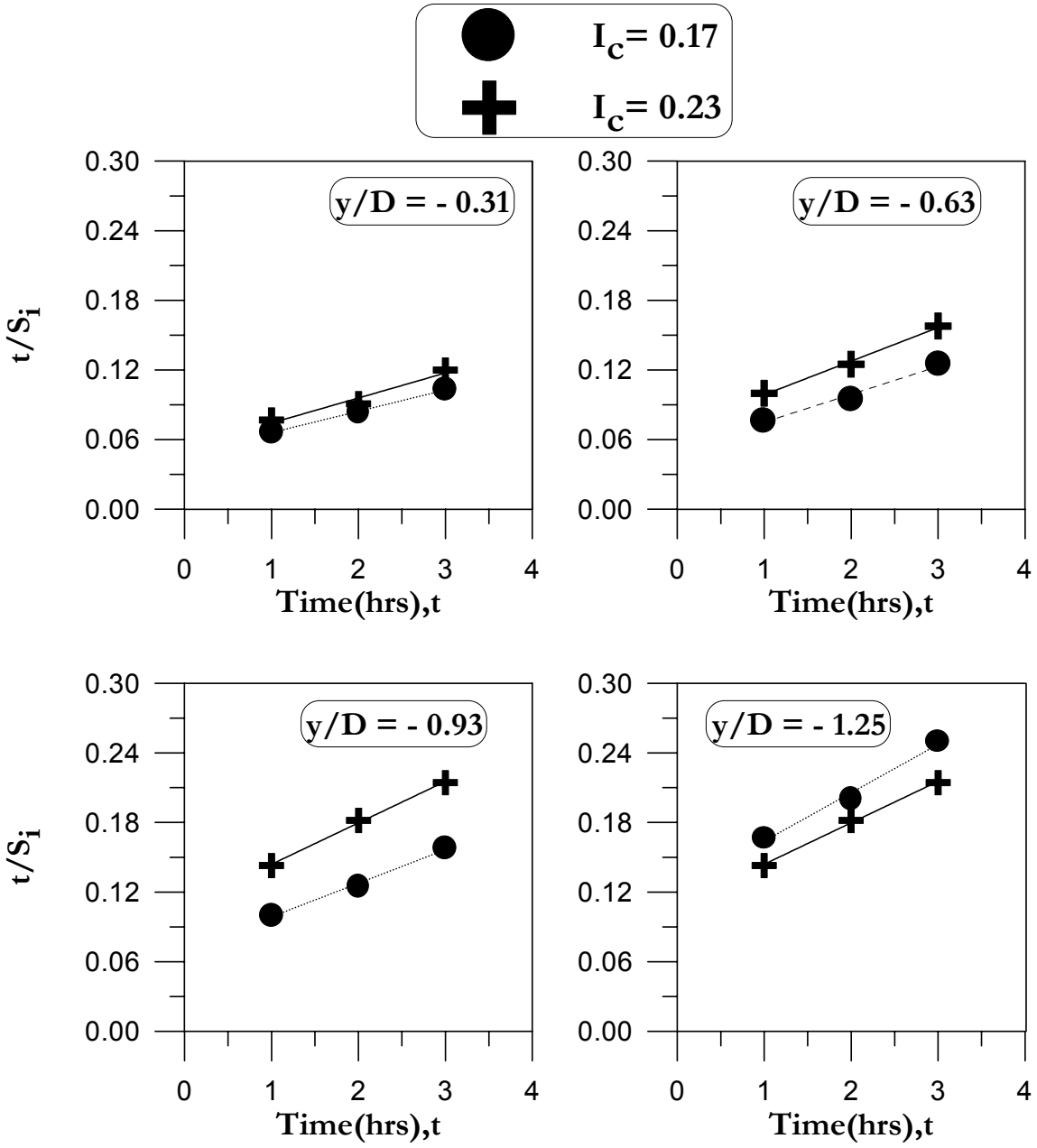

Fig.5 Application of Hperbolic formulation for prediction of ultimate scour depth - An illustration

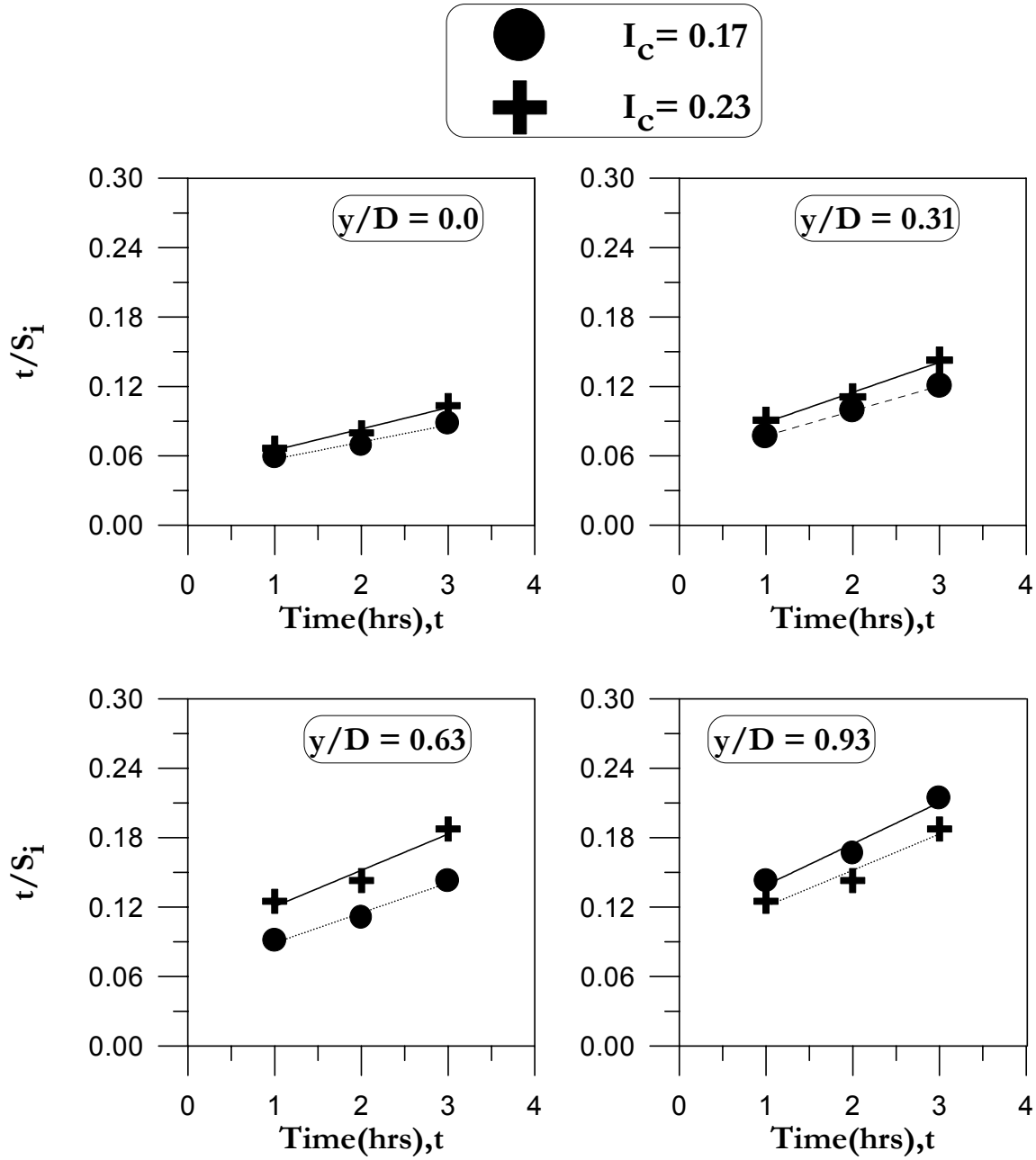

Fig.6 Application of Hperbolic formulation for prediction of ultimate scour depth - An illustration

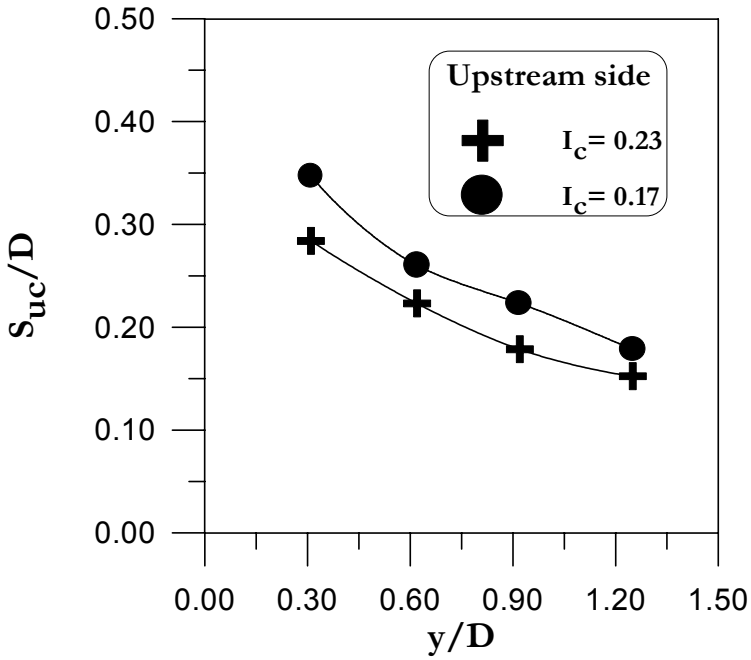

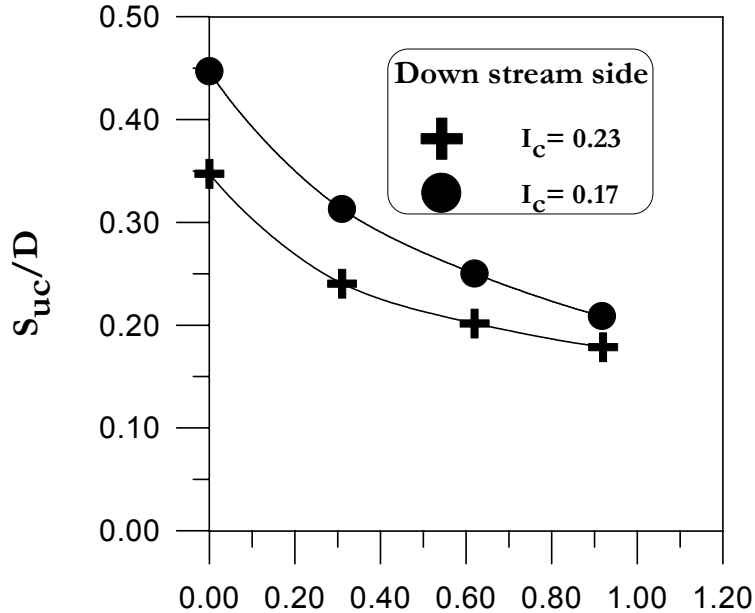

Fig. 7 Effect of I_c on the spatial variation of ultimate scour depth

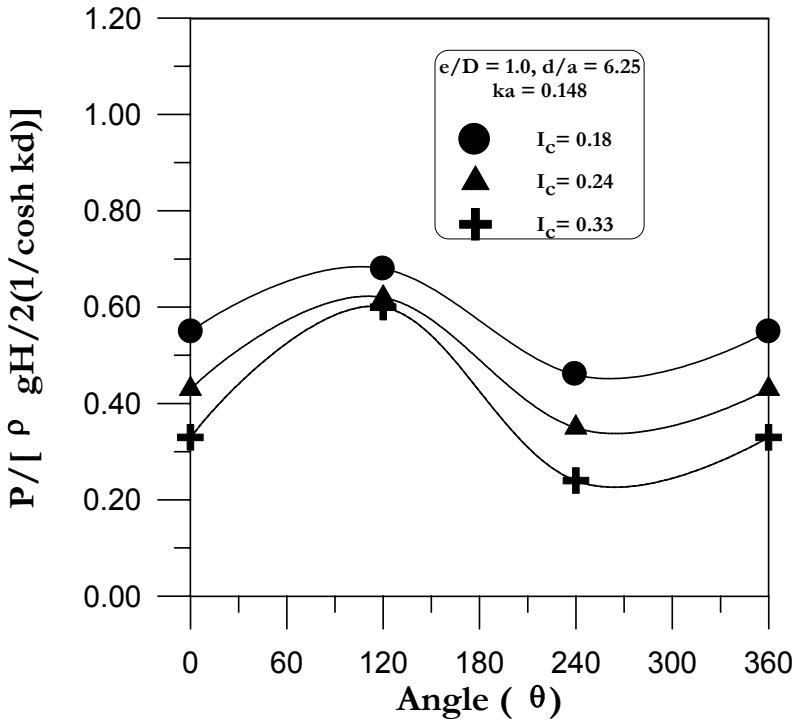

Fig.8 Variation of dimentionless pressure around submarine pipeline for different I_c with e/D =1.0

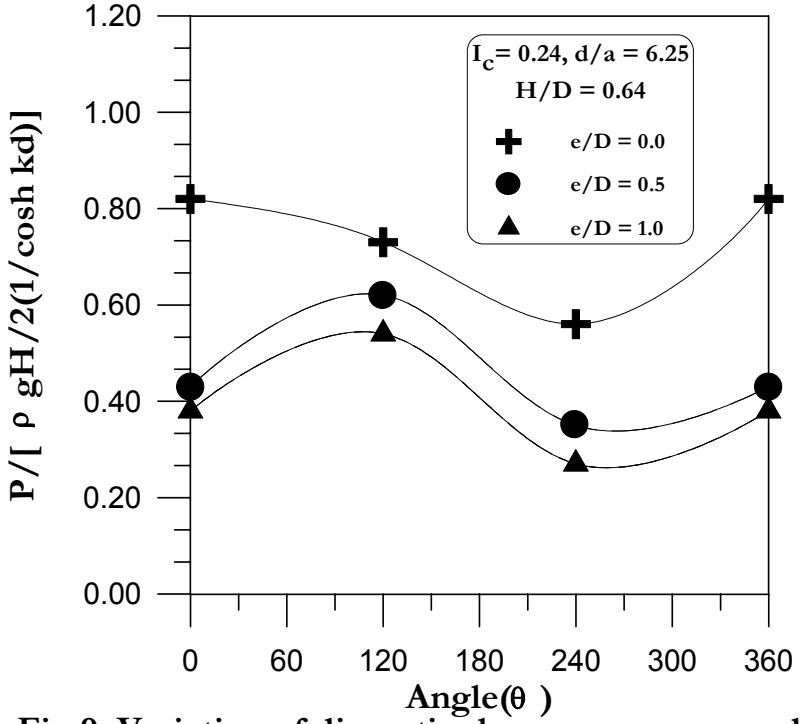

Fig.9 Variation of dimentionless pressure around submarine pipeline for different e/D with I_c= 0.24

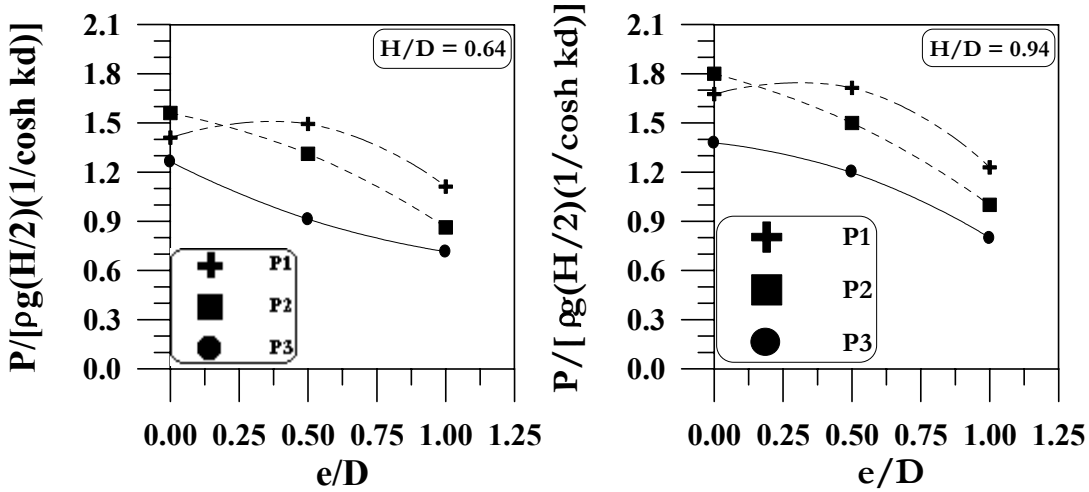

Fig. 10 Effect of H/D on the variation of dimensionless pressure, P/P with relative burial depth, e/D for d/a=5.0 ad I =0.33

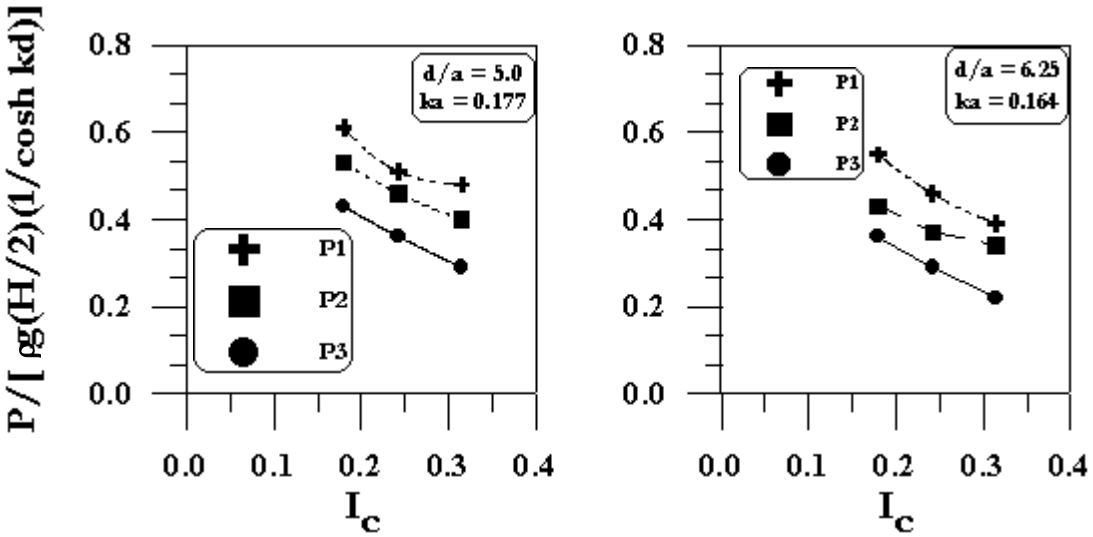

Fig.11 Effect of consistency index on the dimentionless pressure for e/D = 1.0 and H/D = 0.94

GIS-Based Bridge Scour Prioritization

By

Carlton L. Ho[1], Jeffrey M. Di Stasi[2] and Paula Rees[3]

ABSTRACT

A bridge scour prioritization scheme is developed using the advantages of a geographical Information System (GIS) analysis. The scheme was developed to assist in the allocation of resources for bridge remediation and repair. A GIS is created for each New England state to geographically integrate bridge, dam, and gage infrastructure in order to recognize the relation between them. Bridge data are based on known characteristics of the bridges. Because many of the bridges have unknown designs, the Connecticut Comparative Scour Analysis is incorporated in the evaluation of the bridge scour susceptibility. Preliminary analyses have been conducted and compiled into two tables, a gage table and a scour table. The gage table contains data pertinent to recurrence levels at stream gage sites. The scour table contains data pertinent to the flood levels to result in significant scour hazard. The combination of the two data sets results in an analysis that assigns return periods for scour susceptibility. The return periods can be used as a measure of prioritization. The GIS allows for spatially relevant evaluation of the gage data and scour data as well as the presentation of the results in map form.

INTRODUCTION

Bridge scour, or the erosion of the sediments from the streambeds and stream banks, is recognized as the most common cause of bridge failures. According to Shirhole and Holt, sixty percent of all bridge failures since 1950 could be attributed to the effects of flow hydraulics. Annual federal aid for scour related bridge failures and repairs for flood damage to bridges are approximately $30 million to $50 million. The flow regime is made even more complex because of the bridge piers and abutments. When one considers that 84% of the nations 575,000 bridges span a waterway (National Bridge Inventory) the need for a comprehensive and rational means for categorizing the bridges was necessary. To fully characterize the factors that influence bridge scour it is necessary to understand channel and bridge geometry, floodplain characteristics, flow hydraulics, bed material, channel protection, channel stability, riprap placement, ice formations and debris (Richardson and Davis, 1995).

[1] Department of Civil and Environmental Engineering, University of Massachusetts, Amherst, MA, 01003-5205, 1-413-545-9703, 1-413-545-4525 (fax), ho@ecs.umass.edu.
[2] Hayward Baker, Inc., 1130 Annapolis Rd # 202, Odenton, MD 21113-1671, jmdistasi@haywardbaker.com
[3] Department of Civil and Environmental Engineering, 12B Marston Hall, University of Massachusetts, Amherst, MA 01003-5205, 1-413- 577-2337, 1-413-545- 2202 (F), rees@ecs.umass.edu

Although bridge scour has long been observed, the problem first received nationl attention whe the I-90 bridge over Schoharie Creek, New York, failed on 5 April 1987 causing two spans of the bridge to fall into the floodwaters, subsequently resulting in ten deaths. The investigations by the National Transportation Safety Board determined that the cause of the failure was based on inadequate riprap around the piers and a shallow foundation depth, items that could have been addressed if these problems were identified prior to the flood. This resulted in an effort by the Federal Highway Administration (FHWA) to mandate the identification of bridges at risk of scour susctiblity through quantitative and qualitative means.

The FHWA issued technical advisories in 1988 and 1991 (USDOT, 1988, 1991) to provide states with the means for implementing a scour evaluation program for existing bridges and new bridge designs. FHWA issued two Hydraulic Engineering Circulars, HEC-18 and HEC-20) with design, evaluation and inspection procedures for bridge scour (Richardson and Davis 1995). In using the prescribed method of analysis is the development of a single digit rating system of the National Bridge Inspection Standards (NBIS) (USDOT 1995).

Although a logical means for evaluating bridge scour was created, the implementation has not been easy to execute. Bridge scour evaluation requires a multidisciplinary approach. On top of this, the effort requires significant archival research in the design of existing bridges, flow conditions, and hydrological predictive models. Data on as built conditions of bridges is not easily gleaned. Foundations of many older bridges are completely unknown. It isn't always clear how multiple or parallel spans are to be treated when cataloging the bridges. A geographical information system (GIS) is an effective means for spatially storing the database, analyzing the data and presenting results of the analysis.

NBIS rating

Through the NBIS, scour critical bridges are addressed in the Item 113 code in the "Recording and Coding Guide for the Structure Inventory and Appraisal of the Nation's Bridges" (Report No. FHWA-PD-96-001). A bridge is classified as scour critical according to one of the following: (1) observed scour at the bridge site or (2) scour potential as determined by a scour evaluation study. A single digit code is used to describe the stability of the bridge and its vulnerability to scour. Descriptions for all Item 113 codes are presented in Appendix A. Scour critical bridges are identified by a code of 0, 1, 2, or 3, with 0 indicating that the bridge has failed (U.S. Department of Transportation 1995).

Over the past ten years, state DOTs in New England have devoted a large amount of time to assigning Item 113 codes for each bridge. While states have coded the majority of their bridges, no state has completely finished the task as many bridges either still need to be evaluated or were assigned a temporary code until more thorough analyses could be performed. Codes were assigned to many structures after an initial screening was conducted, without the need for a full scour analysis. For other bridges, the initial screening was not sufficient, requiring instead a more comprehensive scour analysis to assign a code. Many of the older structures could not be thoroughly evaluated since no plans were available and the foundations were thus unknown. In other cases, hydraulic or

Federal Emergency Management Agency (FEMA) studies were not available or complex hydraulic conditions at a bridge site necessitated an even more intensive analysis.

There are two approaches for assigning Item 113 codes to bridges with unknown foundations. One is to code the bridge as a 3 (scour critical). This is done to save time and money and is based upon results of other similar bridges that have received full scour evaluations. Another approach is to code the bridge as U (unknown foundation) until subsurface investigations can be performed based upon prioritization. The investigations can be accomplished through borings or geophysical testing methods such as ground penetrating radar. While this approach is more costly, it permits a full scour evaluation to be conducted, potentially removing some bridges from the scour critical list.

HEC-18 Evaluation

DOTs evaluate their bridge inventory for scour susceptibility using a number of different scour methodologies, the most common of which is HEC-18. HEC-18 covers all aspects of scour, including bridge design for scour, scour assessment, inspection procedures, and scour countermeasures. This circular presents a methodology for a detailed scour analysis, commonly referred to as Level 2 scour analysis, which is described in the following paragraphs (Richardson and Davis 1995).

DOTs evaluate their bridge inventory for scour susceptibility using a number of different scour methodologies, the most common of which is HEC-18. HEC-18 covers all aspects of scour, including bridge design for scour, scour assessment, inspection procedures, and scour countermeasures. This circular presents a methodology for a detailed scour analysis, commonly referred to as Level 2 scour analysis, which is described in the following paragraphs (Richardson and Davis 1995).

Three types of scour are addressed in the HEC-18 manual: (1) long-term aggradation and degradation, (2) contraction scour, and (3) local scour. Long-term aggradation and degradation, affected by either natural or man-made causes, refers to changes in streambed elevation over time. Contraction scour is primarily the result of channel constriction at a bridge crossing, where increased velocities scour the channel bed, but can also be caused by a change in local base-level elevation or flow around a bend. Typically, bridge approach abutments that block flow in the floodplain or extend out into the main channel are responsible for this scour type. Local scour is concentrated around piers, abutments, spurs, and embankments. Obstructions in the waterway impede and redirect flow, inducing the formation of vortices that accelerate the removal of bed material around the bases of obstructions. The cumulative sum of these scour types is the total scour (Richardson and Davis 1995).

Additionally, there are two components of both contraction scour and local scour: live-bed scour and clear-water scour. Live-bed scour occurs when bed material is transported from the upstream reach into the bridge crossing. Clear-water scour occurs when either no significant bed material is carried from the upstream reach into the downstream bridge reach or the material transported from the upstream reach is carried mostly in suspension through the bridge crossing to the downstream reach. HEC-18 provides the tools to evaluate both scenarios (Richardson and Davis 1995).

Although HEC-18 is widely used as the model to perform full scour analyses, there are two main problems with the methodology. First, in order to determine flow variables at a bridge, HEC-18 recommends the use of hydraulic modeling programs such as Water-Surface Profile Model (WSPRO) and HEC River Analysis System (HECRAS) (Richardson and Davis 1995). While these programs provide the some of the best estimates of flow variables, they are very costly and time consuming to perform. With large bridge inventories, states are reluctant to employ such time-intensive programs as part of their analyses for many of their bridges. Second, it is well documented that the HEC-18 equations can regularly give overly conservative scour depths. This may be due, among other things, to the inability of researchers to conduct tests on large-scale laboratory models. While it is better to have predictive methods that are conservative, excessive overestimation on a regular basis can increase costs to monitor, remediate, and even design and build bridges. These problems do not preclude the use of HEC-18 equations for scour evaluation, but rather should encourage DOTs to investigate other scour methodologies, in particular those that can generate similar results in a much shorter time period.

Connecticut Comparative Scour Analysis

The Connecticut Department of Transportation (CDOT) initially conducted its scour evaluation studies in general accordance with the aforementioned procedures. After performing Level 2 scour analyses on a few hundred bridges and faced with prohibitive costs and a large number of bridges remaining to be analyzed, CDOT looked to an alternative scour methodology to evaluate its bridges. The CDOT Hydraulic & Drainage Unit (H&D), along with the FHWA and consultants, developed a new, qualitative method that would provide NBIS Item 61, 71, and 113 codes for unanalyzed bridges without requiring full Level 2 scour analyses. This new method, called the comparative scour analysis, utilized the results of previous Level 2 scour analyses while generating time and cost savings (CHA 1998).

The comparative scour analysis is considered an intermediary step in the Comparison Methodology, the revised approach to scour assessment at bridges by CDOT. Its primary purpose is as a screening tool to provide NBIS code recommendations to as many previously unanalyzed bridges as possible during the early phases of the Comparison Methodology, thus eliminating them from further consideration and reducing the number of structures that ultimately receive more time-intensive scour analyses. It should be noted that the comparative scour analysis specifically does not calculate scour depths (CHA 1998).

To aid in the screening process, methodologies were established for collection of information during field visits and office reviews. Field reviews were performed by documenting field observations of site attributes related to the susceptibility of bridges to scour. These observations were quantified using fundamental scour parameters (FSPs) as a means of evaluating bridges according to the same criteria. Rating guidelines for the FSPs were provided to ensure consistent application of the documentation process. The existing 287 Level 2 bridges (i.e. those bridges that already received a full scour analysis) were evaluated and scored for the project according to the FSPs in order to verify that high ratings corresponded to low risk Item 113 ratings and low ratings reflected scour critical Item 113 ratings. Based upon the results, the ratings derived from the scour

parameters were in good correlation with the Item 113 ratings for the Level 2 bridges, and the procedure was affirmed for field use (CHA 1998).

In order to justify the comparison of two bridges, one rated and the other unrated, primary and secondary criteria had to be met. Bridges that were already rated using the Level 2 analysis served as the group of rated bridges with which the unrated bridges would be compared. Primary criteria were considered to be Single vs. Multiple Span and Stream Character Category. Secondary criteria were listed as Estimated Stream Velocity, Foundation Type (at Abutments and Piers), Ratio of the Upstream Channel Width to the Width of the Channel Beneath the Bridge, and Angle of Attack. A valid comparison mandated that, at the very least, all primary criteria were met. The greater the number of secondary criteria met, the closer the similarity of the two bridges (CHA 1998).

The comparative scour analysis was designed so that the field team could make the comparison while at the site of the unanalyzed bridge. Accordingly, the field team was given a laptop, database information, and all other relevant information to assist their efforts. The comparison included not only similarities in primary and secondary criteria between the two bridges, but also incorporated review of FSP scores and office information for the sites along with a detailed look at the structural, hydraulic, and geotechnical characteristics of the Level 2 bridge. Based upon review of all this information and engineering judgment, the field team either recommended NBIS codes for the unrated bridge or recommended additional, more detailed scour analyses (CHA 1998).

Rapid-Estimation Method

Holnbeck and Parrett (1997) addressed the challenges of assessing bridge scour in a timely fashion in a report issued by the USGS and prepared in cooperation with the Montana DOT. As in other states, the large inventory of bridges in Montana, coupled with detailed scour analyses using hydraulic modeling programs, made it difficult to evaluate bridge scour at these sites in a short period of time. The rapid-estimation method was thus created for use as a quick screening tool to identify bridges susceptible to scour. It was also developed to provide results comparable to those from full scour analyses. Scour assessments at bridges using the rapid-estimation method were submitted for review to the Montana DOT, who then decided if a more thorough scour analysis was warranted for any bridge. Results from 122 detailed scour analyses in 10 states were used to justify its application across all regions. Holnbeck and Parrett (1997) emphasize that although this method was developed for use in Montana, it could be applied to other geographic regions.

The rapid-estimation method limits input parameters to those that can easily and quickly be measured in the field, provides reasonable estimates of scour depths without underestimating, and generates results in a period of hours, not days. Scour depth estimations and hydraulic variables are related through simplification of standard Level 2 scour equations and graphical plots. Envelope curves are used in these relations as means to ensure the overestimation, rather than underestimation, of scour depths. The only requirement of this method is knowledge of the discharge at the site, regardless of the recurrence interval corresponding to that flow. Other hydraulic variables are calculated in the field using graphs relating velocity to unit discharge and flow depth to velocity.

Bridge parameters are also determined in the field. Therefore, through the combination of limited site data and envelope curve relations, quick, yet reasonable estimates of scour depth at bridges are made in the field (Holnbeck and Parrett 1997).

GIS APPLICATION

Using a GIS as an assessment tool requires the assimilation of data from a variety of sources. For the purpose of the bridge scour assessment, the GIS is used to integrate and analyze the data. Three categories of data were needed for the GIS: bridges, gages and dams. In order to complete an analysis, the three data sets need to be assembled into coverages. The GIS allows for calculations based on all of the coverages as well as a means for spatially presenting the results of the analysis.

Of the several GIS platforms available, ArcView and ArcInfo (ESRI) were used for the application presented. It must be noted that the bridge scour analysis could be created using any of platform. The ESRI products are used only as one application example. The application was created as part of a study of the bridges in the six New England states For the New England Transportation Consortium (NETC 99-3). The aspects of creating the GIS application can be applied to bridge scour analysis anywhere.

Data Coverages

It is important to understand that the data needed for the bridge scour analysis must be compiled from many different sources. As mentioned earlier the sources are not all consistent and require some effort in coordinating the data. The data may exist in several different forms. Much of the data is still in plan form as many of the bridge designs were done prior to the digital age. Even many of the maps are in original graphical form. These data can be entered into coverages using digitizers or scanners. Fortunately much of geographical material has already been digitized into importable coverages. New England states have created websites for retrieval of the coverages (DiStasi 2001, Ho and DiStasi 2001). A list of the state GIS websites are given in Table 1.

There are numerous coverages available on these websites. The coverages that were used for this study (state boundaries, county boundaries, major river basins, and streams and rivers) were the ones that were used for the scour assessment. Statewide coverages were used when possible. This eliminated the need to tile coverages in order to properly characterize drainage basins and flood plains. Geopolitical boundaries are important to include as the identification of bridges is dependent on the political unit in which the bridge is located. Also, county boundaries were needed to interpret flood warning data as those warnings are generally given on a county by county basis. Stream and rive coverages were needed to confirm that bridges were in fact spanning a waterway.

In some instances, coverages needed to be modified. In particular, the watershed data was often given with too great of a specificity with respect to the density of bridges. Many of the small basins were merged into larger basins in order to be more appropriate for the analysis.

Bridge Coverages

The specific data on bridge design parameters are not generally given in the form of GIS coverages. These data need to be gleaned from other sources. It must be noted that the

state DOT's have compiled extensive databases in the form of spreadsheets containing as much of the data. Even with these databases, many of the bridges are multiple listed, as there are shared jurisdictions (state highways, interstate highways, county roads, etc.).

The DOTs were asked to send bridge attributes they believed to be relevant for inclusion in the bridge scour database, including descriptors (town, county, id), bridge characteristics, stream characteristics, and rankings. There was some difficulty in obtaining the information from DOTs; complete bridge lists were received from Connecticut, Massachusetts, New Hampshire and Vermont. The two most important bridge attributes to collect are a unique bridge id and a bridge location. Any and all other attributes can easily be added or modified at a later time. Emphasis was placed upon including attributes pertinent to bridge scour equations as well as parameters that could be manually queried by the DOTs that would help identify and prioritize bridges generally more susceptible to scour, such as foundation type, scour indices, critical flow events, countermeasures installed (if any), and average daily traffic (ADT). The ability to see the locations of these bridges and use attributes to identify bridges most susceptible to scour during a storm event are vital to earlier and better preparation and response by DOTs and emergency management agencies. Attributes may also be queried to identify trends in infrastructure weakness as well as establish prioritization for bridge remediation.

Once the bridges were entered into the GIS, a cursory check was made to ensure that the sites fell within the state boundaries. In cases where they didn't, the coordinates were checked, and if a discrepancy existed, the DOT was notified and a correction was made.

Stream and Rain Gage Data

Although real-time hydrological data are an important component to this project, the data are not very useful without spatial knowledge of the gage locations. Whether the gage data are monitored throughout the course of a storm or forecast offices provide estimates of precipitation totals or river stages at various gage locations, the user must be aware of gage sites in relation to scour susceptible bridges and dams. Therefore, it was crucial that locations of all active real-time rain and stream gages were identified and entered into a GIS for each state.

An extensive search of the Internet revealed no comprehensive website that included all rain and stream gage networks. Websites with information regarding gage networks typically had their own GIS map showing gage locations, but the map was usually not available to download. The multiple coordinate systems and map formats used by various agencies on their websites also posed difficulties for integrating them within each state GIS. It was thus easier to extract the gage locations and attributes manually and then insert them as new GIS coverages.

Relevant stream gage attributes included general descriptors as well as drainage area into gage. Warning and/or flood thresholds were available for some gages, but were not included as part of the gage attributes. Rain gage attributes were similar to the ones for stream gages, but gage elevation was also added as a parameter.

Dams

It was decided that it would be also useful to incorporate the locations of dams into the GIS, due to their potential impact on the accuracy of stream gages during a significant storm event. This would serve dual purposes: (1) identify gages with regulated flows and (2) aid in the placement of future gages. While thousands of dams have been constructed in New England, only a fraction of these significantly affect the stream gages. The National Inventory of Dams, which is maintained by the Army Corps of Engineers, is available online and contains database information on thousands of dams nationwide ("National Inventory of Dams"). Due to the large number of dams in each state and that fact that no one dam attribute directly impacts bridge scour, all of the dams in the inventory were incorporated into the GIS for the time being. It is better to have too much information than too little and the data can easily be queried to eliminate dams from consideration.

Prediction of Flood Levels

In order to conduct a prioritization of the bridges, archival data needs to be compiled in an accessible and modifiable format. A solution to this is the creation of "gage tables" and "scour tables", which, when used in conjunction with real-time gage data, allow the user to assess scour conditions at bridges in real-time. The use of these tables can be used both as a comparison tool to evaluate the scour potential in real time and to consider the recurrence of scour critical events. Depths could be estimated and catalogued in a database in advance based upon predicted discharges for several return periods. The predicted scour occurring in "real-time" would then be verified using real-time data from nearby gages. Scour depth estimates for bridges will be predetermined and stored in tabular format for a number of flood flow events along with the bridges' scour critical events.

These "gage tables" and "scour tables" would be compiled from existing gage and bridge attributes already stored within the GIS. The intent of these "tables" is to summarize relevant scour attributes for presentation purposes. The user could look at these tables without pulling up extraneous attributes that overall may be important to the gage or bridge, but unimportant within the context of these "tables." These "tables" are of course subject to modification by DOTs.

"Gage tables" would be compiled from statistical analyses of historical gage data or from streamflow statistics made available by websites such as StreamStats. These data would be stored within each gage's attributes in the GIS. "Gage tables" should at least contain various flow return intervals and their corresponding discharge values. "Scour tables" can easily be generated for bridges that have already undergone a full Level 2 analysis in which scour depths were calculated for certain flow events. These "tables" should include various flow return intervals along with corresponding discharge values, predicted scour depths, and determination if the event is scour critical. Many bridges did not receive these intensive analyses, however, meaning scour depths and scour critical events would need to be calculated for hundreds of bridges. This task is made difficult by the cumbersome nature of existing analyses, especially since they require the use of hydraulic modeling programs. A tool like the rapid-estimation method, though, would allow DOTs to quickly and reasonably estimate scour depths at bridges for flow events of

different recurrence intervals. Discharges at bridges could be estimated using a variety of methods as described earlier and the rapid-estimation method would again be used to generate hydraulic variables. Figure 1 presents an envelope curve for estimation of pier scour using the rapid-estimation method. Pier scour can be calculated using this figure along with knowledge of bridge geometry and hydraulic variables, both of which are determined in the field using this method. Even if scour depths are not calculated using the rapid-estimation method, the method can still be used to quickly estimate flow variables for input into different scour algorithms. Regardless of how "scour tables" are created, it is emphasized that if these tables are not available for all bridges, then the potential of prioritization is limited.

Figure 2 presents a map of Connecticut bridges displayed according to their scour critical event determined using HEC-18. The user, though, may want to evaluate the bridges using another equation within the model manager. With equation parameters already stored in the bridge attributes (including flow variables), scour depths can be recalculated (and "scour tables" revised) using the new equation. Regardless of the scour equation, though, the scour depth that would cause factors of safety to fall below acceptable limits would have to be known for each structure. After applying the new equation, a new map would display the same bridges as the first, but the color or symbol scheme for the bridges would be different. The versatility of the model enables discretion to be used, permitting scour to be evaluated a number of different ways and allowing for a more complete analysis.

Analyses should not be limited to comparing bridges using the same equation, though, because equations may be better suited for application to certain bridges based upon the bridges' attributes. The NH USGS report demonstrated that the New York 1996 equation showed some promise as a predictive scour algorithm, but results were largely sensitive to decreases in bed material particle-size (Boehmler and Olimpio, p. 23, 2000). With this knowledge, the user could query all bridges with a minimum median bed particle size and evaluate them using the 1996 New York equation and then analyze the remaining bridges with a smaller median bed particle size using a different equation.

Engineering judgment should always be part of bridge scour analysis. Decisions should not be made solely using quantitative measures. The "gage tables" and "scour tables" are not intended to give exact scour conditions at any given time, but rather provide guidance as to the magnitude of the event and facilitate assessment of scour at bridges in real-time, particularly for prioritization purposes. The importance of engineering judgment is inherent in the SDSS, which allows the user to perform tasks at their discretion.

CONCLUSION

It is important to consider that the prioritization of bridges susceptible to scour can be reasonably accomplished using a GIS scheme. This requires that an understanding of the limited data about the as-built conditions of the bridges is needed. Also, it is important to incorporate appropriate information on stream flow and gage measurements to properly assess the return periods of flood levels.

The combination of the stream gage data and the bridge scour data can be effectively used to make predictions with respect to return periods of scour events. Lower return

period will result in higher scour hazard. Presentation of the return periods can be effectively made using the GIS mapping capabilities.

ACKNOWLEDGEMENTS

The authors would like to acknowledge the New England Transportation Consortium for the funding of the research presented in this paper.

REFERENCES

1. Boehmler, E.M. and Olimpio, J.R. 2000. Evaluation of Pier-scour Measurement Methods and Pier-scour Predictions With Observed Scour Measurements at Selected Bridge Sites in New Hampshire, 1995-98. U.S. Geological Survey, Water-Resources Investigation Report 00-4183, Pembroke, NH.

2. Clough, Harbour & Associates LLP. 1998. "Comparison Methodology." Prepared for Connecticut Department of Transportation.

3. Di Stasi, J.M. Real-time Bridge Scour Assessment and Warning, MSCE Project, Department of Civil and Environmental Engineering, University of Massachusetts, Amherst, May 2001, 12 pp.

4. Ho, C. L. and Di Stasi, J. M., Development Of Priority Based Statewide Scour Monitoring Systems inNew England, Report NETCR 24, NETC, August 2001.

5. Holnbeck, S.R. and Parrett, Charles. 1997. Method for Rapid Estimation of Scour at Highway Bridges Based on Limited Site Data. U.S. Geological Survey, Water-Resources Investigations Report 96-4310, Helena, MT.

6. Richardson, E.V. and Davis, S.R. "Evaluating Scour at Bridges Third Edition," Federal Highway Administration Hydraulic Engineering Circular No. 18, Publication No. FHWA-IP-90-017, Nov. 1995.

7. U.S. Department of Transportation, FHWA. 1988. "Scour at Bridges." Technical Advisory TA5140.20, Office of Engineering, Bridge Division, Washington, D.C.

8. U.S. Department of Transportation, FHWA. 1991. "Evaluating Scour at Bridges." Technical Advisory TA5140.23, Office of Engineering, Bridge Division, Washington, D.C.

9. U.S. Department of Transportation, FHWA. 1995. "Recording and Coding Guide for the Structure Inventory and Appraisal of the Nation's Bridges," Rep. No. FHWA-PD-96-001, Office of Engineering, Bridge Division, Washington, D.C.

Table 1. State GIS websites (DiStasi, 2001, Ho and DiStasi 2001).

State	URL Address
Connecticut	http://magic.lib.uconn.edu/
Maine	http://apollo.ogis.state.me.us/
Massachusetts	http://www.state.ma.us/mgis/massgis.htm
New Hampshire	http://www.granit.sr.unh.edu/
Rhode Island	http://www.edc.uri.edu/rigis/
Vermont	http://geo-vt.uvm.edu/

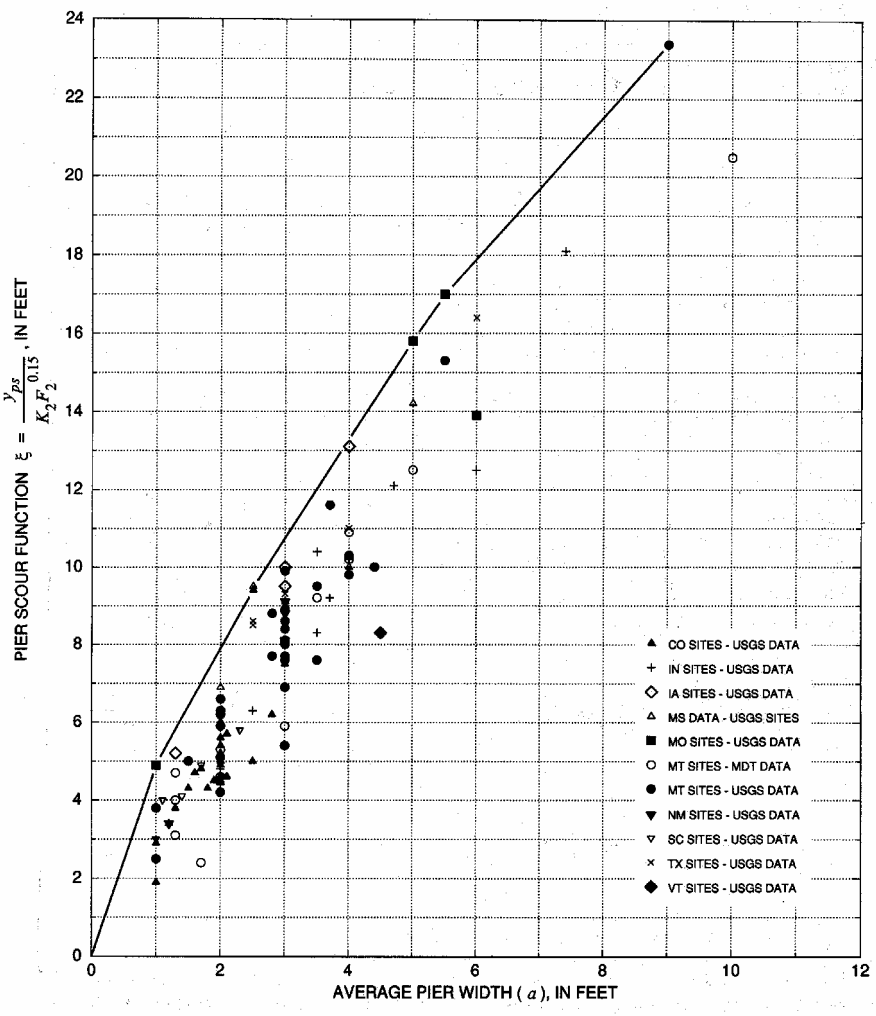

Figure 1. Envelope curve for estimation of pier scour (from Holnbeck and Parrett 1997).

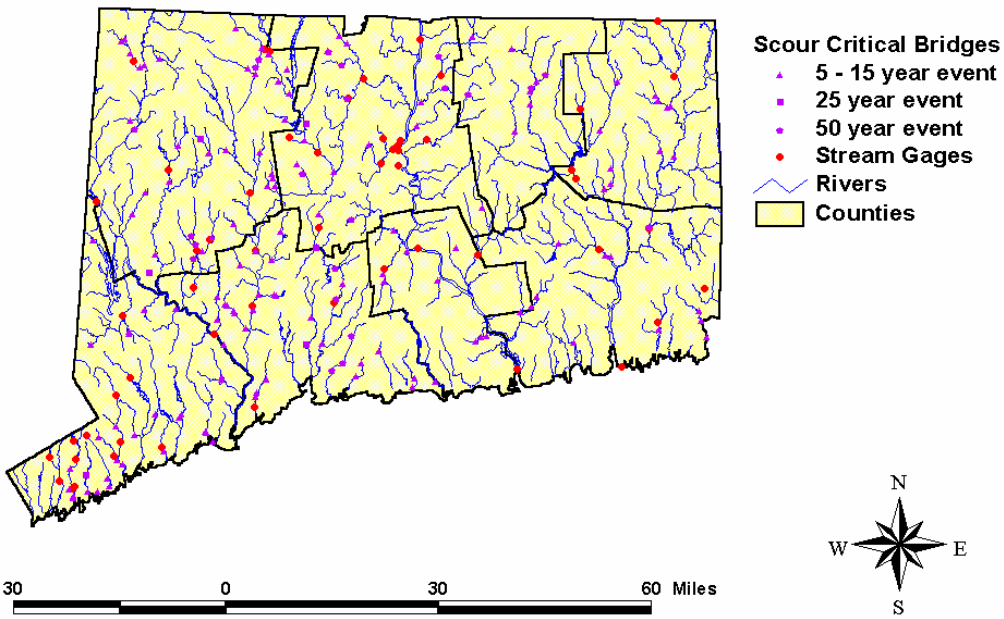

Figure 2. Scour critical bridges in CT (50-year event or smaller).

Erodibility Tests of Shale-Rock Samples Taken from Bridge Pier Construction Site on the Mississippi River

By

Tatsuaki Nakato[1]

Abstract

In 1991 the Iowa Department of Transportation (IADOT) was constructing a new bridge across the Mississippi River (approximately River Mile 404) on U.S. 34 at Burlington, Iowa, when some hazardous material (old coal tar) was found along the right river bank (Iowa side) within a thin sand layer, approximately 2.4 m thick, of the river bottom which overlaid the shale rock. The original design of the bridge-pier scour protection called for placement of riprap materials around the bridge pier. However, the discovery of the coal tar forced a design change of the pier footings to allow for the future clean-up operation of the hazardous material. A re-designed scheme involved possible elimination of proposed riprap. In order to evaluate the entire system's safety against potential scour problems, IADOT decided to extract undisturbed shale samples and test them using prototype velocity scales under a realistic prototype time scale under laboratory conditions. This practical approach was needed because of the uncertainties involved in estimating prototype velocities around bridge piers during extreme flood events, and a scarcity of literature available on the subject. Laboratory scour tests were conducted at IIHR-Hydroscience & Engineering, formerly Iowa Institute of Hydraulic Research (IIHR), The University of Iowa, for two shale specimens which were sampled directly from the bridge construction site. Although the samples were not under the desired undisturbed conditions, the laboratory test results using round jets indicated some potential for scour under high flow velocities. However, because there are so many unknown factors involved, such as true magnitudes of velocities in the scour hole, impact of large-scale eddies within the scour hole on shale-rock stability, surface conditions of shale rock when exposed in the prototype, changes in homogeneity of the shale-rock formation during construction activities, etc., the laboratory erodibility tests could by no means simulate the exact physical phenomena which would occur in the prototype. Instead, the test results reported should be viewed as an indication of probable events that would take place in the prototype.

Introduction

The primary objectives were to investigate through laboratory tests: (1) whether or not the shale would deteriorate and erode under high flow velocities (erodibility); (2)

[1] Research Engineer, IIHR – Hydroscience & Engineering, Adjunct Prof., Civil & Environmental Engineering, The University of Iowa, Iowa City, Iowa 52242, U.S.A.; tatsuaki-nakato@uiowa.edu

if so, at what velocities the shale would deteriorate and erode (critical erodible velocity); and (3) if so, how fast the shale would be eroded (erosion rate).

Samples

Three samples were extracted on 20 August 1991 from Shaft 6 of Pier S-2 that supports Spans S1 and S2 of the new bridge. As shown in Figure 1, the three samples were collected by means of a 61-cm diameter core barrel. According to IADOT (Rost, Field Report dated 29 August 1991), it was noticed that the upper zone of the first extraction was fractured presumably due to seating of the casing and the effect of the screwing process of the core barrel. The second and the third extractions also yielded samples similar to the first one. Large sample specimens were placed on a plastic bag in two separate plywood boxes, and hot wax was poured at a temperature of 49°C between the plastic bags and the samples such that the samples were completely encased at the bridge construction site.

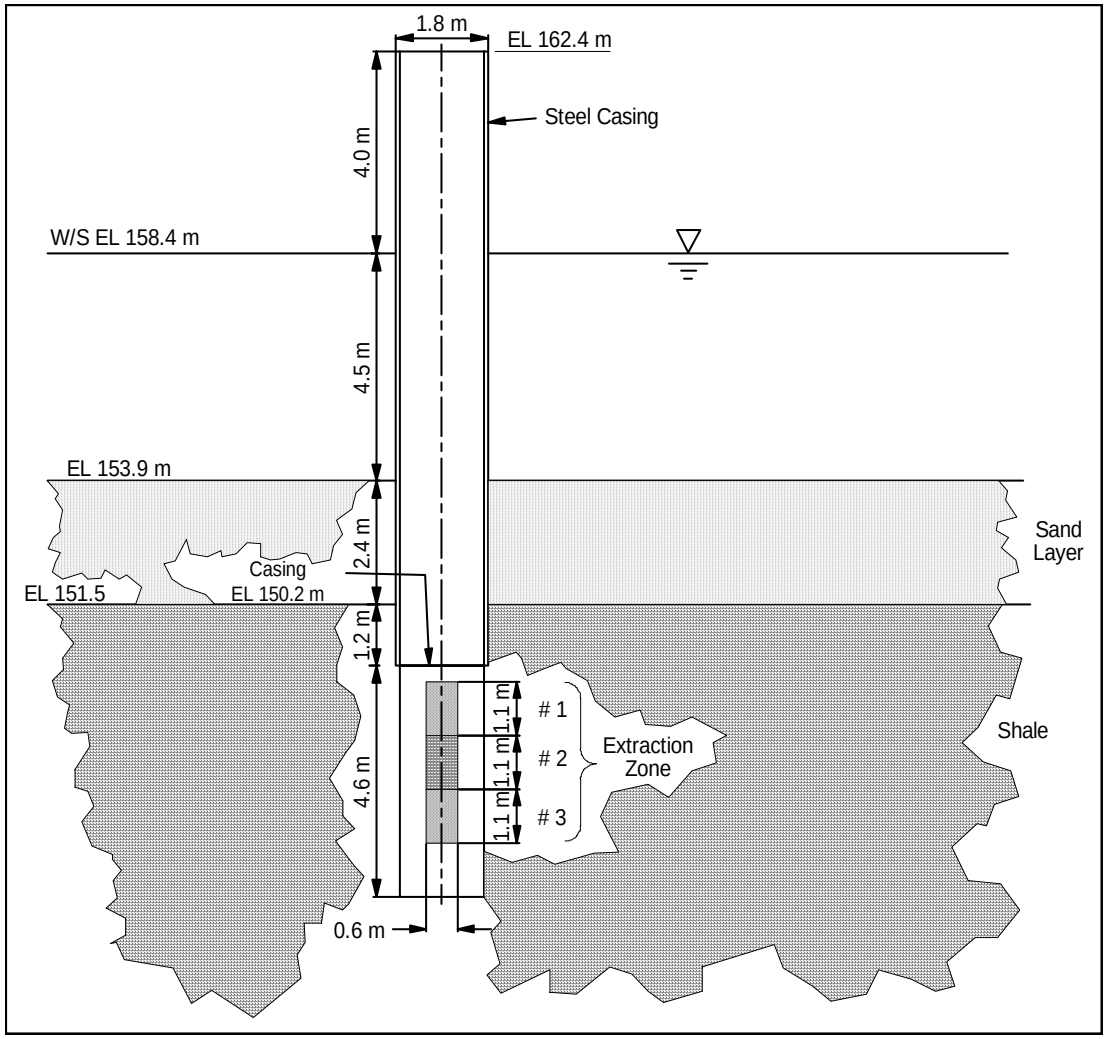

Figure 1. Prototype vertical sample location

Testing Facility

A re-circulating testing facility, as depicted in Figure 2, was constructed and installed on the first floor of the IIHR main building. The flow was re-circulated through a 5.1-cm diameter copper pipe by means of a 2.24-kw centrifugal pump, manufactured by Dunham-Bush Inc. The 5.1-cm piping system was fitted with a calibrated orifice meter for the flow-rate measurement and the discharge was regulated by means of a standard gate valve. Each shale sample container was placed inside the model basin box, which was 1.47-m long, 0.76-m wide, and 0.96-m deep. As shown in Figure 2, the testing box was partitioned by a vertical wall in order to maintain a stable water level within the test compartment. High-velocity jet flow was directed toward the shale surface at a known angle.

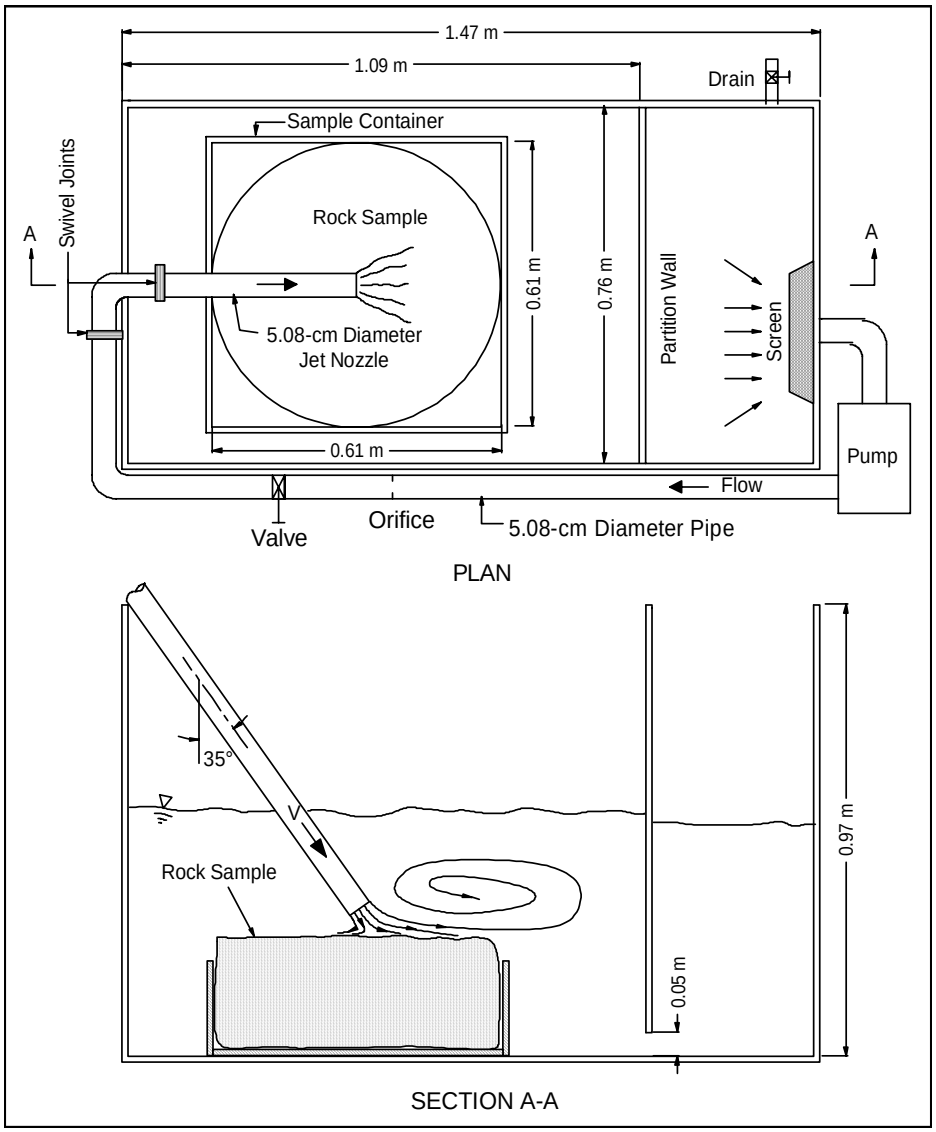

Figure 2. Test set up used to investigate shale-rock erosion

Test Procedure

The portion of wax that covered the top was first removed carefully from each shale sample, and the container holding the shale sample was placed immediately in the testing facility. The testing box was then filled with water, immersing the sample.

In each test, a low velocity jet, for example, 1.5m/s, was first applied, and close visual observations were made at short time intervals to identify any sign of deterioration or erosion of the sample surface. If any erosion was detected, erosion depth, its extent, and time span of exposure to high velocities were recorded, and some still photographs were taken to document the erosion process. In each test case, at least the initial and the final conditions of the sample surface were photographed. Water was drained from the testing facility for several minutes during photographing, but was re-filled promptly.

Test of Extraction 3 Sample (EXT3)

Two boxes containing the Extraction 1 sample and the Extraction 3 sample were delivered to IIHR by IADOT on 12 December 1991. The sample condition was not good, as can be seen in Figure 3 for the Extraction 3 sample. Apparently, the samples were kept outdoors and were exposed to severe cold weather conditions. The wax was cracked due to expansion of the shale. When the wax was removed, the surface of the Extraction 3 sample (EXT3) was found to be wet and soft like clay. In order to obtain a hard surface sample, the soft material was scraped and washed off.

Figure 3. Snow-covered rock sample when delivered

The EXT3 sample was then placed in the testing facility, and the 5.1-cm diameter pipe was installed 7.6 cm above the center of the surface at a jet-impinging angle of 55° from the horizontal plane, as shown in Figure 1. The water depth in the tank was maintained at 53.3 cm. The first test was to run the model at a mean jet velocity of 1.52 m/s. After 21 hrs. of testing, no erosion was detected.

The mean jet-nozzle velocity was then increased to 3.05 m/s in the second run. Small loose shale fragments were peeled off from the sample surface immediately after starting the test. Sometime between 8 hrs. and 27 hrs., several large rock pieces, about 2.5 cm thick, were dislodged from the sample surface. After 64 hrs. of testing, there were some significant erosion patterns that developed over the shale surface. The deepest scour was found around the sample edge, and it was about 5.1 cm deep. Many complex cracks developed in a cascading manner (scour depth increasing in steps) extending outward from the jet nozzle.

The final phase was run for 13.5 hrs. at a jet velocity of 4.57 m/s. Immediately after starting the pump, numerous small shale fragments, 2.5 - 3.8 cm in diameter, were observed peeling off. After 7 hrs. of testing, the tank was dewatered and several photographs were taken. It was clear that significant scour and deterioration of the shale surface occurred with this high jet velocity. This series was stopped after running for 13.5 hrs., at which time the largest scour depth measured was 15.2 cm. The centerline scour profile is depicted in Figure 4, and a plan view of the specimen is shown in Figure 5. Shale flakes which were peeled off the sample were smaller than about 5.1 cm (examine Figure 5 with the fact that the jet pipe diameter was 5.1 cm).

In summary, there was a strong indication that the shale sample tested (EXT3) as provided had scour potential at a jet velocity of 3.05 m/s. However, it must be noted that the sample was apparently frozen and the shale texture had deteriorated somewhat prior to testing.

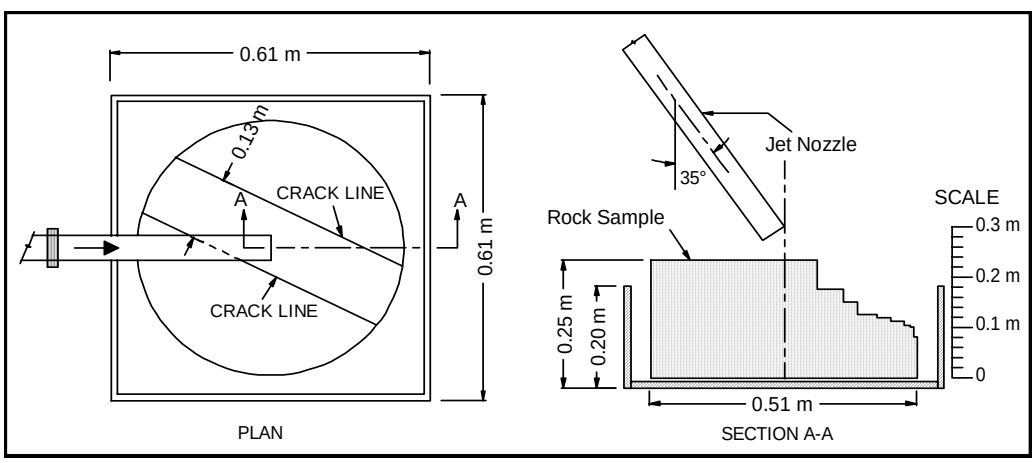

Figure 4. Final scour profile with EXT3 sample (V = 4.57 m/s and t = 13.5 hrs)

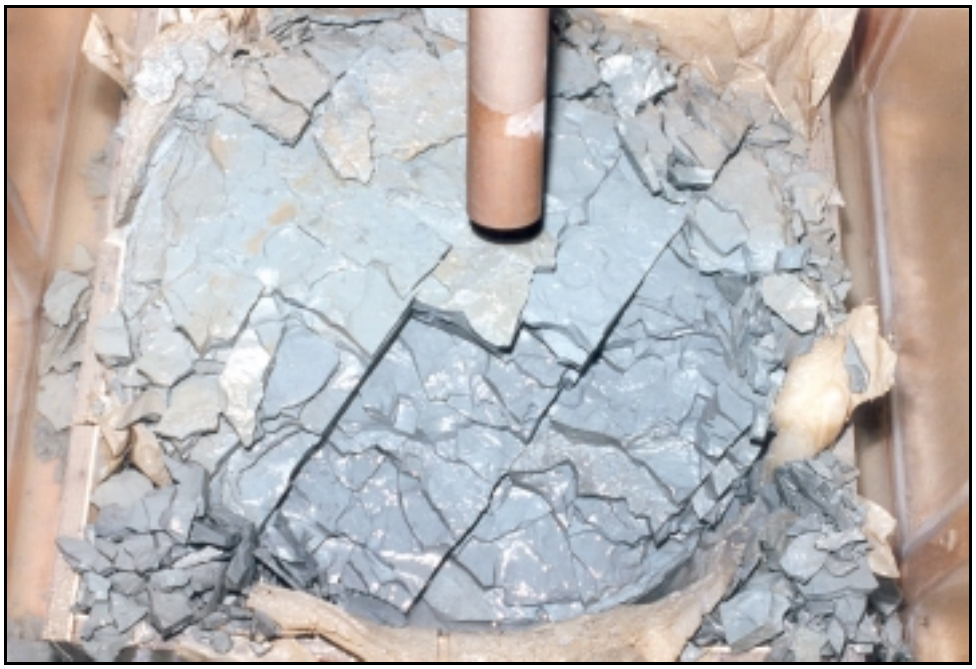

Figure 5. Surface condition of EXT3 sample after 13.5 hrs

Before presenting other test results, it is important to recognize that the terminology "mean jet velocity (V)" used in this report is defined as flow discharge (Q) divided by pipe cross-section area (A). According to Daily and Harleman (1966), a turbulent circular jet may have the following approximate relationships:

$$\frac{V}{V_m} = \frac{1}{\left(1 + \frac{r^2}{0.016z^2}\right)^2} \tag{1}$$

$$\frac{V_m}{V_0} = 6.4\left(\frac{D}{z}\right) \tag{2}$$

and

$$L_0 = 6.4D + 0.6D = 7D \tag{3}$$

where V = jet velocity at point (z,r); z = longitudinal distance from the actual origin of jet defined in Figure 6; r = radial coordinate normal to z axis; V_m = maximum jet velocity along the z axis; V_o = jet core velocity at nozzle; D = pipe diameter; and L_o = distance required for jet to fully develop. Because D = 5.1 cm in this case, the jet core velocity would be expected to extend about 35.6 cm. Although the test condition was such that there was a rigid shale surface on which jet flow impinged and deflected in a complex three-dimensional manner, it can be assumed that the jet core

velocity was maintained at least locally over the sample surface along the jet centerline.

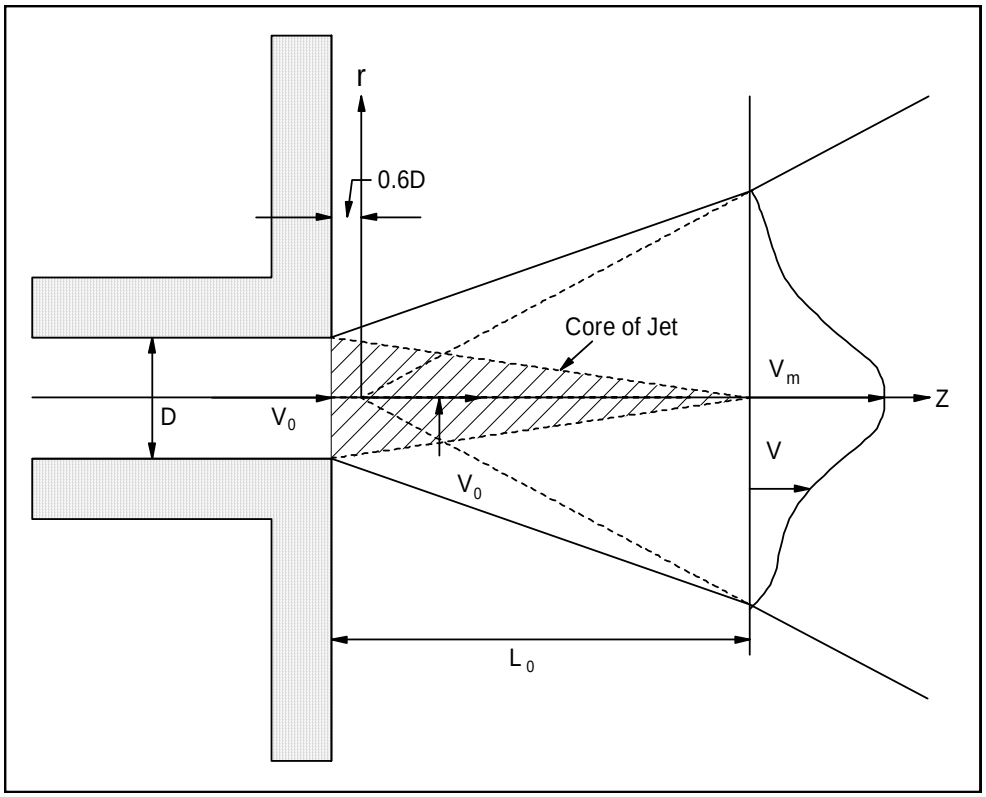

Figure 6. Definition sketch of circular jet

Test of Extraction 1 Sample (EXT1)

Because it was recognized during the test with the EXT3 sample that a minor flaking process occurred with a jet velocity of 3.05 m/s, and severe flaking took place when the jet velocity was increased to 4.57 m/s, it was decided to test the second sample (EXT1) with a starting velocity of 1.83 m/s and to increase jet velocities at a smaller increment.

According to IADOT (Rost, Field Report dated 29 August 1991), the second box contained three shale pieces of varying sizes and shapes. The bottom piece was from Extraction 2, and the other two upper pieces were from Extraction 1. When wax was removed for the first time, no visible sample boundaries were detected. Therefore, this shale sample was called EXT1 for convenience. As done for the EXT3 sample previously, the soft deteriorated top surface was removed first. The sample surface was then washed with a garden hose and fractured surface materials were removed prior to testing. Fortunately, a smooth solid surface layer appeared in this sample, as shown in Figure 7. A smooth initial centerline surface profile was able to be measured this time.

Figure 7. Undisturbed shale surface after removing deteriorated material (EXT1)

Figure 8. Surface condition after 41 hrs. of testing with a jet velocity of 2.44 m/s (EXT1)

The first test was conducted with a jet velocity of 1.83 m/s. Even after 19 hrs. of testing, practically no flaking took place. When the jet velocity was increased to 2.44 m/s, some minor flaking took place, as seen in Figure 8. Although the central

part of the sample surface remained unchanged except for one minor flaking near the jet nozzle, side areas surrounding the central piece deteriorated considerably.

Figure 9. Surface condition after 38.5 hrs. of testing with a jet velocity of 3.05 m/s (EXT1)

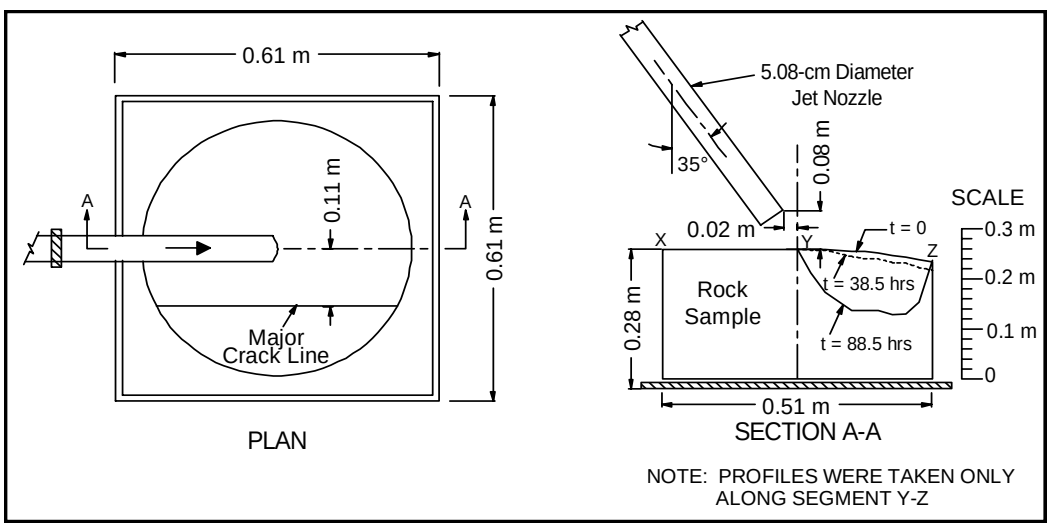

Figure 10. Scour profiles obtained with EXT1 sample with a jet velocity of 3.05 m/s

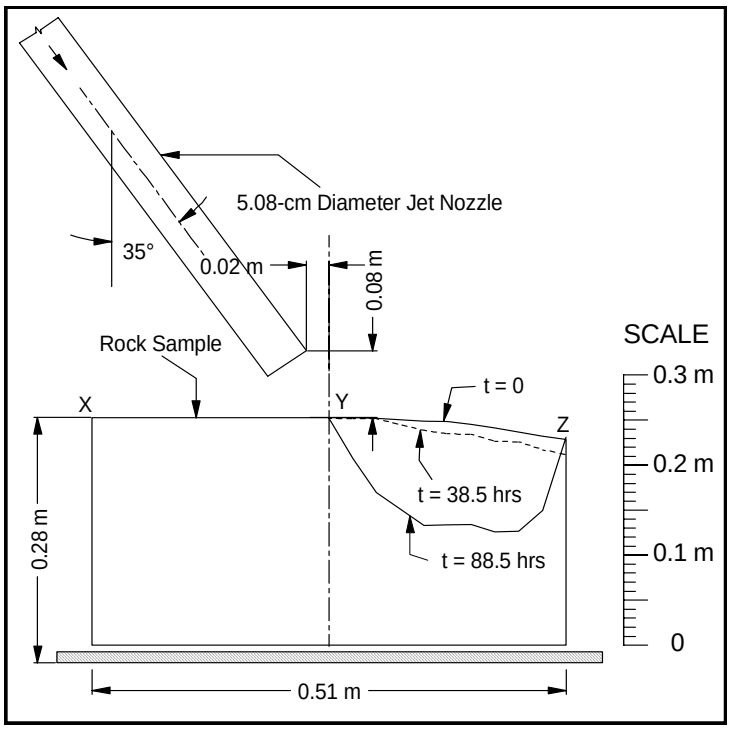

Figure 11. Close-up view of scour profile with EXT1 sample

When the jet velocity was increased to 3.05 m/s, some loose materials peeled off immediately. However, the surface profile of the solid central part remained unchanged even after 31.5 hrs. of continuous testing. At run time of 38.5 hrs., a distinguishable scour was observed, as shown in Figure 9. The measured surface profile is also plotted in Figures 10 and 11. It was determined that approximately, 1.3 cm of the shale material was scoured between 31.5 hrs. and 38.5 hrs. This series of testing was finally stopped after 88.5 hrs. of testing. A large scour hole was discovered, as shown in Figures 10, 11, and 12. The deepest part of the scour hole was approximately 12.7 cm below the original surface elevation.

As stated above, the shale surface did not show any noticeable sign of the scour process during the run time 0 hr. and 31.5 hrs.; and about 1.3 cm deep surface scour was suddenly observed during 31.5 hrs and 38.5 hrs. (overall scouring rate being about 0.033 cm/hr. = 1.3 cm/38.5 hrs.); and a scour hole about 12.7-cm deep was created during 38.5 hrs. and 88.5 hrs. (overall scouring rate being about 0.14 cm/hr = 12.7 cm/88.5 hrs.). This indicates that the shale can withstand for a certain time period high flow velocities as high as 3.05 m/s. However, after a certain time span of exposure, it starts deteriorating, and the scouring action seems to start taking place, the scouring rate appearing to increase in time.

Figure 12. Scour profiles obtained with EXT1 sample with a jet velocity of 3.05 m/s

Conclusions

On the basis of the laboratory tests conducted with the two shale samples, the following conclusions may be drawn:

1. Obviously, the site-specific shale samples, taken from the Mississippi River in Burlington, Iowa, had experienced freezing and thawing processes while kept in the field, and near-surface sample zones, at least the top 5 cm layer from the surface, were severely deteriorated. Although the deteriorated portion was removed as much as possible prior to testing, the exact extent of cracks and internal damage to the sample was not able to be determined. Therefore, the test results presented in this paper should be viewed as a preliminary indication of the deteriorating process of the shale when exposed to a high velocity field.

2. The disturbed shale appeared to deteriorate somewhat when velocities were larger than 2.44 m/s. The shale in good conditions appeared to withstand flow velocities as high as 3.05 m/s for a while (about 30 hrs. in the case of EXT1 sample), but to deteriorate slowly in time. The scouring rate was found to increase in time, and extremely complex fracture patterns seemed to appear.

3. The investigation was the first attempt known to the author to test the physical resistance against scour potential of the shale in a controlled manner. However, there were a number of uncertainties involved in the present study. Therefore, it is strongly recommended that further laboratory investigations similar to this

study be conducted using undisturbed field samples in order to gain more knowledge on general characteristics of the shale or similar erodible rocks.

4. It is recommended that such shale rock samples be kept submersed in river water where samples are taken instead of waxing and that laboratory tests be conducted as soon as samples are extracted to avoid sample deterioration.

Closing Remark

Based on the test results, IADOT decided to protect bridge piers with riprap materials in 1992, which was a truly wise decision because the "Great Flood of '93" hit the Burlington area of the Upper Mississippi River. The average discharge at Burlington, Iowa is about 1,730 m^3/s, and the peak discharge during the '93 flood was estimated to be about 13,600 m^3/s. No damage to the bridge piers was reported during the flood.

References

Daily, J.W., and Harleman, D.R.F., (1966). *Fluid Dynamics*, Addison-Wesley Publishing Company, Inc.

Iowa Department of Transportation, Rost, J.P., (1991). "Shale Samples - Burlington Bridge Site," Ref. No. Des Moines County BRF-34-9(61), August.

The Driving Force on Soil Grains and Its Effect on Scouring the Channel of Foundation

By

Lijun Zhang[1], Duowen Ding[1], Wenbin Zhou[2]

ABSTRACT

Saturated soil is viewed as a multi-phase medium. Based on the motion equation of fluid phase, the viscous constitutive relationship of fluid phase, and the interaction between fluid phase and solid phase, the driving force on soil grains is governed. The effect of the driving force of soil grains on the scoured channel of foundation is investigated. At the same time, on the basis of a two-phase medium, the driving force on soil grains is also discussed by using Darcy's law for relative flow.

INTRODUCTION

Within a saturated aquifer, there is a buoyancy or pressure on a plane surface inside saturated soil, but there are both buoyancy and driving force on soil particles. The driving force on soil particles is caused by the interaction between fluid phase and solid phase. The magnitude of the driving force on soil particles equals the drag force of pore water flow but its direction is opposite to the direction of drag force of pore water flow. Due to the mentioned-above relation of the driving force of soil particles to the drag force of pore water flow, the research on the drag force of pore water flow is often focused on. Many researchers have started a lot of works on a fluid phase in a porous medium. The motion equation for a fluid phase inside the void space of a porous medium has been obtained by Bear (1972), Hassanizadeh and Gray (1979a, b), Bear and Bachmat (1986), Bachmat and Bear (1986), Jiang Li and Donald C. H. etc. In general, the motion equation of pore water flow should include the inertial force term due to acceleration, both local and convective, the viscous resistance term due to internal friction inside the fluid phase, the driving force term due to pressure gradient and gravity, and the drag resistance term caused by the fluid-solid interaction. On the other hand, the motion equation of a two-phase medium has been studied by Macarthur and Schamber (1983), Jeyapalan, Duncan and Seed (1983). The water is considered as fluid phase and the soil particles are considered as solid phase. The motion equations of fluid phase and solid phase are established respectively. The interaction force couples the interaction between fluid phase and solid phase. Finally, the motion equation of a two-phase medium is derived. The paper pays attention to concentrate on both a fluid phase and a two-phase (fluid and solid) medium. The motion equation of fluid phase including interaction between fluid and solid phases is governed. For a special case, the interaction force (the driving force of soil particles or drag force of pore water flow) is discussed. At the same time, saturated soil as a two-phase medium is studied and the driving force on soil particles is governed by introducing a potential function for a two-phase medium.

MOMENTUM EQUATION OF FLUID PHASE INCLUDING THE FLUID-SOLID INTERACTION

---

[1] Research Assistant, Dept. of Civil Engineering, Morgan State University, Baltimore, MD 21286, USA.
[2] Professor, Dept. of Environmental Engineering, East China Geological Institute, Linchuan, Jiangxi 344000, China

In a saturated aquifer, the inertial force, viscous resistance force, driving force, and drag resistance force act on the fluid phase. The motion equation of fluid phase can be expressed as:

$$\boldsymbol{r}_{\mathbf{w}}\mathbf{a}_{\mathrm{w}} + \nabla \mathrm{p} - \nabla \boldsymbol{t} - \boldsymbol{r}_{\mathrm{w}}\mathbf{b} - \mathbf{M} = 0 \tag{1}$$

where ρ_w is fluid density; $\mathbf{a}_w$ is fluid acceleration; p is fluid pressure; τ (a second order tensor) is viscous stress; **b** is body force vector; and **M** is the interaction force vector between fluid and solid phases. The material derivative concept is very useful in analysis of fluid acceleration. Based on the material derivative concept, the acceleration $\mathbf{a}_w$ may be written as:

$$\mathbf{a}_{\mathbf{w}} = \frac{\mathrm{d}\mathbf{v}_{\mathrm{w}}}{\mathrm{dt}} = \frac{\partial \mathbf{v}_{\mathrm{w}}}{\partial \mathrm{t}} + (\mathbf{v}^{\mathrm{p}} \cdot \nabla)\mathbf{v}_{\mathrm{w}} \tag{2}$$

where p is a point in the REV of a saturated aquifer which can be chosen as one point on the macroscopic water phase, or fixed space, or the macroscopic solid phase; $\mathbf{v}_w$ is the velocity of fluid phase; and $\mathbf{v}^p$ is the velocity of the point p. For Newtonian fluids, the viscous stress is linearly related to the rates of deformation and can be expressed as follows:

$$\boldsymbol{t} = \mathrm{D}\dot{\boldsymbol{e}} \tag{3}$$

where D is the viscosity matrix of the fluid; and $\dot{\boldsymbol{e}}$ is strain rate. After equation 3 is taken the operation of divergence, equation 3 becomes:

$$\nabla \boldsymbol{t} = \mathrm{D}\nabla \dot{\boldsymbol{e}} = (\boldsymbol{k} + 3m)\nabla(\nabla \cdot \mathbf{v}_{\mathrm{w}}) + m\nabla^2 \mathbf{v}_{\mathrm{w}} \tag{4}$$

where κ is bulk viscosity; and μ is shear viscosity. Substituting (2) and (4) into (1), the interaction force vector is in the following form:

$$\begin{aligned} \mathbf{M} = \boldsymbol{r}_{\mathrm{w}}[\frac{\partial \mathbf{v}_{\mathrm{w}}}{\partial \mathrm{t}} + (\mathbf{v}^{\mathrm{p}} \cdot \nabla)\mathbf{v}_{\mathrm{w}}] + \nabla \mathrm{p} - (\boldsymbol{k} + 3m) \\ \nabla(\nabla \cdot \mathbf{v}_{\mathrm{w}}) - m\nabla^2 \mathbf{v}_{\mathrm{w}} - \boldsymbol{r}_{\mathrm{w}}\mathbf{b} \end{aligned} \tag{5}$$

In order to simplify equation 5, continuity equation is introduced into equation 5. For steady or unsteady flow, and compressible or incompressible fluids, in vector notation, the equation for conservation of mass can be written as:

$$\frac{\partial \boldsymbol{r}_{\mathbf{w}}}{\partial \mathrm{t}} + \nabla \cdot \boldsymbol{r}_{\mathbf{w}}\mathbf{v}_{\mathrm{w}} = 0 \tag{6}$$

For both steady and unsteady flow of incompressible fluids, the fluid density, ρ_w, is a constant so that equation 6 becomes:

$$\nabla \cdot \mathbf{v}_{\mathrm{w}} = 0 \tag{7}$$

Inserting equation 7 into equation 5, the interaction force vector for incompressible fluid is given below:

$$\mathbf{M} = \rho_w [\frac{\partial \mathbf{v}_w}{\partial t} + (\mathbf{v}^p \cdot \nabla)\mathbf{v}_w] + \nabla p - \mu \nabla^2 \mathbf{v}_w - \rho_w \mathbf{b} \tag{8}$$

It is quite difficult to solve the equation 8 because of their non-linearity arising from the convective terms (i.e., $(\mathbf{v}^p \cdot \nabla)\mathbf{v}_w$ etc.). A special case for which the convective acceleration vanishes will be studied in the following section.

DRIVING FORCE OF SOIL GRAINS FOR STEADY LAMINAR FLOW IN THE SCOURED CHANNEL OF FOUNDATION

The scoured channel of foundation is viewed as fixed parallel plates (its thickness is 2h). The flow is considered as steady laminar flow between fixed parallel plates shown in Figure 1. The equation 8 reduces to:

$$M_x = \frac{\partial p}{\partial x} - \mu \frac{\partial^2 v_{wx}}{\partial x^2} \tag{9}$$

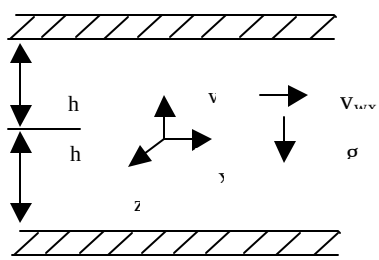

Figure 1 A Model of Scoured Channel

$$M_y = \frac{\partial p}{\partial y} + \rho_w g \tag{10}$$

$$0 = \frac{\partial p}{\partial z} \tag{11}$$

After equations 9, 10, and 11 are solved, the interaction force is given below:

$$M_x = \frac{3q\mu}{2h^3} + \frac{\partial p}{\partial x} \tag{12}$$

where h is half of the thickness between the scoured channel; q is the volume rate of flow. Let Δp_x, and Δp_y represent the pressure drops between two points along x-direction, and y-direction the distances l_x and l_y apart respectively, then

$$\frac{\Delta p_x}{l_x} = -\frac{\partial p}{\partial x} \tag{13}$$

$$\frac{\Delta p_y}{l_y} = -\frac{\partial p}{\partial y} \tag{14}$$

and 12 and 10 can be expressed as

$$M_x = \frac{3q\mu}{2h^3} - \frac{\Delta p_x}{l_x} \tag{15}$$

$$M_y = -\frac{\Delta p_y}{l_y} + \rho_w g \tag{16}$$

M_x, and M_y are the resulting drag resistance force and additional sediment force per unit fluid volume. When the volume of a single soil grain is assumed to be v_{grain}, its equivalent diameter is:

$$d = \left(\frac{6v_{grain}}{\pi}\right)^{\frac{1}{3}} \tag{17}$$

The total number of soil grain per unit volume fluid is given as

$$N = \frac{v_{solid}}{v_{grain}} = \frac{6(1-n)}{n\pi d^3} \tag{18}$$

where N is the total number of soil grain per unit volume fluid; n is the porosity of a saturated soil; and v_{solid} is the total volume of soil solid where the volume of fluid is one unit. The driving force F_d and rising force F_r acting on the single soil grain can be expressed respectively

$$F_d = -\frac{M_x}{N} = \left(\frac{\Delta p_x}{l_x} - \frac{3q\mu}{2h^3}\right)\frac{n\pi d^3}{6(1-n)} \tag{19}$$

$$F_r = -\frac{M_y}{N} = \left(\frac{\Delta p_y}{l_y} - \rho_w g\right)\frac{n\pi d^3}{6(1-n)} \tag{20}$$

when the single grain on the surface of the channel is scoured, the limit equilibrium equation can be given as

$$F_d = [(\rho_{solid} - \rho_w) g \frac{\pi d^3}{6} - F_y] f \tag{21}$$

where f is frictional coefficient. Inserting 19 and 20 into 21, the equation is given

$$\frac{\Delta p_x}{l_x} = [\rho_{solid} g - \frac{1-2n}{1-n} \rho_w g - \frac{\Delta p_y}{l_y} \frac{n}{1-n}] \frac{(1-n) f}{n} + \frac{3qm}{2h^3} \tag{22}$$

When the pressure gradient along x-direction is equal to or larger than $\frac{\Delta p_x}{l_x}$, the soil grain on the surface of channel can be scoured by the pore water flow.

TRANSIENT DRIVING FORCE ON THE SOLID PARTICLES BASED ON A TWO-PHASE FLUID MODEL

Donald C. Helm (1994) introduces a potential function into the two-phase fluid for irrotational flow. Based on the potential function, the bulk flux can be expressed as

$$q_{bi} = - K_{ij} \frac{\partial \theta}{\partial x_j} \tag{23}$$

where K_{ij} is hydraulic conductivity tensor; θ is the potential function of the two-phase fluid; $q_{bi} = nv_{wi} + (1-n)v_{si}$ is the bulk flux; v_{wi} is the velocity of water in *i* direction; and v_{si} is the velocity of solid particles in *i* direction. For an isotropic material, equation 23 can be written as:

$$q_{bx} = - K \frac{\partial \theta}{\partial x} \tag{24}$$

where $q_{bx} = nv_w + (1-n)v_s$. Darcy's law can be given by:

$$q_w = n(v_w - v_s) = - K \frac{\partial h}{\partial x} \tag{25}$$

where q_w is the relative specific discharge; h is a hydraulic head.

By combination of 24 and 25, one has:

$$v_s = - K \frac{\partial(\theta - h)}{\partial x} \tag{26}$$

Based on the equation 26, the bulk driving force on the assemblage of solid is $g\frac{\partial(\boldsymbol{q}-\mathrm{h})}{\partial x}$.

CONCLUSIONS

Based on the fluid phase in a multi-phase medium, the diving force on solid particles is derived by the motion equation of fluid phase, which includes the interaction between solid and fluid phase. The driving force on the solid particles can also be governed by the equations of multi-phase fluid. When the driving force on the solid is equal to or larger than the limit driving force, the solid particles on the scoured channel of foundation starts to move and be scoured.

REFERENCES

Bear, J., 1972, Dynamics of Fluid in Porous Media, Elsevier, New York.

Hassanizadeh, M. and Gray, W. G., 1979a, "General Conservation Equations for Multiphase-Systems, 1. Averaging Procedure", Adv. Water Resour. 2(3), 131-144.

Hassanizadeh, M. and Gray, W. G., 1979a, "General Conservation Equations for Multiphase-systems, 1. Mass, Momentum and Energy Equations", Adv. Water Resour. 2(4), 191-203.

Bachmat, Y. and Bear, J., 1986, "Macroscopic Modeling of Transport Phenomena in Porous Media, 1:the Continuum Approach", Transport in Porous Media 1, 213-240.

Bear, J. and Bachmat, Y., 1986, "Macroscopic Modeling of Transport Phenomena in Porous Media, 2: Applications to Mass, Momentum and Energy Transport", Transport Phenomena in Porous Media 1, 241-269.

Jiang Li and Donald C. H., 1998, "Viscous Drag, Driving Forces, and Their Reduction to Darcy's Law", Water Recourses Research, Vol. 34, No. 7 1675-1684.

Macarthur, R. C. and Schamber, D. R., 1983, "Modeling of slurry flows", Proceedings of Third International Symposium on River Sedimentation, Mississipi.

Jeyapalan, J. K., Duncan, T. M. and Seed, H. B., 1983, "Analyses of Flow Failures of Mines Tailings Dams", Jour. of Geotechnical Engineering, ASCE, Vol. 109, No. 2, 156-171.

Donald C. H., 1994, "Hydraulic Forces That Play a Role in Fissures at Depth", Bulletin of the Association of Engineering Geologists, Vol. XXXI, No. 3, 293-304.

Depth of Mobile Layer Under Severe Wave Conditions: Liquefaction Effect

By

Shinji Sassa

Research Fellow of the Japan Society for the Promotion of Science, Disaster Prevention Research Institute, Kyoto University, Kyoto 611-0011, Japan,(sassa@kaigan.dpri.kyoto-u.ac.jp).

ABSTRACT The wave-induced build-up of pore water pressures that occurs primarily under wave pressure fluctuation rather than oscillatory flow, is shown here to play a vital role in causing transport of fine sediments under waves. Poro-elastic analysis is presented on the depth of mobile layer under waves, and the results are compared with the existing theory in oscillatory flow. The effect of the oscillatory change in effective stress is identified that may manifest itself under severe wave conditions. For soft fine sediments, however, wave-induced liquefaction or fluidization resulting in the complete loss of effective stresses can take place. The simultaneous processes of the wave-induced liquefaction and sediment transport are reproduced here by the poro-elastoplastic finite element analyses. It is found that the thickness of mobile layer can develop rapidly in loose beds of fine sand or silt owing to the build-up of residual pore pressures, under severe yet considerably lower levels of wave loading than in the situation where only oscillatory flow effect is considered.

INTRODUCTION

The depth in which sediment becomes mobile under waves is one of the most fundamental questions in modelling the coastal sediment transport processes. When sediment becomes mobile, the following relation has been assumed to hold at the bottom of the mobile layer (Nielsen, 1992):

$$|\tau_{zx}| = K\sigma'_{z0} \tag{1}$$

where τ_{zx} is a horizontal shear stress, σ'_{z0} is an initial vertical effective stress and K represents a friction coefficient of soil skeleton. The shear stress changes due to the wave-induced oscillatory flow have been well described based on the knowledge of fluid mechanics. However, the changes in effective stresses due to the presence of oscillatory and residual pore pressures in the soil, as shown in Fig. 4 of the present

paper, were out of the scope of fluid mechanics. The integrated use of soil mechanics and fluid mechanics is thus vital for a rational understanding of the wave-induced sediment transport processes.

The paper is aimed at clarifying the role of the build-up of pore water pressures in causing sediment transport under waves. The theoretical background to represent the severity of wave loading will be described first. Then, the paper presents poro-elastic and elastoplastic analyses on the thickness of mobile layer under waves.

REPRESENTATION OF THE SEVERITY OF WAVE LOADING

The passage of wave trains exert two forms of action on the soil surface, namely, wave pressure fluctuation and oscillatory flow, both of which should induce horizontal shear stress in the soil.

The severity of the wave pressure fluctuation on a given horizon of soil may be expressed in terms of the cyclic stress ratio $\chi \equiv \tau / \sigma'_{v0}$ where τ represents the wave-induced maximum shear stress at that horizon and σ'_{v0} the initial vertical effective stress there. With the aid of a poro-elasticity theory (Madsen,1978; Yamamoto et al., 1978), the cyclic stress ratio at the level of the soil surface reduces to the following dimensionless parameter (Sassa and Sekiguchi, 1999)

$$\chi_0 \equiv \left[\frac{\tau}{\sigma'_{v0}}\right]_{z=0} = \frac{\kappa u_0}{\gamma'} \tag{2}$$

where u_0 is the amplitude of the wave-induced pressure fluctuation on the soil surface, κ is the wave number defined by $2\pi/L$ and γ' is the submerged unit weight of soil defined by $(\rho_s - \rho)g/(1+e)$. Here ρ_s is the density of soil particle, ρ is the density of fluid, g is the acceleration due to gravity and e is the void ratio of the soil.

The severity of the wave-induced oscillatory flow may be expressed by the dimensionless parameter S which represents the ratio of inertial to gravity forces acting on individual grains of soil (Sleath, 1994):

$$S = \frac{\rho U_0 \omega}{(\rho_s - \rho) g} \tag{3}$$

where U_0 is the velocity amplitude of the wave-induced oscillatory flow on the soil surface and ω is the angular wave frequency defined by $2\pi/T$.

On the basis of the linear wave theory where $U_0 = \kappa u_0 / (\rho\omega)$, I obtain the following relationship:

$$\chi_0 = S(1+e) \tag{4}$$

Thus, the severity of wave loading can be represented by either χ_0 or S. In the sections that follow, the parameter S will be used to discuss the thickness of mobile layer under waves.

PORO-ELASTIC ANALYSIS AND DISCUSSION

Suppose that small-amplitude sinusoidal fluid wave trains with a wave number κ and an angular wave frequency ω propagate over a plane bed, inducing on the seabed surface both the fluid pressure fluctuation having a pressure amplitude u_0 and the oscillatory flow having a velocity amplitude U_0. The boundary conditions on the soil surface can then be expressed as follows.

$$\begin{aligned} &\tilde{u}_0 = u_0 \cos(\kappa x - \omega t) \\ &\sigma_z = \tilde{u}_0 \\ &\tau_{zx}^{(1)} = \frac{1}{2}\rho f_\omega U_0^{\,2} \cos(\kappa x - \omega t - \phi) \\ &\text{on} \quad z = 0 \end{aligned} \tag{5}$$

where $\tau_{zx}^{(1)}$ is the oscillatory flow-induced shear stress with a phase lead ϕ and f_w is a friction factor defined by Jonsson(1963).

The wave pressure fluctuation $\tilde{u}_0$ which corresponds to the total stress change σ_z is important since it causes changes in stress state in the soil domain ($z \leqq 0$). With the aid of a poro-elasticity theory (Madsen, 1978; Yamamoto et al., 1978), it follows that

$$\tau_{zx}^{(2)} = -u_0 \kappa z \exp(\kappa z) \sin(\kappa x - \omega t) \tag{6}$$

$$\Delta\sigma_z' = -u_0 \kappa z \exp(\kappa z) \cos(\kappa x - \omega t) \tag{7}$$

where $\tau_{zx}^{(2)}$ is the pressure fluctuation-induced horizontal shear stress at a soil depth z and $\Delta\sigma'_z$ is the change in the vertical effective stress at this location z.

The oscillatory flow-induced shear stress $\tau_{zx}^{(1)}$ defined in Eq. (5) is assumed here to hold its value at the shallow depth z. The wave-induced horizontal shear stress τ_{zx} at the location z may then be expressed as $\tau_{zx} = \tau_{zx}^{(1)} + \tau_{zx}^{(2)}$. Let us now consider the sediment mobility on the basis of the relationship $|\tau_{zx}| = K\sigma'_z$. From Eqs. (5) to (7), it

follows at a generic point x=0 that

$$\left|0.5\rho f_w U_0^2 \cos(\omega t+\phi)+\kappa u_0 z\exp(\kappa z)\sin(\omega t)\right| = K\left(-\frac{\rho_s-\rho}{1+e}gz-\kappa u_0 z\exp(\kappa z)\cos(\omega t)\right) \quad (8)$$

Representing the pressure amplitude $u_0 = \rho U_0 \omega / \kappa$ and the mobile layer thickness δ = -z in Eq. (8), I obtain the following form:

$$S^2\left[\left(\frac{\delta}{af_w\exp(\kappa\delta)}\right)^2+0.25+\frac{\delta}{af_w\exp(\kappa\delta)}\sin(\phi)\right]\cos^2(\omega t+\theta)=$$

$$\left(\frac{K}{1+e}\right)^2\left(\frac{\delta}{af_w}\right)^2\left(1+\frac{S(1+e)\cos(\omega t)}{\exp(\kappa\delta)}\right)^2 \quad (9)$$

where a = U_0/ω is the fluid particle semi-excursion, $\kappa\delta = \kappa af_w \times \delta / af_w$ and

$$\tan(\theta)=\tan(\phi)+\frac{2}{\cos(\phi)}\frac{\delta}{af_w\exp(\kappa\delta)} \qquad 0\le\theta\le\pi/2 \quad (10)$$

Eq. (9) can make it possible to predict the variation of the depth of the mobile layer with time in the course of a given wave cycle.

An example calculation using Eq. (9) is shown in Fig. 1. The parameters used, $K/(1+e)=1/3$ and $\phi = 22.5^\circ$, are the same as those used by Zara Flores and Sleath (1998). The predicted form of variation is not sinusoidal, and is consistent with the measurements in oscillatory flow (Zala Flores and Sleath, 1998). The maximum thickness of the mobile layer, δ_{max}, under waves, manifest itself at a particular phase namely near trough of the waves.

The predicted variations of δ_{max} against S are plotted in Fig. 2 with solid curves for four different values of κaf_w. For the purpose of comparison, a theoretical curve developed by Sleath (1994) for a pure oscillatory flow is also plotted in this figure with the dotted curve. The Sleath-curve was shown to conform with the measurements in Zara Fores and Sleath(1998). The present results fall on a single straight line for low values of S. This implies that there is a linear relation between the mobile layer thickness as defined by δ_{max}/D and the Shields parameter $0.5\rho f_w U_0^2/(\rho_s-\rho)gD$, which is in accordance with the previous results by several other investigators (e.g., Asano, 1993).

But, the value of δ_{max} develops rapidly for high values of *S*, depending strongly on the parameter $\kappa a f_w$. A difference can be seen between the present results for $\kappa a f_w = 0$ and the Sleath theoretical curve for A=0. This may represent the effect of the fluctuation in the vertical effective stress under waves. In fact, the threshold value of *S* at which the $\delta_{max} / a f_w$-value increases rapidly, decreases from 0.3 for pure oscillatory flow to 0.25 for waves.

The poro-elastic analysis as described above should correspond to the behaviour of dense and coarse sand in the sense that only oscillatory pore pressures are present in the soil. The next section will clarify the effect of the residual pore pressures in fine sediments on the basis of the poro-elastoplastic finite element analyses.

ELASTO-PLASTIC FINITE ELEMENT ANALYSES

Under severe wave conditions, wave-induced liquefaction due to the build-up of residual pore pressures should occur owing to the cyclic plasticity nature (contractive behaviour) of cohesionless soil. The poro-elastoplastic finite element analysis developed by Sassa and Sekiguchi (2001) can describe the changes in shear stress and effective stresses in the course of the liquefaction. The present study extends the analysis so as to consider the shear stress due to oscillatory flow under waves.

Two sets of the finite element analysis were performed for a total of 15 cycles of wave loading in each set, with the aim of reproducing the observed wave-induced liquefaction in loose beds of silt (mean grain diameter $D_{50} = 0.05mm$) and fine sand ($D_{50} = 0.15mm$). The wave loading and the geometry are shown for each set in Fig.3. It is important here to note that the partial drainage factor Φ (Sassa and Sekiguchi, 1999) is defined by

$$\Phi = \frac{k_D}{m_v \gamma_f \omega} \kappa^2 \tag{11}$$

where k_D is the Darcy coefficient of permeability of the soil, $\gamma_f = \rho g$ is the unit weight of the fluid and m_v is the coefficient of compressibility of the soil skeleton. The Φ-value for the loose fine sand was equal to 4.7×10^{-3}, which was significantly higher than 1.8×10^{-6} for the loose silt. The values of the parameter $\kappa a f_w$ were 0.001 and 0.002 respectively. These parameters were determined with reference to the wave and soil conditions imposed in the experiments by Sassa and Sekiguchi (1999) and Foda and Tzang (1994). The friction factor f_w was calculated from Jonsson's (1963) formula

with a roughness height equal to $2D_{50}$.

A typical set of the results on the variations of stresses at the bottom of the mobile layer is shown in Fig. 4. The fluctuation in the horizontal shear stress τ_{vh} remain unchanged during the first 12 cycles or so, while the vertical effective stress σ'_v decreases continuously owing to the build-up of residual pore pressure $u_e^{(2)}$ in the soil. At the 15th wave loading cycle, liquefaction takes place such that $u_e^{(2)} \cong \sigma'_{v0}$, allowing the sediment to become mobile at this soil depth according to the relationship $|\tau_{vh}| = K\sigma'_v$.

The influence of the severity of wave loading on the development of the liquefaction can be clearly seen in the form of Fig. 5. The wave-induced changes in both the residual pore pressure ratio $u^{(2)}_e/\sigma'_{v0}$ and the effective stress ratio p^*/σ'_v are plotted against the cyclic stress ratio χ_0. For the purpose of discussion, the soil responses to wave pressure fluctuation, namely without the oscillatory flow-induced shear stress, are also plotted in Fig. 5. The results indicate that there exists a critical cyclic stress ratio χ_{cr} below which liquefaction does not occur. It is also noteworthy that there is no significant difference between the results under wave pressure fluctuation and under waves which involve both wave pressure fluctuation and oscillator flow. The wave pressure fluctuation, rather than oscillatory flow, may thus be responsible for the occurrence of the wave-induced liquefaction.

The results of the elastoplastic analysis are superimposed on the results of the elastic analysis, giving a summary plot as shown in Fig. 6. Note here that the elastic response represents the absence of residual pore pressures with only oscillatory pore pressures involved, which may correspond to high values of Φ for dense and coarse sand. For the loose fine sand with $\Phi = 4.7 \times 10^{-3}$ in Fig. 6, however, the δ_{max}-value develops more rapidly owing to the build-up of residual pore pressures in the soil. The liquefaction effect is further significant for the loose silt with $\Phi = 1.8 \times 10^{-6}$.

Verification of the Predicted Depth of Mobile Layer with the Measurements of Wave-Induced Liquefaction

Sassa and Sekiguchi (1999) performed a series of centrifuge wave tank tests on loose beds of fine sand (mean grain size $D_{50} = 0.15mm$) with viscous scaling introduced, such that time scaling laws for wave propagation as well as consolidation of soil were

matched. The critical cyclic stress ratio χ_{cr} for liquefaction to occur was found to be 0.14, in accordance with the predictions as shown in Fig 5. This value corresponds to $S = 0.075$ on the basis of the relationship $S = \chi_0 /(1+e)$. The measured thickness of liquefied zone for the threshold value of S is plotted in Fig. 6. The measured thickness of $\delta_{max} / af_w = 256$ is consistent with the predicted thickness of $\delta_{max} / af_w = 148$.

Foda and Tzang (1994) performed a series of wave flume tests on loose beds of silt ($D_{50} = 0.05mm$) and sand ($D_{50} = 0.29mm$). They observed the occurrence of liquefaction due to the build-up of residual pore pressures in silt. I calculated the S-values for their data and found that liquefaction took place at the value of S as low as 0.03. In contrast, no significant residual pore pressures or sediment transport took place for sand, owing to the high value of Φ. The both measured results for silt and sand conform well with the predictions shown in Fig. 6.

The results described above demonstrate that the poro-elastoplastic finite element analysis combined with the fluid mechanics approach for describing the oscillatory flow-induced shear stresses can predict consistently the maximum thickness of the mobile layer under given wave and soil conditions, emphasizing the effect of the wave-induced liquefaction in beds of silt or fine sand.

CONCLUSIONS

The thickness of mobile layer under waves has been discussed on the basis of poro-elastic and elastoplastic analyses, with the aim of demonstrating the effect of the wave-induced build-up of pore water pressures. It is found that there are three important dimensionless parameters: the wave severity parameter S or χ_0, the partial drainage factor Φ and the newly defined wave friction parameter κaf_w. When the κaf_w-value is low, there could occur a rapid increase in the normalized maximum mobile layer thickness $\delta_{max}/af_{w.}$ The threshold wave condition, namely the critical S-value, depends on the magnitude of Φ for a given sediment. For dense and coarse sediments with high values of Φ, the predicted critical S-value is equal to 0.25 which is slightly lower than the value of 0.3 in pure oscillatory flow. The difference represents the effect of the fluctuating vertical effective stress under waves. The situation changes remarkably when dealing with loose fine sediments with low values of Φ. In fact, the critical S-value reduces to as low as 0.06 for loose beds of fine-grained sand and further to 0.03

for silt, owing to the wave-induced build-up of residual pore water pressures. The wave pressure fluctuation, not oscillatory flow, is responsible for the rapid increase in mobile layer thickness in the fine sediments.

REFERENCES

1. Asano, T., 1993, "Observations of granular-fluid mixture under an oscillatory sheet flow", *Proc. 22th Int. Conf. Coastal Eng., ASCE,* Reston, 1896-1909.
2. Foda, M.A. and S.-Y. Tzang, 1994, "Resonant fluidization of silty soil by water waves", *J. Geophys. Res. 99* (C10), 20,463--20,475.
3. Jonsson, I.G., 1963, "Measurements in the turbulent wave boundary layer", *Proc. 10th Congress IAHR*, London, 85-92.
4. Madsen, O.S., 1978, "Wave-induced pore pressures and effective stresses in a porous bed", *Géotechnique 28* (4), 377-393.
5. Nielsen, P., 1992, "*Coastal bottom boundary layers and sediment transport",* World Scientific, Singapore, pp 324.
6. Sassa, S. and H. Sekiguchi, 1999, "Wave-induced liquefaction of beds of sand in a centrifuge", *Géotechnique 49* (5), 621-638.
7. Sassa, S. and H. Sekiguchi, 2001, "Analysis of wave-induced liquefaction of sand beds", *Géotechnique 51* (2), 115-126.
8. Sleath, J.F.A., 1994, "Sediment transport in oscillatory flow", in *Sediment Transport Mechanisms in Coastal Environments and Rivers* edited by M. Belorgey, R.D.Rajaona and J.F.A. Sleath, World Scientific, Singapore.
9. Yamamoto, T., H.L. Koning., H. Sellmeijer. and E. Hijum, 1978, "On the response of a poro-elastic bed to water waves", *J. Fluid Mech*. *87*, 193-206.
10. Zala Flores, N. and J.F.A. Sleath, 1998, "Mobile layer in oscillatory sheet flow", *J. Geophys. Res. 103*, C6, 12,783-12,786.

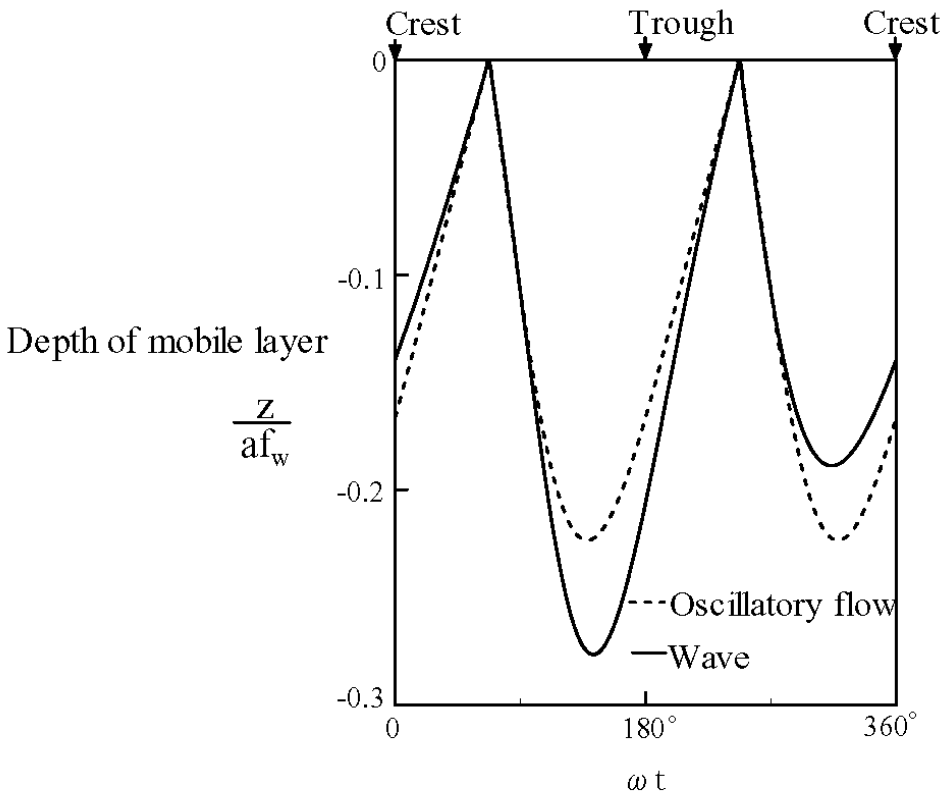

a: Fluid particle semi-excursion U_0 / ω

f_w: Jonsson's friction factor $2 \tau_0 / (\rho U_0^2)$

Fig.1 — Variation of the depth of the mobile layer with time during a wave cycle (S= 0.12, Φ=22.5°, e= 0.6, K=0.53)

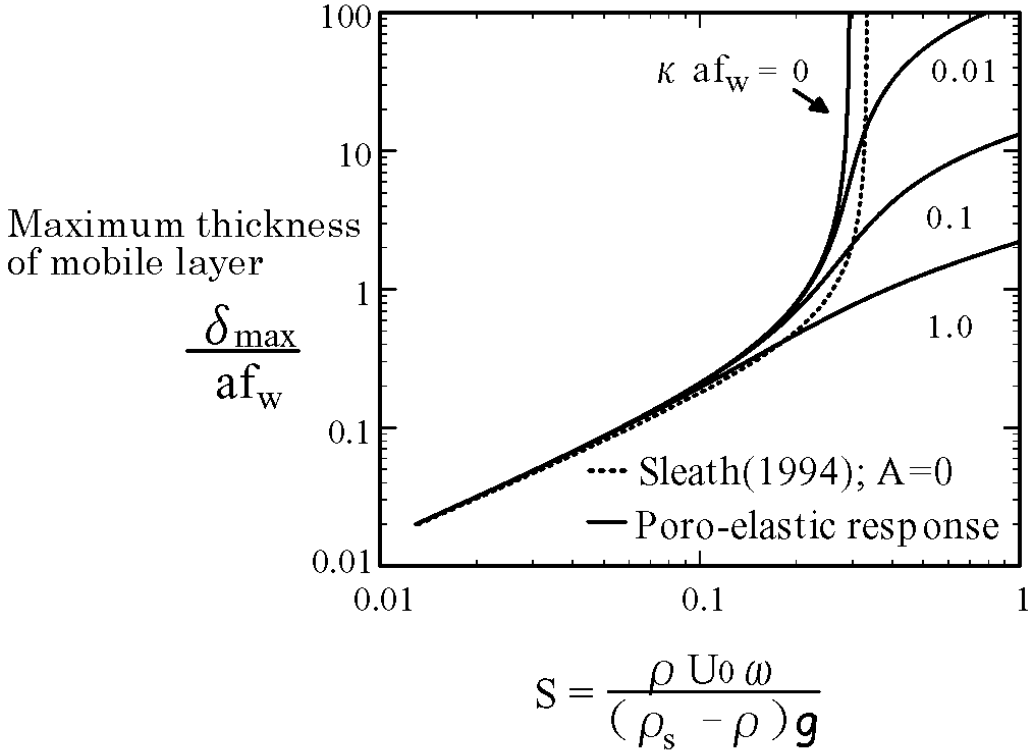

Fig.2 — Variation of normalized maximum mobile-layer thickness with S during a wave cycle

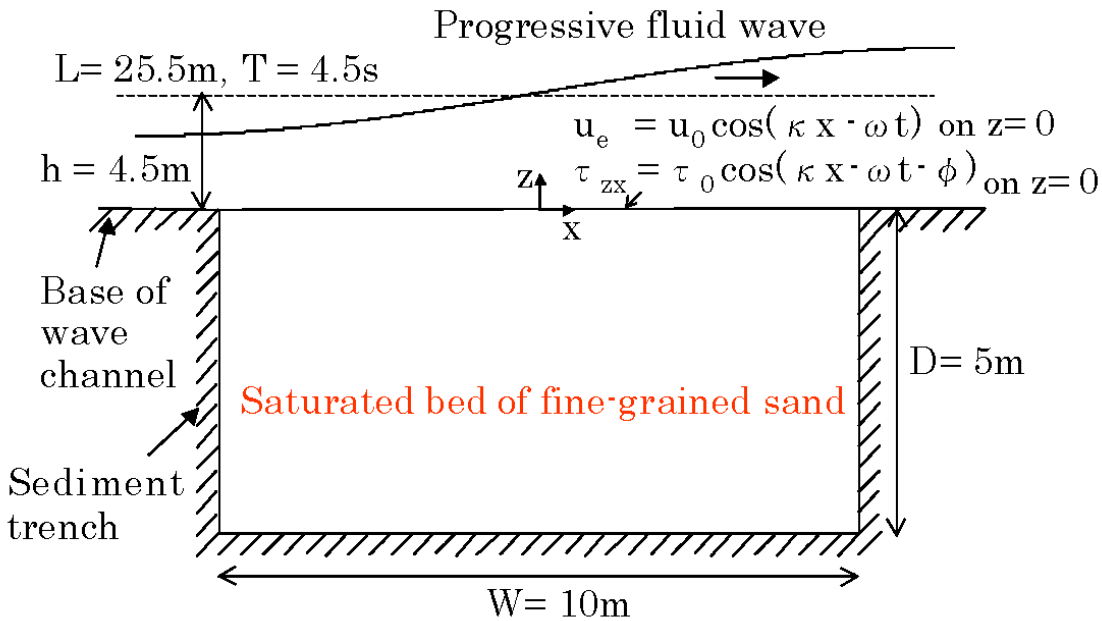

(a) Proto-type for the centrifuge model by Sassa and Sekiguchi(1999)

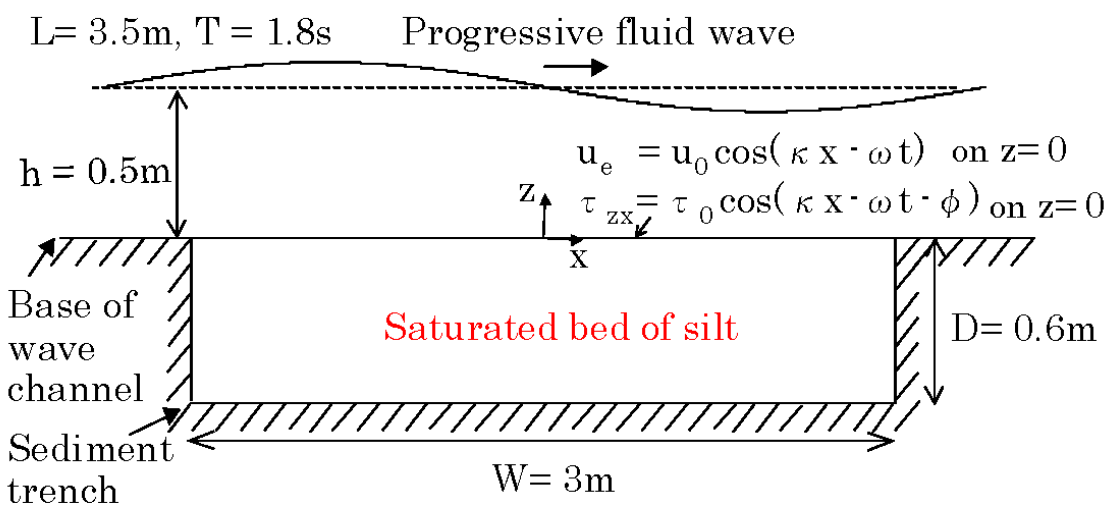

(b) Large scale model by Foda and Tzang(1994)

Fig.3 — Elastoplastic finite element analyses for reproducing the observed wave-induced liquefaction

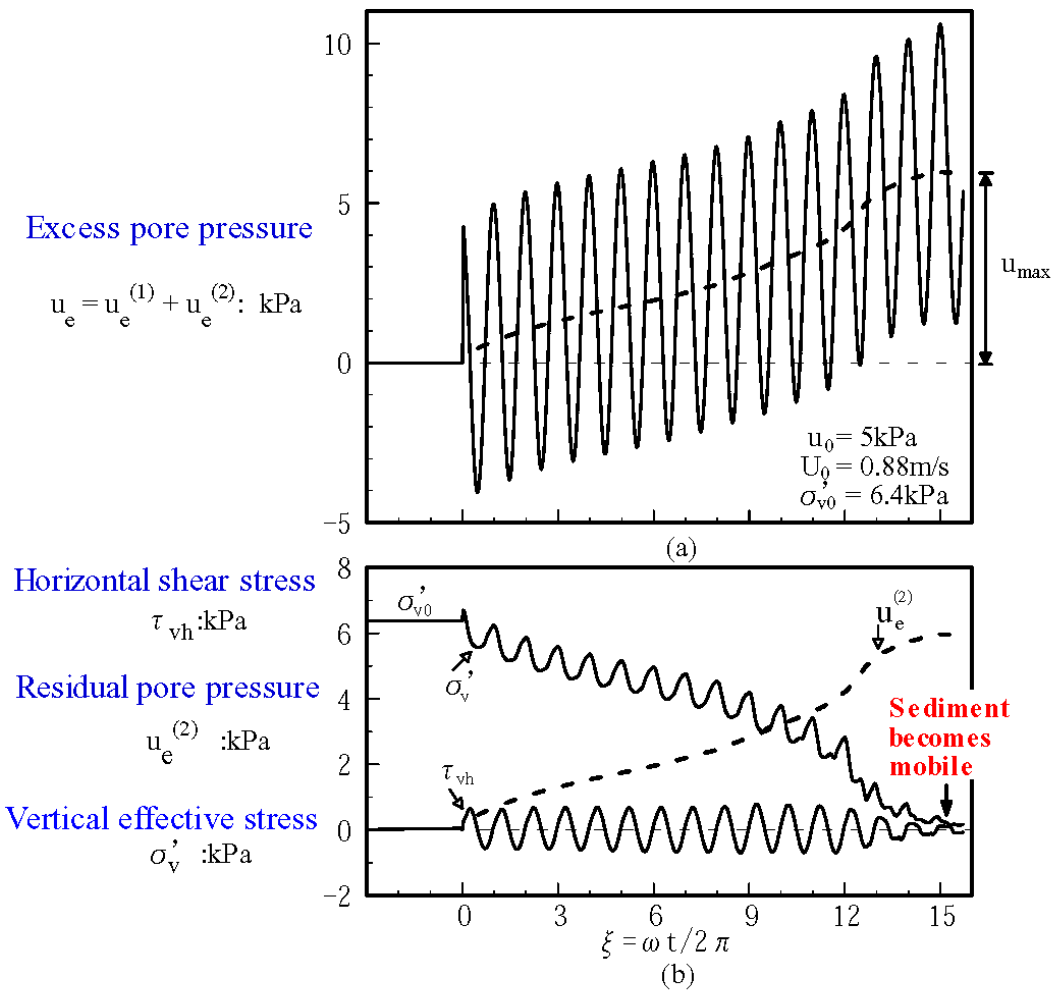

Fig. 4 — Variations with time of τ_{vh}, $u_e^{(2)}$ and σ_v' at the bottom of the mobile layer z = -75cm under waves ($S = 0.075$, $\kappa afw = 0.001$, $\Phi = 4.7 \times 10^{-3}$)

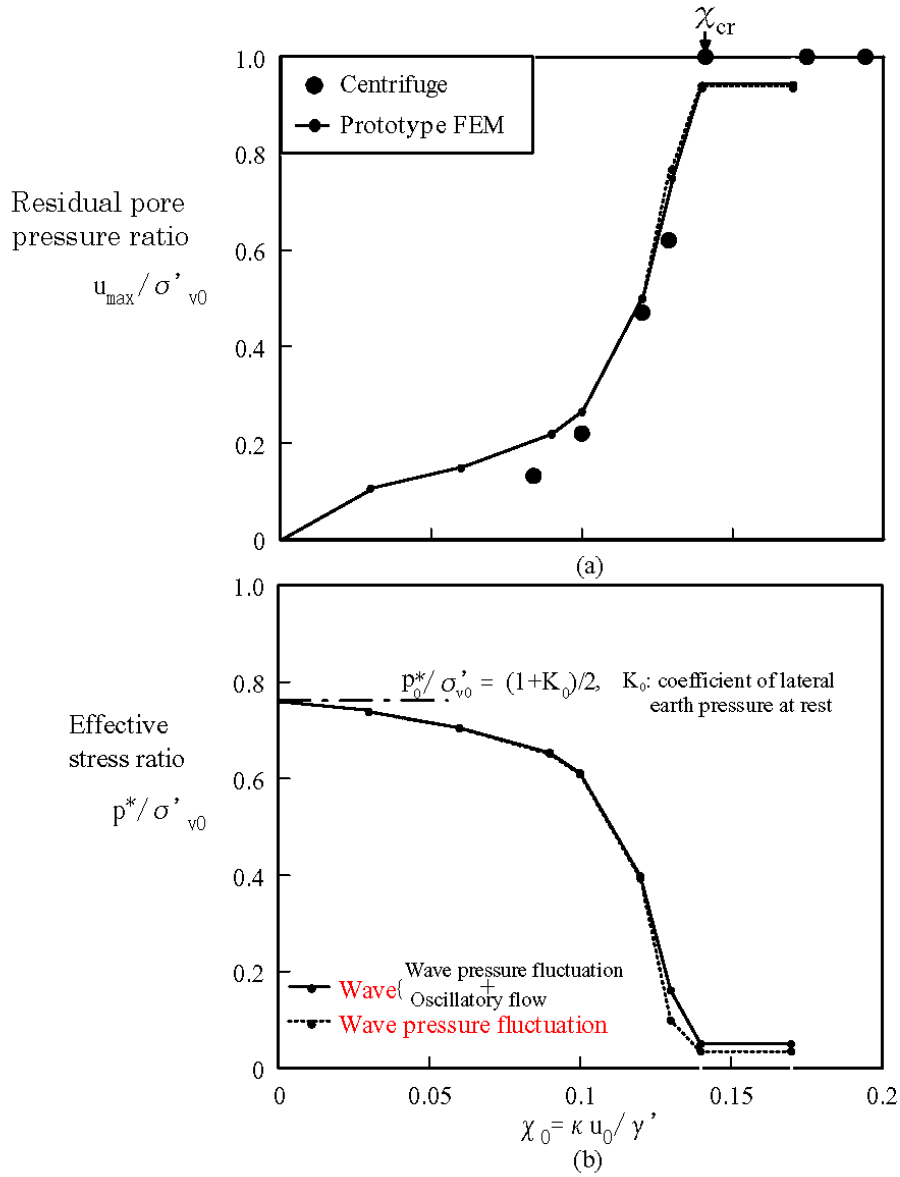

Fig. 5 — Variation with χ_0 of u_{max}/σ'_{v0} and p^*/σ'_{v0} showing the critical cyclic stress ratio for liquefaction to occur

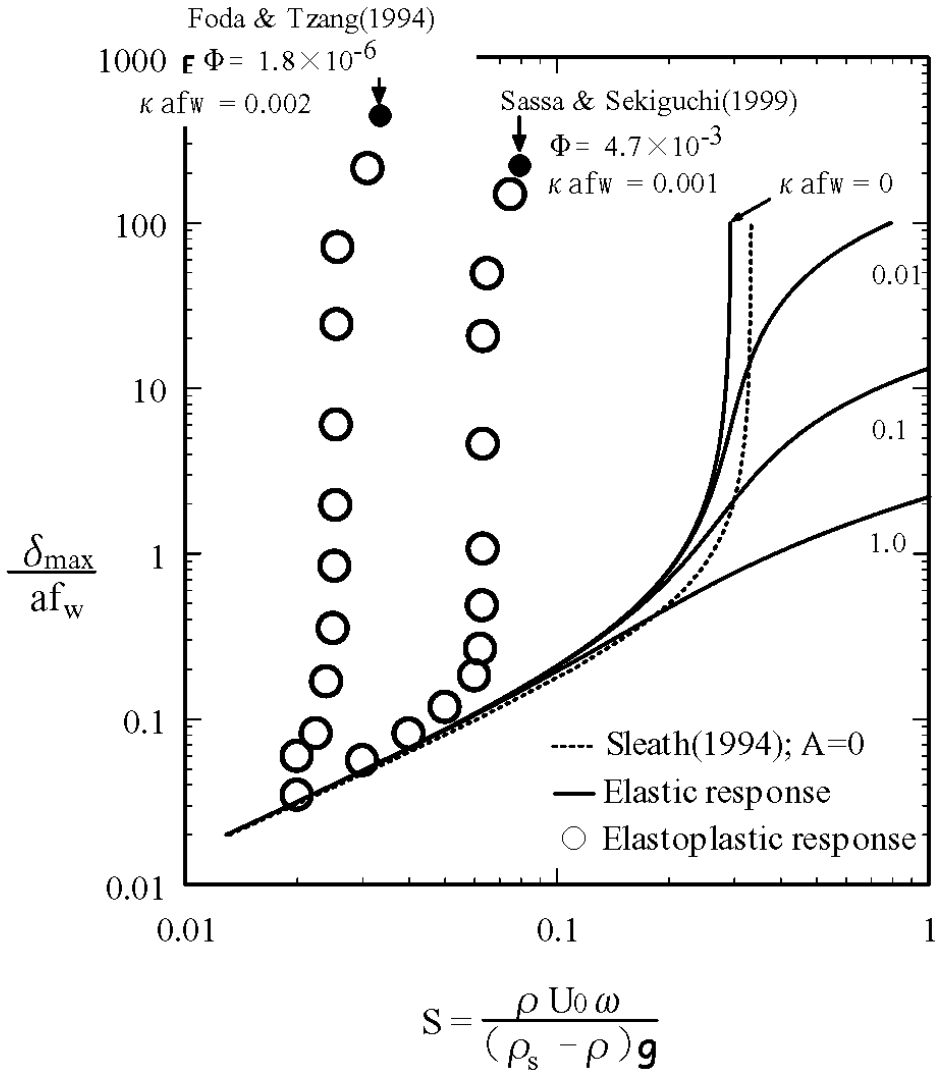

Fig. 6 — Summary plot showing the effect of pore pressure build-up on the maximum thickness of mobile layer under waves

Essence of Silt Factor for Scour Calculation Around Bridge Foundation

By

RK Dhiman[1], DK Mohapatra[2]

ABSTRACT

Foundation of river bridges on alluvial soil is decided largely based on hydraulic data and subsoil strata. The subsoil strata is represented by a numerical value called silt factor. This factor plays vital role as the foundation level depends upon soil strata underneath, which is examined based on the bore log data. Bridges are very costly due to various reasons and the depth of foundation is one of them. There is need to optimise the depth of foundation to a pragmatic level, which can be constructed safely without undue delay as per construction practices. Any variation in foundation level at later date plays crucial role in the overall cost of the bridges and affect the completion time of the project. It is highlighted that pre construction investigation should be given more attention to avoid any lapse in construction programme. Data analysed based on investigation need to be reviewed in term of construction trend in the area. The importance of silt factor has been discussed in this paper. An accurate estimation of the same helps in completing the structure in less time without time and cost over run.

Key words :- Silt factor, scour, Alluvial soil, Soil mixed with boulder, Normal scour depth.

[1] Executive Engineer (C) Dte of Bridges, Dte General Border Roads Seema Sadak Bhawan Ring Road, Delhi Cantt New Delhi-110010, E-mail: d_himan12@yahoo.com
[2] Executive Engineer (C) Dte of Bridges, Dte General Border Roads Seema Sadak Bhawan Ring Road, Delhi Cantt New Delhi-110010, E-mail: dillip_m@hotmail.com

INTRODUCTION

1.0 Foundation level for bridges are finalized based on the hydraulic parameters and the nature of bed material underneath. The subsoil is rated in term of silt factor, which is a numerical value. It indicates the type of bed material from clay to heavy sand. Gravel and Soil Mixed with Boulder (SMB) falls beyond this range. Foundation level is fixed below the scour level after considering the grip length. The scour depth is determined by using the Indian codal formulae which incorporates the silt factor within it or on the basis of results of model study wherever carried out. In bridges the hydraulic parameters such as the discharge, velocity need to be estimated accurately as it has direct bearing on the depth of scour. This involves lot of financial bearing and affects overall completion of bridge Project. Stress has been laid in this paper to highlight the essence of silt factor used for calculation of scour.

SILT FACTOR

2.0 Silt factor plays a significant role in determining the scour depth and also the founding levels for the foundation of the bridge structures. Due to lack of adequate bore hole data and also various uncertainties associated therewith, bridge engineers are confronted with a difficult job of choosing an appropriate value of silt factor. This assumes importance because the present code used for design of bridge foundation guidelines caters for a maximum silt factor of upto 2.42, which is applicable for heavy sand only. Since the silt factor has a significant role to play in finalising foundation depths, it suffices to say that identification of correct silt factor poses a problem wherein the selection of this important parameter is left to the judgement, discretion and experience of the designer. For calculation of silt factor in any type of soil, the soil strata is examined in greater depths and values are calculated in table 1 & 2. A worked out example of silt factor is given below:-

Sample1 **Table 1**

Dia. Of sieve	Weight retained gms	Percentage retained	Average size of sieve	Col. (3) x(4)	(Mean diameter $\frac{\text{Col-5}_{mtr}}{100}$
1	2	3	4	5	6
2.360	293	29.30	-	-	
1.180	313	31.30	1.7700	55.401	79.136/100=0.7913
0.600	172	17.20	0.8900	15.308	
0.425	109	10.90	0.5125	5.586	
0.300	39	3.90	0.3625	1.413	
0.150	59	5.90	0.2250	1.327	$K_f = 1.76\sqrt{m} = 1.5656$
0.075	9	0.90	0.1125	0.101	
Pan	6	0.60	-	-	
	1000	100.00	-	79.136	

Sample2 **Table 2**

1	2	3	4	5	6
2.360	49	4.90	-	-	
1.180	190	19.00	1.7700	33.630	78.424/100=0.7842
0.600	295	29.50	0.8900	26.255	
0.425	253	25.30	0.5125	12.966	$K_f = 1.76\sqrt{m} = 1.5587$
0.300	83	8.30	0.3625	3.008	
0.150	104	10.40	0.2250	2.340	
0.075	20	2.00	0.1125	0.225	
Pan	6	0.60	-	-	
	1000	100.00	-	78.424	

Silt factor = 1.5656 + 1.5587 / 2 = 1.5622

The Sample calculation of mean diameter of silt is based on mathematical expression of averaging.

ROLE OF SILT FACTOR IN ESTIMATION OF SCOUR

3.0 The scour depth is calculated based on Indian Road Congress[1] (IRC) formulae.

$$D_{sm} = 1.34 \left(\frac{D_b^2}{K_{sf}} \right)^{1/3}$$

D_b = Design discharge per meter width
K_{sf} = Silt factor for representative sample of bed material
D_{sm} = Mean scour depth

This formula is applicable upto heavy sand only. For material having heterogeneous stratification in the river where material is comprises soil mixed with boulder, result are compared with actual observation at site or from experience on similar structure nearby and their performance. Model study is also carried out for bridges on requirement and scour depth is finalized accordingly. Trend of normal scour calculation with a fixed discharge of 50 cubic mtr per sec with a different value of silt factor using the IRC formula has been shown in table 3.

TABLE – 3

SCOUR DEPTH FOR DISCHARGE OF 50 M^3/Sec/m (Db)

Silt Factor	Dsm
.50	22.91
.60	21.56
.85	19.19
1.00	18.18
1.25	16.24
1.50	15.88
1.75	15.09
2.00	14.43
2.25	13.87

2.42	13.54
3.00	12.60
4.00	11.45
5.00	10.635
9.00	8.74
13.00	7.73
17.00	7.073
19.00	6.82
20.00	6.70

ESSENCE OF SILT FACTOR

4.0 Essence of silt factor for scour calculation can be further represented in graphical form as indicated below where it is seen that after a value of silt factor of 8 the value of mean scour is not changing much and likely to almost constants for a higher value of discharge.

SCOUR DEPTH VIS-A-VIS SILT FACTOR FOR DISCHARGE OF 50 M³/SEC/M

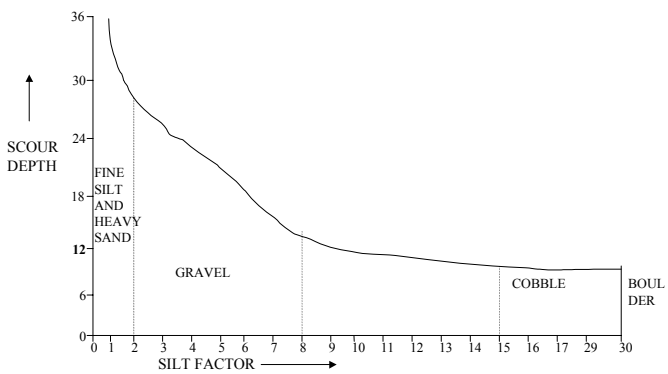

Fig-1

Most of bridges whether already completed or under construction have faced foundation problems especially in sinking of wells of multi span bridges. Whenever problems of sinking of well are faced, case is examined with reference to soil strata actually encountered. The task of subsequent review of foundation levels based on actual strata encountered (review of silt factor) need reprocessing of case. There are certain important points which require attention of bridge engineer for better planning of bridge foundation.

(a) Correct finalisation of silt factor at initial stage will be helpful to optimize cost of the bridge. This will also be helpful to stict to original time schedule as the there is no likely mismatch of strata.

(b) Cost of sinking of foundation can be avoided if there is no variation in soil parameter including silt factor.

(c) Foundation depth is required to be finalised as per the construction technology available in the country.

(d) Infact there is need to take a stock of situation about the construction methodology, in such a way that the proposal finalised should be executable on the ground.

(e) The completion of the particular project and related difficulties encountered be examined with reference to silt factor, as this is the only one major factors affecting the design scour. There are other factors affecting scour around bridge pier viz. Whether the flow is clear water flow or carries sediments, change in depth of flow, shape of pier nose, angle of inclination of pier, opening ratio, bed characteristics, stratification and effect of flow parameters. Apart from this there are other causes leading to scour as given table-4.

TABLE-4

	RIGID BEND	ERODING BEND	ABRUPT CHANGE IN FLOW DIRECTION	OBSTRUCTION (PIER/Abutment)	CONSTRICTION	CONFLUENCE	SUB SURFACE	CONTROL STRUCTURE	BRIDGE PIER
FACTORS AFFLCTING SCOUR	1. Radious of Curvatures 2. Length of bend	1. Raious of curvatures 2. Length of bend 3. Type of bank material	Degree of change in direction	Angle of scour	Degree of narrowing	1. Angle between tributories 2. Flow ratio in each channel	Slope of bedrock	1Downsteam depth	1 Width of pier

(f) Soil strata be studied in details and if required, the help of expert be also sought.

RECOMMENDATIONS

5.0 Various steps to be followed to arrive at correct value of silt factor are as follows:-

(a) Keep a drilling record of the entire bore log and assess the value of silt factor upto foundation level at initial stage.

(b) During construction of foundation better picture of soil strata can be seen and accordingly the silt factor can be further reviewed if it does not match with the calculation as finalised initially during subsoil investigation stage.

(c) Value of different silt factor value can be calculated for 2 to 3 of bore log details and average value can be adpoted.

(d) Wherever the silt factor value is not assessable, the soil strata actually encountered during execution is reviewed and practical aspect is kept in view and final value is arrived at.

CONCLUSION

6.0 Silt factor plays a important role in finalisation of foundation levels. In case of difficulties faced in finalising level of foundation based on silt factor concept, model study can also be reviewed if carried initially otherwise, experienced gained at previous bridges can be dove-tailed for future bridges for finalizing their foundation level. Efforts should be made to assess correct value of silt factor to optimise the depth of foundation and there will be no time and cost over run.

REFERENCE

1. IRC : 78-2000 – Standard Specifications and Code of Practice for Road Bridges, Section VII – Foundations & Substructure (Second Revision).

AUTHOR INDEX

Author	Page
Abghari, A.	684
Adams, J. P.	954
Alonso, C.	349, 734
Anglin, C. D.	582, 978
Annandale, G. W.	449
Awad, M. A.	471
Baig, S. M.	1111
Barkdoll, B.	734
Bermudez, H.	719
Bettencourt, B.	842
Bettess, R.	162
Bixler, M.	918
Boehm, D. W.	609
Bollaert, E.	449
Bos, K. J.	567
Bozo, L.	884
Briaud, J-L.	57, 156, 227, 242, 272, 373, 459, 1061, 1188, 1208
Cao, Y.	227, 459
Casado, J. M.	34
Chang, K-A.	869
Chen, H-C.	14, 156, 242, 373, 459, 1061, 1188,1208
Cheng, L.	175
Chiew, Y-M.	70, 707
Chin, C-O.	968
Chiu, P-H.	869
Choi, S-U.	206
Chung, M-K.	227
Cian, C.	1152,1155
Coleman, S.	749
Curry, J. E.	292
D'Odorico, P.	272
Davies, E. B.	1019
Davis, S.	227
Dennett, K. E.	642, 1008
Dhiman, R. K.	560, 896
Di Stasi, J. M.	516
Ding, D.	540
Dumas, C. E.	112
Edelmann, J.	842
Edgers, L.	842
Escarameia, M.	320
Ettema, R.	364, 383, 734
Farrag, K.	283
Ferrando, G.	1152, 1155
Fredsoe, J.	795
Fricthel, P.	642, 1008
Fukui, J.	47, 410
Gardner, R. W.	623
Guven, O.	292
Hager, W. H.	774
Heibaum, M. H.	1
Ho, C. L.	516
Ho, T-C.	869
Hoe, D.	749
Hoffmans, G.	92
Huessin, M.	918
Hunt, B.	227
Islam, M. S.	684
Itamunoala, F.	582
Jeon, E. J.	272
Jeong, S.	854
Jia, Y.	349, 1181
Johnson, P. A.	678
Jones, J. S.	140, 485, 810
Jung, B-S.	437
Kajima, R.	421
Kandaris, P. M.	954
Kanno, Y.	307
Kant, G.	567, 656
Khan, M. A.	1111
Kim, H.	437
Kirshen, P.	842
Kitsunai, S.	910
Kobayashi, N.	910
Kondziolka, R. E.	954
Krolack, J.	112
Kruisbrink, A. C. H.	567
Kuhnle, R.	349, 734
Kumar, A. V.	500
Kusakabe, O.	1081
Kwak, K.	227
Lachhab, A.	364
Lagasse, P.	1051
Lauchlan, C.	184
Lewandowski, E.	842
Li, W.	968

Author	Page
Li, Y.	156, 242, 373, 459, 1188, 1208
Lim, S-Y.	395, 785
Lin, C.	869
Lindo, M. H.	656
Lindsey, W. B.	699
Link, O.	1160
Lopardo, M. C.	34
Lopardo, R. A.	34
Maeno, S.	218
Martinez, E.	364
Masahiko, S.	337
May, R. W. P.	184, 320
McDonald, J. A.	1019
Melville, B.	120, 734, 749
Melville, J. G.	292
Mercado, E. J.	1019
Mia, F.	218
Michelsen, J.	795
Millen, G.	582
Miller, Jr., W.	827
Mishra, S. K.	699
Mohapatra, D. K.	560
Molinas, A.	485
Morvant, M.	283
Muceku, Y.	884
Mueller, D. S.	257, 1096
Muraishi, H.	337
Murakami, S.	307
Nago, H.	218
Nairn, R. B.	978
Nakajima, D.	337
Nakato, T.	528
Neelamani, S.	500
Nevels, Jr., J. B.	764
Ng, S.	1042
Nishimura, T.	1081
Nishitani, M.	47
Nurtjahyo, P.	156, 242, 373, 459
O'Neill, M. W.	1019
Ogihara, K.	337
Oh, B. C.	437
Oliveto, G.	774
Olson, L. D.	929
Otuka, M.	410
Pagan-Ortiz, J. E.	636
Parchure, T.	734
Park, S.	1061
Parola, A.	734
Percher, M.	842
Phillips, R.	719
Piepers , T	1166
Price, G. R.	1032
Punrattanasin, P.	1081
Rao, S. N.	500
Rausche, F.	918
Razdan, K. K.	896
Rees, P.	516
Richards, D. L.	670
Richardson, E. V.	810, 993
Roulund, A.	795
Sainz, J. A.	597
Sakakiyama, T.	421
Salgado, R.	597
Sassa., S.	546
Schaefer, K. J.	623
Schall, J. D.	1032
Schleiss, A.	449
Sheppard, D. M.	198, 810, 827
Shimamura, M.	910, 945
Siddharthan, R.	642, 1008
Singh, R.	896
Soltani, A.	642, 1008
Spaan, G. B. H.	656
Spitz, W.	1051
Subjarassang, A.	1081
Suh, J.	854
Sultan, N.	719
Sumer, B. M.	795
Suzuki, H.	945
Tan, S-K.	785
Unger, J.	774
Verheij, H. J.	92, 567
Wagner, C. R.	257, 1096
Wang , S. Y	1176, 1181
Wang, J.	156, 242, 373, 459, 1188, 1208
Wang, W.	1188, 1208
Won, J.	854
Wu, Z.	307
Wu,W.	1176
Xu, Y.	1181
Yang, W.	206
Yasuhara, K.	307
Youn, S-Z	437
Yu, G.	395, 785
Zanke, U.	1160
Zarriello, J. J.	1111
Zevenbergen, L.	1051
Zha, J.	684
Zhang, L.	540
Zhou, W.	540